

Научном већу Института за физику Београд

| ИНСТИТУТ ЗА ФИЗИКУ     |       |           |        |
|------------------------|-------|-----------|--------|
| ПРИМЉЕНО: 06. 02. 2020 |       |           |        |
| Рад.јед.               | број  | Арх.шифра | Прилог |
| 0801                   | 157/2 |           |        |

## МОЛБА

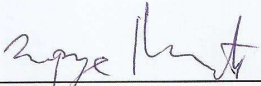
### за покретање поступка реизбора у звање виши научни сарадник

Молим Научно веће Института за физику Београд да, у складу са Правилником о поступку, начину вредновања и квантитативном исказивању научноистраживачких резултата истраживача, покрене поступак за мој реизбор у звање виши научни сарадник.

У прилогу достављам:

1. Мишљење руководиоца лабораторије са предлогом комисије која ће писати извештај.
2. Стручну биографију.
3. Преглед научне активности.
4. Елементе за квалитативну анализу.
5. Елементе за квантитативну анализу.
6. Списак објављених радова и других публикација.
7. Податке о цитираности.
8. Копије објављених радова и других публикација.
9. Решење о претходном избору у звање.
10. Прилоге.

У Београду, 06. фебруара 2020.

  
др Димитрије Малетић  
виши научни сарадник  
Институт за физику Београд

## ИНСТИТУТ ЗА ФИЗИКУ

|                        |       |           |        |
|------------------------|-------|-----------|--------|
| ПРИМЉЕНО: 06. 02. 2020 |       |           |        |
| Рад.јед.               | б р о | Арх.шифра | Прилог |
| 0801                   | 157/1 |           |        |

Научном већу Института за физику Београд

**Мишљење руководиоца лабораторије о reizбору др Димитрија Малетића у звање виши научни сарадник**

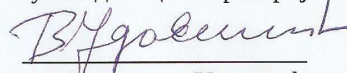
Др Димитрије Малетић је запослен у Нискофонској лабораторији за нуклеарну физику Института за физику Београд, Универзитета у Београду. Бави се истраживањима у областима физике космичког зрачења, физике високих енергија и нуклеарне физике. С обзиром да испуњава све предвиђене услове у складу са Правилником о поступку, начину вредновања и квантитативном исказивању научноистраживачких резултата истраживача МПНТР, сагласан сам са покретањем поступка за reizбор др Димитрија Малетића у звање виши научни сарадник.

За састав комисије за reizбор др Димитрија Малетића у звање виши научни сарадник предлагем:

1. Др Владимир Удовичић, виши научни сарадник, Институт за физику Београд.
2. Др Дејан Јоковић, виши научни сарадник, Институт за физику Београд.
3. Проф. др Марија Димитријевић Ђирић, ванредни професор, Физички Факултет Универзитета у Београду.

У Београду, 06. фебруара 2020.

Руководилац лабораторије



др Владимир Удовичић  
виши научни сарадник  
Институт за физику Београд

## 2. Стручна биографија кандидата

Димитрије Малетић је рођен 21.02.1976. године у Вуковару, р. Хрватска. Завршио је гимназију у Вуковару 1994. године. Основне студије на Физичком факултету Универзитета у Београду на смеру Теоријска и експериментална физика завршио је 2003. године одбранивши дипломски рад под насловом *“Температурска калибрација сензора за контролни систем CMS ECAL детектора”* под руководством проф. др Јована Пузовића. Запошљава се 1. маја 2004. године у Групи за физику елементарних честица Лабораторије за физику (010) Института за нуклеарне науке Винча. Уписује последипломске магистарске студије, и почиње сарадњу са колегама на експерименту CMS у CERN-у, у Женеви, Швајцарска. Магистрира 2006. године на Физичком факултету Универзитета у Београду са темом *„Монте Карло симулација CMS ECAL Preshower детектора и поређење са експерименталним резултатима“* под руководством проф. др Петра Аџића. Учествоје у пројекту основног истраживања у периоду 2006-2009 под називом *„Физика високих енергија на детектору CMS“* под руководством проф. др Петра Аџића. 25. 09. 2006. године је изабран у звање истраживач сарадник у Институту Винча. Наставак рада обележава и веће ангажовање у CMS колаборацији, што резултира израдом докторске дисертације под називом *„Редукација фона двофотонског канала распада  $Higgs$  бозона (SM) на детектору CMS“*, под руководством проф. др Петра Аџића, која је 2009. године одбрањена на Физичком факултету Универзитета у Београду, а која је уједно представљена и CMS колаборацији, и добила статус CERN-ове тезе. У периоду израде докторске тезе блиско је сарађивао са проф. др Аристотелисом Киријакисом из NCSR Демокритос из Института за Нуклеарну и честичну физику у Атини, Грчка, који долази из института које је више пута кандидат посећивао у периоду 2004-2010. Вреди поменути и то да знања о Монте Карло симулацијама, вештачким неуронским мрежама, програмирању и GRID окружењу добро усваја и успешно користи при изради магистарске и докторске тезе. 28.12.2009 изабран је у звање Научни сарадник у Институту Винча. Договорно напушта Институт Винча и CMS колаборацију и 1. маја 2010. године се запошљава у Нискофонској лабораторији за Нуклеарну физику, у Институту за физику Београд, Универзитета у Београду. Учествоје на пројекту основних истраживања МПНТР у периоду 2010-2019 под називом *„Нуклеарне методе истраживања ретких догађаја и космичког зрачења“* под руководством проф. др Иштвана Бикита. Започиње рад на физици космичког зрачења под руководством проф. др Ивана Аничина. Придружује се SHINE колаборацији у CERN-у 2011-2013 године. Започиње рад на проблематици радона под руководством др Владимира Удовичића као и проблематици заштите животне средине. Придружује се MICE колаборацији 2015- и предводи групу сарадника из Института за физику Београд на MICE експерименту у Радерфорд Аплетон лабораторији у Енглеској.

Научне теме којима се кандидат до сада бавио су физика високих и средњих енергија која укључује рад на експериментима CMS, SHINE и MPD/NICA, акцелераторска физика јонизационог хлађења на експерименту MICE, физика космичког зрачења, нуклеарна физика која укључује изучавање особина радиоактивног гаса радона (ИФ, IAEA) и изучавање фонског зрачења које долази од природне радиоактивности, а интерес има и за заштиту од зрачења и заштиту животне средине. По бази SCOPUS има 79 радова са 7142 цитата и х-индекс 30. По Google Scholar има 115 радова са укупно 15806 цитата и х-индекс 40, а по бази <http://inspirehep.net> број цитата искључујући самоцитате је 6,687 и х-индекс је 24. Био је ментор за израду докторске дисертације Михаила Савића, одбрањене 2019. године на Физичком факултету Универзитета у Београду.

### 3. Преглед научне активности

Научноистраживачка активност кандидата обухвата:

- физику високих енергија на детектору CMS,
- изучавања особина атомских језгара на средњим енергијама на експериментима SHINE и NICA,
- акцелераторска физика јонизационог хлађења на MICE експерименту,
- физика космичког зрачења,
- изучавање динамике радона и фонског зрачења
- заштита животне средине.

#### 3.1. Физика високих енергија на детектору CMS

Др Димитрије Малетић се бави физиком на CMS експерименту у периоду од 2003. до 2009. године. Од самог почетка доприноси развоју софтверског пакета за анализу, Монте Карло симулације и реконструкцију експерименталних догађаја Електромагнетског калориметра (ECAL) комплексног детектора CMS који се градио на Великом хадронском сударачу LHC у CERN-у. Значајан део његовог рада сумиран је у докторској дисертацији. У првом делу дисертације, после уводних делова, презентовано је обједињење, анализу и поређење резултата свог сложеног симулационог програма Preshower детектора и резултата реалног експеримента. Успео је да развије, анализира ефикасност, оптимизује и имплементира алгоритам за сепарацију фотона и неутралних пиона, базиран на Вештачким неуронским мрежама, користећи резултате ECAL barrel-а. Анализира добијене резултате из Монте Карло симулација, тј. симулација одговора детектора на упадне честице продукване у протон-протон сударима, са нагласком на детекцију неутралних пиона и фотона, као и анализа до тада једино доступних реалних догађаја из мерења космичког зрачења. Даље је успео да допринесе каснијим анализама података развојем алгоритама као и развојем CMSSW – (симулационог софтвера CMS детектора) – развојем алгоритма читавања и унапређењем описа нове геометрије Preshower детектора. Имплементацијом алгоритма и својим активним учешћем успео је да допринесе званичним анализама двофотонског канала распада Хигс бозона предвиђеног Стандардним моделом. Учествовао је у мерењима протон-протон судара, тј. прикупљању података ECAL детектора, а касније и окидачког система целог CMS детектора. Поред тога, заједно са колегама из института “Democritos” из Атине, радио на адаптирању више генератора догађаја за коришћење при симулацији и анализи аномалних спрезања ( $Z\gamma\gamma$ ) на детектору CMS који би служили за проверу могућности њиховог детектовања, као и помоћ при анализама ових сигнала. Др Димитрије Малетић је у току истраживачког рада на детектору CMS показао способност да потпуно самостално и на ефикасан и брз начин решава сложене проблеме и задатке као и да своје знање успева да у кратком року пренесе другим члановима CMS колаборације и Београдске CMS групе.

### **3.2 Изучавања особина атомских језгара на средњим енергијама на експериментима SHINE и NICA**

Искуство кандидата у Физици високих енергија и рад на CMS експерименту увелико је разлог зашто се укључио у нови експеримент у CERN-у, SHINE (SPS Heavy Ion and Neutrino experiment), као заменик пуководиоца Београдске групе проф. др Јована Пужовића. Првенствено увиђајући потребу млађих колега за помоћ при раду на симулацијама и анализама експерименталних резултата овог експеримента, доста је времена и труда уложио како би колегама помогао да се докажу у новој средини. Поред помоћи млађим колегама у анализама, првенствено K0 и делта++ резонантним сигнаlima са експеримента судара снопа са фиксном метом, веома брзо је преузео вођење званичне реконструкције свих података SHINE (NA61) детектора у грид окружењу. Треба напоменути и покретање компјутерског кластера за потребе NA61 експеримента и потребе симулација у Нискофонској лабораторији у Институту за физику Београд. Интерес у анализи је показивао првенствено за податке мете која је реплика мете T2K експеримента у Јапану, коју види као веза експеримента и истраживаче делатност др Димитрија Малетића у циљу унапређења знања процеса хадронизације која се користи и у симулацијама космичког зрачења, којима се доста бавио у Нискофонској лабораторији Института за физику. Интерес који је имао за експерименте изучавања особина атомских језгара, са нагласком на понашања језгара у близини confinement-а заинтересовао га је за проблематику изучавања кварк-глуон плазме, односно скенирање/употпуњавање графикана такозваних фазних прелаза језгара. Изучавање ове интересантне проблематике наставља радом на MPD детектору NICA сударача у Обједињеном Институту за Нуклеарна истраживања Дубна, Русија, где се укључио у развој софтвера за анализу сигнала електромагнетског калориметра (EMC). Првенствено учествује у развоју софтверских алата за истраживање физике неутралних мезона и промтних фотона који настају у сударима снопова тешких јона.

### **3.3 Акцелераторска физика јонизационог хлађења на MICE експерименту**

Од 2015. године кандидат предводи групу истраживача из Нискофонске лабораторије за нуклеарну физику Института за физику Београд у раду на MICE-у (Muon Ionisation Cooling Experiment). Бавио се анализама губитка енергије миона у метама од течног водоника (LH2) и литијум-хидрида (LiH), на којима је највећи број експерименталних догађаја измерено, и која је у центру проблематике јонизационог хлађења снопа миона. Такође се кандидат бавио развојем софтвера, везано за Монте Карло симулације и реконструкцију мерених догађаја. Учествовао је у оптимизацији симулација проласка честица кроз акцелераторске сегменте. Радио је на развоју програма који омогућују званичну симулацију и реконструкцију догађаја у грид компјутерском систему. Радио је на преласку продукције на „проширење“ грид система ка робустнијем дистрибутивном систему коришћењем Singularity container images. Учествовао у мерењима на MICE експерименту. Кандидат је одговоран за званичну продукцију MICE колаборације тј. за симулацију и реконструкцију експерименталних података.

### **3.4 Физика космичког зрачења**

Кандидат је непосредно након одбрањене докторске дисертације фокус свог истраживачког интересовања усмерио, и већ дао значајан допринос у области космичког зрачења. Треба истаћи да је рад на симулацијама Космичког зрачења помогао да се продубе сазнања о овој проблематици. Такође, развој софтвера за аутоматску обраду података континуалног мониторинга интензитета

космичког зрачења и приказивања података on-line, омогућило је да се Нискофонска лабораторија стави на мапу светских станица за мониторинг космичког зрачења.

### 3.5 Изучавање динамике радона и фонског зрачења

Кандидат је активно укључен у проблематику радијационе физике, прецизније у истраживања везана за проблематику радона и торона, као доминантних извора природне радио-активности. Примена мултиваријантних метода у анализи динамике радона дала је нове резултате у истраживању. Учествоје у првом испитивању концентрација радона у кућама и становима у Републици Србији 2015-2016, као и у испитивању концентрација радона у Школама у Републици Србији 2019, оба везана за Националне пројекте под руководством Директората за радијациону и нуклеарну сигурност и безбедност Србије, а под покровитељством Међународне агенције за атомску енергију са седиштем у Бечу. Учествоје у изради прве Радонске мапе Србије, као и при укључивању ове мапе у Европску радонску мапу. Предмет интересовања др Димитрија Малетића је такође и нискофонска гама спектроскопија. Развојем неопходног и оригиналног софвера за off-line анализу података, и упоредна симулација космичког зрачења и природне радиоактивности доводи до постављање Нискофонске лабораторије у лидерски положај у стручности у области ниско-енергетског природног фона као и у области проучавања варијабилности фона природне радиоактивности и космогеног фона. Бавио се и динамиком, варијабилношћу и симулацијом продукције космогених радионуклида у атмосфери и у земљишту.

### 3.6 Заштита животне средине

Примена мултиваријантних метода у анализи концентрација неких од најзаступљенијих радионуклида у животној средини; радона-222 и олова-210 као и космогеног берилијума-7 дале су добре резултате, и следећи корак је био да се ове методе примене у изучавању динамике и концентрација опасних једињења у животној средини. Добијени резултати усмеравају и охрабрују интезивирање ових истраживања.

## 4. Елементи за квалитативну анализу

### 4.1 Научни ниво и значај резултата, утицај научних радова

Од избора у звање виши научни сарадника кандидат је објавио два рада у категорији M21a, један рад у категорији M21, седам радова у категорији M22 и четири рада у категорији M23.

Као пет најзначајнијих радова кандидата од свих објављених радова могу се узети:

1. Stojic Andreja M, **Maletic Dimitrije M**, Stanisic-Stojic Svetlana M, Mijic Zoran R, Sostaric Andrej I, Forecasting of VOC emissions from traffic and industry using classification and regression multivariate methods, SCIENCE OF THE TOTAL ENVIRONMENT, vol. 521, br. , str. 19-26, 2015. цитиран 18 пута.
2. Forkapic Sofija M, **Maletic Dimitrije M**, Vasin Jovica R, Bikit Kristina I, Mrdja Dusan S, Bikit Istvan S, Udovicic Vladimir I, Banjanac Radomir M, Correlation analysis of the natural radionuclides in soil and indoor radon in Vojvodina, Province of Serbia, JOURNAL OF ENVIRONMENTAL RADIOACTIVITY, vol. 166, br. , str. 403-411, 2017. цитиран 17 пута

3. D.Barney, W.Bialas, P.Kokkas, N.Manthos, **D.Maletic**, I.Papadopoulos, A.Peisert, S.Reynaud, P.Vichoudis, Detection of muons at 150 GeV/c with a CMS Preshower Prototype, Nucl Instrum Meth A, 564, 126-133, 2006. цитиран 6 пута

4. R. Banjanac, **D. Maletić**, D. Joković, N. Veselinović, A. Dragić, V. Udovičić, I. Aničin, On the omnipresent background gamma radiation of the continuous spectrum, Nucl Instrum Meth A, 745, 7-11, 2014. цитиран 2 пута

5. Savic Mihailo R, Dragic Aleksandar L, **Maletic Dimitrije M**, Veselinovic Nikola B, Banjanac Radomir M, Jokovic Dejan R, Udovicic Vladimir I, A novel method for atmospheric correction of cosmic-ray data based on principal component analysis, ASTROPARTICLE PHYSICS, vol. 109, br. , str. 1-11, 2019. није цитиран

Први рад спада у рад кандидата на заштити животне средине. Рад се бави концентрацијама Volatile organic compounds (VOC) који у атмосферу бивају испуштани од извора као што су саобраћај и индустрија. Кандидат је радио на моделовању зависности концентрација ових једињења од атмосферских параметара коришћењем мултиваријантних метода, тј. регресионом мултиваријантном анализом, као и могућношћу предикције концентрације ових једињења. Мултиваријантне методе које су коришћене налазе се имплементирани у скуп програма TMVA (Toolkit for multivariate analysis) унутар ROOT програмског пакета популарног у анализи података у физици високих енергија.

У другом раду је кандидат користио исте мултиваријантне методе као у првом раду за анализу корелација и моделирања концентрација радонама у животним просторима у зависности од састава земљишта и концентрација радионуклида у земљишту, и резултати се поклапају са резултатима других европских земаља, првенствено Велике Британије, чија су истраживања имала много већи број експерименталних резултата.

Трећи рад представља рад на тестовима сноповима, у Х4 експерименталној хали у Превесену у близини Женева, и то Preshower детектора, који је инсталиран у затварачки део електромагнетског калориметра CMS детектора. Кандидат се бавио развојем целокупног програма за Монте Карло симулацију модула за тестирање базирану на популарном Geant4 програмском пакету за симулацију интеракција честица са материјом. Такође се бавио поређењем експерименталних података и симулацијом. Овај рад је издвојен јер је кандидат показао велику самосталност у раду на почетку своје каријере у великој колаборацији CMS. Резултати ових тестова дали су значајне резултате за оптимизацију првенствено електронике, као и софтвера за реконструкцију депоноване енергије и локализацију удара честица у овај детектор.

Четврти рад представља интересантно истраживање нискоенергетског фона зрачења и декомпозицију на фон који долази од радионуклида из земље и грађевинског материјала лабораторије, а који се одбија од зидове лабораторије у којем су вршена мерења, и на космогени фон. Мерења су вршена коришћењем оловом заштићеног, сем са горње стране, HPGe детектора. Овај рад представља и детаљну анализу “тврдоће” меке компоненте фона, коришћењем различитог броја танких абсорбера од лаких метала. Кандидат се бавио детаљном Монте Карло симулацијом и поређењем са експерименталним резултатима.

Пети рад је један од радова чије је резултате Михаило Савић укључио у своју докторску тезу. Кандидат је радио са докторантом на разматрању примене разних модерних мултиваријантних метода. Кандидат је такође радио на методама обраде података, софтверу за аквизицију, развоју база података и припреми експерименталних резултата који долазе од континуалног мониторинга флукса миона коришћењем пластичних сцинтилатора у Нискофонској лабораторији Института за физику Београд.

#### 4.2 Параметри квалитета часописа сумарно

Укупан фактор утицаја (ИФ) свих радова кандидата је 227.4 а од избора у звање виши научни сарадник 70.4.

Додатни библиометријски показатељи у вези са објављеним радовима кандидата од избора у претходно звање дати су у доњој табели. Она садржи импакт факторе (ИФ) радова, М бодове радова по српској категоризацији научноистраживачких резултата, као и импакт фактор нормализован по импакту цитирајућег чланка (СНИП). У табели су дате укупне вредности, као и вредности свих фактора усредњених по броју чланака и по броју аутора по чланку, за радове објављене у категоријама М20.

|                     | ИФ    | М    | СНИП  |
|---------------------|-------|------|-------|
| Укупно              | 70.44 | 75   | 22.56 |
| Усредњено по чланку | 5.03  | 5.77 | 1.61  |
| Усредњено по аутору | 3.24  | 7.46 | 1.55  |

#### 4.3 Награде

- Награда за најбољи постер међународна конференција РАД 2014.

У прилогу изглед странице са објављеним добитницима награда на сајту конференције.

- Иако не спада у награде, интересантно је поменути да кандидат има забележена достигнућа на сајту Researchgate, и то да су током 9 недеља његове публикације биле најчитаније од свих аутора из институција р. Србије, и 40 недеља најчитаније публикације од аутора из Института за физику Београд.

У прилогу стилизована листа достигнућа на сајту Researchgate.

#### 4.4 Ангажованост у формирању научних кадрова

После избора у вишег научног сарадника:

- кандидат је био ментор Михаилу Савићу при изради докторске тезе на Физичком факултету, Универзитета у Београду, одбрањене 4. јула 2019. године.

У прилогу део реферата Михаила Савића и скенирано решење о одбрани докторске дисертације.

### Пре избора у вишег научног сарадника:

- помагао је у изради теза - налази се поменут у захвалници докторских дисертација за: Дејана Јоковића, под називом: *“Детекција и спектроскопија миона из Космичког зрачења пластичним сцинтилационим детекторима”*, на Физичком факултету, Универзитета у Београду и Радомира Бањанца, под називом: *„Временски променење комбинованог фона у Нискофонској подземној лабораторији“* на Физичком факултету, Универзитета у Београду.

Био је ментор два одбрањена дипломска рада, (по старом систему – у еквиваленцији мастер рада) Радована Ковачевића и Биљане Савић на Физичком факултету, Универзитет у Београду.

2004.-2005. Држао је експерименталне вежбе из предмета: Физика језгра и честица.

2005.-2006. Држао је рачунске вежбе из предмета: Нуклеарна физика, Физика језгра и честица.

2007.-2008. Држао је рачунске вежбе из предмета: Нуклеарна физика, Физика језгра и честица и експерименталне вежбе из предмета: Нуклеарна физика

Ментор два матурска рада за ученике Математичке гимназије у Београду. Један од кандидата потом уписао Физички факултет у Београду.

Сарадња са Центром за таленте Земун. Ментор рада Наталије Ђорђевић, ученице 1 разреда Девете београдске гимназије, која је освојила 3. место на републичкој смотри за таленте 2014 године.

### **Радио је на популаризација науке**

#### После избора у вишег научног сарадника:

20. новембар 2015. одржао је колоквијум на Департману за физику, ПМФ Нови Сад.  
У прилогу део странице на којој је колоквијум најављен.

#### Пре избора у вишег научног сарадника:

2008. Учешће на Фесивалу науке.

2009. и 2010. Члан локалног организационог комитета и предавач на Masterclass-у одржаном на Физичком факултету у Београду.

2009. Популарно предавање о CERN-у на семинару за професоре физике, у Новом Саду.

2009. Популарно предавање на скупу “CERN у Димитровграду”.

2009. “*Serbian and Montenegrin Teachers Programme 2009*”. Посета професора физике из Србије и Црне Горе CERN-у. Члан организационог одбора и предавач: “*Physics with the CMS ECAL*”

2012. “*Novi Sad University Students*” посета студената Универзитета у Новом Саду ЦЕРН-у. Водич посете CERN-овом компјутерском центру.

2010-2014. Посета професора Физике и студената Физичког факултета ИФ-у. Упознавање са Нискофонском лабораторијом.

2014 аутор текстова у часопису “Млади физичар”

#### **4.5 Нормирање броја коауторских радова, патената и техничких решења**

Сви радови са више од седам коаутора нормирани су коришћењем формуле за експерименталне радове наведене у Правилнику. Колаборациони радови су такође овако нормирани, јер кандидат није увидео потребу да се процедура компликује укључењем процене доприноса кандидата на колаборационим радовима од стране Комисије за CERN, јер је број овако нормираних бодова од колаборационих радова и/или са потпуно искљученим колаборационим радовима из разматрања значајно превазилази број потребних бодова за реизбор у звање виши научни сарадник.

Након нормирања на горе наведен начин, број М бодова које је кандидат остварио након претходног избора у звање са 114.5 смањује се на 80.08, а током каријере са 552.5 на 151.7.

Нормирање не утиче на значајан начин на број бодова за реизбор кандидата.

#### **4.6 Руковођење пројектима, потпројектима и пројектним задацима**

После избора у вишег научног сарадника:

- Води учешће сарадника Института за физику Београд у МІСЕ колаборацији, корисници Transnational access fund, EuCARD2 део ЕУ програма FP7.

У прилогу: листа представника институција у колаборацији,  
листа учесника у колаборацији и  
писмо о одобравању средстава.

- Руководи учешћем сарадника из Института за физику Београд у билатералном пројекту на експерименту MPD/NICA у Обједињеном институту за нуклеарна страживања у Дубни, Русија. Учесће финансирано од стране МПНТР, преко Заједничког комитета за сарадњу са ОИНИ Дубна и р. Србије, чији је кандидат члан задужен за сарадњу у области физике високих енергија.

У прилогу доказ о чланству у комитету.

Пре избора у вишег научног сарадника:

- 2011. Пројектни задатак покретања on-line обраде података континуалног мониторинга Београдске мионске станице.
- 2012. Пројектни задатак покретања компјутерског кластера добијеног на поклон од CERN-а на ИФ-у за потребе SHINE колаборације и Нискофонске лабораторије.

#### 4.7 Активност у научним и научно-стручним друштвима

##### После избора у вишег научног сарадника:

2017- Члан Заједничког комитета за сарадњу са ОИНИ Дубна и р. Србије, задужен за сарадњу у области физике високих енергија

У прилогу доказ о чланству у комитету.

Фебруар 2015 – Члан колаборационог борда MICE Experiment Management Office (CB)

У прилогу: листа представника институција у колаборацији.

Фебруар 2019 – Члан Joint MICE Experiment Management Office (МИМО)

У прилогу позивно писмо и страница.

Рецензент је у међународним часописима: *Nuclear Technology and Radiation Protection*, *Fuel*, *Environmental Pollution*, *Atmospheric Pollution Research*, *Building and Environment*

У прилогу сертификати рецензија и више листа рецензената за *Nuclear Technology and Radiation Protection*.

2017. Рецензирао је билатерални пројекат са Мађарском.

27-29. јуна 2017. Водио локални организациони одбор састанка MICE колаборације у Београду.

У прилогу докази о одржаном састанку у Београду.

##### Пре избора у вишег научног сарадника:

2012-2014. Представник Института за физику у одсеку Физике језгра, елементарних честица и основних интеракција одељења Друштва Физичара Србије за Научна истраживања и високо образовање (НИВОДФС)

2012. Члан локалној организационој одбора једнодневне научне скупине одржане у згради САНУ под називом: “100 година од открића атомског језира”.

Рецензент је у међународним часописима: *Nuclear Technology and Radiation Protection*, *Applied Radiation and Isotopes*

#### **4.8 Конкретан допринос кандидата у реализацији радова у научним центрима у земљи и иностранству**

2004-2010. Члан Београдске CMS групе. (Рад на експерименту CMS у CERN-у)

2011-2013. Члан Београдског SHINE тима (Рад на експерименту NA61 у CERN-у)

2015- Води учешће сарадника Института за физику Београд у MICE коалборацији.

2016-2017 Учесник билатералног пројекта са р. Белорусијом: RADON MAPS PREPARING AND DOSE ASSESSMENT OF THE PUBLIC EXPOSURE TO RADON IN BELARUS AND SERBIA

2015- Активности: учествовање на радним састанцима регионалних пројекта IAEA;

1. SRB/9/003 “Enhancing the Regulatory Infrastructure and Legislative System” Expert Mission to assist Serbia in designing a National Radon Survey. Belgrade, 2-4 February 2015

2. RER/9/136. “Reducing Public Exposure to Radon by Supporting the Implementation and Further Development of National Strategies” Expert Mission to assist Serbia On Measures To Reduce Radon Levels In Buildings. Belgrade, 15-16 November 2016

3. SRB/9/006 Planning and kick-off meeting. Belgrade, Serbia. 22nd February 2018

4. RER/9/153-1706076 "Enhancing the Regional Capacity to Control Long Term Risk to the Public due to Radon in Dwellings and Workplaces", Regional Workshop on Database and Statistical Analysis, Harmonization of Protocols and Procedures for the Measurement of Radon, Bosnia & Hercegovina, Sarajevo, 12-14 June 2018

5. RER9153 – Enhancing the Regional Capacity to Control Long Term Risks to the Public due to Radon in Dwellings and Workplaces: Regional Workshop on Development of Radon Maps and the Definition of Radon-Prone Areas (EVT1807175), Vilnius, Lithuania, 09-11 July 2019.

#### **4.9 Уводна предавања на конференцијама и друга предавања**

18. Septembar 2017 COOL 2017 conference in Gustav-Stresemann-Institut, Bonn

1) „Measurement of phase-space density evolution in MICE“. 50 минутно предавање.

2) „Recent results from MICE on multiple Coulomb scattering and energy loss“. 40 минутно предавање.

У прилогу.

Интересантно је поменути:

7. Mart 2017 - MICE Project Board Review, „Bulk production of Monte Carlo“

У прилогу.

## 5. Елементи за квантитативну анализу

**Остварени резултати у периоду након одлуке Научног већа о предлогу за стицање претходног научног звања:**

| Категорија | М бодова по раду | Број радова | Укупно М бодова | Нормирани број М бодова |
|------------|------------------|-------------|-----------------|-------------------------|
| M21a       | 10               | 2           | 20              | 10.37                   |
| M21        | 8                | 1           | 8               | 0.3                     |
| M22        | 5                | 7           | 35              | 26.86                   |
| M23        | 3                | 4           | 12              | 7.15                    |
| M32        | 1.5              | 2           | 3               | 2.44                    |
| M33        | 1                | 28          | 28              | 25.72                   |
| M34        | 0.5              | 17          | 8.5             | 7.24                    |

**Поређење са минималним квантитативним условима за реизбор у звање виши научни сарадник (половина од минималног броја за избор у звање виши научни сарадник):**

| Минимални број М бодова         |    | Остварено, М бодова без нормирања | Остварено, нормирани број М бодова |
|---------------------------------|----|-----------------------------------|------------------------------------|
| Укупно                          | 25 | 114.5                             | 80.08                              |
| M10+M20+M31+M32+M33+M41+M42+M90 | 20 | 106                               | 72.84                              |
| M11+M12+M21a+M21+M22+M23        | 15 | 75                                | 44                                 |

## 6. Списак објављених радова и других публикација

### 6.1 Радови у међународним часописима изузетних вредности (M21a)

#### Радови објављени након претходног избора у звање:

1. Bogomilov, M., Tsenov, R., Vankova-Kirilova, G.,..., Maletic, D.,..., *et al.* Demonstration of cooling by the Muon Ionization Cooling Experiment. *Nature* **578**, 53–59, 2020.
2. Stojic Andreja M, Maletic Dimitrije M, Stanisic-Stojic Svetlana M, Mijic Zoran R, Sostaric Andrej I, Forecasting of VOC emissions from traffic and industry using classification and regression multivariate methods, *SCIENCE OF THE TOTAL ENVIRONMENT*, vol. 521, br. , str. 19-26, 2015.

#### Радови објављени пре претходног избора у звање:

3. N. Abgrall, A. Aduszkiewicz, ..., D. Maletić, ..., W. Zipper, Measurements of production properties of K<sup>0</sup>S mesons and  $\Lambda$  hyperons in proton-carbon interactions at 31 GeV/c, *Phys Rev C*, **89**, 025205, 2014.
4. Khachatryan V,...,Adzic Petar R, Djordjevic Milos P, Krpic Dragomir K, Maletic Dimitrije, Milosevic Jovan, Puzovic Jovan M, Measurement of the charge ratio of atmospheric muons with the CMS detector, *Phys Lett B*, **692**, 83-104, 2010.
5. Chatrchyan S,...,Adzic Petar R,Djordjevic Milos P,Jovanovic Dragoslav,Krpic Dragomir K,Maletic Dimitrije,Puzovic Jovan M,Smiljkovic Nebojsa,..., Measurement of the muon stopping power in lead tungstate, *J Instrum*, **5**, P03007, 2010.
6. Chatrchyan S,..., Adzic Petar R, Djordjevic Milos P, Jovanovic Dragoslav, Krpic Dragomir K, Maletic Dimitrije, Puzovic Jovan M, Smiljkovic Nebojsa, Alignment of the CMS silicon tracker during commissioning with cosmic rays, *J Instrum*, **5**, T03009, 2010.
7. Chatrchyan S,...,Adzic Petar R,Djordjevic Milos P,Jovanovic Dragoslav,Krpic Dragomir K,Maletic Dimitrije,Puzovic Jovan M,Smiljkovic Nebojsa, Performance of the CMS cathode strip chambers with cosmic rays, *J Instrum*, **5**, T03018, 2010.
8. Adzic Petar R, Almeida N, Andelin D, Anicin Ivan V,..., Djordjevic Milos P,..., Drndarevic Snezana L,..., Jovanovic Dragoslav,..., Krpic Dragomir K,..., Maletic Dimitrije,..., Milenovic Predrag,..., Puzovic Jovan M, Radiation hardness qualification of PbWO<sub>4</sub> scintillation crystals for the CMS Electromagnetic Calorimeter, *J Instrum*, **5**, P03010, 2010.
9. Chatrchyan S,..., Adzic Petar R, Djordjevic Milos P, Jovanovic Dragoslav, Krpic Dragomir K, Maletic Dimitrije, Puzovic Jovan M, Smiljkovic Nebojsa, Performance study of the CMS barrel resistive plate chambers with cosmic rays, *J Instrum*, **5**, T03017, 2010
10. Chatrchyan S,..., Adzic Petar R, Djordjevic Milos P, Jovanovic Dragoslav, Krpic Dragomir K, Maletic Dimitrije, Puzovic Jovan M, Smiljkovic Nebojsa, Time reconstruction and performance of the CMS electromagnetic calorimeter, *J Instrum*, **5**, T03011, 2010.

11. Chatrchyan S,..., Adzic Petar R, Djordjevic Milos P, Jovanovic Dragoslav, Krpic Dragomir K, Maletic Dimitrije, Puzovic Jovan M, Smiljkovic Nebojsa, Performance of CMS muon reconstruction in cosmic-ray events, J Instrum, 5, T03022, 2010.
12. Chatrchyan S,...,Adzic Petar R, Djordjevic Milos P, Jovanovic Dragoslav, Krpic Dragomir K, Maletic Dimitrije, Puzovic Jovan M, Smiljkovic Nebojsa, Performance of CMS hadron calorimeter timing and synchronization using test beam, cosmic ray, and LHC beam data, J Instrum, 5, T03013, 2010.
13. Chatrchyan S,..., Adzic Petar R, Djordjevic Milos P, Jovanovic Dragoslav, Krpic Dragomir K, Maletic Dimitrije, Puzovic Jovan M, Smiljkovic Nebojsa, Commissioning of the CMS High-Level Trigger with cosmic rays, J Instrum, 5, T03005 , 2010.
14. Chatrchyan S,..., Adzic Petar R, Djordjevic Milos P, Jovanovic Dragoslav, Krpic Dragomir K, Maletic Dimitrije, Puzovic Jovan M, Smiljkovic Nebojsa, Performance of the CMS drift-tube chamber local trigger with cosmic rays, J Instrum, 5, T03015, 2010.
15. Chatrchyan S,..., Adzic Petar R, Djordjevic Milos P, Jovanovic Dragoslav, Krpic Dragomir K, Maletic Dimitrije, Puzovic Jovan M, Smiljkovic Nebojsa,..., Milenovic Predrag, Commissioning and Performance of the CMS Pixel Tracker with Cosmic Ray Muons, J Instrum, 5, T03007, 2010.
16. Chatrchyan S,..., Adzic Petar R, Djordjevic Milos P, Jovanovic Dragoslav, Krpic Dragomir K, Maletic Dimitrije, Puzovic Jovan M, Smiljkovic Nebojsa, Performance of the CMS Level-1 trigger during commissioning with cosmic ray muons and LHC beams, J Instrum, 5, T03002, 2010.
17. Chatrchyan S,..., Adzic Petar R, Djordjevic Milos P, Jovanovic Dragoslav, Krpic Dragomir K, Maletic Dimitrije, Puzovic Jovan M, Smiljkovic Nebojsa,..., Milenovic Predrag, Calibration of the CMS drift tube chambers and measurement of the drift velocity with cosmic rays, J Instrum, 5, T03016, 2010.
18. Chatrchyan S,..., Adzic Petar R, Djordjevic Milos P, Jovanovic Dragoslav, Krpic Dragomir K, Maletic Dimitrije, Puzovic Jovan M, Smiljkovic Nebojsa, Precise mapping of the magnetic field in the CMS barrel yoke using cosmic rays, J Instrum, 5, T03021, 2010.
19. Chatrchyan S,..., Adzic Petar R, Djordjevic Milos P, Jovanovic Dragoslav, Krpic Dragomir K, Maletic Dimitrije, Puzovic Jovan M, Smiljkovic Nebojsa, Commissioning and performance of the CMS silicon strip tracker with cosmic ray muons, J Instrum, 5, T03008, 2010.
20. Chatrchyan S,...,Adzic Petar R, Djordjevic Milos P, Jovanovic Dragoslav, Krpic Dragomir K, Maletic Dimitrije, Puzovic Jovan M, Smiljkovic Nebojsa, Commissioning of the CMS experiment and the cosmic run at four tesla, J Instrum, 5,T03001, 2010.
21. Chatrchyan S,..., Adzic Petar R, Djordjevic Milos P, Jovanovic Dragoslav, Krpic Dragomir K, Maletic Dimitrije, Puzovic Jovan M, Smiljkovic Nebojsa, Performance of the CMS drift tube chambers with cosmic rays, J Instrum, 5, T03015, 2010.

22. Chatrchyan S,..., Adzic Petar R, Djordjevic Milos P, Jovanovic Dragoslav, Krpic Dragomir K, Maletic Dimitrije, Puzovic Jovan M, Smiljkovic Nebojsa, Identification and filtering of uncharacteristic noise in the CMS hadron calorimeter, *J Instrum*, 5, T03014, 2010.
23. Chatrchyan S,..., Adzic Petar R, Djordjevic Milos P, Jovanovic Dragoslav, Krpic Dragomir K, Maletic Dimitrije, Puzovic Jovan M, Smiljkovic Nebojsa, Performance and operation of the CMS electromagnetic calorimeter, *J Instrum*, 5, T03010, 2010.
24. Chatrchyan S,..., Adzic Petar R, Djordjevic Milos P, Jovanovic Dragoslav, Krpic Dragomir K, Maletic Dimitrije, Puzovic Jovan M, Smiljkovic Nebojsa, Alignment of the CMS muon system with cosmic-ray and beam-halo muons, *J Instrum*, 5, T03020, 2010.
25. Chatrchyan S,..., Adzic Petar R, Djordjevic Milos P, Jovanovic Dragoslav, Krpic Dragomir K, Maletic Dimitrije, Puzovic Jovan M, Smiljkovic Nebojsa, Aligning the CMS muon chambers with the muon alignment system during an extended cosmic ray run, *J Instrum*, 5, T03019, 2010.
26. Chatrchyan S,..., Adzic Petar R, Djordjevic Milos P, Jovanovic Dragoslav, Krpic Dragomir K, Maletic Dimitrije, Puzovic Jovan M, Smiljkovic Nebojsa, Performance of the CMS hadron calorimeter with cosmic ray muons and LHC beam data, *J Instrum*, 5, T03012, 2010.
27. Chatrchyan S,..., Adzic Petar R, Djordjevic Milos P, Jovanovic Dragoslav, Krpic Dragomir K, Maletic Dimitrije, Puzovic Jovan M, Smiljkovic Nebojsa, Fine synchronization of the CMS muon drift-tube local trigger using cosmic rays, *J Instrum*, 5, T03004, 2010.
28. Chatrchyan S,..., Adzic Petar R, Djordjevic Milos P, Jovanovic Dragoslav, Krpic Dragomir K, Maletic Dimitrije, Puzovic Jovan M, Smiljkovic Nebojsa,..., Milenovic Predrag, CMS data processing workflows during an extended cosmic ray run, *J Instrum*, 5, T03006, 2010.
29. Khachatryan V,..., Adzic Petar R, Djordjevic Milos P, Krpic Dragomir K, Maletic Dimitrije, Milosevic Jovan, Puzovic Jovan M, First Measurement of Bose-Einstein Correlations in Proton-Proton Collisions at  $\sqrt{s}=0.9$  and 2.36 TeV at the LHC, *Phys Rev Lett*, 105, 032001, 2010.
30. ..., Adzic Petar R, Djordjevic Milos P, Krpic Dragomir K, Maletic Dimitrije, Milosevic Jovan Z, Puzovic Jovan M,..., Milenovic Predrag, Search for Dijet Resonances in 7 TeV pp Collisions at CMS, *Phys Rev Lett*, 105, 211801, 2010.
31. Khachatryan V,..., Adzic Petar R, Djordjevic Milos P, Krpic Dragomir K, Maletic Dimitrije, Milosevic Jovan, Puzovic Jovan M, Transverse-Momentum and Pseudorapidity Distributions of Charged Hadrons in pp Collisions at  $\sqrt{s}=7$  TeV, *Phys Rev Lett*, 105, 022002, 2010.
32. David G. d'Enterria et al. (with D. Maletic) CMS Collaboration, CMS physics technical design report: Addendum on high density QCD with heavy ions, *J Phys G*, 34, 2307-2455, 2007.
33. G.L. Bayatian et al. (with D. Maletic) CMS Collaboration, CMS technical design report, volume II: Physics performance, *J Phys G*, 34, 995-1579, 2007.

## 6.2 Радови у врхунским међународним часописима (M21)

### Радови објављени након претходног избора у звање:

34. Adams D,..., Jokovic Dejan R, ..., Maletic Dimitrije M, ..., Savic Mihailo R, ..., First particle-by-particle measurement of emittance in the Muon Ionization Cooling Experiment, EUROPEAN PHYSICAL JOURNAL C, vol. 79, br. 3, 2019.

### Радови објављени пре претходног избора у звање:

35. R. Banjanac, A. Dragić, V. Udovičić, D. Joković, D. Maletić, N. Veselinović, M. Savić, Variations of gamma-ray background in the Belgrade shallow underground low-level laboratory, Appl Radiat Isotopes, 87, 70, 2014.

36. R. Banjanac, D. Maletić, D. Joković, N. Veselinović, A. Dragić, V. Udovičić, I. Aničin, On the omnipresent background gamma radiation of the continuous spectrum, Nucl Instrum Meth A, 745, 7-11, 2014.

37. N. Abgrall, O. Andreeva, ..., D. Maletić, ..., W. Zipper, NA61/SHINE facility at the CERN SPS: beams and detector system, J Instrum, 9, 06005, 2014.

38. M. Krmar, J. Hansman, N. Jovančević, N. Lalović, J. Slivka, D. Joković, D. Maletić, A method to estimate a contribution of Ge(n,n') reaction to the low-energy part of gamma spectra of HPGe detectors, Nucl Instrum Meth A, 709, 8-11, 2013.

39. Abgrall N,...,Grabez Bojana S,...,Maletic Dimitrije,...,Puzovic Jovan M,...,Savic Mihailo, Pion emission from the T2K replica target: Method, results and application, Nucl Instrum Meth A, 701, 99-114, 2013.

40. Khachatryan V,..., Adzic Petar R, Djordjevic Milos P, Krpic Dragomir K, Maletic Dimitrije, Milosevic Jovan, Puzovic Jovan M, Observation of long-range, near-side angular correlations in proton-proton collisions at the LHC, JHEP, 1009, 091, 2010.

41. Khachatryan V,...,Adzic Petar R, Djordjevic Milos P, Maletic Dimitrije, Puzovic Jovan M,..., Milenovic Predrag, Transverse-momentum and pseudorapidity distributions of charged hadrons in pp collisions at root s=0.9 and 2.36 TeV, JHEP, 1002, 041, 2010.

42. R. Adolphi et al. (with D. Maletic) CMS Collaboration, The CMS experiment at the CERN LHC, J Instrum 3, S08004, 2008.

43. P. Adzic et al.(with D. Maletic) CMS Electromagnetic Calorimeter Group, Intercalibration of the barrel electromagnetic calorimeter of the CMS experiment at start-up, J Instrum 3, P10007, 2008.

44. P. Adzic et al.(with D. Maletic) CMS Electromagnetic Calorimeter Group, Energy resolution of the barrel of the CMS electromagnetic calorimeter, J Instrum, 2, P04004, 2007.

45. D.Barney, W.Bialas, P.Kokkas, N.Manthos, D.Maletic, I.Papadopoulos, A.Peisert, S.Reynaud, P.Vichoudis, Detection of muons at 150 GeV/c with a CMS Preshower Prototype, Nucl Instrum Meth A, 564, 126-133, 2006.

46. P. Milenovic, J. Puzovic, D. Jovanovic, D. Maletic, G. Dissertori, P. Adzic, Performance of the CMS-ECAL Safety System for Super Modules SM0 and SM1, Nucl Instrum Meth A, 554, 427-436, 2005.

### **6.3 Радови у истакнутим међународним часописима (M22)**

#### **Радови објављени након претходног избора у звање:**

47. Knezevic David, Jovancevic Nikola, Sukhovoj Anatoly M, Dragic Aleksandar L, Mitsyna Ludmila V, Revay Zsolt, Stieghorst Christian, Stephan Oberstedt, Krmar Miodrag D, Arsenic Ilija D, Maletic Dimitrije M, Jokovic Dejan R. Study of gamma ray transitions and level scheme of Mn-56(25) using the Mn-55(25)(n(th),2 gamma) reaction, NUCLEAR PHYSICS A, vol. 992, 2019.

48. Savic Mihailo R, Dragic Aleksandar L, Maletic Dimitrije M, Veselinovic Nikola B, Banjanac Radomir M, Jokovic Dejan R, Udovicic Vladimir I, A novel method for atmospheric correction of cosmic-ray data based on principal component analysis, ASTROPARTICLE PHYSICS, vol. 109, br. , str. 1-11, 2019.

49. Savic Mihailo R, Veselinovic Nikola B, Dragic Aleksandar L, Maletic Dimitrije M, Jokovic Dejan R, Banjanac Radomir M, Udovicic Vladimir I, Rigidity dependence of Forbush decreases in the energy region exceeding the sensitivity of neutron monitors, ADVANCES IN SPACE RESEARCH, vol. 63, br. 4, str. 1483-1489, 2019.

50. Veselinovic Nikola B, Dragic Aleksandar L, Savic Mihailo R, Maletic Dimitrije M, Jokovic Dejan R, Banjanac Radomir M, Udovicic Vladimir I, An underground laboratory as a facility for studies of cosmic-ray solar modulation, NUCLEAR INSTRUMENTS & METHODS IN PHYSICS RESEARCH SECTION A-ACCELERATORS SPECTROMETERS DETECTORS AND ASSOCIATED EQUIPMENT, vol. 875, br. , str. 10-15, 2017

51. Bogomilov M,..., Jokovic Dejan R, Maletic Dimitrije M, Savic Mihailo R,..., Lattice design and expected performance of the Muon Ionization Cooling Experiment demonstration of ionization cooling, PHYSICAL REVIEW ACCELERATORS AND BEAMS, vol. 20, br. 6, 2017.

52. Perisic Mirjana D, Maletic Dimitrije M, Stanisic-Stojic Svetlana M, Rajsic Slavica F, Stojic Andreja M, Forecasting hourly particulate matter concentrations based on the advanced multivariate methods, INTERNATIONAL JOURNAL OF ENVIRONMENTAL SCIENCE AND TECHNOLOGY, vol. 14, br. 5, str. 1047-1054, 2017.

53. Forkapic Sofija M, Maletic Dimitrije M, Vasin Jovica R, Bikit Kristina I, Mrdja Dusan S, Bikit Istvan S, Udovicic Vladimir I, Banjanac Radomir M, Correlation analysis of the natural radionuclides in soil and indoor radon in Vojvodina, Province of Serbia, JOURNAL OF ENVIRONMENTAL RADIOACTIVITY, vol. 166, br. , str. 403-411, 2017.

### **Радови објављени пре претходног избора у звање:**

54. Dimitrije M. Maletić, Vladimir I. Udovičić, Radomir M. Banjanac, Dejan R. Joković, Aleksandar L. Dragić, Nikola B. Veselinović, Jelena Filipović, Correlative and multivariate analysis of increased radon concentration in underground laboratory, *Radiation Protection Dosimetry*, 162, 1-2, 148-151, 2014.
55. D. Maletić, V. Udovičić, R. Banjanac, D. Joković, A. Dragić, N. Veselinović, J. Filipović, Comparison of multivariate classification and regression methods for the indoor radon measurements, *Nucl Technol Radiat*, 29, 17-23, 2014.
56. V. Udovičić, J. Filipović, A. Dragić, R. Banjanac, D. Joković, D. Maletić, B. Grabež, N. Veselinović Daily and seasonal radon variability in the underground low-background laboratory in Belgrade, Serbia, *Radiation Protection Dosimetry*, doi: 10.1093/rpd/ncu109, 2014.
57. A. Dragić, V. Udovičić, R. Banjanac, D. Joković, D. Maletić, N. Veselinović, M. Savić, J. Puzović, I. Aničin, The new set-up in the Belgrade low-level and cosmic-ray laboratory, *Nucl Technol Radiat*, 26, 181-192, 2011.
58. Khachatryan V,..., Adzic Petar R, Djordjevic Milos P, Krpic Dragomir K, Maletic Dimitrije, Milosevic Jovan, Puzovic Jovan M,..., CMS tracking performance results from early LHC operation, *Eur Phys J C*, 70, 1165-1192, 2010.
59. Khachatryan V,..., Adzic Petar R, Djordjevic Milos P, Krpic Dragomir K, Maletic Dimitrije, Milosevic Jovan, Puzovic Jovan M,..., First measurement of the underlying event activity at the LHC with root  $s=0.9$  TeV, *Eur Phys J C*, 70, 555-572, 2010.
60. S. Abdullin et al. (with D. Maletic) CMS HCAL/ECAL Collaborations, The CMS barrel calorimeter response to particle beams from 2 to 350 GeV/c, *Eur Phys J C*, 60, 359-373, 2009.
61. P. Adzic et al., (with D. Maletic) ECAL/CMS Collaboration, Results of the first performance tests of the CMS electromagnetic calorimeter, *Eur Phys J C*, 44S02, 1–10, 2006.

### **6.4 Радови у међународним часописима (M23)**

#### **Радови објављени након претходног избора у звање:**

62. Asfandiyarov R,..., Maletic Dimitrije M,..., Savic Mihailo R,..., MAUS: the MICE analysis user software, *JOURNAL OF INSTRUMENTATION*, vol. 14, 2019.

63. Udovicic Vladimir I, Maletic Dimitrije M, Banjanac Radomir M, Jokovic Dejan R, Dragic Aleksandar L, Veselinovic Nikola B, Zivanovic Jelena Z, Savic Mihailo R, Forkapic Sofija M, Multiyear Indoor Radon Variability in a Family House - a Case Study in Serbia, NUCLEAR TECHNOLOGY & RADIATION PROTECTION, vol. 33, br. 2, str. 174-179. 2018.
64. Udovicic Vladimir I, Maletic Dimitrije M, Eremic-Savkovic Maja M, Pantelic Gordana K, Ujic Predrag N, Celikovic Igor T, Forkapic Sofija M, Nikezic Dragoslav R, Markovic Vladimir MM, Arsic Vesna, Ilic Jovana, First steps towards national radon action plan in Serbia, NUKLEONIKA, vol. 61, br. 3, str. 361-365, 2016.
65. Filipovic Jelena Z, Maletic Dimitrije M, Udovicic Vladimir I, Banjanac Radomir M, Jokovic Dejan R, Savic Mihailo R, Veselinovic Nikola B, The use of multivariate analysis of the radon variability in the underground laboratory and indoor environment, NUKLEONIKA, vol. 61, br. 3, str. 357-360, 2016.

#### **Радови објављени пре претходног избора у звање:**

66. Maletic Slavica B, Maletic Dimitrije, Petronijevic Ivan M, Dojcilovic Jablan R, Popovic Dusan M (2014) Dielectric and infrared properties of SrTiO<sub>3</sub> single crystal doped by 3d (V, Mn, Fe, Ni) and 4f (Nd, Sm, Er) ions, Chinese Physics B, 23, 026102, 2014.
67. V. Udovičić, N. Veselinović, D. Joksimović, R. Banjanac, D. Maletić, D. Joković, D. Lukić, Plasma focus studies in Serbia, Journal of Modern Physics, 5, 82-88, 2014.
68. R. Banjanac, V. Udovičić, A. Dragić, D. Joković, D. Maletić, N. Veselinović, B. Grabež, Daily variations of gamma-ray background and radon concentration, Romanian Journal of Physics, 58, S14-S21, 2013.
69. A. Dragić, I. Aničin, R. Banjanac, V. Udovičić, D. Joković, D. Maletić, J. Puzović, Forbush decreases – clouds relation in the neutron monitor era, Astrophysics and Space Science Transactions, 7, 315-318, 2011.

#### **6.5 Предавања по позиву с међународних скупова штампана у изводу (M32)**

##### **Радови објављени након претходног избора у звање:**

70. Vladimir Udovičić, Dimitrije Maletić, Maja Eremić Savković, Sofija Forkapić, From motivation through the national radon survey to European Indoor Radon Map, 2nd International Workshop on the European Atlas of Natural Radiation IWEANR 2017, Verbania, Italy, 6-9 November 2017.
71. Vladimir Udovičić, Dimitrije Maletić, Maja Eremić Savković, Gordana Pantelić, Predrag Ujić, Igor Čeliković, Sofija Forkapić, Dragoslav Nikezić, Vladimir Marković, Vesna Arsić, SAMPLING DESIGN OF THE FIRST NATIONAL INDOOR RADON SURVEY IN SERBIA, International Workshop on the European Atlas of Natural Radiation, Verbania, Italy, 9-13 November 2015.

#### **6.6 Саопштења са међународних скупова штампана у целини (M33)**

**Радови објављени након претходног избора у звање:**

72. Drielsma, F. and Maletic, D., Measurement of Phase Space Density Evolution in MICE, Proceedings, International Workshop on Beam Cooling and Related Topics (COOL'17): Bonn, Germany, September 18-22, 2018.
73. Vladimir Udovičić, Dimitrije Maletić, Aleksandar Dragić, Radomir Banjanac, Dejan Joković, Mihailo Savić, Nikola Veselinović, AN OVERVIEW OF THE RADON RESEARCH IN THE INSTITUTE OF PHYSICS BELGRADE, Proceedings of 11th Symposium of the Croatian Radiation Protection Association, Osijek, Croatia, April 5 - 7, 2017.
74. N.Veselinović A. Dragić, M. Savić, D. Maletić, D. Joković, R. Banjanac, V. Udovičić, Utilization of a shallow underground laboratory for studies of the energy dependent CR solar modulation, XXV European Cosmic Ray Symposium, Torino, Sept. 4-9, 2016.
75. M. Savic, A. Dragic, N. Veselinovic, V. Udovicic, R. Banjanac, D. Jokovic, D. Maletic, Effect of pressure and temperature corrections on muon flux variability at ground level and underground, XXV European Cosmic Ray Symposium, Torino, Sept. 4-9, 2016.
76. Ajtic Jelena V, Maletic Dimitrije M, Stratimirovic Djordje I, Blesic Suzana M, Nikolic Jelena D, Djurdjevic Vladimir S, Todorovic Dragana J, Predictability of Lead-210 in Surface Air Based on Multivariate Analysis, RAD 2015: THE THIRD INTERNATIONAL CONFERENCE ON RADIATION AND APPLICATIONS IN VARIOUS FIELDS OF RESEARCH, vol. , br. , str. 317-322, 2015.
77. Banjanac Radomir M, Udovicic Vladimir I, Jokovic Dejan R, Maletic Dimitrije M, Veselinovic Nikola B, Savic Mihailo R, Dragic Aleksandar L, Anicin Ivan V, Background Spectrum Characteristics of the HPGE Detector Long-Term Measurement in the Belgrade Low-Background Laboratory, RAD 2015: THE THIRD INTERNATIONAL CONFERENCE ON RADIATION AND APPLICATIONS IN VARIOUS FIELDS OF RESEARCH, vol. , br. , str. 151-153, 2015.
78. Maletic Dimitrije M, Banjanac Radomir M, Jokovic Dejan R, Udovicic Vladimir I, Dragic Aleksandar L, Savic Mihailo R, Veselinovic Nikola B, Correlative and Periodogram Analysis of Dependence of Continuous Gamma Spectrum in the Shallow Underground Laboratory on Cosmic Ray and Climate Variables, RAD 2015: THE THIRD INTERNATIONAL CONFERENCE ON RADIATION AND APPLICATIONS IN VARIOUS FIELDS OF RESEARCH, vol. , br. , str. 47-50, 2015.
79. Savic Mihailo R, Maletic Dimitrije M, Jokovic Dejan R, Veselinovic Nikola B, Banjanac Radomir M, Udovicic Vladimir I, Dragic Aleksandar L, Pressure and temperature effect corrections of atmospheric muon data in the Belgrade cosmic-ray station, 24TH EUROPEAN COSMIC RAY SYMPOSIUM (ECRS), vol. 632, 2015.
80. Veselinovic Nikola B, Dragic Aleksandar L, Maletic Dimitrije M, Jokovic Dejan R, Savic Mihailo R, Banjanac Radomir M, Udovicic Vladimir I, Anicin Ivan V, Cosmic Rays Muon Flux Measurements at Belgrade Shallow Underground Laboratory, EXOTIC NUCLEI AND NUCLEAR/PARTICLE ASTROPHYSICS (V). FROM NUCLEI TO STARS, vol. 1645, br. , str. 421-425, 2015.

81. V. Udovičić, D. Maletić, M. Eremić Savković, G. Pantelić, P. Ujić, I. Čeliković, S. Forkapić, D. Nikezić, V. M. Marković, V. Arsić, NATIONAL PROGRAMME FOR THE CONTROL OF PUBLIC EXPOSURE TO RADON IN SERBIA, V International Congress BIOMEDICINE AND GEOSCIENCES – INFLUENCE OF ENVIRONMENT ON HUMAN HEALTH, Hotel Crowne Plaza, Belgrade, March 3-4, 32-39, 2015.

82. N. Veselinović, A. Dragić, D. Maletić, D. Joković, M. Savić, R. Banjanac, V. Udovičić and I. Aničin, Cosmic rays muon flux measurements at Belgrade shallow underground laboratory, Exotic Nuclei and Nuclear/Particle Astrophysics (V). From Nuclei to Stars, 13–26 July 2014, Sinaia, Romania. AIP Conf. Proc. 1645, 421-425, 2015.

83. Dimitrije Maletić, Radomir Banjanac, Dejan Joković, Vladimir Udovičić, Aleksandar Dragić, Mihailo Savić, Nikola Veselinović, CORRELATIVE AND PERIODOGRAM ANALYSIS OF DEPENDENCE OF CONTINUOUS GAMMA SPECTRUM IN THE SHALLOW UNDERGROUND LABORATORY ON COSMIC RAY AND CLIMATE VARIABLES, PROCEEDINGS OF THIRD INTERNATIONAL CONFERENCE ON RADIATION AND DOSIMETRY IN VARIOUS FIELDS OF RESEARCH RAD2015, JUNE 8 – 12, 47-50, 2015.

84. Radomir Banjanac, Vladimir Udovičić, Dejan Joković, Dimitrije Maletić, Nikola Veselinović, Mihailo Savić, Aleksandar Dragić, Ivan Aničin, BACKGROUND SPECTRUM CHARACTERISTICS OF THE HPGE DETECTOR LONG-TERM MEASUREMENT IN THE BELGRADE LOW-BACKGROUND LABORATORY, PROCEEDINGS OF THIRD INTERNATIONAL CONFERENCE ON RADIATION AND DOSIMETRY IN VARIOUS FIELDS OF RESEARCH RAD2015, JUNE 8 – 12, 151-153, 2015.

**Радови објављени пре претходног избора у звање:**

85. Dimitrije Maletić, Jelena Ajtić, Vladimir Đurđević, Dragana Todorović, Jelena Nikolić, Radomir Banjanac, and Vladimir Udovičić, Multivariate analysis of climate variables, teleconnection indices and activities of Lead-210 and Beryllium-7 in surface air in Belgrade, Serbia, Proceedings - The Second International Conference on Radiation and Dosimetry in Various Fields of Research, RAD 2014, May 27-30, 2014, Niš, Serbia, pp. 13-16., 2014.

86. R. Banjanac, V. Udovičić, J. Filipović, D. Joković, D. Maletić, M. Savić, N. Veselinović, P.Kolarž, A. Dragić, Relation between daily gamma-ray background and radon variability in the nderground low-level laboratory in Belgrade, Proceedings - The Second International Conference on Radiation and Dosimetry in Various Fields of Research, RAD 2014, May 27-30, 2014, Niš, Serbia, pp.99-102, 2014.

87. Vladimir Udovičić, Dimitrije Maletić, Radomir Banjanac, Dejan Joković, Bojana Grabež, Nikola Veselinović, Jelena Filipović, Comprehensive analysis of long-term variations of low radon concentration in underground laboratory , Proceedings - The Second International Conference on Radiation and Dosimetry in Various Fields of Research, RAD 2014, May 27-30, 2014, Niš, Serbia, pp.35-38, 2014.

88. R. Banjanac, A. Dragić, V. Udovičić, D. Joković, D. Maletić, N. Veselinović, M. Savić, Comparative study of gamma-ray background and radon concentration inside ground level and underground low-level laboratories, Proceedings of the VII Hungarian Radon Forum, Veszprém, Hungary p.9-12, 2013.

89. D. Joković, V. Udovičić, R. Banjanac, D. Maletić, A. Dragić, N. Veselinović, B. Grabež, J. Nikolov, A simple Monte Carlo simulation method for estimating radon induced background of germanium detectors, Proceedings of the VII Hungarian Radon Forum, Veszprém, Hungary p.95-97, 2013.
90. V. Udovičić, A. Dragić, R. Banjanac, D. Joković, D. Maletić, N. Veselinović, J. Filipović, Influence of ventilation systems on indoor radon variability, Proceedings of the VII Hungarian Radon Forum, Veszprém, Hungary p.179-183, 2013.
91. A. Dragić, I. Aniĉin, R. Banjanac, V. Udovičić, D. Joković, D. Maletić, M. Savić, N. Veselinović, J. Puzović, Neutrons produced by muons at 25 mwe, 23rd European Cosmic Ray Symposium, Moscow, Russia (2012); Journal of Physics: Conference Series, 409, 012054, 2013.
92. I. Aniĉin, D. Maletić, A. Dragić, R. Banjanac, D. Joković, N. Veselinović, V. Udovičić, M. Savić, J. Puzović, Stopped cosmic ray muons in plastic scintillators on the surface and at the depth of 25 m.w.e., 23rd European Cosmic Ray Symposium, Moscow, Russia (2012); Journal of Physics: Conference Series, 409, 012142, 2013.
93. D. Maletić, V. Udovičić, R. Banjanac, A. Dragić, D. Joković, M. Savić, N. Veselinović, J. Puzović, Semi-empirical simulation of natural background in underground laboratory, Proceedings of the 3rd International Conference on Environmental Protection, Veszprém, Hungary, p. 83-88, 2012
94. P. Adzic, F. Beaudette, G. Dissertori, R.G. Garrido, G. Leshev, A. Lister, D. Maletic, P. Milenovic, R. Ofierzynski, J. Puzovic, A. Sytin, S. Zelepoukine, The detector control system for the electromagnetic calorimeter of the CMS experiment at the LHC, 10th International Conference on Accelerator and Large Experimental Physics Control Systems (ICALPCS 2005), Geneva, Switzerland, Europhysics Conference Abstracts, 29J, MO3\_4-10, 2005.

## **6.7 Саопштења са међународних скупова штампана у изводу (М34)**

### **Радови објављени након претходног избора у звање:**

95. Vladimir Udovičić, Nikola Veselinovic, Dimitrije Maletic, Radomir Banjanac, Aleksandar Dragic, Dejan Jokovic, Mihailo Savic, David Knezevic, Maja Eremic Savkovic, RADON VARIABILITY DUE TO FLOOR LEVEL IN THE TWO TYPICAL RESIDENTIAL BUILDINGS IN SERBIA, BOOK of ABSTRACTS, 3 rd International Conference “Radon in the Environment 2019” 27-31 May 2019, Kraków, Poland. 2019.
96. Maja Eremic-Savkovic, Vladimir Udovicic, Dimitrije Maletic, Aleksandar Djordjevic, PILOT STUDY ON MITIGATION SOLUTIONS FOR BUILDINGS WITH AN ELEVATED RADON LEVELS IN SERBIA, BOOK of ABSTRACTS, 3 rd International Conference “Radon in the Environment 2019” 27-31 May 2019, Kraków, Poland, 2019.
97. Vladimir Udovičić, Dimitrije Maletić, Maja Eremić Savković, Slađan Velinov, Bojana Spasić, Branko Markoski, FIRST SERBIAN INDOOR RADON MAP, III East European Radon Symposium TEERAS 2017, Sofia, Bulgaria, 15-19 May, 2017, Book of Abstracts 16. 2017.

98. Dimitrije Maletic, Vladimir Udovicic, Radomir Banjanac, Dejan Jokovic, Mihailo Savic, Nikola Veselinovic, Jelena Zivanovic, Aleksandar Dragic, Correlative, multivariate and periodicity analysis of the variations of low radon concentrations in an shallow underground laboratory, III East European Radon Symposium TEERAS 2017, Sofia, Bulgaria, 15-19 May, 2017, Book of Abstracts 48. 2017.
99. D. Maletic, V. Udovicic, M. E. Savkovic, G. Pantelic, P. Ujic, I. Celikovic, S. Forkapic, D. Nikezic, V. Markovic, V. Arsic, J. Ilic, REPRESENTATIVENESS OF THE FIRST NATIONAL INDOOR RADON SURVEY IN SERBIA, V. TERRESTRIAL RADIOISOTOPES IN ENVIRONMENT, International Conference on Environmental Protection, Veszprém-Hungary, May 17-20, (2016) Book of Abstracts, pp. 11, 2016.
100. D. Joković, R. Banjanac, D. Maletić, V. Udovičić, M. Keržlin, S. Stošić, M. Serdar, A STUDY ON RADIOACTIVITY OF ENVIRONMENTAL SAMPLES FROM THE VICINITY OF THE OBRENOVAC POWER PLANT, V. TERRESTRIAL RADIOISOTOPES IN ENVIRONMENT, International Conference on Environmental Protection, Veszprém-Hungary, May 17-20, (2016) Book of Abstracts, pp. 70, 2016.
101. Dimitrije Maletic, Dejan Jokovic, Radomir Banjanac, Vladimir Udovicic, Aleksandar Dragic, Nikola Veselinovic, Mihailo Savic, VARIATION OF MUON COSMIC RAY FLUX RECORDED BY BELGRADE COSMIC RAY STATION DURING DECEMBER 2015 AND COMPARISON WITH EUROPEAN NEUTRON FLUX MONITORS, BOOK OF ABSTRACTS OF FOURTH INTERNATIONAL CONFERENCE ON RADIATION AND DOSIMETRY IN VARIOUS FIELDS OF RESEARCH RAD2016, MAY 23 – 27, 306, 2016.
102. Dejan Joković, Nikola Veselinović, Radomir Banjanac, Dimitrije Maletić, Vladimir Udovičić, Mihailo Savić, Marija Keržlin, Slaviša Stošić, A STUDY ON NATURAL RADIOACTIVITY OF VARIOUS ENVIRONMENTAL SAMPLES FROM THE VICINITY OF THE OBRENOVAC POWER PLANT, BOOK OF ABSTRACTS OF FOURTH INTERNATIONAL CONFERENCE ON RADIATION AND DOSIMETRY IN VARIOUS FIELDS OF RESEARCH RAD2016, MAY 23 – 27, 429, 2016.
103. Vladimir Udovicic, Dimitrije Maletic, Maja Eremic Savkovic, Gordana Pantelic, Predrag Ujic, Igor Celikovic, Dragoslav Nikezic, Vladimir Markovic, Per Nilsson, Sofija Forkapic, Vesna Arsic, Jovana Ilic, FIRST NATIONAL INDOOR RADON SURVEY IN SERBIA, BOOK OF ABSTRACTS OF FOURTH INTERNATIONAL CONFERENCE ON RADIATION AND DOSIMETRY IN VARIOUS FIELDS OF RESEARCH RAD2016, MAY 23 – 27, 490, 2016.
104. Vladimir Udovicic, Dimitrije Maletic, Radomir Banjanac, Dejan Jokovic, Gordan Nisevic, Vesna Manic, Goran Manic, IN-FIELD INTERCOMPARISON INDOOR RADON MEASUREMENTS IN RADON-PRONE AREAS OF NISKA BANJA, SERBIA, BOOK OF ABSTRACTS OF FOURTH INTERNATIONAL CONFERENCE ON RADIATION AND DOSIMETRY IN VARIOUS FIELDS OF RESEARCH RAD2016, MAY 23 – 27, 497, 2016.
105. Vladimir Udovicic, Dimitrije Maletic, Maja Eremic Savkovic, Gordana Pantelic, Predrag Ujic, Igor Celikovic, Sofija Forkapic, Dragoslav Nikezic, Vladimir Markovic, Vesna Arsic, Jovana Ilic, Per Nilsson, Preliminary results of the first national indoor radon survey in Serbia, 8th Conference of Protection against Radon at Home and at Work, 12 - 14 of September 2016, Prague, Czech Republic, Book of Abstracts, pp. 61., 2016.

106. Vladimir Udovicic, Dimitrije Maletic, Jelena Zivanovic, Aleksandar Dragic, Radomir Banjanac, Dejan Jokovic, Sofija Forkapic, Long-term indoor radon measurements in a family house – a case study in Serbia, 8th Conference of Protection against Radon at Home and at Work, 12 - 14 of September 2016, Prague, Czech Republic, Book of Abstracts, pp. 79. 2016.
107. Jokovic, D., Maletic, D., Savic, M., Veselinovic, N., Banjanac, R., Udovicic, V., Dragic, A., Pressure and temperature correction of atmospheric muon data, 24th European Cosmic Ray Symposium, Kiel, Germany, September 1 - 5, 2014, Book of Abstracts, pp. 74., 2015.
108. Veselinovic, N., Dragic, A., Maletic, D., Jokovic, D., Savic, M., Banjanac, R., Udovicic, V., Anicin, I., Muon measurements at Belgrade shallow underground laboratory, 24th European Cosmic Ray Symposium, Kiel, Germany, September 1 - 5, 2014, Book of Abstracts, pp. 74., 2015.
109. Jelena Z. Filipović, Vladimir I. Udovičić, Dimitrije M. Maletić, Radomir M. Banjanac, Dejan R. Joković, Mihailo R. Savić, Nikola B. Veselinović, The Use of Multivariate Analysis and Modeling of the Radon Variation in Laboratory and Real Environment, 2nd INTERNATIONAL CONFERENCE „RADON in the ENVIRONMENT 2015”; KRAKÓW, POLAND, May 25-29. 2015, Book of Abstracts, pp. 66, 2015.
110. Vladimir Udovičić, Dimitrije Maletić, Maja Eremić Savković, Gordana Pantelić, Predrag Ujić, Sofija Forkapić, Nenad Stevanović, Vladimir M. Marković, Vesna Arsić, First Steps Towards a National Radon Action Plan in Serbia, 2nd INTERNATIONAL CONFERENCE „RADON in the ENVIRONMENT 2015”; KRAKÓW, POLAND, May 25-29. 2015, Book of Abstracts, pp. 75, 2015.
111. R. Banjanac, D. Joković, D. Maletić, V. Udovičić, N. Veselinović, M. Savić, A. Dragić, Long-term background measurements in the Belgrade low-level underground laboratory, 20th International Conference on Radionuclide Metrology and its Applications, June 8 – 11, 2015, Vienna, Austria, Book of Abstracts, pp. P-161., 2015.

**Радови објављени пре претходног избора у звање:**

112. D. Joković, R. Banjanac, D. Maletić, V. Udovičić, N. Veselinović, B. Grabež, A GEANT4 based method to estimate radon concentration inside lead castle of shielded germanium detectors, Book of Abstracts - The Second International Conference on Radiation and Dosimetry in Various Fields of Research, RAD 2014, May 27-30, 2014, Niš, Serbia, p. 246, 2014.
113. N. Veselinović, D. Maletić, D. Joković, R. Banjanac, V. Udovičić, M. Savić, J. Puzović, I.V. Aničin, A. Dragić, Some peculiarities of digital  $\gamma$ -ray spectroscopy with germanium detectors performed in presence of neutrons, GAMMA-2, Scientific Workshop on Nuclear Fission Dynamics and the Emission of Prompt Neutrons and Gamma Rays; Book of Abstracts p30, 2013.
114. R. Banjanac, A. Dragić, V. Udovičić, D. Joković, D. Maletić, N. Veselinović, M. Savić, Variations of gamma-ray background in the Belgrade shallow underground low-level laboratory, 19th International Conference on Radionuclide Metrology and its Applications, Antwerp, Belgium; Book of Abstracts p142, 2013.

115. V. Udovičić, J. Filipović, A. Dragić, R. Banjanac, D. Joković, D. Maletić, B. Grabež, Daily radon variability in the underground low-background laboratory in Belgrade, Serbia, 7th International Conference on Protection Against Radon at Home and at Work, Prague; Czech Republic, Book of Abstracts, p122, 2013.
116. V. Udovičić, A. Dragić, R. Banjanac, D. Joković, D. Maletić, B. Grabež, J. Filipović, Effects of the air conditioning system usage on the indoor radon variability, 7th International Conference on Protection Against Radon at Home and at Work, Prague; Czech Republic, Book of Abstracts, p70, 2013.
117. R. Banjanac, V. Udovičić, A. Dragić, D. Joković, D. Maletić, N. Veselinović, J. Puzović, Correlation of daily variation between gamma-ray background and radon concentration, 1st East European Radon Symposium, Cluj-Napoca, Romania; Book of Abstracts, p94, 2012.

## **Нема ИФ**

### **Радови објављени пре претходног избора у звање:**

118. K. Karafasoulis, A. Kyriakis and D. Maletic, *Neutral Pion rejection for isolated and unconverted photon candidates using CMS ECAL and Preshower detector*, CMS Analysis Note 2008/036, 2008.

## **6.8 Саопштења са скупова националног значаја штампана у целини (M63)**

### **Радови објављени након претходног избора у звање:**

119. Vladimir UDOVIČIĆ, Dimitrije MALETIĆ, Aleksandar DRAGIĆ, Radomir BANJANAC, Dejan JOKOVIĆ, Nikola VESELINOVIĆ, Mihailo SAVIĆ, David KNEZEVIĆ, Maja EREMIĆ-SAVKOVIĆ, DISTRIBUCIJA KONCENTRACIJE RADONA PO SPRATNOSTI STAMBENIH ZGRADA, XXX СИМПОЗИЈУМ ДЗЗСЦГ Дивчибаре 2- 4. октобар 2019. године, 2019.
120. Mihailo SAVIĆ, Vladimir UDOVIČIĆ, Dimitrije MALETIĆ, Aleksandar DRAGIĆ, Radomir BANJANAC, Dejan JOKOVIĆ, Nikola VESELINOVIĆ i David KNEZEVIĆ, PROCENA TEMPERATURSKOG PROFILA ATMOSFERE NA OSNOVU DETEKTOVANOG FLUKSA KOSMIČKIH MIONA, XXX СИМПОЗИЈУМ ДЗЗСЦГ Дивчибаре 2- 4. октобар 2019. године, 2019.
121. Vladimir UDOVIČIĆ, Dimitrije MALETIĆ, Aleksandar DRAGIĆ, Radomir BANJANAC, Dejan JOKOVIĆ i Sofija FORKAPIĆ, STUDIJA SLUČAJA SEZONSKE VARIJACIJE KONCENTRACIJE RADONA U PORODIČNOJ KUĆI U SRBIJI, XXIX SIMPOZIJUM DRUŠTVA ZA ZAŠTITU OD ZRAČENJA SRBIJE I CRNE GORE, Srebrno jezero, Srbija, 27.-29. Septembar 2017, Zbornik radova 179-182., 2017.
122. Sofija FORKAPIĆ, Dimitrije MALETIĆ, Jovica VASIN, Kristina BIKIT, Dušan MRĐA, Ištvan BIKIT, Vladimir UDOVIČIĆ, Radomir BANJANAC, KORIŠĆENJE MULTIVARIJANTNE

ANALIZE ZA PREDVIĐANJE GEOGENOG RADONSKOG POTENCIJALA, XXIX SIMPOZIJUM DRUŠTVA ZA ZAŠTITU OD ZRAČENJA SRBIJE I CRNE GORE, Srebrno jezero, Srbija, 27.-29. Septembar 2017, Zbornik radova 210-218., 2017.

123. Владимир УДОВИЧИЋ, Александар ДРАГИЋ, Радомир БАЊАНАЦ, Дејан ЈОКОВИЋ, Димитрије МАЛЕТИЋ, Никола ВЕСЕЛИНОВИЋ, Михаило САВИЋ, Давид КНЕЖЕВИЋ, НИСКОФОНСКА ЛАБОРАТОРИЈА ИНСТИТУТА ЗА ФИЗИКУ - ПРВИХ ДВАДЕСЕТ ГОДИНА, XXIX СИМПОЗИЈУМ ДРУШТВА ЗА ЗАШТИТУ ОД ЗРАЧЕЊА СРБИЈЕ И ЦРНЕ ГОРЕ, Сребрно језеро, Србија, 27.-29. Септембар 2017, Зборник радова 429-437. 2017.

124. Dimitrije MALETIĆ, Vladimir UDOVIČIĆ, Dejan JOKOVIĆ, Radomir BANJANAC, Aleksandar DRAGIĆ, Mihailo SAVIĆ, Nikola VESELINOVIĆ, MONTE KARLO SIMULACIJA FONA HPGE DETEKTORA OD RADIONUKLIDA, KOSMIČKOG I SKYSHINE ZRAČENJA. XXIX SIMPOZIJUM DRUŠTVA ZA ZAŠTITU OD ZRAČENJA SRBIJE I CRNE GORE, Srebrno jezero, Srbija, 27.-29. Septembar 2017, Zbornik radova 438-442. 2017.

125. Dimitrije MALETIĆ, Dejan JOKOVIĆ, Radomir BANJANAC, Nikola VESELINOVIĆ, Mihailo SAVIĆ, Aleksandar DRAGIĆ, Vladimir UDOVIČIĆ, KORIŠĆENJE MOBILNOG TELEFONA ZA TESTIRANJE I OPTIMIZACIJU LABORATORIJSKIH MERENJA FOTOMULTIPLIKATORIMA. XXVIII Simpozijum DZZSCG, Vršac, Zbornik radova (2015) 589-593, 2015.

126. Dimitrije MALETIĆ, Dejan JOKOVIĆ, Mihailo SAVIĆ, Aleksandar DRAGIĆ, Radomir BANJANAC, Vladimir UDOVIČIĆ, Nikola VESELINOVIĆ, AUTOMATSKA OBRADA PODATAKA KOSMIKE I EVALUACIJA KONCENTRACIJE RADONA NA INTERNET (WEB) SERVERU, XXVIII Simpozijum DZZSCG, Vršac, Zbornik radova (2015) 584-588. 2015.

127. Dimitrije MALETIĆ, Nikola VESELINOVIĆ, Dejan JOKOVIĆ, Vladimir UDOVIČIĆ, Radomir BANJANAC, Mihailo SAVIĆ, Aleksandar DRAGIĆ, MONTE KARLO SIMULACIJA KREIRANJA KOSMOGENIH RADIONUKLIDA U LESU. XXVIII Simpozijum DZZSCG, Vršac, Zbornik radova (2015) 481-486, 2015.

128. Jelena FILIPOVIĆ, Vladimir UDOVIČIĆ, Dimitrije MALETIĆ, Radomir BANJANAC, Dejan JOKOVIĆ, Mihailo SAVIĆ, Nikola VESELINOVIĆ, KORELACIONA I REGRESIONA ANALIZA VARIJABILNOSTI RADONA PRIMENOM MULTIVARIJANTNIH METODA, XXVIII Simpozijum DZZSCG, Vršac, Zbornik radova (2015) 254-259, 2015.

129. Mihailo SAVIĆ, Dimitrije MALETIĆ, Dejan JOKOVIĆ, Nikola VESELINOVIĆ, Aleksandar DRAGIĆ, Radomir BANJANAC, Vladimir UDOVIČIĆ, ODREĐIVANJE TEMPERATURSKOG PROFILA ATMOSFERE MERENJEM INTENZITETA KOSMIČKOG ZRAČENJA NA POVRŠINI ZEMLJE, XXVIII Simpozijum DZZSCG, Vršac, Zbornik radova (2015) 577-583, 2015.

130. Radomir BANJANAC, Vladimir UDOVIČIĆ, Jelena FILIPOVIĆ, Dejan JOKOVIĆ, Dimitrije MALETIĆ, Gordan NIŠEVIĆ, KORELACIJA VARIJACIJA FONA GAMA ZRAČENJA I RADONA U NISKOFONSKOJ PODZEMNOJ LABORATORIJI U BEOGRADU, XXVIII Simpozijum DZZSCG, Vršac, Zbornik radova (2015) 248-253, 2015.

131. Radomir BANJANAC, Aleksandar DRAGIĆ, Vladimir UDOVIČIĆ, Dejan JOKOVIĆ, Dimitrije MALETIĆ, Nikola VESELINOVIĆ, Mihailo SAVIĆ. GLEDANJE U KUGLU-25 GODINA POSLE, XXVIII Simpozijum DZZSCG, Vršac, Zbornik radova (2015) 548-554, 2015.

132. Vladimir UDOVIČIĆ, Mihailo SAVIĆ, Dejan JOKOVIĆ, Dimitrije MALETIĆ, Radomir BANJAC, Nikola VESELINOVIĆ, Marina ŽIKIĆ, MERENJE KONCENTRACIJE RADONA I PROCENA IZLOŽENOSTI U BOGOVINSKOJ PEĆINI, XXVIII Simpozijum DZZSCG, Vršac, Zbornik radova (2015) 207-211, 2015.

133. Vladimir UDOVIČIĆ, Dimitrije MALETIĆ, Maja EREMIĆ SAVKOVIĆ, Gordana PANTELIĆ, Predrag UJIĆ, Igor ČELIKOVIĆ, Sofija FORKAPIĆ, Dragoslav NIKEZIĆ, Vladimir MARKOVIĆ, Vesna ARSIĆ, Jovana ILIĆ, NACIONALNI PROGRAM MERENJA RADONA U SRBIJI, XXVIII Simpozijum DZZSCG, Vršac, Zbornik radova (2015) 173-180, 2015.

#### **Радови објављени пре претходног избора у звање:**

134. V. Udovičić, J. Filipović, A. Dragić, R. Banjanac, D. Joković, D. Maletić, B. Grabež, Z.S. Žunić, Merenje niskih koncentracija radona u podzemnoj niskofonskoj laboratoriji u Zemunu, XII Kongres fizičara Srbije, Vrnjačka Banja, Zbornik radova, p457-460, 2013.

135. V. Udovičić, N. Veselinović, A. Dragić, R. Banjanac, D. Joković, D. Maletić, D. Joksimović, Zavisnost prinosa neutrona od pritiska radnog gasa u uređaju plazma fokus, XII Kongres fizičara Srbije, Vrnjačka Banja, Zbornik radova, p260-263, 2013.

136. J. Puzović, B. Grabež, D. Maletić, D. Joković, M. Savić, D. Manić, NA61/SHINE eksperiment i detektorski sistem, XII Kongres fizičara Srbije, Vrnjačka Banja, Zbornik radova, p244-247, 2013.

137. D. Maletić, V. Udovičić, R. Banjanac, A. Dragić, D. Joković, N. Veselinović, B. Grabež, M. Savić, J. Puzović, I. Aničin, Semi-empirijska simulacija prirodnog fona u podzemnoj laboratoriji, XII Kongres fizičara Srbije, Vrnjačka Banja, Zbornik radova, p228-231, 2013.

138. D. Maletić, A. Dragić, R. Banjanac, D. Joković, N. Veselinović, V. Udovičić, B. Grabež, M. Savić, J. Puzović, I. Aničin, Polarizacija miona kosmičkog zračenja na površini Zemlje i u podzemnoj laboratoriji, XII Kongres fizičara Srbije, Vrnjačka Banja, Zbornik radova, p224-227, 2013.

139. D. Maletić, A. Dragić, R. Banjanac, D. Joković, N. Veselinović, V. Udovičić, B. Grabež, M. Savić, J. Puzović, I. Aničin, Paket programa za spektralnu i vremensku analizu podataka u digitalnoj nuklearnoj i spektroskopiji kosmičkog zračenja, XII Kongres fizičara Srbije, Vrnjačka Banja, Zbornik radova, p220-223, 2013.

140. A. Dragić, D. Maletić, D. Joković, R. Banjanac, N. Veselinović, V. Udovičić, I. Aničin, Vreme života miona kosmičkog zračenja zaustavljenih u olovu, XII Kongres fizičara Srbije, Vrnjačka Banja, Zbornik radova, p201-203, 2013.

141. A. Dragić, D. Maletić, R. Banjanac, D. Joković, V. Udovičić, B. Grabež, N. Veselinović, M. Savić, J. Puzović, I. Aničin, Produkcija neutrona mionima iz kosmičkog zračenja na dubini od 25 m.w.e, XII Kongres fizičara Srbije, Vrnjačka Banja, Zbornik radova, p197-200, 2013.

142. A. Dragić, D. Maletić, R. Banjanac, D. Joković, V. Udovičić, B. Grabež, N. Veselinović, M. Savić, J. Puzović, I. Aničin, Indeks devijacije DTR i kosmički zraci, XII Kongres fizičara Srbije, Vrnjačka Banja, Zbornik radova, p193-196, 2013.

143. A. Dragić, N. Veselinović, D. Maletić, D. Joković, R. Banjanac, V. Udovičić, I. Aničin, O vezi između intenziteta kosmičkog zračenja i klime na Zemlji, XII Kongres fizičara Srbije, Vrnjačka Banja, Zbornik radova, p189-192, 2013.
144. R. Banjanac, D. Maletić, D. Joković, N. Veselinović, A. Dragić, V. Udovičić, I. Aničin, O svuda prisutnom fonskom zračenju kontinuirang spektra, XII Kongres fizičara Srbije, Vrnjačka Banja, Zbornik radova, p181-184, 2013.
145. R. Banjanac, A. Dragić, V. Udovičić, D. Joković, D. Maletić, N. Veselinović, M. Savić, B. Grabež, I. Aničin, J. Puzović, Varijacije radona i kosmičkog zračenja kao izvori vremenske varijacije fona gama zračenja u niskofonskoj gama spektrometriji, XII Kongres fizičara Srbije, Vrnjačka Banja, Zbornik radova, p177-180, 2013.
146. D. Maletić, D. Joković, R. Banjanac, A. Dragić, V. Udovičić, N. Veselinović, I. Aničin, Kompozicija kosmičkog zračenja zaustavljenog u veto detektorima, XXVII Simpozijum DZZSCG, Vrnjačka Banja, Zbornik radova, p394-397, 2013.
147. D. Maletić, A. Dragić, D. Joković, R. Banjanac, V. Udovičić, N. Veselinović, I. Aničin Spektralna i vremenska analiza u digitalnoj spektroskopiji – razvoj softvera i primeri, XXVII Simpozijum DZZSCG, Vrnjačka Banja, Zbornik radova, p390-393, 2013.
148. V. Udovičić, A. Dragić, R. Banjanac, D. Joković, D. Maletić, B. Grabež, J. Filipović. Korelaciona analiza uticaja atmosfere na varijaciju koncentracije radona u različitim sredinama XXVII Simpozijum DZZSCG, Vrnjačka Banja, Zbornik radova, p171-174, 2013.
149. V. Udovičić, D. Maletić, A. Dragić, R. Banjanac, D. Joković, N. Veselinović, J. Filipović Primena različitih metoda u analizi vremenskih serija koncentracije radona, XXVII Simpozijum DZZSCG, Vrnjačka Banja, Zbornik radova, p167-170, 2013.
150. D. Joković, J. Nikolov, R. Banjanac, V. Udovičić, D. Maletić, A. Dragić, B. Grabež, Monte Karlo simulacija za procenu radonske aktivnosti unutar olovne zaštite germanijumskih detektora, XXVII Simpozijum DZZSCG, Vrnjačka Banja, Zbornik radova, p143-146, 2013.
151. R. Banjanac, A. Dragić, V. Udovičić, D. Joković, D. Maletić, N. Veselinović, I. Aničin, Kompozicija niskoenergijskog dela fonskog spektra gama zračenja u nadzemnoj i podzemnoj niskofonskoj laboratoriji, XXVII Simpozijum DZZSCG, Vrnjačka Banja, Zbornik radova, p126-129, 2013.
152. R. Banjanac, A. Dragić, V. Udovičić, D. Joković, D. Maletić, N. Veselinović, I. Aničin, Vremenski promenljive komponente fona gama zračenja i merenje malih aktivnosti, XXVII Simpozijum DZZSCG, Vrnjačka Banja, Zbornik radova, p122-125, 2013.
153. D. Maletić, R. Banjanac, A. Dragić, D. Joković, V. Udovičić, J. Puzović, Semiempirijska simulacija prirodnog fona sendvič detektora, XXVI Simpozijum DZZSCG, Tara, Zbornik radova, p335-339, 2011.
154. D. Joković, R. Banjanac, V. Udovičić, A. Dragić, D. Maletić, N. Veselinović, I. Aničin, Monte Karlo simulacija apsolutne efikasnosti detekcije od 46.5 keV za određivanje koncentracije Pb-210 u

postojećoj olovnoj zaštiti HPGe detektora, XXVI Simpozijum DZZSCG, Tara, Zbornik radova, p311-315, 2011.

155. V. Udovičić, A. Dragić, R. Banjanac, D. Joković, B. Grabež, Z.S. Žunić, Periodičnost koncentracije radona u niskofonskoj podzemnoj laboratoriji u Beogradu, XXVI Simpozijum DZZSCG, Tara, Zbornik radova, p155-159, 2011.

156. Đorđević M., Lazić D., Maletić D., Adžić P.R., Particle identification in the combined test beam ECAL/HCAL of the CMS detector using Cherenkov counters in the experimental line H2 at CERN, Journal of Research in Physics, 31/2, 48-51, 2007

157. Maletić D., Creation and distribution of 'Monarc' files during the 'LoadTest07' exercise within the CMS experiment, Journal of Research in Physics, 31/2, 52-56, 2007

158. Maletić D., Đorđević M., Adžić P.R., Algorithmic XML geometry description of the CMS ECAL Preshower detector, Journal of Research in Physics, 31/2, 44-47, 2007

159. Maletić D., Đorđević M., Adžić P.R., Aničin I.V., Drndarević S., Jovanović D., Krpić D., Milenović P., Puzović J., Background reduction of two photon Higgs decay based on unconverted photon reconstruction in the central part of the ECAL of CMS detector, Journal of Research in Physics, 31/2, 40-43, 2007

160. Adžić P.R., Aničin V., Đorđević M., Drndarević S., Krpić D., Maletić D., Milenović P., Jovanović D., Puzović J., Smiljković N., The CMS experiment and participation of the CMS Belgrade group, Journal of Research in Physics, 31/2, 16-21, 2007

## **6.9 магистарске и докторске тезе (М 70)**

### **М 71**

#### **Радови објављени пре претходног избора у звање:**

161. 2009. докторирао на Физичком Факултету Универзитета у Београду са темом:  
“*Редуција фона двофотонског канала распада  $H_{i\bar{i}}$  дозона (СМ) на гејекџору CMS*”

### **М 72**

#### **Радови објављени пре претходног избора у звање:**

162. 2006. магистрирао на Физичком Факултету Универзитета у Београду са темом: “*Монџе Карло симулација CMS ECAL Preshower гејекџора и њорешјење са експерименталним резултатима*”

## 7. Подаци о цитираности кандидата

По бази SCOPUS кандидат има 79 радова са 7142 цитата и х-индекс 30.  
SCOPUS: <https://www.scopus.com/authid/detail.uri?authorId=15728244200>

По Google Scholar има 115 радова са укупно 15806 цитата и х-индекс 40,  
Google Scholar: <https://scholar.google.com/citations?user=zdY0NXwAAAAJ&hl=en>

а по бази <http://inspirehep.net> број цитата искључујући самоцитате је 6,687 и х-индекс је 24.



Generated on 2020-02-07

74 papers found, 68 of them citeable (published or arXiv)

| Citation summary results                 | Citeable papers | Citeable papers excluding self cites | Citeable papers excluding RPP | Published only | Published only excluding self cites | Published only excluding RPP |
|--|-----------------|--------------------------------------|-------------------------------|----------------|-------------------------------------|------------------------------|
| <b>Total number of papers analyzed:</b>  | 68              | 68                                   | 68                            | 52             | 52                                  | 52                           |
| <b>Total number of citations:</b>        | 13723           | 6687                                 | 13723                         | 12789          | 6030                                | 12789                        |
| <b>Average citations per paper:</b>      | 201.8           | 98.3                                 | 201.8                         | 245.9          | 116                                 | 245.9                        |
| <b>Breakdown of papers by citations:</b> |                 |                                      |                               |                |                                     |                              |
| Renowned papers (500+)                   | 4               | 4                                    | 4                             | 3              | 3                                   | 3                            |
| Famous papers (250-499)                  | 3               | 2                                    | 3                             | 3              | 2                                   | 3                            |
| Very well-known papers (100-249)         | 7               | 3                                    | 7                             | 7              | 3                                   | 7                            |
| Well-known papers (50-99)                | 13              | 5                                    | 13                            | 13             | 5                                   | 13                           |
| Known papers (10-49)                     | 19              | 21                                   | 19                            | 18             | 21                                  | 18                           |
| Less known papers (1-9)                  | 11              | 20                                   | 11                            | 4              | 14                                  | 4                            |
| Unknown papers (0)                       | 11              | 13                                   | 11                            | 4              | 4                                   | 4                            |
| hHEP index [?]                           | 31              | 24                                   | 31                            | 30             | 23                                  | 30                           |

Bogomilov, M., Tsenov, R., Vankova-Kirilova, G. *et al.* Demonstration of cooling by the Muon Ionization Cooling Experiment. *Nature* **578**, 53–59 (2020). <https://doi.org/10.1038/s41586-020-1958-9>

<https://www.nature.com/articles/s41586-020-1958-9>

Часопис забрањује дистрибуцију pdf-а или копија рада у наредних 6 месеци. Рад може да се преузме као Open access.

The screenshot shows a web browser displaying the article page on the Nature website. At the top, there is a cookie consent banner. Below it is the Nature logo and navigation icons for Search, E-alert, Submit, and Login. The article title is prominently displayed, along with its publication date (05 February 2020) and 'Open Access' status. A 'Download PDF' button is visible. The 'Associated Content' section lists related articles, including 'Muon colliders come a step closer'. The 'Sections' tab is active, showing a list of sections: Abstract, High-quality muon beams, and MICE cooling apparatus. The abstract text is partially visible at the bottom of the page.

Demonstration of cooling by the Muon Ionization Cooling Experiment

Article | [Open Access](#) | Published: 05 February 2020

**Demonstration of cooling by the Muon Ionization Cooling Experiment**

[MICE collaboration](#)

[Nature](#) **578**, 53–59(2020) | [Cite this article](#)

145 [Altmetric](#) | [Metrics](#)

**Abstract**

The use of accelerated beams of electrons, protons or ions has furthered the development of nearly every scientific discipline. However, high-

[Download PDF](#)

**Associated Content**

[Nature](#) | [News & Views](#)

**Muon colliders come a step closer**

Robert D. Ryne

**Sections** | [Figures](#) | [References](#)

- [Abstract](#)
- [High-quality muon beams](#)
- [MICE cooling apparatus](#)



Contents lists available at ScienceDirect

# Science of the Total Environment

journal homepage: [www.elsevier.com/locate/scitotenv](http://www.elsevier.com/locate/scitotenv)

## Forecasting of VOC emissions from traffic and industry using classification and regression multivariate methods



Andreja Stojić<sup>a,\*</sup>, Dimitrije Maletić<sup>a</sup>, Svetlana Stanišić Stojić<sup>b</sup>, Zoran Mijić<sup>a</sup>, Andrej Šoštarčić<sup>c</sup>

<sup>a</sup> Institute of Physics Belgrade, University of Belgrade, Pregrevica 118, 11080 Belgrade, Serbia

<sup>b</sup> Singidunum University, Danijelova 32, 11010 Belgrade, Serbia

<sup>c</sup> Institute of Public Health Belgrade, Bulevar Despota Stefana 54, 11000 Belgrade, Serbia

### HIGHLIGHTS

- Receptor models were applied for the purpose of VOC source apportionment.
- MVA methods were used for forecasting contributions from traffic and industry.
- Forecast was based on inorganic pollutant concentrations and meteorological data.
- Predicted values were consistent with the results of receptor modeling.
- The highest forecast accuracy was achieved with relative error of only 6%.

### ARTICLE INFO

#### Article history:

Received 19 December 2014

Received in revised form 21 March 2015

Accepted 22 March 2015

Available online xxxx

Editor: P. Kassomenos

#### Keywords:

VOC

PTR-MS

Receptor modeling

Forecasting

MVA

### ABSTRACT

In this study, advanced multivariate methods were applied for VOC source apportionment and subsequent short-term forecast of industrial- and vehicle exhaust-related contributions in Belgrade urban area (Serbia). The VOC concentrations were measured using PTR-MS, together with inorganic gaseous pollutants (NO<sub>x</sub>, NO, NO<sub>2</sub>, SO<sub>2</sub>, and CO), PM<sub>10</sub>, and meteorological parameters. US EPA Positive Matrix Factorization and Unmix receptor models were applied to the obtained dataset both resolving six source profiles. For the purpose of forecasting industrial- and vehicle exhaust-related source contributions, different multivariate methods were employed in two separate cases, relying on meteorological data, and on meteorological data and concentrations of inorganic gaseous pollutants, respectively. The results indicate that Boosted Decision Trees and Multi-Layer Perceptrons were the best performing methods. According to the results, forecasting accuracy was high (lowest relative error of only 6%), in particular when the forecast was based on both meteorological parameters and concentrations of inorganic gaseous pollutants.

© 2015 Published by Elsevier B.V.

### 1. Introduction

Volatile organic compounds (VOC) comprise a diverse group of species which are of concern due to their potentially detrimental impact on human health and the environment. Under sufficiently conducive meteorological conditions, they are important precursors in the formation of ozone, the abundant and reactive gaseous pollutant, capable of inducing oxidative damage to living cells (Kampa and Castanas, 2008). In addition, several VOC species such as styrene and benzene have been identified as toxic or mutagenic, while epidemiological evidence indicates that repetitive daily or intermittent exposure is associated with

numerous adverse health effects, mainly respiratory and heart disorders (Musselman and Korfmacher, 2014; Hsieh and Tsai, 2003). As regards environmental issues, the significant impact of VOC on climate change is observed in spite of their low concentrations in ambient air, and arises from their ability to form secondary aerosol and their properties as greenhouse gases (Chin and Batterman, 2012).

The ubiquity of VOC results from both biogenic and anthropogenic emissions, whereas the latter often dominate in heavily populated areas and are associated with vehicle transport, industrial activities, fossil fuel refining and distribution, biomass burning, solvent usage, etc. (Lee et al., 2002; Na et al., 2004). The abundance and spatial distribution of gaseous pollutants originating from remote emission sources mostly depend on their atmospheric lifetimes (Jobson et al., 1999), whereas, in the case of locally generated pollution, this relationship is no longer sustained, and VOC levels and variability are mainly controlled by emission rates and meteorological factors (Liu et al., 2012).

\* Corresponding author at: Pregrevica 118, 11080 Belgrade, Serbia.

E-mail addresses: [andreja.stojic@ipb.ac.rs](mailto:andreja.stojic@ipb.ac.rs) (A. Stojić), [dimitrije.maletic@ipb.ac.rs](mailto:dimitrije.maletic@ipb.ac.rs) (D. Maletić), [sstanic@singidunum.ac.rs](mailto:ssstanic@singidunum.ac.rs) (S. Stanišić Stojić), [zoran.mijic@ipb.ac.rs](mailto:zoran.mijic@ipb.ac.rs) (Z. Mijić), [andrej.sostaric@zdravlje.org.rs](mailto:andrej.sostaric@zdravlje.org.rs) (A. Šoštarčić).

Apart from being an important regional traffic hub with a population of 1.6 million residents, the capital of Serbia, Belgrade, and its suburban area is home to network of coal-fired power plants and different industrial facilities, such as the petrochemical complex, chemical plant, and oil refinery. In such complex urban environments with the prevalence of local emission sources, meteorological conditions play a significant role in the VOC mixing and distribution. The methods which simulate the variations of VOC emissions with sufficient reliability, based solely on meteorological data, can be used to forecast temporal distribution of VOC species, which is essential for development of efficient abatement strategies (Liu et al., 2012).

In this study several multivariate (MVA) methods were employed to assess the impact of traffic- and industry-related sources on VOC levels in Belgrade urban area, and predict their contribution dynamics. The petrochemical/chemical industry (PC) and vehicle exhaust emissions (VE) present one of the most significant emission sources. Their contributions were estimated using widely applied receptor models, Positive Matrix Factorization (PMF) and Unmix, based on the assumption that, in a complex VOC mixture, species emitted from the same source are statistically interrelated (Song et al., 2008). Subsequently, classification and regression MVA methods were applied in order to predict the source contribution dynamics on the basis of meteorological dataset and concentrations of inorganic gaseous pollutants (IG) – NO<sub>x</sub>, NO, NO<sub>2</sub>, SO<sub>2</sub> and CO. The supervised learning algorithms for classification and regression analyses were specifically designed within Toolkit for Multivariate Analysis (TMVA) (Hoecker et al., 2007) within the ROOT framework (Brun and Rademakers, 1997), for extensive data processing in high-energy physics, but their applications are not restricted to these requirements (Maletić et al., 2014). The best performing MVA methods were Boosted Decision Trees (BDT and BDTG), designed for the purpose of MiniBooNE neutrino experiment (Yang et al., 2005), and based on complex method of cuts, and Multi-Layer Perceptrons (MLP), based on artificial neural networks (ANN) (Rojas, 1996).

Nowadays, the forecasting of air pollutant concentrations is an essential issue in environmental research due to a wide range of potential benefits. Besides providing information for early public warnings to the susceptible populations, as well as assistance in the assessment of regulation policies, the accurate and reliable forecast could be useful for development of preventive approaches and considerable reduction in the number of measurement sites over the area. This study reveals that presented MVA methods can be successfully used for forecasting the contributions of different emission sources in the investigated area.

## 2. Materials and methods

The measurement site is located at the Institute of Public Health in Belgrade (44°49' N, 20°28' E), in the urban canyon street with heavy and slow traffic. Proton Transfer Reaction Mass Spectrometer (Standard PTR-quad-MS, Ionicon Analytik, GmbH, Austria) was used for on-line measurements of concentrations of 36 VOC-related masses in the period from January 22nd to March 24th 2014. A detailed description of the method is given elsewhere (Lindinger et al., 1998; de Gouw and Warneke, 2007). The inlet of the instrument, 3 m heated (70 °C) silcosteel line inner diameter 3 mm, was placed 3 m above ground. VOC data, with 0.5 s dwell time, and five control parameters (m/z 21, m/z 25, m/z 30, m/z 32, and m/z 37) were obtained in 24 s cycles.

Drift tube parameters included: pressure, ranging from 2.08 to 2.11 mbar; temperature, 60 °C; voltage, 600 V; E/N parameter, 145 Td providing reaction time of 90 μs. The count rate of H<sub>3</sub>O<sup>+</sup>H<sub>2</sub>O was 1 to 7% of the 5.1 · 10<sup>6</sup> counts s<sup>-1</sup> count rate of primary H<sub>3</sub>O<sup>+</sup> ions. The calibration was done according to Taipale et al. (2008). For this purpose, TO-15 Supelco gas mixture (m/z 57, m/z 79, m/z 93, m/z 107, and m/z 121) was diluted with ASGU 370-p HORIBA system zero air to five concentrations in the range from 0.5 to 100 ppb. Normalized sensitivities were in the range from 6.2 to 14.3 npcs ppb<sup>-1</sup>. Detection limit of 1-h

averaged VOC concentrations was less than 0.5 ppb, except for methanol (2.0 ppb) and acetone (1.1 ppb). Key m/z-signals in the dataset, identified using a method developed by Galbally et al. (2008), were observed for 29 out of 36 masses, and used for further analysis.

The concentrations of IG, PM<sub>10</sub>, and meteorological data (atmospheric pressure, temperature, humidity, precipitation, wind speed and direction) were obtained from the automatic monitoring station at the measurement site (Institute of Public Health Belgrade).

US EPA Unmix 6.0 (USEPA, 2007) and Positive Matrix Factorization (Version 3.0) (USEPA, 2008) receptor models were applied to the 1169 observations of 1-hour-averaged concentrations of 29 species in order to identify emission sources (Table 1). The usages of these models as well as the theoretical background are detailed in literature (Henry, 2003). Briefly, Unmix is based on an eigenvalue analysis and does not allow down weighting of individual data points (Henry, 1997), while PMF decomposes a matrix of ambient data into two matrices representing source contribution and source profile (Paatero and Tapper, 1994). A value equal to the half of the method detection limit (DL) for each variable was used for concentrations below the DL. The number of pollutants selected as Unmix and PMF input variables was chosen using a combination of trial and error with the general goal of maximizing the number of input variables that produced feasible and physically interpretable solutions and following additional fit diagnostics criteria (Chan et al., 2011). After selecting the base run, 100 bootstrap runs with R<sup>2</sup>-value of 0.6 were performed to evaluate the uncertainty of the PMF resolved profiles. In addition, PMF was run with different Fpeak values to explore the rotational freedom and reported results were for its value adjusted to 0.2.

Statistical analyses, including bivariate polar plot and bivariate cluster (k-means clustering, grouping similar conditions together) analysis, were performed with the statistical software environment R (Team, 2012), using the Openair package (Carslaw and Ropkins, 2012). The

**Table 1**

Basic statistics for measured parameters: VOC related masses [ppb], NO<sub>x</sub>, NO<sub>2</sub>, NO, SO<sub>2</sub> [μg m<sup>-3</sup>], and CO [mg m<sup>-3</sup>] concentrations.

| Parameter              | Mean   | Median | Min   | Max    | 10th  | 90th   | St. dev. |
|------------------------|--------|--------|-------|--------|-------|--------|----------|
| NO <sub>x</sub>        | 149.69 | 121.01 | 11.24 | 912.42 | 37.14 | 301.52 | 116.19   |
| NO <sub>2</sub>        | 62.94  | 54.96  | 8.86  | 239.09 | 21.36 | 115.61 | 38.17    |
| NO                     | 86.76  | 58.67  | 1.19  | 673.33 | 11.12 | 205.61 | 88.32    |
| CO                     | 0.68   | 0.59   | 0.16  | 3.42   | 0.36  | 1.10   | 0.38     |
| SO <sub>2</sub>        | 21.54  | 17.43  | 3.85  | 236.46 | 7.74  | 39.94  | 16.70    |
| Ethylbenzene           | 2.31   | 1.76   | <DL   | 36.93  | 0.37  | 4.63   | 2.41     |
| mp-Xylene              | 8.99   | 6.86   | <DL   | 124.62 | 1.41  | 17.25  | 9.52     |
| o-Xylene               | 1.88   | 1.46   | <DL   | 18.52  | 0.28  | 3.79   | 1.72     |
| m/z 41 (propylene)     | 1.89   | 1.66   | 0.34  | 19.88  | 0.80  | 2.94   | 1.43     |
| m/z 43                 | 4.87   | 4.42   | 1.27  | 28.40  | 2.32  | 7.84   | 2.52     |
| m/z 45 (acetaldehyde)  | 5.04   | 4.29   | 1.31  | 38.85  | 2.28  | 7.92   | 3.53     |
| m/z 47 (ethanol)       | 7.81   | 3.02   | <DL   | 177.33 | <DL   | 17.39  | 15.55    |
| m/z 57 (MTBE)          | 1.94   | 1.63   | 0.26  | 28.82  | 0.75  | 2.92   | 1.93     |
| m/z 59 (acetone)       | 7.16   | 5.67   | <DL   | 30.79  | 1.61  | 15.57  | 5.42     |
| m/z 61 (acetic acid)   | 4.85   | 4.48   | 1.36  | 25.98  | 2.58  | 7.24   | 2.36     |
| m/z 71                 | 0.63   | 0.58   | 0.11  | 5.32   | 0.29  | 0.94   | 0.39     |
| m/z 73                 | 0.87   | 0.78   | 0.17  | 7.89   | 0.46  | 1.32   | 0.52     |
| m/z 75                 | 1.28   | 0.97   | 0.26  | 45.29  | 0.54  | 1.80   | 2.09     |
| m/z 79 (benzene)       | 1.35   | 1.10   | 0.05  | 6.95   | 0.50  | 2.44   | 0.90     |
| m/z 81                 | 0.81   | 0.68   | 0.07  | 9.88   | 0.25  | 1.33   | 0.78     |
| m/z 83                 | 14.4   | 10.16  | 0.37  | 92.44  | 3.05  | 31.65  | 11.99    |
| m/z 85                 | 9.43   | 6.73   | 0.17  | 65.12  | 1.96  | 20.52  | 7.85     |
| m/z 87                 | 2.53   | 2.20   | 0.49  | 12.36  | 1.03  | 4.55   | 1.48     |
| m/z 93 (toluene)       | 3.36   | 2.63   | 0.19  | 29.66  | 1.15  | 6.11   | 2.62     |
| m/z 99                 | 0.49   | 0.43   | <DL   | 2.32   | 0.17  | 0.91   | 0.31     |
| m/z 101                | 1.25   | 1.05   | 0.37  | 5.34   | 0.58  | 2.33   | 0.71     |
| m/z 105 (styrene)      | 0.53   | 0.43   | 0.11  | 16.39  | 0.22  | 0.76   | 0.81     |
| m/z 121 (C9 aromatics) | 4.32   | 3.13   | 0.28  | 24.96  | 1.19  | 8.59   | 3.88     |
| m/z 137 (monoterpenes) | 0.89   | 0.65   | <DL   | 8.50   | 0.19  | 1.67   | 0.90     |

DL – detection limit.

results were used for analysis of source contribution dynamics, the impact of potential emission sources, as well as wind speed and direction, on the air quality at the measurement site.

The impact of planetary boundary layer (PBL) height on VOC source contribution dynamics was also taken into consideration. PBL height was obtained combining Raman Lidar system case study observations (Banks et al., 2014) performed within the framework of EARLINET network (Belgrade station), and calculations using MeteorInfo software (Wang, 2014) and GDAS1 (Global Data Assimilation System) data.

Subsequently, MVA methods were used for forecasting of PC and VE source contribution dynamics in two separate cases: they either used meteorological values as inputs, or meteorological values and IG concentrations, while the VOC distributions and evaluated VOC values were not used as inputs. In addition to this, all MVA methods training and testing were conducted once more with the additional input variable *i.e.*, previously predicted source contribution values. The results obtained this way have “Prev” suffix. All MVA methods were used both for classification, which served to differentiate between pollution indicators of high and low significance for the source contribution dynamics, and regression methods, which were used to obtain mapped functional behavior of dependency of the source contribution on the examined variables. A sample of events, each consisting of source contribution value and input (meteorological, or meteorological and IG concentration) data, was used to train and test methods. The MVA methods used in the analysis were: Boosted Decision Trees (BDT, BDTG), Artificial Neural Network Multilayer Perceptron (MLP), MLP with Bayesian Extension (MLPBNN), Support Vector Machine (SVM), Linear Discriminant (LD), Fisher Discriminant (Fisher), Multidimensional Probability Density Estimator Range Search Method (PDERS), Function Discrimination Analysis with Genetic Algorithm Converger (FDA\_GA), Likelihood Method and Function Discriminant Analysis (FDA).

### 3. Results and discussion

Both receptor models, PMF and Unmix resolved six-profile solution including 29 compounds, and for the purpose of this study, the profiles which correspond to VE and PC were analyzed and compared (Fig. 1). In depth analysis of all Unmix- and PMF-resolved profiles is presented in our previous study (Stojić et al., 2015). In the expanded seven-source solution, Unmix resolved two VE profiles instead of one, with total contribution of 31.2%, whereas one of them did not include majority of IG. Similarly, expansion of PMF model to seven profiles resulted in further division and three VE profiles, all comprising dominant portions of different species associated with vehicle emissions. The attempts to obtain five-profile solutions also failed to provide reasonable results.

The Unmix resolved source which can be attributed to VE ( $VE_{Unmix}$ ) exhibits very high correlations with related PMF resolved profiles (both  $VE_{PMF1}$  and  $VE_{PMF2}$ , as separated, and  $VE_{PMF}$  in total, summed as in Hopke et al., 2006), 0.83, 0.88, and 0.89, respectively (Fig. 2). The significant share of benzene, toluene, *o*-xylene, *m*-xylene and ethylbenzene is apportioned to these profiles, together with IG suggesting the relationship with combustion processes. Unlike gasoline, diesel emissions are associated with 15 times less CO, seven times more  $NO_x$  and 10–14 times less BTEX (Thornhill et al., 2010). The shares of CO and  $NO_x$  are in the same range, which together with considerable portions of benzene, toluene, and extremely high portions of *o*-xylene, *m*-xylene and ethylbenzene indicates that the observed pollutants mainly originate from gasoline combustion, at least in the surrounding of the measurement site. Toluene to benzene (T/B) ratio for the analyzed profiles ranges from 2.16 to 2.49, which complies with the results from previous studies on VE emissions in winter season (from 2 to 5) (Lough et al., 2005).

The estimated average contribution of  $VE_{Unmix}$  to total observed concentrations (27.6%) significantly exceeds the total contribution of two PMF resolved profiles,  $VE_{PMF1}$  and  $VE_{PMF2}$  (20.31%). This is probably due to the fact that significant shares of certain VOC species included

in Unmix solution, such as gasoline additive, methyl tertiary butyl ether (MTBE) and C9 aromatics, which are known to be tracers of mobile or gasoline evaporative emissions, were apportioned between PC and the profile assigned to gasoline evaporation in the PMF model solution.

Similarly, the compounds detected at *m/z* 71 (methyl vinyl ketone, methacrolein, isoprene oxidation products) and *m/z* 73 (methyl ethyl ketone, butanal) with moderate contributions to  $VE_{Unmix}$ , 29.8 and 26.0%, respectively, are not included in PMF profiles assigned to VE, while their dominant shares are apportioned to PC. Since both of the species are positively correlated with propylene, MTBE, benzene, toluene, and styrene (from 0.64 to 0.89), as well as with monoterpenes and isoprene (from 0.47 to 0.91), their origin can be recognized as anthropogenic in VE profiles, or biogenic in profiles related to PC, which contain certain amount of biogenic tracers. Finally, in Unmix resolved profiles, the dominant shares of benzene, toluene, and styrene are apportioned to VE source, whereas in PMF model solution these species mainly contribute to PC. Therefore, the estimated contribution of industrial emissions also differs, and is 7% higher for PMF than for Unmix resolved profile.

The contributions of all VE profiles exhibited a regular diurnal pattern, characterized by prominent morning and late afternoon peak (6:00–09:00 AM, 6:00–10:00 PM), which is consistent with the expected rush hour and accumulation of pollutants in the shallow boundary layer (Fig. 2) (Bon et al., 2011). The decrease in traffic intensity and expansion of daytime boundary layer result in lowest values of profile contributions in the afternoon (12:00–5:00 PM). The traffic load is significantly decreased on weekends, thus being compliant with the expected tendency in city's central zone.

The prevailing wind direction changed from NE in January to W, SW and E in March which was followed by gradual increase in contribution of VE profiles, since the western sectors belong to central traffic-congested area. It should also be noted that the registered episode of extreme wind, blowing up to  $20.6 \text{ m s}^{-1}$  from NE direction (from January, 30th to February, 2nd) had a significant impact on profile contributions, which suggests that the dominant share arises from local sources distributed around the measurement site, as expected. According to the results of bivariate cluster analysis between 55.0 and 64.4% of vehicle emissions are mainly related to locally generated pollution concentrated in the stagnant zone across the canyon street (Fig. 2).

As regards the PC, the significant decrease in contribution of all related profiles was observed in March, with the change in wind direction, since the major local source of petrochemical evaporation is Petrohemija, located in the industrial zone of Pančevo, about 13 km of air distance in the NE direction. It is one of the largest chemical industrial complexes in Southeastern Europe with annual production of more than six hundred thousand tons of propylene, 1,3-butadiene, MTBE, plastic and rubber polymers, and other petrochemicals. In compliance with this, the results of bivariate cluster analysis show that the contributions of industrial profiles are mainly associated with moderate wind blowing from the N/E sector (from 72.7 to 81.5%) (Fig. 2). The contribution of regional transport is estimated to be around 25%, as determined by using air back trajectory sector analysis (TSA) (Zhu et al., 2011) and PBL height (Stojić et al., 2015).

The PC profiles resolved by Unmix ( $PC_{Unmix}$ ) and PMF ( $PC_{PMF}$ ) exhibit relatively good correlation, particularly in domain of source contributions less than 1 (Fig. 2). They are distinguished mainly by significant portions of propylene, MTBE, benzene, toluene, styrene, and propionic acid (*m/z* 75) produced by the ethylene hydrocarboxylation. The presence of acetic acid, its fragments detected at *m/z* 43, and its intermediate precursor, acetaldehyde, can be associated with the emissions from a large Methanol and Acetic Acid Complex, Kikinda, located in the N/NE sector, about 100 km of air distance from the measurement site. Since the pollutants mainly originate from evaporative processes, gaseous oxides do not contribute to these profiles, excluding moderate share of CO apportioned to  $PC_{PMF}$ .

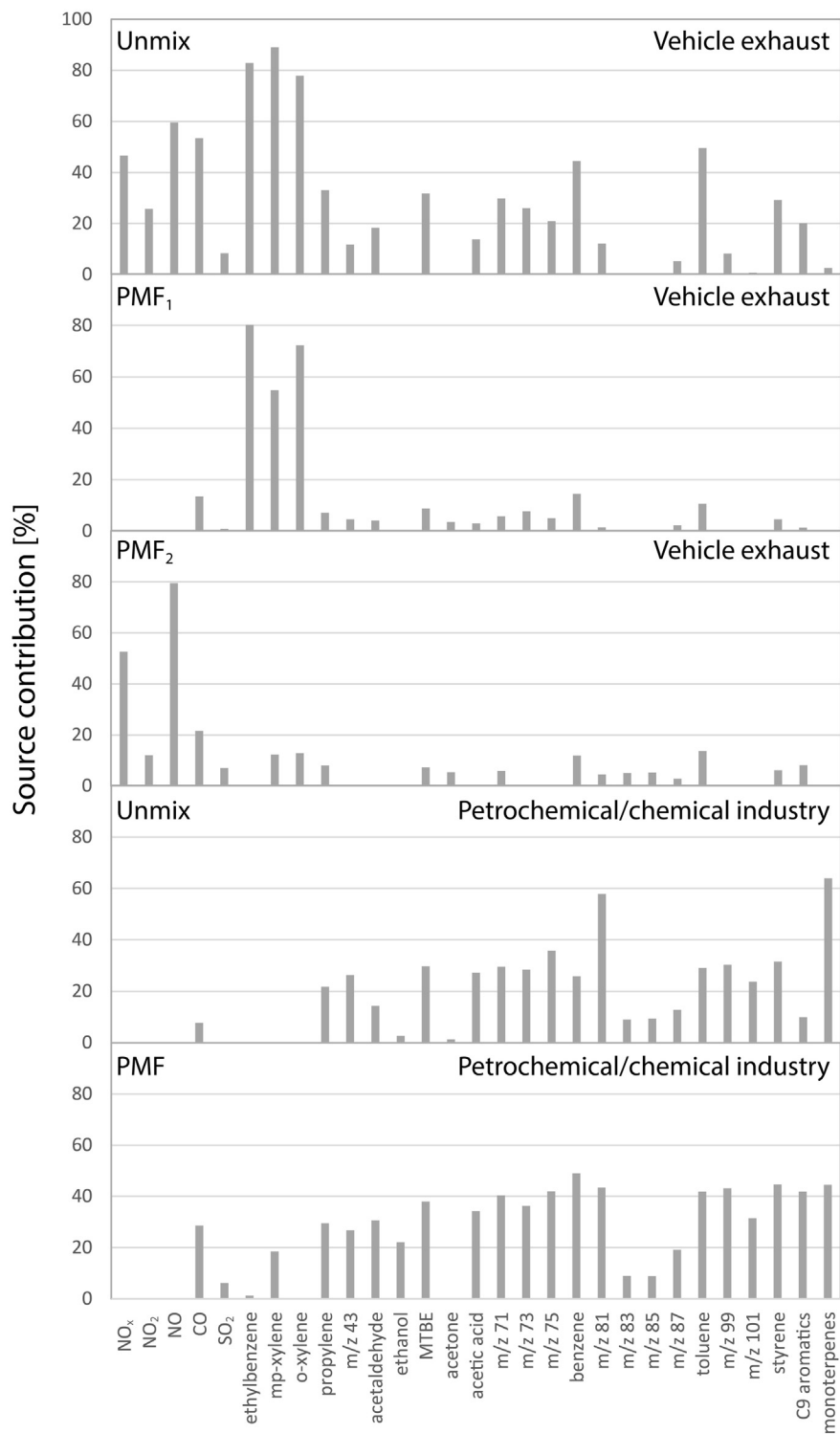


Fig. 1. Unmix- and PMF-resolved VE and PC source profiles [%].

Unlike traffic-related emissions, diurnal patterns of PC profiles exhibit a gradual increase during working hours (9:00 AM–6:00 PM) on weekdays and Saturdays, whereas on Sundays their contributions are decreased to minimum, as expected for industrial activities (Fig. 2).

Eventually, no model solution resolved profile which can be assigned exclusively to biogenic emissions, which clearly reflects the negligible significance of biosphere, particularly in urban areas and

winter season. Nevertheless, significant shares of monoterpenes, monoterpene oxidation products (m/z 81), and other species identified of probable biogenic origin (m/z 71, m/z 73, m/z 99, and m/z 101) are apportioned to industrial profiles. The reason for this is probably Botanical garden, a large area of vegetation located about 150 m from the measurement site, on the pathway of air masses coming from the NE and encompassing chemical and petrochemical industrial complexes.

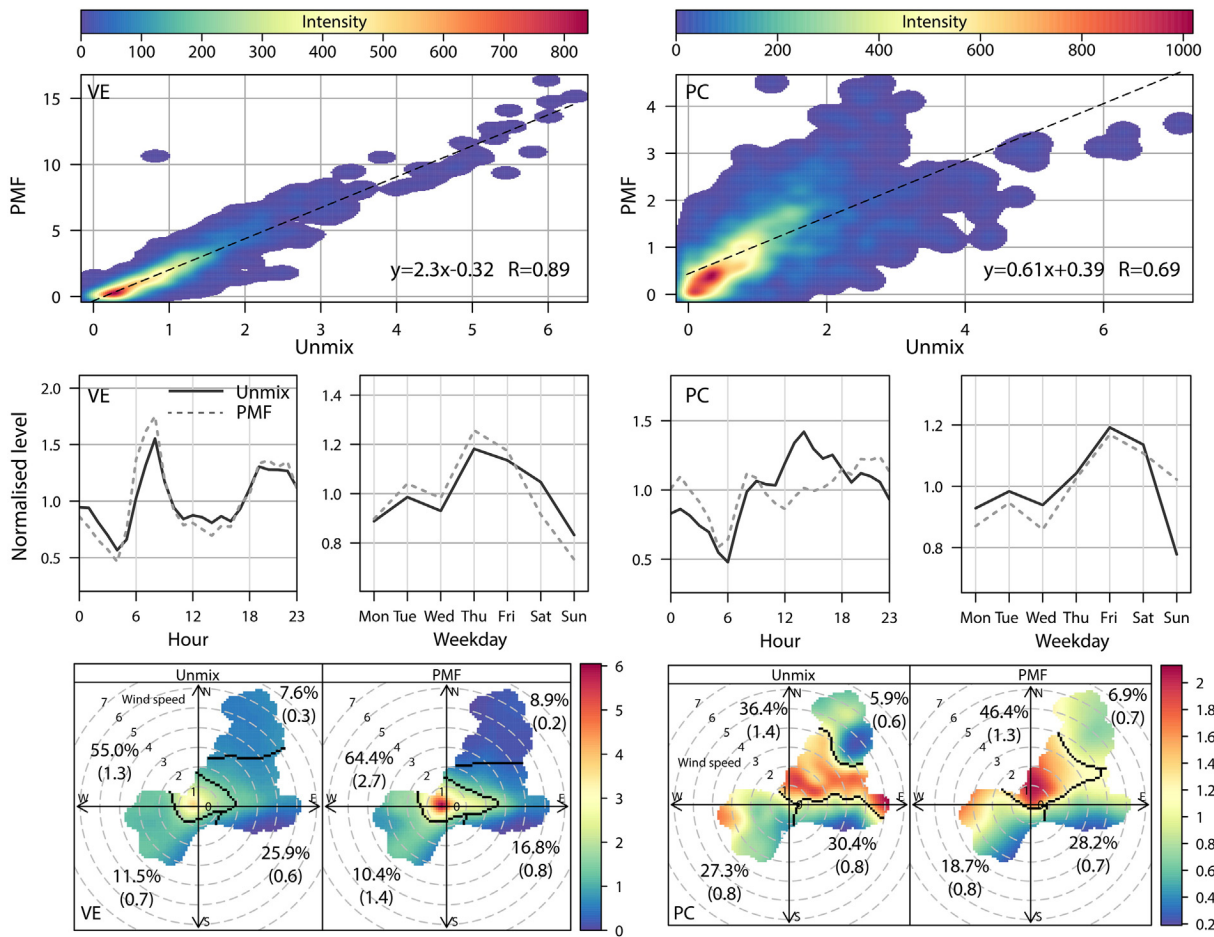


Fig. 2. Characteristics of PMF- and Unmix-resolved VE and PC normalized source contributions: intensity plot and linear fit (above); daily, weekly variations (middle), and bivariate and cluster plot (below).

3.1. Classification MVA methods

All MVA methods were applied for forecast of both industrial- (PMF and Unmix) and traffic-related (PMF<sub>2</sub> and Unmix) source contributions and prediction of potentially health-damaging events. For the purpose of this study the forecasting of both VE<sub>PMF1</sub> and VE<sub>PMF2</sub>, and VE<sub>PMF</sub> in total, was conducted, and herein presented results are related to VE<sub>PMF2</sub> only, to demonstrate how accurate forecasts can be produced.

The necessity to urge caution was estimated on the basis of the predicted source contributions, as follows: the values above 60% are considered to require the increased level of caution, whereas those exceeding

75% are considered as extremely high-alarm triggering values. Both values were chosen as arbitrary limits. Prior to method trainings and analyses of their performances, the input variables that did not exhibit significant linear correlations with source contributions were excluded. Also, one input variable was excluded for every two that were observed to be highly correlated. Therefore, the number of meteorological variables having significant impact on profile contributions is reduced to two per source. For both vehicle exhaust profiles, wind speed is ranked first, followed by temperature. For industrial profiles, the first and second ranked were temperature and wind speed (PC<sub>PMF</sub>), and pressure and temperature (PC<sub>Unmix</sub>), respectively.

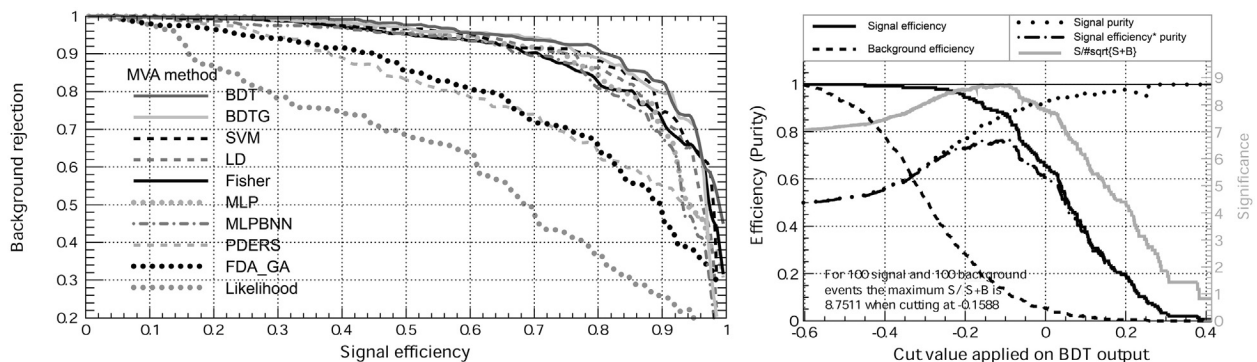


Fig. 3. ROC curve for various MVA methods used as VE<sub>PMF</sub> (25%) classifiers (left), and cut efficiencies and optimum cut value for BDT method evaluating (right) on the basis of meteorological data only.

**Table 2**

The best performing MVA methods for alarm triggering value (25%) and level of caution (40%) forecasting (10% of background inhibition in signal).

| Sources                   | M-IG-Prev <sup>a</sup> |            | M-IG   |            | M-Prev |            | M      |            |
|---------------------------|------------------------|------------|--------|------------|--------|------------|--------|------------|
|                           | Method                 | Sig. eff.  | Met.   | Sig. eff.  | Met.   | Sig. eff.  | Method | Sig. eff.  |
| VE <sub>PMF2</sub> (25%)  | MLPBNN                 | 0.997 (04) | BDT    | 0.999 (01) | BDT    | 0.814 (32) | BDT    | 0.813 (32) |
|                           | BDT                    | 0.989 (08) | LD     | 0.986 (09) | SVM    | 0.783 (34) | BDTG   | 0.755 (35) |
| VE <sub>Unmix</sub> (25%) | LD                     | 0.890 (25) | BDT    | 0.853 (29) | BDT    | 0.743 (36) | BDT    | 0.686 (38) |
|                           | BDT                    | 0.885 (26) | SVM    | 0.845 (29) | SVM    | 0.743 (36) | BDTG   | 0.656 (39) |
| PC <sub>PMF</sub> (25%)   | BDT                    | 0.859 (29) | BDT    | 0.769 (35) | BDT    | 0.832 (31) | BDT    | 0.621 (41) |
|                           | LD                     | 0.894 (26) | MLPBNN | 0.730 (37) | LD     | 0.861 (29) | BDTG   | 0.642 (40) |
| PC <sub>Unmix</sub> (25%) | BDT                    | 0.841 (30) | MLPBNN | 0.855 (29) | BDT    | 0.801 (33) | BDT    | 0.661 (39) |
|                           | LD                     | 0.875 (27) | BDT    | 0.787 (33) | LD     | 0.831 (31) | BDTG   | 0.707 (37) |
| VE <sub>PMF2</sub> (40%)  | MLPBNN                 | 0.988 (07) | MLPBNN | 0.999 (01) | BDT    | 0.700 (29) | BDT    | 0.677 (30) |
|                           | BDTG                   | 0.975 (10) | BDT    | 0.977 (09) | BDTG   | 0.683 (30) | BDTG   | 0.623 (31) |
| VE <sub>Unmix</sub> (40%) | BDT                    | 0.797 (26) | BDT    | 0.787 (26) | BDT    | 0.650 (31) | BDTG   | 0.540 (32) |
|                           | SVM                    | 0.795 (26) | MLPBNN | 0.825 (24) | SVM    | 0.600 (32) | BDT    | 0.575 (32) |
| PC <sub>PMF</sub> (40%)   | BDT                    | 0.866 (22) | BDT    | 0.760 (27) | BDT    | 0.847 (23) | BDT    | 0.650 (31) |
|                           | LD                     | 0.855 (23) | BDTG   | 0.757 (28) | Fisher | 0.833 (24) | MLPBNN | 0.593 (32) |
| PC <sub>Unmix</sub> (40%) | BDT                    | 0.852 (23) | BDT    | 0.757 (28) | BDT    | 0.826 (24) | BDTG   | 0.691 (30) |
|                           | SVM                    | 0.830 (24) | BDTG   | 0.727 (29) | SVM    | 0.803 (26) | BDT    | 0.626 (31) |

<sup>a</sup> Input variables: M – meteorological parameters, IG – inorganic gaseous pollutants, Prev – MVA method had information of forecast for previous hours.

The estimation of classification method performances was done using the Receiver Operating Characteristic (ROC) curve (Fig. 3, left). The method with the largest integral is considered the best performing method, provided that signal efficiency is high (close to 1), and the highest possible background rejection (the significant distinction between background levels and predicted source contributions) is achieved. In general, better performance was observed when both meteorological and IG concentrations were used (Table 2). As regards VE<sub>PMF2</sub>, the predicted contributions and background were almost completely separated when using both input variables, whereas BDT method based on meteorological data only, exhibited the best performance for prediction of higher values (Fig. 4). In comparison to this, somewhat poorer method predictions were obtained for VE<sub>Unmix</sub>, PC<sub>PMF</sub> and PC<sub>Unmix</sub>. This could suggest that certain variables which were not used as input data would assist to improve the predictive method performances.

As shown in Fig. 3 (right), the optimum cut value was determined on the basis of the value of significance. The comparison of method performance is conducted by evaluating signal efficiencies (Table 2). Thereby, more accurate predictions are obtained in cases where hysteresis-like curves, formed by source contribution and background efficiency curves, cover large area.

If only 10% of signal background inhibition is allowed for predictions based on meteorology and IG concentrations, all episodes of high VE<sub>PMF2</sub> contribution would be properly identified as alarm triggering values (Table 2). However, if only meteorological data were used, the percentage of the accurately identified alarm triggering values decrease to 81%.

The prediction of industry-related pollution episodes was efficient for both resolved profiles, PC<sub>PMF</sub> and PC<sub>Unmix</sub>, although the negligibly better solution was obtained for PC<sub>Unmix</sub> predicted on the basis of meteorological data only.

Table 2 shows that certain MVA methods are capable of forecasting the source contribution values which are considered to require the increased level of caution. The overall performance was satisfying, while the methods using meteorological and IG concentration data provided more accurate predictions.

According to the results, the forecast of vehicle exhaust-related pollution was more precise when using PMF-derived source contributions for classification. As regards industry-related pollution, the results are not straightforward to interpret. In case that MVA method had information of forecast for previous hours, most accurate prediction was mainly obtained for PMF source contributions, whereas in the case of forecast relying on input data exclusively, most accurate prediction was predominantly obtained for Unmix source contributions.

### 3.2. Regression MVA methods

Regression MVA methods were applied to interpret the dependency of the source contributions on the examined meteorological data, and both meteorological data and IG concentrations. As described in previous section, the statistical relationships were examined and certain number of variables was excluded from the input dataset.

Median and standard deviations were calculated respectively to be: 1.05 and 1.30 for VE<sub>PMF2</sub>, 1.03 and 0.94 for VE<sub>Unmix</sub>, 1.02 and 0.86 for

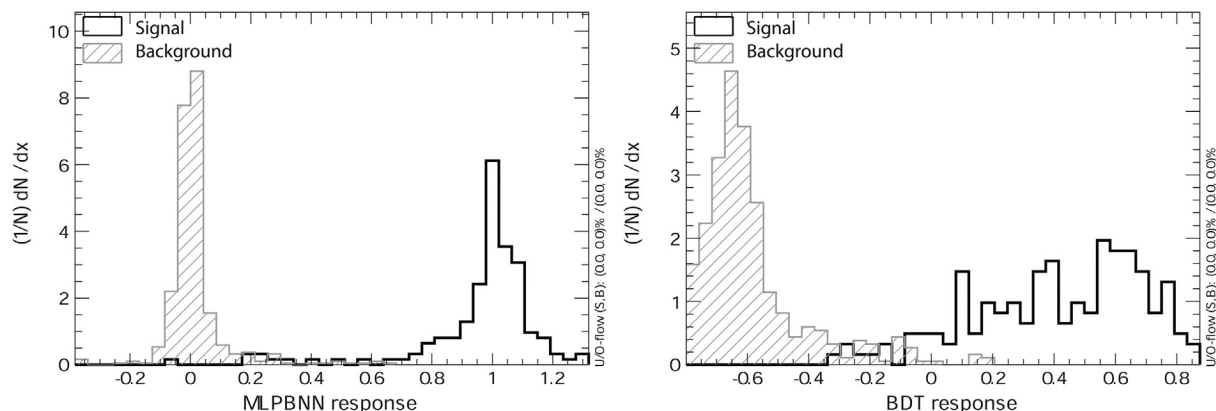
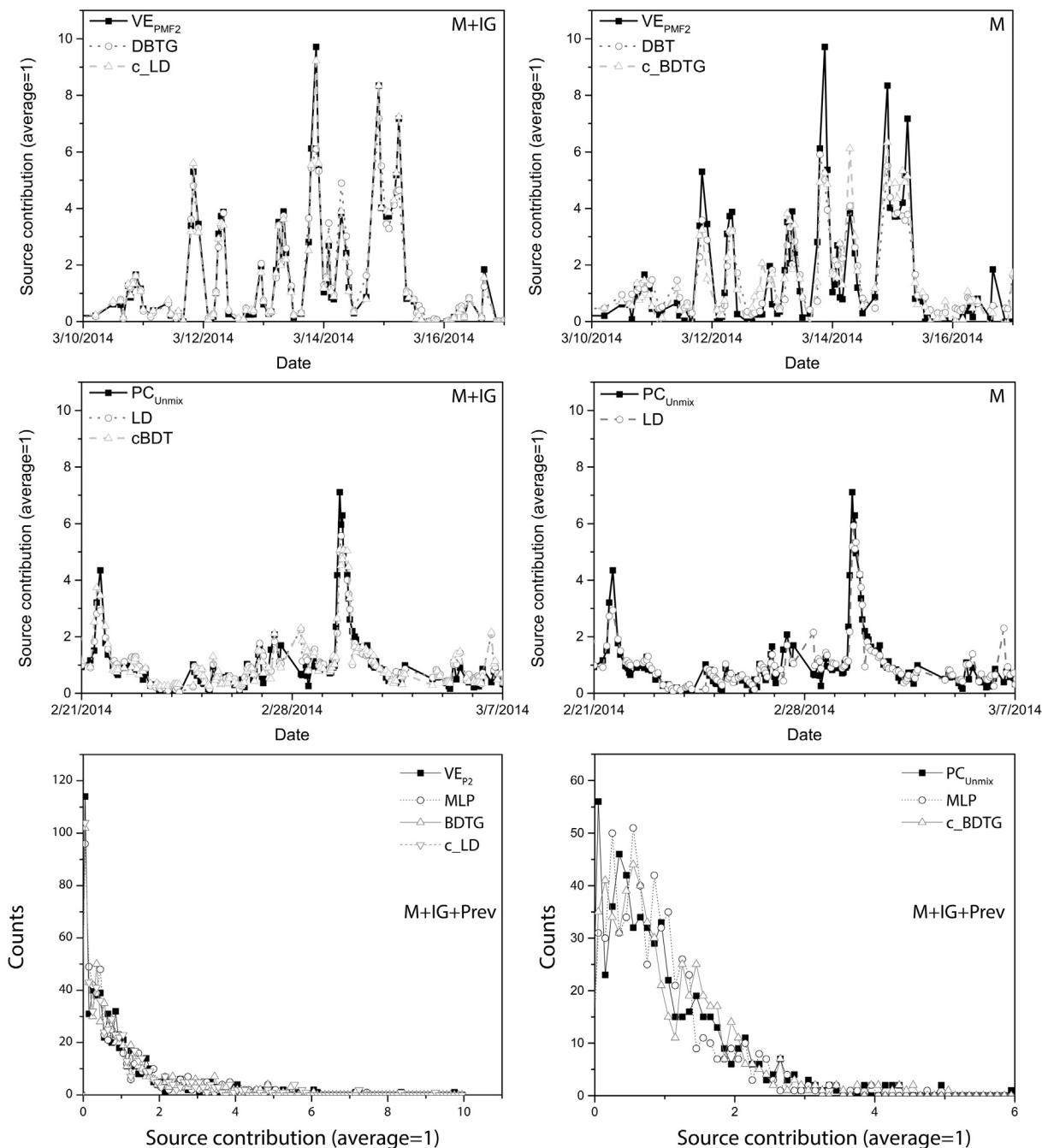


Fig. 4. VE<sub>PMF2</sub> TMVA response for classifiers: MLPBNN (left) and BDT (right). Meteorological parameters and inorganic gaseous pollutant concentrations were used as input data.

**Table 3**  
Absolute errors of best performing regression methods.

| Target              | M-IG-Prev |        | M-IG  |        | M-Prev |        | M     |        |
|---------------------|-----------|--------|-------|--------|--------|--------|-------|--------|
|                     | Value     | Method | Value | Method | Value  | Method | Value | Method |
| VE <sub>PMF2</sub>  | 0.07      | BDTG   | 0.06  | MLP    | 0.25   | BDT    | 0.35  | BDT    |
| VE <sub>PMF2</sub>  | 0.08      | c_LD   | 0.07  | c_LD   | 0.35   | c_BDTG | 0.48  | c_BDTG |
| VE <sub>Unmix</sub> | 0.22      | BDT    | 0.22  | c_BDTG | 0.24   | c_BDT  | 0.29  | BDTG   |
| VE <sub>Unmix</sub> | 0.22      | c_MLP  | 0.25  | LD     | 0.29   | BDTG   | 0.41  | BDT    |
| PC <sub>Unmix</sub> | 0.18      | LD     | 0.32  | c_BDTG | 0.24   | LD     | 0.35  | c_BDTG |
| PC <sub>Unmix</sub> | 0.23      | c_BDT  | 0.37  | BDT    | 0.26   | MLP    | 0.44  | BDT    |
| PC <sub>PMF</sub>   | 0.26      | LD     | 0.34  | BDT    | 0.31   | LD     | 0.43  | BDT    |
| PC <sub>PMF</sub>   | 0.31      | c_BDT  | 0.42  | c_MLP  | 0.33   | c_BDTG | 0.45  | c_BDTG |

PC<sub>PMF</sub> and 1.02 and 0.95 for PC<sub>Unmix</sub>. Low absolute errors obtained for the best performing regression methods (Table 3) indicate that source contributions were successfully evaluated, particularly when both meteorological and IG were used as input data. The same conclusion can be drawn from Fig. 5, in which PC<sub>Unmix</sub> and VE<sub>PMF2</sub>-derived source contributions and variations predicted using regression methods produce almost identical time-series plot. In contrast to this, VE<sub>Unmix</sub> appears to be more robust to changes in input variables, which suggests that it is less dependent on meteorological data. Similar to classification methods, most successful regression methods are the BDT and MLP based. In some MVA methods, corrections were done to adjust linear regression coefficients between source contributions and evaluated



**Fig. 5.** The comparison of receptor model-derived normalized source contributions and contributions obtained by the use of the best performing MVA methods. Meteorological parameters and inorganic gaseous pollutant concentrations (M + IG), meteorological parameters (M) and previously predicted source contribution values (Prev) are used as input data.

values to be closer to 1, using test samples only. If corrections are done using training sample, evaluated values can be considered as extension of training process. The MVA methods corrected this way are presented with prefix “c”.

As previously mentioned, the predictions based on meteorological data exclusively were less accurate, although still satisfying. In this case, minor differences in time-series plots of source contributions and regression method predictions as well as higher absolute errors were observed, particularly for PC<sub>PMF</sub>. In general, forecasting of industry-related contributions is more accurate when both meteorological data and IG concentrations were used (Fig. 5, middle).

In addition to previously mentioned indicators, the similarity of source contribution and evaluated values confirms that presented methods may become an efficient tool for forecasting of source contributions (Fig. 5, below).

Finally, it should be emphasized that the results are promising in both cases, for forecasting contributions of local origin as in the case of vehicle exhaust, as well as for forecasting contributions which are to certain extent (25%) associated with regional transport as in the case of industry-related source. Related to this, it can be assumed that slightly lower performance of MVA methods in the case of industry-related contribution forecast is probably associated with the impact of transported pollution.

#### 4. Conclusion

Given the fact that timely information on occurrence of dangerous air pollutant levels is very important for prevention of human health damage, particularly for the protection of vulnerable categories of people, design and implementation of early warning systems is an issue of high relevance in environmental science. The multivariate methods herein presented are capable of identifying emission sources, estimating their contributions and providing reliable prediction of source contribution dynamics which is the most important. In this study, two receptor models, Unmix and PMF, are used for the purpose of VOC source apportionment in Belgrade urban area, and the profiles identified as vehicle exhaust and industrial emissions with contributions ranging from 18 to 28%, are analyzed and compared. Subsequently, classification and regression MVA methods were used for prediction of the source contribution dynamics using registered meteorological parameters and IG as input data. According to the results, all examined methods show satisfying forecast capabilities, in the case of local source contributions as well as of contributions which are to certain extent (25%) associated with regional transport. Thereby, the best regression methods are considered to provide the most accurate prediction of hourly source contributions, closest possible to the receptor model-derived values with relative errors starting from 6%. The use of advanced MVA methods for forecasting of episodes of dangerous pollutant concentrations may support air quality management on a day-to-day basis, although it should be emphasized that, in this case, the reliable public warning highly depends on accurate meteorological forecast.

#### Acknowledgments

This study was carried out as part of project Nos. III43007 and OI171002, financed by the Ministry of Education, Science and Technological Development of the Republic of Serbia for the period 2011–15.

#### References

- Banks, R.F., Tiana-Alsina, J., Baldasano, J.M., Rocadenbosch, F., 2014. Retrieval of boundary layer height from lidar using extended Kalman filter approach, classic methods, and backtrajectory cluster analysis. *SPIE Remote Sensing. International Society for Optics and Photonics* (92420 F-92420 F, October).
- Bon, D.M., Ulbrich, I.M., de Gouw, J.A., Warneke, C., Kuster, W.C., Alexander, M.L., Vargas, O., 2011. Measurements of volatile organic compounds at a suburban ground site (T1) in Mexico City during the MILAGRO 2006 campaign: measurement comparison, emission ratios, and source attribution. *Atmos. Chem. Phys.* 11 (6), 2399–2421.
- Brun, R., Rademakers, F., 1997. ROOT—an object oriented data analysis framework. *Nucl. Instrum. Methods Phys. Res., Sect. A* 389, 81–86.
- Carlsaw, D.C., Ropkins, K., 2012. openair—an R package for air quality data analysis. *Environ. Model. Softw.* 27, 52–61.
- Chan, Y.C., Hawas, O., Hawker, D., Vowles, P., Cohen, D.D., Stelcer, E., Simpson, R., Golding, G., Christensen, E., 2011. Using multiple type composition data and wind data in PMF analysis to apportion and locate sources of air pollutants. *Atmos. Environ.* 45, 439–449.
- Chin, J.Y., Batterman, S.A., 2012. VOC composition of current motor vehicle fuels and vapors, and collinearity analyses for receptor modeling. *Chemosphere* 86, 951–958.
- de Gouw, J., Warneke, C., 2007. Measurements of volatile organic compounds in the earth's atmosphere using proton-transfer-reaction mass spectrometry. *Mass Spectrom. Rev.* 26, 223–257.
- Galbally, I.E., Hibberd, M.F., Lawson, S.J., Bentley, S.T., Cheng, M., Weeks, I.A., Gillett, R.W., Selleck, P.W., 2008. A study of VOCs during winter 2006 at Wagerup, Western Australia. Report to Alcoa World Alumina Australia. CSIRO, Aspendale.
- Henry, R.C., 1997. History and fundamentals of multivariate air quality receptor models. *Chemom. Intell. Lab. Syst.* 37, 37–42.
- Henry, R.C., 2003. Multivariate receptor modeling by N-dimensional edge detection. *Chemom. Intell. Lab. Syst.* 65, 179–189.
- Hoecker, A., Speckmayer, P., Stelzer, J., Therhaag, J., Von Toerne, E., Voss, H., Backes, M., Carli, T., Cohen, O., Christov, A., Dannheim, D., Danilowski, K., Henrot-Versille, S., Jachowski, M., Kraszewski, K., Krasznahorkay, A., Kruk, M., Mahalalel, Y., Ospanov, R., Prudent, X., Robert, A., Schouten, D., Tegenfeldt, F., Voigt, A., Voss, K., Wolter, M., Zemla, A., 2007. TMVA Users Guide – Toolkit for Multivariate Data Analysis, PoSACAT 040. <http://arxiv.org/abs/physics/0703039>.
- Hopke, P.K., Ito, K., Mar, T., Christensen, W.F., Eatough, D.J., Henry, R.C., Kim, E., Laden, F., Lall, R., Larson, T.V., Liu, H., Neas, L., Pinto, J., Stolzel, M., Suh, H., Paatero, P., Thurston, G.D., 2006. PM source apportionment and health effects: 1. Intercomparison of source apportionment results. *J. Expo. Sci. Environ. Epidemiol.* 16 (3), 275–286.
- Hsieh, C.C., Tsai, J.H., 2003. VOC concentration characteristics in Southern Taiwan. *Chemosphere* 50, 545–556.
- Institute of Public Health in Belgrade, d. [http://www.beoeko.com/?page\\_id=595&stanica=1](http://www.beoeko.com/?page_id=595&stanica=1) (Accessed: 29th August, 2014).
- Jobson, B.T., McKeen, S.A., Parrish, D.D., Fehsenfeld, F.C., Blake, D.R., Goldstein, A.H., Schauffler, S.M., Elkins, J.W., 1999. Trace gas mixing ratio variability versus lifetime in the troposphere and stratosphere: observations. *J. Geophys. Res. Atmos.* 104 (D13), 16091–16113.
- Kampa, M., Castanas, E., 2008. Human health effects of air pollution. *Environ. Pollut.* 151, 362–367.
- Lee, S.C., Chiu, M.Y., Ho, K.F., Zou, S.C., Wang, X., 2002. Volatile organic compounds (VOCs) in urban atmosphere of Hong Kong. *Chemosphere* 48, 375–382.
- Lindinger, W., Hansel, A., Jordan, A., 1998. On-line monitoring of volatile organic compounds at pptv levels by means of proton-transfer-reaction mass spectrometry (PTR-MS) medical applications, food control and environmental research. *Int. J. Mass Spectrom. Ion Process.* 173, 191–241.
- Liu, W.T., Hsieh, H.C., Chen, S.P., Chang, J.S., Lin, N.H., Chang, C.C., Wang, J.L., 2012. Diagnosis of air quality through observation and modeling of volatile organic compounds (VOCs) as pollution tracers. *Atmos. Environ.* 55, 56–63.
- Lough, G.C., Schauer, J.J., Lonneman, W.A., Allen, M.K., 2005. Summer and winter nonmethane hydrocarbon emissions from on-road motor vehicles in the Midwestern United States. *J. Air Waste Manage. Assoc.* 55, 629–646.
- Maletić, D.M., Udovičić, V.I., Banjanac, R.M., Joković, D.R., Dragić, A.L., Veselinović, N.B., Filipović, J.Z., 2014. Comparison of multivariate classification and regression methods for the indoor radon measurements. *Nucl. Technol. Radiat. Prot.* 29, 17–23.
- Musselman, R.C., Korfmacher, J.L., 2014. Ozone in remote areas of the Southern Rocky Mountains. *Atmos. Environ.* 82, 383–390.
- Na, K., Kim, Y.P., Moon, I., Moon, K.C., 2004. Chemical composition of major VOC emission sources in the Seoul atmosphere. *Chemosphere* 55, 585–594.
- Paatero, P., Tapper, U., 1994. Positive matrix factorization: a non-negative factor model with optimal utilization of error estimates of data values. *Environmetrics* 5, 111–126.
- Rojas, R., 1996. *Neural Networks*. Springer-Verlag, Berlin.
- Song, Y., Dai, W., Shao, M., Liu, Y., Lu, S., Kuster, W., Goldan, P., 2008. Comparison of receptor models for source apportionment of volatile organic compounds in Beijing, China. *Environ. Pollut.* 156, 174–183.
- Stojić, A., Stojić, S.S., Mijić, Z., Šoštarić, A., Rajšić, S., 2015. Spatio-temporal distribution of VOC emissions in urban area based on receptor modeling. *Atmos. Environ.* 106, 71–79.
- Taipale, R., Ruuskanen, T.M., Rinne, J., Kajos, M.K., Hakola, H., Pohja, T., Kulmala, M., 2008. Technical note: quantitative long-term measurements of VOC concentrations by PTR-MS—measurement, calibration, and volume mixing ratio calculation methods. *Atmos. Chem. Phys.* 8, 6681–6698.
- Team, R.C., 2012. R: a language and environment for statistical computing. <http://cran.case.edu/web/packages/dpLR/vignettes/timeseries-dpLR.pdf> (Accessed: 4th April, 2014).
- Thornhill, D.A., Williams, A.E., Onasch, T.B., Wood, E., Herndon, S.C., Kolb, C.E., Marr, L.C., 2010. Application of positive matrix factorization to on-road measurements for source apportionment of diesel- and gasoline-powered vehicle emissions in Mexico City. *Atmos. Chem. Phys.* 10 (8), 3629–3644.
- USEPA, 2007. EPA Unmix 6.0 Fundamentals and User guide. USEPA Office of Research and Development.
- USEPA, 2008. EPA Positive Matrix Factorization (PMF) 3.0 Fundamentals and User guide. USEPA Office of Research and Development.
- Wang, Y.Q., 2014. *MeteoInfo: GIS software for meteorological data visualization and analysis*. *Meteorol. Appl.* 21, 360–368.
- Yang, H.J., Roe, B.P., Zhu, J., 2005. Studies of boosted decision trees for MiniBooNE particle identification. *Nucl. Instrum. Methods Phys. Res., Sect. A* 555, 370–385.
- Zhu, L., Huang, X., Shi, H., Cai, X., Song, Y., 2011. Transport pathways and potential sources of PM<sub>10</sub> in Beijing. *Atmos. Environ.* 45, 594–604.



# First particle-by-particle measurement of emittance in the Muon Ionization Cooling Experiment

MICE Collaboration

D. Adams<sup>15</sup>, D. Adey<sup>25,34</sup>, R. Asfandiyarov<sup>13</sup>, G. Barber<sup>18</sup>, A. de Bari<sup>6</sup>, R. Bayes<sup>16</sup>, V. Bayliss<sup>15</sup>, R. Bertoni<sup>4</sup>, V. Blackmore<sup>18,a</sup>, A. Blondel<sup>13</sup>, J. Boehm<sup>15</sup>, M. Bogomilov<sup>1</sup>, M. Bonesini<sup>4</sup>, C. N. Booth<sup>20</sup>, D. Bowring<sup>25</sup>, S. Boyd<sup>22</sup>, T. W. Bradshaw<sup>15</sup>, A. D. Bross<sup>25</sup>, C. Brown<sup>15,23</sup>, G. Charnley<sup>14</sup>, G. T. Chatzitheodoridis<sup>16,21</sup>, F. Chignoli<sup>4</sup>, M. Chung<sup>10</sup>, D. Cline<sup>30</sup>, J. H. Cobb<sup>19</sup>, D. Colling<sup>18</sup>, N. Collomb<sup>14</sup>, P. Cooke<sup>17</sup>, M. Courthold<sup>15</sup>, L. M. Cremaldi<sup>28</sup>, A. DeMello<sup>26</sup>, A. J. Dick<sup>21</sup>, A. Dobbs<sup>18</sup>, P. Dornan<sup>18</sup>, F. Drielsma<sup>13</sup>, K. Dumbell<sup>14</sup>, M. Ellis<sup>23</sup>, F. Filthaut<sup>11,32</sup>, P. Franchini<sup>22</sup>, B. Freemire<sup>27</sup>, A. Gallagher<sup>14</sup>, R. Gamet<sup>17</sup>, R. B. S. Gardener<sup>23</sup>, S. Gourlay<sup>26</sup>, A. Grant<sup>14</sup>, J. R. Greis<sup>22</sup>, S. Griffiths<sup>14</sup>, P. Hanlet<sup>27</sup>, G. G. Hanson<sup>29</sup>, T. Hartnett<sup>14</sup>, C. Heidt<sup>29</sup>, P. Hodgson<sup>20</sup>, C. Hunt<sup>18</sup>, S. Ishimoto<sup>9</sup>, D. Jokovic<sup>12</sup>, P. B. Jurj<sup>18</sup>, D. M. Kaplan<sup>27</sup>, Y. Karadzhov<sup>13</sup>, A. Klier<sup>29</sup>, Y. Kuno<sup>8</sup>, A. Kurup<sup>18</sup>, P. Kyberd<sup>23</sup>, J.-B. Lagrange<sup>18</sup>, J. Langlands<sup>20</sup>, W. Lau<sup>19</sup>, D. Li<sup>26</sup>, Z. Li<sup>3</sup>, A. Liu<sup>25</sup>, K. Long<sup>18</sup>, T. Lord<sup>22</sup>, C. Macwaters<sup>15</sup>, D. Maletic<sup>12</sup>, B. Martlew<sup>14</sup>, J. Martyniak<sup>18</sup>, R. Mazza<sup>4</sup>, S. Middleton<sup>18</sup>, T. A. Mohayai<sup>27</sup>, A. Moss<sup>14</sup>, A. Muir<sup>14</sup>, I. Mullacrane<sup>14</sup>, J. J. Nebrensky<sup>23</sup>, D. Neuffer<sup>25</sup>, A. Nichols<sup>15</sup>, J. C. Nugent<sup>16</sup>, A. Oates<sup>14</sup>, D. Orestano<sup>7</sup>, E. Overton<sup>20</sup>, P. Owens<sup>14</sup>, V. Palladino<sup>5</sup>, M. Palmer<sup>24</sup>, J. Pasternak<sup>18</sup>, V. Pec<sup>20</sup>, C. Pidcott<sup>22,33</sup>, M. Popovic<sup>25</sup>, R. Preece<sup>15</sup>, S. Prestemon<sup>26</sup>, D. Rajaram<sup>27</sup>, S. Ricciardi<sup>15</sup>, M. Robinson<sup>20</sup>, C. Rogers<sup>15</sup>, K. Ronald<sup>21</sup>, P. Rubinov<sup>25</sup>, H. Sakamoto<sup>8,31</sup>, D. A. Sanders<sup>28</sup>, A. Sato<sup>8</sup>, M. Savic<sup>12</sup>, P. Snopok<sup>27</sup>, P. J. Smith<sup>20</sup>, F. J. P. Soler<sup>16</sup>, Y. Song<sup>2</sup>, T. Stanley<sup>15</sup>, G. Stokes<sup>14</sup>, V. Suezaki<sup>27</sup>, D. J. Summers<sup>28</sup>, C. K. Sung<sup>10</sup>, J. Tang<sup>2</sup>, J. Tarrant<sup>15</sup>, I. Taylor<sup>22</sup>, L. Tortora<sup>7</sup>, Y. Torun<sup>27</sup>, R. Tsenov<sup>1</sup>, M. Tucker<sup>14</sup>, M. A. Uchida<sup>18</sup>, S. Virostek<sup>26</sup>, G. Vankova-Kirilova<sup>1</sup>, P. Warburton<sup>14</sup>, S. Wilbur<sup>20</sup>, A. Wilson<sup>15</sup>, H. Witte<sup>24</sup>, C. White<sup>14</sup>, C. G. Whyte<sup>21</sup>, X. Yang<sup>30</sup>, A. R. Young<sup>21</sup>, M. Zisman<sup>26</sup>

<sup>1</sup> Department of Atomic Physics, St. Kliment Ohridski University of Sofia, Sofia, Bulgaria

<sup>2</sup> Institute of High Energy Physics, Chinese Academy of Sciences, Beijing, China

<sup>3</sup> Sichuan University, Chengdu, China

<sup>4</sup> Dipartimento di Fisica G. Occhialini, Sezione INFN Milano Bicocca, Milan, Italy

<sup>5</sup> Sezione INFN Napoli and Dipartimento di Fisica, Università Federico II, Complesso Universitario di Monte S. Angelo, Naples, Italy

<sup>6</sup> Sezione INFN Pavia and Dipartimento di Fisica, Pavia, Italy

<sup>7</sup> INFN Sezione di Roma Tre and Dipartimento di Matematica e Fisica, Università Roma Tre, Rome, Italy

<sup>8</sup> Department of Physics, Graduate School of Science, Osaka University, Toyonaka, Osaka, Japan

<sup>9</sup> High Energy Accelerator Research Organization (KEK), Institute of Particle and Nuclear Studies, Tsukuba, Ibaraki, Japan

<sup>10</sup> UNIST, Ulsan, Korea

<sup>11</sup> Nikhef, Amsterdam, The Netherlands

<sup>12</sup> Institute of Physics, University of Belgrade, Belgrade, Serbia

<sup>13</sup> DPNC, Section de Physique, Université de Genève, Geneva, Switzerland

<sup>14</sup> STFC Daresbury Laboratory, Daresbury, Cheshire, UK

<sup>15</sup> STFC Rutherford Appleton Laboratory, Harwell Oxford, Didcot, UK

<sup>16</sup> School of Physics and Astronomy, The University of Glasgow, Kelvin Building, Glasgow, UK

<sup>17</sup> Department of Physics, University of Liverpool, Liverpool, UK

<sup>18</sup> Blackett Laboratory, Department of Physics, Imperial College London, London, UK

<sup>19</sup> Department of Physics, University of Oxford, Denys Wilkinson Building, Oxford, UK

<sup>20</sup> Department of Physics and Astronomy, University of Sheffield, Sheffield, UK

<sup>21</sup> SUPA and the Department of Physics, University of Strathclyde, Glasgow, UK

<sup>22</sup> Department of Physics, University of Warwick, Coventry, UK

<sup>23</sup> Brunel University, Uxbridge, UK

<sup>24</sup> Brookhaven National Laboratory, Upton, NY, USA

<sup>25</sup> Fermilab, Batavia, IL, USA

<sup>26</sup> Lawrence Berkeley National Laboratory, Berkeley, CA, USA

<sup>27</sup> Illinois Institute of Technology, Chicago, IL, USA

<sup>28</sup> University of Mississippi, Oxford, MS, USA

<sup>29</sup> University of California, Riverside, CA, USA

<sup>30</sup> University of California, Los Angeles, CA, USA

<sup>31</sup> *Current address:* RIKEN, Wako, Japan

<sup>32</sup> *Also at* Radboud University, Nijmegen, The Netherlands

<sup>33</sup> *Current address:* Department of Physics and Astronomy, University of Sheffield, Sheffield, UK

<sup>34</sup> *Current address:* Institute of High Energy Physics, Chinese Academy of Sciences, Beijing, China

Received: 31 October 2018 / Accepted: 11 February 2019 / Published online: 21 March 2019

© The Author(s) 2019

**Abstract** The Muon Ionization Cooling Experiment (MICE) collaboration seeks to demonstrate the feasibility of ionization cooling, the technique by which it is proposed to cool the muon beam at a future neutrino factory or muon collider. The emittance is measured from an ensemble of muons assembled from those that pass through the experiment. A pure muon ensemble is selected using a particle-identification system that can reject efficiently both pions and electrons. The position and momentum of each muon are measured using a high-precision scintillating-fibre tracker in a 4 T solenoidal magnetic field. This paper presents the techniques used to reconstruct the phase-space distributions in the upstream tracking detector and reports the first particle-by-particle measurement of the emittance of the MICE Muon Beam as a function of muon-beam momentum.

## 1 Introduction

Stored muon beams have been proposed as the source of neutrinos at a neutrino factory [1,2] and as the means to deliver multi-TeV lepton-antilepton collisions at a muon collider [3,4]. In such facilities the muon beam is produced from the decay of pions generated by a high-power proton beam striking a target. The tertiary muon beam occupies a large volume in phase space. To optimise the muon yield for a neutrino factory, and luminosity for a muon collider, while maintaining a suitably small aperture in the muon-acceleration system requires that the muon beam be ‘cooled’ (i.e., its phase-space volume reduced) prior to acceleration. An alternative approach to the production of low-emittance muon beams through the capture of  $\mu^+\mu^-$  pairs close to threshold in electron-positron annihilation has recently been proposed [5]. To realise the luminosity required for a muon collider using this scheme requires the substantial challenges presented by the accumulation and acceleration of the intense positron beam, the high-power muon-production target, and the muon-capture system to be addressed.

A muon is short-lived, with a lifetime of  $2.2\mu\text{s}$  in its rest frame. Beam manipulation at low energy ( $\leq 1\text{ GeV}$ ) must be carried out rapidly. Four cooling techniques are in use at particle accelerators: synchrotron-radiation cooling [6]; laser cooling [7–9]; stochastic cooling [10]; and electron cooling [11]. In each case, the time taken to cool the beam is long compared to the muon lifetime. In contrast, ionization cooling is a process that occurs on a short timescale. A muon beam passes through a material (the absorber), loses energy, and is then re-accelerated. This cools the beam efficiently with modest decay losses. Ionization cooling is therefore the technique by which it is proposed to increase the number of particles within the downstream acceptance for a neutrino factory, and the phase-space density for a muon collider [12–14]. This technique has never been demonstrated experimentally and such a demonstration is essential for the development of future high-brightness muon accelerators or intense muon facilities.

The international Muon Ionization Cooling Experiment (MICE) has been designed [15] to perform a full demonstration of transverse ionization cooling. Intensity effects are negligible for most of the cooling channels conceived for the neutrino factory or muon collider [16]. This allows the MICE experiment to record muon trajectories one particle at a time. The MICE collaboration has constructed two solenoidal spectrometers, one placed upstream, the other downstream, of the cooling cell. An ensemble of muon trajectories is assembled offline, selecting an initial distribution based on quantities measured in the upstream particle-identification detectors and upstream spectrometer. This paper describes the techniques used to reconstruct the phase-space distributions in the spectrometers. It presents the first measurement of the emittance of momentum-selected muon ensembles in the upstream spectrometer.

## 2 Calculation of emittance

Emittance is a key parameter in assessing the overall performance of an accelerator [17]. The luminosity achieved by a collider is inversely proportional to the emittance of the colliding beams, and therefore beams with small emittance are required.

D. Cline, M. Zisman: Deceased.

<sup>a</sup> e-mail: [v.blackmore@imperial.ac.uk](mailto:v.blackmore@imperial.ac.uk)

A beam travelling through a portion of an accelerator may be described as an ensemble of particles. Consider a beam that propagates in the positive  $z$  direction of a right-handed Cartesian coordinate system,  $(x, y, z)$ . The position of the  $i^{\text{th}}$  particle in the ensemble is  $\mathbf{r}_i = (x_i, y_i)$  and its transverse momentum is  $\mathbf{p}_{Ti} = (p_{xi}, p_{yi})$ ;  $\mathbf{r}_i$  and  $\mathbf{p}_{Ti}$  define the coordinates of the particle in transverse phase space. The normalised transverse emittance,  $\varepsilon_N$ , of the ensemble approximates the volume occupied by the particles in four-dimensional phase space and is given by

$$\varepsilon_N = \frac{1}{m_\mu} \sqrt[4]{\det \mathcal{C}}, \tag{1}$$

where  $m_\mu$  is the rest mass of the muon,  $\mathcal{C}$  is the four-dimensional covariance matrix,

$$\mathcal{C} = \begin{pmatrix} \sigma_{xx} & \sigma_{xp_x} & \sigma_{xy} & \sigma_{xp_y} \\ \sigma_{xp_x} & \sigma_{p_x p_x} & \sigma_{yp_x} & \sigma_{p_x p_y} \\ \sigma_{xy} & \sigma_{yp_x} & \sigma_{yy} & \sigma_{yp_y} \\ \sigma_{xp_y} & \sigma_{p_x p_y} & \sigma_{yp_y} & \sigma_{p_y p_y} \end{pmatrix}, \tag{2}$$

and  $\sigma_{\alpha\beta}$ , where  $\alpha, \beta = x, y, p_x, p_y$ , is given by

$$\sigma_{\alpha\beta} = \frac{1}{N-1} \left( \sum_i^N \alpha_i \beta_i - \frac{(\sum_i^N \alpha_i)(\sum_i^N \beta_i)}{N} \right), \tag{3}$$

and  $N$  is the number of muons in the ensemble.

The MICE experiment was operated such that muons passed through the experiment one at a time. The phase-space coordinates of each muon were measured. An ensemble of muons that was representative of the muon beam was assembled using the measured coordinates. The normalised transverse emittance of the ensemble was then calculated by evaluating the sums necessary to construct the covariance matrix,  $\mathcal{C}$ , and using Eq. 1.

### 3 The Muon Ionization Cooling Experiment

The muons for MICE came from the decay of pions produced by an internal target dipping directly into the circulating proton beam of the ISIS synchrotron at the Rutherford Appleton Laboratory (RAL) [18, 19]. The burst of particles resulting from one target dip is referred to as a ‘spill’. A transfer line of nine quadrupoles, two dipoles and a superconducting ‘decay solenoid’ selected a momentum bite and transported the beam into the experiment [20]. The small fraction of pions that remained in the beam were rejected during analysis using the time-of-flight hodoscopes, TOF0 and TOF1, and Cherenkov counters that were installed in the MICE Muon Beam line upstream of the cooling experiment [21, 22]. A ‘diffuser’ was installed at the upstream end of the experiment to vary the initial emittance of the beam by introducing a changeable amount of tungsten and brass, which are high- $Z$  materials, into the beam path [20].

A schematic diagram of the experiment is shown in Fig. 1. It contained an absorber/focus-coil module sandwiched between two spectrometer-solenoid modules that provided a uniform magnetic field for momentum measurement. The focus-coil module had two separate windings that were operated with the same, or opposed, polarities. A lithium-hydride or liquid-hydrogen absorber was placed at the centre of the focus-coil module. An iron Partial Return Yoke (PRY) was installed around the experiment to contain the field produced by the solenoidal spectrometers (not shown in Fig. 1). The PRY was installed at a distance from the beam axis such that its effect on the trajectories of particles travelling through the experiment was negligible.

The emittance was measured upstream and downstream of the absorber and focus-coil module using scintillating-fibre tracking detectors [26] immersed in the solenoidal field provided by three superconducting coils E1, C, and E2. The

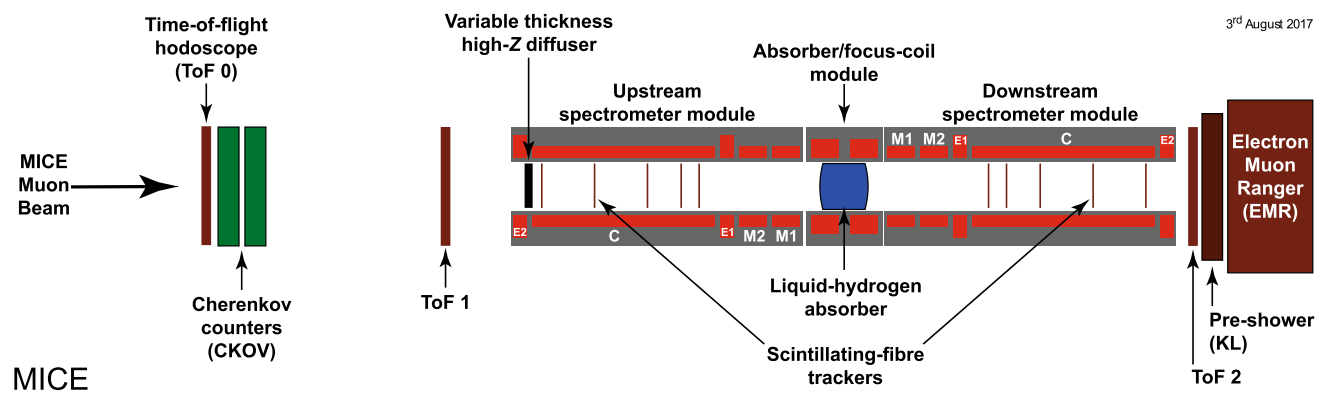


**Fig. 1** Schematic diagram of the MICE experiment. The red rectangles represent the coils of the spectrometer solenoids and focus-coil module. The individual coils of the spectrometer solenoids are labelled E1, C, E2, M1 and M2. The various detectors (time-of-flight hodoscopes

(TOF0, TOF1) [23, 24], Cherenkov counters [25], scintillating-fibre trackers [26], KLOE-Light (KL) calorimeter [20, 27], and Electron Muon Ranger (EMR) [28, 29]) are also represented. The Partial Return Yoke (PRY) is not shown

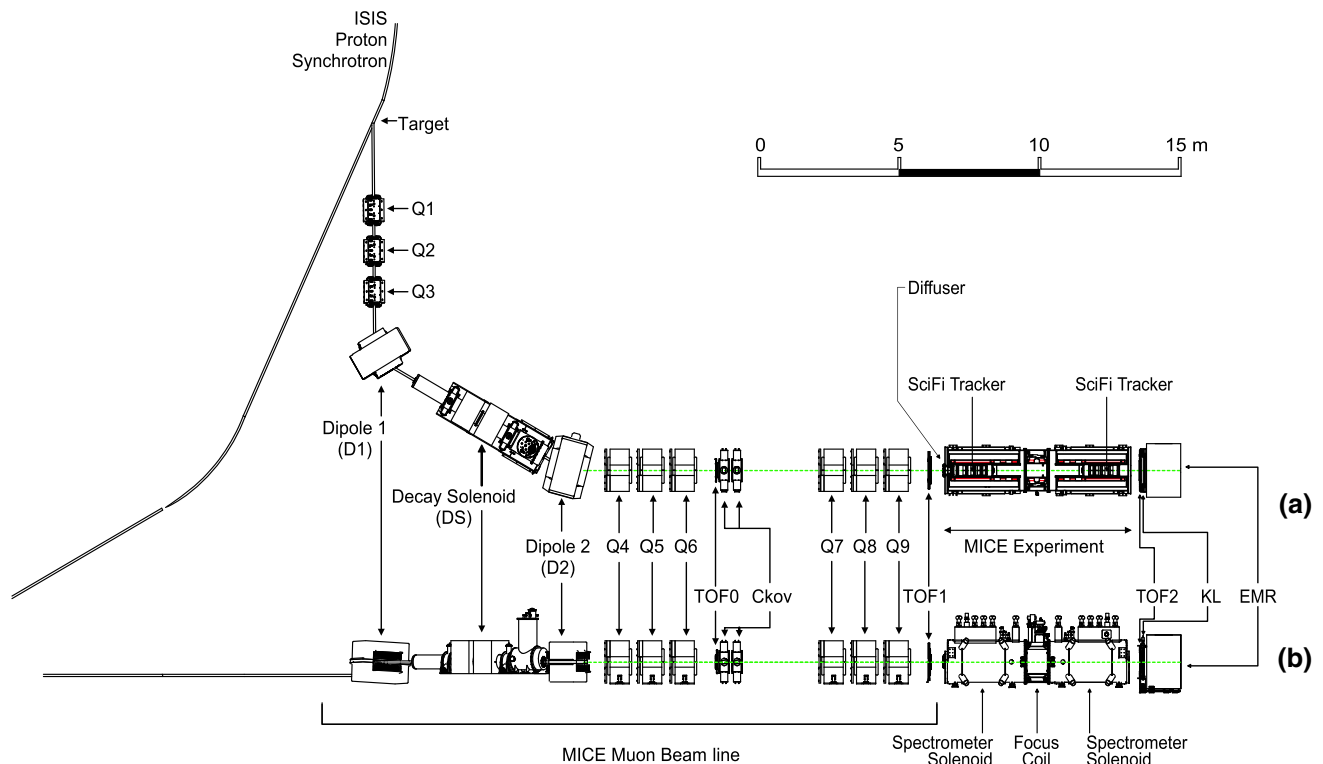


**Fig. 2** **a** Top and **b** side views of the MICE Muon Beam line, its instrumentation, and the experimental configuration. A titanium target dipped into the ISIS proton synchrotron and the resultant spill of particles was captured with a quadrupole triplet (Q1–3) and transported

trackers were used to reconstruct the trajectories of individual muons at the entrance and exit of the absorber. The trackers were each constructed from five planar stations of scintillating fibres, each with an active radius of 150 mm. The track parameters were reported at the nominal reference plane: the surface of the scintillating-fibre plane closest to the absorber [30]. Hall probes were installed on the tracker to measure the magnetic-field strength in situ. The instrumentation up- and downstream of the spectrometer module was used to select a pure sample of muons. The reconstructed tracks of the selected muons were then used to measure the muon-beam emittance at the upstream and downstream tracker reference planes. The spectrometer-solenoid modules also contained two superconducting ‘matching’ coils (M1, M2) that were used to match the optics between the uniform-field region and the neighbouring focus-coil module. The MICE coordinate system is such that the  $z$  axis is coincident with the beam direction, the  $y$  axis points vertically upward, and the  $x$  axis completes a right-handed co-ordinate system. This paper discusses the measurement of emittance using only the tracker and beam-line instrumentation upstream of the absorber. The diffuser was fully retracted for the data presented here, i.e. no extra material was introduced into the centre of the beam line, so that the incident particle distribution could be assessed.

through momentum-selecting dipoles (D1, D2). The quadrupole triplets (Q4–6, Q7–9) transported particles to the upstream spectrometer module. The time-of-flight of particles, measured between TOF0 and TOF1, was used for particle identification

#### 4 MICE Muon beam line

The MICE Muon Beam line is shown schematically in Fig. 2. It was capable of delivering beams with normalised transverse emittance in the range  $3 \lesssim \varepsilon_N \lesssim 10$  mm and mean momentum in the range  $140 \lesssim p_\mu \lesssim 240$  MeV/ $c$  with a root-mean-squared (RMS) momentum spread of  $\sim 20$  MeV/ $c$  [20] after the diffuser (Fig. 1).

Pions produced by the momentary insertion of a titanium target [18, 19] into the ISIS proton beam were captured using a quadrupole triplet (Q1–3) and transported to a first dipole magnet (D1), which selected particles of a desired momentum bite into the 5 T decay solenoid (DS). Muons produced in pion decay in the DS were momentum-selected using a second dipole magnet (D2) and focused onto the diffuser by a quadrupole channel (Q4–6 and Q7–9). In positive-beam running, a borated polyethylene absorber of variable thickness was inserted into the beam just downstream of the decay solenoid to suppress the high rate of protons that were produced at the target [31].

The composition and momentum spectra of the beams delivered to MICE were determined by the interplay between the two bending magnets D1 and D2. In ‘muon mode’, D2 was set to half the current of D1, selecting backward-going

muons in the pion rest frame. This produced an almost pure muon beam.

Data were taken in October 2015 in muon mode at a nominal momentum of 200 MeV/c, with ISIS in operation at 700 MeV. These data [32] are used here to characterise the properties of the beam accepted by the upstream solenoid with all diffuser irises withdrawn from the beam. The upstream E1-C-E2 coils in the spectrometer module were energised and produced a field of 4 T, effectively uniform across the tracking region, while all other coils were unpowered. Positively charged particles were selected due to their higher production rate in 700 MeV proton-nucleus collisions.

## 5 Simulation

Monte Carlo simulations were used to determine the accuracy of the kinematic reconstruction, to evaluate the efficiency of the response of the scintillating-fibre tracker, and to study systematic uncertainties. A sufficient number of events were generated to ensure that statistical uncertainties from the simulations were negligible in comparison to those of the data.

The beam impinging on TOF0 was modelled using G4beamline [33]. Particles were produced at the target using a parameterised particle-production model. These particles were tracked through the MICE Muon Beam line taking into account all material in and surrounding the beam line and using realistic models of the fields and apertures of the various magnets. The G4beamline simulation was tuned to reproduce the observed particle distributions at TOF0.

The MICE Analysis User Software (MAUS) [34] package was used to simulate the passage of particles from TOF0 through the remainder of the MICE Muon Beam line and through the solenoidal lattice. This simulation includes the response of the instrumentation and used the input distribution produced using G4beamline. MAUS was also used for offline reconstruction and to provide fast real-time detector reconstruction and data visualisation during MICE running. MAUS uses GEANT4 [35, 36] for beam propagation and the simulation of detector response. ROOT [37] was used for data visualisation and for data storage. The particles generated were subjected to the same trigger requirements as the data and processed by the same reconstruction programs.

## 6 Beam selection

Data were buffered in the front-end electronics and read out at the end of each spill [20]. For the reconstructed data presented here, the digitisation of analogue signals received from the detectors was triggered by a coincidence of signals in the PMTs serving a single scintillator slab in TOF1. Any slab in TOF1 could generate a trigger.

The following cuts were used to select muons passing through the upstream tracker:

- *One reconstructed space-point in TOF0 and TOF1* Each TOF hodoscope was composed of two perpendicular planes of scintillator slabs arranged to measure the  $x$  and  $y$  coordinates. A space-point was formed from the intersection of hits in the  $x$  and  $y$  projections. Figure 3a, b show the hit multiplicity in TOF0 plotted against the hit multiplicity in TOF1 for reconstructed data and reconstructed Monte Carlo respectively. The sample is dominated by events with one space-point in both TOF0 and TOF1. This cut removes events in which two particles enter the experiment within the trigger window.
- *Relative time-of-flight between TOF0 and TOF1,  $t_{\text{rel}}$ , in the range  $1 \leq t_{\text{rel}} \leq 6 \text{ ns}$*  The time of flight between TOF0 and TOF1,  $t_{01}$ , was measured relative to the mean positron time of flight,  $t_e$ . Figure 3c shows the relative time-of-flight distribution in data (black, circles) and simulation (filled histogram). All cuts other than the relative time-of-flight cut have been applied in this figure. The time-of-flight of particles relative to the mean positron time-of-flight is calculated as

$$t_{\text{rel}} = t_{01} - (t_e + \delta t_e) ,$$

where  $\delta t_e$  accounts for the difference in transit time, or path length travelled, between electrons and muons in the field of the quadrupole triplets [21]. This cut removes electrons from the selected ensemble as well as a small number of pions. The data has a longer tail compared to the simulation, which is related to the imperfect simulation of the longitudinal momentum of particles in the beam (see Sect. 7.1).

- *A single track reconstructed in the upstream tracker with a track-fit  $\chi^2$  satisfying  $\frac{\chi^2}{N_{\text{DOF}}} \leq 4$*   $N_{\text{DOF}}$  is the number of degrees of freedom. The distribution of  $\frac{\chi^2}{N_{\text{DOF}}}$  is shown in Fig. 3d. This cut removes events with poorly reconstructed tracks. Multi-track events, in which more than one particle passes through the same pixel in TOF0 and TOF1 during the trigger window, are rare and are also removed by this cut. The distribution of  $\frac{\chi^2}{N_{\text{DOF}}}$  is broader and peaked at slightly larger values in the data than in the simulation.
- *Track contained within the fiducial volume of the tracker* The radius of the track measured by the tracker,  $R_{\text{track}}$ , is required to satisfy  $R_{\text{track}} < 150 \text{ mm}$  to ensure the track does not leave and then re-enter the fiducial volume. The track radius is evaluated at 1 mm intervals between the stations. If the track radius exceeds 150 mm at any of these positions, the event is rejected.

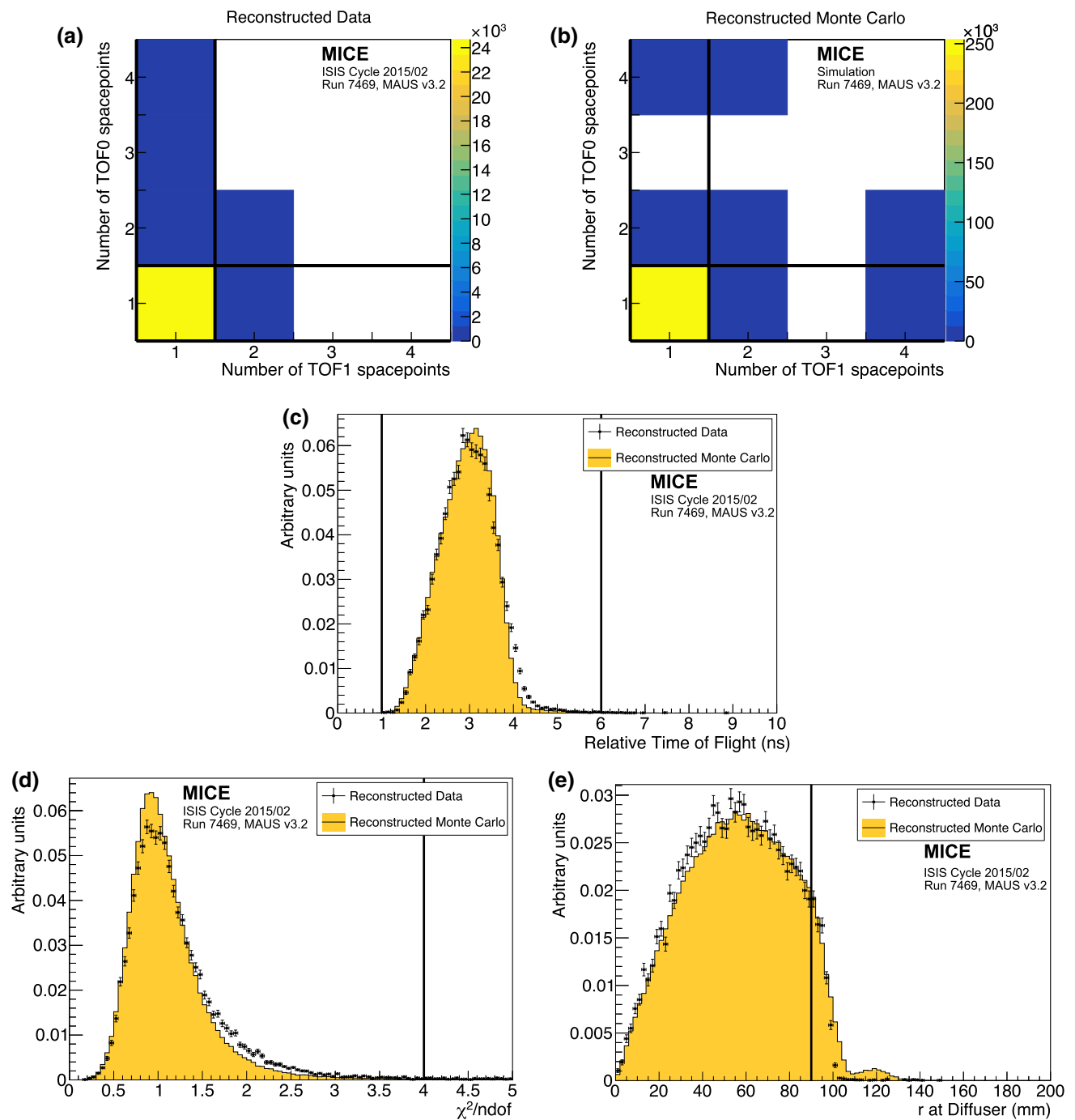


**Fig. 3** Distribution of the quantities that were used to select the sample used to reconstruct the emittance of the beam: **a** the number of space-points in TOF0 plotted against the number of space-points in TOF1 for reconstructed data, and **b** reconstructed simulation; **c** distribution of the relative time-of-flight,  $t_{rel}$ ; **d** distribution of  $\frac{\chi^2}{N_{DOF}}$ ; and **e** distribution

of  $R_{diff}$ . The 1D distributions show reconstructed data as solid (black) circles and reconstructed MAUS simulation as the solid (yellow) histogram. The solid (black) lines indicate the position of the cuts made on these quantities. Events enter these plots if all cuts other than the cut under examination are passed

– *Extrapolated track radius at the diffuser,  $R_{diff} \leq 90$  mm* Muons that pass through the annulus of the diffuser, which includes the retracted irises, lose a substantial amount of energy. Such muons may re-enter the track-

ing volume and be reconstructed but have properties that are no longer characteristic of the incident muon beam. The aperture radius of the diffuser mechanism (100 mm) defines the transverse acceptance of the beam injected

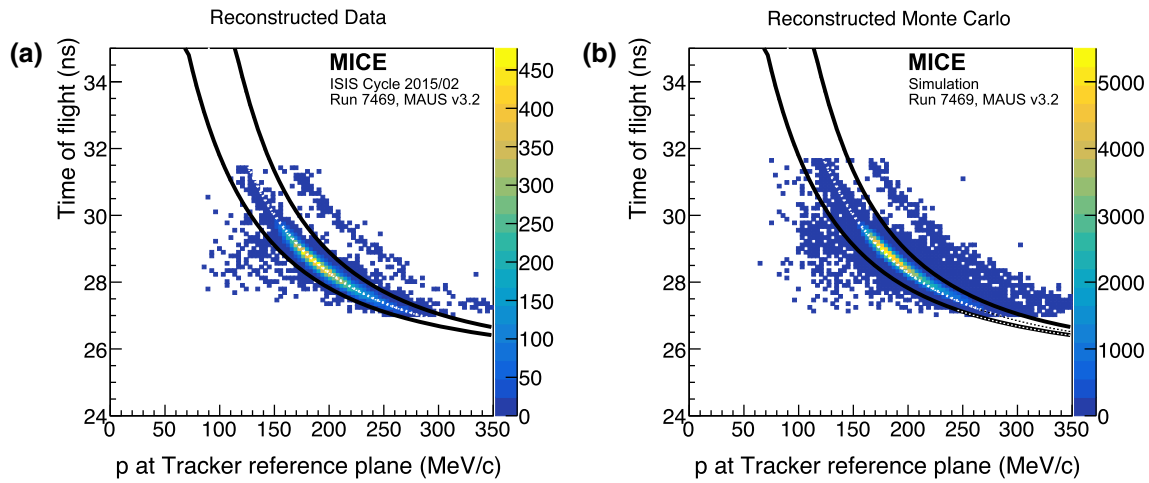


**Fig. 4** Time of flight between TOF0 and TOF1 ( $t_{01}$ ) plotted as a function of the muon momentum,  $p$ , measured in the upstream tracker. All cuts other than the muon hypothesis have been applied. Particles within the black lines are selected. The white dotted line is the trajectory of

a muon that loses the most probable momentum (20 MeV/c) between TOF1 and the tracker in **a** reconstructed data, and **b** reconstructed Monte Carlo

**Table 1** The number of particles that pass each selection criterion. A total of 24,660 particles pass all of the cuts

| Cut   | No. surviving particles | Cumulative surviving particles |
|---|-------------------------|--------------------------------|
| None  | 53 276                  | 53 276                         |
| One space-point in TOF0 and TOF1                                | 37 619                  | 37 619                         |
| Relative time of flight in range 1–6 ns                         | 37 093                  | 36 658                         |
| Single reconstructed track with $\frac{\chi^2}{N_{DOF}} \leq 4$ | 40 110                  | 30 132                         |
| Track within fiducial volume of tracker                         | 52 039                  | 29 714                         |
| Extrapolated track radius at diffuser $\leq 90$ mm              | 42 592                  | 25 310                         |
| Muon hypothesis   | 34 121                  | 24 660                         |
| All   | 24 660                  | 24 660                         |

into the experiment. Back-extrapolation of tracks to the exit of the diffuser yields a measurement of  $R_{diff}$  with a resolution of  $\sigma_{R_{diff}} = 1.7$  mm. Figure 3e shows the distribution of  $R_{diff}$ , where the difference between data and simulation lies above the accepted radius. These differences are due to approximations in modelling the outer material of the diffuser. The cut on  $R_{diff}$  accepts particles that passed at least  $5.9\sigma_{R_{diff}}$  inside the aperture limit of the diffuser.

- *Particle consistent with muon hypothesis* Figure 4 shows  $t_{01}$ , the time-of-flight between TOF0 and TOF1, plotted as a function of  $p$ , the momentum reconstructed by the upstream tracking detector. Momentum is lost between TOF1 and the reference plane of the tracker in the material of the detectors. A muon that loses the most probable momentum,  $\Delta p \simeq 20$  MeV/c, is shown as the dotted (white) line. Particles that are poorly reconstructed, or have passed through support material upstream of the tracker and have lost significant momentum, are excluded

by the lower bound. The population of events above the upper bound are ascribed to the passage of pions, or mis-reconstructed muons, and are also removed from the analysis.

A total of 24,660 events pass the cuts listed above. Table 1 shows the number of particles that survive each individual cut. Data distributions are compared to the distributions obtained using the MAUS simulation in Figs. 3 and 4. Despite minor disagreements, the agreement between the simulation and data is sufficiently good to give confidence that a clean sample of muons has been selected.

The expected pion contamination of the unselected ensemble of particles has been measured to be  $\leq 0.4\%$ [22]. Table 2 shows the number of positrons, muons, and pions in the MAUS simulation that pass all selection criteria. The criteria used to select the muon sample for the analysis presented here efficiently reject electrons and pions from the Monte Carlo sample.

**Table 2** The number of reconstructed electrons, muons, and pions at the upstream tracker that survive each cut in the Monte Carlo simulation. Application of all cuts removes almost all positrons and pions in the reconstructed Monte Carlo sample. In the Monte Carlo simulation, a total of 253,504 particles pass all of the cuts described in the text

| Cut  | $e$    | $\mu$   | $\pi$ | Total   |
|--|--------|---------|-------|---------|
| None   | 14,912 | 432,294 | 1610  | 463,451 |
| One space-point in TOF0 and TOF1                                       | 11,222 | 353,613 | 1213  | 376,528 |
| Relative Time of flight in range 1–6 ns                                | 757    | 369,337 | 1217  | 379,761 |
| Single reconstructed track with $\frac{\chi^2}{N_{\text{DOF}}} \leq 4$ | 10,519 | 407,276 | 1380  | 419,208 |
| Track within fiducial volume of tracker                                | 14,527 | 412,857 | 1427  | 443,431 |
| Tracked radius at diffuser $\leq 90$ mm                                | 11,753 | 311,076 | 856   | 334,216 |
| Muon hypothesis (above lower limit)                                    | 3225   | 362,606 | 411   | 367,340 |
| Muon hypothesis (below upper limit)                                    | 12,464 | 411,283 | 379   | 424,203 |
| Muon hypothesis (overall)  | 2724   | 358,427 | 371   | 361,576 |
| All  | 22     | 253,475 | 5     | 253,504 |

## 7 Results

### 7.1 Phase-space projections

The distributions of  $x$ ,  $y$ ,  $p_x$ ,  $p_y$ ,  $p_z$ , and  $p = \sqrt{p_x^2 + p_y^2 + p_z^2}$  are shown in Fig. 5. The total momentum of the muons that make up the beam lie within the range  $140 \lesssim |p| \lesssim 260 \text{ MeV}/c$ . The results of the MAUS simulation, which are also shown in Fig. 5, give a reasonable description of the data. In the case of the longitudinal component of momentum,  $p_z$ , the data are peaked to slightly larger values than the simulation. The difference is small and is reflected in the distribution of the total momentum,  $p$ . As the simulation began with particle production from the titanium target, any difference between the simulated and observed particle distributions would be apparent in the measured longitudinal and total momentum distributions. The scale of the observed disagreement is small, and as such the simulation adequately describes the experiment. The distributions of the components of the transverse phase space ( $x$ ,  $p_x$ ,  $y$ ,  $p_y$ ) are well described by the simulation. Normalised transverse emittance is calculated with respect to the means of the distributions (Eq. 2), and so is unaffected by this discrepancy.

The phase space occupied by the selected beam is shown in Fig. 6. The distributions are plotted at the reference surface of the upstream tracker. The beam is moderately well centred in the ( $x$ ,  $y$ ) plane. Correlations are apparent that couple the position and momentum components in the transverse plane. The transverse position and momentum coordinates are also seen to be correlated with total momentum. The correlation in the ( $x$ ,  $p_y$ ) and ( $y$ ,  $p_x$ ) plane is due to the solenoidal field, and is of the expected order. The dispersion and chromaticity of the beam are discussed further in Sect. 7.2.

### 7.2 Effect of dispersion, chromaticity, and binning in longitudinal momentum

Momentum selection at D2 introduces a correlation, dispersion, between the position and momentum of particles. Figure 7 shows the transverse position and momentum with respect to the total momentum,  $p$ , as measured at the upstream-tracker reference plane. Correlations exist between all four transverse phase-space co-ordinates and the total momentum.

Emittance is calculated in  $10 \text{ MeV}/c$  bins of total momentum in the range  $185 \leq p \leq 255 \text{ MeV}/c$ . This bin size was chosen as it is commensurate with the detector resolution. Calculating the emittance in momentum increments makes the effect of the optical mismatch, or chromaticity, small compared to the statistical uncertainty. The range of  $185 \leq p \leq 255 \text{ MeV}/c$  was chosen to maximise the number of particles in each bin that are not scraped by the aperture of the diffuser.

### 7.3 Uncertainties on emittance measurement

#### 7.3.1 Statistical uncertainties

The statistical uncertainty on the emittance in each momentum bin is calculated as  $\sigma_\epsilon = \frac{\epsilon}{\sqrt{2N}}$  [38–40], where  $\epsilon$  is the emittance of the ensemble of muons in the specified momentum range and  $N$  is the number of muons in that ensemble. The number of events per bin varies from  $\sim 4000$  for  $p \sim 190 \text{ MeV}/c$  to  $\sim 700$  for  $p \sim 250 \text{ MeV}/c$ .

### 7.4 Systematic uncertainties

#### 7.4.1 Uncorrelated systematic uncertainties

Systematic uncertainties related to the beam selection were estimated by varying the cut values by an amount correspond-

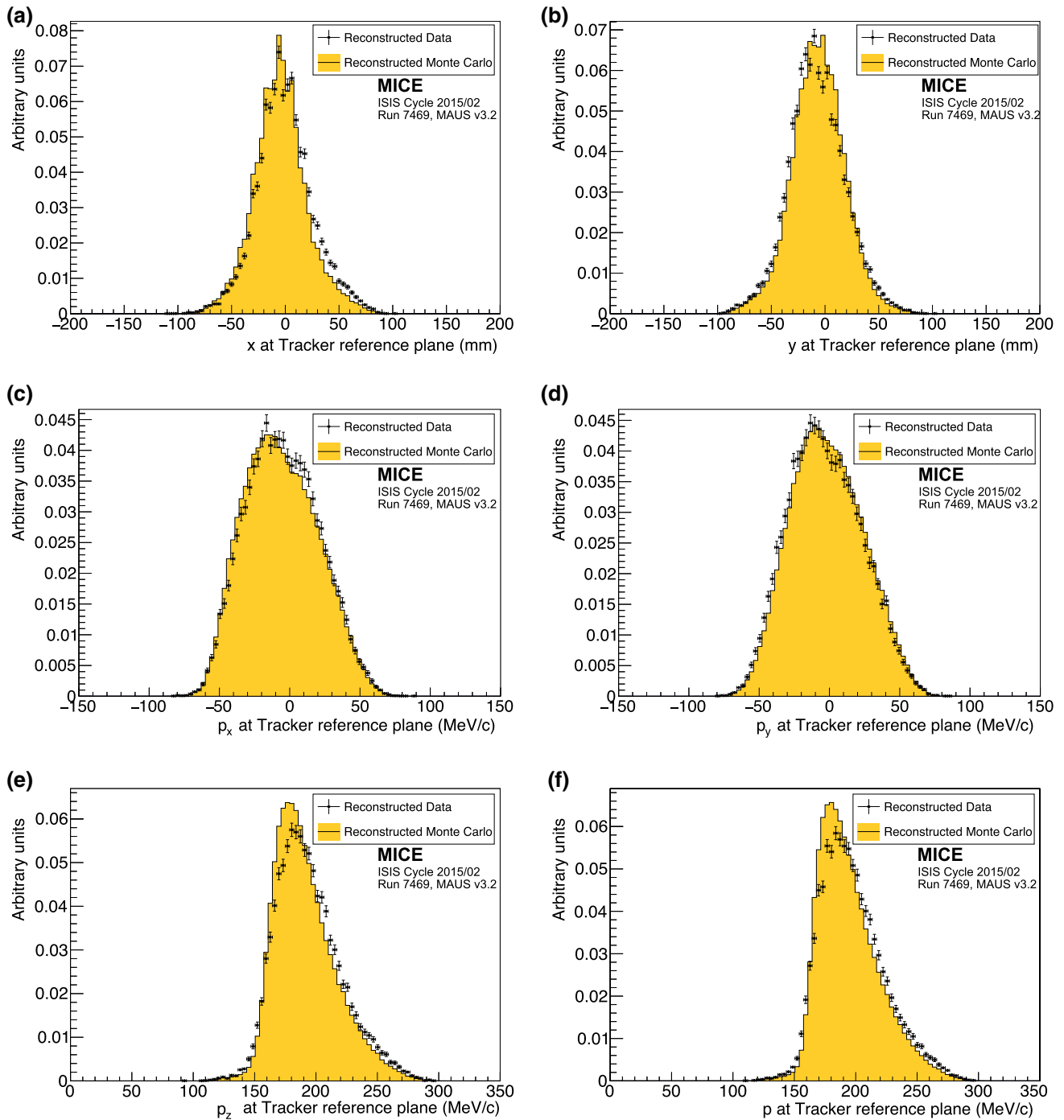


**Fig. 5** Position and momentum distributions of muons reconstructed at the reference surface of the upstream tracker: **a**  $x$ , **b**  $y$ , **c**  $p_x$ , **d**  $p_y$ , **e**  $p_z$ , and **f**  $p$ , the total momentum. The data are shown as the solid circles while the results of the MAUS simulation are shown as the yellow histogram

ing to the RMS resolution of the quantity in question. The emittance of the ensembles selected with the changed cut values were calculated and compared to the emittance calculated using the nominal cut values and the difference taken as the uncertainty due to changing the cut boundaries. The overall uncertainty due to beam selection is summarised in Table 3. The dominant beam-selection uncertainty is in the

selection of particles that successfully pass within the inner 90 mm of the diffuser aperture.

Systematic uncertainties related to possible biases in calibration constants were evaluated by varying each calibration constant by its resolution. Systematic uncertainties related to the reconstruction algorithms were evaluated using the MAUS simulation. The positive and negative deviations

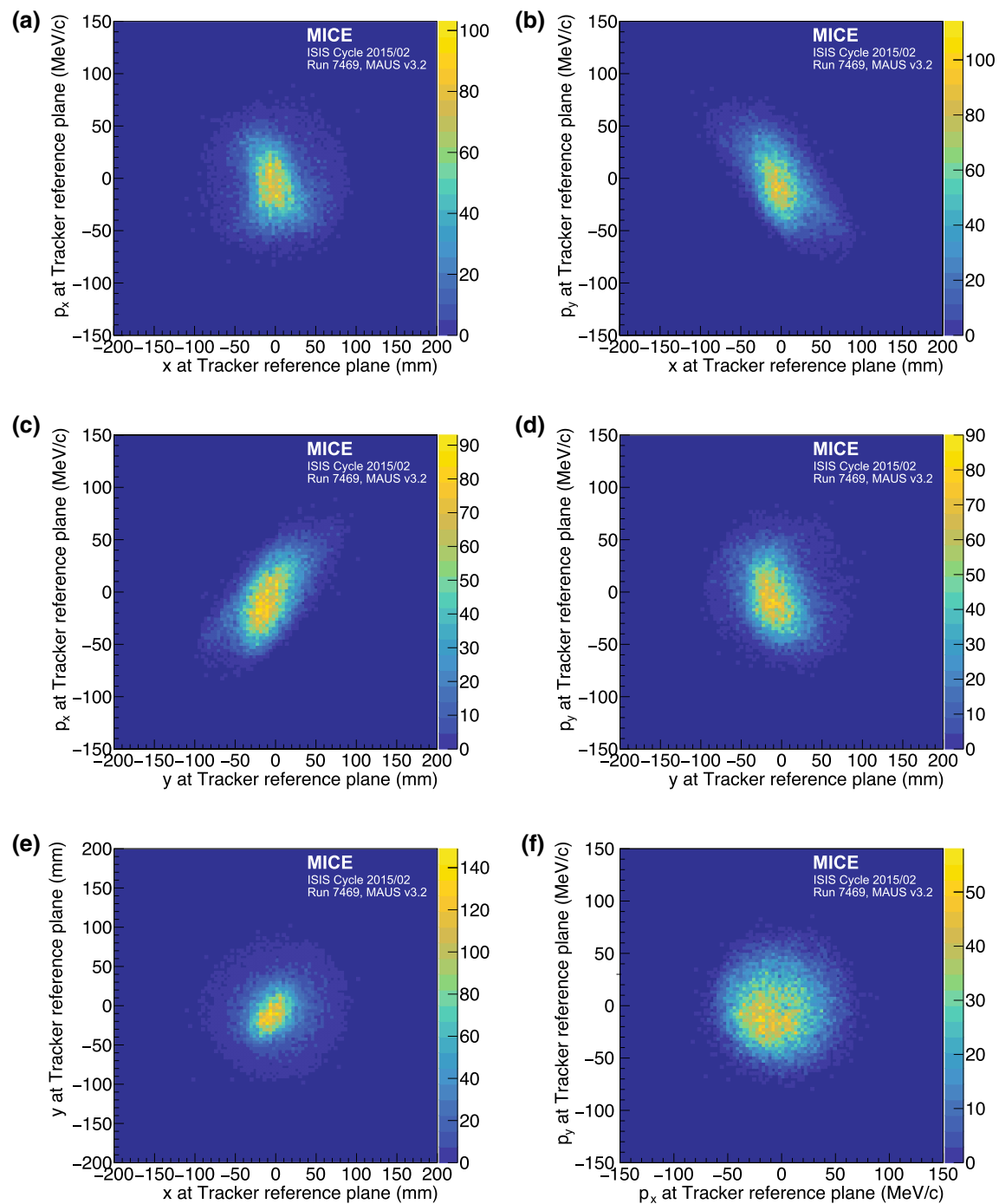


**Fig. 6** Transverse phase space occupied by selected muons transported through the MICE Muon Beam line to the reference plane of the upstream tracker. **a** ( $x, p_x$ ), **b** ( $x, p_y$ ), **c** ( $y, p_x$ ), **d** ( $y, p_y$ ), **e** ( $x, y$ ), and **f** ( $p_x, p_y$ )

from the nominal emittance were added in quadrature separately to obtain the total positive and negative systematic uncertainty. Sources of correlated uncertainties are discussed below.

#### 7.4.2 Correlated systematic uncertainties

Some systematic uncertainties are correlated with the total momentum,  $p$ . For example, the measured value of  $p$  dictates the momentum bin to which a muon is assigned for the emittance calculation. The uncertainty on the emittance reconstructed in each bin has been evaluated by allowing the

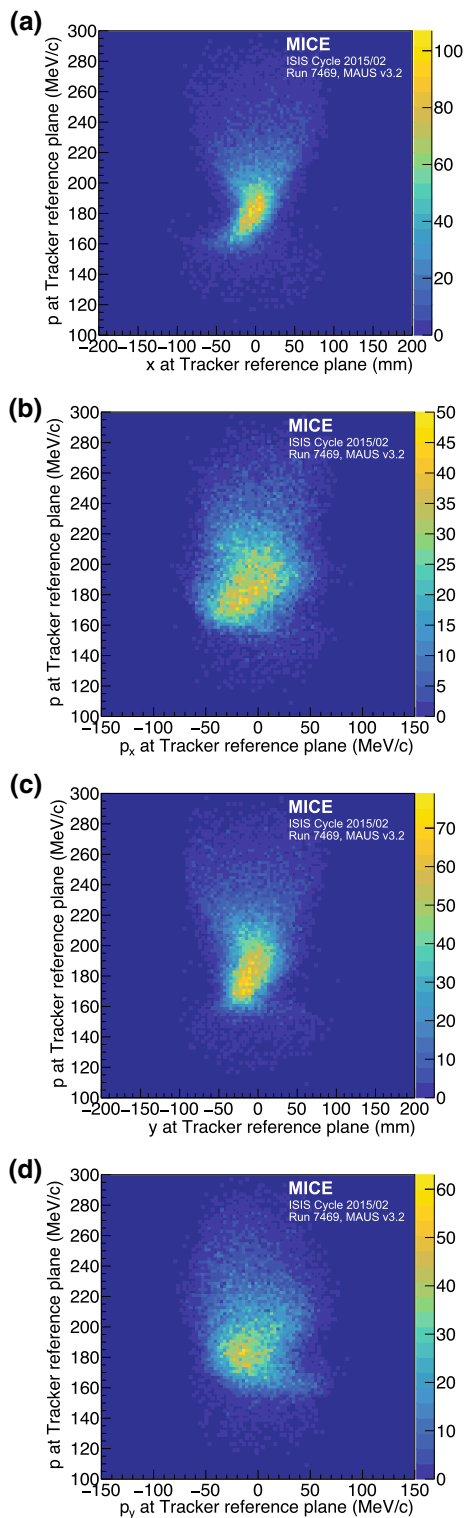


**Fig. 7** The effect of dispersion, the dependence of the components of transverse phase space on the momentum,  $p$ , is shown at the reference surface of the upstream tracker: **a**) ( $x, p$ ); **b**) ( $p_x, p$ ); **c**) ( $y, p$ ); **d**) ( $p_y, p$ )

momentum of each muon to fluctuate around its measured value according to a Gaussian distribution of width equal to

the measurement uncertainty on  $p$ . In Table 3 this uncertainty is listed as ‘Binning in  $p$ ’.

A second uncertainty that is correlated with total momentum is the uncertainty on the reconstructed  $x$ ,  $p_x$ ,  $y$ , and  $p_y$ . The effect on the emittance was evaluated with the same procedure used to evaluate the uncertainty due to binning in total momentum. This is listed as ‘Tracker resolution’ in Table 3.

Systematic uncertainties correlated with  $p$  are primarily due to the differences between the model of the apparatus used in the reconstruction and the hardware actually used in the experiment. The most significant contribution arises from the magnetic field within the tracking volume. Particle tracks are reconstructed assuming a uniform solenoidal field, with no fringe-field effects. Small non-uniformities in the magnetic field in the tracking volume will result in a disagreement between the true parameters and the reconstructed values. To quantify this effect, six field models (one optimal and five additional models) were used to estimate the deviation in reconstructed emittance from the true value under realistic conditions. Three families of field model were investigated, corresponding to the three key field descriptors: field scale, field alignment, and field uniformity. The values of these descriptors that best describe the Hall-probe measurements were used to define the optimal model and the uncertainty in the descriptor values were used to determine the  $1\sigma$  variations.

#### 7.4.3 Field scale

Hall-probes located on the tracker provided measurements of the magnetic field strength within the tracking volume at known positions. An optimal field model was produced with a scale factor of 0.49% that reproduced the Hall-probe measurements. Two additional field models were produced which used scale factors that were one standard deviation,  $\pm 0.03\%$ , above and below the nominal value.

#### 7.4.4 Field alignment

A field-alignment algorithm was developed based on the determination of the orientation of the field with respect to the mechanical axis of the tracker using coaxial tracks with  $p_T \approx 0$  [41]. The field was rotated with respect to the tracker by  $1.4 \pm 0.1$  mrad about the  $x$  axis and  $0.3 \pm 0.1$  mrad about the  $y$  axis. The optimal field model was created such that the simulated alignment is in agreement with the measurements. Two additional models that vary the alignment by one standard deviation were also produced.

#### 7.4.5 Field uniformity

A COMSOL [42] model of the field was used to generate the optimal model which includes the field generated by each coil

**Table 3** Emittance together with the statistical and systematic uncertainties and biases as a function of mean total momentum,  $\langle p \rangle$

| Source                                 | $\langle p \rangle$ (MeV/c) | 190                      | 200                      | 210                      | 220                      | 230                      | 240                      | 250                      |
|--|-----------------------------|--------------------------|--------------------------|--------------------------|--------------------------|--------------------------|--------------------------|--------------------------|
| Measured emittance (mm rad)            |                             | 3.40                     | 3.65                     | 3.69                     | 3.65                     | 3.69                     | 3.62                     | 3.31                     |
| Statistical uncertainty                |                             | $\pm 3.8 \times 10^{-2}$ | $\pm 4.4 \times 10^{-2}$ | $\pm 5.0 \times 10^{-2}$ | $\pm 5.8 \times 10^{-2}$ | $\pm 7.0 \times 10^{-2}$ | $\pm 8.4 \times 10^{-2}$ | $\pm 9.2 \times 10^{-2}$ |
| Beam selection:                        |                             |                          |                          |                          |                          |                          |                          |                          |
| Diffuser aperture                      |                             | $4.9 \times 10^{-2}$     | $5.3 \times 10^{-2}$     | $4.9 \times 10^{-2}$     | $4.7 \times 10^{-2}$     | $4.2 \times 10^{-2}$     | $11.0 \times 10^{-2}$    | $4.4 \times 10^{-2}$     |
|  |                             | $-3.5 \times 10^{-2}$    | $-5.1 \times 10^{-2}$    | $-5.7 \times 10^{-2}$    | $-5.0 \times 10^{-2}$    | $-3.5 \times 10^{-2}$    | $-5.0 \times 10^{-2}$    | $-9.6 \times 10^{-2}$    |
| $\frac{\chi^2}{\text{NDOF}} \leq 4$    |                             | $5.1 \times 10^{-3}$     | $2.0 \times 10^{-3}$     | $1.0 \times 10^{-2}$     | $4.1 \times 10^{-3}$     | $1.2 \times 10^{-3}$     | $5.5 \times 10^{-3}$     | $7.9 \times 10^{-3}$     |
|  |                             | $-4.8 \times 10^{-3}$    | $-1.3 \times 10^{-3}$    | $-1.8 \times 10^{-3}$    | $-3.3 \times 10^{-3}$    | $-2.8 \times 10^{-4}$    | $-6.5 \times 10^{-3}$    | $-4.7 \times 10^{-4}$    |
| Muon hypothesis                        |                             | $4.5 \times 10^{-3}$     | $2.2 \times 10^{-4}$     | $6.4 \times 10^{-3}$     | $3.1 \times 10^{-3}$     | $1.4 \times 10^{-3}$     | $2.6 \times 10^{-3}$     | $1.3 \times 10^{-3}$     |
|  |                             | $-3.2 \times 10^{-3}$    | $-6.8 \times 10^{-3}$    | $-8.8 \times 10^{-4}$    | $-4.7 \times 10^{-3}$    | $-1.1 \times 10^{-2}$    | $-6.7 \times 10^{-2}$    | $-4.1 \times 10^{-3}$    |
| Beam selection (Overall)               |                             | $4.9 \times 10^{-2}$     | $5.3 \times 10^{-2}$     | $5.0 \times 10^{-2}$     | $4.7 \times 10^{-2}$     | $4.2 \times 10^{-2}$     | $1.1 \times 10^{-1}$     | $4.5 \times 10^{-2}$     |
|  |                             | $-3.6 \times 10^{-2}$    | $-5.2 \times 10^{-2}$    | $-5.8 \times 10^{-2}$    | $-5.0 \times 10^{-2}$    | $-3.9 \times 10^{-2}$    | $-8.4 \times 10^{-2}$    | $-9.6 \times 10^{-2}$    |
| Binning in $p$                         |                             | $\pm 1.8 \times 10^{-2}$ | $\pm 2.1 \times 10^{-2}$ | $\pm 2.3 \times 10^{-2}$ | $\pm 2.9 \times 10^{-2}$ | $\pm 3.5 \times 10^{-2}$ | $\pm 4.3 \times 10^{-2}$ | $\pm 5.2 \times 10^{-2}$ |
| Magnetic field misalignment and scale: |                             |                          |                          |                          |                          |                          |                          |                          |
| Bias                                   |                             | $-1.3 \times 10^{-2}$    | $-1.4 \times 10^{-2}$    | $-1.5 \times 10^{-2}$    | $-1.6 \times 10^{-2}$    | $-1.6 \times 10^{-2}$    | $-1.7 \times 10^{-2}$    | $-1.6 \times 10^{-2}$    |
| Uncertainty                            |                             | $\pm 2.0 \times 10^{-4}$ | $\pm 2.9 \times 10^{-4}$ | $\pm 8.0 \times 10^{-4}$ | $\pm 4.8 \times 10^{-4}$ | $\pm 5.5 \times 10^{-4}$ | $\pm 4.8 \times 10^{-4}$ | $\pm 4.9 \times 10^{-4}$ |
| Tracker resolution                     |                             | $\pm 1.6 \times 10^{-3}$ | $\pm 2.1 \times 10^{-3}$ | $\pm 2.8 \times 10^{-3}$ | $\pm 3.8 \times 10^{-3}$ | $\pm 5.3 \times 10^{-3}$ | $\pm 7.0 \times 10^{-3}$ | $\pm 9.5 \times 10^{-3}$ |
| Total systematic uncertainty           |                             | $5.2 \times 10^{-2}$     | $5.7 \times 10^{-2}$     | $5.5 \times 10^{-2}$     | $5.6 \times 10^{-2}$     | $5.5 \times 10^{-2}$     | $11.7 \times 10^{-2}$    | $6.9 \times 10^{-2}$     |
|  |                             | $-4.0 \times 10^{-2}$    | $-5.6 \times 10^{-2}$    | $-6.2 \times 10^{-2}$    | $-5.8 \times 10^{-2}$    | $-5.2 \times 10^{-2}$    | $-9.5 \times 10^{-2}$    | $-11.0 \times 10^{-2}$   |
| Corrected emittance (mm rad)           |                             | 3.41                     | 3.66                     | 3.71                     | 3.67                     | 3.71                     | 3.65                     | 3.34                     |
| Total uncertainty                      |                             | $\pm 0.06$               | $\pm 0.07$               | $+0.07$                  | $\pm 0.08$               | $\pm 0.09$               | $+0.14$                  | $+0.12$                  |
|  |                             | $-0.08$                  | $-0.08$                  | $-0.08$                  | $-0.08$                  | $-0.08$                  | $-0.13$                  | $-0.14$                  |
| Total uncertainty (%)                  |                             | $+1.90$                  | $+1.96$                  | $+2.01$                  | $+2.19$                  | $+2.40$                  | $+3.97$                  | $+3.47$                  |
|  |                             | $-1.63$                  | $-1.94$                  | $-2.15$                  | $-2.34$                  | $-2.37$                  | $-3.49$                  | $-4.30$                  |

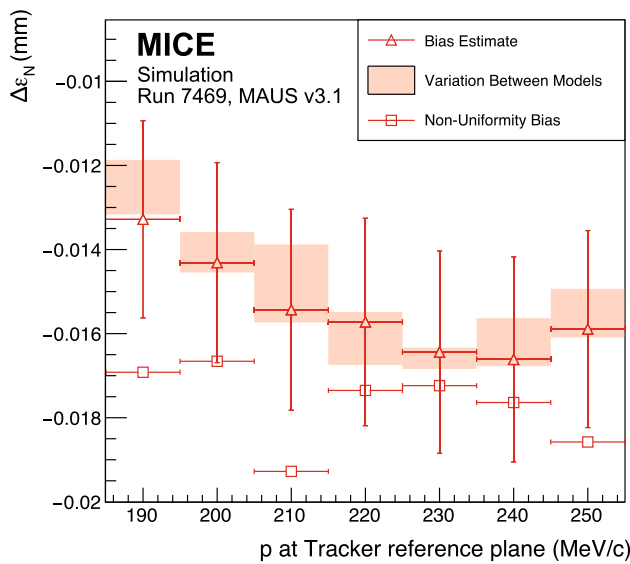


**Fig. 8** The systematic bias and uncertainty on the reconstructed emittance under different magnetic field model assumptions. The bias estimate (open triangles) includes the non-uniformity bias (open squares). The variation between the models (see text) is indicated by the shaded bands

using the ‘as-built’ parameters and the partial return yoke. A simple field model was created using only the individual coil geometries to provide additional information on the effect of field uniformity on the reconstruction. The values for the simple field model were normalised to the Hall-probe measurements as for the other field models. This represents a significant deviation from the COMSOL model, but demonstrates the stability of the reconstruction with respect to changes in field uniformity, as the variation in emittance between all field models is small (less than 0.002 mm).

For each of the 5 field models, multiple 2000-muon ensembles were generated for each momentum bin. The deviation of the calculated emittance from the true emittance was found for each ensemble. The distribution of the difference between the ensemble emittance and the true emittance was assumed to be Gaussian with mean  $\epsilon$  and variance  $s^2 = \sigma^2 + \theta^2$ , where  $\sigma$  is the statistical uncertainty and  $\theta$  is an additional systematic uncertainty. The systematic bias for each momentum bin was then calculated as [43]

$$\Delta\epsilon_N = \langle \epsilon \rangle - \epsilon_{\text{true}}, \tag{4}$$

where  $\epsilon_{\text{true}}$  is the true beam emittance in that momentum bin and  $\langle \epsilon \rangle$  is the mean emittance from the  $N$  ensembles. The systematic uncertainty was calculated assuming that the distribution of residuals of  $\epsilon_i$  from the mean,  $\langle \epsilon \rangle$ , satisfies a  $\chi^2$  distribution with  $N - 1$  degrees of freedom,

$$\chi_{N-1}^2 = \sum_i^N \frac{(\epsilon_i - \langle \epsilon \rangle)^2}{\sigma^2 + \theta^2}, \tag{5}$$

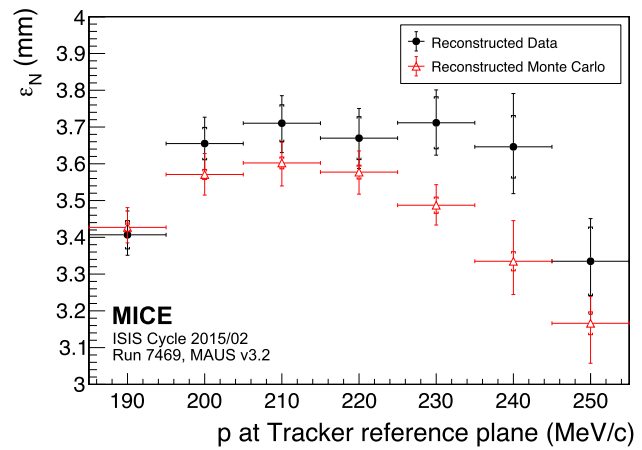


**Fig. 9** Normalised transverse emittance as a function of total momentum,  $p$ , for data (black, filled circle) and reconstructed Monte Carlo (red, open triangle). The inner error bars show the statistical uncertainty. The outer error bars show the quadratic sum of the statistical and systematic uncertainties

and  $\theta$  was estimated by minimising the expression  $(\chi_{N-1}^2 - (N - 1))^2$  [43].

The uncertainty,  $\theta$ , was consistent with zero in all momentum bins, whereas the bias,  $\Delta\epsilon_N$ , was found to be momentum dependent as shown in Fig. 8. The bias was estimated from the mean difference between the reconstructed and true emittance values using the optimal field model. The variation in the bias was calculated from the range of values reconstructed for each of the additional field models. The model representing the effects of non-uniformities in the field was considered separately due to the significance of the deviation from the optimal model.

The results show a consistent systematic bias in the reconstructed emittance of  $\approx -0.015$  mm that is a function of momentum (see Table 3). The absolute variation in the mean values between the models that were used was smaller than the expected statistical fluctuations, demonstrating the stability of the reconstruction across the expected variations in field alignment and scale. The effect of the non-uniformity model was larger but still demonstrates consistent reconstruction. The biases calculated from the optimal field model were used to correct the emittance values in the final calculation (Sect. 7.5).

### 7.5 Emittance

The normalised transverse emittance as a function of  $p$  is shown in Fig. 9. The emittance has been corrected for the systematic bias shown in Table 3. The uncertainties plotted are those summarised in Table 3, where the inner bars represent the statistical uncertainty and outer bars the total uncertainty. The emittance of the measured muon ensembles (black, filled circle) is approximately flat in the range

$195 \leq p \leq 245 \text{ MeV}/c$ , corresponding to the design momentum of the experiment. The mean emittance in this region is  $\approx 3.7 \text{ mm}$ . The emittance of the reconstructed Monte Carlo is consistently lower than that of the data, and therefore gives only an approximate simulation of the beam.

## 8 Conclusions

A first particle-by-particle measurement of the emittance of the MICE Muon Beam was made using the upstream scintillating-fibre tracking detector in a 4 T solenoidal field. A total of 24,660 muons survive the selection criteria. The position and momentum of these muons were measured at the reference plane of the upstream tracking detector. The muon sample was divided into  $10 \text{ MeV}/c$  bins of total momentum,  $p$ , from  $185\text{--}255 \text{ MeV}/c$  to account for dispersion, chromaticity, and scraping in apertures upstream of the tracking detector. The emittance of the measured muon ensembles is approximately flat from  $195 \leq p \leq 245 \text{ MeV}/c$  with a mean value of  $\approx 3.7 \text{ mm}$  across this region.

The total uncertainty on this measurement ranged from  $+1.9\%$  to  $-4.3\%$ , increasing with total momentum,  $p$ . As  $p$  increases, the number of muons in the reported ensemble decreases, increasing the statistical uncertainty. At the extremes of the momentum range, a larger proportion of the input beam distribution is scraped on the aperture of the diffuser. This contributes to an increase in systematic uncertainty at the limits of the reported momentum range. The systematic uncertainty introduced by the diffuser aperture highlights the need to study ensembles where the total momentum,  $p$ , is close to the design momentum of the beam line. The total systematic uncertainty on the measured emittance is larger than that on a future measurement of the ratio of emittance before and after an absorber. The measurement is sufficiently precise to demonstrate muon ionization cooling.

The technique presented here represents the first precise measurement of normalised transverse emittance on a particle-by-particle basis. This technique will be applied to muon ensembles up- and downstream of a low- $Z$  absorber, such as liquid hydrogen or lithium hydride, to measure emittance change across the absorber and thereby to study ionization cooling.

**Acknowledgements** The work described here was made possible by grants from Department of Energy and National Science Foundation (USA), the Istituto Nazionale di Fisica Nucleare (Italy), the Science and Technology Facilities Council (UK), the European Community under the European Commission Framework Programme 7 (AIDA project, grant agreement no. 262025, TIARA project, grant agreement no. 261905, and EuCARD), the Japan Society for the Promotion of Science, the National Research Foundation of Korea (No. NRF-2016R1A5A1013277), and the Swiss National Science Foundation, in the framework of the SCOPES programme. We gratefully acknowledge all sources of support. We are grateful for the support given to us by the

staff of the STFC Rutherford Appleton and Daresbury Laboratories. We acknowledge the use of Grid computing resources deployed and operated by GridPP in the UK, <http://www.gridpp.ac.uk/>.

**Data Availability Statement** This manuscript has associated data in a data repository. [Authors' comment: The data that support the findings of this study are publicly available on the GridPP computing Grid via the data DOIs (the MICE unprocessed data: 10.17633/rd.brunel.3179644; the MICE reconstructed data: 10.17633/rd.brunel.5955850). Publications using the MICE data must contain the following statement: "We gratefully acknowledge the MICE collaboration for allowing us access to their data. Third-party results are not endorsed by the MICE collaboration and the MICE collaboration does not accept responsibility for any errors in the third-party's understanding of the MICE data."]

**Open Access** This article is distributed under the terms of the Creative Commons Attribution 4.0 International License (<http://creativecommons.org/licenses/by/4.0/>), which permits unrestricted use, distribution, and reproduction in any medium, provided you give appropriate credit to the original author(s) and the source, provide a link to the Creative Commons license, and indicate if changes were made. Funded by SCOAP<sup>3</sup>.

## References

1. S. Geer, Phys. Rev. D **57**, 6989 (1998). <https://doi.org/10.1103/PhysRevD.57.6989>
2. M. Apollonio, et al., Oscillation physics with a neutrino factory (2002). [arXiv:hep-ph/0210192](https://arxiv.org/abs/hep-ph/0210192)
3. D.V. Neuffer, R.B. Palmer, Conf. Proc. C **940627**, 52 (1995)
4. R.B. Palmer, Rev. Accel. Sci. Tech. **7**, 137 (2014). <https://doi.org/10.1142/S1793626814300072>
5. M. Boscolo, M. Antonelli, O.R. Blanco-Garcia, S. Guiducci, S. Liuzzo, P. Raimondi, F. Collamati, Low emittance muon accelerator studies with production from positrons on target (2018). <https://doi.org/10.1103/PhysRevAccelBeams.21.061005>. [arXiv:1803.06696](https://arxiv.org/abs/1803.06696) [physics.acc-ph]
6. S.Y. Lee, *Accelerator Physics*, 3rd edn. (World Scientific Publishing Co, Singapore, 2012). <https://doi.org/10.1142/8335>
7. S. Schröder, R. Klein, N. Boos, M. Gerhard, R. Grieser, G. Huber, A. Karafillidis, M. Krieg, N. Schmidt, T. Kühl, R. Neumann, V. Balykin, M. Grieser, D. Habs, E. Jaeschke, D. Krämer, M. Kristensen, M. Music, W. Petrich, D. Schwalm, P. Sigray, M. Steck, B. Wanner, A. Wolf, Phys. Rev. Lett. **64**, 2901 (1990). <https://doi.org/10.1103/PhysRevLett.64.2901>
8. J.S. Hangst, M. Kristensen, J.S. Nielsen, O. Poulsen, J.P. Schiffer, P. Shi, Phys. Rev. Lett. **67**, 1238 (1991). <https://doi.org/10.1103/PhysRevLett.67.1238>
9. P.J. Channell, J. Appl. Phys. **52**(6), 3791 (1981). <https://doi.org/10.1063/1.329218>
10. J. Marriner, Nucl. Instrum. Methods A **532**, 11 (2004). <https://doi.org/10.1016/j.nima.2004.06.025>
11. V.V. Parkhomchuk, A.N. Skrinsky, Physics-Uspekhi **43**(5), 433 (2000)
12. A.N. Skrinsky, V.V. Parkhomchuk, Sov. J. Part. Nucl. **12**, 223 (1981) [**Fig. Elem. Chast. Atom. Yadra** **12**,557 (1981)]
13. D. Neuffer, Conf. Proc. C **830811**, 481 (1983)
14. D. Neuffer, Part. Accel. **14**, 75 (1983)
15. The MICE collaboration, International MUON Ionization Cooling Experiment. <http://mice.iit.edu>. Accessed 4 Mar 2019
16. M. Apollonio et al., JINST **4**, P07001 (2009). <https://doi.org/10.1088/1748-0221/4/07/P07001>
17. J.B. Rosenzweig, *Fundamentals of Beam Physics* (Oxford University Press, Oxford, 2003)

18. C.N. Booth et al., JINST **8**, P03006 (2013). <https://doi.org/10.1088/1748-0221/8/03/P03006>
19. C.N. Booth et al., JINST **11**(05), P05006 (2016). <https://doi.org/10.1088/1748-0221/11/05/P05006>
20. M. Bogomilov et al., JINST **7**, P05009 (2012). <https://doi.org/10.1088/1748-0221/7/05/P05009>
21. D. Adams et al., Eur. Phys. J. C **73**(10), 2582 (2013). <https://doi.org/10.1140/epjc/s10052-013-2582-8>
22. M. Bogomilov et al., JINST **11**(03), P03001 (2016). <https://doi.org/10.1088/1748-0221/11/03/P03001>
23. R. Bertoni, Nucl. Instrum. Methods A **615**, 14 (2010). <https://doi.org/10.1016/j.nima.2009.12.065>
24. R. Bertoni, M. Bonesini, A. de Bari, G. Cecchet, Y. Karadzhov, R. Mazza, The construction of the MICE TOF2 detector (2010). <http://mice.iit.edu/micenotes/public/pdf/MICE0286/MICE0286.pdf>. Accessed 4 Mar 2019
25. L. Cremaldi, D.A. Sanders, P. Sonnek, D.J. Summers, J. Reidy Jr., I.E.E.E. Trans, Nucl. Sci. **56**, 1475 (2009). <https://doi.org/10.1109/TNS.2009.2021266>
26. M. Ellis, Nucl. Instrum. Methods A **659**, 136 (2011). <https://doi.org/10.1016/j.nima.2011.04.041>
27. F. Ambrosino, Nucl. Instrum. Methods A **598**, 239 (2009). <https://doi.org/10.1016/j.nima.2008.08.097>
28. R. Asfandiyarov et al., JINST **11**(10), T10007 (2016). <https://doi.org/10.1088/1748-0221/11/10/T10007>
29. D. Adams et al., JINST **10**(12), P12012 (2015). <https://doi.org/10.1088/1748-0221/10/12/P12012>
30. A. Dobbs, C. Hunt, K. Long, E. Santos, M.A. Uchida, P. Kyberd, C. Heidt, S. Blot, E. Overton, JINST **11**(12), T12001 (2016). <https://doi.org/10.1088/1748-0221/11/12/T12001>
31. S. Blot, *Proceedings 2nd International Particle Accelerator Conference (IPAC 11) 4–9 September 2011* (San Sebastian, 2011) <https://accelconf.web.cern.ch/accelconf/IPAC2011/papers/mopz034.pdf>. Accessed 4 Mar 2019
32. The MICE Collaboration, The MICE RAW Data. <https://doi.org/10.17633/rd.brunel.3179644> (**MICE/Step4/07000/07469.tar**)
33. T. Roberts, et al., G4beamline; a “Swiss Army Knife” for Geant4, optimized for simulating beamlines. <http://public.muonsinc.com/Projects/G4beamline.aspx>. Accessed 17 Sept 2018
34. D. Rajaram, C. Rogers, The mice offline computing capabilities (2014). <http://mice.iit.edu/micenotes/public/pdf/MICE0439/MICE0439.pdf> (**MICE Note 439**)
35. S. Agostinelli, Nucl. Instrum. Methods Phys. Res. A **506**, 250 (2003)
36. J. Allison et al., IEEE Trans. Nucl. Sci. **53**, 270 (2006). <https://doi.org/10.1109/TNS.2006.869826>
37. R. Brun, F. Rademakers, Nucl. Instrum. Methods A **389**, 81 (1997). [https://doi.org/10.1016/S0168-9002\(97\)00048-X](https://doi.org/10.1016/S0168-9002(97)00048-X)
38. J. Cobb, Statistical errors on emittance measurements (2009). <http://mice.iit.edu/micenotes/public/pdf/MICE341/MICE268.pdf>. Accessed 4 Mar 2019
39. J. Cobb, Statistical errors on emittance and optical functions (2011). <http://mice.iit.edu/micenotes/public/pdf/MICE341/MICE341.pdf>. Accessed 4 Mar 2019
40. J.H. Cobb, Statistical Errors on Emittance (2015, Private communication)
41. C. Hunt, Private communication Publication-in-progress
42. COMSOL Multiphysics software Webpage: <https://www.comsol.com>. Accessed 4 Mar 2019
43. L. Lyons, J. Phys. A Math. Gen. **25**(7), 1967 (1992). <http://stacks.iop.org/0305-4470/25/i=7/a=035>



Available online at [www.sciencedirect.com](http://www.sciencedirect.com)

ScienceDirect



Nuclear Physics A 992 (2019) 121628

[www.elsevier.com/locate/nuclphysa](http://www.elsevier.com/locate/nuclphysa)

## Study of gamma ray transitions and level scheme of $^{56}_{25}\text{Mn}$ using the $^{55}_{25}\text{Mn}(n_{th}, 2\gamma)$ reaction

David Knezevic<sup>a,b,\*</sup>, Nikola Jovancevic<sup>b</sup>, Anatoly M. Sukhovoj<sup>c</sup>,  
Aleksandar Dragic<sup>a</sup>, Liudmila V. Mitsyna<sup>c</sup>, Zsolt Revay<sup>d</sup>,  
Christian Stieghorst<sup>d</sup>, Stephan Oberstedt<sup>e</sup>, Miodrag Krmar<sup>b</sup>,  
Ilija Arsenic<sup>f</sup>, Dimitrije Maletic<sup>a</sup>, Dejan Jokovic<sup>a</sup>

<sup>a</sup> University of Belgrade, Institute of Physics Belgrade, Pregrevica 118, 11080 Zemun, Serbia

<sup>b</sup> University of Novi Sad, Faculty of Science, Department of Physics, Trg Dositeja Obradovica 3, 21000 Novi Sad, Serbia

<sup>c</sup> Joint Institute for Nuclear Research, 141980 Moscow region, Dubna, Russia

<sup>d</sup> Technische Universität München, Heinz Maier-Leibnitz Zentrum (MLZ), Lichtenbergstr. 1, D-85747 Garching, Germany

<sup>e</sup> European Commission, Joint Research Centre, Directorate G – Nuclear Safety and Security, Unit G.2, Retieseweg 111, B-2440 Geel, Belgium

<sup>f</sup> University of Novi Sad, Faculty of Agriculture, Trg Dositeja Obradovica 8, 21000 Novi Sad, Serbia

Received 20 May 2019; received in revised form 9 September 2019; accepted 12 September 2019

Available online 18 September 2019

### Abstract

This work provides new data about the level scheme of  $^{56}_{25}\text{Mn}$  studied by the  $^{55}_{25}\text{Mn}(n_{th}, 2\gamma)$  reaction. The spectroscopic information were collected using the gamma-gamma coincidence spectrometer at the Technische Universität München, Heinz Maier-Leibnitz Zentrum (MLZ), Garching, Germany. The intensities, energies of primary and secondary transitions of 71 energy-resolved cascades, as well as intermediate cascade levels were determined. The updated level scheme of  $^{56}_{25}\text{Mn}$  was obtained from analyzing the intensity spectra of the strongest cascades. The comparison with the existing data in the ENSDF database shows that 23 primary transitions, 24 intermediate cascades levels as well as 32 secondary transitions determined in this work can be recommended as new nuclear data.

2019 Published by Elsevier B.V.

\* Corresponding author at: University of Belgrade, Institute of Physics Belgrade, Pregrevica 118, 11080 Zemun, Serbia.  
E-mail addresses: [davidk@ipb.ac.rs](mailto:davidk@ipb.ac.rs) (D. Knezevic), [nikola.jovancevic@df.uns.ac.rs](mailto:nikola.jovancevic@df.uns.ac.rs) (N. Jovancevic).

*Keywords:* Gamma ray spectrometry; Thermal neutron capture; Level scheme; Gamma ray cascades

---

## 1. Introduction

Accurate data about the nuclear level scheme play an important role in the understanding of the nuclear properties. They are necessary for studying nuclear reactions as well as for determining nuclear structure parameters. In this work we chose to study the level scheme of the  $^{56}_{25}\text{Mn}$ . For that purpose, we used the two-step gamma-cascade method based on measurements of coincident prompt gamma rays following thermal neutron capture [1–4]. An advantage of this technique is a low Compton background in collected spectra owing to the use of the background-subtraction algorithm [1].

The properties of  $^{56}_{25}\text{Mn}$  nucleus have been studied by means of thermal and resonance neutron capture [5–24] but also by other methods, such as the  $^{56}\text{Cr}$   $\beta^-$  decay [25],  $^{48}\text{Ca}(^{11}\text{B}, 3n\gamma)$  [26],  $^{54}\text{Cr}(^3\text{He}, p)$  [27],  $^{54}\text{Cr}(\alpha, d)$  [28],  $^{55}\text{Mn}(d, p)$  [29–32],  $^{56}\text{Fe}(\mu^-, \nu\gamma)$  [33],  $^{56}\text{Fe}(t, ^3\text{He})$  [34],  $^{56}\text{Fe}(^{12}\text{C}, ^{12}\text{N})$  [35,36],  $^{58}\text{Fe}(d, \alpha)$  [37]. The overview of excitation data shows the need for collecting new accurate spectroscopic data on  $^{56}_{25}\text{Mn}$ .

In this work, we present new information on the  $^{56}_{25}\text{Mn}$  nucleus (levels, gamma ray transition energies and their intensities per capture). The obtained results were compared with the existing ENSDF data [38]. As it is an odd-odd nucleus, the  $^{56}_{25}\text{Mn}$  can also be interesting from a theoretical point of view, such as studying the level density and the radiative strength function. Since the two-step gamma ray-cascades method provides the possibility to estimate simultaneously the level density and radiative strength functions, in a future work, these nuclear parameters may be obtained for this nuclei as well, as it was done in [39–44] for other investigated nuclei.

## 2. Experimental setup and measurement

The objective of this experiment was the detection of two-step gamma ray cascades in  $^{56}_{25}\text{Mn}$  following thermal neutron capture on  $^{55}_{25}\text{Mn}$ ,  $^{55}_{25}\text{Mn}(n_{th}, 2\gamma)^{56}_{25}\text{Mn}$ . The measurement was carried out at the PGAA station of Technische Universität München, Heinz Maier-Leibnitz Zentrum (MLZ), Garching, Germany [45,46].

The experimental setup consisted of two HPGe detectors with relative efficiencies of 60% and 30%. The distance between detectors was 22.5 cm (this distance is the distance between the detector cap of the 60% detector and the point on the axis of the 30% detector that lies on the line determined by the detector cap of the 60% detector and the position of the sample). Target was placed at 9 cm from the detector with a 30% efficiency (distance measured on the above mentioned line) as shown in Fig. 1. The other detector was surrounded by an active anti-Compton suppression made of bismuth germanate (BGO). The shielding against scattered neutrons consisted of a 1 mm thick boron-containing plastic tube that was built around the detectors. The detector was also surrounded by 10 cm of lead shielding to reduce background gamma ray radiation. The necessary experimental data for the analysis (energy of both detected coincident photons and time difference between their detection) were collected by a N1728B CAEN ADC digitizer. For the mono-isotopic manganese ( $^{55}_{25}\text{Mn}$ ) the preparation of a high-purity target for the experiment is considerably easier compared to nuclei of more complex isotopic composition. The target was high-purity (99.9%) natural manganese powder with the mass of 50 mg. The relative efficiency of the detectors was determined from single gamma ray spectra accumulated using a PVC tar-

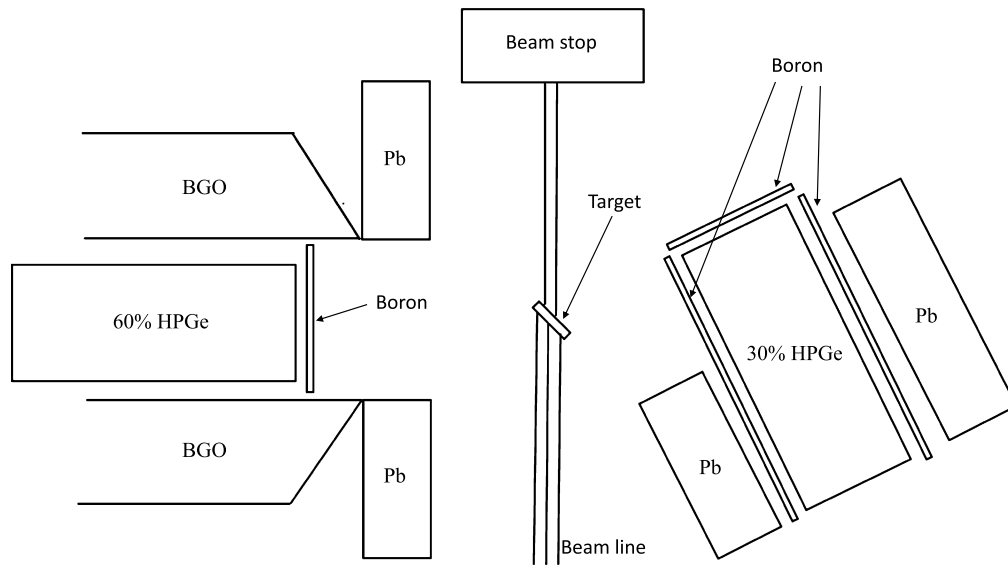


Fig. 1. Sketch of the experimental setup.

get (the  $^{35}\text{Cl}(n,\gamma)^{36}\text{Cl}$  reaction) [47]. For the 30% detector the efficiency curve was  $\ln(\epsilon) = -1.124210 \cdot \ln(E_\gamma) - 2.01161 \cdot \ln(E_\gamma/1022) + 0.453523 \cdot \ln^2(E_\gamma/1022)$ , and for the 60% detector it was  $\ln(\epsilon) = -0.751695 \cdot \ln(E_\gamma) + 0.150324 \cdot \ln(E_\gamma/1022) - 0.177287 \cdot \ln^2(E_\gamma/1022)$ . Manganese two gamma ray events were recorded for 105.6 h.

### 3. Result and discussion

Only a short description of the applied procedure to extract the cascade events and intensities is presented here. The detailed description can be found in Ref. [1].

The most important part of the collected spectrum of sums of amplitudes for coincident pulses (SACP) is shown in Fig. 2. The five marked peaks in Fig. 2 present the two-step cascade peaks of  $^{56}\text{Mn}$  for transitions from the neutron binding energy (7270.0(5) keV) to the ground state and to the first four excited states with the energies of 26.5, 110.4, 212.0 and 341.0 keV. In Table 1, the core information about these five cascade peaks is presented. The remaining unmarked peaks in the SACP spectrum correspond to background events (Fig. 2). They may come from recording of coincidences of the first with the third or fourth quantum of the multiple-step gamma ray cascades or from neutron interaction with surrounding materials. In Table 1, there is also information about part of the resolved intensity, that represents the fraction of the total intensity (% per decay) observed in the spectra  $E_{\gamma,1} + E_{\gamma,2} = \text{const}$  in the form of pairs of intense energy-resolved peaks in Fig. 3 and Fig. 4. These cascades are observed in the form of pairs of standard peaks. Their intensity is given in column 4 of Table 2 in the form of  $I_{\gamma\gamma}$ . The concept of “part of resolved cascade intensity” is used in further analysis to determine the ratio of the sum of the intensity of only resolved peaks to the total sum of the intensities of all resolved and unresolved cascades. The total sum includes all cascades without exception, primary and secondary transitions that satisfy the rules of selection by multiplicity. The cascades to other spins and multipolarities are impossible to determine in this type of experiment.

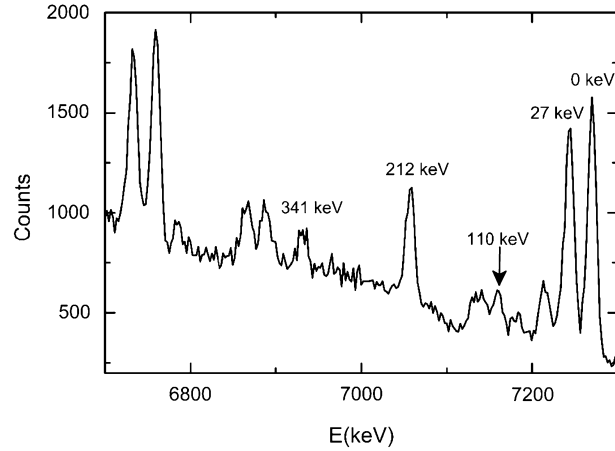


Fig. 2. Spectrum of sums of amplitudes for coincident pulses (SACP) at the radiative capture of thermal neutrons in  $^{55}\text{Mn}$  nucleus. Peaks of the full capture of two quanta are labeled by energy of the final level of the resolved cascades.

Table 1

Information about the two-step cascades to the ground state and the first four excited states collected in the experiment. The spin values of the final levels were taken from [38].

| Gamma ray cascade total energy (keV) | Final level ( $E_f$ ) of the cascade (keV) | Spin of level $E_f$ | Part of resolved cascade intensity | Full intensities % per decay |
|--------------------------------------|--|---------------------|------------------------------------|------------------------------|
| 7270                                 | 0  | 3+                  | 70(5)                              | 17(3)                        |
| 7243                                 | 26.5                                       | 2+                  | 70(7)                              | 13(3)                        |
| 7160                                 | 110.4                                      | 1+                  | 51(9)                              | 5.0(10)                      |
| 7058                                 | 212.0                                      | 4+                  | 49(5)                              | 16.0(20)                     |
| 6929                                 | 341.0                                      | 3+                  | 40(6)                              | 6.0(10)                      |
| Sum of total                         |  |                     | 56(3)                              | 57(5)                        |

From collected SACP spectra the two-step-cascade (TSC) spectra were obtained. This was done for five energy-resolved amplitude peaks. The obtained TSC spectra represent the cascades from the initial state to the defined low-lying final levels of the  $^{56}\text{Mn}$  nucleus. The elimination of Compton background and random coincidences was done by gating on the region nearby the peaks of interest in Fig. 2. Figs. 3 and 4 show examples of the obtained TSC spectra for cascade total energies of 6929 and 7058 keV. The background in the two-step-cascade (TSC) spectra of mono-isotopic manganese is practically absent.

The mirror-symmetrical peaks [2] in the TSC spectra represent primary and secondary transitions of the investigated two-step gamma ray cascade. The peaks' positions correspond to the energies,  $E_{\gamma,1}$  and  $E_{\gamma,2}$ , of primary and secondary quanta of the cascades. The relative intensity of each peak is proportional to its area. The criteria for selecting if the structure in the TSC spectrum is a peak is based on searching for the peak structures with non zero count across multiple channels, and then verifying the existence of the peak using the fitting procedure. All energy-resolved peaks are approximated by the Gauss function, and the background is approximated by a constant or a weakly varying linear function. The ratio of the area of all peaks to the sum of the spectrum gives the value of the proportion of resolved peaks detected in the experiment. The remainder is a continuum of the unresolved cascades.

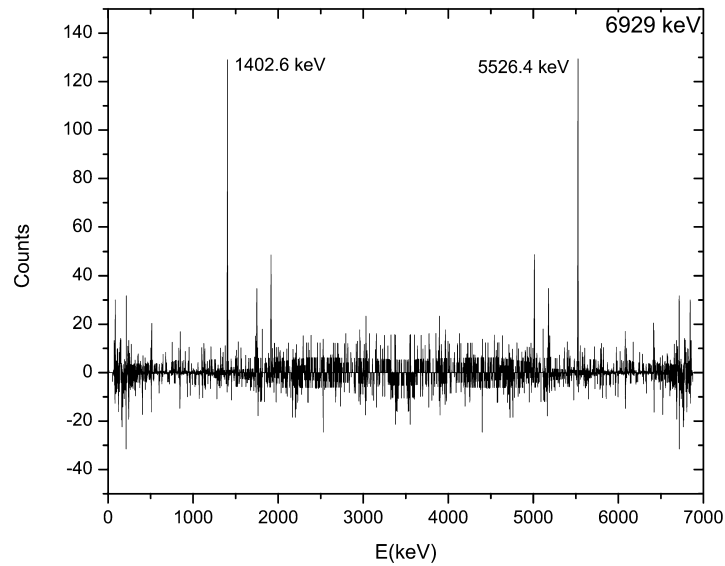


Fig. 3. Two step cascade (TSC) spectrum with the total energy of 6930 keV. The final level of the cascade is 340.957(6) keV (value taken from [38]). This spectrum represents the TSC spectrum with low number of cascades (8 pairs of gamma rays). The energies of the most intense pair of gamma rays are labeled.

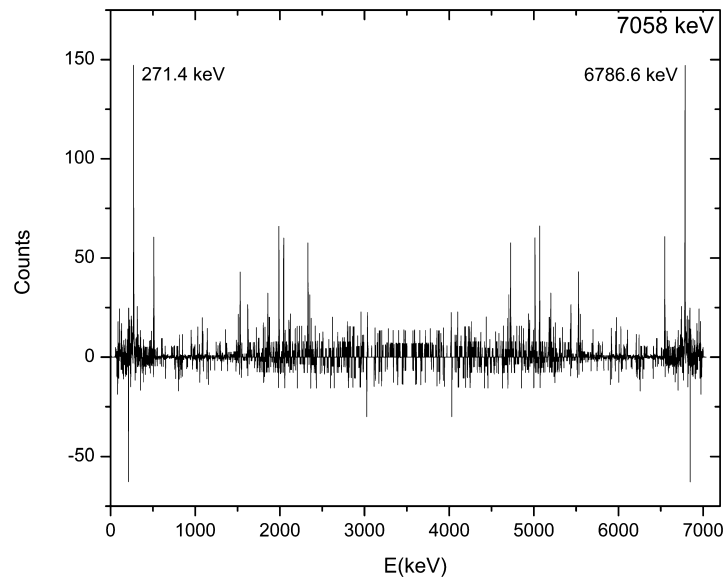


Fig. 4. Two step cascade (TSC) spectrum with the total energy of 7058 keV. The final level of the cascade is 212.004(5) keV (value taken from [38]). This spectrum represents the TSC spectrum with high number of cascades (22 pairs of gamma rays). The energies of the most intense pair of gamma rays are labeled.

Details of the method and the maximum likelihood function used to determine the energies of primary and secondary cascade transitions were presented in [1,4]. The intensities of 71 resolved cascades are determined from five TSC distributions. In all investigated cascades, primary tran-

sitions (except for 7 of them) have the higher energy in comparison with the energy of secondary quanta. All detected primary and secondary gamma ray transitions and their intensities as well as the energies of intermediate levels are presented in Table 2.

In order to compare the data of the cascade spectra (Figs. 3 and 4) with the experimental data for strongest primary transitions with  $E_{\gamma,1}=7058, 7160, 6929, 6784, 5527$  and  $5181$  keV, the branching coefficients ( $Br$ ) of their secondary transitions were obtained independently (using existing ENSDF data), which gave data of absolute intensity of the cascades for normalization of the data from Table 2.

The intensities of primary gamma transitions to individual low-lying levels  $i_1$  are generally known. The product  $i_1 \cdot Br$  is the absolute intensity of one of these cascades to the intermediate level. Then, from the proportion with three known values  $i_1, i_2, i_1 \cdot Br$  and the total sum of the intensity of all transitions of the given stages  $i_{\gamma\gamma} = 100\%$ , we obtain the ratio  $I_{\gamma\gamma} = i_1 \cdot Br \cdot i_1 i_2 / 100$ . It is equal to the sum of  $I_{\gamma\gamma}$  of all two-quantum cascades (resolved and unresolved energetically for the cascade with the corresponding finite level). The values of the total intensity  $I_{\gamma\gamma}$  obtained in such a way (Table 1), which include both the resolved cascades and unresolved cascade continuum with sub-threshold intensity, show that, for the investigated nucleus, we have obtained in this experiment 57% of total intensity of all two-step cascades. At that, 56% of this intensity  $I_{\gamma\gamma}$  falls to the share of the energy-resolved cascades (Table 2).

The data were compared with the existing ones in the ENSDF database [38]. From this comparison, 22 primary transitions that existed in the ENSDF data set were determined. 23 primary transitions, which are not included in the ENSDF library, can be therefore recommended as new data. 21 intermediate levels are identified in our experiment and already listed in the ENSDF database. However, for 24 levels observed in this study, there are no data in the ENSDF library yet. The difference between number of primary gamma rays and levels comes from the fact that in some cases, as is the case of gamma ray with energy (database value [38]) 5432.9 keV, that is identified as primary gamma-ray corresponding to experimental value of 5431.5 keV, gamma-rays exist in the database, but do not have a scheme position assigned to them, so the authors tentatively assigned the scheme position for a number of gamma rays as the primary gamma rays of the cascades. Same is the case for gamma ray with energies (database values [38]) 6019.2, 4324.1 and 3034.1 keV. In this work, we observed 32 secondary gamma ray transitions for which there is no information in the ENSDF database. 14 of these new observed secondary transitions come from the levels already in the ENSDF library, and 18 from levels determined for the first time in this work. Also, 11 secondary gamma rays observed in this study are listed in the ENSDF database, but do not have an assigned position in the decay scheme. In this paper we assigned the decay scheme positions for gamma rays with energies (database values [38]) of 1140.4, 2147.3, 2437.8, 2582.0, 2864.4, 2832.9, 2740.3, 2937.6, 3135.6, 4127.7 and 4024.5 keV.

The comparison of determined energies of levels and gamma rays with the ones from the ENSDF database shows an average deviation of about 1.5 keV. For levels and gamma rays where the deviation was larger than 2 keV, ENSDF values were in some cases assigned tentatively by the authors. This relatively large discrepancy can be explained by insufficient statistics in the present TSC spectra, as well as by the keV/Ch difference between the two detectors during measurement, which can cause uncertainty in the determination of the energy.

The level scheme of  $^{56}_{25}\text{Mn}$  obtained in this work is presented in Figs. 5 and 6.

Spin of the neutron capture level is determined by the ground state spin of the capturing nuclei  $\pm$  the  $1/2$  spin of the neutron. This state decays primarily via dipole transition, predominantly of electric multipolarity. As the compound-state of  $^{55}_{25}\text{Mn}$  is  $5/2^-$ , after a capture of a thermal neutron primary gamma ray transitions can be emitted from the decay of levels with spins  $2^-$  or

Table 2

Comparison of the experimental data with the ENSDF database.  $E_{\gamma,1}$  and  $E_{\gamma,2}$  are the energies of the first and second quanta of the cascade, respectively,  $E_i$  is the energy of the intermediate level and  $E_f$  are the final levels of the two step gamma ray cascade.  $I_{\gamma\gamma}$  is the intensity of the cascade (per 100 decays) observed in the experiment. The experimental uncertainty of  $E_{\gamma,2}$  has the same absolute values as for  $E_{\gamma,1}$  (listed in the table). Values in bold are values for which there is no data in the ENSDF library.

| Present work         |                      |                   |                    | ENSDF       |                      |                      |             |
|----------------------|----------------------|-------------------|--------------------|-------------|----------------------|----------------------|-------------|
| $E_{\gamma,1}$ (keV) | $E_{\gamma,2}$ (keV) | $E_i$ (keV)       | $I_{\gamma\gamma}$ | $E_f$ (keV) | $E_{\gamma,1}$ (keV) | $E_{\gamma,2}$ (keV) | $E_i$ (keV) |
| 7160.6(3)            | 82.9                 | 109.0(6)          | 4.8(6)             | 26.516(3)   | 7159.7(2)            | 83.8990(15)          | 110.428(3)  |
| 7058.80(21)          | 211.20               | 211.2(5)          | 9.2(8)             | g.s.        | 7057.8(2)            | 212.017(6)           | 212.004(5)  |
| <b>7053.1(13)</b>    | 106.5                | 216.9(14)         | 0.9(4)             | 110.428(3)  | –                    | 104.6234(20)         | 215.057(3)  |
| 6925.1(12)           | 344.9                | 344.9(13)         | 0.10(5)            | g.s.        | 6928.7(2)            | 340.990(25)          | 340.957(6)  |
| 6929.9(6)            | 313.6                | 340.1(8)          | 1.3(4)             | 26.516(3)   | 6928.7(2)            | 314.395(10)          | 340.957(6)  |
| 6786.6(7)            | 271.4                | 483.4(9)          | 1.3(4)             | 212.004(5)  | 6783.3(2)            | 271.175(9)           | 486.251(8)  |
| 6786.6(17)           | 142.4                | 483.4(18)         | 0.22(15)           | 340.957(6)  | 6783.3(2)            | 145.320(20)          | 486.251(8)  |
| <b>6733.0(8)</b>     | <b>510.5</b>         | <b>537.0(9)</b>   | 0.55(17)           | 26.516(3)   | –                    | –                    | –           |
| <b>6699.7(27)</b>    | 229.3                | <b>570.3(27)</b>  | 0.15(17)           | 340.957(6)  | –                    | 229.867(7)           | –           |
| 6101.8(12)           | 1141.7               | 1168.2(13)        | 0.25(16)           | 26.516(3)   | 6103.9(2)            | 1140.4(10)           | 1166.54(21) |
| 6101.8(9)            | <b>1057.8</b>        | 1168.2(10)        | 0.16(5)            | 110.428(3)  | 6103.9(2)            | –                    | 1166.54(21) |
| 6101.8(14)           | <b>956.2</b>         | 1168.2(15)        | 0.09(4)            | 212.004(5)  | 6103.9(2)            | –                    | 1166.54(21) |
| 6021.8(20)           | <b>1221.7</b>        | <b>1248.2(21)</b> | 0.08(6)            | 26.516(3)   | 6019.2(8)            | –                    | –           |
| 5919.4(15)           | <b>1324.1</b>        | 1350.6(16)        | 0.18(11)           | 26.516(3)   | 5920.5(2)            | –                    | 1349.95(21) |
| <b>5916.7(13)</b>    | <b>1141.3</b>        | <b>1353.3(14)</b> | 0.08(4)            | 212.004(5)  | –                    | –                    | –           |
| <b>5789.8(27)</b>    | <b>1453.7</b>        | <b>1480.2(27)</b> | 0.09(8)            | 26.516(3)   | –                    | –                    | –           |
| 5759.7(4)            | <b>1510.3</b>        | 1510.3(6)         | 0.79(14)           | g.s.        | 5760.9(2)            | –                    | 1509.55(21) |
| 5759.7(13)           | <b>1298.3</b>        | 1510.3(14)        | 0.07(3)            | 212.004(5)  | 5760.9(2)            | –                    | 1509.55(21) |
| 5759.7(17)           | 1169.3               | 1510.3(18)        | 0.034(24)          | 340.957(6)  | 5760.9(2)            | 1169.71(13)          | 1509.55(21) |
| <b>5547.5(10)</b>    | <b>1510.5</b>        | <b>1722.5(11)</b> | 0.10(4)            | 212.004(5)  | –                    | –                    | –           |
| 5526.4(13)           | 1717.1               | 1743.6(14)        | 0.12(8)            | 26.516(3)   | 5527.4(2)            | 1716.63(14)          | 1744.3(10)  |
| 5526.4(5)            | <b>1531.6</b>        | 1743.6(7)         | 0.46(8)            | 212.004(5)  | 5527.4(2)            | –                    | 1744.3(10)  |
| 5526.4(6)            | 1402.6               | 1743.6(8)         | 0.82(24)           | 340.957(6)  | 5527.4(2)            | 1401.7(10)           | 1744.3(10)  |
| 5438.7(12)           | <b>1720.9</b>        | 1831.3(13)        | 0.07(3)            | 110.428(3)  | 5437.0(2)            | –                    | 1833.67(21) |
| 5438.7(16)           | <b>1619.3</b>        | 1831.3(17)        | 0.08(5)            | 212.004(5)  | 5437.0(2)            | –                    | 1833.67(21) |
| 5431.5(24)           | <b>1626.5</b>        | <b>1838.5(25)</b> | 0.10(7)            | 212.004(5)  | 5432.9(2)            | –                    | –           |
| <b>5313.6(16)</b>    | <b>1956.4</b>        | <b>1956.4(17)</b> | 0.07(5)            | g.s.        | –                    | –                    | –           |
| <b>5270.3(11)</b>    | <b>1889.3</b>        | <b>1999.7(12)</b> | 0.17(7)            | 110.428(3)  | –                    | –                    | –           |
| <b>5250.8(16)</b>    | 2019.2               | 2019.2(17)        | 0.13(8)            | g.s.        | –                    | 2016.5(2)            | 2016.39(15) |
| <b>5201(3)</b>       | 2042.5               | <b>2069(3)</b>    | 0.12(11)           | 26.516(3)   | –                    | 2044.7(2)            | –           |
| 5197.8(14)           | <b>1961.8</b>        | 2072.2(15)        | 0.08(4)            | 110.428(3)  | 5199.1(2)            | –                    | 2071.39(15) |
| 5197.8(11)           | <b>1860.2</b>        | 2072.2(12)        | 0.17(9)            | 212.004(5)  | 5199.1(2)            | –                    | 2071.39(15) |
| <b>5182.7(11)</b>    | 2060.8               | <b>2087.3(12)</b> | 0.46(23)           | 26.516(3)   | –                    | 2063.2(2)            | –           |
| 5180.6(7)            | 2089.7               | 2089.7(9)         | 0.54(10)           | g.s.        | 5181.6(2)            | 2090.4(2)            | 2089.38(15) |
| 5180.6(17)           | 1877.7               | 2089.7(18)        | 0.18(9)            | 212.004(5)  | 5181.6(2)            | 1876.2(10)           | 2089.38(15) |
| 5180.6(7)            | 1748.7               | 2089.7(9)         | 0.49(14)           | 340.957(6)  | 5181.6(2)            | 1747.0(10)           | 2089.38(15) |
| <b>5064.4(13)</b>    | 2179.1               | 2205.6(14)        | 0.40(20)           | 26.516(3)   | –                    | 2176.6(2)            | 2202.73(15) |
| <b>5064.4(16)</b>    | <b>1993.6</b>        | 2205.6(17)        | 0.22(12)           | 212.004(5)  | –                    | –                    | 2202.73(15) |
| <b>5030.8(23)</b>    | <b>2128.8</b>        | 2239.2(24)        | 0.07(5)            | 110.428(3)  | –                    | –                    | 2235.14(21) |
| 5013.5(9)            | 2044.5               | 2256.5(10)        | 0.26(13)           | 212.004(5)  | 5015.0(2)            | 2044.7(2)            | 2255.24(15) |
| 5013.5(5)            | 1915.5               | 2256.5(7)         | 0.5(11)            | 340.957(6)  | 5015.0(2)            | 1915.2(10)           | 2255.24(15) |
| 4950.9(12)           | 2292.6               | 2319.1(13)        | 0.31(14)           | 26.516(3)   | 4949.4(2)            | 2294.8(2)            | 2321.15(10) |
| 4950.9(14)           | 2208.7               | 2319.1(15)        | 0.12(7)            | 110.428(3)  | 4949.4(2)            | 2211.3(2)            | 2321.15(10) |
| 4907.4(11)           | 2252.2               | 2362.6(12)        | 0.12(7)            | 110.428(3)  | 4907.9(2)            | 2254.8(2)            | 2362.62(21) |
| 4907.4(11)           | 2150.6               | 2362.6(12)        | 0.054(22)          | 212.004(5)  | 4907.9(2)            | 2147.3(2)            | 2362.62(21) |

(continued on next page)

Table 2 (continued)

| Present work         |                      |                   |                    | ENSDF       |                      |                      |             |
|----------------------|----------------------|-------------------|--------------------|-------------|----------------------|----------------------|-------------|
| $E_{\gamma,1}$ (keV) | $E_{\gamma,2}$ (keV) | $E_i$ (keV)       | $I_{\gamma\gamma}$ | $E_f$ (keV) | $E_{\gamma,1}$ (keV) | $E_{\gamma,2}$ (keV) | $E_i$ (keV) |
| 4831.9(13)           | 2438.1               | 2438.1(14)        | 0.23(11)           | g.s.        | 4829.7(2)            | 2437.8(2)            | 2441.27(15) |
| 4831.9(25)           | 2327.7               | 2438.1(25)        | 0.10(7)            | 110.428(3)  | 4829.7(2)            | 2331.2(2)            | 2441.27(15) |
| <b>4730.2(14)</b>    | <b>2539.8</b>        | <b>2539.0(15)</b> | 0.14(10)           | g.s.        | –                    | –                    | –           |
| 4726.3(5)            | 2331.7               | 2543.7(7)         | 0.64(12)           | 212.004(5)  | 4725.0(2)            | 2331.2(2)            | 2545.65(20) |
| <b>4659(3)</b>       | 2584                 | <b>2611(3)</b>    | 0.17(26)           | 26.516(3)   | –                    | 2582.0(2)            | –           |
| 4551.1(19)           | <b>2506.9</b>        | 2718.9(20)        | 0.07(5)            | 212.004(5)  | 4550.6(2)            | –                    | 2719.96(21) |
| 4379.0(14)           | 2864.5               | 2891.0(15)        | 0.15(11)           | 26.516(3)   | 4381.0(2)            | 2864.4(2)            | 2889.57(21) |
| <b>4341.3(16)</b>    | <b>2716.7</b>        | <b>2928.7(17)</b> | 0.09(5)            | 212.004(5)  | –                    | –                    | –           |
| 4325.1(22)           | 2834.5               | <b>2944.9(23)</b> | 0.05(4)            | 110.428(3)  | 4324.1(2)            | 2832.9(2)            | –           |
| 4317.7(20)           | 2740.3               | 2952.3(21)        | 0.06(5)            | 212.004(5)  | 4319.5(2)            | 2740.3(8)            | 2951.07(21) |
| <b>4263.3(16)</b>    | 3006.9               | <b>3006.9(17)</b> | 0.17(10)           | g.s.        | –                    | 3003.4(2)            | –           |
| <b>4263.3(23)</b>    | <b>2794.9</b>        | <b>3006.9(24)</b> | 0.06(4)            | 212.004(5)  | –                    | –                    | –           |
| 4224.5(16)           | 3045.5               | 3045.5(17)        | 0.19(10)           | g.s.        | 4223.5(2)            | 3047.5(2)            | 3047.34(15) |
| 4224.5(14)           | 2935.1               | 3045.5(15)        | 0.09(5)            | 110.428(3)  | 4223.5(2)            | 2937.6(8)            | 3047.34(15) |
| <b>4134.8(22)</b>    | 3135.2               | <b>3135.2(23)</b> | 0.16(10)           | g.s.        | –                    | 3135.6(2)            | –           |
| <b>3879(4)</b>       | <b>3391</b>          | <b>3391(4)</b>    | 0.07(9)            | g.s.        | –                    | –                    | –           |
| 3871.6(14)           | 3057.4               | 3398.4(15)        | 0.09(5)            | 340.957(6)  | 3873.0(2)            | 3058.2(2)            | 3397.61     |
| 3751.1(13)           | <b>3408.5</b>        | 3518.9(14)        | 0.22(10)           | 110.428(3)  | 3752.3(2)            | –                    | 3518.32(21) |
| <b>3592.8(14)</b>    | <b>3465.2</b>        | <b>3677.2(15)</b> | 0.12(6)            | 212.004(5)  | –                    | –                    | –           |
| 3035.0(11)           | 4124.6               | <b>4235.0(12)</b> | 0.20(7)            | 110.428(3)  | 3034.1(2)            | 4127.7(8)            | –           |
| 3035.0(20)           | 4023.0               | <b>4235.0(21)</b> | 0.13(9)            | 212.004(5)  | 3034.1(2)            | 4024.5(10)           | –           |
| 3035.0(17)           | <b>3894.0</b>        | <b>4235.0(18)</b> | 0.13(7)            | 340.957(6)  | 3034.1(2)            | –                    | –           |
| <b>2959.5(14)</b>    | <b>4200.1</b>        | <b>4310.5(15)</b> | 0.06(3)            | 110.428(3)  | –                    | –                    | –           |
| <b>2959(5)</b>       | <b>4098</b>          | <b>4311(5)</b>    | 0.05(6)            | 212.004(5)  | –                    | –                    | –           |
| <b>2588(3)</b>       | <b>4571</b>          | <b>4682(3)</b>    | 0.08(10)           | 110.428(3)  | –                    | –                    | –           |
| <b>2179.7(9)</b>     | <b>4878.3</b>        | <b>5090.3(10)</b> | 0.12(4)            | 212.004(5)  | –                    | –                    | –           |

$3^-$ , exciting the levels with spins from  $J=1$  to  $J=4$ . Cross section for the neutron resonance with a spin of  $2^-$  is 8.36 b, for spin  $3^-$  this cross section is 3.57 b, and for boundary resonance with cross section of 1.39 b, the spin is unknown [22]. Spin interval for the nuclear levels that are excited by secondary transitions of the cascade is from  $J=0$  to  $J=5$ . Such limitation on the possible values of spins is due to decay of excited nucleus by mainly dipole E1- and M1-transitions, at least, if cascade energy is larger than 6930 MeV. Cascades of less total energy with  $\Delta J=3$  were not observed in our experiment. A contribution of quadrupole gamma ray transitions to the total gamma ray spectrum is negligible.

Insufficient resolution of HPGe-detectors did not allow to uncouple the two-step cascades to doublets of final levels 212.026/215.128 keV and 335.529/340.989 keV. But small shift of average of total-energy sum of these doublets (7058 and 6934 keV) give us the reason to think that cascades to the final levels with the energies of 212 and 340 keV and corresponded to them spins  $4^+$  and  $3^+$  are dominated in the decay scheme.

#### 4. Conclusion

In this paper, new spectroscopic information was obtained for  $^{56}_{25}\text{Mn}$  by investigating two-step gamma ray cascades following thermal-neutron capture on  $^{55}_{25}\text{Mn}$ . The level scheme and gamma ray transitions for the  $^{56}_{25}\text{Mn}$  nucleus were obtained. The data show good agreement with the ones from the ENSDF library. 24 new levels were observed with 23 new primary and 32 secondary



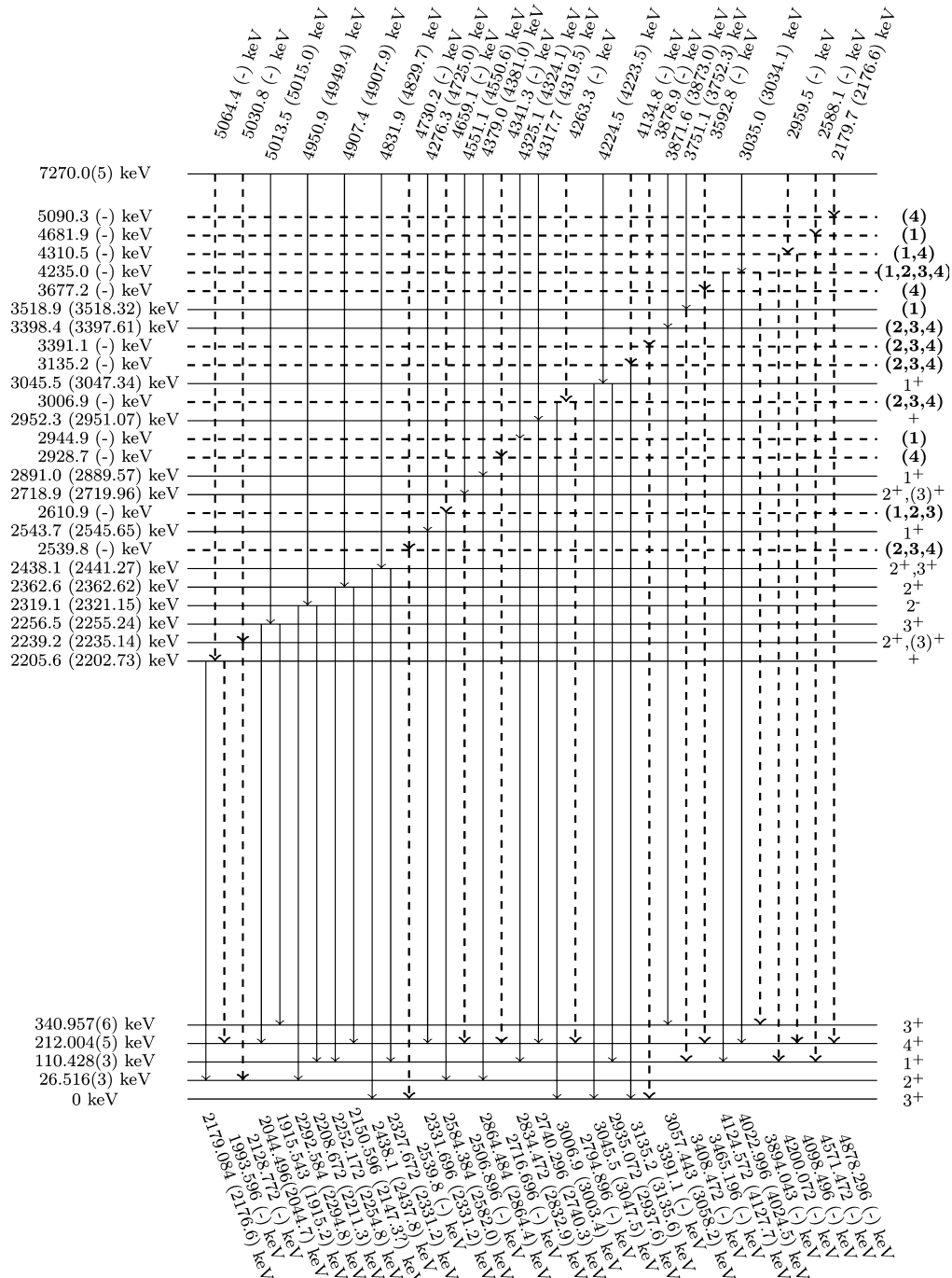


Fig. 6. Experimental level scheme of  $^{56}\text{Mn}$  with intermediate level energies from 2200 to 5100 keV. Dashed lines – levels and gamma rays not found in the ENSDF library; bold spin values – values suggested by the authors for the levels without spin information in the ENSDF library. All energy values, except the energy values for the first 4 low-lying levels are given in the form: Experimental value(ENSDF value).

gamma ray transitions in the energy range between 0.3 MeV and 7.1 MeV. These new results can be useful for future investigations of nuclear structure parameters such as the nuclear level density and radiative strength function.

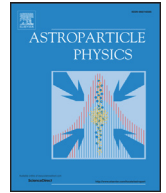
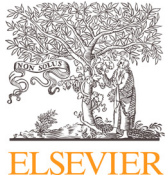
### Acknowledgement

The authors gratefully acknowledge the financial support provided by the FRM II to perform the experiment at the Heinz Maier-Leibnitz Zentrum (MLZ), Garching, Germany.

### References

- [1] S. Boneva, E. Vasil'eva, Y.P. Popov, A. Sukhovoij, V. Khitrov, Two-quantum cascades of radiative neutron capture I. Spectroscopy of excited states of complex nuclei in the neutron binding energy region, *Sov. J. Part. Nucl.* 22 (2) (1991) 232–248 (English Translation).
- [2] Y.P. Popov, A. Sukhovoij, V. Khitrov, Y.S. Yazvitskij, Study on the  $\gamma$  decay of 165 Dy with the help of the  $(n, 2\gamma)$  reaction, *Izv. Akad. Nauk SSSR, Ser. Fiz.* 48 (5) (1984) 891–900.
- [3] A. Sukhovoij, V. Khitrov, Method of improving the amplitude resolution of the spectra of gamma-transition cascades in the computer processing of encoded coincidence data, *Instrum. Exp. Tech.* 27 (5) (1985) 1071–1074.
- [4] E. Vasilieva, A. Sukhovoij, V. Khitrov, Direct experimental estimate of parameters that determine the cascade gamma decay of compound states of heavy nuclei, *Phys. At. Nucl.* 64 (2) (2001) 153–168.
- [5] R.W. Bauer, M. Deutsch, Nuclear orientation of Mn-56, *Phys. Rev.* 117 (2) (1960) 519.
- [6] S. Du Toit, L. Bollinger, Lifetimes of energy levels in Al-28, Mn-56, Cu-64, Rh-104, and I-128 excited by slow neutron capture, *Phys. Rev.* 123 (2) (1961) 629.
- [7] I. Estulin, A. Melioransky, L. Kalinkin, Transitions between low-lying excited states of Mn-54 and Ho-166, *Nucl. Phys.* 24 (1) (1961) 118–125.
- [8] P. Carlos, H. Nifenecker, J. Fagot, J. Matuszek, Étude de cascades  $\gamma$ — $\gamma$  dans la capture thermique de neutrons par les isotopes 55Mn, 56Fe, 59Co, 199Hg, *J. Phys.* 25 (11) (1964) 957–960.
- [9] L. Hughes, T. Kennett, W. Prestwich, A study of the 55Mn  $(n, \gamma)$  56Mn reaction, *Nucl. Phys.* 80 (1) (1966) 131–144.
- [10] D. Dorioman, M. Popa, M. Cristu, Gamma Rays from Thermal Neutron Capture in Manganese, Germanium, and Iridium Nuclei, *Tech. Rep.*, Inst. of Atomic Physics, Bucharest, 1967.
- [11] R. Alves, J. Kuchly, J. Julien, C. Samour, J. Morgenstern, Capture radiative partielle des neutrons de résonance dans le chlore, le manganèse, le fer, le cuivre, le thulium et le mercure, *Nucl. Phys. A* 135 (2) (1969) 241–280.
- [12] J. Kopecký, E. Warming, Circular polarization measurements with a Ge (Li) detector, *Nucl. Phys. A* 127 (2) (1969) 385–398.
- [13] J. Mellema, H. Postma, Investigation of nuclear level spins of 56Mn by means of nuclear orientation, *Nucl. Phys. A* 154 (2) (1970) 385–406.
- [14] V. Orphan, N.C. Rasmussen, T. Harper, Line and Continuum Gamma-Ray Yields from Thermal-Neutron Capture in 75 Elements, *Tech. Rep.*, Gulf Energy And Environmental Systems INC San Diego CA, 1970.
- [15] J. Boulter, W. Prestwich, Lifetimes of the 26 and 110 keV levels in 56Mn, *Can. J. Phys.* 49 (23) (1971) 2911–2916.
- [16] P. Van Assche, H. Baader, H. Koch, B. Maier, U. Gruber, O. Schult, J. McGrory, J. Comfort, R. Rimawi, R. Chrien, et al., Energy levels of 56Mn, *Nucl. Phys. A* 160 (2) (1971) 367–384.
- [17] F. Stecher-Rasmussen, K. Abrahams, J. Kopecky, W. Ratynski, Circular polarization of neutron-capture gamma-rays from Mn, Ni, Ga and W, *Nucl. Phys. A* 1 (1972) 250.
- [18] H. Börner, O. Schult, Resonance neutron capture in 55Mn and levels in 56Mn, *Z. Naturforsch. A* 29 (3) (1974) 385–388.
- [19] A. Colenbrander, T. Kennett, An investigation of the reaction 55Mn  $(n, \gamma)$  56Mn, *Can. J. Phys.* 53 (3) (1975) 236–250.
- [20] P. Delheij, K. Abrahams, W. Huiskamp, H. Postma, The 55Mn  $(n, \gamma)$  56Mn reaction studied with polarized neutrons and polarized manganese nuclei, *Nucl. Phys. A* 341 (1) (1980) 45–55.
- [21] M. Islam, T. Kennett, S. Kerr, W. Prestwich, A self-consistent set of neutron separation energies, *Can. J. Phys.* 58 (2) (1980) 168–173.
- [22] S. Mughabghab, Neutron Cross Sections: Neutron Resonance Parameters and Thermal Cross Sections, Part A: Z=1-60, vol. 1, Elsevier, 2012.
- [23] R. Macklin, Resonance neutron capture by manganese below 2.5 keV, *Nucl. Sci. Eng.* 89 (4) (1985) 362–365.

- [24] A. Wapstra, G. Audi, The 1983 atomic mass evaluation: (i). atomic mass table, Nucl. Phys. A 432 (1) (1985) 1–54.
- [25] B. Dropesky, A. Schardt, T. Shull, Note on the decay of the new nuclide Cr-56, Nucl. Phys. 16 (2) (1960) 357–359.
- [26] A.M. Nathan, J.W. Olness, E.K. Warburton, J.B. McGrory, Yrast decay schemes from heavy ion +  $^{48}\text{Ca}$  fusion-evaporation reactions. i.  $^{54-56}\text{Mn}$ ,  $^{56}\text{Cr}$ , and  $^{52-53}\text{V}$ , Phys. Rev. C 16 (1977) 192–214, <https://doi.org/10.1103/PhysRevC.16.192>.
- [27] T. Caldwell, D. Pullen, T. Mulligan, O. Hansen, (tau, p) reactions on Cr. ii. 54 Cr (tau, p), 56 Mn, Tech. Rep., Univ. of Pennsylvania, Philadelphia, 1971.
- [28] U. Fister, R. Jahn, P. von Neumann-Cosel, P. Schenk, T. Trelle, D. Wenzel, U. Wienands, Stretched proton-neutron configurations in fp-shell nuclei:(i). experimental results of the ( $\alpha$ , d) reaction, Nucl. Phys. A 569 (3) (1994) 421–440.
- [29] J. Green, A. Smith, W. Buechner, M. Mazari, Excited states in Mn 56, Phys. Rev. 108 (3) (1957) 841.
- [30] J. Bjerregaard, P. Dahl, O. Hansen, G. Sidenius, Energy levels from (p, p'), (d, p) and (d,  $\alpha$ ) reactions on the stable isotopes between Sc-45 and Ni-58, Nucl. Phys. 51 (1964) 641–666.
- [31] J.R. Comfort, Nuclear structure of manganese-56, Phys. Rev. 177 (4) (1969) 1573.
- [32] A. Garcia, A. Lopez, F. Senent, The  $^{55}\text{Mn}$  (d, p)  $^{56}\text{Mn}$  reaction, An. Fis. 67 (1971) 181.
- [33] D.F. Measday, T.J. Stocki,  $\gamma$  rays from muon capture in natural Ca, Fe, and Ni, Phys. Rev. C 73 (4) (2006) 045501.
- [34] F. Ajzenberg-Selove, R.E. Brown, E.R. Flynn, J.W. Sunier, ( $t, ^3\text{He}$ ) reactions on  $^{56}\text{Fe}$ ,  $^{58}\text{Fe}$ , and  $^{58}\text{Ni}$ , Phys. Rev. C 31 (1985) 777–786, <https://doi.org/10.1103/PhysRevC.31.777>.
- [35] N. Anantaraman, S.M. Austin, J. Winfield, Heavy ion reactions as probes for spin strength, Nucl. Phys. A 482 (1–2) (1988) 331–342.
- [36] S. Albergo, S. Costa, R. Potenza, J. Romanski, C. Tuvé, L. Jarczyk, B. Kamys, A. Magiera, A. Strzalkowski, R. Barna, V. D'Amico, D. De Pasquale, G. Mannino, Elastic transfer in the  $^{11}\text{B}+^{12}\text{C}$  system in the c.m. energy range 5–40 MeV, Phys. Rev. C 43 (1991) 2704–2710, <https://doi.org/10.1103/PhysRevC.43.2704>.
- [37] H. Kelleter, D. Bachner, B. Schmidt, W. Seliger, Level investigation by means of the (d,  $\alpha$ ) reaction (ii).  $^{52}\text{Mn}$  and  $^{56}\text{Mn}$ , Nucl. Phys. A 183 (3) (1972) 509–522.
- [38] H. Junde, H. Su, Y. Dong, Nuclear data sheets for A=56, Nucl. Data Sheets 112 (6) (2011) 1513–1645.
- [39] V. Khitrov, A. Sukhovej, New technique for a simultaneous estimation of the level density and radiative strength functions of dipole transitions at  $E_{ex} < B_n - 0.5$  MeV, arXiv preprint, arXiv:nucl-ex/0110017.
- [40] A. Sukhovej, L. Mitsyna, N. Jovancevic, Overall picture of the cascade gamma decay of neutron resonances within a modified practical model, Phys. At. Nucl. 79 (3) (2016) 313–325.
- [41] D. Vu, A. Sukhovej, L. Mitsyna, S. Zeinalov, N. Jovancevic, D. Knezevic, M. Krmar, A. Dragic, Representation of radiative strength functions within a practical model of cascade gamma decay, Phys. At. Nucl. 80 (2) (2017) 237–250.
- [42] A. Sukhovej, New model of the cascade gamma decay of neutron resonances for practitioners: basic concepts and attainable precision, Phys. At. Nucl. 78 (2) (2015) 230–245.
- [43] A.M. Sukhovej, L.V. Mitsyna, The next-generation practical model of the cascade gamma-decay of neutron resonance and expected parameters for an arbitrary nucleus, in: Proceedings, 22nd International Seminar on Interaction of Neutrons with Nuclei: Fundamental Interactions and Neutrons, Nuclear Structure, Ultracold Neutrons, Related Topics (ISINN 22), Dubna, Russia, May 27–30, 2014, 2015.
- [44] S. Boneva, V. Khitrov, A. Sukhovej, A. Vojnov, Excitation study of high-lying states of differently shaped heavy nuclei by the method of two-step cascades, Nucl. Phys. A 589 (2) (1995) 293–306.
- [45] Z. Revay, PGAA: Prompt gamma and in-beam neutron activation analysis facility, J. Large-Scale Res. Fac. JLSRF 1 (2015) 20.
- [46] Z. Révay, P. Kudějová, K. Kleszcz, S. Söllradl, C. Genreith, In-beam activation analysis facility at MLZ, Garching, Nucl. Instrum. Methods Phys. Res., Sect. A, Accel. Spectrom. Detect. Assoc. Equip. 799 (2015) 114–123.
- [47] B. Krusche, K. Lieb, H. Daniel, T. Von Egidy, G. Barreau, H. Börner, R. Brissot, C. Hofmeyr, R. Rascher, Gamma ray energies and  $^{36}\text{Cl}$  level scheme from the reaction  $^{35}\text{Cl}(n, \gamma)$ , Nucl. Phys. A 386 (2) (1982) 245–268.



# A novel method for atmospheric correction of cosmic-ray data based on principal component analysis

M. Savić, A. Dragić\*, D. Maletić, N. Veselinović, R. Banjanac, D. Joković, V. Udovičić

Institute of Physics, University of Belgrade, Pregrevica 118, Zemun 11080, Serbia

## ARTICLE INFO

### Article history:

Received 23 August 2018  
Revised 8 December 2018  
Accepted 29 January 2019  
Available online 29 January 2019

### Keywords:

Cosmic rays  
Muons  
Atmospheric corrections  
Principal component analysis

## ABSTRACT

A new method for atmospheric correction of cosmic ray data is designed. It's fully empirical, based on the principal component analysis. The method requires knowledge of the pressure and the temperature profile of the atmosphere. It's applicable to all muon detectors. The method is tested on muon data from two detectors in Belgrade cosmic ray station, one located on the ground level and the other at the depth of 25 mwe. Correction reduces variance by 64.5% in ground level detector data and 38.1% in underground data. At the same time, the amplitude of the annual variation is reduced by 86.0% at ground level and 54.9% underground. With the same data sets the presented method performs better than the integral correction method.

© 2019 Elsevier B.V. All rights reserved.

## 1. Introduction

Count rates of ground based or underground cosmic-ray (CR) muon detectors are affected by atmospheric parameters (air pressure and temperature at different heights). The proper description of atmospheric effects is necessary for understanding primary CR variations, originating outside of the atmosphere.

Early studies in CR temporal variations [1,2] revealed the existence of a variation caused by the change of air pressure, the so called "barometric effect". With the increase in pressure the atmosphere represents thicker absorber, resulting in reduced number of muons reaching the ground level. Therefore, muon flux is expected to be anti-correlated with atmospheric pressure.

Observed negative correlation between muon flux and atmospheric temperature, the so called "negative temperature effect", has been explained by Blackett [3] to be a consequence of muon decay. During warm periods the atmosphere is expanded and the main layer of muon production (~100 mb) is higher, resulting in longer muon path and lower surviving probability to the ground level. Low energy muons are more affected, while the flux of high energy muons, capable of penetrating great depth, does not suffer. At deep underground experiments another type of temperature effect, "positive temperature effect" is pronounced [4]. Development of nuclear emulsions capable of detecting energetic charged particles lead to discovery of charged pions in CRs and  $\pi - \mu$  decay [5–7]. The positive temperature effect is interpreted as a conse-

quence of latter process [8,9]. Pions created in the interactions of primary CR particles with the atmospheric nuclei can decay into muons or interact with air nuclei. Higher temperature in the production layer means lower air density and consequently, lower interaction probability and higher muon production.

In most cases linear regression is sufficient to account for the barometric effect. The temperature effects are treated by empirical and theoretical methods. In addition to the barometric coefficient  $\beta$ , **the method of effective level of generation** [8] introduces two empirical parameters:  $\alpha_H$  to encounter for muon intensity variations  $\delta I_\mu$  correlated with the change of the height of generation level  $\delta H$  (negative effect) and  $\alpha_T$  for the changes of the temperature of this level (positive temperature effect).

$$\delta I_\mu = \beta \delta p + \alpha_H \delta H + \alpha_T \delta T \quad (1)$$

Duperier method has been successfully used in many studies for the atmospheric corrections of muon data ([10–15] etc.).

It's been argued [16,17] that for correct temperature correction of muon detectors count rate the vertical temperature profile of the entire atmosphere needs to be known. In the so called **integral method** the muon intensity variations caused by the temperature are described by the equation:

$$\frac{\delta I_\mu}{I_\mu} = \int_0^{h_0} W_T(h) \delta T(h) dh \quad (2)$$

where  $\delta T(h)$  is the variation of temperature at isobaric level  $h$  with respect to the referent value and  $W_T(h)$  is the temperature coefficient density. The coefficients are calculated theoretically and the best known calculations are given in references [18,19].

\* Corresponding author.

E-mail address: [dragic@ipb.ac.rs](mailto:dragic@ipb.ac.rs) (A. Dragić).

The **mass-average temperature method** [20] is a variant of the integral method, based on the assumption of small changes of the temperature coefficient density  $W_T(h)$  with the atmospheric depth  $h$  allowing its average value  $\overline{W}_T$  to be put in front of the integral in the Eq. (2) and on determination of the mass-averaged temperature  $T_m$ :

$$\frac{\delta I_\mu}{I_\mu} = \overline{W}_T(h) \int_0^{h_0} \delta T(h) dh = \overline{W}_T(h) \cdot \delta T_m \quad (3)$$

The method was used in numerous studies ([21–23] to name a few).

Another form of the integral method is the **effective temperature method** [24]. By introducing the temperature coefficient  $\alpha_T$ :

$$\alpha_T = \int_0^{h_0} W_T(h) dh$$

the Eq. (2) can be normalized as:

$$\frac{\delta I_\mu}{I_\mu} = \int_0^{h_0} W_T(h) dh \cdot \frac{\int_0^{h_0} W_T(h) \delta T(h) dh}{\int_0^{h_0} W_T(h) dh} = \alpha_T \cdot \delta T_{eff} \quad (4)$$

where the effective temperature  $T_{eff}$  is defined as:

$$T_{eff} = \frac{\int_0^{h_0} W_T(h) T(h) dh}{\int_0^{h_0} W_T(h) dh}$$

The latter method is popular with the underground muon telescopes [25,26].

Different methods of atmospheric correction might be compared on the basis of several criteria. One is requirement of the lowest variance of corrected data. Since the most prominent temperature effect on CR time series is seasonal variation, another criterion is the smallest residual amplitude of seasonal variation after correction is applied. The latter does not take into account possible genuine seasonal variation of non-atmospheric origin.

Early studies comparing Duprier's empirical and Dorman's theoretical methods ([27] and references therein) found similar accuracy of two methods, with essentially the same corrections at sea level, but with the integral method overestimating the temperature effect.

A more recent study [28] compared different methods of atmospheric correction for data from Nagoya and Tibet supertelescopes, as well as Yakutsk, Moscow and Novosibirsk telescopes. They found the mass-averaged temperature method to practically coincide with the integral method. On the other hand, the effective level of generation method for Nagoya shows discrepancy from the integral method in winter time, being able to eliminate only 50% of the temperature effect. Even with the integral method in the case of Tibet muon telescope the removal of temperature effect is achieved with the density of temperature coefficients 3 times higher than calculated ones. The precise origin of disagreement is unknown.

The method of the effective level of generation takes care of key physical causes of the temperature effect. However, it does not make optimal use of the temperature data. Also, the assumption of a single level of main muon production is a simplification. Detailed CORSIKA simulation of the shower development in the atmosphere reveals the actual distribution of the muon generation heights (see Fig. 1).

Different implementations of the integral method exist, employing different approximations, choice of parameters, models of the atmosphere, whether kaon contribution is taken into account, leading to differences in calculated density temperature coefficients (see for instance discussion in [29]). As already mentioned, on the case of Tibet telescope [28] theoretical calculations do not fully correspond to the local experimental conditions and the origin of disagreement is difficult to trace.

The effective temperature method lacks universality, since it works best with the data from deep underground detectors.

Here we propose a new method for atmospheric corrections. It's fully empirical, makes use of the available temperature data through entire atmosphere and it's applicable to arbitrary detector irrespective to energy sensitivity and is simple to implement. The method is based on the principal component analysis, thus reducing dimensionality of the problem, exploiting correlations between atmospheric variables and ensuring mutual independence of correction parameters. The price is loss of clear physical interpretation of these parameters, since the pressure and the temperature at different levels are treated on equal footing.

## 2. Method description

### 2.1. Meteorological data

Set of variables that enter principal component decomposition consists of atmospheric temperature profile for the given location as well as locally measured atmospheric pressure. Meteorological balloon soundings for Belgrade are not done frequently enough to be used for suggested analysis. As a consequence, modeled temperatures were used instead. However, there were enough balloon sounding data for testing consistency of the modeled temperatures.

There are several weather and global climate numerical models available today. Here, Global Forecast System [30] data was used. GFS is a weather forecast model, developed by National Centers for Environmental Prediction [31], which is able to predict large number of atmospheric and land-soil parameters. Apart from forecast data, GFS also provides retrospective data produced taking into account most recent measurements by a world wide array of meteorological stations. Retrospective data are produced four times a day at 00:00, 06:00, 12:00 and 18:00 UTC. Data with finer temporal resolution are obtained by cubic spline interpolation. Temperatures for the following 25 isobaric levels (in mb) were used for initial analysis: 10, 20, 30, 50, 70, 100, 150, 200, 250, 300, 350, 400, 450, 500, 550, 600, 650, 700, 750, 800, 850, 900, 925, 975, 1000. Horizontal spatial resolution for modeled data is 0.5 degrees, so coordinates closest to the experiment location (latitude 44.86, longitude 20.39), were selected with this precision. Before any further analysis was done, GFS modeled temperature profiles were compared to local meteorological balloon soundings for Belgrade, where balloon data was available. Fig. 2 shows profile of differences between modeled and measured values for different isobaric levels. Disagreement was found between measured and modeled temperature at the lowest level. As a result, it was decided not to use temperature data for isobaric level of 1000 mb in further analysis. Ground temperature data measured by local meteorological stations was used for lowest layer instead. Similar problem with the GFS data was reported before by [28] who found 5° C deviation in the summer time near ground level at Yakutsk location.

Atmospheric pressure and ground level temperature from the Republic Hydro-meteorological Service of Serbia was used to compose unique local pressure and temperature time series.

### 2.2. Cosmic-ray data

The analysis is performed on data from Belgrade muon detectors. The Belgrade cosmic-ray station, together with the present detector arrangement is described in details elsewhere [32]. Two muon detectors are located in the laboratory, one at the ground level and the other at the depth of 25 mwe. Data are recorded on the event-by event basis and can be integrated into the time series with the arbitrary time resolution. For most purposes hourly data are used. Muon detectors are sensitive to primary cosmic rays

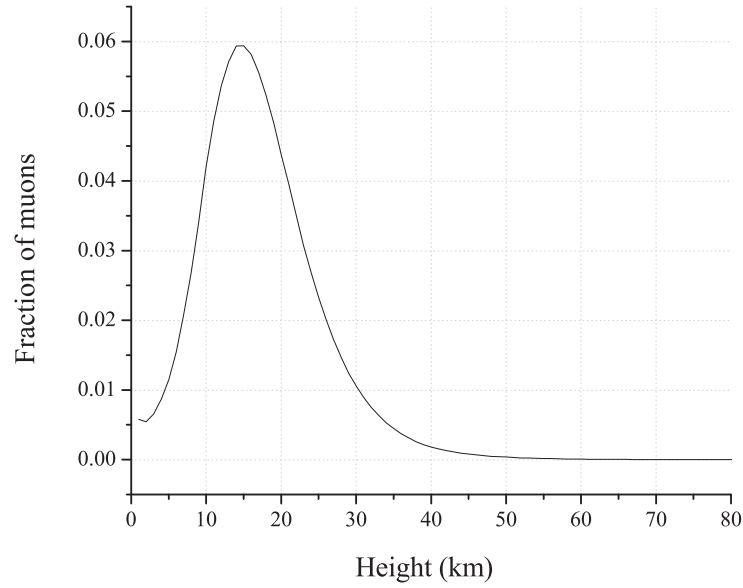


Fig. 1. Distribution of muon generation at different heights in the atmosphere, according to CORSIKA simulation.

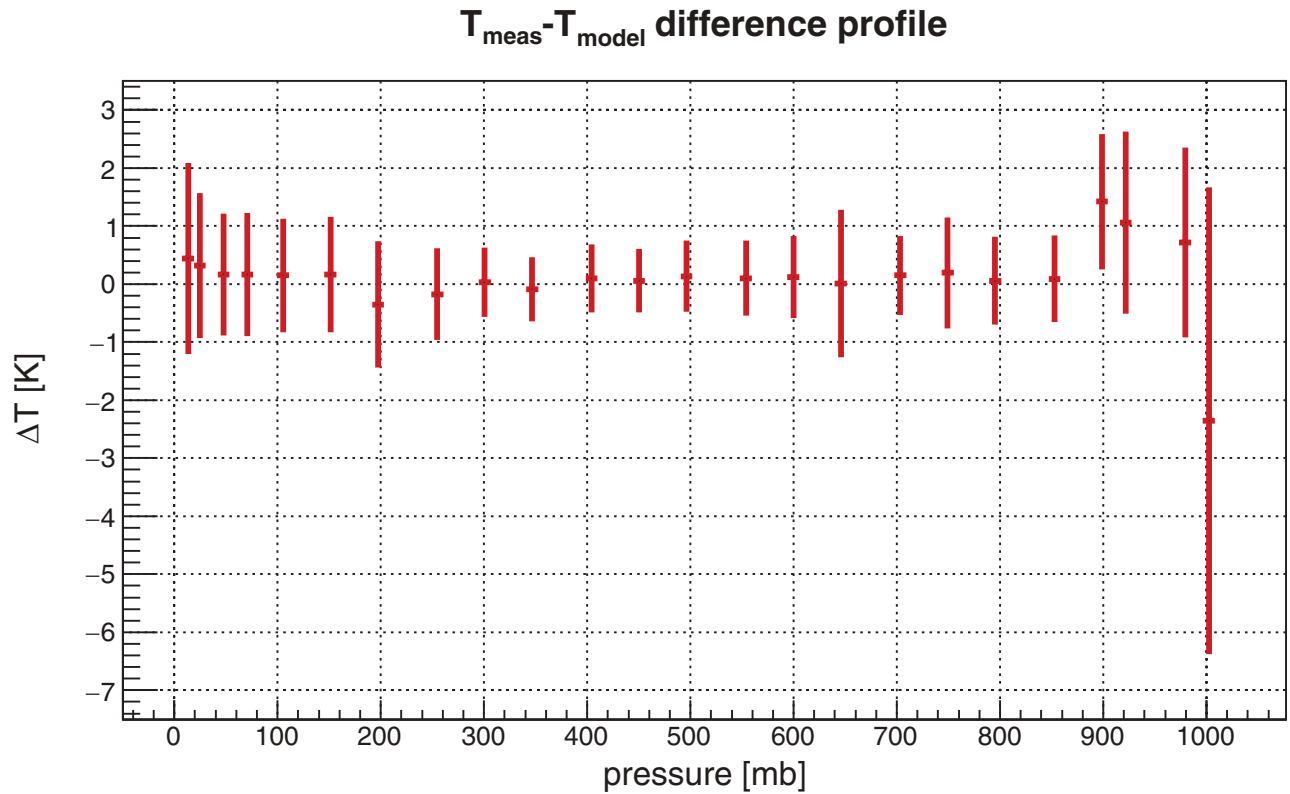


Fig. 2. Distribution of differences between measured temperatures and modeled by GFS.

of 59 GeV median energy in the case of ground level detector and 137 GeV for underground detector.

### 2.3. Principal component decomposition

Principal component analysis is a convenient and widely used data reduction method when dealing with strongly correlated

data. It transforms the original set of variables into a set of uncorrelated variables (called principal components (PC)). The principal components are ordered according to decreasing variance. In our case, there are 26 input variables: 24 modeled temperatures (isobaric level 1000 mb temperature excluded), locally measured ground level temperature and local atmospheric pressure. Initial variables were centered and normalized before

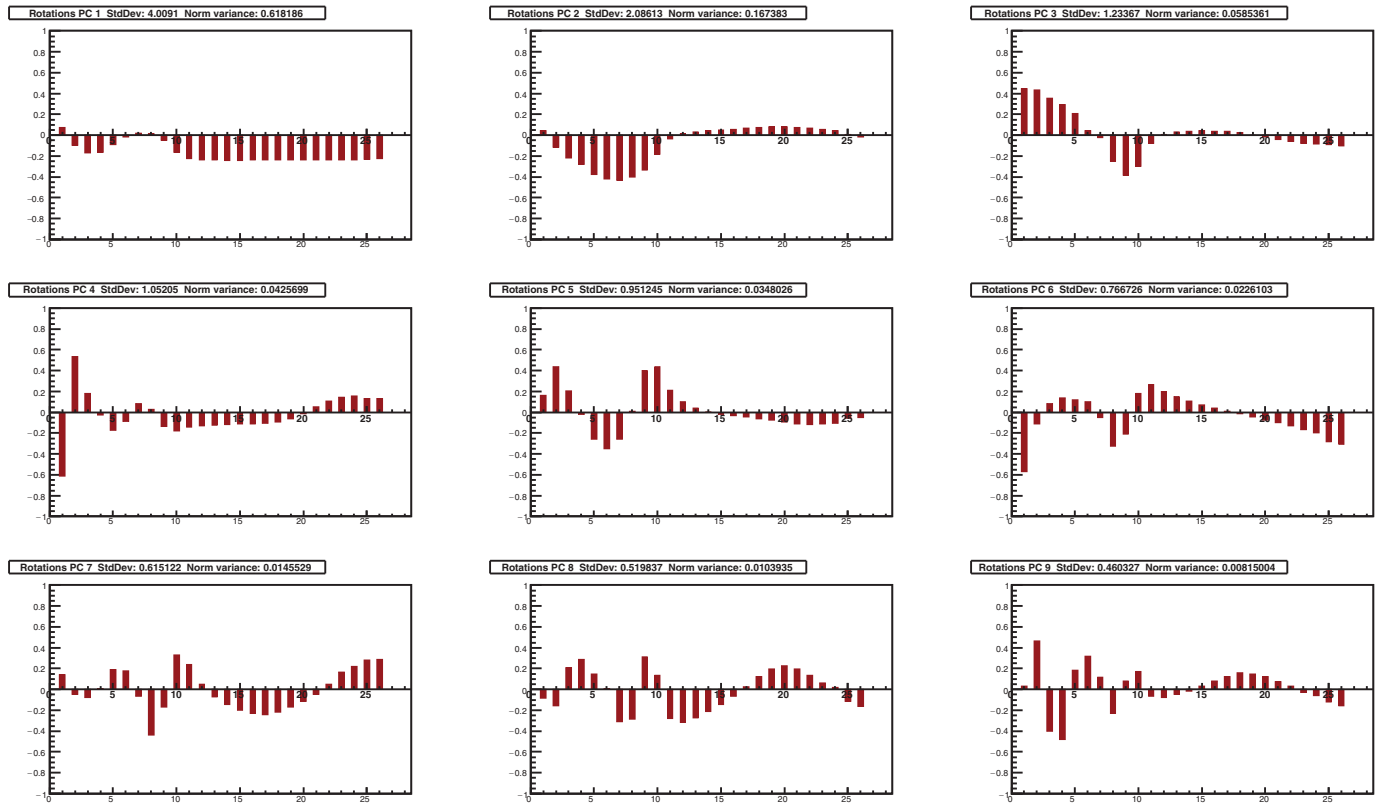


**Fig. 3.** Composition of nine principal components with largest variance (in decreasing order). Input variables are displayed on X-axis: 1 being pressure, 2 temperature of 10 mb isobaric level, 26 being local ground level temperature. Y-axis represents rotations.

decomposition. After decomposition, a new set of 26 principal components was obtained. Decomposition should not be regarded as universal, but it should be redone for every location and period under study.

One year was selected as a suitable time period for the analysis, in order to reduce possible seasonal bias, due to atmospheric temperature annual variation. Additional criteria were quality and consistency of muon data. Taking this into account, final time interval selected for analysis was from 01.06.2010 to 31.05.2011.

Fig. 3 shows composition plots for the first nine principal components, that account for 98% of total variance. X-axis represents input atmospheric variables, first being atmospheric pressure, followed by 10 mb layer temperature, last being ground level local temperature. Y-axis represents decomposition rotations for a given principal component. Interesting features observed on these plots are that first two principal components depend almost exclusively on temperature. The first one is mostly combination of temperatures in the troposphere (isobaric levels 250–1000 mb) with almost equal weights. The second eigenvector accounts for significant variance of temperatures in higher atmospheric levels (10–250 mb), with the strongest contribution centered in the tropopause. Components 3 to 6 have mixed p-T composition. The correlation of atmospheric pressure and temperature at different heights is not surprising. The diurnal and semi-diurnal oscillations of pressure are attributed to the warming of the upper atmosphere by the Sun [33]. This correlation makes it impossible to define a single barometric parameter in PCA based method of atmospheric corrections. It's worth mentioning that Dorman [34] recognizes three different barometric effects: absorption, decay and genera-

tion effect. It also indicates that empirical methods with separated pressure and temperature corrections might lead to overcorrection.

The values of the eigenvectors for these first nine components are also given in Table 1.

Fig. 4 shows plot of proportion of variance as well as plot of cumulative variance for obtained principal components. Corresponding numerical values are given in Table 2.

Usually, only a first few principal components (containing high fraction of total variance) are of practical interest. There are various different methods and rules for choosing how many PCs to retain in the analysis, none completely free of subjectivity (see for example a thorough discussion in [35]). A rule based on cumulative percentage of total variation usually recommends to retain PCs responsible for 70–90% of total variation. When one or two components are dominant, higher value (95%) is appropriate. In our case it would mean keeping first 6 PCs. According to Kaiser's rule only PCs with the eigenvalue  $\lambda > 1$  should be retained. Jolliffe [35] suggested 0.7 as correct level, exceeded by six of our PCs. Another rule proposes to retain components with the eigenvalue above mean, a condition satisfied by first seven of our PCs. Another popular model is broken stick, but in application to our problem is too restrictive, leading to only two relevant PCs. The scree graph or log-eigenvalue diagram don't provide clean cut with our set of PCs.

To test the meaningfulness of potentially relevant PCs, the time series from PC data are constructed and tested whether they are distinguishable from white noise. The procedure is often done when principal component analysis is applied to atmospheric physics problems [36]. The time series with hourly resolution for the first three PCs are plotted on Fig. 5.

**Table 1**  
Definition of first nine principal components.

| Variables | Principal components |          |          |          |          |          |          |          |          |
|-----------|----------------------|----------|----------|----------|----------|----------|----------|----------|----------|
|           | PC1                  | PC2      | PC3      | PC4      | PC5      | PC6      | PC7      | PC8      | PC9      |
| $p$       | 0.07699              | 0.04117  | 0.44694  | -0.61285 | 0.16301  | -0.57121 | 0.14028  | -0.08106 | 0.03443  |
| $T(10)$   | -0.0947              | -0.11603 | 0.43488  | 0.5344   | 0.43741  | -0.11036 | -0.04499 | -0.15825 | 0.46469  |
| $T(20)$   | -0.16947             | -0.21766 | 0.35754  | 0.18029  | 0.20527  | 0.08546  | -0.07719 | 0.20635  | -0.40309 |
| $T(30)$   | -0.16476             | -0.27825 | 0.29593  | -0.02505 | -0.02204 | 0.14134  | 0.00634  | 0.28574  | -0.47812 |
| $T(50)$   | -0.09124             | -0.37682 | 0.20969  | -0.17322 | -0.25798 | 0.12084  | 0.19349  | 0.14645  | 0.18493  |
| $T(70)$   | -0.01483             | -0.42304 | 0.04507  | -0.08651 | -0.3472  | 0.09965  | 0.18155  | 0.01024  | 0.31886  |
| $T(100)$  | 0.02192              | -0.43132 | -0.02451 | 0.08228  | -0.25692 | -0.04937 | -0.06464 | -0.3103  | 0.1183   |
| $T(150)$  | 0.01487              | -0.40127 | -0.24673 | 0.03037  | 0.012    | -0.32566 | -0.43658 | -0.28393 | -0.23316 |
| $T(200)$  | -0.04737             | -0.33404 | -0.38636 | -0.13563 | 0.40141  | -0.2069  | -0.16852 | 0.31181  | 0.07995  |
| $T(250)$  | -0.16218             | -0.17984 | -0.29739 | -0.18123 | 0.43708  | 0.18013  | 0.32866  | 0.13662  | 0.17389  |
| $T(300)$  | -0.22473             | -0.03266 | -0.07561 | -0.14073 | 0.21179  | 0.26504  | 0.23807  | -0.27931 | -0.06785 |
| $T(350)$  | -0.2369              | 0.01439  | 0.00488  | -0.12991 | 0.0998   | 0.1988   | 0.05306  | -0.31612 | -0.0771  |
| $T(400)$  | -0.23956             | 0.03362  | 0.02958  | -0.12159 | 0.04075  | 0.14932  | -0.06959 | -0.27189 | -0.04852 |
| $T(450)$  | -0.24028             | 0.04271  | 0.0402   | -0.11503 | 0.00384  | 0.10744  | -0.14772 | -0.21165 | -0.01823 |
| $T(500)$  | -0.24005             | 0.04935  | 0.0428   | -0.11304 | -0.02187 | 0.07218  | -0.19893 | -0.14512 | 0.03068  |
| $T(550)$  | -0.23958             | 0.05695  | 0.03965  | -0.11295 | -0.03254 | 0.0388   | -0.23263 | -0.06843 | 0.08056  |
| $T(600)$  | -0.23881             | 0.06549  | 0.03681  | -0.10649 | -0.04369 | 0.01102  | -0.24562 | 0.02401  | 0.12499  |
| $T(650)$  | -0.23854             | 0.07279  | 0.0236   | -0.09184 | -0.06132 | -0.01542 | -0.21788 | 0.12597  | 0.15977  |
| $T(700)$  | -0.23835             | 0.0801   | 0.00429  | -0.06052 | -0.07601 | -0.04668 | -0.16785 | 0.19559  | 0.14932  |
| $T(750)$  | -0.23842             | 0.08071  | -0.01837 | -0.01332 | -0.09245 | -0.07308 | -0.11295 | 0.22563  | 0.12401  |
| $T(800)$  | -0.23814             | 0.07557  | -0.03907 | 0.05036  | -0.10989 | -0.09943 | -0.04696 | 0.19596  | 0.07735  |
| $T(850)$  | -0.23701             | 0.0675   | -0.06202 | 0.1081   | -0.11988 | -0.12745 | 0.04989  | 0.13672  | 0.0304   |
| $T(900)$  | -0.23535             | 0.05462  | -0.07977 | 0.14776  | -0.11454 | -0.16955 | 0.16551  | 0.06204  | -0.02952 |
| $T(925)$  | -0.23414             | 0.04606  | -0.08313 | 0.15641  | -0.10257 | -0.19925 | 0.21877  | 0.01715  | -0.05804 |
| $T(975)$  | -0.23108             | 0.00789  | -0.08827 | 0.13022  | -0.05888 | -0.28046 | 0.284    | -0.11523 | -0.12249 |
| $T(1000)$ | -0.22494             | -0.01582 | -0.10092 | 0.13401  | -0.04977 | -0.30749 | 0.28553  | -0.16516 | -0.15908 |

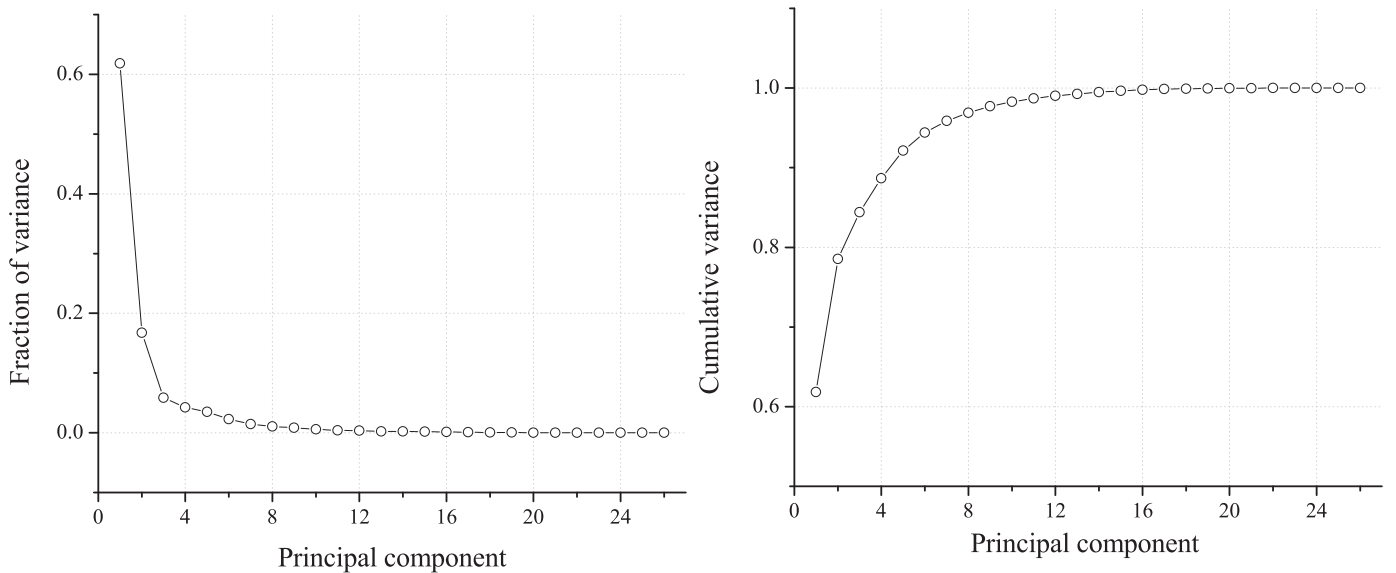


**Fig. 4.** Proportion of variance (left) and cumulative proportion of variance (right) for all 26 principal components.

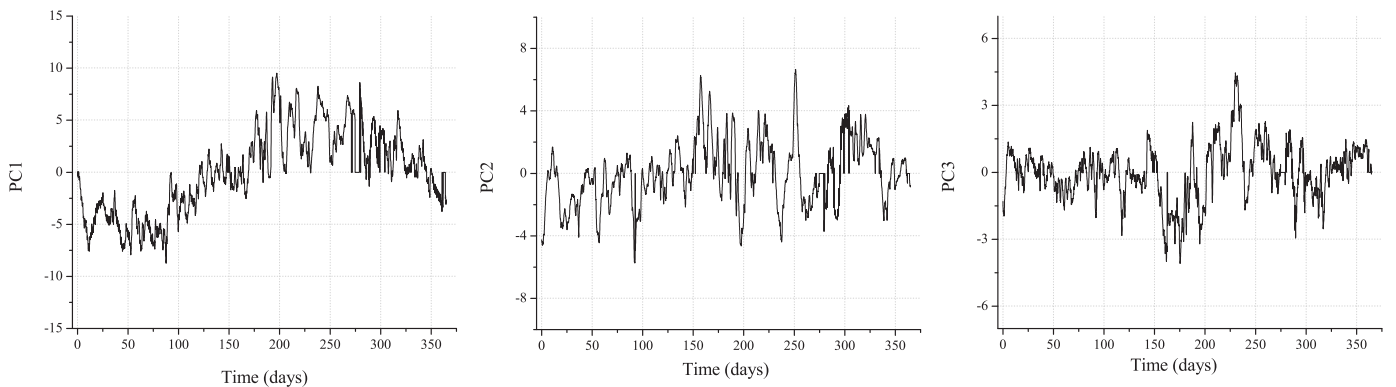


**Fig. 5.** Time series of the first 3 PCs.

**Table 2**  
Variance (individual and cumulative) for all 26 PCs.

| Principal component | Eigenvalue | Percentage of variance | Cumulative variance (%) |
|---------------------|------------|------------------------|-------------------------|
| 1                   | 4.0091     | 0.618186               | 0.618186                |
| 2                   | 2.08613    | 0.167383               | 0.785569                |
| 3                   | 1.23367    | 0.0585361              | 0.844105                |
| 4                   | 1.05205    | 0.0425699              | 0.886675                |
| 5                   | 0.951245   | 0.0348026              | 0.921478                |
| 6                   | 0.766726   | 0.0226103              | 0.944088                |
| 7                   | 0.615122   | 0.0145529              | 0.958641                |
| 8                   | 0.519837   | 0.0103935              | 0.969034                |
| 9                   | 0.460327   | 0.00815004             | 0.977184                |
| 10                  | 0.382006   | 0.00561263             | 0.982797                |
| 11                  | 0.32832    | 0.00414592             | 0.986943                |
| 12                  | 0.294489   | 0.00333553             | 0.990278                |
| 13                  | 0.247876   | 0.00236317             | 0.992642                |
| 14                  | 0.239462   | 0.00220546             | 0.994847                |
| 15                  | 0.206157   | 0.00163465             | 0.996482                |
| 16                  | 0.184453   | 0.00130857             | 0.99779                 |
| 17                  | 0.144657   | 8.04834E-4             | 0.998595                |
| 18                  | 0.119676   | 5.5086E-4              | 0.999146                |
| 19                  | 0.0938189  | 3.38538E-4             | 0.999485                |
| 20                  | 0.0739496  | 2.10328E-4             | 0.999695                |
| 21                  | 0.0586253  | 1.32189E-4             | 0.999827                |
| 22                  | 0.0414996  | 6.62391E-5             | 0.999893                |
| 23                  | 0.0338811  | 4.41511E-5             | 0.999937                |
| 24                  | 0.0281359  | 3.04472E-5             | 0.999968                |
| 25                  | 0.0219102  | 1.84637E-5             | 0.999986                |
| 26                  | 0.0188263  | 1.36319E-5             | 1                       |

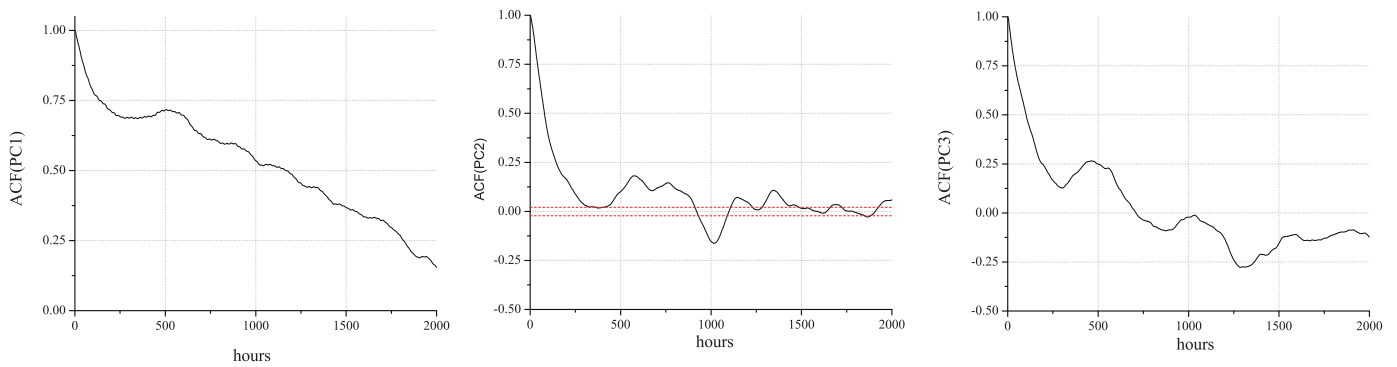


**Fig. 6.** Autocorrelation function of the first 3 PCs. Time lag is given in hours. In the case of PC2, 95% significance level is indicated by dashed red line. (For interpretation of the references to color in this figure legend, the reader is referred to the web version of this article.)

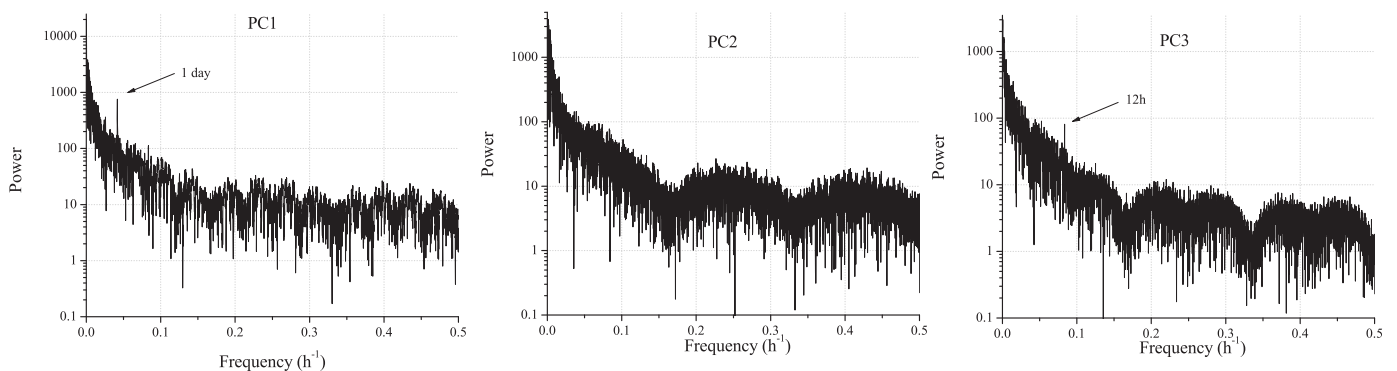


**Fig. 7.** Spectral analysis of time series of the first 3 PCs.

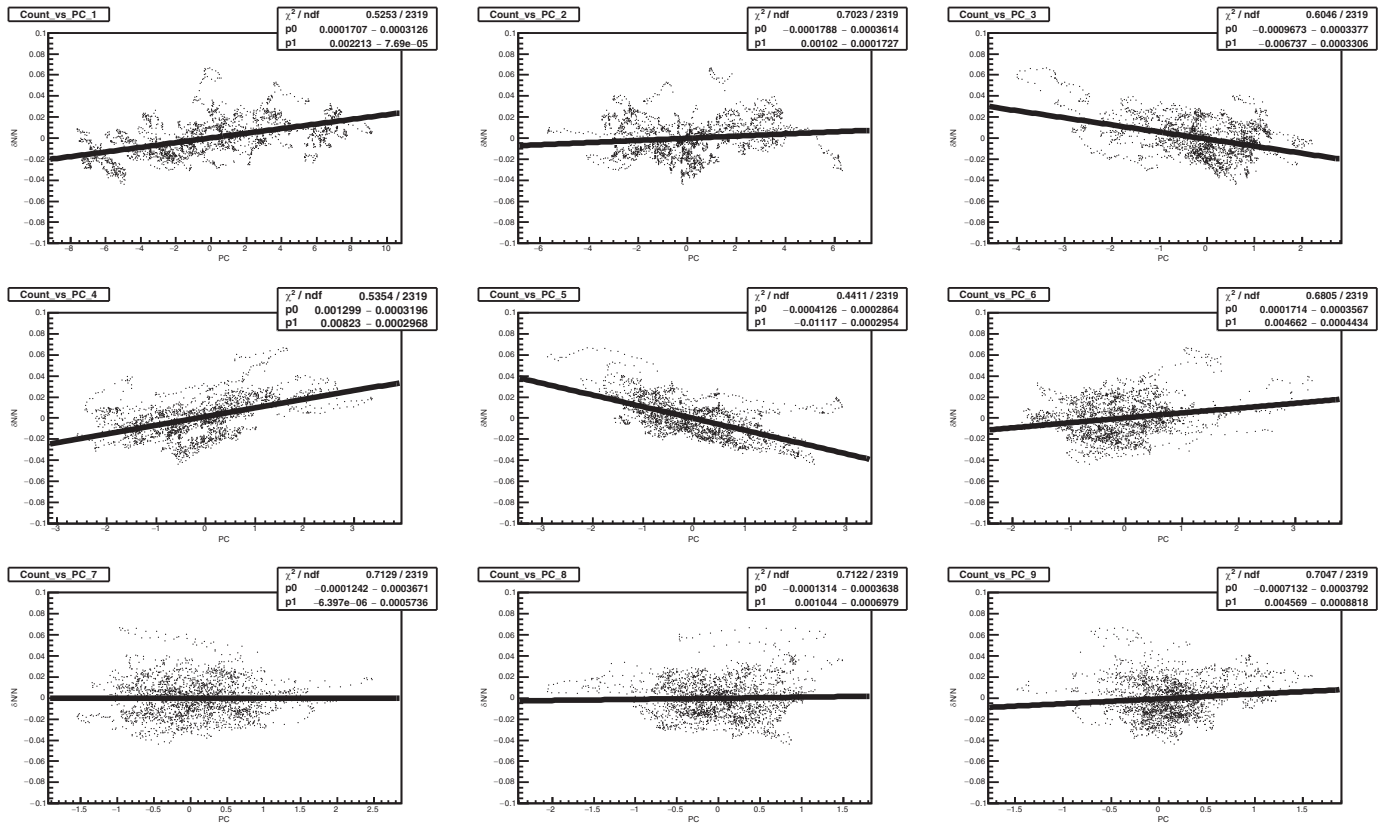


Fig. 8. Muon count dependence on principal components for the first nine principal components (GLL).

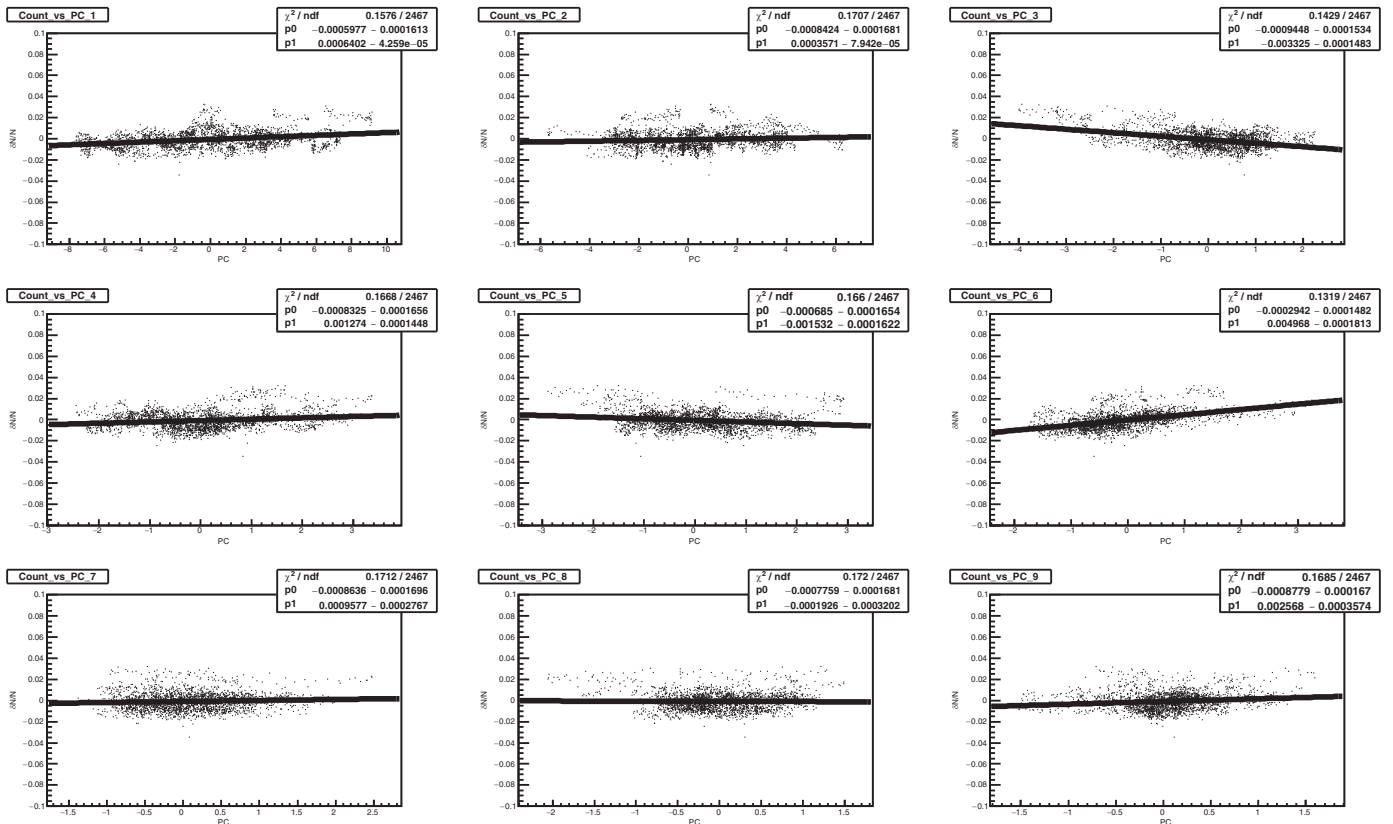


Fig. 9. Muon count dependence on principal components for the first nine principal components (UL).

The subsequent temperature and pressure measurements are highly correlated, as evident from autocorrelation function plot for selected PCs (Fig. 6).

The spectral analysis of the PC time series reveals, for PCs with the strong pressure component, semi-diurnal periodicity in addition to diurnal (Fig. 7).

Since our purpose is the regression of muon data with principal components, selecting the components with significantly high variance is not the main issue. It is more important to identify PCs with high correlation with CR data. Components with relatively low variance, can have high predictive power.

#### 2.4. Correlation of principal components with CR muon count rate and correction of muon data

Scatter plot of muon count rate vs. PCs, together with the linear fit for the first nine principal components are shown on Fig. 8 (GLL) and Fig. 9 (UL). In the analysis hourly summed muon counts and principal component values for the respective hour were used. To minimize the effect of geomagnetic disturbances, only data for International Quiet Days were taken into account. The International Quiet Days are the days with minimum geomagnetic activity for each month. The selection of quiet days is deduced from  $K_p$  index. In our analysis 5 quietest days for each month are considered. The values of correlation coefficients are listed in Table 3.

Principal components PC1, PC3, PC4, PC5 and PC6 have been identified as ones with significant contribution to the muon flux variation. Interestingly enough, the PC2, responsible for 16.7% variance of the meteorological data has very little effect on muon flux, at neither ground nor underground level. Ground level muon flux variation is more affected by the first principal component, depending chiefly on the temperature in the troposphere. The finding agrees with usual negative temperature effect. The other PCs are difficult to compare with traditional correction parameters. Yet, the effect of PC3, that is composed more from upper atmosphere temperatures and hence could be loosely associated with positive temperature effect, is more pronounced for the underground muon flux. Fourth and fifth principal components with strong pressure contribution affect more ground level muon flux. On the other hand, PC6, also the one with high pressure component, has more pronounced influence on underground muon flux.

Gradients obtained from the fits for the significant principal components 1, 3, 4, 5 and 6 were then used to calculate the PCA corrected muon count according to the formula:

$$N_{\mu}^{(corr)} = N_{\mu} - \langle N_{\mu} \rangle + \sum_i k_i PC_i, \quad i = 1, 3, 4, 5, 6 \quad (5)$$

where  $N_{\mu}^{(corr)}$  corr is the corrected muon count,  $N_{\mu}$  is the raw muon count,  $\langle N_{\mu} \rangle$  is the mean count for the whole period,  $k_i$  are the gradients and  $PC_i$  are the corresponding principal components. Resulting corrected muon count time series are plotted on Figs. 10 (GLL) and 11 (UL) along with raw and pressure only corrected time series. Pressure corrected time series are produced for reference. Barometric coefficient was determined by applying linear regression to the same data set used for PCA. Data was previously corrected for temperature effect using integral method, as in Ref. [37]. Pressure corrected and PCA corrected time series are fitted with sine function with annual period in order to illustrate how PCA correction affects yearly variation induced by temperature effect.

PCA based atmospheric corrections remove 64.5% of total variance in GLL time series and 38.1% in UL time series. Pressure corrected CR time series exhibit annual variation, a consequence of

**Table 3**  
Correlation coefficients between principal components and muon count rate in the ground level laboratory (GLL) and underground laboratory (UL).

|     | PC 1 | 2    | 3     | 4    | 5     | 6    | 7     | 8    | 9     | 10   | 11   | 12    | 13    | 14   | 15    | 16    | 17   | 18    | 19    | 20   | 21    | 22   | 23   | 24    | 25   | 26   |
|-----|------|------|-------|------|-------|------|-------|------|-------|------|------|-------|-------|------|-------|-------|------|-------|-------|------|-------|------|------|-------|------|------|
| GLL | 0.43 | 0.01 | -0.37 | 0.48 | -0.55 | 0.30 | -0.01 | 0.03 | -0.01 | 0.06 | 0.00 | -0.04 | 0.00  | 0.01 | 0.02  | -0.01 | 0.00 | -0.01 | -0.01 | 0.03 | -0.03 | 0.00 | 0.02 | -0.01 | 0.04 | 0.02 |
| UL  | 0.26 | 0.02 | -0.48 | 0.21 | -0.19 | 0.52 | 0.02  | 0.04 | 0.07  | 0.04 | 0.01 | -0.04 | -0.07 | 0.06 | -0.02 | -0.05 | 0.04 | 0.04  | -0.02 | 0.00 | 0.00  | 0.01 | 0.00 | -0.03 | 0.01 | 0.01 |

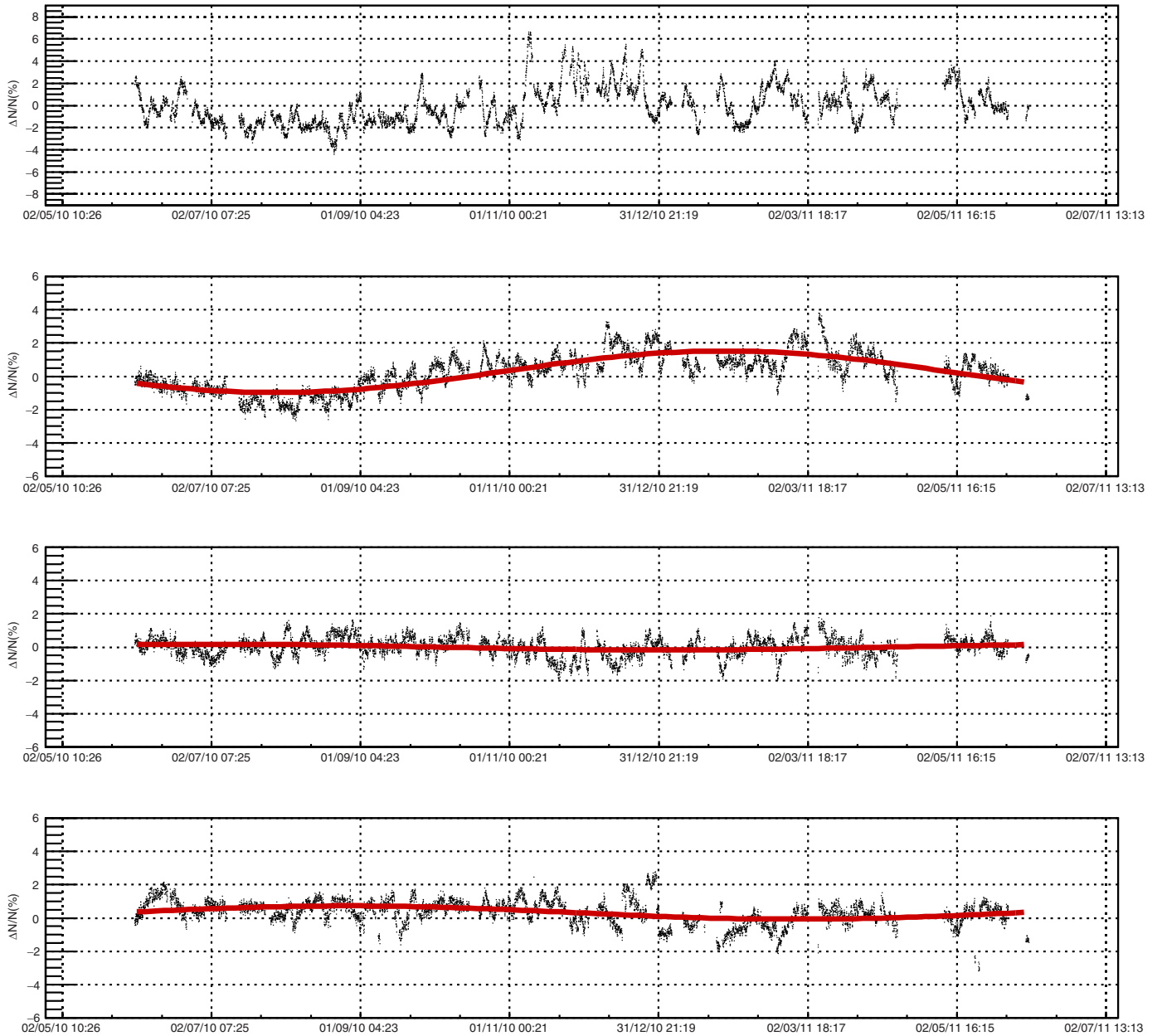


**Fig. 10.** Raw (upper panel), pressure corrected (middle panel), pressure+temperature corrected with PCA method (3rd panel from the top) and pressure+temperature corrected with integral method (lower panel) normalized muon count rate for GLL. The sine function with one year period is fitted to the data.

the temperature effect. The performance of the temperature correction may be tested by comparing the amplitude of the annual variation before and after correction. With presented method the amplitude of the annual variation is reduced by 86% (54.9%) in the case of GLL (UL) with respect to the pressure only corrected time series.

To further test the new method, the atmospheric correction of GLL data are performed by the integral method. The correction resulted in 56.25% of variance reduction and 68.1% of reduction of the amplitude of the annual wave. At least in the case of our CR data set the new method performs somewhat better than the integral method.

### 3. Conclusion

The principal component analysis is successfully used to construct a new empirical method for the atmospheric corrections of CR muon data. The method is equally applicable to all muon detectors, irrespective to location: ground level, shallow or deep underground. It requires knowledge of the atmospheric pressure and temperatures along the entire atmosphere, which is nowadays available in databases such as GFS. The method is suitable for the near real-time correction, with the delay defined by the availability of the atmospheric data (one day in the case of present GFS data). When applied to Belgrade muon data from two detectors

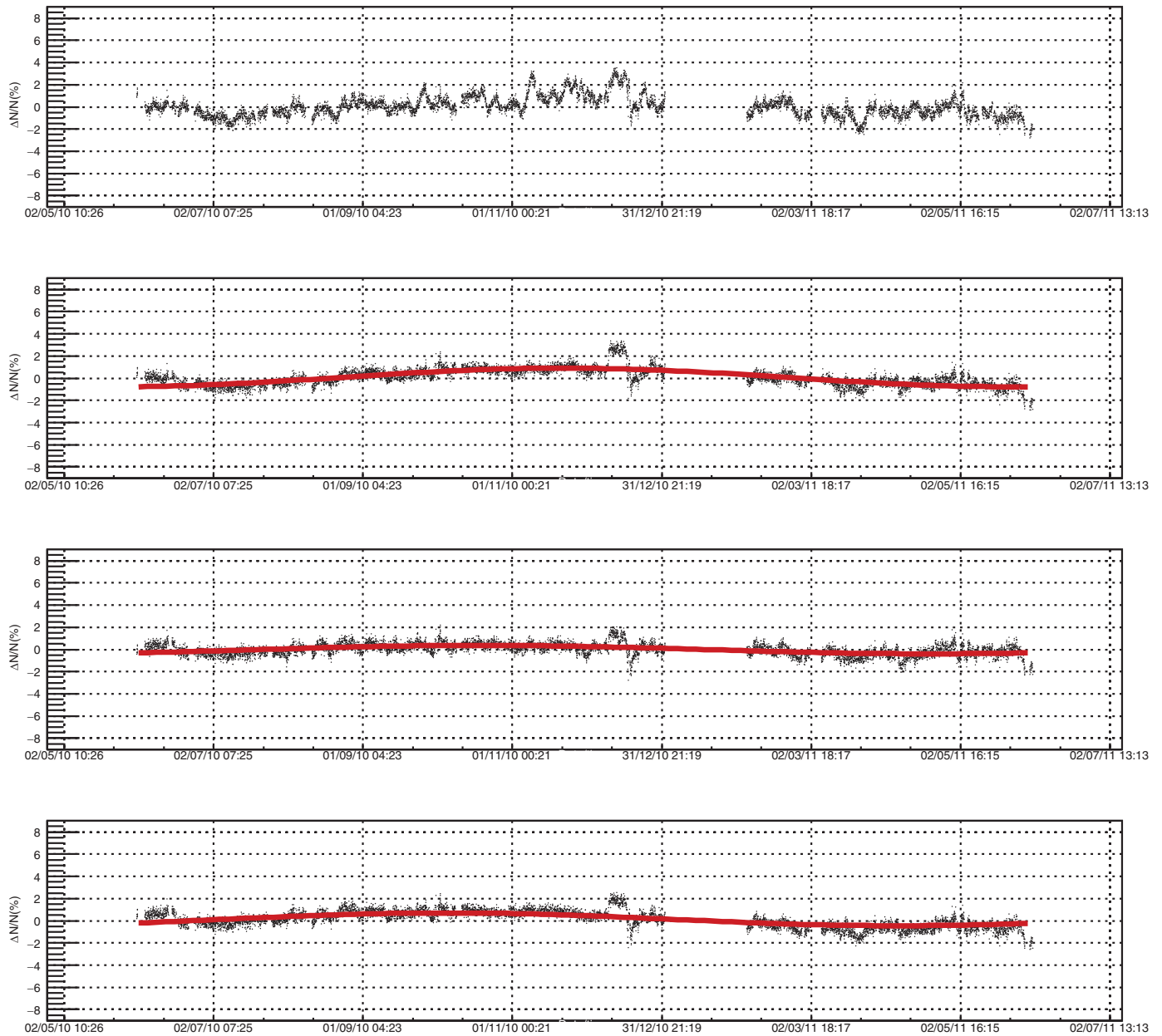


**Fig. 11.** Raw (upper panel), pressure corrected (middle panel), pressure+temperature corrected with PCA method (3rd panel from the top) and pressure+temperature corrected with integral method (lower panel) normalized muon count rate for UL. The sine function with one year period is fitted to the data.

(ground level and at 25 mwe), the method requires correction to five parameters, determined from linear regression. With the same CR dataset, the present method yields results superior to the integral method in terms of variance reduction and reduction of the annual variation. The new method is also suitable for temperature corrections of the neutron monitor data, which is seldom done in practice.

### Acknowledgments

The authors are deeply grateful to Dr. Viktor Yanke for the encouragement and useful advice. The present work was funded by the Ministry of Education, Science and Technological Development of the Republic of Serbia, under the Project no. 171002.

### References

- [1] L. Myssowsky, L. Tuwim, Unregelmäßige intensitätsschwankungen der höhenstrahlung in geringer seehöhe, *Zeitsch. Phys.* 39 (2–3) (1926) 146–150.
- [2] E. Steinke, Über schwankungen und barometereffekt der kosmischen ultrastrahlung im meeresniveau, *Zeitsch. Phys.* 64 (1–2) (1930) 48–63.
- [3] P.M. Blackett, On the instability of the barytron and the temperature effect of cosmic rays, *Phys. Rev.* 54 (11) (1938) 973.
- [4] M. Forro, Temperature effect of cosmic radiation at 1000-m water equivalent depth, *Phys. Rev.* 72 (9) (1947) 868.
- [5] C.M.G. Lattes, G.P. Occhialini, C.F. Powell, Observations on the tracks of slow mesons in photographic emulsions, *Nature* 160 (4067) (1947) 486.
- [6] C.M.G. Lattes, H. Muirhead, G.P. Occhialini, C.F. Powell, Processes involving charged mesons, *Nature* 159 (4047) (1947) 694.
- [7] G. Occhialini, C. Powell, Nuclear disintegrations produced by slow charged particles of small mass, *Nature* 159 (4032) (1947) 186.
- [8] A. Duperier, The meson intensity at the surface of the earth and the temperature at the production level, *Proc. Phys. Soc. Lond. Sect. A* 62 (11) (1949) 684.
- [9] A. Duperier, Temperature of the upper atmosphere and meson production, *Nature* 167 (4243) (1951) 312.

- [10] C. Baker, D. Hall, J. Humble, M. Duldig, Atmospheric correction analysis for the Mawson muon telescopes, in: International Cosmic Ray Conference, 3, 1993, p. 753.
- [11] A. Maghrabi, M. Almutayri, Atmospheric effect on cosmic ray muons at high cut-off rigidity station, *Adv. Astron.* 2016 (2016).
- [12] C.R. Braga, A. Dal Lago, T. Kuwabara, N.J. Schuch, K. Munakata, Temperature effect correction for the cosmic ray muon data observed at the Brazilian Southern Space Observatory in São Martinho da Serra, *J. Phys.* 409 (2013) 012138 IOP Publishing.
- [13] G.C. Castagnoli, M. Dodero, Temperature effect of the muon component underground and pion attenuation length, *Il Nuovo Cimento B* (1965–1970) 51 (2) (1967) 525–534.
- [14] A. Fenton, R. Jacklyn, R. Taylor, Cosmic ray observations at 42 m we underground at hobart, tasmania, *Il Nuovo Cimento* (1955–1965) 22 (2) (1961) 285–295.
- [15] M. Zazyan, M. Ganeva, M. Berkova, V. Yanke, R. Hippler, Atmospheric effect corrections of mustang data, *J. Space Weather Space Clim.* 5 (2015) A6.
- [16] L. Dorman, The temperature effect of the hard component of cosmic rays, *Doklady Akad. Nauk SSSR* 95 (1954).
- [17] E. Feinberg, On the nature of cosmic ray barometric and temperature effects, *DAN SSSR* 53 (5) (1946) 421–424.
- [18] L.I. Dorman, Cosmic ray variations, Technical Report, Foreign Technology Div Wright-Patterson AFB OHIO, 1957.
- [19] K. Maeda, M. Wada, Atmospheric temperature effect upon the cosmic-ray intensity at sea level, *J. Sci. Res. Inst.* 48 (1954).
- [20] V. Dvornikov, Y.Y. Krest'yannikov, A. Sergeev, Determination of the variation of average-mass temperature of the atmosphere by data of cosmic ray intensity, *Geomag. Aeron.* 16 (1976) 923–925.
- [21] V. Yanchukovsky, G.Y. Filimonov, R. Hisamov, Atmospheric variations in muon intensity for different zenith angles, *Bull. Russ. Acad. Sci.* 71 (7) (2007) 1038–1040.
- [22] R. De Mendonça, C. Braga, E. Echer, A. Dal Lago, K. Munakata, T. Kuwabara, M. Kozai, C. Kato, M. Rockenbach, N. Schuch, et al., The temperature effect in secondary cosmic rays (muons) observed at the ground: analysis of the Global MUON Detector Network data, *Astrophys. J.* 830 (2) (2016) 88.
- [23] A. Dmitrieva, I. Astapov, A. Kovylyayeva, D. Pankova, Temperature effect correction for muon flux at the earth surface: estimation of the accuracy of different methods, *J. Phys.* 409 (2013) 012130. IOP Publishing.
- [24] P.H. Barrett, L.M. Bollinger, G. Cocconi, Y. Eisenberg, K. Greisen, Interpretation of cosmic-ray measurements far underground, *Rev. Mod. Phys.* 24 (3) (1952) 133.
- [25] S. Tilav, P. Desiati, T. Kuwabara, D. Rocco, F. Rothmaier, M. Simmons, H. Wissing, et al., Atmospheric variations as observed by IceCube, arXiv:1001.0776 (2010).
- [26] P. Adamson, C. Andreopoulos, K. Arms, R. Armstrong, D. Auty, D. Ayres, C. Backhouse, J. Barnett, G. Barr, W. Barrett, et al., Observation of muon intensity variations by season with the Minos far detector, *Phys. Rev. D* 81 (1) (2010) 012001.
- [27] H. Carmichael, M. Bercovitch, J.F. Steljes, Introduction of meteorological corrections into meson monitor data, *Tellus* 19 (1) (1967) 143–160, doi:10.1111/j.2153-3490.1967.tb01468.x.
- [28] M.D. Berkova, A.V. Belov, E.A. Eroshenko, V.G. Yanke, Temperature effect of the muon component and practical questions for considering it in real time, *Bull. Russ. Acad. Sci.* 75 (6) (2011) 820–824, doi:10.3103/S1062873811060086.
- [29] A. Dmitrieva, R. Kokoulin, A. Petrukhin, D. Timashkov, Corrections for temperature effect for ground-based muon hodoscopes, *Astropart. Phys.* 34 (6) (2011) 401–411, doi:10.1016/j.astropartphys.2010.10.013.
- [30] Global forecast system (GFS), <https://www.ncdc.noaa.gov/data-access/modeldata/model-datasets/global-forecast-system-gfs>.
- [31] National centers for environmental prediction (NCEP), <http://www.ncep.noaa.gov/>.
- [32] A. Dragić, V. Udovičić, R. Banjanac, D. Joković, D. Maletić, N. Veselinović, M. Savić, J. Puzović, I.V. Aničin, The new setup in the Belgrade low-level and cosmic-ray laboratory, *Nucl. Technol. Radiat. Protect.* 26 (3) (2011) 181–192.
- [33] B. Haurwitz, The diurnal surface-pressure oscillation, *Arch. Meteorol. Geophys. Bioklimatol. Ser. A* 14 (4) (1965) 361–379, doi:10.1007/BF02253483.
- [34] L.I. Dorman, Cosmic Rays in the Earth's Atmosphere and Underground, Springer Netherlands, 2004, doi:10.1007/978-1-4020-2113-8.
- [35] I. Jolliffe, Principal Component Analysis, Springer-Verlag, 2002, doi:10.1007/b98835.
- [36] R.W. Preisendorfer, D.M. Curtis, Principal component analysis in meteorology and oceanography, Elsevier, Amsterdam, 1988.
- [37] M. Savić, D. Maletić, D. Joković, N. Veselinović, R. Banjanac, V. Udovičić, A. Dragić, Pressure and temperature effect corrections of atmospheric muon data in the belgrade cosmic-ray station, *J. Phys. Conf. Ser.* 632 (1) (2015) 012059.



# An underground laboratory as a facility for studies of cosmic-ray solar modulation

N. Veselinović, A. Dragić\*, M. Savić, D. Maletić, D. Joković, R. Banjanac, V. Udovičić

*Institute of Physics, University of Belgrade, Pregrevica 118, 11080 Zemun, Serbia*

## ARTICLE INFO

### Keywords:

Cosmic ray muons  
Forbush decrease  
Response function

## ABSTRACT

The possibility of utilizing a shallow underground laboratory for the study of energy dependent solar modulation process is investigated. The laboratory is equipped with muon detectors at ground level and underground (25mwe), and with an underground asymmetric muon telescope to have a single site detection system sensitive to different median energies of primary cosmic-ray particles. The detector response functions to galactic cosmic rays are determined from Monte Carlo simulation of muon generation and propagation through the atmosphere and soil, based on CORSIKA and GEANT4 simulation packages. The present setup is suitable for studies of energy dependence of Forbush decreases and other transient or quasi-periodic cosmic-ray variations.

© 2017 Elsevier B.V. All rights reserved.

## 1. Introduction

Galactic cosmic rays (GCR) arriving at Earth after propagating through the heliosphere interact with nuclei in the atmosphere. These interactions of primary CRs lead to production of a cascade (shower) of secondary particles: hadrons, electrons, photons, muons, neutrinos. Ground based CR detectors are designed to detect some species of secondary cosmic radiation. Widely in use are neutron monitors [1,2], muon telescopes [3,4], various types of air shower arrays [5],  $\gamma$ -ray air Cherenkov detectors [6], air fluorescence detectors [7] etc.

The flux and energy spectra of GCR are modulated by the solar magnetic field, convected by the solar wind. Particularly affected are GCR at the low energy side of the spectrum (up to  $\sim 100$  GeV). Therefore, secondary CRs generated in the atmosphere can be used for studying solar and heliospheric processes. Among the best known effects of the solar modulation are CR flux variations with 11 year period of the solar cycle, 22 year magnetic cycle, diurnal variation and Forbush decrease. The so called corotation with the solar magnetic field results in the flux variation with the 27-day period of solar rotation.

Modulation effects have been studied extensively by neutron monitors (NM) [8,9], sensitive up to several tens of GeV, depending on their geomagnetic location and atmospheric depth. Muon detectors at ground level are sensitive to primary particles of higher energies than NMs. Underground muon detectors correspond to even higher energy primaries. For this reason muon observations complement NM observations in studies of long-term CR variations, CR anisotropy and gradients

or rigidity spectrum of Forbush decreases. However, muon observations suffer from difficulties to disentangle variations of atmospheric origin. While the effect of atmospheric pressure is similar to NMs and easy to account for, the temperature effect is more complicated. The entire temperature profile of the atmosphere is contributing, with different net temperature effect on muon flux at different atmospheric layers, as a result of interplay of positive and negative temperature effects. The positive temperature effect is a consequence of reduced atmospheric density with the temperature increase, resulting in less pion interactions and more decays into muons [10]. The negative temperature effect comes from the increased altitude of muon production at the periods of high temperature, with the longer muon path length and the higher decay probability before reaching the ground level [11]. Both effects are accounted for by the integral method of Dorman [12]. The negative temperature effect is dominant for low energy muons (detected at ground level) and the positive for high energy muons (detected deep underground). At shallow depth of several tens of meters of water equivalent both temperature effects contribute to the overall temperature effect. Several detector systems with different sensitivity to primaries at the same location have the advantage of sharing common atmospheric and geomagnetic conditions.

Belgrade CR station is equipped with muon detectors at ground level and at the depth of 25 m.w.e. Underground laboratory is reached only by muons exceeding energy threshold of 12 GeV. The existing detectors are recently amended by additional setup in an attempt to fully exploit laboratory's possibilities to study solar modulation at different

\* Corresponding author.

E-mail address: [dragic@ipb.ac.rs](mailto:dragic@ipb.ac.rs) (A. Dragić).

median rigidities. In the present paper the detector systems at the Belgrade CR station are described. Response functions of muon detectors to galactic cosmic rays are calculated. The detector system represents useful extension of modulation studies with neutron monitors to higher energies, as it is demonstrated in the case of a recent Forbush event.

## 2. Description of Belgrade CR station

The Belgrade cosmic-ray station, situated at the Low Background Laboratory for Nuclear Physics at Institute of Physics, is located at near-sea level at the altitude of 78 m a.s.l. Its geographic position is: latitude  $44^{\circ}51'N$  and longitude  $20^{\circ}23'E$ , with vertical cut-off rigidity 5.3 GV. It consists of the ground level lab (GLL) and the underground lab (UL) which has useful area of  $45 \text{ m}^2$ , dug at a depth of 12 m. The soil overburden consists of loess with an average density  $2.0 \pm 0.1 \text{ g/cm}^3$ . Together with the 30 cm layer of reinforced concrete the laboratory depth is equivalent to 25 m.w.e. At this depth, practically only the muonic component of the atmospheric shower is present [13].

### 2.1. Old setup

The experimental setup [14] consists of two identical sets of detectors and read out electronics, one situated in the GLL and the other in the UL. Each setup utilizes a plastic scintillation detector with dimensions  $100 \text{ cm} \times 100 \text{ cm} \times 5 \text{ cm}$  equipped with 4 PMTs optically attached to beveled corners of a detector. Preamplifier output of two diagonally opposing PMTs are summed and fed to a digitizer input (CAEN FADC, type N1728B). FADC operates at 100 MHz frequency with 14 bit resolution. The events generating enough scintillation light to produce simultaneous signals in both inputs exceeding the given threshold are identified as muon events. The simulated total energy deposit spectrum is presented on the left panel of Fig. 1. After the appropriate threshold conditions are imposed on the signals from two diagonals, the spectrum is reduced to the one represented on the right panel of the same figure. Contribution from different CR components are indicated on both graphs and experimentally recorded spectrum is plotted as well.

Particle identification is verified by a two-step Monte Carlo simulation. In the first step development of CR showers in the atmosphere is traced, starting from the primary particles at the top of the atmosphere by CORSIKA simulation package. CORSIKA output contains information on generated particles (muons, electrons, photons, etc.) and their momenta at given observation level. More details on CORSIKA simulation will be given in Section 3. This output serves as an input for the second step in simulation, based on GEANT4. In the later step energy deposit by CR particles in the plastic scintillator detector are determined, together with the light collection at PMTs. Contributions from different CR components to recorded spectrum are also shown in Fig. 1.

According to the simulation, 87.5% of events in the coincident spectrum originate from muons. To account for the contribution from other particles to the experimental spectrum not all the events in the spectrum are counted when muon time series are constructed. Muon events are defined by setting the threshold corresponding to muon fraction of recorded spectrum. Threshold is set in terms of “constant fraction” of the spectrum maximum, which also reduces count rate fluctuations due to inevitable shifts of the spectrum during long-term measurements.

### 2.2. Upgrade of the detector system

Existing detectors enable monitoring of CR variations at two different median energies. An update is contemplated that would provide more differentiated response. Two ideas are considered. First one was to extend the sensitivity to higher energies with detection of multi-muon events underground. An array of horizontally oriented muon detectors ought to be placed in the UL. Simultaneous triggering of more than

one detector is an indication of a multi-muon event. The idea was exploited in the EMMA underground array [15], located at the deeper underground laboratory in Pyhasalmi mine, Finland, with the intention to reach energies in the so called knee region. For a shallow underground laboratory, exceeding the energy region of solar modulation would open the possibility to study CR flux variations originating outside the heliosphere. Second idea is an asymmetric muon telescope separating muons with respect to zenith angle. Later idea is much less expensive to be put into practice.

Both ideas will be explained in detail and response function to GCR for existing and contemplated detectors calculated in the next section.

## 3. Calculation of response functions

Nature of variations of primary cosmic radiation can be deduced from the record of ground based cosmic ray detectors provided relation between the spectra of primary and secondary particles at surface level are known with sufficient accuracy. Relation can be expressed in terms of rigidity or kinetic energy.

Total detector count rate can be expressed as:

$$N(E_{th}, h, t) = \sum_i \int_{E_{th}}^{\infty} Y_i(E, h) \cdot J_i(E, t) dE \quad (1)$$

where  $E$  is primary particle energy,  $i$  is type of primary particle (we take into account protons and  $\alpha$  particles),  $J_i(E, t)$  is energy spectrum of primary particles,  $h$  is atmospheric depth and  $Y_i(E, h)$  is the so called yield function.  $E_{th}$  is the threshold energy of primary particles. It depends on location (geomagnetic latitude and atmospheric altitude) and detector construction details. At a given location on Earth, only particles with rigidity above vertical rigidity cut-off contribute to the count rate. Also, detector construction often prevents detection of low energy particles. For instance, muon detectors are sometimes covered with a layer of lead. In present configuration our detectors are lead free.

Historically, yield functions were calculated empirically, often exploiting the latitude variations of neutron and muonic CR component [16–18]. With the advancement of computing power and modern transport simulation codes it became possible to calculate yield functions from the interaction processes in the atmosphere [19,20]. The yield function for muons is calculated as:

$$Y_i(E, h) = \int_{E_{th}}^{\infty} \int S_i(\theta, \phi) \cdot \Phi_{i,\mu}(E_i, h, E, \theta, \phi) dE d\Omega \quad (2)$$

where  $S(\theta, \phi)$  is the effective detector area and integration is performed over upper hemisphere.  $\Phi_{i,\mu}(E_i, h, E, \theta, \phi)$  is the differential muon flux per primary particle of the type  $i$  with the energy  $E_i$ .

Total differential response function:

$$W(E, h, t) = \sum_i Y_i(E, h) \cdot J_i(E, t) \quad (3)$$

when normalized to the total count rate gives the fraction of count rate originating from the primary particles with the energy in the infinitesimal interval around  $E$ . Integration of differential response function gives the cumulative response function.

The response functions of our CR detectors are calculated using Monte Carlo simulation of CR transport through the atmosphere with CORSIKA simulation package. Simulation was performed with protons and  $\alpha$ -particles as primary particles. They make  $\sim 94\%$  ( $79\% + 14.7\%$ ) of all primaries [21]. Implemented hadron interaction models were FLUKA for energies below 80 GeV, and QGSJET II-04 for higher energies. If the old version of QGSJET is used, a small discontinuity in response function is noticed at the boundary energy between two models. Geomagnetic field corresponds to the location of Belgrade  $B_x = 22.61 \mu\text{T}$ ,  $B_z = 42.27 \mu\text{T}$ . Power law form of differential energy spectrum of galactic cosmic rays  $J_p(E) \sim E^{-2.7}$  is assumed. Energy range of primary particles is between 1 GeV and  $2 \cdot 10^7$  GeV. Interval of zenith angles is  $0^\circ < \theta < 70^\circ$ . Low energy thresholds for secondary particles are: 150 MeV for hadrons and muons and 15 MeV for electrons

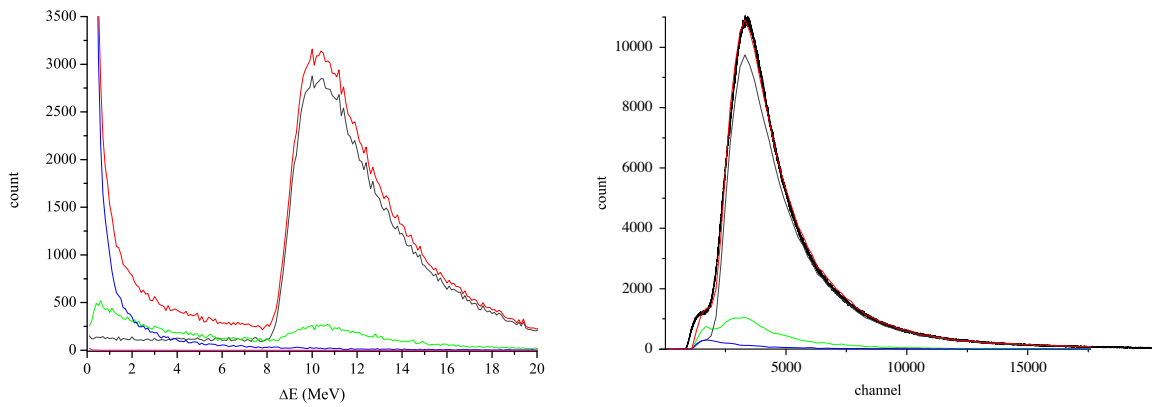


**Fig. 1.** Left —  $\Delta E$  spectrum in the plastic scintillator detector, derived from GEANT simulation; right — the same, but for the events exceeding threshold on both diagonals. Contribution of different CR components to the total energy deposit in the detector: muons-gray line, photons-blue line, electrons-green line and sum of all contributions — red line. The black curve on the right panel is the experimental spectrum. (For interpretation of the references to color in this figure legend, the reader is referred to the web version of this article.)

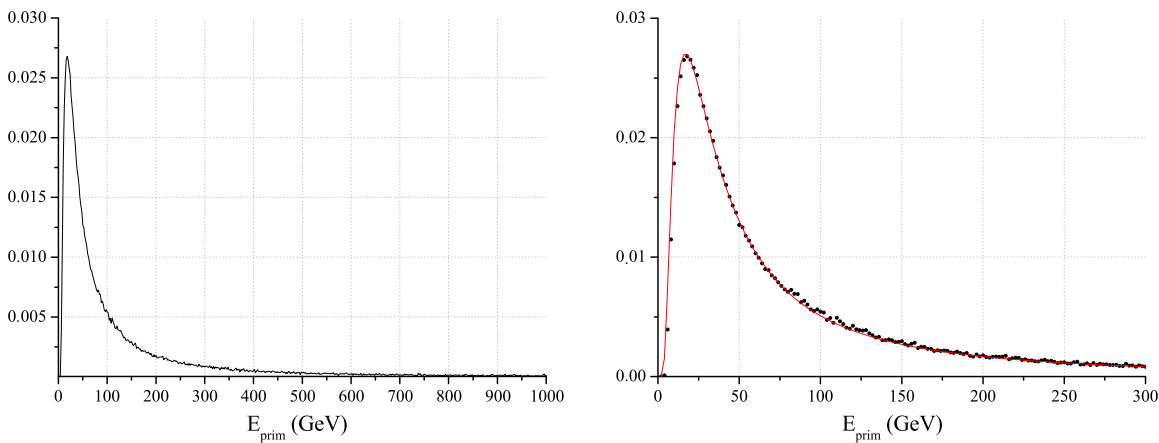


**Fig. 2.** Left: normalized total response function of ground level muon detector to galactic cosmic rays; right: same as left, fitted with Dorman function (red line). (For interpretation of the references to color in this figure legend, the reader is referred to the web version of this article.)

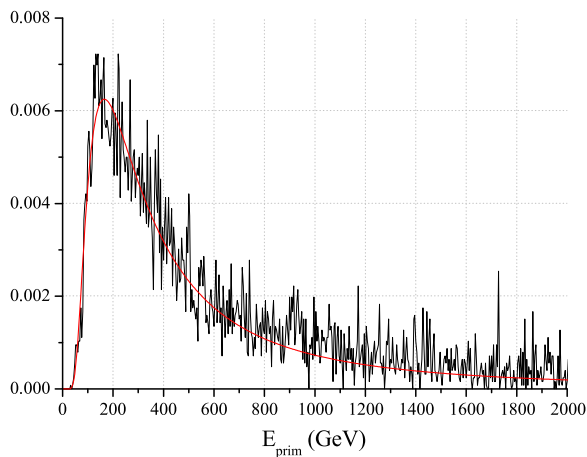


**Fig. 3.** Response function for multi-muon events in UL to galactic cosmic rays.

and photons. Selected atmospheric model is AT511 (Central European atmosphere for May 11 1993). Observational level is at 78m a.s.l.

For calculation of response functions for underground detectors, simulation of particle propagation through the soil overburden is performed using the code based on GEANT4 package. For precise calculation of energy loss, chemical composition of the soil needs to be known. The

composition used in our work is taken from a geochemical study of neighboring loess sections of Batajnica and Stari Slankamen [22]. Most abundant constituents are quartz ( $\text{SiO}_2$ ) 70%, alumina ( $\text{Al}_2\text{O}_3$ ) 15% and quicklime ( $\text{CaO}$ ) 10%, while others include  $\text{Fe}_2\text{O}_3$ ,  $\text{MgO}$ ,  $\text{TiO}_2$ ,  $\text{K}_2\text{O}$ , ... Inaccuracy of our knowledge of the soil chemical composition should not strongly affect our results since, at relevant energies, dominant energy loss mechanism for muons is ionization which, according to Bethe-Bloch formula depends mostly on  $\langle Z \rangle / \langle A \rangle$ . Soil density profile is probed during laboratory construction. It varies slowly with depth and average density is found to be  $(2.0 \pm 0.1) \text{ g/cm}^3$ .

In the simulation, the effective area and angular acceptance of different modes of asymmetric muon telescope (single, coincident and anticoincident) are taken into account.

According to Dorman [12], response function can be parametrized as:

$$W(E) = \begin{cases} 0, & \text{if } E < E_{th}; \\ \frac{a \cdot k \cdot \exp(-aE^{-k})}{E^{(k+1)}(1 - aE_{th}^{-k})}, & \text{otherwise;} \end{cases} \quad (4)$$

with the high energy asymptotics:  $W(E) \approx a \cdot k \cdot E^{-(k+1)}$ .

### 3.1. Ground level

Calculated response function for ground level muon detector is presented on Fig. 2, together with fitted Dorman function (4).

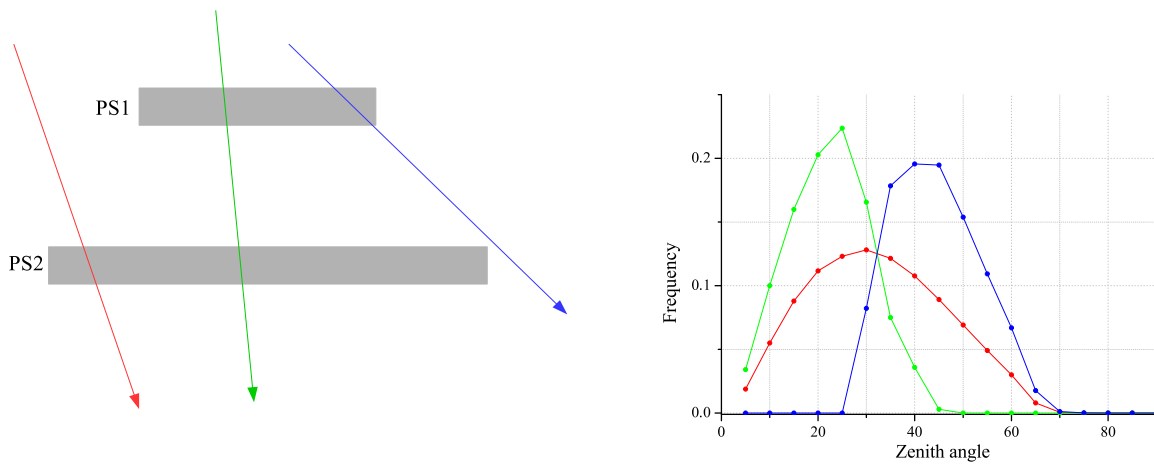


Fig. 4. Left: Schematic view of the asymmetric muon telescope; PS1 — plastic scintillator detector 1, PS2 — plastic scintillator detector 2. Right: angular distribution of detected muons in single mode (red), coincident mode (green) and anticoincident mode (blue), normalized to number of counts in each mode. (For interpretation of the references to color in this figure legend, the reader is referred to the web version of this article.)

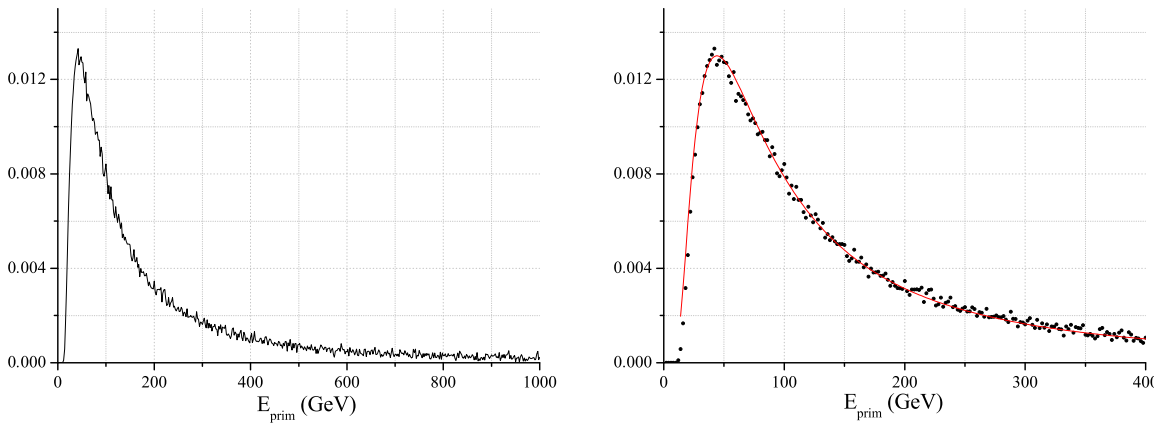


Fig. 5. Response function of single mode of ASYMUT in the UL to galactic cosmic rays. On the right panel the energy interval of interest is enlarged and Dorman function fit is plotted (red line). (For interpretation of the references to color in this figure legend, the reader is referred to the web version of this article.)

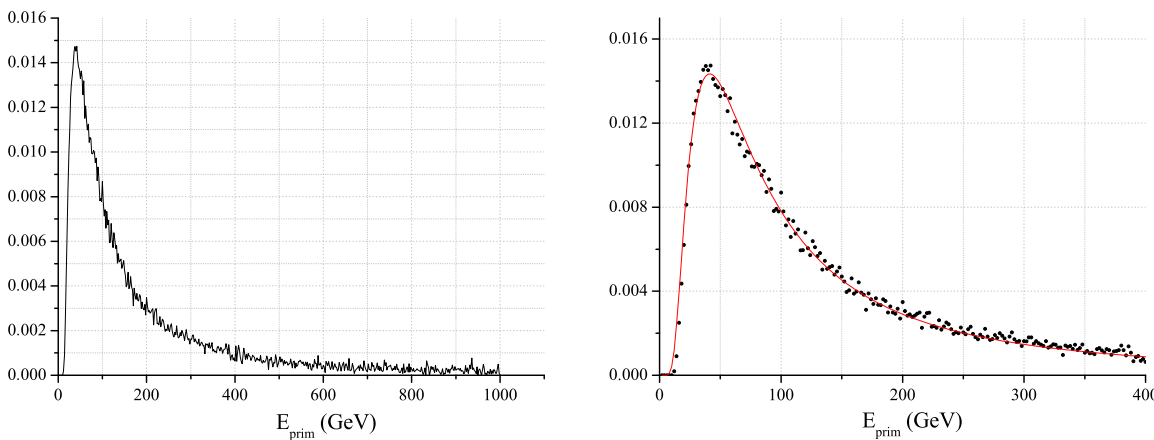


Fig. 6. Response function of coincident mode of asymmetric muon telescope in the UL to galactic cosmic rays. On the right panel the interesting energy interval is enlarged and Dorman function fit is plotted (red line). (For interpretation of the references to color in this figure legend, the reader is referred to the web version of this article.)

### 3.2. Underground

#### 3.2.1. Multi-muon events

Count rate of multi-muon events underground turned out to be too low for the above mentioned array detector experiment to be feasible in our laboratory. To collect enough events for construction of the response function (Fig. 3), allowed muon separation is 200 m, fairly

exceeding laboratory dimensions. Under these conditions calculated median energy is 270 GeV.

#### 3.2.2. ASYmmetric MUon Telescope (ASYMUT)

Asymmetric muon telescope is an inexpensive detector, constructed from components already available in the laboratory. It consists of two plastic scintillators of unequal dimensions. The lower is identical to the

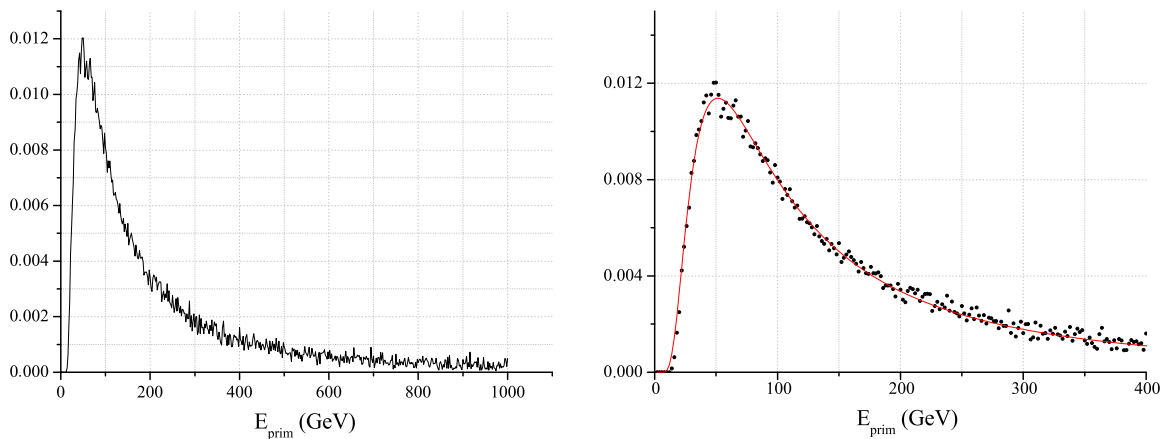


Fig. 7. Response function of anticoincident mode of asymmetric muon telescope in the UL to galactic cosmic rays. On the right panel the interesting energy interval is enlarged and Dorman function fit is plotted (red line). (For interpretation of the references to color in this figure legend, the reader is referred to the web version of this article.)

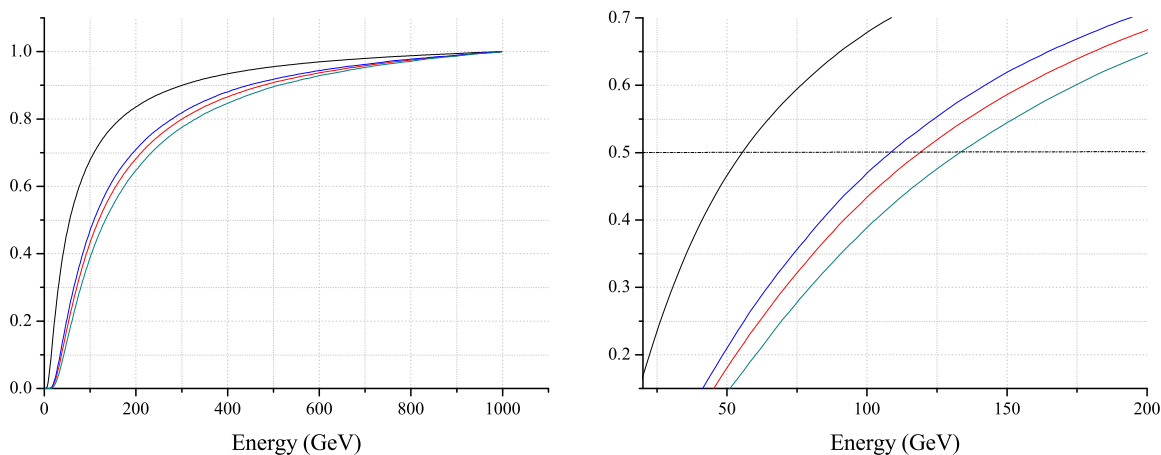


Fig. 8. Cumulative response function to galactic cosmic rays of different muon detectors in the Belgrade CR station: black curve — GLL; red curve — single UL; green curve — CC mode and blue curve — ANTI CC mode of asymmetric muon telescope. The 0.5 level corresponds to median energy. Cumulative response function with enlarged region around this level is shown in the right picture. (For interpretation of the references to color in this figure legend, the reader is referred to the web version of this article.)

one located in the GLL ( $100 \times 100 \times 5$  cm) and upper one is  $50 \times 46 \times 5$  cm. Detectors are separated vertically by 78 cm, as depicted in Fig. 4, to have roughly the same count rate in the coincident and anticoincident mode. Lower detector in single mode operates in the same manner as the one in the GLL, with wide angular acceptance. The coincident mode is composed of the events registered in both upper and lower detector. In the anticoincident mode, muons passing through the upper but not the lower detector are counted. Therefore, the later mode favors inclined muon paths. Different angular distribution means different path length of muons registered in three modes of ASYMUT (right part of Fig. 4) and also different energy distribution of parental primary particles.

The response functions to GCR of three modes of ASYMUT are shown on Figs. 5–7 and respective cumulative response functions are shown on Fig. 8.

Important parameters describing shapes of response functions are summarized in Table 1. The most often used characteristics of a detector system is its median energy  $E_{med}$ . Primary particles with the energy below  $E_{med}$  give 50% contribution to detector count rate. The energy interval  $(E_{0.05}, E_{0.95})$  is responsible for 90% of registered events. Fitted value of the parameter  $k$  from Dorman function (Eq. (4)) is also presented. The parameters  $E_{0.05}$  and  $E_{med}$  are determined with 1 GeV accuracy, while the uncertainty of  $E_{0.95}$  is much higher due to small number of very high energy events and is conservatively estimated as 10%.

Table 1

Sensitivity of Belgrade CR detectors (GLL — ground level; UL — underground based ASYMUT single mode; CC — ASYMUT coincident mode; ANTI — ASYMUT anticoincident mode) to GCR primary particles. Primaries with the energy below  $E_{0.05}$  (and above  $E_{0.95}$ ) contribute with 5% to the count rate of a corresponding detector.  $E_{med}$  is median energy,  $E_{th}$  threshold energy and  $k$  is Dorman parameter.

| det  | $E_{th}$ (GeV) | $E_{0.05}$ (GeV) | $E_{med}$ (GeV) | $E_{0.95}$ (GeV) | $k$      |
|------|----------------|------------------|-----------------|------------------|----------|
| GLL  | 5              | 11               | 59              | 915              | 0.894(1) |
| UL   | 12             | 31               | 137             | 1811             | 0.971(4) |
| CC   | 12             | 27               | 121             | 1585             | 1.015(3) |
| ANTI | 14             | 35               | 157             | 2031             | 0.992(4) |

### 3.3. Conclusions

Usefulness of our setup for solar modulation studies is tested on the example of investigation of a Forbush decrease of 8 March 2012. In the first half of March 2012 several M and X class solar flares erupted from the active region 1429 on the Sun. The strongest were two X class flares that bursted on March 7. The first one is the X5.4 class flare (peaked at 00:24 UT) and the second one is the X1.3 class flare (peaked at 01:14 UT). The two flares were accompanied by two fast CMEs, one of which was Earth-directed [23]. Several magnetic storms were also registered on Earth, and a series of Forbush decreases is registered. The most pronounced one was registered on March 8. Characteristics of this event as recorded by various neutron monitors and our detectors are compared.

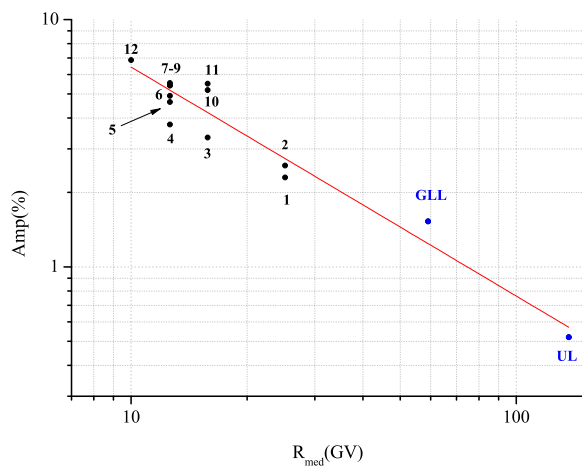


Fig. 9. Rigidity spectrum of FD from 12 March 2012. Black points represent the amplitude of the event as seen by twelve NMs: 1 — Athens, 2 — Mexico City; 3 — Almaty, 4 — Lomnický štít; 5 — Moscow; 6 — Kiel; 7 — Yakutsk; 8 — Apatity; 9 — Inuvik; 10 — McMurdo; 11 — Thul; 12 — South Pole. Blue points are from Belgrade CR station: GLL — ground level and UL — underground. (For interpretation of the references to color in this figure legend, the reader is referred to the web version of this article.)

Amplitude of a Forbush decrease is one of its main characteristics. Dependence of FD amplitude on median rigidity (or energy) is expected to follow the power law:  $\Delta N/N \sim R^{-\gamma}$  [12].

For investigation of rigidity spectrum of mentioned FD data from 12 NMs are combined with the data from our two detectors (GLL and UL) that were operational at the time of the event. Neutron monitor data in the period between 1 March 2012 and 1 April 2012 are taken from the NMDB database ([www.nmdb.eu](http://www.nmdb.eu)) [24]. The exponent of the rigidity spectrum of this FD  $\gamma$  is obtained by the least-square fitting of the data with the power function (Fig. 9) and found to be  $\gamma = 0.92 \pm 0.18$ . Presented analysis illustrates applicability of our setup for studies of consequences of CR solar modulation process in the energy region exceeding sensitivity of neutron monitors.

## Acknowledgments

We are very grateful to late Prof. Ivan Aničin for his enthusiastic contributions, deep insights and valuable advice not just regarding work presented in this paper but also for being a real spiritus agens of our lab. We acknowledge the NMDB database ([www.nmdb.eu](http://www.nmdb.eu)), founded under the European Union's FP7 programme (contract no. 213007) for providing NM data. The present work was funded by the Ministry of Education, Science and Technological Development of the Republic of Serbia, under the Project No. 171002.

## References

- [1] J.A. Simpson, The cosmic ray nucleonic component: The invention and scientific uses of the neutron monitor, *Cosmic Rays Earth* (2000) 11–32.
- [2] J.W. Bieber, Neutron monitoring: Past, present, future, in: Jonathan F.O. (Ed.) AIP Conference Proceedings, vol. 1516, No. 1, 2013.
- [3] M.L. Duldig, Muon observations, in: *Cosmic Rays and Earth*, Springer, Netherlands, 2000, pp. 207–226.
- [4] S. Cecchini, M. Spurio, Atmospheric muons: experimental aspects, *Geosci. Instrum. Methods Data Syst. Discuss.* 2 (2012) 603–641.
- [5] K.-H. Kampert, A.A. Watson, Extensive air showers and ultra high-energy cosmic rays: a historical review, *Eur. Phys. J. H* 37 (3) (2012) 359–412.
- [6] A. de Angelis, O. Mansutti, M. Persic, Very-high energy gamma astrophysics, *Riv. Nuovo Cimento* 31 (4) (2008) 187–246. <http://dx.doi.org/10.1393/ncr/i2008-10032-2>.
- [7] F. Arqueros, J.R. Hörandel, B. Keilhauer, Air fluorescence relevant for cosmic-ray detection — review of pioneering measurements, *Nucl. Instrum. Methods A* 597 (2008) 23–31. <http://dx.doi.org/10.1016/j.nima.2008.08.055>.
- [8] J.A. Lockwood, W.R. Webber, The 11 year solar modulation of cosmic rays as deduced from neutron monitor variations and direct measurements at low energies, *J. Geophys. Res.* 72 (23) (1967) 5977–5989.
- [9] I.G. Usoskin, G.A. Bazilevskaia, G.A. Kovaltsov, Solar modulation parameter for cosmic rays since 1936 reconstructed from ground-based neutron monitors and ionization chambers, *J. Geophys. Res.* 116 (2011) A02104. <http://dx.doi.org/10.1029/2010JA016105>.
- [10] A. Duperier, The meson intensity at the surface of the earth and the temperature at the production level, *Proc. Phys. Soc. A* 62 (11) (1949) 684.
- [11] P.M. Blackett, On the instability of the barytron and the temperature effect of cosmic rays, *Phys. Rev.* 54 (11) (1938) 973.
- [12] L. Dorman, *Cosmic Rays in the Earth's Atmosphere and Underground*, Springer Science + Business Media, LLC., New York, 2004.
- [13] G. Hausser, Cosmic ray-induced background in ge-spectrometry, *Nucl. Instrum. Methods B* 83 (1–2) (1993) 223–228.
- [14] A. Dragić, V. Udovičić, R. Banjanac, D. Joković, D. Maletić, N. Veselinović, M. Savić, J. Puzović, I.V. Aničin, The new setup in the Belgrade low-level and cosmic-ray laboratory, *Nucl. Technol. Radiat. Prot.* 26 (3) (2011) 181–192. <http://dx.doi.org/10.2298/NTRP1101064N>.
- [15] T. Kalliokoski, L. Bezrukov, T. Enqvist, H. Fynbo, L. Inzhechik, P. Jones, J. Joutsenvaara, J. Karjalainen, P. Kuusiniemi, K. Loo, B. Lubsandorzhev, V. Petkov, T. Rih, J. Sarkamo, M. Slupezki, W. Trzaska, A. Virkajrvi, Can EMMA solve the puzzle of the knee? *Prog. Part. Nucl. Phys.* 66 (2011) 468–472.
- [16] W.H. Fonger, Cosmic radiation intensity-time variations and their origin. II. Energy dependence of 27-day variations, *Phys. Rev.* 91 (2) (1953) 351.
- [17] E.E. Brown, Neutron yield functions for the nucleonic component of cosmic radiation, *Il Nuovo Cimento* (1955–1965) 6 (4) (1957) 956–962.
- [18] L. Dorman, *Cosmic Ray Variations*, State Publishing House for Technical and Theoretical Literature, 1957.
- [19] E.O. Fluckiger, et al., A parameterized neutron monitor yield function for space weather applications, in: *Proceedings of the 30th International Cosmic Ray Conference*, Mexico City, Mexico, vol. 1 (SH), 2008, pp. 289–292.
- [20] M. Zazyan, A. Chilingarian, Calculations of the sensitivity of the particle detectors of ASEC and SEVAN networks to galactic and solar cosmic rays, *Astropart. Phys.* 32 (2009) 185–192.
- [21] K. Nakamura, et al., 24. Cosmic rays, *J. Phys. G* 37 (2010) 075021.
- [22] B. Bugge, B. Glaser, L. Zoller, U. Hambach, S. Markovic, I. Glaser, N. Gerasimenko, Geochemical characterization and origin of Southeastern and Eastern European loesses (Serbia, Romania, Ukraine), *Quat. Sci. Rev.* 27 (2008) 1058–1075.
- [23] NASA Goddard Space Weather Research Center, Summary of the space weather event associated with the X5.4 and X1.3 flare on March 7.
- [24] H. Mavromichalaki, et al., Applications and usage of the real-time Neutron Monitor Database, *Adv. Space Res.* 47 (12) (2011) 2210–2222.



# Rigidity dependence of Forbush decreases in the energy region exceeding the sensitivity of neutron monitors

M. Savić, N. Veselinović\*, A. Dragić, D. Maletić, D. Joković, R. Banjanac, V. Udovičić

*Institute of Physics, University of Belgrade, Pregrevica 118, 11080 Zemun, Serbia*

Received 2 May 2018; received in revised form 14 September 2018; accepted 24 September 2018

Available online 28 September 2018

## Abstract

Applicability of our present setup for solar modulation studies in a shallow underground laboratory is tested on four prominent examples of Forbush decrease during solar cycle 24. Forbush decreases are of interest in space weather application and study of energy-dependent solar modulation, and they have been studied extensively. The characteristics of these events, as recorded by various neutron monitors and our detectors, were compared, and rigidity spectrum was found. Linear regression was performed to find power indices that correspond to each event. As expected, a steeper spectrum during more intense extreme solar events with strong X-flares shows a greater modulation of galactic cosmic rays. Presented comparative analysis illustrates the applicability of our setup for studies of solar modulation in the energy region exceeding the sensitivity of neutron monitors.

© 2018 COSPAR. Published by Elsevier Ltd. All rights reserved.

*Keywords:* Forbush decrease; Muon CR station; Median rigidity

## 1. Introduction

Galactic cosmic rays (GCRs) traverse the heliosphere; this leads to variation in the cosmic ray (CR) flux due to solar activity. The influence of solar and heliospheric modulation is pronounced for primary CR particles with low rigidity or momentum over unit charge. CRs interact, upon arrival, with Earth's atmosphere causing electromagnetic and hadronic showers. A network of ground-based CR detectors, neutron monitors (NMs), and muon detectors, located at various locations around the globe, as well as airborne balloons and satellites, provide valuable data to study the effect of these modulations on the integrated CR flux with time. Energies of the primary particles in NMs are sensitive to the state of solar activity and reach up to 40 GeV. Muon detectors have a significant response from 10 GeV up to several hundred GeV for surface, and

one order of magnitude greater for underground detectors, depending on the depth (Duldig, 2000). This energy interval allows muon detectors to monitor not only modulation effects on lower-energy CRs but also galactic effects on primary CRs with high energies where solar modulation is negligible. Because of the sensitivity to different energies of the primary particle flux, observations of muon detectors complement those of NMs in studies of long-term CR variations, CR anisotropy, and gradients or rigidity spectrum of Forbush decreases (FDs).

FDs (Forbush, 1954) represent decreases of the observed GCR intensity under the influence of coronal mass ejections (CMEs) and interplanetary counterparts of coronal mass ejections (ICMEs) and/or high-speed streams of solar wind (HSS) from the coronal holes (Belov, 2008). FDs belong to two types depending on the drivers: non-recurrent and recurrent decreases. This work addresses several non-recurrent FDs.

These sporadic FDs are caused by ICMEs. As the matter with its magnetic field moves through the solar system,

\* Corresponding author.

E-mail address: [veselinovic@ipb.ac.rs](mailto:veselinovic@ipb.ac.rs) (N. Veselinović).

it suppresses the CR intensity. FDs of this kind have an asymmetric profile, and the intensity of GCRs has a sudden onset and recovers gradually. Sometimes an early phase of FD prior to the dip (precursor of FD) shows an increase in CR intensity. These precursors of FDs are caused by GCR acceleration at the front of the advancing disturbance on the outer boundary of the ICME, as the primary CR particles are being reflected from the approaching shock (Papailiou et al., 2013). The FD profile depends on the area, velocity, and intensity of CME magnetic field produced in extreme events that originate at the Sun (Chauhan et al., 2008).

Data from observed modulation of GCR intensity contain information regarding the transport of GCRs through the interplanetary environment. GCR transport parameters are connected with the interplanetary magnetic field (IMF) in the heliosphere. It is empirically established that the radial diffusion coefficient is proportional to the rigidity of CR (Ahluwalia, 2005). In this article, we present an analysis of the amplitude of FD during four events, which were recorded by plastic scintillator muon detectors, located at the Belgrade muon station, as well as by a network of NMs.

## 2. Belgrade CR station

The Low-Background Laboratory for Nuclear Physics (LBLNP) is a part of the Institute of Physics, University of Belgrade. It is composed of two separate laboratory facilities, ground-level laboratory (GLL) and underground laboratory (UL), dug into a cliff. The overburden of the UL is approximately 12 m of loess soil, which is equivalent to 25 m of water (m.w.e). Laboratory is dedicated to measurements of low radiation activities and studies of muon and electromagnetic components of CRs at ground and shallow underground levels. The geographic position of the laboratory is at 75 m a.s.l., at 44°51'N latitude and 20°23'E longitude; geomagnetic vertical rigidity cutoff is 5.3 GV at the surface. The equipment was upgraded in 2008, and now, it consists of two identical sets of detectors and accompanying data processing electronics: one is situated in GLL and the other in UL. Detectors are a pair of plastic scintillator detectors, with dimensions of 100 cm × 100 cm × 5 cm and four PMTs that are directly coupled to the corners. Signals from two opposite PMTs on a single detector are summed, and the coincidence of the two diagonals is found. Fig. 1 presents the coincident sum spectra of two diagonals of large scintillator detectors.

Summing over diagonals suppresses the acquisition of electromagnetic component of the secondary CR shower and collects mainly the muon component of secondary CRs. A well-defined peak in the energy spectra corresponds to a muon energy loss of ~11 MeV. The average muon flux measured in the laboratory is 137(6) muons/m<sup>2</sup>s for GLL and 45(2) muons/m<sup>2</sup>s for UL. For more detailed description, see Dragić et al. (2011). Integral of this distribution, without low energy part, is used to form time series of this

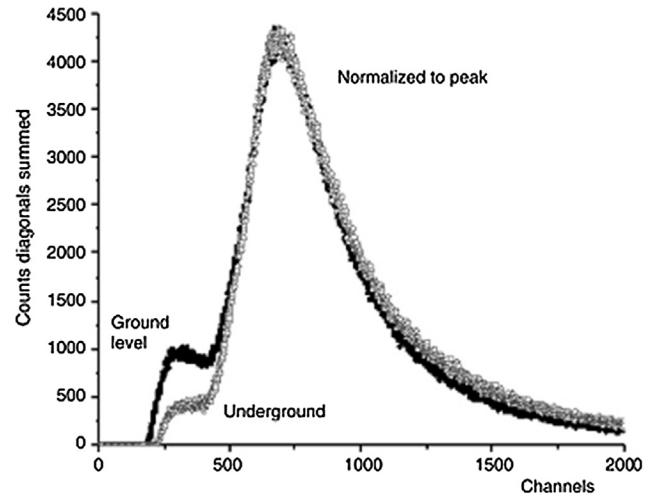


Fig. 1. The coincident spectra of two diagonals of large plastic detectors in UL and GLL normalized for comparison.

CR muons spectrum integrated over different time intervals. This time series is then corrected for efficiency, atmospheric pressure, and temperature (Savić et al., 2015).

The CR flux measured at the ground level varies because of changes in atmospheric conditions. Effects of the atmospheric pressure can be easily accounted for, similar like for NMs, but the temperature effect is somewhat more difficult to treat. The difficulties arise from the interplay of positive and negative temperature effects. With temperature increase, the atmospheric density decreases; hence, less pions interact and more muons are created from decay. The result is a positive effect of more muons at the ground level. On the other hand, the altitude of muon production level is high due to the expansion of the atmosphere when the temperature is high, muon path length is long, and decay probability of muons is high before they reach the ground level. Negative effect is dominant for low-energy muons (mostly detected in GLL) and positive for high-energy muons. A proper treatment of the temperature effect requires knowledge of the entire temperature profile of the atmosphere. This meteorological variation must be corrected to study CR variations originating outside the atmosphere.

For ground (and underground)-based CR detectors, the response function, i.e., the relation between particles of GCR spectra at the top of the atmosphere and recorded secondary particles at the surface level, should be accurately known. The total detector count rate can be expressed as follows (Caballero-Lopez and Moraal, 2012):

$$\begin{aligned}
 N(R_0, h, t) &= \sum_i \int_{R_0}^{\infty} (S_i | (R, h) j_i(R, t)) dR \\
 &= \int_{R_0}^{\infty} W(R, h, t) dR
 \end{aligned} \quad (1)$$

where  $N(R_0, h, t)$  is the detector counting rate,  $R_0$  is the geomagnetic cutoff rigidity,  $h$  is the atmospheric depth, and  $t$  represents time.  $S_i(R, h)$  represents the detector yield

function for primary particles of type  $i$  and  $j_i(R, t)$  represents the primary particle rigidity spectrum of type  $i$  at time  $t$ . The total response function  $W(R, h, t)$  is the sum of  $S_i(R, h)$  and  $j_i(R, t)$ . The maximum value of this function is in the range of 4–7 GV at sea level, depending on the solar modulation epoch at time  $t$  (Clem and Dorman, 2000). One of the methods to find this response function is to use the numerical simulation of propagation of CRs through the atmosphere. CORSIKA simulation package (Heck et al., 1998) was to simulate CR transport through the atmosphere and GEANT4 (Agostinelli et al., 2003) to simulate the propagation of secondary CRs through overburden and response of the detectors to find the relationship between the count rate at our site and the flux of primary particles on top of the atmosphere.

The excellent agreement of the simulated and measured flux (Fig. 2) allows us to establish that the cutoff energy for primary CR protons for showers detected in GLL is caused by its geomagnetic rigidity, and the median energy is  $\sim 60$  GeV. For UL, the cutoff energy due to earth overburden is 12 GeV, and the median energy is  $\sim 120$  GeV. These values give us opportunity to study solar modulation at energies exceeding energies detected with a NM. Observation of the solar activity and related magnetic disturbances in the heliosphere that create transient CR intensity variation at several different energies can provide an energy-dependent description of these phenomena.

### 3. Data analysis

The new setup in the LBLNP, presented by Dragić et al. (2011) coincides with the start of the 24th solar cycle, thus allowing us to observe the increase and decrease in solar activity and the effect of solar modulation at energies higher than ones studied using NMs.

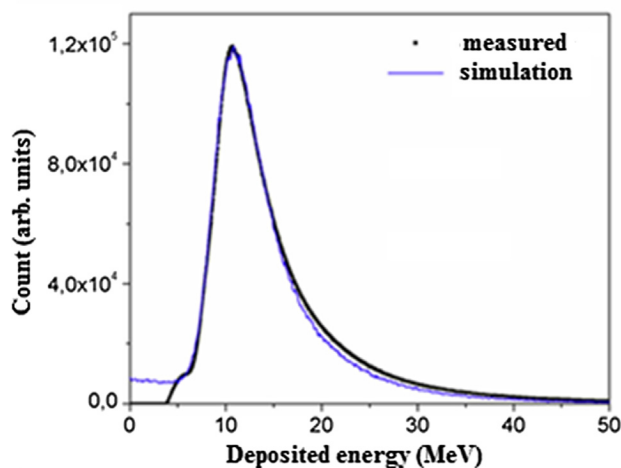


Fig. 2. Simulated (blue line) and measured spectra (black line) for muon detectors in UL. (For interpretation of the references to colour in this figure legend, the reader is referred to the web version of this article.)

Muon time series was searched for days where the average muon flux was significantly lower than the background level. The background level is determined from the moving averages of hourly count rates 10 days before the event. These decreases in the count rate, in GLL and UL, are then compared with space weather events of solar cycle 24. Data collected in UG and GLL are compared with four NM stations from the neutron monitor database [<http://www.nmdb.eu/>]. Three of these NMs (Athens, Rome, and Jungfraujoch) have cutoff rigidity and geographic proximity similar to the Belgrade CR station.

A high correlation is found between the count rates measured by the NMs in the LBLNP in March 2012 (Table 1), but for GLL and UL, as the cutoff energy of the primary flux increases, the correlation slightly decreases.

#### 3.1. Selected Forbush decreases

The Belgrade CR station has detected, both in GLL and UL, several significant structures connected to some extreme solar effects. Several, more prominent, Forbush decreases occurred in March 2012, September 2014, June 2015, and most recently in September 2017.

The FD that occurred on March 8, 2012 was recorded at the Belgrade CR station as well as at other stations (Fig. 3). This FD was separated into two following two CMEs. These CMEs produced an intense disturbance in the interplanetary space and caused a severe geomagnetic storm when the shockwave reached Earth on March 8, 2012. During this event, a very complex combination of modulation occurs (Lingri et al., 2016). Two CMEs from the same active region as the September 10 (X1.6) flare produced FD on September 12, 2014. There was a relatively fast partial halo CME and a larger and rapidly moving halo CME trailing behind the first one on September 10. These two gave rise to the FD that was first detected by NMs on September 12, 2014. This FD was not a classical two-step FD as expected, probably due to the interaction of slower and faster CMEs. The FD profile (Fig. 3) showed a small second step several hours after the first, similar to the FD that occurred in February 2011 (Papaioannou et al., 2013). In June 2015, a large activity occurred in the Sun from powerful AR 2371 that produced several CMEs from the Sun. These CMEs induced a complex modulation of GCRs that led to an FD occurrence on June 22, 2015 with an unusual structure (Samara et al., 2018).

A sudden burst of activity from the Sun early in September 2017, after a prolonged period of low solar activity, produced several flares, including the largest solar flare seen from Earth since 2006, an X9.3 flare. This activity produced several Earth-directed CMEs. Throughout this time, Earth experienced a series of geomagnetic storms, which started promptly after the first CME. This unusual activity produced an FD, which was recorded with detectors in terms of ground level enhancement (GLE) on Earth and Mars (Guo et al., 2018).

Table 1

Correlation matrix of the linear correlation coefficient (in%) for recorded hourly flux at the Belgrade CR station with its temperature- and pressure-corrected underground and ground-level detectors (UL\_tpc and GLL\_tpc), only pressure-corrected detectors (UL\_pc, GLL\_pc), and raw data detectors (UL\_raw and GLL\_raw) and recordings at Rome, Oulu, Jungfraujoch (Jung.) and Athens NMs for March 2012.

|         |        |      |       |      |         |        |         |        |       |        |
|---------|--------|------|-------|------|---------|--------|---------|--------|-------|--------|
| UL_tpc  | 75     | 81   | 80    | 81   | 76      | 73     | 78      | 86     | 97    | 100    |
| UL_pc   | 77     | 83   | 83    | 83   | 73      | 78     | 72      | 84     | 100   | 97     |
| UL_raw  | 57     | 71   | 70    | 74   | 94      | 49     | 51      | 100    | 84    | 86     |
| GLL_tpc | 86     | 86   | 84    | 83   | 59      | 90     | 100     | 51     | 72    | 78     |
| GLL_pc  | 90     | 92   | 90    | 89   | 56      | 100    | 90      | 49     | 78    | 73     |
| GLL_raw | 63     | 79   | 78    | 81   | 100     | 56     | 59      | 94     | 73    | 76     |
| Oulu    | 90     | 98   | 98    | 100  | 81      | 89     | 83      | 74     | 83    | 81     |
| Jung.   | 91     | 98   | 100   | 98   | 78      | 92     | 84      | 70     | 83    | 80     |
| Rome    | 91     | 100  | 98    | 98   | 79      | 92     | 86      | 71     | 83    | 81     |
| Athens  | 100    | 91   | 91    | 90   | 63      | 90     | 86      | 57     | 77    | 75     |
|         | Athens | Rome | Jung. | Oulu | GLL_raw | GLL_pc | GLL_tpc | UL_raw | UL_pc | UL_tpc |

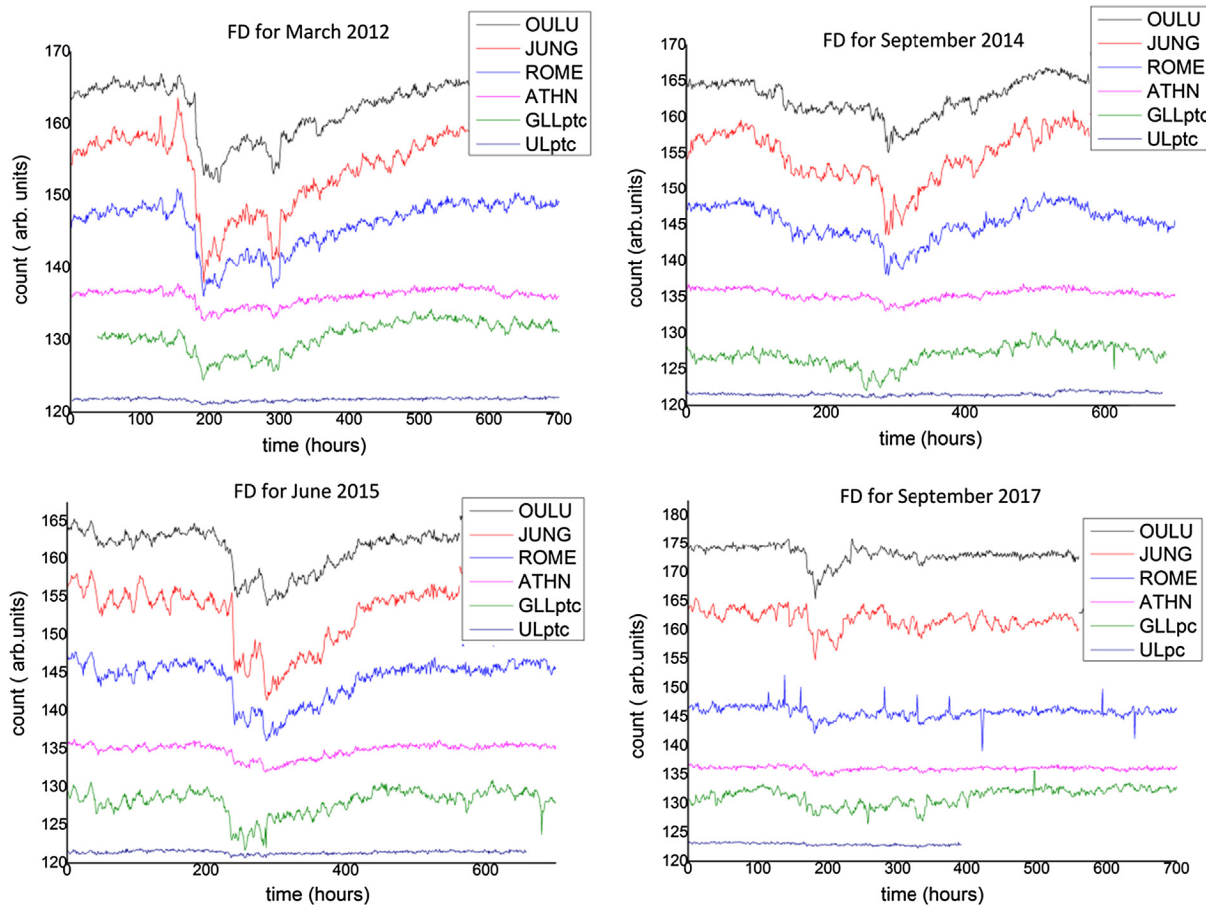


Fig. 3. Comparison of hourly time series over one month period for pressure- and temperature-corrected count rates of the Belgrade muon monitor station (GLL<sub>ptc</sub> and UL<sub>ptc</sub>) and NMs at Athens (ATHN), Rome (ROME), Jungfraujoch (JUNG), and Oulu (OULU) for extreme solar events in March 2012, September 2014, and June 2015. Count rates are shifted for comparison. For extreme solar event in September 2017, for GLL and UL, the count rate is pressure-corrected only.

#### 4. FD and median rigidity

For each event, we study the energy dependence of FD amplitude. The energy dependence of FD amplitude is

expected to follow the power law:  $\Delta N/N \sim R^{-\gamma}$  (Cane, 2000). To obtain reliable values of amplitudes, we defined amplitude as a relative decrease in the hourly count rate of the minimum compared with the average of seven days'

Table 2  
Median and cutoff rigidity for several stations.

| Stations      | Median rigidity $R_m$ (GV) | Min. rigidity $R_0$ (GV) |
|---------------|----------------------------|--------------------------|
| Athens        | 25.1                       | 8.53                     |
| Mexico        | 25.1                       | 8.28                     |
| Almaty        | 15.8                       | 6.69                     |
| Lomnický štít | 12.6                       | 3.84                     |
| Moscow        | 15.8                       | 2.43                     |
| Kiel          | 15.8                       | 2.36                     |
| Yakutsk       | 12.6                       | 1.65                     |
| Apatity       | 12.6                       | 0.65                     |
| Inuvik        | 12.6                       | 0.3                      |
| Mc Murdo      | 12.6                       | 0.3                      |
| Thule         | 12.6                       | 0.3                      |
| South Pole    | 10                         | 0.1                      |
| UL            | 122                        | 12.3                     |
| GLL           | 63                         | 5.3                      |

count rate before FDs (not including possible precursory increases). Such a long base period was used because of the higher activity of the Sun prior to registered FDs and sensitivity of the muon detectors.

Amplitudes are determined for two of our detectors and for 12 NMs. To investigate the rigidity spectrum of

Table 3  
Power indices of the median rigidity dependence of the dip of the FD. Power indices are obtained for NMs only, NMs and the Belgrade muon station, and Belgrade station only.

| $\gamma$   | NM only         | NM + Belgrade   | Belgrade station only |
|------------|-----------------|-----------------|-----------------------|
| March 2012 | $0.82 \pm 0.08$ | $0.78 \pm 0.03$ | 0.715                 |
| Sept. 2014 | $0.79 \pm 0.16$ | $0.67 \pm 0.06$ | 0.744                 |
| June 2015  | $0.57 \pm 0.05$ | $0.58 \pm 0.02$ | 0.764                 |
| Sept. 2017 | $1.27 \pm 0.16$ | $0.86 \pm 0.07$ | 0.739                 |

mentioned FDs, the median rigidity  $R_m$  is defined.  $R_m$  is the rigidity of the response of the detector to GCR spectrum where 50% of the detector counting rate lies below  $R_m$  (Ahluwalia and Fikani, 2007). For this study, we used a list of  $R_m$  for 12 NM stations given by Minamino et al. (2014). For an NM, the median rigidity can be computed from the detector response function derived from surveys for particulate station, usually around the minima of solar activity; this is because the intensity of lowest rigidity GCRs is maximum at that time.

For the Belgrade muon station,  $R_m$  was found using the response function acquired by the Monte Carlo method of

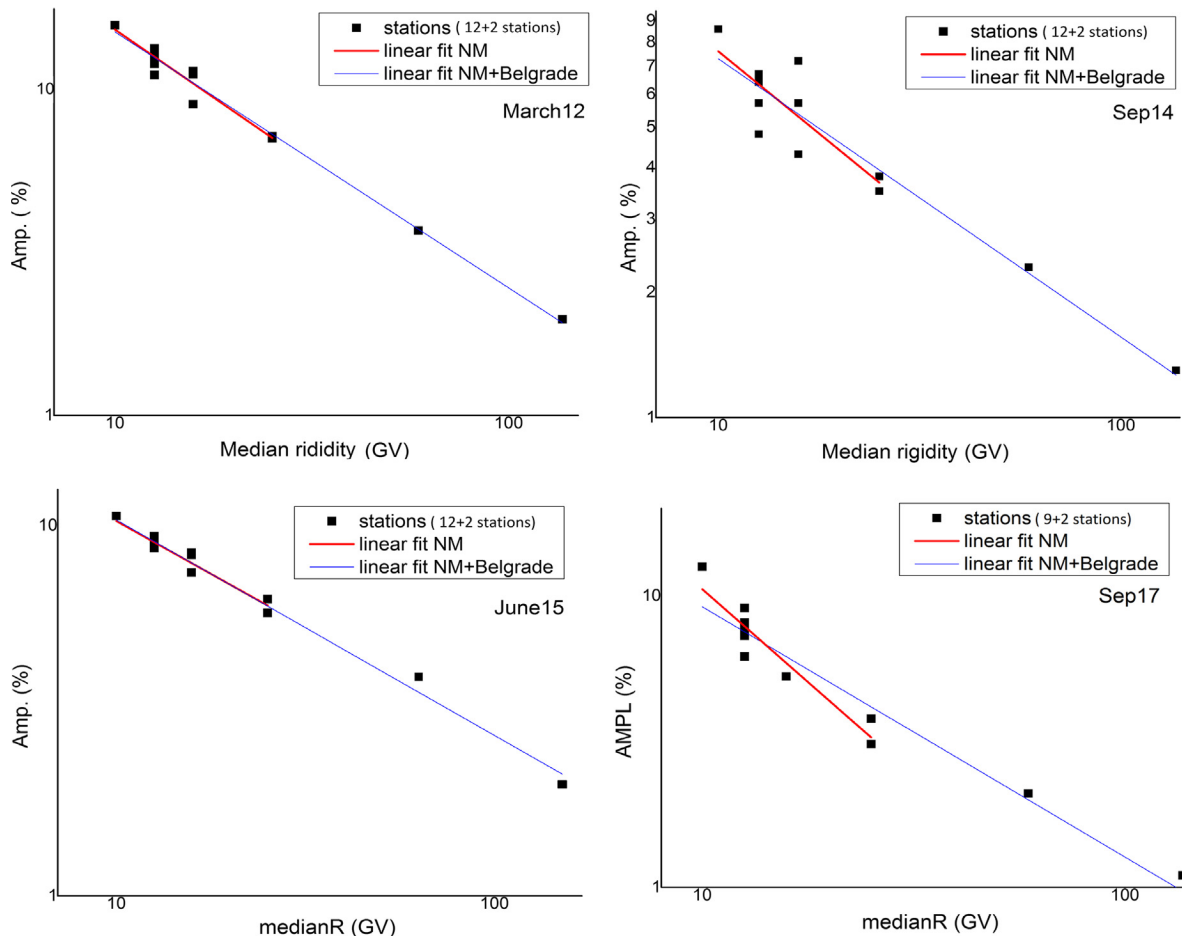


Fig. 4. Rigidity spectrum of FD from March 8, 2012, September 12, 2014, June 22, 2015, and September 8, 2017. Points represent the amplitude of the event as seen by NMs and the Belgrade CR station.

CR transport. Approximate values of  $R_m$  for the detectors used in this study are provided in Table 2.

For every selected event, a scatter plot is drawn (Fig. 4). All plots show, plotted in log-log scale, a clear median rigidity dependence of the amplitude of FD decrease.

Linear regression was performed to find power indices corresponding to each event. Power indices are given in Table 3.

Higher power indices can be due to more complex variations in GCRs. This more complex variation is a result of a series of CMEs during this event that leads to large compound ICME structure with multiple shocks and transient flow (Zhao and Zhang, 2016). Results obtained from the power law are generally consistent with those obtained in previous studies (Ahluwalia and Fikani, 2007, Lingri et al., 2016, Klyueva et al., 2017) conducted for NMs only.

A more significant difference observed for indices during the 2017 event was because we used only pressure-corrected data for the muon flux recorded at the Belgrade station. For all other events and data, we performed both pressure and temperature correction. Without temperature corrections, variation in the count rate in muon detectors is higher and it can affect the results.

We expect that when the newly improved, internally developed technique for temperature correction of the CR flux is implemented, the amplitude of the FD measured at the Belgrade muon station will be more consistent with other events and measurements. More data points on the graphs are needed to understand indices better, particularly in an energy region between NM and our laboratory. Similar work (Braun et al., 2009) discussed the extension up to 15 and 33 GeV, but there are no data available for FDs during cycle 24 and cannot be incorporated into this work. As for other operating muon telescopes, there is an agreement between the data obtained at our stations data and the URAGAN data for FD in June 2015 (Barbashina et al., 2016), but we have no data on other FDs and/or median energies of other stations. Our new experimental setup described elsewhere (Veselinović et al. 2017) will provide two additional median energies (121 and 157 GeV) to monitor variations in the CR flux.

## 5. Conclusion

The Belgrade CR station, with both ground level and underground setups, monitors the effect of solar modulation on the CR flux since 2008. Extreme solar events, like Forbush decreases, were detected during solar cycle 24 at the site, suggesting that these phenomena can be studied at energies higher than typical ones detected with NMs. GLL and UL data, as well as data from several NM stations, were used to analyze four intense FDs. The magnitude of FDs is energy (rigidity) dependent and follows the power law. Data used to find the rigidity dependence of these transient solar modulation of GCR were obtained over much higher range of rigidities than region NMs are

sensitive in, thus allowing more extensive studies of CR solar modulation processes.

## Acknowledgements

We acknowledge the NMDB ([www.nmdb.eu](http://www.nmdb.eu)), founded under the European Union's FP7 programme (contract no. 213007), for providing data. We acknowledge individual monitors for following the information given on the respective station information page. *Athens NM data were kindly provided by the Physics Department of the National and Kapodistrian University of Athens. Jungfrauoch NM data were kindly provided by the Physikalisches Institut, University of Bern, Switzerland. Oulu NM data were kindly provided by <http://cosmicrays oulu.fi> and Sodankyla Geophysical Observatory. Rome NM data were kindly provided by SVIRCO NM, supported by INAF/IAPS-UNIRoma3 COLLABORATION.* We thank the anonymous referees for useful advices.

The present work was funded by the Ministry of Education, Science and Technological Development of the Republic of Serbia, under Project No. 171002.

## References

- Agostinelli, S., et al., GEANT4—A Simulation Toolkit, 2003. Nuclear Instruments and Methods in Physics Research Section A 506, pp. 250–303. [https://doi.org/10.1016/S0168-9002\(03\)01368-8](https://doi.org/10.1016/S0168-9002(03)01368-8).
- Ahluwalia, H.S., 2005. Cycle 20 solar wind modulation of galactic cosmic rays: understanding the challenge. *J. Geophys. Res.* 110, A10106. <https://doi.org/10.1029/2005JA011106>.
- Ahluwalia, H.S., Fikani, M.M., 2007. Cosmic ray detector response to transient solar modulation: Forbush decreases. *J. Geophys. Res.* 112 (A8), A08105. <https://doi.org/10.1029/2006JA011958>.
- Barbashina, N.S., Ampilogov, N.V., Astapov, I.I., Borog, V.V., Dmitrieva, A.N., Petrukhin, A.A., Sitko, O.A., Shutenko, V.V., Yakovleva, E.I., 2016. Characteristics of the Forbush decrease of 22 June 2015 measured by means of the muon hodoscope URAGAN. *J. Phys.: Conf. Ser.* 675 (3). <https://doi.org/10.1088/1742-6596/675/3/032038>, article id. 032038.
- Belov, A.V., 2008. Forbush effects and their connection with solar, interplanetary and geomagnetic phenomena. In: Proceedings of the International Astronomical Union 4.S257, pp. 439–450. <https://doi.org/10.1017/S1743921309029676>.
- Braun, I., Engler, J., Hörandela, J.R., Milke, J., 2009. Forbush decreases and solar events seen in the 10–20 GeV energy range by the Karlsruhe Muon Telescope. *Adv. Space Res.* 43 (4), 480–488. <https://doi.org/10.1016/j.asr.2008.07.012>.
- Caballero-Lopez, R.A., Moraal, H., 2012. Cosmic-ray yield and response functions in the atmosphere. *J. Geophys. Res. Space Phys.* 117 (A12), 7461–7469. <https://doi.org/10.1029/2012JA017794>.
- Cane, H.V., 2000. Coronal mass ejections and Forbush decreases. *Space Sci. Rev.* 93 (1–2), 55–77. <https://doi.org/10.1023/1026532125747>.
- Chauhan, M.L., Jain Manjula, S.K., Shrivastava, S.K., 2008. Study of two major Forbush decrease events of 2005. In: Proceedings of the 30th International Cosmic Ray Conference, Mexico City, vol. 1 (SH), pp. 307–310. <https://doi.org/10.7529/ICRC2011/V10/0097>.
- Clem, J.M., Dorman, L.I., 2000. Neutron monitor response functions, cosmic rays and earth. *Space Sci. Rev.* 93 (1/2), 335–359. <https://doi.org/10.1023/A:1026515722112>.
- Dragić, A., Udovičić, V., Banjanac, R., Joković, D., Maletić, D., Veselinović, N., Savić, M., Puzović, J., Aničin, I.V., 2011. The new setup in the Belgrade low-level and cosmic-ray laboratory. *Nucl.*

- Technol. Radiat. Protect. 26 (3), 181–192. <https://doi.org/10.2298/NTRP1101064N>.
- Duldig, M.L., 2000. Muon observations. In: Bieber, J.W., Eroshenko, E., Evenson, P., Flückiger, E.O., Kallenbach, R. (Eds.), *Cosmic Rays and Earth. Space Sciences Series of ISSI*. Springer, Dordrecht, pp. 207–226. [https://doi.org/10.1007/978-94-017-1187-6\\_1](https://doi.org/10.1007/978-94-017-1187-6_1).
- Forbush, S.E., 1954. World-wide cosmic ray variations, 1937–1952. *J. Geophys. Res.* 59 (4), 525–542. <https://doi.org/10.1029/JZ059i004p00525>.
- Guo, J., Dumbović, M., Wimmer-Schweingruber, R.F., Temmer, M., Lohf, H., Wang, Y., Veronig, A., Hassler, D.M., Leila, M., Mays, L. M., Zeitlin, C., Ehresmann, B., Witasse, O., Freiherr von Forstner, J. L., Heber, B., Holmström, M., Posner, A., 2018. Modeling the evolution and propagation of the 2017 September 9th and 10th CMEs and SEPs arriving at Mars constrained by remote-sensing and in-situ measurement. Also Available at: arXiv preprint arXiv:1803.00461.
- Heck, D., Knapp, J., Capdevielle, J.N., Schatz, G., Thouw, T., 1998. *CORSIKA: a Monte Carlo code to simulate extensive air showers*. Forschungszentrum Karlsruhe GmbH, p. V +90, TIB Hannover, D-30167 Hannover.
- Klyueva, A.I., Belov, A.V., Eroshenko, E.A., 2017. Specific features of the rigidity spectrum of Forbush effects. *Geomag. Aeron.* 57 (2), 177–189. <https://doi.org/10.1134/S0016793217020050>.
- Lingri, D., Mavromichalaki, H., Belov, A., Eroshenko, E., Yanke, V., Abunin, A., Abunina, M., 2016. Solar activity parameters and associated Forbush decreases during the minimum between cycles 23 and 24 and the ascending phase of cycle 24. *Sol. Phys.* 291 (3), 1025–1041. <https://doi.org/10.1007/s11207-016-0863-8>.
- Minamino, Mohanty, Morishita, et al. for the GRAPES-3 Collaboration, 2014. Rigidity Dependence of Forbush Decreases, Poster #654. In: *Proceedings of the 33rd International Cosmic Ray Conference, Rio de Janeiro, Brazil*, pp. 3612–3615.
- Papailiou, M., Mavromichalaki, H., Abunina, M., Belov, A., Eroshenko, E., Yanke, V., Kryakunova, O., 2013. Forbush decreases associated with western solar sources and geomagnetic storms: a study on precursors. *Sol. Phys.* 283 (2), 557–563. <https://doi.org/10.1007/s11207-013-0231-x>.
- Papaioannou, A., Belov, A.A., Mavromichalaki, H., Eroshenko, E., Yanke, V., Asvestari, E., Abunin, A., Abunina, M., 2013. The first Forbush decrease of solar cycle 24. *J. Phys. Conf. Ser.* 409 (1). <https://doi.org/10.1088/1742-6596/409/1/012202>.
- Samara, E., Smpontias, I.A., Lytrosyngounis, I., Lingri, D., Mavromichalaki, H., Sgouropoulos, C., 2018. Unusual cosmic ray variations during the Forbush decreases of June 2015. *Sol. Phys.* 293 (67). <https://doi.org/10.1007/S11207-018-1290-9>.
- Savić, M., Maletić, D., Joković, D., Veselinović, N., Banjanac, R., Udovičić, V., Dragić, V., 2015. Pressure and temperature effect corrections of atmospheric muon data in the Belgrade cosmic-ray station. *J. Phys. Conf. Ser.* 632 (1). <https://doi.org/10.1088/1742-6596/632/1/012059>, article id. 012059.
- Veselinović, N., Dragić, A., Savić, M., Maletić, D., Joković, D., Banjanac, R., Udovičić, V., 2017. An underground laboratory as a facility for studies of cosmic-ray solar modulation. *Nucl. Instrum. Meth.* A875, 10–15. <https://doi.org/10.1016/j.nima.2017.09.008>.
- Zhao, L.-L., Zhang, H., 2016. Transient galactic cosmic-ray modulation during solar cycle 24: a comparative study of two prominent forbush decrease events. *Astrophys. J.* 827 (1). <https://doi.org/10.3847/0004-637X>.



## Lattice design and expected performance of the Muon Ionization Cooling Experiment demonstration of ionization cooling

M. Bogomilov,<sup>1</sup> R. Tsenov,<sup>1</sup> G. Vankova-Kirilova,<sup>1</sup> Y. Song,<sup>2</sup> J. Tang,<sup>2</sup> Z. Li,<sup>3</sup> R. Bertoni,<sup>4</sup> M. Bonesini,<sup>4</sup> F. Chignoli,<sup>4</sup> R. Mazza,<sup>4</sup> V. Palladino,<sup>5</sup> A. de Bari,<sup>6</sup> G. Cecchet,<sup>6</sup> D. Orestano,<sup>7</sup> L. Tortora,<sup>7</sup> Y. Kuno,<sup>8</sup> S. Ishimoto,<sup>9</sup> F. Filthaut,<sup>10</sup> D. Jokovic,<sup>11</sup> D. Maletic,<sup>11</sup> M. Savic,<sup>11</sup> O. M. Hansen,<sup>12</sup> S. Ramberger,<sup>12</sup> M. Vretenar,<sup>12</sup> R. Asfandiyarov,<sup>13</sup> A. Blondel,<sup>13</sup> F. Drielsma,<sup>13</sup> Y. Karadzhov,<sup>13</sup> G. Charnley,<sup>14</sup> N. Collomb,<sup>14</sup> K. Dumbell,<sup>14</sup> A. Gallagher,<sup>14</sup> A. Grant,<sup>14</sup> S. Griffiths,<sup>14</sup> T. Hartnett,<sup>14</sup> B. Martlew,<sup>14</sup> A. Moss,<sup>14</sup> A. Muir,<sup>14</sup> I. Mullacrane,<sup>14</sup> A. Oates,<sup>14</sup> P. Owens,<sup>14</sup> G. Stokes,<sup>14</sup> P. Warburton,<sup>14</sup> C. White,<sup>14</sup> D. Adams,<sup>15</sup> R. J. Anderson,<sup>15</sup> P. Barclay,<sup>15</sup> V. Bayliss,<sup>15</sup> J. Boehm,<sup>15</sup> T. W. Bradshaw,<sup>15</sup> M. Courthold,<sup>15</sup> V. Francis,<sup>15</sup> L. Fry,<sup>15</sup> T. Hayler,<sup>15</sup> M. Hills,<sup>15</sup> A. Lintern,<sup>15</sup> C. Macwaters,<sup>15</sup> A. Nichols,<sup>15</sup> R. Preece,<sup>15</sup> S. Ricciardi,<sup>15</sup> C. Rogers,<sup>15</sup> T. Stanley,<sup>15</sup> J. Tarrant,<sup>15</sup> M. Tucker,<sup>15</sup> A. Wilson,<sup>15</sup> S. Watson,<sup>16</sup> R. Bayes,<sup>17</sup> J. C. Nugent,<sup>17</sup> F. J. P. Soler,<sup>17</sup> R. Gamet,<sup>18</sup> G. Barber,<sup>19</sup> V. J. Blackmore,<sup>19</sup> D. Colling,<sup>19</sup> A. Dobbs,<sup>19</sup> P. Dornan,<sup>19</sup> C. Hunt,<sup>19</sup> A. Kurup,<sup>19</sup> J.-B. Lagrange,<sup>19,\*</sup> K. Long,<sup>19</sup> J. Martyniak,<sup>19</sup> S. Middleton,<sup>19</sup> J. Pasternak,<sup>19</sup> M. A. Uchida,<sup>19</sup> J. H. Cobb,<sup>20</sup> W. Lau,<sup>20</sup> C. N. Booth,<sup>21</sup> P. Hodgson,<sup>21</sup> J. Langlands,<sup>21</sup> E. Overton,<sup>21</sup> M. Robinson,<sup>21</sup> P. J. Smith,<sup>21</sup> S. Wilbur,<sup>21</sup> A. J. Dick,<sup>22</sup> K. Ronald,<sup>22</sup> C. G. Whyte,<sup>22</sup> A. R. Young,<sup>22</sup> S. Boyd,<sup>23</sup> P. Franchini,<sup>23</sup> J. R. Greis,<sup>23</sup> C. Pidcott,<sup>23</sup> I. Taylor,<sup>23</sup> R. B. S. Gardener,<sup>24</sup> P. Kyberd,<sup>24</sup> J. J. Nebrensky,<sup>24</sup> M. Palmer,<sup>25</sup> H. Witte,<sup>25</sup> A. D. Bross,<sup>26</sup> D. Bowring,<sup>26</sup> A. Liu,<sup>26</sup> D. Neuffer,<sup>26</sup> M. Popovic,<sup>26</sup> P. Rubinov,<sup>26</sup> A. DeMello,<sup>27</sup> S. Gourlay,<sup>27</sup> D. Li,<sup>27</sup> S. Prestemon,<sup>27</sup> S. Virostek,<sup>27</sup> B. Freemire,<sup>28</sup> P. Hanlet,<sup>28</sup> D. M. Kaplan,<sup>28</sup> T. A. Mohayai,<sup>28</sup> D. Rajaram,<sup>28</sup> P. Snopok,<sup>28</sup> V. Suezaki,<sup>28</sup> Y. Torun,<sup>28</sup> Y. Onel,<sup>29</sup> L. M. Cremaldi,<sup>30</sup> D. A. Sanders,<sup>30</sup> D. J. Summers,<sup>30</sup> G. G. Hanson,<sup>31</sup> and C. Heidt<sup>31</sup>

(The MICE collaboration)

<sup>1</sup>*Department of Atomic Physics, St. Kliment Ohridski University of Sofia, Sofia 1164, Bulgaria*

<sup>2</sup>*Institute of High Energy Physics, Chinese Academy of Sciences, Beijing 100039, China*

<sup>3</sup>*Sichuan University, Sichuan Sheng 610000, China*

<sup>4</sup>*Sezione INFN Milano Bicocca, Dipartimento di Fisica G. Occhialini, Milano 20126, Italy*

<sup>5</sup>*Sezione INFN Napoli and Dipartimento di Fisica, Università Federico II, Complesso Universitario di Monte S. Angelo, Napoli 80126, Italy*

<sup>6</sup>*Sezione INFN Pavia and Dipartimento di Fisica, Pavia 27100, Italy*

<sup>7</sup>*INFN Sezione di Roma Tre and Dipartimento di Matematica e Fisica, Università Roma Tre, 00146 Roma, Italy*

<sup>8</sup>*Osaka University, Graduate School of Science, Department of Physics, Toyonaka, Osaka 565-0871, Japan*

<sup>9</sup>*High Energy Accelerator Research Organization (KEK), Institute of Particle and Nuclear Studies, Tsukuba 305-0801, Ibaraki, Japan*

<sup>10</sup>*Nikhef, Amsterdam, The Netherlands and Radboud University, Nijmegen 1098, The Netherlands*

<sup>11</sup>*Institute of Physics, University of Belgrade, Belgrade 11080, Serbia*

<sup>12</sup>*CERN, Geneva 1217, Switzerland*

<sup>13</sup>*DPNC, Section de Physique, Université de Genève, Geneva 1205, Switzerland*

<sup>14</sup>*STFC Daresbury Laboratory, Daresbury, Cheshire WA4 4AD, United Kingdom*

<sup>15</sup>*STFC Rutherford Appleton Laboratory, Harwell Oxford, Didcot OX11 0QX, United Kingdom*

<sup>16</sup>*STFC Rutherford UK Astronomy Technology Centre, Royal Observatory, Edinburgh, Blackford Hill, Edinburgh EH9 3HJ, United Kingdom*

<sup>17</sup>*School of Physics and Astronomy, Kelvin Building, The University of Glasgow, Glasgow G12 8SU, United Kingdom*

<sup>18</sup>*Department of Physics, University of Liverpool, Liverpool L69 7ZE, United Kingdom*

<sup>19</sup>*Department of Physics, Blackett Laboratory, Imperial College London, London SW7 2BB, United Kingdom*

<sup>20</sup>*Department of Physics, University of Oxford, Denys Wilkinson Building, Oxford OX1 3PJ, United Kingdom*

<sup>21</sup>*Department of Physics and Astronomy, University of Sheffield, Sheffield S10 2TN, United Kingdom*

<sup>22</sup>*SUPA and the Department of Physics, University of Strathclyde, Glasgow G1 1XQ, United Kingdom and Cockcroft Institute, United Kingdom*

<sup>23</sup>*Department of Physics, University of Warwick, Coventry CV4 7AL, United Kingdom*

<sup>24</sup>*Brunel University, Uxbridge UB8 3PH, United Kingdom*

<sup>25</sup>*Brookhaven National Laboratory, New York NY 11967, USA*

<sup>26</sup>*Fermilab, Batavia, Illinois 60510, USA*

<sup>27</sup>*Lawrence Berkeley National Laboratory, Berkeley, California 94720, USA*<sup>28</sup>*Illinois Institute of Technology, Chicago, Illinois 60616, USA*<sup>29</sup>*Department of Physics and Astronomy, University of Iowa, Iowa City, Iowa 52242, USA*<sup>30</sup>*University of Mississippi, Oxford, Mississippi 38677, USA*<sup>31</sup>*University of California, Riverside, California 92521, USA*

(Received 30 January 2017; published 19 June 2017)

Muon beams of low emittance provide the basis for the intense, well-characterized neutrino beams necessary to elucidate the physics of flavor at a neutrino factory and to provide lepton-antilepton collisions at energies of up to several TeV at a muon collider. The international Muon Ionization Cooling Experiment (MICE) aims to demonstrate ionization cooling, the technique by which it is proposed to reduce the phase-space volume occupied by the muon beam at such facilities. In an ionization-cooling channel, the muon beam passes through a material in which it loses energy. The energy lost is then replaced using rf cavities. The combined effect of energy loss and reacceleration is to reduce the transverse emittance of the beam (transverse cooling). A major revision of the scope of the project was carried out over the summer of 2014. The revised experiment can deliver a demonstration of ionization cooling. The design of the cooling demonstration experiment will be described together with its predicted cooling performance.

DOI: [10.1103/PhysRevAccelBeams.20.063501](https://doi.org/10.1103/PhysRevAccelBeams.20.063501)

## I. INTRODUCTION

Stored muon beams have been proposed as the source of neutrinos at a neutrino factory [1,2] and as the means to deliver multi-TeV lepton-antilepton collisions at a muon collider [3,4]. In such facilities the muon beam is produced from the decay of pions generated by a high-power proton beam striking a target. The tertiary muon beam occupies a large volume in phase space. To optimize the muon yield while maintaining a suitably small aperture in the muon-acceleration system requires that the muon beam be “cooled” (i.e., its phase-space volume reduced) prior to acceleration. A muon is short-lived, decaying with a lifetime of  $2.2 \mu\text{s}$  in its rest frame. Therefore, beam manipulation at low energy ( $\leq 1 \text{ GeV}$ ) must be carried out rapidly. Four cooling techniques are in use at particle accelerators: synchrotron-radiation cooling [5]; laser cooling [6–8]; stochastic cooling [9]; and electron cooling [10]. Synchrotron-radiation cooling is observed only in electron or positron beams, owing to the relatively low mass of the electron. Laser cooling is limited to certain ions and atomic beams. Stochastic cooling times are dependent on the bandwidth of the stochastic-cooling system relative to the frequency spread of the particle beam. The electron-cooling time is limited by the available electron density and the electron-beam energy and emittance. Typical cooling times are between seconds and hours, long compared with the muon lifetime. Ionization cooling proceeds by passing a muon beam through a material, the absorber, in which it

loses energy through ionization, and subsequently restoring the lost energy in accelerating cavities. Transverse and longitudinal momentum are lost in equal proportions in the absorber, while the cavities restore only the momentum component parallel to the beam axis. The net effect of the energy-loss/reacceleration process is to decrease the ratio of transverse to longitudinal momentum, thereby decreasing the transverse emittance of the beam. In an ionization-cooling channel the cooling time is short enough to allow the muon beam to be cooled efficiently with modest decay losses. Ionization cooling is therefore the technique by which it is proposed to cool muon beams [11–13]. This technique has never been demonstrated experimentally and such a demonstration is essential for the development of future high-brightness muon accelerators.

The international Muon Ionization Cooling Experiment (MICE) collaboration proposes a two-part process to perform a full demonstration of transverse ionization cooling. First, the “Step IV” configuration [14] will be used to study the material and beam properties that determine the performance of an ionization-cooling lattice. Second, a study of transverse-emittance reduction in a cooling cell that includes accelerating cavities will be performed.

The cooling performance of an ionization-cooling cell depends on the emittance and momentum of the initial beam, on the properties of the absorber material and on the transverse betatron function ( $\beta_{\perp}$ ) at the absorber. These factors will be studied using the Step IV configuration. Once this has been done, “sustainable” ionization cooling must be demonstrated. This requires restoring energy lost by the muons as they pass through the absorber using rf cavities. The experimental configuration with which the MICE collaboration originally proposed to study ionization cooling was presented in [15]. This configuration was revised to accelerate the timetable on which a demonstration of ionization cooling could be delivered and to reduce

\*[j.lagrange@imperial.ac.uk](mailto:j.lagrange@imperial.ac.uk)

cost. This paper describes the revised lattice proposed by the MICE collaboration for the demonstration of ionization cooling and presents its performance.

## II. COOLING IN NEUTRINO FACTORIES AND MUON COLLIDERS

At production, muons occupy a large volume of phase space. The emittance of the initial muon beam must be reduced before the beam is accelerated. A neutrino factory [16] requires the transverse emittance to be reduced from 15–20 mm to 2–5 mm. A muon collider [17] requires the muon beam to be cooled in all six phase-space dimensions; to achieve the desired luminosity requires an emittance of  $\sim 0.025$  mm in the transverse plane and  $\sim 70$  mm in the longitudinal direction [18,19].

Ionization cooling is achieved by passing a muon beam through a material with low atomic number ( $Z$ ), in which it loses energy by ionization, and subsequently accelerating the beam. The rate of change of the normalized transverse emittance,  $\varepsilon_{\perp}$ , is given approximately by [12,20,21]:

$$\frac{d\varepsilon_{\perp}}{dz} \simeq -\frac{\varepsilon_{\perp}}{\beta^2 E_{\mu}} \left\langle \frac{dE}{dz} \right\rangle + \frac{\beta_{\perp} (13.6 \text{ MeV}/c)^2}{2\beta^3 E_{\mu} m_{\mu} X_0}; \quad (1)$$

where  $z$  is the longitudinal coordinate,  $\beta c$  is the muon velocity,  $E_{\mu}$  the energy,  $\langle \frac{dE}{dz} \rangle$  the mean rate of energy loss per unit path-length,  $m_{\mu}$  the mass of the muon,  $X_0$  the radiation length of the absorber and  $\beta_{\perp}$  the transverse betatron function at the absorber. The first term of this equation describes “cooling” by ionization energy loss and the second describes “heating” by multiple Coulomb scattering. Equation (1) implies that the equilibrium emittance, for which  $\frac{d\varepsilon_{\perp}}{dz} = 0$ , and the asymptotic value of  $\frac{d\varepsilon_{\perp}}{dz}$  for large emittance are functions of muon-beam energy.

In order to have good performance in an ionization-cooling channel,  $\beta_{\perp}$  needs to be minimized and  $X_0 \langle \frac{dE}{dz} \rangle$

maximised. The betatron function at the absorber is minimized using a suitable magnetic focusing channel (typically solenoidal) [22,23] and  $X_0 \langle \frac{dE}{dz} \rangle$  is maximized using a low- $Z$  absorber such as liquid hydrogen ( $\text{LH}_2$ ) or lithium hydride ( $\text{LiH}$ ) [24].

## III. THE MUON IONIZATION COOLING EXPERIMENT

The muons for MICE come from the decay of pions produced at an internal target dipping directly into the circulating proton beam in the ISIS synchrotron at the Rutherford Appleton Laboratory (RAL) [25,26]. A beam line of 9 quadrupoles, 2 dipoles and a superconducting “decay solenoid” collects and transports the momentum-selected beam into the experiment [27]. The small fraction of pions that remain in the beam may be rejected during analysis using the time-of-flight hodoscopes and Cherenkov counters that are installed in the beam line upstream of the experiment [28]. A diffuser is installed at the upstream end of the experiment to vary the initial emittance of the beam. Ionization cooling depends on momentum through  $\beta$ ,  $E_{\mu}$  and  $\langle \frac{dE}{dz} \rangle$  as shown in Eq. (1). It is therefore proposed that the performance of the cell be measured for momenta in the range 140 MeV/ $c$  to 240 MeV/ $c$  [15].

### A. The configuration of the ionization-cooling experiment

The configuration proposed for the demonstration of ionization cooling is shown in Fig. 1. It contains a cooling cell sandwiched between two spectrometer-solenoid modules. The cooling cell is composed of two 201 MHz cavities, one primary (65 mm) and two secondary (32.5 mm) LiH absorbers placed between two superconducting “focus-coil” (FC) modules. Each FC has two separate windings that can be operated either with the same or in opposed polarity.

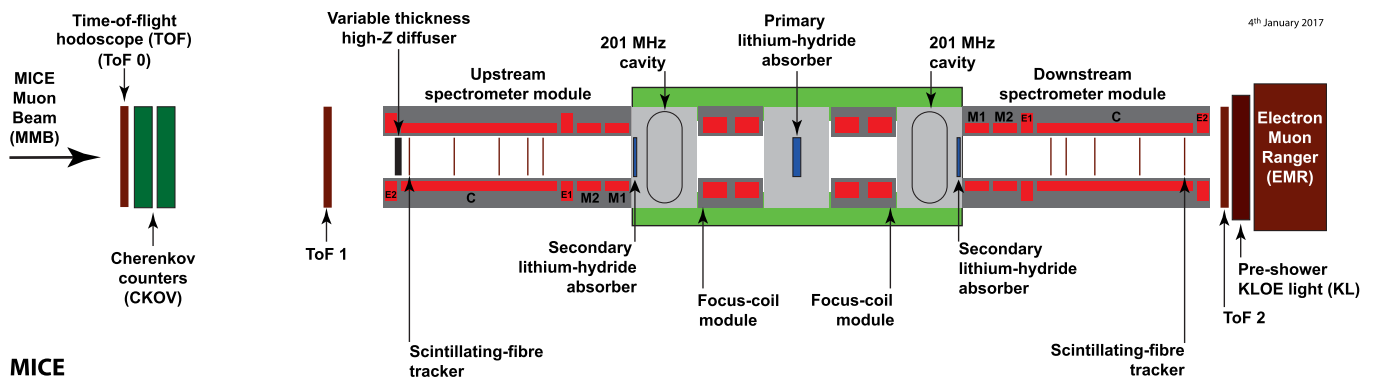


FIG. 1. Layout of the lattice configuration for the cooling demonstration. The red rectangles represent the solenoids. The individual coils in the spectrometer solenoids are labeled E1, C, E2, M1 and M2. The ovals represent the rf cavities and the blue rectangles the absorbers. The various detectors (time-of-flight hodoscopes [29,30], Cherenkov counters [31], scintillating-fibre trackers [32], KLOE Light (KL) calorimeter [27,33], electron muon ranger [34]) used to characterize the beam are also represented. The green-shaded box indicates the cooling cell.

The emittance is measured upstream and downstream of the cooling cell using scintillating-fiber tracking detectors [32] immersed in the uniform 4 T magnetic field provided by three superconducting coils (E1, C, E2). The trackers are used to reconstruct the trajectories of individual muons at the entrance and exit of the cooling cell. The reconstructed tracks are combined with information from instrumentation upstream and downstream of the spectrometer modules to measure the muon-beam emittance at the upstream and downstream tracker reference planes. The instrumentation upstream and downstream of the spectrometer modules serves to select a pure sample of muons. Time-of-flight hodoscopes are used to determine the time at which the muon crosses the rf cavities. The spectrometer-solenoid magnets also contain two superconducting “matching” coils (M1, M2) that are used to match the optics between the uniform field region and the neighboring FC.

The secondary LiH absorbers (SAs) are introduced between the cavities and the trackers to minimize the exposure of the trackers to “dark-current” electrons originating from the rf cavities. Experiments at the MuCool Test Area (MTA) at Fermilab [35] have observed that the rate of direct x-ray production from the rf cavities can be managed to ensure it does not damage the trackers [36]. The SAs are introduced to minimize the exposure of the trackers to energetic dark-current electrons that could produce background hits. The SAs are positioned between the trackers and the cavities such that they can be removed to study the empty channel. The SAs increase the net transverse-cooling effect since the betatron functions at these locations are small.

Retractable lead radiation shutters will be installed on rails between the spectrometer solenoids and the rf modules to protect the trackers against dark-current induced radiation during cavity conditioning. The SAs will be mounted on a rail system similar to that which will be used for the lead shutters and will be located between the cavities and the lead shutters. Both mechanisms will be moved using linear piezoelectric motors that operate in vacuum and magnetic field. The design of both the radiation shutter and the movable SA inside the vacuum chamber is shown in Fig. 2.

The rf cavities are 201 MHz “pillbox” resonators, 430 mm in length, operating in the  $TM_{010}$  mode with large diameter apertures to accommodate the high emittance beam. The apertures are covered by thin (0.38 mm) beryllium windows to define the limits for the accelerating rf fields whilst minimizing the scattering of muons. The cavity is excited by two magnetic-loop couplers on opposite sides of the cavity. At the particle rate expected in MICE there is no beam-loading of the rf fields. An effective peak field of 10.3 MV/m is expected for a drive power of 1.6 MW to each cavity. This estimate was used to define the gradient in the simulations described below.

The original configuration of the MICE cooling cell described in [15] was composed of three focus-coil modules, each of which housed a liquid-hydrogen absorber, and two,

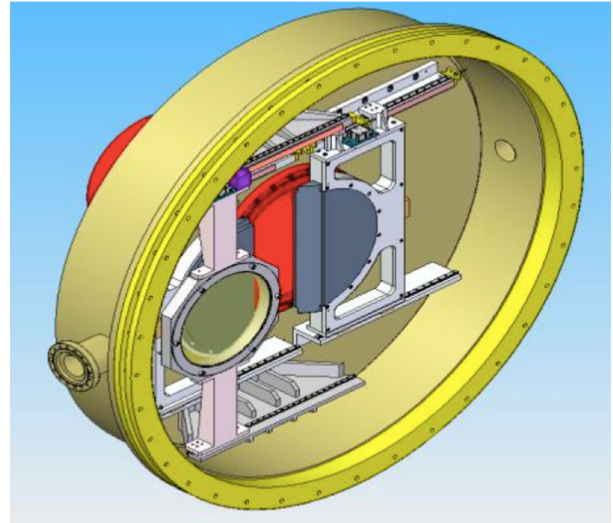


FIG. 2. Design of the movable frame for the secondary absorber (front) and the lead radiation shutter (back). The half discs of the lead shutter (grey) can be seen together with the rails (white) inside the vacuum chamber (yellow).

four-cavity, linac modules. Each linac module incorporated a large, superconducting “coupling coil” to transport the beam. The configuration described in this paper was developed to simplify the lattice described in [15] such that the coupling coils are not required and acceleration is provided by two single-cavity modules. The revision of the magnetic lattice substantially reduces the technical risks associated with the implementation of the experiment since all of the superconducting solenoids required to transport and focus the beam have been commissioned on the beam line. Further, by reducing the number of cavities from eight to two and reconfiguring the rf-power-distribution system the cost of implementing the experiment has been reduced and the timetable on which the experiment can be mounted has been advanced. The present configuration was optimized to maximize its cooling performance as described in Sec. IV. The performance of the optimized lattice, though reduced compared to that described in [15], is sufficient for the principle of ionization-cooling to be demonstrated (see Sec. VI).

## IV. LATTICE DESIGN

### A. Design parameters

The lattice has been optimized to maximize the reduction in transverse emittance. The optimum is obtained by matching the betatron function to a small value in the central absorber while minimizing its maximum values in the FC modules; limiting the size of the betatron function in the FCs helps to reduce the influence of nonlinear terms in the magnetic-field expansion. The matching accounts for the change in energy of the muons as they pass through the cooling cell by adjusting currents in the upstream and

downstream FCs and in the matching coils in the spectrometer solenoids independently while maintaining the field in the tracking volumes at 4 T. In this configuration, it is also possible to keep the betatron function relatively small at the position of the secondary absorbers whilst maintaining an acceptable beam size at the position of the cavities.

Chromatic aberrations caused by the large momentum spread of the beam ( $\sim 5\%$  rms) lead to a chromatic mismatch of the beam in the downstream solenoid unless the phase advance across the cooling cell (i.e., the rate of rotation of the phase-space ellipse) is chosen appropriately. The phase advance of the cell is obtained by integrating the inverse of the beta-function along the beam axis from the reference plane in the upstream spectrometer-solenoid to the reference plane in the downstream spectrometer-solenoid. Such a mismatch reduces the effective transverse-emittance reduction through the chromatic decoherence that results from the superposition of beam evolutions for the different betatron frequencies that result from the range of momenta in the beam. For beams with a large input emittance, spherical aberrations may lead to phase-space filamentation. The chromatic and spherical aberrations were studied by tracking samples of muons through the lattice using the ‘‘MICE Analysis User Software’’ (MAUS, see Sec. V). The betatron-function and emittance evolution of a 200 MeV/ $c$  beam with the

TABLE I. General parameters of the initial beam conditions used in the simulations.

| Parameter  | Value        |
|--|--------------|
| Particle   | muon $\mu^+$ |
| Number of particles                                | 10000        |
| Longitudinal position [mm]                         | -4612.1      |
| Central energy (140 MeV/ $c$ settings) [MeV]       | 175.4        |
| Central energy (200 MeV/ $c$ settings) [MeV]       | 228.0        |
| Central energy (240 MeV/ $c$ settings) [MeV]       | 262.2        |
| Transverse Gaussian distribution:                  |              |
| $\alpha_{\perp}$                                   | 0            |
| $\beta_{\perp}$ (140 MeV/ $c$ settings) [mm]       | 233.5        |
| $\varepsilon_{\perp}$ (140 MeV/ $c$ settings) [mm] | 4.2          |
| $\beta_{\perp}$ (200 MeV/ $c$ settings) [mm]       | 339.0        |
| $\varepsilon_{\perp}$ (200 MeV/ $c$ settings) [mm] | 6.0          |
| $\beta_{\perp}$ (240 MeV/ $c$ settings) [mm]       | 400.3        |
| $\varepsilon_{\perp}$ (240 MeV/ $c$ settings) [mm] | 7.2          |
| Longitudinal Gaussian distribution:                |              |
| Longitudinal emittance [mm]                        | 20           |
| Longitudinal $\beta$ [ns]                          | 11           |
| Longitudinal $\alpha$                              | -0.7         |
| rms momentum spread (140 MeV/ $c$ settings)        | 4.8%         |
| rms time spread (140 MeV/ $c$ settings) [ns]       | 0.40         |
| rms momentum spread (200 MeV/ $c$ settings)        | 4.0%         |
| rms time spread (200 MeV/ $c$ settings) [ns]       | 0.34         |
| rms momentum spread (240 MeV/ $c$ settings)        | 3.6%         |
| rms time spread (240 MeV/ $c$ settings) [ns]       | 0.31         |

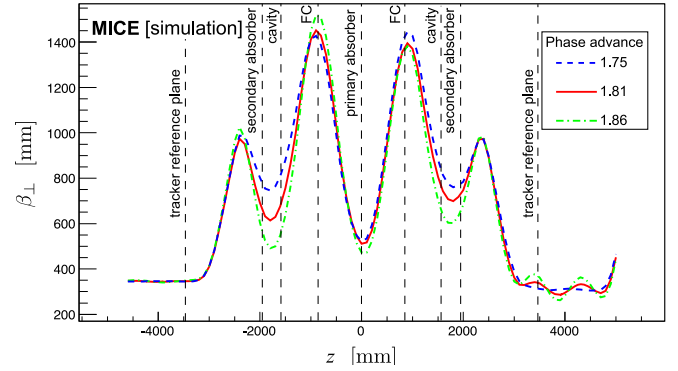


FIG. 3. Transverse 4D beta-function versus longitudinal coordinate  $z$  in the cooling-demonstration lattice for 200 MeV/ $c$  settings with a phase advance of  $2\pi \times 1.75$  (dashed blue line),  $2\pi \times 1.81$  (solid red line) and  $2\pi \times 1.86$  (dot-dashed green line). The vertical dashed lines with labels show the positions of the tracker reference planes and the centers of the absorbers, rf cavities, and focus coil modules.

initial parameters given in Table I are shown, for different phase advances, in Figs. 3 and 4, respectively. The phase advance of  $2\pi \times 1.81$  showed the largest transverse-emittance reduction and was therefore chosen. The lattice parameters for this phase advance are presented in Table II.

The currents that produce the optimum magnetic lattice were obtained using the procedure described above for three momentum settings: 140 MeV/ $c$ , 200 MeV/ $c$ , and 240 MeV/ $c$ . The magnetic field on axis for each of these settings is shown in Fig. 5. The fields in the downstream FC and spectrometer are opposite to those in the upstream FC and spectrometer, the field changing sign at the primary absorber. Such a field flip is required in an ionization cooling channel to reduce the build-up of canonical angular momentum [37]. The currents required to produce the magnetic fields shown in Fig. 5 are listed in Table III. All currents are within the proven limits of operation for the

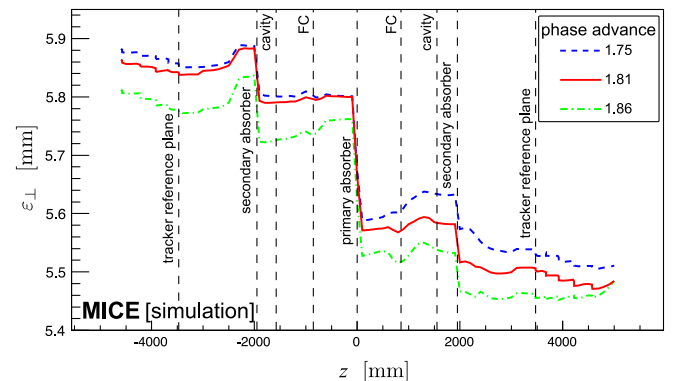


FIG. 4. 4D emittance evolution in the cooling-demonstration lattice for 200 MeV/ $c$  settings with a phase advance of  $2\pi \times 1.75$  (dashed blue line),  $2\pi \times 1.81$  (solid red line) and  $2\pi \times 1.86$  (dot-dashed green line). The vertical dashed lines with labels show the positions of the tracker reference planes and the centers of the absorbers, rf cavities, and focus coil modules.

TABLE II. Parameters of the cooling-demonstration lattice.  $L_{SS \rightarrow FC}$  is the distance between the center of the spectrometer solenoid and the center of the neighboring FC,  $L_{FC \rightarrow FC}$  the distance between the centers of the FCs, and  $L_{RF \text{ module} \rightarrow FC}$  the distance between the rf module and the neighboring FC.

| Parameter  | Value  |
|--|--------|
| Length $L_{SS \rightarrow FC}$ [mm]                | 2607.5 |
| Length $L_{FC \rightarrow FC}$ [mm]                | 1678.8 |
| Length $L_{rf \text{ module} \rightarrow FC}$ [mm] | 784.0  |
| rf Gradient [MV/m]                                 | 10.3   |
| Number of rf cavities                              | 2      |
| Number of primary absorbers                        | 1      |
| Number of secondary absorbers                      | 2      |

individual coil windings. The magnetic forces acting on the coils have been analyzed and were found to be acceptable. Configurations in which there is no field flip can also be considered.

Figure 6 shows matched betatron functions versus longitudinal position for beams of different initial momentum. These betatron functions are constrained, within the fiducial-volume of the trackers, by the requirements on the Courant-Snyder parameters  $\alpha_{\perp} = 0$  and  $\beta_{\perp} = \frac{2p_z}{eB_z}$  (where  $p_z$  is the mean longitudinal momentum of the beam,  $e$  the elementary charge and  $B_z$  the longitudinal component of the magnetic field). A small betatron-function “waist” in the central absorber is achieved. Betatron-function values at relevant positions in the different configurations are summarized in Table IV.

## V. SIMULATION

Simulations to evaluate the performance of the lattice have been performed using the official MICE simulation

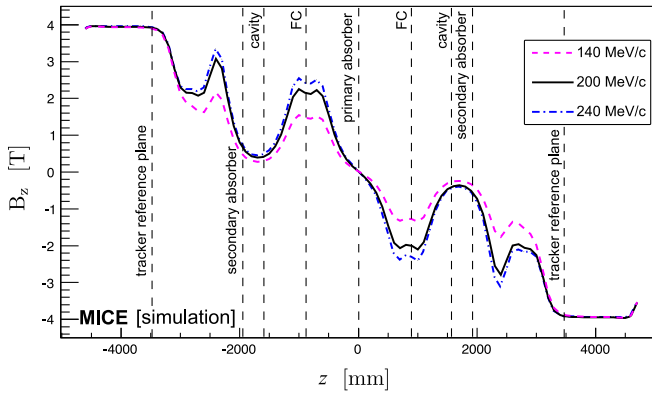


FIG. 5. Magnetic field  $B_z$  on-axis versus the longitudinal coordinate  $z$  for the cooling-demonstration lattice design for 200 MeV/c (solid black line), 140 MeV/c (dashed purple line), and 240 MeV/c (dot-dashed blue line) settings. The vertical dashed lines with labels show the positions of the tracker reference planes and the centres of the absorbers, rf cavities, and focus coil modules.

TABLE III. Coil currents used for 140 MeV/c, 200 MeV/c, and 240 MeV/c lattice settings.

| Coil                 | 140 MeV/c Lattice [A] | 200 MeV/c Lattice [A] | 240 MeV/c Lattice [A] |
|----------------------|-----------------------|-----------------------|-----------------------|
| Upstream E2          | +253.00               | +253.00               | +253.00               |
| Upstream C           | +274.00               | +274.00               | +274.00               |
| Upstream E1          | +234.00               | +234.00               | +234.00               |
| Upstream M2          | +126.48               | +155.37               | +163.50               |
| Upstream M1          | +175.89               | +258.42               | +280.72               |
| Upstream FC-coil 1   | +54.14                | +79.35                | +89.77                |
| Upstream FC-coil 2   | +54.14                | +79.35                | +89.77                |
| Downstream FC-coil 1 | -47.32                | -74.10                | -85.35                |
| Downstream FC-coil 2 | -47.32                | -74.10                | -85.35                |
| Downstream M1        | -140.43               | -231.60               | -261.71               |
| Downstream M2        | -100.12               | -149.15               | -159.21               |
| Downstream E1        | -234.00               | -234.00               | -234.00               |
| Downstream C         | -274.00               | -274.00               | -274.00               |
| Downstream E2        | -253.00               | -253.00               | -253.00               |

and reconstruction software MAUS (MICE Analysis User Software) [38]. In addition to simulation, MAUS also provides a framework for data analysis. MAUS is used for offline analysis and to provide fast real-time detector reconstruction and data visualisation during MICE running. MAUS uses GEANT4 [39,40] for beam propagation and the simulation of detector response. ROOT [41] is used for data visualisation and for data storage.

Particle tracking has been performed for several configurations. The parameters of the initial beam configurations used for the simulations are summarized in Table I.

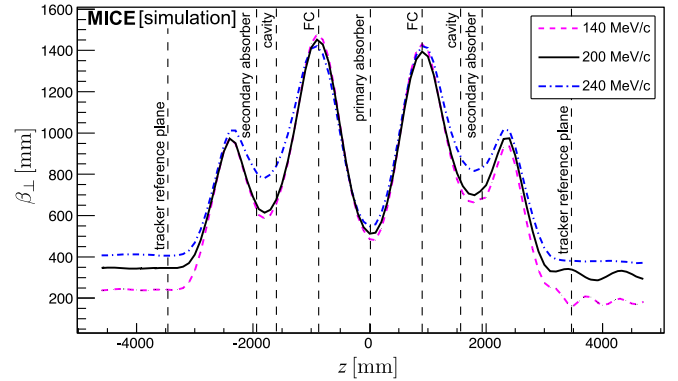


FIG. 6.  $\beta_{\perp}$  versus the longitudinal coordinate  $z$  for 200 MeV/c (solid black line), 140 MeV/c (dashed purple line) and 240 MeV/c (dot-dashed blue line) in the cooling-demonstration lattice. The vertical dashed lines with labels show the positions of the tracker reference planes and the centers of the absorbers, rf cavities, and focus coil modules.

TABLE IV. Beta-function values at relevant positions for an initial beam at 140 MeV/c, 200 MeV/c, and 240 MeV/c in the cooling-demonstration lattice design.

| Parameter   | Value for 140 MeV/c | Value for 200 MeV/c | Value for 240 MeV/c |
|---|---------------------|---------------------|---------------------|
| $\beta_{\perp}$ at primary absorber [mm]              | 480                 | 512                 | 545                 |
| $\beta_{\perp}$ at upstream secondary absorber [mm]   | 660                 | 710                 | 840                 |
| $\beta_{\perp}$ at downstream secondary absorber [mm] | 680                 | 740                 | 850                 |
| $\beta_{\perp \text{ max}}$ at FC [mm]                | 1480                | 1450                | 1430                |

The simulation of the beam starts at a point between the diffuser and the first plane of the tracker. The beam is generated by a randomizing algorithm with a fixed seed. The number of particles launched for each simulation is a compromise between the statistical uncertainty required ( $\approx 1\%$ ) and computing time. Each cavity is simulated by a TM<sub>010</sub> ideal cylindrical pillbox with a peak effective gradient matched to that expected for the real cavities. The reference particle is used to set the phase of the cavities so that it is accelerated “on crest.” The initial distributions defined in Table I are centred on the reference particle in both time and momentum. Table V lists the acceptance criteria applied to all analyses presented here. Trajectories that fail to meet the acceptance criteria are removed from the analysis.

The normalized transverse emittance is calculated by taking the fourth root of the determinant of the four-dimensional phase-space covariance matrix [20,21]. The MICE collaboration plans to take data such that the statistical uncertainty on the relative change in emittance for a particular setting is 1%. The MICE instrumentation was designed such that the systematic uncertainty related to the reconstruction of particle trajectories would contribute at the  $\sim 0.3\%$  level to the overall systematic uncertainty [15]; such uncertainties would thus be negligible.

## VI. PERFORMANCE

Figure 7 shows the evolution of the mean energy of a muon beam as it traverses the lattice. Beams with initial normalised transverse emittance  $\varepsilon_{\perp} = 4.2$  mm,

TABLE V. Acceptance criteria for analysis.

| Parameter                             | Acceptance condition             |
|---------------------------------------|----------------------------------|
| Particle                              | muon $\mu^+$                     |
| Transmission: pass through two planes | $z = -4600$ mm and $z = 5000$ mm |
| Radius at $z = -4600$ mm              | $\leq 150.0$ mm                  |
| Radius at $z = 5000$ mm               | $\leq 150.0$ mm                  |

$\varepsilon_{\perp} = 6$  mm, and  $\varepsilon_{\perp} = 7.2$  mm for initial muon beam momenta of 140 MeV/c, 200 MeV/c, and 240 MeV/c respectively are shown. The initial normalized transverse emittance is chosen such that the geometrical emittance of the three beams is the same. A 200 MeV/c muon passing through two 32.5 mm thick secondary LiH absorbers and one 65 mm thick primary LiH absorber loses an energy of 18.9 MeV. Including losses in the scintillating-fiber

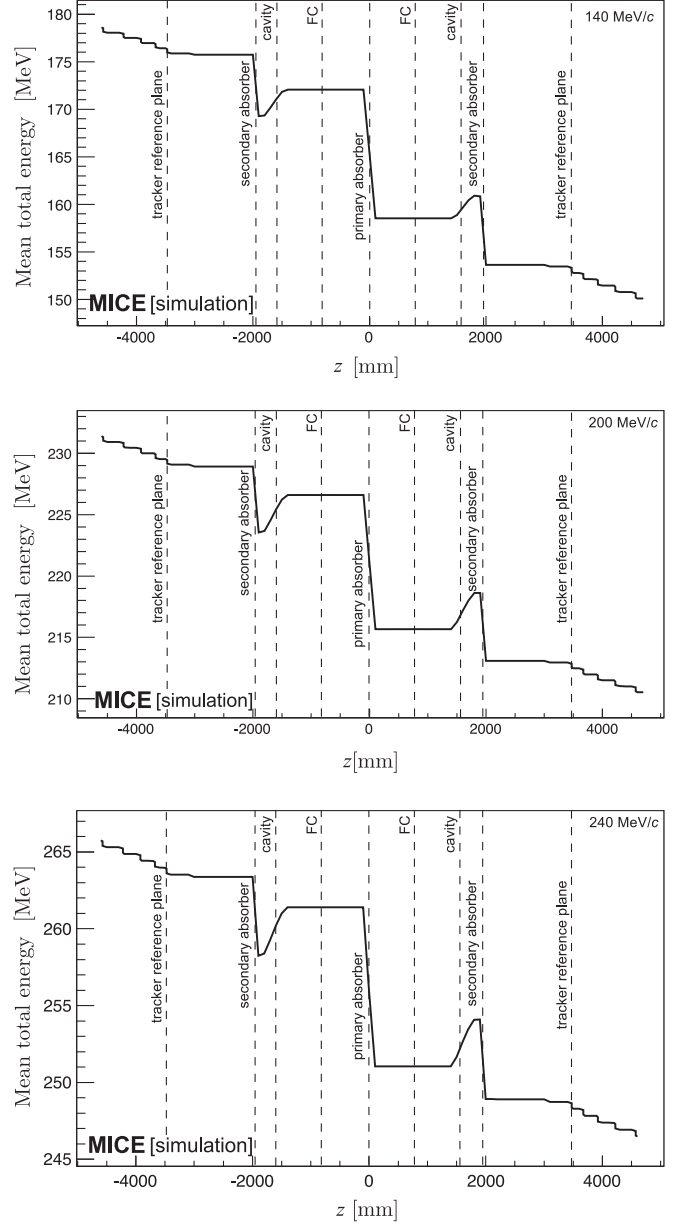


FIG. 7. Mean energy of the beam versus longitudinal coordinate ( $z$ ) in the cooling-demonstration lattice. Top: the 140 MeV/c configuration for initial emittance  $\varepsilon_{\perp} = 4.2$  mm. Middle: the 200 MeV/c configuration for initial emittance  $\varepsilon_{\perp} = 6$  mm. Bottom: the 240 MeV/c configuration for initial emittance  $\varepsilon_{\perp} = 7.2$  mm. The vertical dashed lines with labels show the positions of the tracker reference planes, and the centers of the absorbers, rf cavities, and focus coil modules.

trackers and windows, this increases to 24.3 MeV. The accelerating gradient that can be achieved in each of the two cavities is constrained by the available rf power and is insufficient to replace all the lost energy. Therefore, a comparison of beam energy with and without acceleration is required. With acceleration an energy

deficit of  $\langle \Delta E \rangle = 19$  MeV will be observed. This measurable difference will be used to extrapolate the measured cooling effect to that which would pertain if all the lost energy were restored.

The evolution of normalized transverse emittance across the lattice is shown in Fig. 8. The beam is subject to nonlinear effects in regions of high  $\beta_{\perp}$ , which cause the normalized transverse emittance to grow, especially in the 140 MeV/c configuration. This phenomenon can be seen in three different regions of the lattice: a moderate increase in emittance is observed at  $z \approx -2500$  mm and  $z \approx 1000$  mm while a larger increase is observed at  $z \approx 3000$  mm. The nonlinear effects are mainly chromatic in origin, since they are greatly lessened when the initial momentum spread is reduced. This is illustrated for the 140 MeV/c case for which the evolution of normalized emittance for beams with an rms momentum spread of 6.7 MeV/c and 2.5 MeV/c are shown. Nonetheless, in all cases a reduction in emittance is observed between the upstream and downstream trackers ( $z = \pm 3473$  mm). The lattice is predicted to achieve an emittance reduction between the tracker reference planes of  $\approx 8.1\%$ ,  $\approx 5.8\%$  and  $\approx 4.0\%$  in the 140 MeV/c, 200 MeV/c, and 240 MeV/c cases, respectively. A reduction as large as  $\approx 10\%$  can be reached in the 140 MeV/c configuration with an rms momentum spread of 1.4%.

The transmission of the cooling-demonstration lattice for beams of mean momentum 140 MeV/c, 200 MeV/c, and 240 MeV/c is shown in Fig. 9. Transmission is computed as the ratio of the number of particles that satisfy the acceptance criteria observed downstream of the cooling cell divided by the number that enter the cell. This accounts

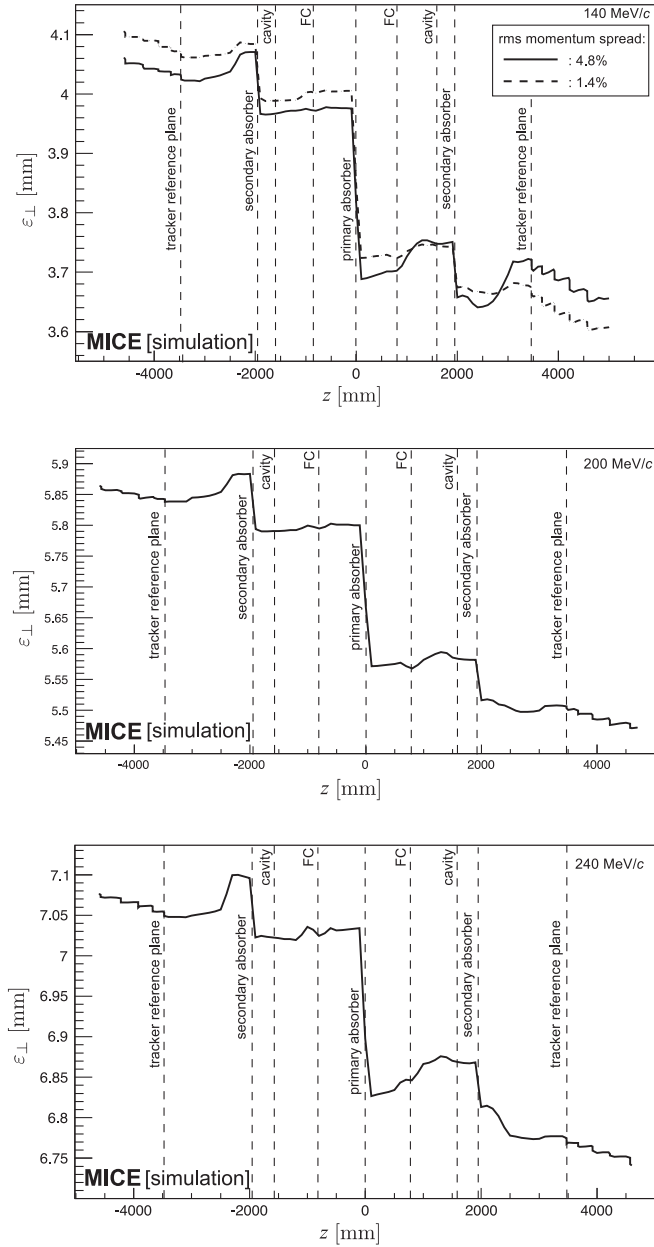


FIG. 8. Emittance variation versus the longitudinal coordinate ( $z$ ) for the cooling-demonstration lattice design. Top: 140 MeV/c beam with initial  $\epsilon_{\perp} = 4.2$  mm with an rms momentum spread of 6.7 MeV/c (rms spread 4.8%, solid line) and 2.5 MeV/c (rms spread 1.8%, dashed line). Middle: 200 MeV/c beam with initial  $\epsilon_{\perp} = 6$  mm (rms spread 4.0%). Bottom: 240 MeV/c beam with initial  $\epsilon_{\perp} = 7.2$  mm (rms spread 3.6%). The vertical dashed lines with labels show the positions of the tracker reference planes, and the centers of the absorbers, rf cavities, and focus coil modules.

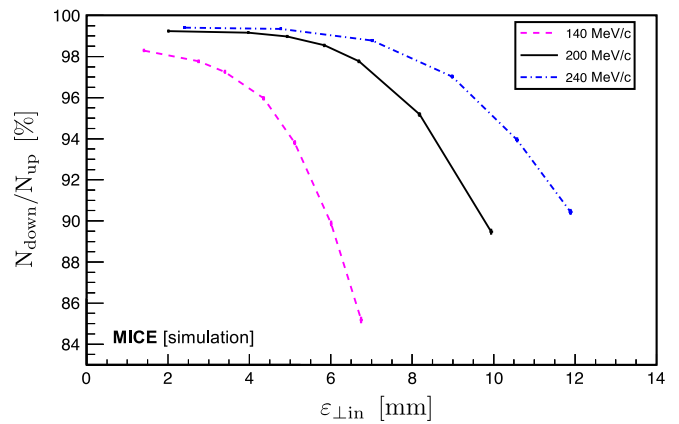


FIG. 9. Transmission (defined as the ratio of good muons observed downstream of the cooling cell,  $N_{\text{down}}$ , to those observed upstream,  $N_{\text{up}}$ ) in percent versus initial emittance ( $\epsilon_{\perp, \text{in}}$ ) for the cooling-demonstration lattice. The transmission of the 140 MeV/c, 200 MeV/c, and 240 MeV/c lattices are shown as the purple-dashed, solid black, and dot-dashed blue lines respectively. The error bars indicate the statistical precision that would be achieved using a sample of 100,000 muons.

for decay losses and implies that, in the absence of scraping or acceptance losses, the maximum transmission for beams of mean momentum 140 MeV/c, 200 MeV/c, and 240 MeV/c is 98.9%, 99.2%, and 99.5%, respectively. The lattice delivers transmission close to the maximum for 200 MeV/c and 240 MeV/c beams with input emittance below  $\approx 5$  mm and  $\approx 7$  mm, respectively. For beams of larger input emittance, the transmission gradually decreases with increasing initial emittance due to the scraping of high amplitude muons. The beam is subject to chromatic effects in regions of high  $\beta_{\perp}$ , which causes nonlinear emittance growth and limits the transmission. The behavior of the transmission for the various beam energies results from the different geometrical emittance values of the beam for the same initial normalised emittance and the energy dependence of the energy loss and scattering in the material through which the beam passes.

The fractional change in normalized transverse emittance with respect to the input emittance for beams of mean momentum 140 MeV/c, 200 MeV/c, and 240 MeV/c is shown in Fig. 10. The different values of the equilibrium emittance and the asymptote at large emittance for each momentum are clearly visible in Fig. 10. A maximum cooling effect of 15%, 8%, and 6% can be observed for beams with 140 MeV/c, 200 MeV/c, and 240 MeV/c, respectively.

The performance of the configuration proposed here is comparable to that described in [15]. In the ‘‘Step V’’ configuration, that incorporated two liquid-hydrogen absorbers each placed within a focus-coil module capable of providing a value  $\beta_{\perp}$  smaller than that which can be achieved with the present lattice, the maximum cooling effect with an input momentum and emittance of

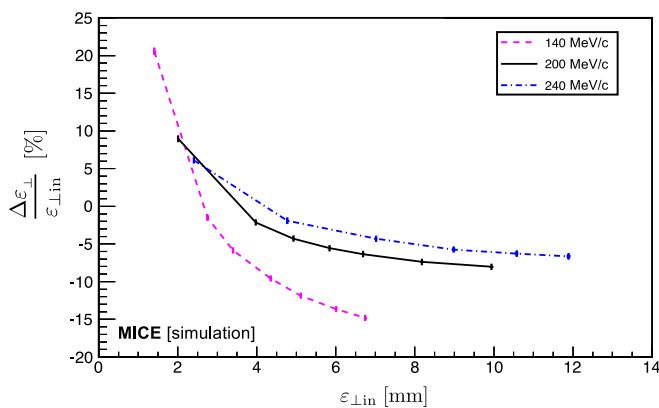


FIG. 10. Fractional change in emittance versus initial emittance ( $\epsilon_{\perp\text{in}}$ ) for the cooling-demonstration lattice design measured at the tracker reference planes. The fractional change in emittance of the 140 MeV/c, 200 MeV/c, and 240 MeV/c lattices are shown as the purple-dashed, solid black, and dot-dashed blue lines, respectively. The error bars indicate the statistical precision that would be achieved using a sample of 100,000 muons.

200 MeV/c and 10 mm respectively, was  $\sim 10\%$ . Figures 9 and 10 show the statistical uncertainties that will result from the reconstruction of a sample of 100,000 muons [42] with the configuration proposed in this paper. The instrumentation was specified to ensure that no single source of systematic uncertainty would contribute more than one third of the statistical uncertainty on the fractional change in emittance [15]. All of the instrumentation has been commissioned on the beam-line and performs to specification. The emittance-change evolution presented in Fig. 10 can therefore be measured with high significance.

## VII. CONCLUSION

An experiment by which to demonstrate ionization cooling has been described that is predicted by simulations to exhibit cooling over a range of momentum. The demonstration is performed using lithium-hydride absorbers and with acceleration provided by two 201 MHz cavities. The equipment necessary to mount the experiment is either in hand (the superconducting magnets and instrumentation), or at an advanced stage of preparation. The configuration of the demonstration of ionization cooling has been shown to deliver the performance required for the detailed study of the ionization-cooling technique.

The demonstration of ionization cooling is essential to the future development of muon-based facilities that would provide the intense, well characterized low-emittance muon beams required to elucidate the physics of flavor at a neutrino factory or to deliver multi-TeV lepton-antilepton collisions at a muon collider. The successful completion of the MICE programme would therefore herald the establishment of a new technique for particle physics.

## ACKNOWLEDGMENTS

The work described here was made possible by grants from the Science and Technology Facilities Council (UK), the Department of Energy and National Science Foundation (USA), the Istituto Nazionale di Fisica Nucleare (Italy), the Bulgarian Academy of Sciences, the Chinese Academy of Sciences, the Dutch National Science Foundation, the Ministry of Education, Science and Technological Development of the Republic of Serbia, the European Community under the European Commission Framework Programme 7 (AIDA project, Grant Agreement No. 262025, TIARA project, Grant Agreement No. 261905, and EuCARD), the Japan Society for the Promotion of Science and the Swiss National Science Foundation in the framework of the SCOPES programme. We gratefully acknowledge all sources of support. We are grateful to the support given to us by the staff of the STFC Rutherford Appleton and Daresbury Laboratories. We acknowledge the use of Grid computing resources deployed and operated by GridPP in the UK, <http://www.gridpp.ac.uk/>.

- [1] S. Geer, Neutrino beams from muon storage rings: Characteristics and physics potential, *Phys. Rev. D* **57**, 6989 (1998).
- [2] M. Apollonio *et al.*, Oscillation Physics with a Neutrino Factory, [arXiv:hep-ph/0210192](https://arxiv.org/abs/hep-ph/0210192).
- [3] D. V. Neuffer and R. B. Palmer, A high-energy high-luminosity  $\mu^+\mu^-$  collider in *Proceedings of the Fourth European Particle Accelerator Conference EPAC 94, London, England* (World Scientific, River Edge, NJ, 1994), p. 52.
- [4] R. B. Palmer, Muon colliders, *Rev. Accel. Sci. Technol.* **07**, 137 (2014).
- [5] S. Y. Lee, *Accelerator Physics*, 3rd ed., edited by S. Y. Lee (World Scientific, Singapore, 2012).
- [6] S. Schröder *et al.*, First laser cooling of relativistic ions in a storage ring, *Phys. Rev. Lett.* **64**, 2901 (1990).
- [7] J. S. Hangst, M. Kristensen, J. S. Nielsen, O. Poulsen, J. P. Schiffer, and P. Shi, Laser cooling of a stored ion beam to 1 mK, *Phys. Rev. Lett.* **67**, 1238 (1991).
- [8] P. J. Channell, Laser cooling of heavy ion beams, *J. Appl. Phys.* **52**, 3791 (1981).
- [9] J. Marriner, Stochastic cooling overview, *Nucl. Instrum. Methods Phys. Res., Sect. A* **532**, 11 (2004).
- [10] V. V. Parkhomchuk and A. N. Skrinsky, Electron cooling: 35 years of development, *Phys. Usp.* **43**, 433 (2000).
- [11] A. N. Skrinsky and V. V. Parkhomchuk, Cooling methods for beams of charged particles, *Fiz. Elem. Chastits At. Yadra* **12**, 557 (1981) [*Sov. J. Part. Nucl.* **12**, 223 (1981)].
- [12] D. Neuffer, Principles and applications of muon cooling, in *Proceedings, 12th International Conference on High-Energy Accelerators, HEACC 1983: Fermilab, Batavia, 1983*, Vol. C830811 (Fermi National Accelerator Laboratory, Batavia, 1983), p. 481–484.
- [13] D. Neuffer, Principles and applications of muon cooling, *Part. Accel.* **14**, 75 (1983).
- [14] D. Rajaram and V. C. Palladino, The status of MICE Step IV, in *Proceedings, 6th International Particle Accelerator Conference (IPAC 2015): Richmond, Virginia, USA, 2015* (JACoW, Geneva, 2015), p. 4000.
- [15] MICE Collaboration, MICE: An International Muon Ionization Cooling Experiment, <http://mice.iit.edu/micenotes/public/pdf/MICE0021/MICE0021.pdf> (2003), MICE Note 21.
- [16] M. Apollonio *et al.* (ISS Accelerator Working Group Collaboration), Accelerator design concept for future neutrino facilities, *J. Instrum.* **4**, P07001 (2009).
- [17] C. M. Ankenbrandt *et al.*, Status of muon collider research and development and future plans, *Phys. Rev. ST Accel. Beams* **2**, 081001 (1999).
- [18] M. M. Alsharoa *et al.* (Neutrino Factory and Muon Collider Collaboration), Recent progress in neutrino factory and muon collider research within the Muon collaboration, *Phys. Rev. ST Accel. Beams* **6**, 081001 (2003).
- [19] R. B. Palmer, J. S. Berg, R. C. Fernow, J. C. Gallardo, H. G. Kirk, Y. Alexahin, D. Neuffer, S. A. Kahn, and D. Summers, A complete scheme of ionization cooling for a muon collider, in *Proceedings of the 22nd Particle Accelerator Conference, PAC-2007, Albuquerque, NM* (IEEE, New York, 2007), p. 3193.
- [20] G. Penn and J. S. Wurtele, Beam Envelope Equations for Cooling of Muons in Solenoid Fields, *Phys. Rev. Lett.* **85**, 764 (2000).
- [21] C. Rogers, Ph.D. dissertation, Imperial College of London, 2008.
- [22] D. Stratakis and R. B. Palmer, Rectilinear six-dimensional ionization cooling channel for a muon collider: A theoretical and numerical study, *Phys. Rev. ST Accel. Beams* **18**, 031003 (2015).
- [23] D. Neuffer, H. Sayed, T. Hart, and D. Summers, Final Cooling for a High-Energy High-Luminosity Lepton Collider, [arXiv:1612.08960](https://arxiv.org/abs/1612.08960).
- [24] A. V. Tollestrup and J. Monroe, Fermi National Accelerator Laboratory Technical Report No. FERMILAB-MUCOOL-176, 2000.
- [25] C. N. Booth *et al.*, The design, construction and performance of the MICE target, *J. Instrum.* **8**, P03006 (2013).
- [26] C. N. Booth *et al.*, The design and performance of an improved target for MICE, *J. Instrum.* **11**, P05006 (2016).
- [27] M. Bogomilov *et al.* (MICE Collaboration), The MICE Muon Beam on ISIS and the beam-line instrumentation of the Muon Ionization Cooling Experiment, *J. Instrum.* **7**, P05009 (2012).
- [28] D. Adams *et al.* (MICE Collaboration), Characterisation of the muon beams for the Muon Ionisation Cooling Experiment, *Eur. Phys. J. C* **73**, 2582 (2013).
- [29] R. Bertoni *et al.*, The design and commissioning of the MICE upstream time-of-flight system, *Nucl. Instrum. Methods Phys. Res., Sect. A* **615**, 14 (2010).
- [30] R. Bertoni, M. Bonesini, A. de Bari, G. Cecchet, Y. Karadzhev, and R. Mazza, The construction of the MICE TOF2 detector, <http://mice.iit.edu/micenotes/public/pdf/MICE0286/MICE0286.pdf> (2010).
- [31] L. Cremaldi, D. A. Sanders, P. Sonnek, D. J. Summers, and J. Reidy, Jr., A Cherenkov radiation detector with high density aerogels, *IEEE Trans. Nucl. Sci.* **56**, 1475 (2009).
- [32] M. Ellis *et al.*, The design, construction and performance of the MICE scintillating fibre trackers, *Nucl. Instrum. Methods Phys. Res., Sect. A* **659**, 136 (2011).
- [33] F. Ambrosino *et al.*, Calibration and performances of the KLOE calorimeter, *Nucl. Instrum. Methods Phys. Res., Sect. A* **598**, 239 (2009).
- [34] R. Asfandiyarov *et al.*, The design and construction of the MICE Electron-Muon Ranger, *J. Instrum.* **11**, T10007 (2016).
- [35] M. Leonova *et al.*, MICE cavity installation and commissioning/operation at MTA, in *Proceedings, 6th International Particle Accelerator Conference (IPAC 2015): Richmond, Virginia, USA, 2015* (JACoW, Geneva, 2015), p. 3342–3344.
- [36] Y. Torun *et al.*, Final commissioning of the MICE RF module prototype with production couplers, in *Proceedings, 7th International Particle Accelerator Conference (IPAC 2016): Busan, Korea, 2016* (JACoW, Geneva, 2016), p. 474.
- [37] R. C. Fernow and R. B. Palmer, Solenoidal ionization cooling lattices, *Phys. Rev. ST Accel. Beams* **10**, 064001 (2007).
- [38] C. D. Tunnell and C. T. Rogers, MAUS: MICE Analysis User Software, in *Proceedings of the 2nd International Particle Accelerator Conference, San Sebastián, Spain* (EPS-AG, Spain, 2011), p. 850.

- 
- [39] S. Agostinelli *et al.* (GEANT4 Collaboration), GEANT4: A simulation toolkit, *Nucl. Instrum. Methods Phys. Res., Sect. A* **506**, 250 (2003).
- [40] J. Allison *et al.*, Geant4 developments and applications, *IEEE Trans. Nucl. Sci.* **53**, 270 (2006).
- [41] R. Brun and F. Rademakers, ROOT: An object oriented data analysis framework, *Nucl. Instrum. Methods Phys. Res., Sect. A* **389**, 81 (1997).
- [42] C. Hunt, Ph.D. dissertation, Imperial College of London, 2017.

# Forecasting hourly particulate matter concentrations based on the advanced multivariate methods

M. Perišić<sup>1</sup> · D. Maletić<sup>1</sup> · S. S. Stojić<sup>2</sup> · S. Rajšić<sup>1</sup> · A. Stojić<sup>1</sup>

Received: 22 April 2016/Revised: 11 July 2016/Accepted: 19 November 2016  
© Islamic Azad University (IAU) 2016

**Abstract** In this study, several multivariate methods were used for forecasting hourly PM<sub>10</sub> concentrations at four locations based on SO<sub>2</sub> and meteorological data from the previous period. According to the results, boosted decision trees and multi-layer perceptrons yielded the best predictions. The forecasting performances were similar for all examined locations, despite the additional PM<sub>10</sub> spatio-temporal analysis showed that the sites were affected by different emission sources, topographic and microclimatic conditions. The best prediction of PM<sub>10</sub> concentrations was obtained for industrial sites, probably due to the simplicity and regularity of dominant pollutant emissions on a daily basis. Conversely, somewhat weaker forecast accuracy was achieved at urban canyon avenue, which can be attributed to the specific urban morphology and most diverse emission sources. In conclusion to this, the integration of advanced multivariate methods in air quality forecasting systems could enhance accuracy and provide the basis for efficient decision-making in environmental regulatory management.

**Keywords** Air quality · Environmental pollution · Regulatory management · Supervised learning algorithms

## Introduction

Over the last century, changes in emission sources, methane concentrations and climate have affected atmospheric composition and led to the significant increase in the levels of particulate matter (PM) and gaseous pollutants, particularly in developing countries (Fang et al. 2013). According to recent estimates, about 3.5 million cardiopulmonary deaths annually and globally can be attributed to exposure to anthropogenic PM<sub>2.5</sub>, and the projections are that this number could double by 2050 (Lelieveld et al. 2015). In addition to stringent abatement measures, the accurate and reliable prediction of air pollutant episodes and establishment of an early public warning system is of vital importance for the increase in life expectancy and reduction of health care expenditures.

Despite the fact that significant progress has been made through integration of different scientific approaches, modeling of air pollution data remains a challenge, due to complexity and non-linear nature of atmospheric phenomena and processes (Pai et al. 2013). The variety of techniques and tools described in the literature for air quality forecasting covers simple empirical approaches, statistical approaches including artificial neural networks and fuzzy logic methods, and physically-based approaches including deterministic methods and ensemble and probabilistic methods (Zhang et al. 2012). The deterministic approach mostly refers to meteorological and chemical transport models, such as sophisticated Community Air Quality Modelling System (CMAQ) for prediction of air quality index at locations with no real-time measurements.

---

Editorial responsibility: An-Lei Wei.

---

**Electronic supplementary material** The online version of this article (doi:10.1007/s13762-016-1208-8) contains supplementary material, which is available to authorized users.

---

✉ M. Perišić  
mirjana.perisic@ipb.ac.rs

<sup>1</sup> Institute of Physics Belgrade, University of Belgrade, Pregrevica 118, 11080 Belgrade, Serbia

<sup>2</sup> Singidunum University, Danijelova 32, 11010 Belgrade, Serbia

The chemical transport models were first used in Germany for air quality forecasting purposes, and soon many other developed countries became aware of the benefits of such implementation and launched the centralized air quality forecasting systems based on different tools, from simple empirical to online-coupled meteorology and chemistry models. While deterministic models don't require a large quantity of observational data, they do demand sufficient knowledge and understanding of pollutant emission sources, transport and atmospheric reactions and transformations under the planetary boundary layer (Feng et al. 2015). Since crucial knowledge in this area is often limited and some processes are too complex to be presented within a model, deterministic models are computationally expensive and time-consuming for routine predictions and often employ approximations and simplifications that lead to strong biases and inaccuracy, thus making the forecasts useless for timely management of critical situations (Cobourn 2010; Russo and Soares 2014).

Over the last decade, the parametric or non-parametric statistical approaches have been proposed as a more economical alternative for discovering the underlying site-specific dependencies between pollutant concentrations and potential predictors (Feng et al. 2015). The most commonly examined were artificial neural networks, based on artificial neurons or nodes capable of learning relationships between the routinely-measured pollutant data and selected predictors through embedded functions and data from the previous period (Fernando et al. 2012). Unlike deterministic models, artificial neural networks provide more accurate air quality forecasts, whereas their major disadvantages are associated with "black box" nature and poor generalization performance (Moustris et al. 2013). Furthermore, both statistical and deterministic approaches show satisfactory or good performance in forecasting concentrations closer to average values, whereas the prediction of extreme pollution events is more challenging.

As summarized by Zhang et al. (2012), the integration of advanced statistical methods in future air quality forecasting systems could considerably reduce forecasting biases and further enhance accuracy. In our previous study, MVA methods were successfully applied for forecasting the contributions of industry and vehicle exhaust to volatile organic compound (VOC) levels in the urban area, with smallest relative forecast error of only 6% (Stojić et al. 2015a). In this study, we compared the performance of twelve advanced multivariate (MVA) methods for PM<sub>10</sub> forecasting relying on meteorological data and SO<sub>2</sub> concentrations. The analysis was based on a multi-year dataset collected at four different locations, affected by traffic or

industry emissions. The herein employed MVA classification and regression methods belong to the supervised learning algorithms designed within Toolkit for Multivariate Analysis (TMVA; Hoecker et al. 2007) within the ROOT framework (Brun and Rademakers 1997), for extracting the maximum available information from the extensive data in high-energy physics.

## Materials and methods

The analyzed dataset comprising 5-year (2011–2015) hourly concentrations of PM<sub>10</sub>, SO<sub>2</sub> and meteorological data (atmospheric pressure, temperature, humidity, wind speed and direction), was obtained from the automatic monitoring stations within the Institute of Public Health network, at four different sites (Fig. 1, Supplementary Material). In the urban area, mostly affected by vehicle-exhaust emissions, measurements were conducted at the Institute of Public Health and New Belgrade, the sites characterized as being urban canyon avenue (UCA) and urban boulevard (UB), respectively, due to their topographic configuration. In the area influenced by emissions from fossil fuel burning for industry and heating operations, the data were collected in Obrenovac and Grabovac, the sites corresponding to urban industry (UI) and rural industry (RI), respectively. The measurements at industrial sites were incomplete due to severe floods that affected the area in 2014. The concentrations of PM<sub>10</sub> and SO<sub>2</sub> were measured by means of referent beta-ray attenuation (Thermo FH 62-IR) sampler and referent sampling device Horiba APSA 360, respectively. The meteorological data were obtained by using Lufft WS500-UMB Smart Weather Sensor. The accuracy and precision of detection methods are provided in Stojic et al. (2016).

The analyses of daily, weekly, seasonal and annual dynamics, trend (Pretty 2015) and periodicity were performed by means of Openair (Carslaw and Ropkins 2012) and Lomb (Ruf 1999) packages within the Statistical Software Environment R (Team 2012). The relationships between pollutant concentrations and wind characteristics were investigated by the use of bivariate polar plot and bivariate cluster analyses within the Openair package. The contribution of local emission sources, background and transport to the observed PM<sub>10</sub> pollution was analyzed using the 72-h air mass back trajectories and trajectory sector analysis (TSA) as described in Stojić et al. (2016).

The following MVA methods were used for PM<sub>10</sub> forecasting: Boosted decision trees (BDT, BDTG, BDTMitFisher), Artificial Neural Network Multilayer

Perceptron (MLP), MLP with Bayesian Extension (MLPBNN), Support Vector Machine (SVM), k-nearest neighbor (KNN), Linear Discriminant (LD), Boosted Fisher Discriminant (BoostedFisher), Multidimensional Probability Density Estimator Range Search Method (PDERS), Predictive Learning via Rule Ensembles (Rule-Fit) and Function Discriminant Analysis (FDA). All methods were used for both classification and regression. The five-year dataset was divided into two equal subsets, each consisting of  $PM_{10}$  concentrations and input data (meteorological and  $SO_2$ ). One subset was used for method trainings, either to differentiate between high and low importance indicators for  $PM_{10}$  concentrations (classification), or to determine an approximation of the underlying functional behavior defining  $PM_{10}$  concentrations (regression). The other subset was utilized for method performance testing.

## Results and discussion

Previous studies aimed at investigating the origin and spatio-temporal distribution of different pollutant species converge on the conclusion that poor air quality presents an important health risk factor in Belgrade area (Perišić et al. 2015; Stojić et al. 2015b). In the previous years, the mean annual  $PM_{10}$  concentrations in Belgrade area were in the range from 39.74 to 62.32  $\mu g m^{-3}$ , whereas the exceedances of the proposed air quality guideline value of 50  $\mu g m^{-3}$  were registered during 20.5–42.2% of total number of days (Stanišić Stojić et al. 2016).

### Specifics of measurement sites

In order to examine the MVA forecasting performances,  $PM_{10}$  observational data from four measurement sites affected by different emission sources were collected and analyzed (Fig. 1, Supplementary Material). The two locations defined as urban were affected by traffic emissions throughout the year. However, specific microclimatic conditions associated with contrasting urban morphology between UCA and UB plays an important role in spatial distribution of particles. The presence of tall buildings along both sides of the canyon avenue induces a complex wind flow that does not enhance the pollutant dispersion due to terrain configuration, but it facilitates suspension, particularly fine PM fraction (Vardoulakis et al. 2003). Furthermore, frequent congestions in the canyon avenue compared to free flowing traffic in the wide boulevard contributed to higher  $PM_{10}$  concentrations at UCA

throughout the year, with the exception of winter season, when the air quality at UB was additionally affected by fuel burning from the neighboring heating plant.

The herein presented industrial locations were affected either by fuel burning emissions only (RI), or by emissions from both industrial activities and vehicle exhaust (UI). Within the range of 15–20 km in NW/N and SE/S direction around the two industrial sites, the strong emission sources including three thermal power plants, four open-pit mines of high-sulfur lignite and several coal ash disposal sites are located.

As can be seen, the highest mean  $PM_{10}$  concentration for the entire period was registered at UI (Table 1, Supplementary Material), which was partly driven by extreme pollutant loadings in 2012 (Fig. 2, Supplementary Material). It should be noted that the  $PM_{10}$  variations at two industrial locations exhibited similar pattern, only with less significant deviations at rural site, which points to the prevalence of the same emission sources.

Daily mean  $PM_{10}$  exceedances ( $>50 \mu g m^{-3}$ ) were commonly observed, whereas the episodes of extreme pollutant levels were registered only at UI (Fig. 3, Supplementary Material). The winter  $PM_{10}$  concentrations were considerably higher at all examined locations, which can be partly attributed to heating operations, but also to lower planetary boundary layer (PBL) height in winter season. Unsurprisingly, the lowest  $PM_{10}$  levels for the entire period were observed at rural site, particularly during spring and summer season, with the values of 29.15 and 32.09  $\mu g m^{-3}$  being registered, respectively. Conversely, the highest concentrations in warm season were measured at UCA, the only site predominately affected by traffic. The differences between the summer and winter concentrations were relatively small at UCA and RI, whereas the inter-seasonal variations at two other sites exposed to the emissions from two strong sources were almost two times higher.

In Fig. 4, Supplementary Material, daily, weekly and seasonal  $PM_{10}$  variations are displayed. Accordingly, the lowest concentrations were registered in May and June, probably due to intense precipitations. The particle resuspension processes and atmospheric photochemical reactions in dry summer months starting from July, led to the rising pollutant levels, particularly at industrial sites in the vicinity of ash disposals. The accumulation of particles during working days was followed by a significant decrease at the weekend at two locations dominated by vehicle exhaust emissions, whereas the weekday/weekend difference was not observed at UI and RI sites. As regards diurnal  $PM_{10}$  variations, the same pattern was detected at all locations: daytime levels tended to be low with the exception of

morning and afternoon rush hours, whereas the pronounced increase in nighttime concentrations could be attributed to stable atmospheric conditions and shallow PBL.

According to bivariate and cluster analysis, the average contributions of the surrounding emission sources were dominant at all locations (Fig. 1), particularly at UCA (59.5  $\mu\text{g m}^{-3}$ ), due to limited pollutant dispersion, and UI (73.1  $\mu\text{g m}^{-3}$ ), which has been directly exposed to emissions from the thermal plant which produces more than 50% of electricity for the Serbian market. The UCA is located in the central city area and thus, the polluted air masses were observed to come from all directions, whereas at UB, the impact of heating plant emissions from S and intersections with intensive traffic coming from E can be noted. In the case of industrial locations, local sources appeared to be particularly significant during the heating season, whereas in spring and summer, both UI and RI were affected by emissions from ash disposals and lignite mining sites in NW/N and SE/S. The dynamics of cluster contributions on a daily, weekly and seasonal basis are shown in Fig. 5, Supplementary Material. As can be seen, local emissions, corresponding to cluster 4 at industrial sites, exhibited extremely regular daily variations, which suggests the prominent role of anthropogenic sources. The rush hour peaks were noticeable only in the variations of locally-emitted  $\text{PM}_{10}$  concentrations at UCA (cluster 4), since the site has been dominated by traffic emissions.

The analysis was also performed to determine the impact of local emissions, transported pollution and background on the air quality at examined locations. According to TSA results, the estimated share of background was highest at rural site (48%), whereas the contribution of local production was the most significant factor (43%) for  $\text{PM}_{10}$  concentrations at UI, as previously shown by bivariate and cluster analysis.

Upon the presented analysis, we have reached the conclusion that the selected locations are substantially different in terms of air quality and factors closely associated with it, including micro-climatic conditions, topographic features and proximity of strong sources. This was considered a prerequisite for examining the dependency between the efficiency of MVA methods for air quality forecasting and site characteristics.

### Classification MVA methods

As previously mentioned, the 5-year dataset, including  $\text{PM}_{10}$  and  $\text{SO}_2$  concentrations, and meteorological data, was divided into two subsets equal in size, used for training and testing of MVA methods, respectively. In order to account for seasonal, *i.e.* weekday/weekend variations, two new variables were introduced for classification purposes: Yearreal is a quotient of the ordinal number of a day and total number of days per year, while Weekreal represents

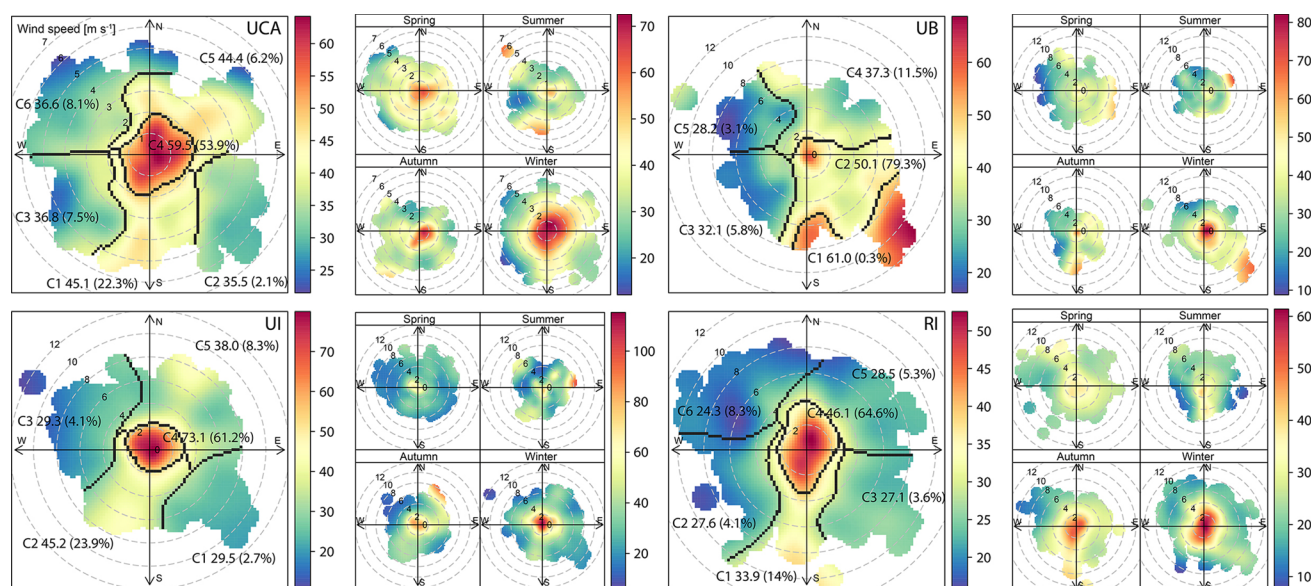


**Fig. 1** The relationship between  $\text{PM}_{10}$  concentrations and wind characteristics: bivariate cluster plot [frequency (%) and average contributions ( $\mu\text{g m}^{-3}$ )] for the entire period (left) and seasonal variations ( $\mu\text{g m}^{-3}$ ) (right)



the quotient of the ordinal number of a day and number 7. Correlation and mutual information of input variables and the observed PM<sub>10</sub> mass concentrations for all sampling sites are presented in Table 1.

For the purposes of classification, the PM<sub>10</sub> levels above 50 µg m<sup>-3</sup> are considered to require the increased level of caution, whereas those exceeding 100 µg m<sup>-3</sup> are considered extremely high—alarm triggering values, both of which are chosen as arbitrary limits. The estimation of classification method performances by using the Receiver Operating Characteristic (ROC) curve is presented in

**Table 1** Correlation (C) and mutual information (MI) of input variables (P, pressure; T, temperature; Rh, relative humidity; ws, wind speed; Yearreal, day of year; Weekreal, day of week) and measured PM<sub>10</sub> concentrations at all sampling sites

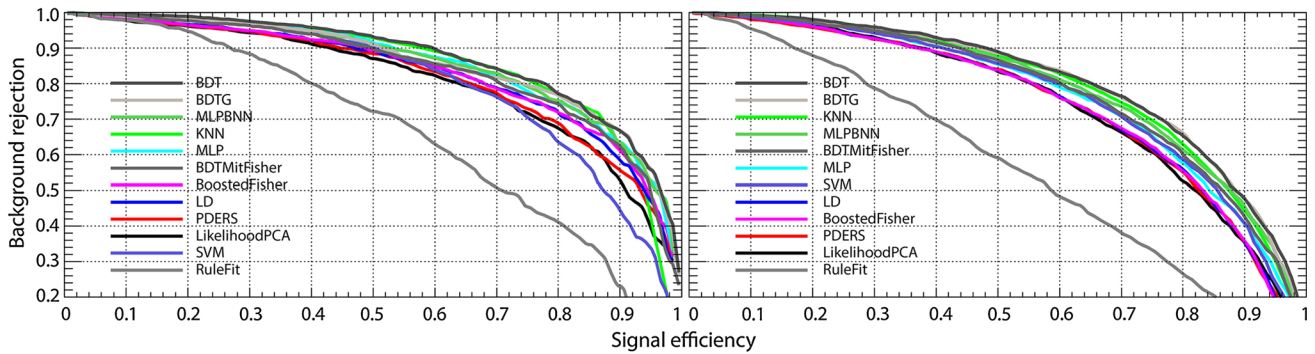
| Variable        | UCA  |      | UB   |      | UI   |      | RI   |      |
|-----------------|------|------|------|------|------|------|------|------|
|                 | C    | MI   | C    | MI   | C    | MI   | C    | MI   |
| P               | 0.18 | 1.31 | 0.26 | 0.97 | 0.20 | 1.49 | 0.29 | 1.26 |
| T               | 0.21 | 1.40 | 0.30 | 1.21 | 0.28 | 1.69 | 0.22 | 1.39 |
| Rh              | 0.24 | 1.47 | 0.24 | 1.29 | 0.22 | 1.86 | 0.19 | 1.60 |
| ws              | 0.29 | 1.39 | 0.25 | 0.82 | 0.26 | 1.57 | 0.32 | 1.18 |
| SO <sub>2</sub> | 0.25 | 1.63 | 0.09 | 1.39 | 0.20 | 1.87 | 0.32 | 1.59 |
| Yearreal        | 0.04 | 1.49 | 0.05 | 1.31 | 0.09 | 1.86 | 0.12 | 1.53 |
| Weekreal        | 0.02 | 0.12 | 0.03 | 0.11 | 0.02 | 0.18 | 0.02 | 0.14 |

Fig. 2. The highest separation between background and predicted PM<sub>10</sub> concentrations was observed when PM<sub>10</sub> classifier value of 100 µg m<sup>-3</sup> was taken into account (Fig. 3), whereas somewhat poorer results were obtained for 50 µg m<sup>-3</sup>, which suggests that including additional meteorological or pollutant variables as input data might further enhance classification performance.

The comparison of the results by evaluating signal and background efficiencies revealed that certain MVA methods are capable of classifying the PM<sub>10</sub> levels which are considered to require a high degree of caution (Table 2, left). The results showed that BDTG and MLP exhibit the best results for all examined locations. Signal and background separation was most efficiently performed for RI and UB, and to a somewhat lower extent for UCA.

**Regression MVA methods**

Regression MVA methods were applied to interpret the relationships between pollutant concentrations and the examined input data. Similar to classification methods, BDTG and MLP exhibited the most satisfying performances with absolute and relative errors presented in Table 2, right. The MVA method performance was best for PM<sub>10</sub> loadings at industrial sites, around 25%, while the forecast quality could be clearly seen at RI location, Fig. 4. It can be assumed that more accurate air quality forecasts can be



**Fig. 2** ROC curves for MVA classification methods with PM<sub>10</sub> classifier value of 100 µg m<sup>-3</sup> (left) and 50 µg m<sup>-3</sup> (right) for all sampling sites

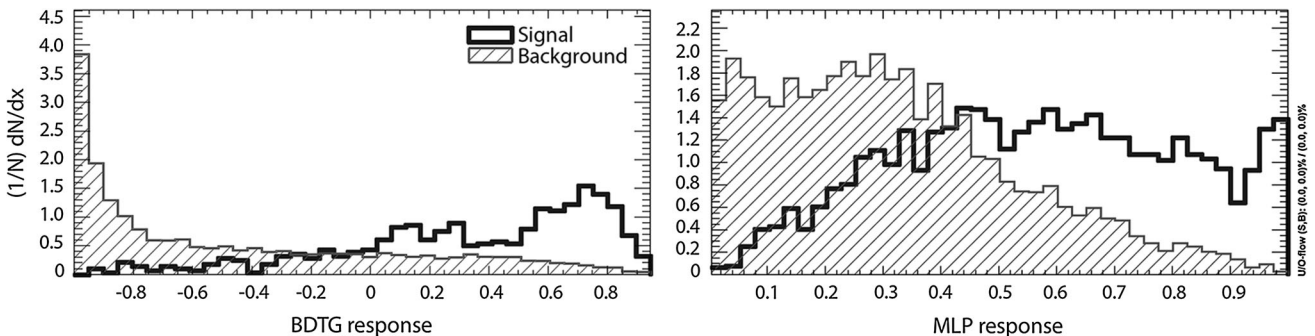


**Fig. 3** MVA classification method response for PM<sub>10</sub> classifier value of 100 µg m<sup>-3</sup> (left) and 50 µg m<sup>-3</sup> (right) for UCA site

**Table 2** The comparison of best performing methods for ROC, separation and significance values for all measurement sites (left) and absolute ( $\mu\text{g m}^{-3}$ ) and relative (%) errors of the best performing regression methods (right)

| Sampling site | Method | Classification |            |              | Regression     |                |
|---------------|--------|----------------|------------|--------------|----------------|----------------|
|               |        | ROC            | Separation | Significance | Absolute error | Relative error |
| UCA           | BDTG   | 0.806          | 0.282      | 0.883        | 17.2           | 29.6           |
|               | MLP    | 0.772          | 0.226      | 0.755        | 21.8           | 37.5           |
| UB            | BDTG   | 0.868          | 0.408      | 1.12         | 13.9           | 26.8           |
|               | MLP    | 0.841          | 0.352      | 1.015        | 17.4           | 33.5           |
| UI            | BDTG   | 0.855          | 0.379      | 1.059        | 15.6           | 24.6           |
|               | MLP    | 0.826          | 0.323      | 0.956        | 24.0           | 37.9           |
| RI            | BDTG   | 0.867          | 0.412      | 1.172        | 10.6           | 25.2           |
|               | MLP    | 0.837          | 0.345      | 0.962        | 15.1           | 36.0           |

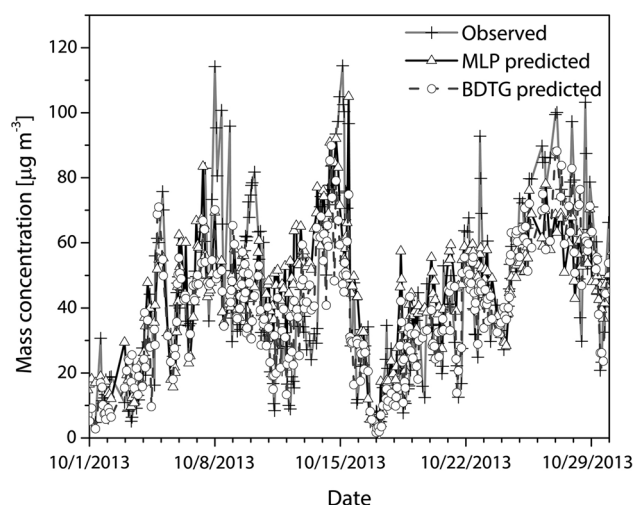


**Fig. 4** The comparison of time series of the observed and best performing MVA-predicted  $\text{PM}_{10}$  concentrations ( $\mu\text{g m}^{-3}$ ) at RI site

achieved at the locations such as RI, which are affected by less significant number of emission sources. Furthermore, the simplicity and regularity of dominant pollutant emissions on a daily, weekly and seasonal basis, as registered at UI location, as well as minor deviations from the commonly observed pollutant loadings, which is particularly evident for air quality forecasting at rural site, are probably the additional factors associated with forecast accuracy.

Conversely, the weakest MVA method performance was derived for  $\text{PM}_{10}$  concentrations at UCA, probably because the urban morphology of the canyon avenue represents the additional factor modifying the pollutant levels in a less predictable manner. Furthermore, the emission sources in the central city zone are diverse and primarily refer to traffic congestions and intense atmospheric reactions that take place in stagnant conditions of the canyon street. Moreover, they also relate to local fireboxes in residential area where lignite is burned

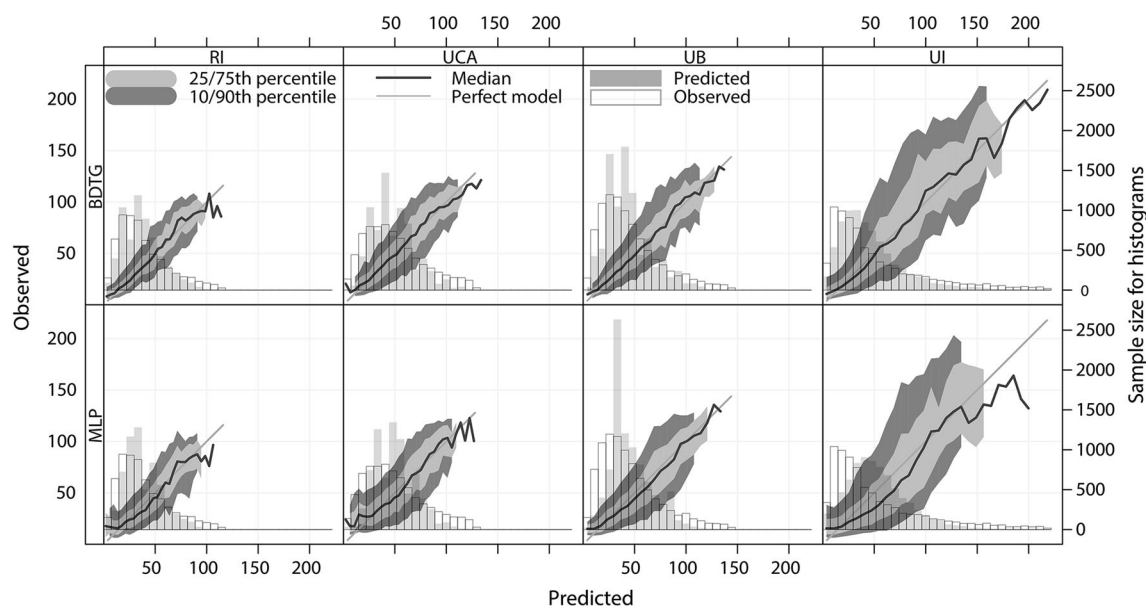


**Fig. 5** The comparison of the observed and best performing MVA-predicted  $\text{PM}_{10}$  mass concentrations ( $\mu\text{g m}^{-3}$ )



during autumn and winter season and local manufactures that are associated with pollutant emissions highly variable in time and intensity.

As can be seen in Fig. 5, the PM<sub>10</sub> time series evaluated by means of MVA regression methods correlated very well with the observed concentrations at all sampling sites. Mutual information obtained for BDTG-predicted and the observed PM<sub>10</sub> mass concentrations were 0.71, 0.7, 0.65 and 0.64 for RI, UB, UCA and UI, respectively. This suggests that significant input variables were used for the forecasting process. In addition, it could be noted that their distributions are relatively well.

Although the other MVA methods employed in the present study generated similar results when being used for classification, they generated the significant PM<sub>10</sub> forecast errors when being used for regression, at least based on the observed input variables. The herein presented errors are mostly in compliance with the findings of our previous study, aimed at forecasting the contributions from traffic and industry to the observed VOC concentrations in the urban area, which suggests that both PM and VOC, as important air quality indicators, can be predicted using the MVA methods.

## Conclusion

In this study, the performances of MVA methods for forecasting PM<sub>10</sub> concentrations and prediction of related health-damaging events were evaluated on the basis of datasets from traffic- and industry-affected locations with substantial differences in air quality, which has also been verified through additional analyses. The results of both classification and regression methods were rather promising, particularly considering the fact that the presented forecast accuracy referred to hourly concentrations. The quality of the prediction might be partly dependent on microclimatic conditions, topographic characteristics, presence of strong emission sources and other site characteristics, as well as on the input data. All that implies that the selection of additional or different variables could enhance the method forecasting performances. The importance of accurate air quality forecasts as part of the management system is reflected in the potential applications, including health alerts for susceptible categories, operational planning, as well as amendment of pollutant time-series and reduction of regular monitoring expenditures.

**Acknowledgements** This study was carried out as part of the Project No. III43007, III41011 and OI171002, financed by the Ministry of Education, Science and Technological Development of the Republic of Serbia for the period 2011–2016.

## References

- Brun R, Rademakers F (1997) ROOT—an object oriented data analysis framework. *Nucl Instrum Methods A* 389:81–86
- Carslaw DC, Ropkins K (2012) Openair—an R package for air quality data analysis. *Environ Model Softw* 27:52–61
- Cobourn WG (2010) An enhanced PM<sub>2.5</sub> air quality forecast model based on nonlinear regression and back-trajectory concentrations. *Atmos Environ* 44:3015–3023
- Fang Y, Mauzerall DL, Liu J, Fiore AM, Horowitz LW (2013) Impacts of 21st century climate change on global air pollution-related premature mortality. *Clim Change* 121:239–253
- Feng X, Li Q, Zhu Y, Hou J, Jin L, Wang J (2015) Artificial neural networks forecasting of PM<sub>2.5</sub> pollution using air mass trajectory based geographic model and wavelet transformation. *Atmos Environ* 107:118–128
- Fernando HJS, Mammarella MC, Grandoni G, Fedele P, Di Marco R, Dimitrova R, Hyde P (2012) Forecasting PM<sub>10</sub> in metropolitan areas: efficacy of neural networks. *Environ Pollut* 163:62–67
- Hoecker A, Speckmayer P, Stelzer J, Therhaag J, Von Toerne E, Voss H, Backes M, Carli T, Cohen O, Christov A, Dannheim D, Danilowski K, Henrot-Versille S, Jachowski M, Kraszewski K, Krasznahorkay A, Kruk M, Mahalalel Y, Ospanov R, Prudent X, Robert A, Schouten D, Tegenfeldt F, Voigt A, Voss K, Wolter M, Zemla A (2007) TMVA users guide—toolkit for multivariate data analysis, PoSACAT 040. <http://arxiv.org/abs/physics/0703039>. Accessed 14 June 2015
- Lelieveld J, Evans JS, Fnais M, Giannadaki D, Pozzer A (2015) The contribution of outdoor air pollution sources to premature mortality on a global scale. *Nature* 525:367–371
- Moustris KP, Larissi IK, Nastos PT, Koukouletsos KV, Paliatsos AG (2013) Development and application of artificial neural network modeling in forecasting PM<sub>10</sub> levels in a Mediterranean city. *Water Air Soil Pollut* 224:1–11
- Pai TY, Hanaki K, Chiou RJ (2013) Forecasting hourly roadside particulate matter in Taipei County of Taiwan based on first-order and one-variable grey model. *CLEAN Soil Air Water* 41:737–742
- Perišić M, Stojić A, Stojić SS, Šošćarić A, Mijić Z, Rajšić S (2015) Estimation of required PM<sub>10</sub> emission source reduction on the basis of a 10-year period data. *Air Qual Atmos Health* 8:379–389
- Pretty R (2015) TheilSen {openair} tests for trends using Theil–Sen estimates. <http://www.inside-r.org/packages/cran/openair/docs/TheilSen>. Accessed 12 Dec 2015
- Ruf T (1999) The Lomb-Scargle periodogram in biological rhythm research: analysis of incomplete and unequally spaced time-series. *Biol Rhythm Res* 30:178–201
- Russo A, Soares AO (2014) Hybrid model for urban air pollution forecasting: a stochastic spatio-temporal approach. *Math Geosci* 46:75–93
- Stanišić Stojić S, Stanišić N, Stojić A, Šošćarić A (2016) Single and combined effects of air pollutants on circulatory and respiratory system-related mortality in Belgrade, Serbia. *J Toxicol Environ Health A* 79:17–27
- Stojić A, Maletić D, Stojić SS, Mijić Z, Šošćarić A (2015a) Forecasting of VOC emissions from traffic and industry using classification and regression multivariate methods. *Sci Total Environ* 521:19–26
- Stojić A, Stojić SS, Mijić Z, Šošćarić A, Rajšić S (2015b) Spatio-temporal distribution of VOC emissions in urban area based on receptor modeling. *Atmos Environ* 106:71–79
- Stojić A, Stanišić Stojić S, Reljin I, Čabarkapa M, Šošćarić A, Perišić M, Mijić Z (2016) Comprehensive analysis of PM<sub>10</sub> in Belgrade urban area on the basis of long term measurements. *Environ Sci Pollut Res*. doi:10.1007/s11356-016-6266-4

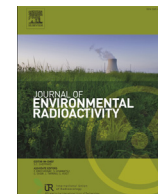


Team RC (2012) R: a language and environment for statistical computing. <http://cran.case.edu/web/packages/dplr/vignettes/timeseries-dplr.pdf>. Accessed 10 June 2015

Vardoulakis S, Fisher BE, Pericleous K, Gonzalez-Flesca N (2003) Modelling air quality in street canyons: a review. *Atmos Environ* 37:155–182

Zhang Y, Bocquet M, Mallet V, Seigneur C, Baklanov A (2012) Real-time air quality forecasting, part I: history, techniques, and current status. *Atmos Environ* 60:632–655





## Correlation analysis of the natural radionuclides in soil and indoor radon in Vojvodina, Province of Serbia



S. Forkapic <sup>a,\*</sup>, D. Maletić <sup>b</sup>, J. Vasin <sup>c</sup>, K. Bikit <sup>a</sup>, D. Mrdja <sup>a</sup>, I. Bikit <sup>a</sup>, V. Udovičić <sup>b</sup>, R. Banjanac <sup>b</sup>

<sup>a</sup> University of Novi Sad, Faculty of Sciences, Department of Physics, Laboratory for Radioactivity and Dose Measurements, 21000 Novi Sad, Serbia

<sup>b</sup> Institute of Physics Belgrade, University of Belgrade, Belgrade, Serbia

<sup>c</sup> Institute of Field and Vegetable Crops, 21000 Novi Sad, Serbia

### ARTICLE INFO

#### Article history:

Received 8 November 2015

Received in revised form

8 July 2016

Accepted 21 July 2016

Available online 29 July 2016

#### Keywords:

Radon

Soil characteristics

Correlative and multivariate analysis

### ABSTRACT

The most dominant source of indoor radon is the underlying soil, so the enhanced levels of radon are usually expected in mountain regions and geology units with high radium and uranium content in surface soils. Laboratory for radioactivity and dose measurement, Faculty of Sciences, University of Novi Sad has rich databases of natural radionuclides concentrations in Vojvodina soil and also of indoor radon concentrations for the region of Vojvodina, Northern Province of Serbia. In this paper we present the results of correlative and multivariate analysis of these results and soil characteristics in order to estimate the geogenic radon potential. The correlative and multivariate analysis were done using Toolkit for Multivariate Analysis software package TMVA package, within ROOT analysis framework, which uses several comparable multivariate methods for our analysis. The evaluation ranking results based on the best signal efficiency and purity, show that the Boosted Decision Trees (BDT) and Multi Layer Preceptor (MLP), based on Artificial Neural Network (ANN), are multivariate methods which give the best results in the analysis. The BDTG multivariate method shows that variables with the highest importance are radionuclides activity on 30 cm depth. Moreover, the multivariate regression methods give a good approximation of indoor radon activity using full set of input variables. On several locations in the city of Novi Sad the results of indoor radon concentrations, radon emanation from soil, gamma spectrometry measurements of underlying soil and geology characteristics of soil were analyzed in detail in order to verify previously obtained correlations for Vojvodina soil.

© 2016 Elsevier Ltd. All rights reserved.

### 1. Introduction

It is well known that radon and their short lived progenies have the most impact to the population effective dose from radioactive sources (UNSCEAR, 2008). Recent epidemiological studies show that the radiation risk due to radon exists on concentrations that were considered negligible (WHO, 2009). In most European countries radon mapping has been carried out and the results are summing in the publications of Joint Research Centre of European Commission (JRC EC) which coordinates of the project of European Natural Radioactivity Atlas (De Cort et al., 2011). Therefore, all member states (including candidate countries) must propose the

reference level of radon in dwellings and working places and identify radon priority areas with high radon potential according to EU directive (EURATOM, 2013). There are two different concepts in definition of radon potential: the first one relative to number of houses with indoor radon concentrations above the reference value (depends of construction types, living habits and meteorology) and the other one geogenic radon potential relative to local geophysical parameters (radon concentration in soil and the permeability of soil) (Gruber et al., 2013). Geogenic radon emanates from radium and uranium rich minerals into the soil pore space and it migrates through the soil by diffusion and convection due to the gradient in concentrations. Geogenic radon potential (GRP) therefore describes radon in the subsurface soil as the main contributor to radon buildup in houses and in contrast to indoor radon potential (IRP) it is independent on human influence and temporally constant over a geological timescale. In the lack of soil gas radon and soil gas permeability measurements, our first steps toward the geogenic

\* Corresponding author. University of Novi Sad, Faculty of Sciences, Department of Physics, Trg Dositeja Obradovića 4, 21000 Novi Sad, Serbia.

E-mail address: [sofija@df.uns.ac.rs](mailto:sofija@df.uns.ac.rs) (S. Forkapic).

radon map are to find correlations between available radio-geochemical data and indoor radon concentration measurements in order to predict radon prone areas and validate geogenic prognosis.

In Serbian Northern Province Vojvodina several indoor radon surveys were performed in the period of four years from 2002 to 2005 by Laboratory for radioactivity and dose measurement, Faculty of Sciences, University of Novi Sad (Forkapic et al., 2007). The same laboratory during this period carried out radioactivity monitoring of soil on 50 different locations in Vojvodina region (Bikit et al., 2005) in cooperation with the Institute of Field and Vegetable Crops who determined the geochemical soil characteristics, mechanical composition and content of total N, CaCO<sub>3</sub> and available phosphorus P<sub>2</sub>O<sub>5</sub> and potassium K<sub>2</sub>O. The locations were

selected in a way to proportionally represent all geomorphological units (Koščal et al., 2005): two mountains, four loess plateaus, three loess terraces, four alluvial plains, two sandstone terrains and all soil types (IUSS, 2014): Chernozem, Vertisol, Fluvisol, Cambisol, Planosol, Solonchak and Solonetz. The influence of clay and humus content and humidity of soil on radon adsorption to the soil grains were discussed and analyzed using correlative and multivariate analysis with indoor radon concentrations.

The demand for detailed analyses of large amount of data in high-energy physics resulted in wide and intense development and usage of multivariate methods. Many of multivariate methods and algorithms for classification and regression are already integrated into the analysis framework ROOT (Brun and Rademakers, 1997), more specifically, into the Toolkit for Multivariate analysis (TMVA)

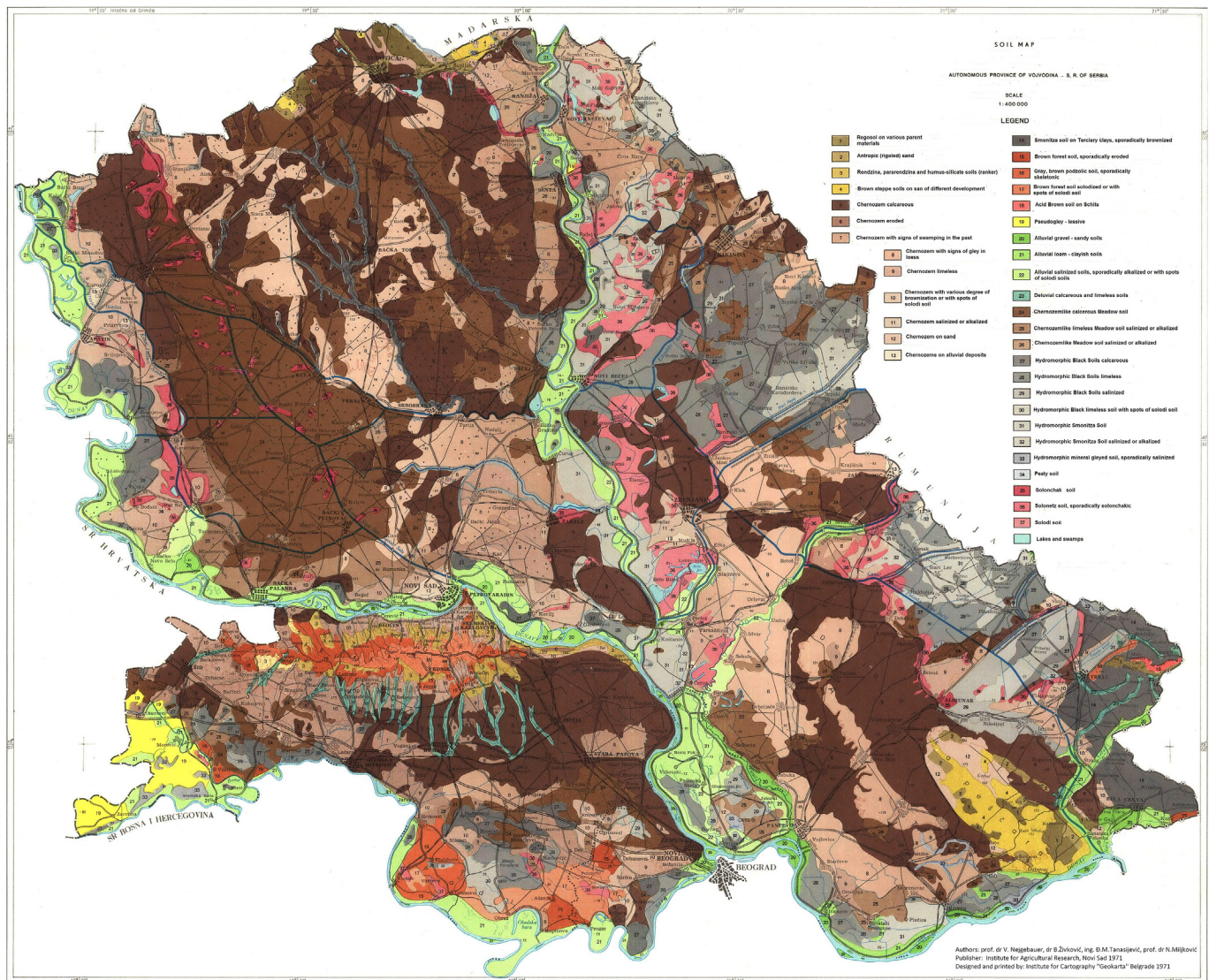


**Fig. 1.** Soil map of Vojvodina Province (Neugebauer et al., 1971): 1 – Regosol on various parent materials; 2 – Antropic (rigoled) sand; 3 – Rendzina, pararendzina and humus-silicate soils (ranker); 4 – Brown steppe soils on sand of different development; 5 – Chernozem calcareous; 6 – Chernozem eroded; 7 – Chernozem with signs of swamping in the past; 8 – Chernozem with signs of clay in loess; 9 – Chernozem limeless; 10 – Chernozems with various degree of brownization or with spots of solodi soil; 11 – Chernozem salinized or alkalized; 12 – Chernozem on sand; 13 – Chernozems on alluvial deposits; 14 – Smonitza soil on Tertiary clays, sporadically brownized; 15 – Brown Forest soil, sporadically eroded; 16 – Gray, brown podzolic soil sporadically skeletal; 17 – Brown Forest soil solodized or with spots of solodi soil; 18 – Acid Brown Soil on Schits; 19 – Pseudogley – lessive; 20 – Alluvial gravel – sandy soils; 21 – Alluvial loam – clayish soils; 22 – Alluvial salinized soils, sporadically alkalized or with spots of solodi soils; 23 – Deluvial calcareous and limeless soils; 24 – Chernozemlike calcareous Meadow Soil; 25 – Chernozemlike limeless Meadow Soil salinized or alkalized; 26 – Chernozemlike Meadow soil salinized or alkalized; 27 – Hydromorphic Black Soils calcareous; 28 – Hydromorphic Black Soils limeless; 29 – Hydromorphic Black Soils salinized; 30 – Hydromorphic Black limeless soil with spots of solodi soil; 31 – Hydromorphic Smonitza Soil; 32 – Hydromorphic Smonitza Soil salinized or alkalized; 33 – Hydromorphic mineral gleyed soil, sporadically salinized; 34 – Peaty Soil; 35 – Solonchak Soil; 36 – Solonetz soil, sporadically solonchakic; 37 – Solodi Soil.

(Hoecker et al., 2007). Institute of Physics Belgrade used these multivariate methods to create, test and apply all available classifiers and regression methods implemented in the TMVA in order to find the method that would be the most appropriate and yield maximum information on the dependence of radon concentrations on the multitude of input variables.

The first step is to calculate and rank the correlation coefficients between all the variables involved, what will help in setting up and testing the framework for running the various multivariate methods contained in the TMVA. Although these correlation rankings will later be superseded by method-specific variable rankings, they are useful at the beginning of the analysis.

The next step is to use and compare the multivariate methods in order to find out which one is best suited for classification (division) of indoor radon concentrations into what would be considered acceptable and what would be considered increased concentration.

In order to be able to use the multivariate classification, the set of input events used, have to be split into those the correspond to

the signal (the indoor radon concentrations that are considered increased) and to the background (consisting of indoor radon concentrations that are declared acceptable). This splitting of the set of input events is for the purposes of this preliminary analysis performed at the limiting value of 120 Bq/m<sup>3</sup>. This value is used for classification analyses, and is selected because this splitting ensures maximum employment of multivariate comparison methods, and this particular value reflects the fact that in our test case the statistics on higher radon concentration values are lower. The method of multivariate regression, however, does not require preliminary splitting of input events, and is therefore a more general one. Main aim is to find out which method can, if any, on the basis of input variables only, give an output that would satisfactorily close match the observed variations of indoor radon concentrations.

In this paper we proposed and analyzed the application of multivariate techniques developed at CERN for experiments with particle physics for correlation analysis of experimental indoor radon data and soil characteristics. Obtained results were verified

**Table 1**  
Classification of soil types for 50 locations of sampling.

| No | Locality            | Soil type (national classification) (Škorić et al., 1985) | Soil group (FAO-WRB) (IUSS, 2014)          |
|----|---------------------|---|--|
| 1  | Horgoš              | Arenosol  | Protic ARENOSOL (Calcic, Aridic)           |
| 2  | Palić               | Solonchak   | Haplic SOLONCHAK (Siltic)                  |
| 3  | Žednik              | Chernozem   | Calcic CHERNOZEM (Loamic, Pachic)          |
| 4  | Aleksa Šantić       | Chernozem   | Haplic CHERNOZEM (Loamic, Pachic)          |
| 5  | Tornjoš             | Chernozem   | Gleyic CHERNOZEM (Loamic, Pachic)          |
| 6  | Gakovo              | Chernozem   | Haplic CHERNOZEM (Loamic, Pachic)          |
| 7  | Kula                | Chernozem   | Calcic, Gleyic CHERNOZEM (Loamic, Pachic)  |
| 8  | Becej               | Humoglej  | Mollic Oxigleyic GLEYSOL (Clayic)          |
| 9  | Srbobran            | Chernozem   | Calcic, Gleyic CHERNOZEM (Loamic, Pachic)  |
| 10 | Srpski Miletić      | Chernozem   | Gleyic CHERNOZEM (Loamic, Pachic)          |
| 11 | Bogojevo            | Humoglej – marsh swamp soil                               | Mollic Oxigleyic GLEYSOL (Loamic)          |
| 12 | Nadalj              | Chernozem   | Gleyic CHERNOZEM (Loamic, Pachic)          |
| 13 | Ruski Krstur        | Chernozem   | Gleyic CHERNOZEM (Loamic, Pachic)          |
| 14 | Parage              | Chernozem   | Gleyic CHERNOZEM (Loamic, Pachic)          |
| 15 | Rimski Šančevi      | Chernozem   | Haplic CHERNOZEM (Clayic, Pachic)          |
| 16 | Žabalj              | Chernozem   | Gleyic CHERNOZEM (Loamic, Pachic)          |
| 17 | Maglić              | Chernozem   | Gleyic CHERNOZEM (Loamic, Pachic)          |
| 18 | Kač                 | Fluvisol  | Gleyic FLUVISOL (Loamic, Salic)            |
| 19 | Bačko Novo Selo     | Fluvisol  | Gleyic FLUVISOL (Loamic)                   |
| 20 | Banatsko Arandelovo | Humoglej – marsh swamp soil                               | Mollic Oxigleyic GLEYSOL (Clayic)          |
| 21 | Sanad               | Fluvisol  | Stagnic FLUVISOL (Clayic)                  |
| 22 | Crna Bara – Čoka    | Chernozem   | Gleyic CHERNOZEM (Clayic, Pachic)          |
| 23 | Kikinda             | Chernozem   | Haplic CHERNOZEM (Clayic, Pachic)          |
| 24 | Rusko Selo          | Humoglej – marsh swamp soil                               | Mollic Oxigleyic GLEYSOL (Clayic)          |
| 25 | Torda               | Humoglej – marsh swamp soil                               | Mollic Oxigleyic GLEYSOL (Clayic)          |
| 26 | Kumane              | Solonetz  | Gleyic, Salic SOLONETZ (Clayic)            |
| 27 | Begejci             | Chernozem   | Gleyic CHERNOZEM (Clayic, Pachic)          |
| 28 | Zrenjanin           | Chernozem   | Calcic CHERNOZEM (Clayic, Pachic)          |
| 29 | Boka                | Solonetz  | Haplic SOLONETZ (Clayic)                   |
| 30 | Orlovat             | Chernozem   | Gleyic CHERNOZEM (Loamic, Pachic)          |
| 31 | Vršački Ritovi      | Humoglej – marsh swamp soil                               | Mollic Oxigleyic GLEYSOL (Clayic)          |
| 32 | Kozjak              | Chernozem   | Gleyic CHERNOZEM (Loamic, Pachic)          |
| 33 | Ilandža             | Humoglej – marsh swamp soil                               | Mollic Oxigleyic GLEYSOL (Clayic)          |
| 34 | Idvor               | Chernozem   | Gleyic CHERNOZEM (Clayic, Pachic)          |
| 35 | Padina              | Chernozem   | Haplic CHERNOZEM (Loamic, Pachic)          |
| 36 | Vrsac               | Eutric Cambisol   | Eutric CAMBISOL (Clayic)                   |
| 37 | Crepaja             | Chernozem   | Haplic CHERNOZEM (Loamic, Pachic)          |
| 38 | Deliblato           | Chernozem   | Haplic CHERNOZEM (Arenic, Pachic)          |
| 39 | Bavanište           | Chernozem   | Haplic CHERNOZEM (Loamic, Pachic)          |
| 40 | Petrovaradin        | Eutric Cambisol   | Eutric CAMBISOL (Clayic)                   |
| 41 | Šid                 | Chernozem   | Haplic CHERNOZEM (Loamic, Pachic, Stagnic) |
| 42 | Rivica              | Chernozem   | Haplic CHERNOZEM (Clayic, Pachic)          |
| 43 | Ruma                | Chernozem   | Haplic CHERNOZEM (Clayic, Pachic)          |
| 44 | Indija              | Chernozem   | Haplic CHERNOZEM (Loamic, Pachic)          |
| 45 | Morović             | Pseudoglej  | Gleyic, Fluvic, Luvic PLANOSOL (Loamic)    |
| 46 | Višnjićevo          | Pseudoglej  | Gleyic, Fluvic, Luvic PLANOSOL (Loamic)    |
| 47 | Sremska Mitrovica   | Chernozem   | Haplic CHERNOZEM (Clayic, Pachic)          |
| 48 | Popinci             | Chernozem   | Gleyic CHERNOZEM (Clayic, Pachic)          |
| 49 | Donji Tovarnik      | Humoglej – marsh swamp soil                               | Mollic Oxigleyic GLEYSOL (Clayic)          |
| 50 | Kupinovo            | Fluvisol  | Haplic FLUVISOL (Loamic)                   |



Fig. 2. The RAD7 complete for soil gas measurements (Durrige, 2014).

**Table 2**  
Correlation coefficients between indoor radon concentration and input variables.

| Number | Parameter                     | Correlation coefficient |
|--------|-------------------------------|-------------------------|
| 1      | Elevation                     | +0.11                   |
| 2      | pH                            | 0                       |
| 3      | CaCO <sub>3</sub>             | -0.03                   |
| 4      | Humus                         | +0.15                   |
| 5      | Total N                       | +0.13                   |
| 6      | P <sub>2</sub> O <sub>5</sub> | -0.01                   |
| 7      | K <sub>2</sub> O              | +0.01                   |
| 8      | Coarse sand                   | -0.08                   |
| 9      | Fine sand                     | -0.19                   |
| 10     | Powder                        | +0.16                   |
| 11     | Clay                          | +0.17                   |
| 12     | Ra-226 30 cm                  | +0.27                   |
| 13     | U-238 30 cm                   | +0.17                   |
| 14     | Th-232 30 cm                  | +0.22                   |
| 15     | K-40 30 cm                    | +0.10                   |
| 16     | U-238 surface                 | -0.17                   |
| 17     | Ra-226 surface                | +0.04                   |
| 18     | Th-232 surface                | 0                       |
| 19     | K-40 surface                  | +0.02                   |
| 20     | Cs-137 surface                | -0.17                   |

and discussed on measured soil gas data for Novi Sad districts.

## 2. Study area

Vojvodina region is located in the Pannonian Basin of Central Europe. The choice of sampling locations was made on the basis of the presence of certain soil types (Škorić et al., 1985) on the Pedological Map of Vojvodina (Nejgebauer et al., 1971) which is shown on Fig. 1. The observed soil types were classified in Table 1 according to the FAO-WRB classification (IUSS, 2014). The dominant soil type at the examined area is Chernozem. Parent material (geological substrate) for this type of soil, and for the largest part of the surface of Vojvodina, is loess – loose sedimentary rock deposited by wind-accumulation in the Pleistocene (during interglacial periods).

## 3. Materials and methods

Indoor radon mapping of Vojvodina Province was performed using the etched track detectors CR39 on about 3000 locations in ground floor rooms during three years from 2002 to 2005. The time of exposure was 90 days during the winter seasons, from December

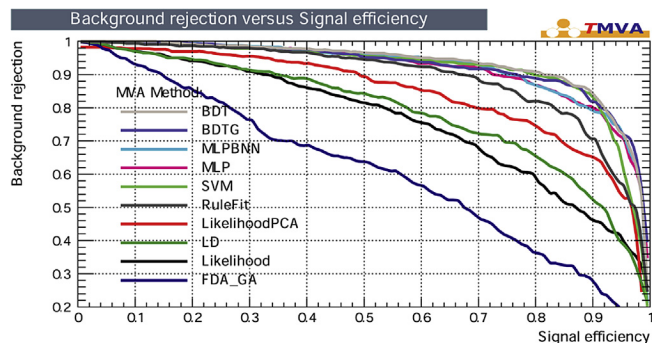


Fig. 3. Receiver operating characteristic (ROC) for all Multivariate methods used for classification of indoor radon concentration using climate variables. It shows that BDT and MLP methods are the best ones for radon.

to March. The etching and counting of tracks were performed by Radosys Company. For this study the average indoor radon concentrations in the nearest village or city to locations of soil sampling were calculated and used in correlation analysis. The results of intercomparison of radon CR-39 detector systems conducted in CLOR's accredited calibration laboratory and quality control data of commercially available Hungarian RadoSys systems are presented and discussed in (Mamont-Ciesla et al., 2010).

For radioactivity measurements from each location of an approximately area  $10 \times 10$  m, 10 subsamples of soil were collected, mixed and homogenized. The soil was sampled from the surface layer (0–10 cm). For chemical analysis soil was sampled by agrochemical probe to a depth of 30 cm. Soil samples were dried at 105 °C to constant mass. After that all mechanical contaminants, mainly small stone peaces and plant material were removed. Dried soil samples were homogenized as fine powder and measured in cylindrical geometry 62 mm  $\times$  67 mm on the cap of HPGe detector. Typical mass of samples was 200 g–300 g and measurement time was 80 ks. Activity concentrations of radionuclides gamma emitters were determined by the method of low-level gamma spectrometry on actively and passively shielded germanium detectors with maximal background reduction. Detector calibrations and quality control measurements were done with certified reference material in cylindrical geometry type CBSS2 supplied by Czech Metrology Institute. Every year laboratory participates with accepted results in world-wide open proficiency tests for gamma spectrometry organized by IAEA Reference Materials Group, Terrestrial Environment Laboratory. The gamma spectra were acquired and analyzed using the Canberra Genie 2000 software. The program calculates the activity concentration of an isotope from all prominent gamma lines after peaked background subtraction. All measurement uncertainties are presented at 95% confidence level. A special procedure developed in the Novi Sad laboratory was used for the determination of the <sup>238</sup>U activity concentration from gamma-lines of the first progeny of this radionuclide, <sup>234</sup>Th (Bikit et al., 2003).

pH-value was measured in the suspension of soil with water (10 g: 25 cm<sup>3</sup>) by pH meter PHM62 standard- Radiometar Copenhagen. Content of humus was determined according to method of Tjurin. The total nitrogen content was determined by Kjeldahl on the system for digestion and titration Tacator. The available phosphorus and potassium were measured using the extraction with ammonium lactate. For soil characterization purposes, removal of organic matter by H<sub>2</sub>O<sub>2</sub> and of carbonates by HCl was carried out. Then, the sample is shaken with a dispersing agent and sand is separated from clay and powder with a 63  $\mu$ m sieve. The sand is fractionated by dry sieving, and by the pipette method the clay and powder fractions are determined (IUSS, 2014). Particle size in the soil

**Table 3**

Evaluation results ranked by best signal efficiency and purity (area) It shows that BDT and MLP methods are the best ones for radon. @B is part of Background events classified as Signal events.

| MVA method    | Signal efficiency at bkg eff.(error): |           |           |           | Separation | Significance |
|---------------|---------------------------------------|-----------|-----------|-----------|------------|--------------|
|               | @B = 0.01                             | @B = 0.10 | @B = 0.30 | ROC-integ |            |              |
| BDT           | 0.212(16)                             | 0.814(16) | 0.959(08) | 0.932     | 0.609      | 1.614        |
| BDTG          | 0.243(17)                             | 0.767(17) | 0.966(07) | 0.927     | 0.611      | 1.676        |
| MLPBNN        | 0.224(17)                             | 0.754(17) | 0.957(08) | 0.922     | 0.600      | 1.579        |
| MLP           | 0.228(17)                             | 0.728(18) | 0.955(08) | 0.919     | 0.577      | 1.540        |
| SVM           | 0.211(16)                             | 0.797(16) | 0.938(09) | 0.918     | 0.587      | 1.611        |
| RuleFit       | 0.162(15)                             | 0.671(19) | 0.906(12) | 0.891     | 0.482      | 1.263        |
| LikelihoodPCA | 0.000(00)                             | 0.491(20) | 0.845(14) | 0.843     | 0.404      | 1.099        |
| LD            | 0.047(08)                             | 0.348(19) | 0.744(18) | 0.789     | 0.271      | 0.806        |
| Likelihood    | 0.031(07)                             | 0.328(19) | 0.674(19) | 0.764     | 0.208      | 0.589        |
| FDA_GA        | 0.031(07)                             | 0.147(14) | 0.363(19) | 0.611     | 0.093      | 0.353        |

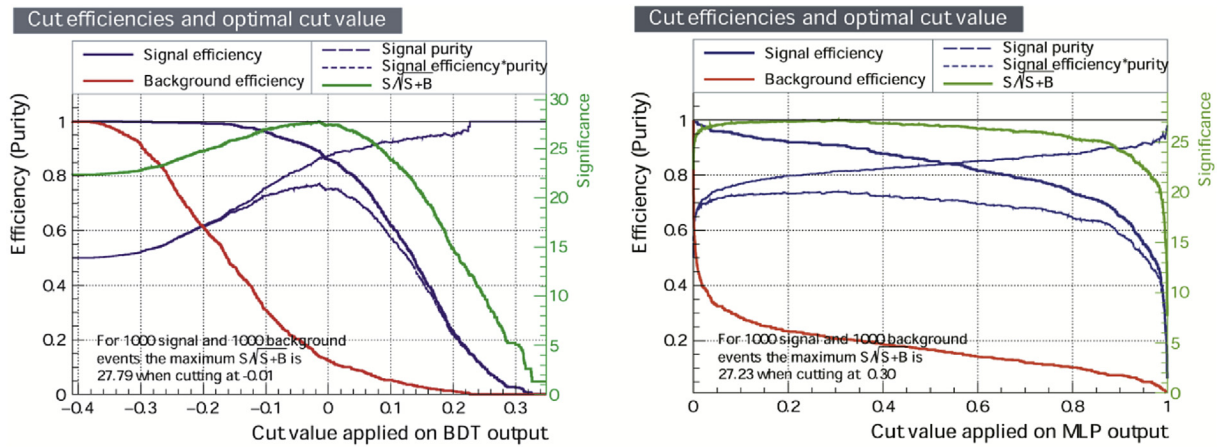


Fig. 4. Cut efficiency and optimal cut value of BDT (left) and MLP (right) classification MVA method for indoor radon concentration.

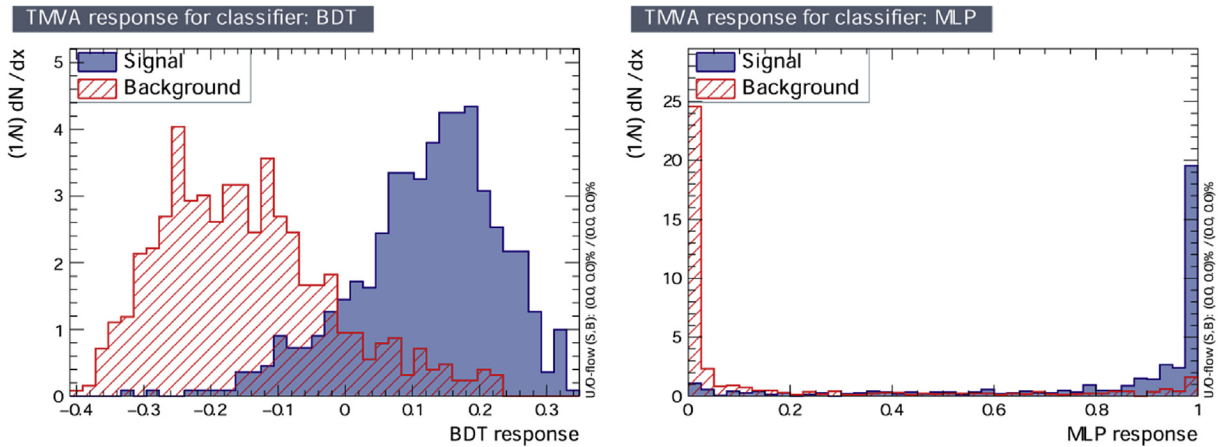


Fig. 5. Distribution of BDT and ANN MLP classification method outputs for input signal and background events.

samples was determined by the pipette method with sodium pyrophosphate as peptizing agent. Based on particle size analysis the following fractions were determined according to IUSS classification: coarse sand (0.2–2 mm), fine sand (0.02–0.2 mm), powder (0.002–0.02 mm) and clay (<0.002 mm).

Soil gas radon activity concentration was measured in situ by RAD7 alpha-spectrometer (DURRIDGE Company) with stainless soil gas probe using grab protocol (Fig. 2). While pumping, the air flow rate is about 0.7 l/min and therefore 3.5 l of soil gas is extracted from the soil at the depth of 70 cm. The last calibration of used

device was performed in radon chamber at the accredited trial metrological Lab. SUJCHBO Kamenna, Czech Republic. Calibration laboratory is traceable to PTB Braunschweig, Germany. After that calibration laboratory participated with RAD7 device in the 2015 NRPI Intercomparison of Radon gas Measurement Instruments with satisfactory results ( $|\text{zeta score}| < 2$  – Report number NRPI REG 01-2016, January 2016).

The Toolkit for Multivariate Analysis (TMVA) provides a ROOT-integrated environment for the processing, parallel evaluation and application of multivariate classification and multivariate

**Table 4**  
Variable importance for BDTG MVA method for indoor radon.

| BDTG rank | Variable                      | Variable importance $\times 10^{-2}$ |
|-----------|-------------------------------|--------------------------------------|
| 1         | Total N                       | 6.490                                |
| 2         | U-238 30 cm                   | 6.425                                |
| 3         | K-40 30 cm                    | 6.040                                |
| 4         | Th-232 30 cm                  | 5.495                                |
| 5         | Humus                         | 5.490                                |
| 6         | K <sub>2</sub> O              | 5.406                                |
| 7         | Clay                          | 5.360                                |
| 8         | U-238 surface                 | 5.218                                |
| 9         | Fine                          | 5.116                                |
| 10        | CaCO <sub>3</sub>             | 5.081                                |
| 11        | P <sub>2</sub> O <sub>5</sub> | 5.003                                |
| 12        | Cs-137 surface                | 4.715                                |
| 13        | Ra-226 30 cm                  | 4.656                                |
| 14        | Elevation                     | 4.595                                |
| 15        | K-40 surface                  | 4.509                                |
| 16        | pH                            | 4.435                                |
| 17        | Ra-226 surface                | 4.188                                |
| 18        | Powder                        | 4.082                                |
| 19        | Th-232 surface                | 4.026                                |
| 20        | Coarse                        | 3.671                                |

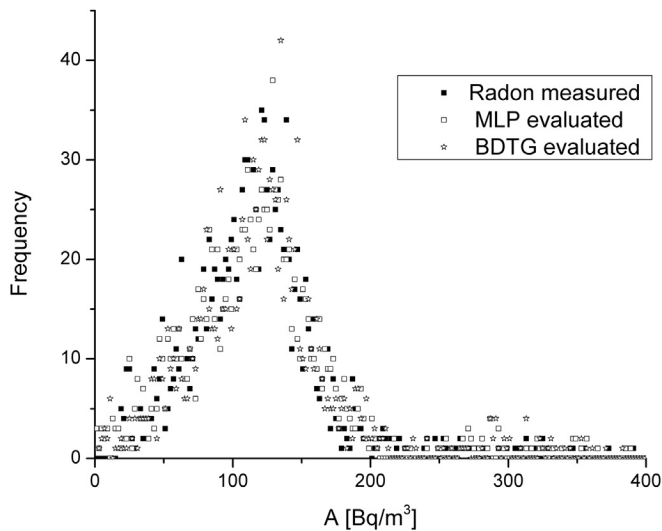


**Fig. 6.** Distribution of indoor radon concentrations and outputs from MLP Multivariate regression method's evaluation for of indoor radon concentration.

regression methods. All multivariate methods in TMVA belong to the family of “supervised learning” algorithms. They make use of training events, for which the desired output is known, to determine the mapping function that either describes a decision boundary (classification) or an approximation of the underlying functional behavior defining the target value (regression). The two most important Multivariate methods for our purposes are “Boosted Decision Trees” (BDT) and “Artificial Neural Networks” (ANN).

Boosted Decision Trees (BDT) have been successfully used in High Energy Physics analysis for example by the MiniBooNE experiment (Hai-Jun et al., 2005). In BDT, the selection is done on a majority vote on the result of several decision trees. However, the advantage of the straightforward interpretation of the decision tree is lost.

An Artificial Neural Network (ANN) (Rojas, 1996) is most generally speaking any simulated collection of interconnected neurons, with each neuron producing a certain response at a given set of input signals. ANNs in TMVA belong to the class of Multilayer Perceptrons (MLP), which are feed-forward neural networks.

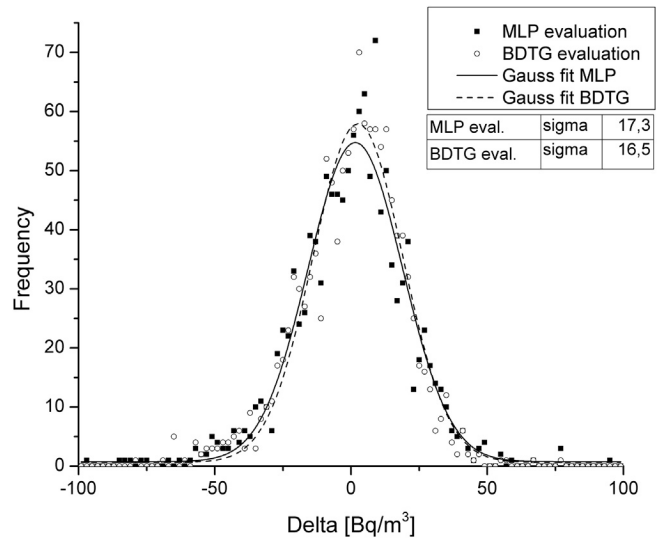


**Fig. 7.** Distributions of differences of outputs from MLP Multivariate regression method and measured indoor radon concentrations.

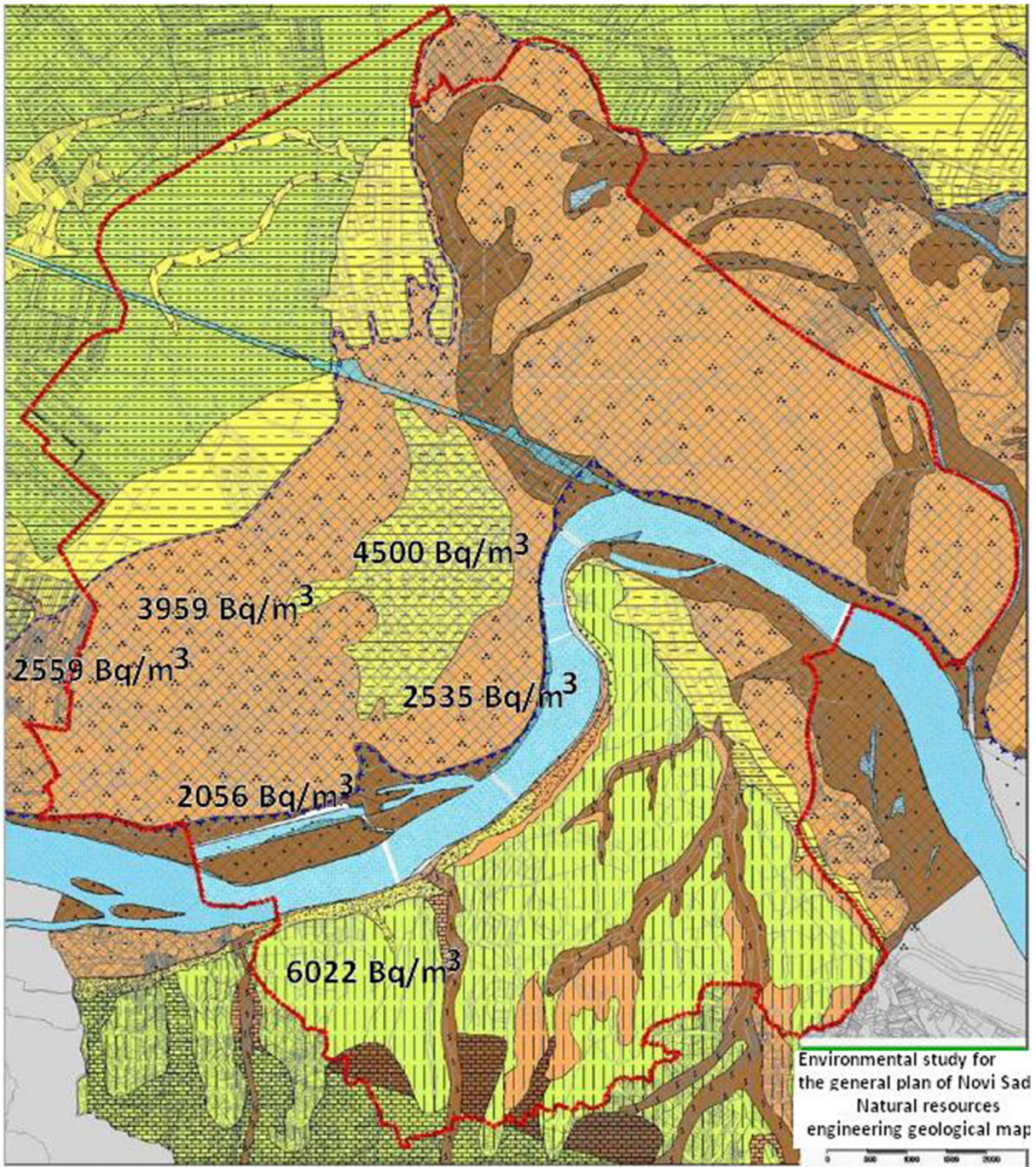
#### 4. Results and discussion

Table 2 shows linear correlation coefficients, which tells us how big is the correlation of input variable and indoor radon concentration. We can notice that radon is more correlated to radioisotopes at depth of 30 cm.

In order to use MVA methods, the sample has to have significant statistics. Since set intended to be used in this analysis does not have enough statistics, we artificially increased the sample by introducing of copy of same sample events, but with modified values of input and measured radon concentrations multiplying initial value with  $1 + \text{random Gaussian values with sigma } 1/10$ . We are using the input events (set of soil sample properties and radionuclides activity in 30 cm depth and on surface) to train, test and evaluate the 12 multivariate methods implemented in TMVA. The graph presenting the “Receiver operating characteristic” (ROC) for each multivariate method (Fig. 3) may be considered as the most indicative in comparing the different methods used for classification of radon concentrations using climate variables. On this graph one can read the dependence of background rejection on signal efficiency. The best method is the one that holds maximum value of background rejection for highest Signal efficiency (Table 3), i.e. the best method has ROC curve closest to the upper right corner on the graph presented in Fig. 3. It turns out that the method best suited for our purpose is the Boosted Decision Trees (BDT) method. This means that BDT gives most efficient classification of input events. This is seen in Fig. 4, which shows the distribution of BDT classification method outputs for input signal and background events. The second best method is the implementation of ANN Multilayer Perceptrons (MLP).

In Fig. 4, one can see the values of signal and background efficiency and significance. Significance, calculated as  $N(\text{Signal}) / \sqrt{N(\text{Signal}) + N(\text{Background})}$ , can be used as the value for comparison of various multivariate methods, and also for comparison of method efficiencies for different sets of input variables.

Fig. 5 shows the distribution of BDT classification method outputs for input signal and background events. These figures again demonstrate that classification methods work well i.e. that the separation of signal and background works very good. Also, the significance value for BDT is higher for higher cut values for splitting of input events. Interestingly, it appears that other multivariate



**Lithological classification**

- |   |  |   |   |
|---|--|---|---|
|  | contemporary riverbanks<br>fine sandy                    |  | loess clay  |
|  | older riverbanks<br>sandy clay                           |  | unchanged loess                                       |
|  | sediments old lakes and swamps<br>rich in organic matter |  | Delluvial gravel-sandy clay                           |
|  | sediments of new swamps                                  |  | Tertiary (clay, marl,<br>conglomerates, clays, sands) |
|  | sediments of loess valley                                |  | Mesozoic flysch                                       |
|  | redeposited loess  |  | Eruptive rocks  |

Fig. 8. Lithological map of Novi Sad city (Obrknežev et al., 2009) with maximal soil gas radon activity concentrations measured in six parts of the city.

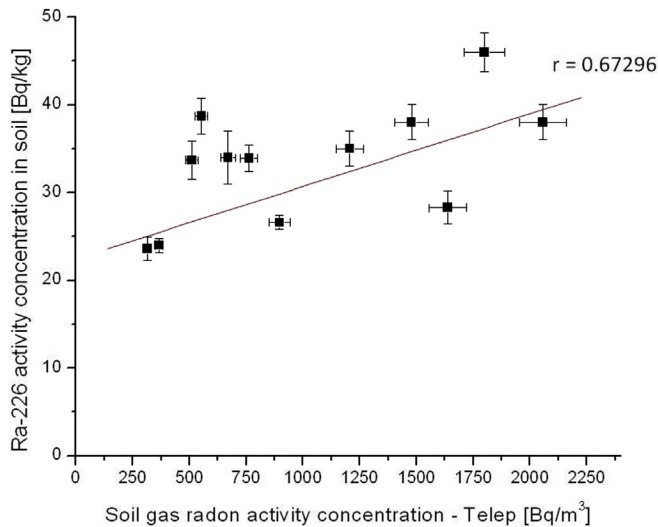


Fig. 9. Correlation between radium activity concentrations in the soil and soil gas activity concentrations for Telep district.

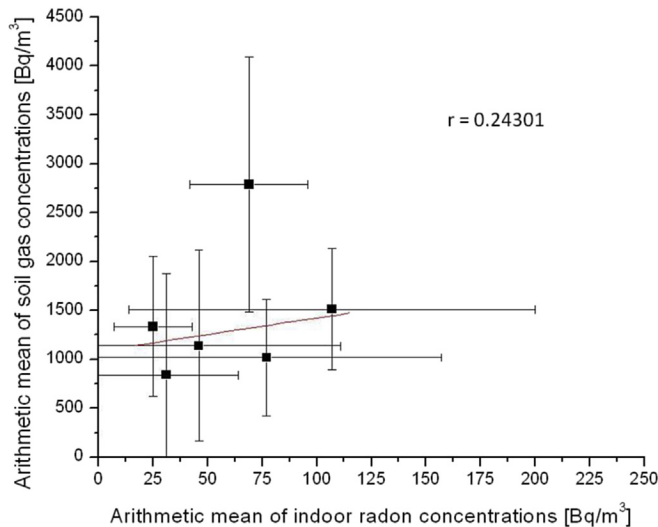


Fig. 10. Correlations between arithmetic means of soil gas concentrations and indoor radon activity concentrations with standard deviations (error bars) for six districts of Novi Sad city.

methods also give better results under these new conditions.

Ranking of the BDTG input variables (Table 4) is derived by counting how often the variables are used to split decision tree nodes, and by weighting each split occurrence by the separation it has achieved and by the number of events in the node. As seen from Table 4, besides Total N, radionuclides on 30 cm depth appears to be the most important variables for indoor radon.

Regression is the approximation of the underlying functional behavior defining the target value. We tried to find the best regression method that will give output values (predicted indoor radon concentration) closest to the actual concentrations that corresponds to specific input variables. The best multivariate regression method is found to be BDT, and the second one is MLP, same as in case of multivariate classifiers. Fig. 6 presents the distribution of indoor radon concentrations and outputs from the MPL multivariate regression method evaluation of radon concentration using all input variables.

To best way to estimate the quality of the method is to look at the differences between the output values from MLP multivariate regression method and the values of measured indoor radon concentrations (Fig. 7). The figure indicates the good predictive power of multivariate regression methods as applied for prediction of variations of indoor radon concentrations based on full set of input variables.

In the city of Novi Sad Laboratory for dose and radioactivity measurements performed soil gas measurements by active device RAD7 coupled with soil gas probe on about 100 locations divided in 6 districts of the city. In order to verify previously obtained correlations we analyzed in detail all available parameters: radionuclide contents of the soil, average indoor radon concentrations in each district, maximal and average soil gas concentrations for each district and geomorphologic units. Results are shown on Figs. 8–10 and in Table 5. Indoor radon concentrations were measured by gamma spectrometry method using charcoal canisters for radon adsorption. The MDA for this technique of indoor radon measurement is about 2 Bq/m<sup>3</sup> and the measurement uncertainty depends on count rates in post radon gamma lines, detector efficiency and charcoal water gain.

The effects of radium activity concentrations in deep layers of examined soil to indoor radon concentrations were analyzed through linear correlations and the results are shown on Figs. 9 and 10. We used Pearson correlation coefficient based on a comparison of the actual impact of observed variables to one another in relation to the maximum potential impact of the two variables (1) and obtained almost high positive correlation between radium activity concentrations in soil and soil gas concentrations ( $r = 0.67296$ ) and low positive correlation between arithmetic means of soil gas concentrations and indoor radon activity concentrations ( $r = 0.24301$ ).

$$r = \frac{\sum_i x_i y_i - \frac{1}{n} \sum_i x_i \sum_i y_i}{\sqrt{\left[ \sum_i y_i^2 - \left( \frac{1}{n} \right) \left( \sum_i y_i \right)^2 \right] \left[ \sum_i x_i^2 - \left( \frac{1}{n} \right) \left( \sum_i x_i \right)^2 \right]}} \quad (1)$$

## 5. Conclusion

In the paper the possibility of multivariate analysis application for radon potential estimation is described in detailed. The most appropriate multivariate method of analysis of indoor radon measurements is selected from a wide spectrum of multivariate methods developed for data analysis in high-energy physics and implemented in the Toolkit for Multivariate Analysis software package. The evaluation ranking results based on the best signal efficiency and purity, show that the Boosted Decision Trees (BDT) and Multi Layer Perceptron (MLP), based on Artificial Neural Network (ANN), are multivariate methods which give the best results in the analysis. Further multivariate analysis results give insight into the dependence of indoor radon concentrations with other radionuclides activity both 30 cm underground and on surface during the time of measurements, as well as soil properties variables. The BDTG multivariate method shows that variables with the highest importance are radionuclides activity in deep layers compared with the activity of surface layer, but also the humus and clay content (Table 4). Moreover, the multivariate regression methods give a good approximation of indoor radon activity using full set of input variables.

This study showed that radiogeochemical data are useful to generate maps of radon priority areas. We confirmed the assumption that the soil types which contain the highest content of clay

**Table 5**

Comparison of available data for each analyzed district of Novi Sad city with the description of geomorphologic unit and the number of samples that were considered. Numbers in brackets are the standard deviations for the average values and the measurement uncertainties for measured values in the range column.

| City district (Geomorphologic unit)                    | Average of soil gas concentrations [Bq/m <sup>3</sup> ] | Range of soil gas concentrations [Bq/m <sup>3</sup> ] | Average of indoor radon concentrations [Bq/m <sup>3</sup> ] | Range of indoor radon concentrations [Bq/m <sup>3</sup> ] | Average of Ra-226 concentrations in soil [Bq/kg] | Range of Ra-226 concentrations in soil [Bq/kg] |
|--|---|---|---|---|--|--|
| Telep (Contemporary riverbanks, fine sandy) 13 samples | 1020(596)   | 315(16)–2056(105)                                     | 77(80)  | 4(2)–313(8)   | 33(7)  | 23,6(13)–46,0(22)                              |
| Detelinara (Loess clay) 29 samples                     | 1138(976)   | 312(17)–4500(220)                                     | 46(65)  | 4(2)–345(14)  | 30(7)  | 14,1(14)–45(2)                                 |
| Liman (Older riverbanks, sandy clay) 17 samples        | 1334(715)   | 230(12)–2535(130)                                     | 25(18)  | 6(2)–74(5)  | 27(7)  | 14,9(14)–40,5(21)                              |
| Veternik (Older riverbanks, sandy clay) 16 samples     | 1512(616)   | 104(7)–2559(132)                                      | 107(93)   | 34(4)–276(8)  | 32(5)  | 22,3(14)–41(2)                                 |
| Novo Naselje (Older riverbanks, sandy clay) 19 samples | 840(1033)   | 122(8)–3959(198)                                      | 31(33)  | 4(2)–92(6)  | 31(6)  | 19(2)–44(2)                                    |
| Sremska Kamenica (Unchanged loess) 14 samples          | 2787(1306)  | 1582(80)–6022(302)                                    | 69(27)  | 38(4)–110(6)  | 36(7)  | 19,9(16)–43,5(17)                              |

and humus best adsorb and retain radon which is reflected in elevated soil gas radon concentrations and higher geogenic radon potential. This conclusion could be used for selection of locations for planning radon permeability measurements. The best correlation of radon concentrations with total nitrogen amount in the soil is very interested result and it will be studied in next research.

The results of detailed analysis of databases for radon and soil radioactivity measurements for the city of Novi Sad validated geogenic prognosis that soil gas radon concentrations mostly depend on geomorphologic units and litologic distribution in study area. Good agreement of radium content in soil samples and radon soil gas activity concentrations obtained.

The multivariate regression methods used gives as a result a "mapped" functional behavior of indoor radon and input variables. Using this "mapped" function, the search for radon priority areas is straightforward. The best performing multivariate methods identified most important variables, and help with simplification of "mapped" function which then requires smaller number of input variables. Further analysis of "mapped" function can point to which are the most important mechanisms for increase of indoor radon concentrations.

So the multivariate methods can be used in identifying the most significant variables, help identify radon priority areas, and help with physics analysis of processes of radon emanation.

## Acknowledgements

The authors acknowledge the financial support of the Provincial Secretariat for Environmental Protection and Sustainable Development (grant number 401-00088/2003) and Ministry of Science, Technology and Development of Serbia within the projects: Nuclear Methods Investigations of Rare Processes and Cosmic Rays (grant number 171002) and Biosensing Technologies and Global System for Continuous Research and Integrated Management (grant number 43002).

## References

- Bikit, I., et al., 2003. Simple method for depleted uranium determination. *Jpn. J. Appl. Phys.* 42, 5269–5273.
- Bikit, I., et al., 2005. Radioactivity of the soil in Vojvodina (northern province of Serbia and Montenegro). *J. Environ. Radioact.* 78, 11–19.
- Brun, R., Rademakers, F., 1997. Root – an object oriented data analysis framework. *Nucl. Inst. Meth. Phys. Res. A* 389, 81.
- De Cort, M., et al., 2011. Towards a European atlas of natural radiation: goal, status and future perspectives. *Radioprotection* 46, 737–743.
- Durrige, 2014. RAD7 Radon Detector User Manual, Revision 7.26. DURRIDGE Company. <http://www.durrige.com/documentation/RAD7Manual.pdf>.
- EURATOM, 2013. Council Directive 2013/59/EURATOM of 5 December 2013 Laying Down Basic Safety Standards for Protection against the Dangers Arising from Exposure to Ionising Radiation, and Repealing Directives 89/618/Euratom, 90/641/Euratom, 96/29/Euratom, 97/43/Euratom and 2003/122/Euratom, Article 74 Indoor Exposure to Radon. <http://eur-lex.europa.eu/LexUriServ/LexUriServ.do?uri=OJ:L:2014:013:0001:0073:EN:PDF>.
- Forkapic, S., et al., 2007. Indoor radon in rural dwellings of the south-Pannonian region. *Radiat. Prot. Dosim.* 123, 378–383.
- Gruber, V., et al., 2013. The European map of geogenic radon potential. *J. Radiol. Prot.* 33, 51–60.
- Hai-Jun, Y., et al., 2005. Studies of boosted decision trees for MiniBooNE particle identification. *Nucl. Instrum. Meth.* A555, 370–385. <http://arxiv.org/abs/physics/0508045>.
- Hoecker, A., et al., 2007. TMVA – Toolkit for Multivariate Data Analysis. *PoS ACAT* 040, arXiv:physics/070303.
- IUSS Working Group WRB, 2014. World reference base for soil resources 2014. In: International Soil Classification System for Naming Soils and Creating Legends for Soil Maps. *World Soil*, 106. FAO, Rome.
- Košćal, M., et al., 2005. Geomorphological Map of Vojvodina with Legends. *Geozavod – Gemini*, Beograd.
- Mamont-Ciešla, K., et al., 2010. Intercomparison of radon CR-39 detector systems conducted in CLOR's calibration chamber. *Nukleonika* 55 (4), 598–593.
- Nejgebauer, V., et al., 1971. The Pedological Map of Vojvodina (R 1 : 50.000). Institute for Agricultural Research, Novi Sad.
- Obrknežev, R., et al., 2009. The Study of Environmental Protection in the City of Novi Sad, Public Enterprise "Urbanizam". Department of Urban Planning, Novi Sad.
- Rojas, R., 1996. *Neural Networks*. Springer-Verlag, Berlin.
- Skorić, A., et al., 1985. Classification of soils in Yugoslavia, academy of Sciences and arts of Bosnia and Herzegovina special editions, book LXXVIII, Sarajevo.
- UNSCEAR, 2008. Ionizing Radiation: Sources and Effects, UNSCEAR 2008 REPORT, VOLUME II. United Nations, New York. [http://www.unscear.org/unscear/en/publications/2008\\_1.html](http://www.unscear.org/unscear/en/publications/2008_1.html).
- WHO, 2009. In: Handbook on Indoor Radon – a Public Health Perspective. [www.who.int/ionizing\\_radiation/env/radon/en/imdex1.html](http://www.who.int/ionizing_radiation/env/radon/en/imdex1.html).

## MAUS: the MICE analysis user software

To cite this article: R. Asfandiyarov *et al* 2019 *JINST* **14** T04005

View the [article online](#) for updates and enhancements.

### Recent citations

- [Demonstration of cooling by the Muon Ionization Cooling Experiment](#)



**IOP | ebooks™**

Bringing you innovative digital publishing with leading voices to create your essential collection of books in STEM research.

Start exploring the collection - download the first chapter of every title for free.

## MUON ACCELERATORS FOR PARTICLE PHYSICS — MUON

## MAUS: the MICE analysis user software

R. Asfandiyarov,<sup>a</sup> R. Bayes,<sup>b</sup> V. Blackmore,<sup>c</sup> M. Bogomilov,<sup>d</sup> D. Colling,<sup>c</sup> A.J. Dobbs,<sup>c</sup> F. Drielsma,<sup>a</sup> M. Drews,<sup>h</sup> M. Ellis,<sup>c</sup> M. Fedorov,<sup>e</sup> P. Franchini,<sup>f</sup> R. Gardener,<sup>g</sup> J.R. Greis,<sup>f</sup> P.M. Hanlet,<sup>h</sup> C. Heidt,<sup>i</sup> C. Hunt,<sup>c</sup> G. Kafka,<sup>h</sup> Y. Karadzov,<sup>a</sup> A. Kurup,<sup>c</sup> P. Kyberd,<sup>g</sup> M. Littlefield,<sup>g</sup> A. Liu,<sup>j</sup> K. Long,<sup>c,n</sup> D. Maletic,<sup>k</sup> J. Martyniak,<sup>c</sup> S. Middleton,<sup>c</sup> T. Mohayai,<sup>h,j</sup> J.J. Nebrensky,<sup>g</sup> J.C. Nugent,<sup>b</sup> E. Overton,<sup>l</sup> V. Pec,<sup>l</sup> C.E. Pidcott,<sup>f</sup> D. Rajaram,<sup>h,1</sup> M. Rayner,<sup>m</sup> I.D. Reid,<sup>g</sup> C.T. Rogers,<sup>n</sup> E. Santos,<sup>c</sup> M. Savic,<sup>k</sup> I. Taylor,<sup>f</sup> Y. Torun,<sup>h</sup> C.D. Tunnell,<sup>m</sup> M.A. Uchida,<sup>c</sup> V. Verguilov,<sup>a</sup> K. Walaron,<sup>b</sup> M. Winter<sup>h</sup> and S. Wilbur<sup>l</sup>

<sup>a</sup>DPNC, section de Physique, Université de Genève, Geneva, Switzerland

<sup>b</sup>School of Physics and Astronomy, Kelvin Building, The University of Glasgow, Glasgow, U.K.

<sup>c</sup>Department of Physics, Blackett Laboratory, Imperial College London, London, U.K.

<sup>d</sup>Department of Atomic Physics, St. Kliment Ohridski University of Sofia, Sofia, Bulgaria

<sup>e</sup>Radboud University of Nijmegen, Netherlands

<sup>f</sup>Department of Physics, University of Warwick, Coventry, U.K.

<sup>g</sup>Brunel University, Uxbridge, U.K.

<sup>h</sup>Physics Department, Illinois Institute of Technology, Chicago, IL, U.S.A.

<sup>i</sup>University of California, Riverside, CA, U.S.A.

<sup>j</sup>Fermilab, Batavia, IL, U.S.A.

<sup>k</sup>Institute of Physics, University of Belgrade, Serbia

<sup>l</sup>Department of Physics and Astronomy, University of Sheffield, Sheffield, U.K.

<sup>m</sup>Department of Physics, University of Oxford, Denys Wilkinson Building, Oxford, U.K.

<sup>n</sup>STFC Rutherford Appleton Laboratory, Harwell Oxford, Didcot, U.K.

E-mail: [durga@fnal.gov](mailto:durga@fnal.gov)

**ABSTRACT:** The Muon Ionization Cooling Experiment (MICE) collaboration has developed the MICE Analysis User Software (MAUS) to simulate and analyze experimental data. It serves as the primary codebase for the experiment, providing for offline batch simulation and reconstruction as well as online data quality checks. The software provides both traditional particle-physics functionalities such as track reconstruction and particle identification, and accelerator physics functions, such as calculating transfer matrices and emittances. The code design is object orientated, but has a top-level structure based on the Map-Reduce model. This allows for parallelization to support live data reconstruction during data-taking operations. MAUS allows users to develop in

<sup>1</sup>Corresponding author.

either Python or C++ and provides APIs for both. Various software engineering practices from industry are also used to ensure correct and maintainable code, including style, unit and integration tests, continuous integration and load testing, code reviews, and distributed version control. The software framework and the simulation and reconstruction capabilities are described.

**KEYWORDS:** Data reduction methods; Simulation methods and programs; Software architectures (event data models, frameworks and databases); Accelerator modelling and simulations (multi-particle dynamics; single-particle dynamics)

ARXIV EPRINT: [1812.02674](https://arxiv.org/abs/1812.02674)

2019 JINST 14 T04005

---

## Contents

|          |                                      |           |
|----------|--------------------------------------|-----------|
| <b>1</b> | <b>Introduction</b>                  | <b>1</b>  |
| 1.1      | The MICE experiment                  | 1         |
| 1.2      | Software requirements                | 3         |
| <b>2</b> | <b>MAUS</b>                          | <b>3</b>  |
| 2.1      | Code design                          | 3         |
| 2.2      | Data structure                       | 6         |
| 2.2.1    | Physics data                         | 6         |
| 2.2.2    | Top level data organization          | 10        |
| 2.3      | Data flow                            | 10        |
| 2.4      | Testing                              | 10        |
| <b>3</b> | <b>Monte Carlo</b>                   | <b>12</b> |
| 3.1      | Beam generation                      | 12        |
| 3.2      | Geant4                               | 12        |
| 3.3      | Geometry                             | 13        |
| 3.4      | Tracking, field maps and beam optics | 14        |
| 3.5      | Detector response and digitization   | 15        |
| <b>4</b> | <b>Reconstruction</b>                | <b>15</b> |
| 4.1      | Time of flight                       | 15        |
| 4.2      | Scintillating-fiber trackers         | 16        |
| 4.3      | KL calorimeter                       | 17        |
| 4.4      | Electron-muon ranger                 | 17        |
| 4.5      | Cherenkov                            | 18        |
| 4.6      | Global reconstruction                | 18        |
| 4.6.1    | Global track matching                | 18        |
| 4.6.2    | Global PID                           | 18        |
| 4.7      | Online reconstruction                | 19        |
| <b>5</b> | <b>Summary</b>                       | <b>19</b> |

---

## 1 Introduction

### 1.1 The MICE experiment

The Muon Ionization Cooling Experiment (MICE) sited at the STFC Rutherford Appleton Laboratory (RAL) has delivered the first demonstration of muon ionization cooling [1] — the reduction of the phase-space of muon beams. Muon-beam cooling is essential for future facilities based on

muon acceleration, such as the Neutrino Factory or Muon Collider [2, 3]. The experiment was designed to be built and operated in a staged manner. In the first stage, the muon beamline was commissioned [4] and characterized [5]. A schematic diagram of the configuration used to study the factors that determine the performance of an ionization-cooling channel is shown in figure 1. The MICE experiment was operated such that muons passed through the experiment one at a time. The experiment included instrumentation to identify particle species (the particle-identification detectors, PID) [6–11] and to measure the phase-space coordinates of each muon. An ensemble of muons that was representative of the muon beam was then assembled using the measured coordinates. The techniques used to reconstruct the ensemble properties of the beam are described in [12] and the first observation of the ionization-cooling of a muon beam is presented in [1].

The configuration shown in figure 1 was used to study the factors that determine the performance of an ionization-cooling channel and to observe for the first time the reduction in transverse emittance of a muon beam.

The MICE Muon Beam line is described in detail in [4]. There are 5 different detector systems present on the beamline: time-of-flight (TOF) scintillators [6], threshold Cherenkov (Ckov) counters [13], scintillating-fiber trackers [14], a sampling calorimeter (KL) [8, 9], and the Electron Muon Ranger (EMR) — a totally active scintillating calorimeter [10, 11]. The TOF, Ckov, KL and EMR detectors are used for particle identification (PID), and the scintillating-fiber trackers are used to measure position and momentum. The TOF detector system consists of three detector stations, TOF0, TOF1 and TOF2, each composed of two orthogonal layers of scintillator bars. The TOF system determines PID via the time-of-flight between the stations. Each station also provides a low-resolution image of the beam profile. The Ckov system consists of two aerogel threshold Cherenkov stations, CkovA and CkovB. The KL and EMR detectors, the former using scintillating fibers embedded in lead sheets, and the latter scintillating bars, form the downstream calorimeter system.

The tracker system consists of two scintillating-fiber detectors, one upstream of the MICE cooling cell, the other downstream, in order to measure the change in emittance across the cooling cell. Each detector consists of 5 stations, each station having 3 fiber planes, allowing precision measurement of momentum and position to be made on a particle-by-particle basis.

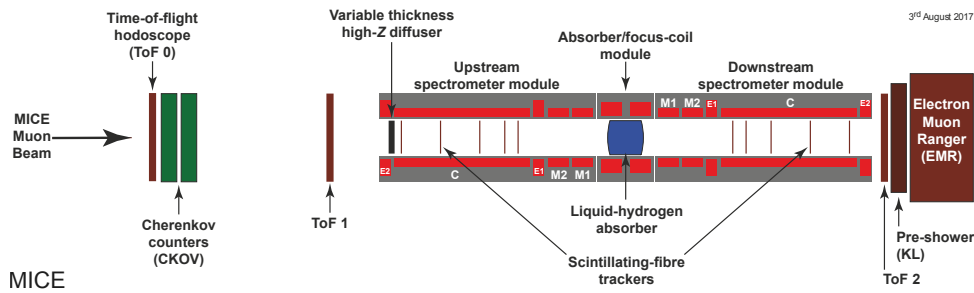


**Figure 1.** Schematic diagram of the MICE experiment. The red rectangles represent the coils of the spectrometer solenoids and focus-coil module. The individual coils of the spectrometer solenoids are labelled E1, C, E2, M1 and M2. The various detectors (time-of-flight hodoscopes (TOF0, TOF1) [6], Cherenkov counters [13], scintillating-fiber trackers [14], KLOE-Light (KL) calorimeter [7, 8], and Electron Muon Ranger (EMR) [10, 11]) are also represented.

## 1.2 Software requirements

The MICE software must serve both the accelerator-physics and the particle-physics needs of the experiment. Traditional particle-physics functionality includes reconstructing particle tracks, identifying them, and simulating the response from various detectors, while the accelerator-physics aspect includes the calculation of transfer matrices and Twiss parameters and propagating the beam envelopes. All of these items require a detailed description of the beamline, the geometries of the detectors, and the magnetic fields, as well as functionality to simulate the various detectors and reconstruct the detector outputs. MICE aims to measure the change in emittance to 1%, which imposes requirements on the performance of the track reconstruction, particle identification and measurements of scattering widths. In addition, the computational performance of the software was also important in order to ensure that the software can reconstruct data with sufficient speed to support live online monitoring of the experiment.

## 2 MAUS

The MICE Analysis User Software (MAUS) is the collaboration's simulation, reconstruction, and analysis software framework. MAUS provides a Monte Carlo (MC) simulation of the experiment, reconstruction of tracks and identification of particles from simulations and real data, and provides monitoring and diagnostics while running the experiment.

Installation is performed via a set of shell scripts with SCons [15] as the tool for constructing and building the software libraries and executables. The codebase is maintained with GNU Bazaar [16], a distributed version control system, and is hosted on Launchpad [17], a website that provides functionalities to host and maintain the software repository. MAUS has a number of dependencies on standard packages such as Python, ROOT [18] and Geant4 [19] which are built as “third party” external libraries during the installation process. The officially supported platform is Scientific Linux 6 [20] though developers have successfully built on CentOS [21], Fedora [22], and Ubuntu [23] distributions.

Each of the MICE detector systems, described in section 1.1, is represented within MAUS. Their data structures are described in section 2.2 and their simulation and reconstruction algorithms in sections 3 and 4. MAUS also provides “global” reconstruction routines, which combine data from individual detector systems to identify particle species by the likelihood method and perform a global track fit. These algorithms are also described in section 4.

### 2.1 Code design

MAUS is written in a mixture of Python and C++. C++ is used for complex or low-level algorithms where processing time is important, while Python is used for simple or high-level algorithms where development time is a more stringent requirement. Developers are allowed to write in either Python or C++ and Python bindings to C++ are handled through internal abstractions. In practice, all the reconstruction modules are written in C++ but support is provided for legacy modules written in Python.

MAUS has an Application Programming Interface (API) that provides a framework on which developers can hang individual routines. The MAUS API provides MAUS developers with a well-defined environment for developing reconstruction code, while allowing independent development of the back-end and code-sharing of common elements, such as error handling.

The MAUS data processing model is inspired by the Map-Reduce framework [24], which forms the core of the API design. Map-Reduce, illustrated in figure 2 is a useful model for parallelizing data processing on a large scale. A *map* process takes a single object as an input, transforms it, and returns a new object as the output (in the case of MAUS this input object is the *spill* class, see section 2.2).

A module is the basic building block of the MAUS API framework. Four types of module exist within MAUS:

1. **Inputters** generate input data either by reading data from files or over a network, or by generating an input beam;
2. **Mappers** modify the input data, for example by reconstructing signals from detectors, or tracking particles to generate MC hits;
3. **Reducers** collate the mapped data and provide functionality that requires access to the entire data set; and
4. **Outputters** save the data either by streaming over a network or writing to disk.

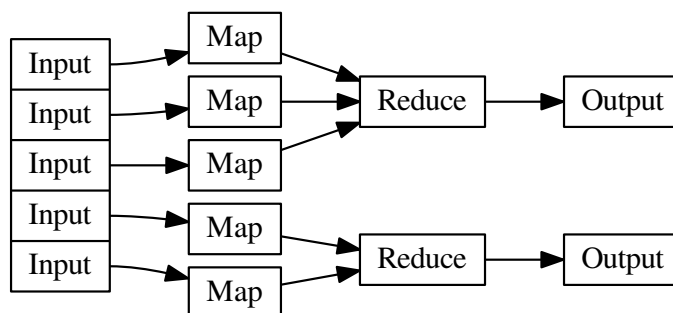


**Figure 2.** A Map-Reduce framework.

Each module type follows a common, extensible, object-orientated class hierarchy, shown for the case of the *map* and *reduce* modules in figure 3.

There are some objects that sit outside the scope of this modular framework but are nevertheless required by several of the modules. For instance, the detector geometries, magnetic fields, and calibrations are required by the reconstruction and simulation modules, and objects such as the electronics-cabling maps are required in order to unpack data from the data acquisition (DAQ) source, and error handling functionality is required by all of the modules. All these objects are accessed through a static singleton *globals* class.

MAUS has two execution concepts. A *job* refers to a single execution of the code, while a *run* refers to the processing of data for a DAQ run or MC run. A job may contain many runs. Since data are typically accessed from a single source and written to a single destination, *inputters* and *outputters* are initialized and destroyed at the beginning and end of a job. On the other hand, *mappers*

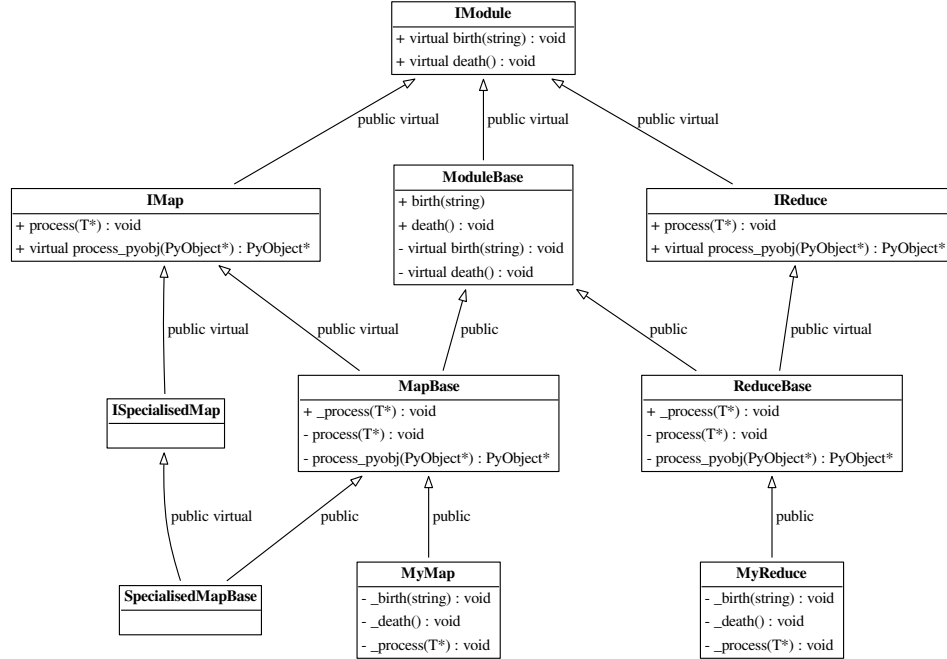


**Figure 3.** The MAUS API class hierarchy for Map and Reduce modules. The input and output modules follow related designs.  $T$  represents a templated argument. “+” indicates the introduction of a virtual void method, defining an interface, while “-” indicates that a class implements that method, fulfilling that aspect of the interface. The *process\_pyobj* functions are the main entry points for Python applications, and *process* the entry points for C++ applications. The framework can be extended as many times as necessary, as exemplified by the “SpecialisedMap” classes.

and *reducers* are initialized at the beginning of a run in order to allow run-specific information such as electronics cabling maps, fields, calibrations and geometries to be loaded.

The principal data type in MAUS, which is passed from module to module, is the *spill*. A single spill corresponds to data from the particle burst associated with a dip of the MICE target [4]. A spill lasts up to  $\sim 3$  ms and contains several DAQ triggers. Data from a given trigger define a single MICE *event*. In the language of the Input-Map-Reduce-Output framework, an *Input* module creates an instance of spill data, a *Map* module processes the spill (simulating, reconstructing, etc.), a *Reduce* module acts on a collection of spills when all the *mappers* finish, and finally an *Output* module records the data to a given file format.

Modules can exchange spill data either as C++ pointers or JSON [25] objects. In Python, the data format can be changed by using a converter module, and in C++ *mappers* are templated to a MAUS data type and an API handles any necessary conversion to that type (see figure 3).

Data contained within the MAUS data structure (see section 2.2) can be saved to permanent storage in one of two formats. The default data format is a ROOT [18] binary and the secondary format is JSON. ROOT is a standard high-energy physics analysis package, distributed with MAUS, through which many of the analyses on MICE are performed. Each spill is stored as a single entry in a ROOT TTree object. JSON is an ASCII data-tree format. Specific JSON parsers are available — for example, the Python *json* library, and the C++ *JsonCpp* [26] parser come prepackaged with MAUS.

In addition to storing the output from the *map* modules, MAUS is also capable of storing the data produced by *reducer* modules using a special *Image* class. This class is used by *reducers* to store images of monitoring histograms, efficiency plots, etc. *Image* data may only be saved in JSON format.

## 2.2 Data structure

### 2.2.1 Physics data

At the top of the MAUS data structure is the spill class which contains all the data from the simulation, raw real data and the reconstructed data. The spill is passed between modules and written to permanent storage. The data within a spill is organized into arrays of three possible event types: an *MCEvent* contains data representing the simulation of a single particle traversing the experiment and the simulated detector responses; a *DAQEvent* corresponds to the real data for a single trigger; and a *ReconEvent* corresponds to the data reconstructed for a single particle event (arising either from a Monte Carlo(MC) particle or a real data trigger). These different branches of the MAUS data structure are shown diagrammatically in figures 4–9.

The sub-structure of the MC event class is shown in figure 5. The class is subdivided into events containing detector hits (energy deposited, position, momentum) for each of the MICE detectors (see section 1.1). The event also contains information about the primary particle that created the hits in the detectors.

The sub-structure of the reconstruction event class is shown in figure 6. The class is subdivided into events representing each of the MICE detectors, together with the data from the trigger, and data for the global event reconstruction. Each detector class and the global-reconstruction class has several further layers of reconstruction data. This is shown in figures 7–9.

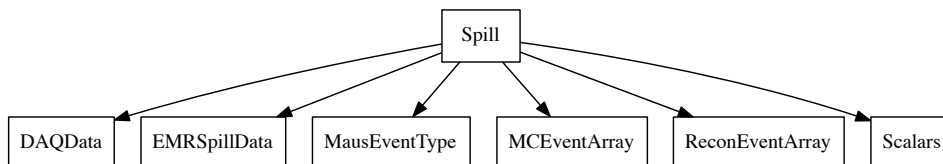


**Figure 4.** The MAUS output structure for a spill event. The label in each box is the name of the C++ class.

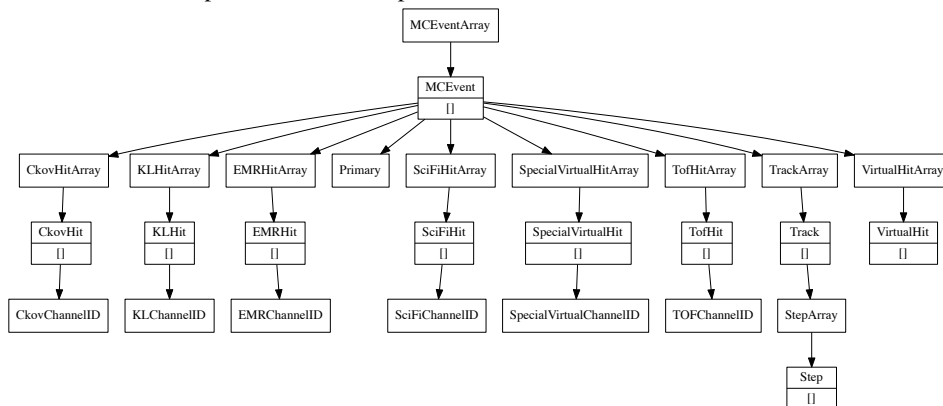


**Figure 5.** The MAUS data structure for MC events. The label in each box is the name of the C++ class and [] indicates that child objects are array items.

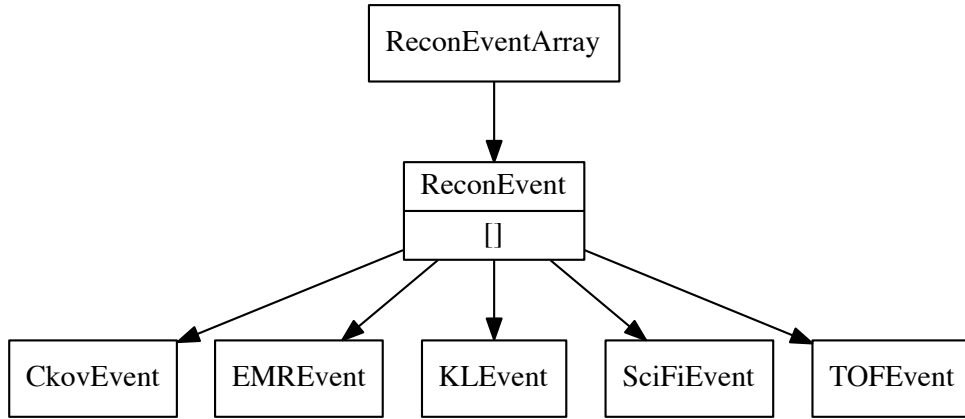


**Figure 6.** The MAUS data structure for reconstructed events. The label in each box is the name of the C++ class.

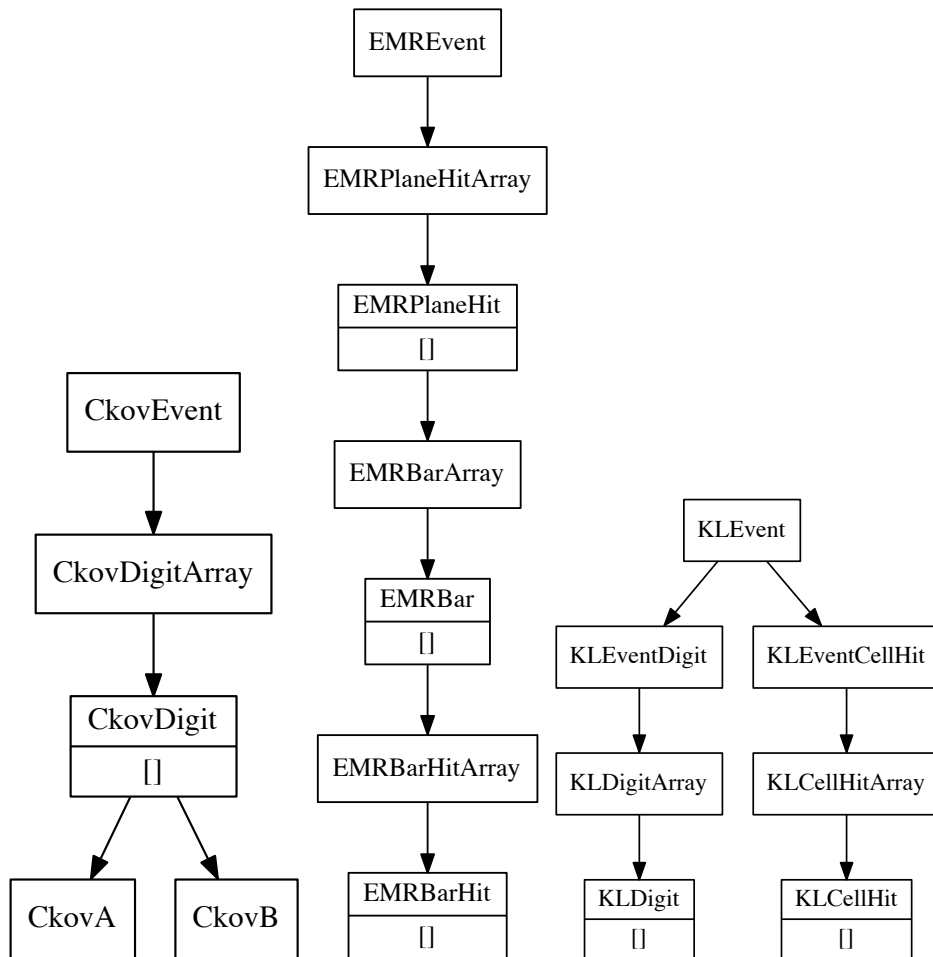


**Figure 7.** The MAUS data structure for CKOV (left), EMR (middle) and KL (right) reconstructed events. The label in each box is the name of the C++ class [] indicates that child objects are array items.

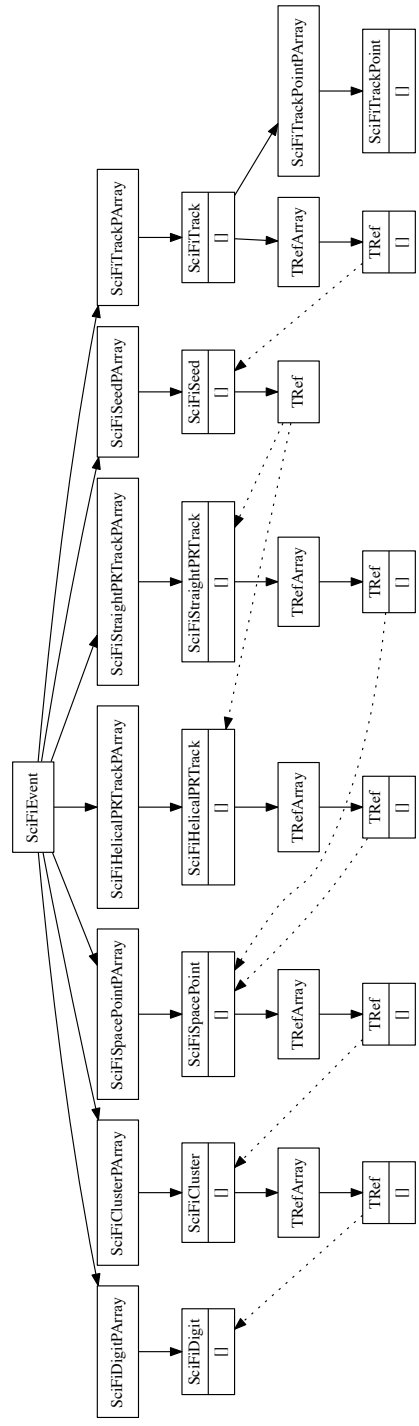


**Figure 8.** The MAUS data structure for the tracker. The label in each box is the name of the C++ class and [] indicates that child objects are array items.

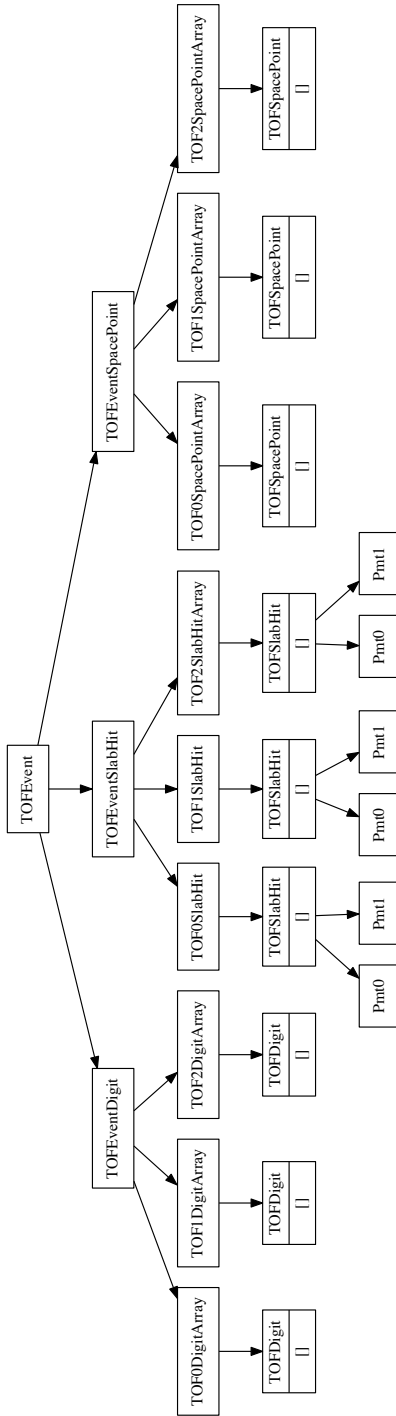


**Figure 9.** The MAUS data structure for the TOFs. The label in each box is the name of the C++ class and [] indicates that child objects are array items.

## 2.2.2 Top level data organization

In addition to the spill data, MAUS also contains structures for storing supplementary information for each run and job. These are referred to as *JobHeader* and *JobFooter*, and *RunHeader* and *RunFooter*. The *JobHeader* and *JobFooter* represent data, such as the MAUS release version, associated with the start and end of a job, and the *RunHeader* and *RunFooter* represent data, such as the geometry and calibrations associated with a run, associated with the start and end of a run. These are saved to the output along with the spill.

In order to interface with ROOT, particularly in order to save data in the ROOT format, thin wrappers for each of the top level classes, and a templated base class, were introduced. This allows the ROOT TTree, in which the output data is stored (see section 2.2.1), to be given a single memory address to read from. The wrapper for Spill is called *Data*, while for each of *RunHeader*, *RunFooter*, *JobHeader* and *JobFooter*, the respective wrapper class is just given the original class name with “Data” appended, e.g., *RunHeaderData*. The base class for each of the wrappers is called *MAUSevent*. The class hierarchy is illustrated in figure 10.

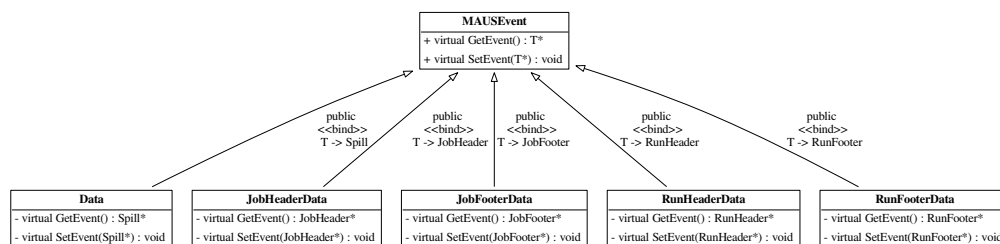


**Figure 10.** Class hierarchy for the wrappers and base class of the top-level classes of the MAUS data structure.

## 2.3 Data flow

The MAUS data-flow, showing the reconstruction chain for data originating from MC or real data, is depicted in figure 11. Each item in the diagram is implemented as an individual module. The data flow is grouped into three principal areas: the simulation data flow used to generate digits (electronics signals) from particle tracking; the real data flow used to generate digits from real detector data; and the reconstruction data flow which illustrates how digits are built into higher level objects and converted to parameters of interest. The reconstruction data flow is the same for digits from real data and simulation. In the case of real data, separate input modules are provided to read either directly from the DAQ, or from archived data stored on disk. A *reducer* module for each detector provides functionality to create summary histograms.

## 2.4 Testing

MAUS has a set of tests at the unit level and the integration level, together with code-style tests for both Python and C++. Unit tests are implemented to test a single function, while integration tests operate on a complete workflow. Unit tests check that each function operates as intended

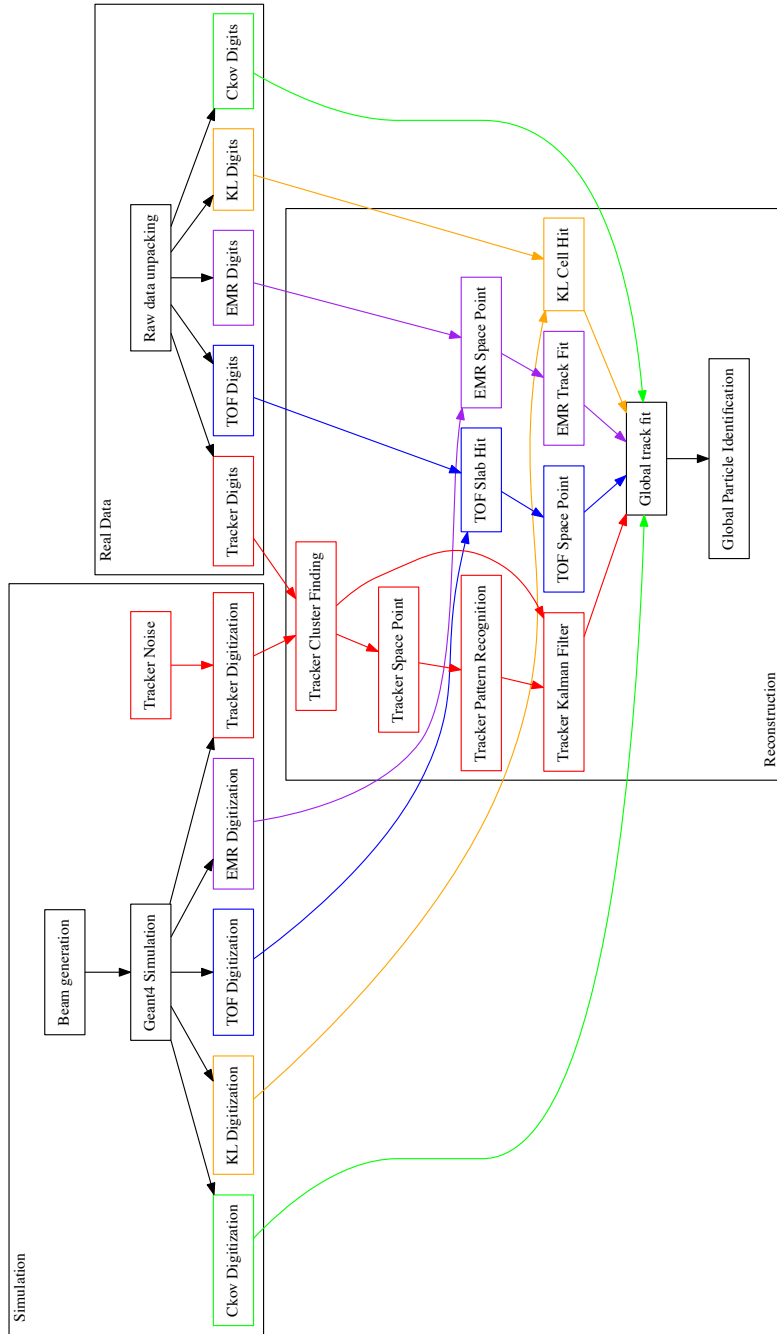


**Figure 11.** Data flow for the MAUS project. The data flow is color-coded by detector: Ckov — green, EMR — purple, KL — orange, TOF — blue, Tracker — red.

by the developer. Tests are run automatically for every version committed to the repository and results show that a high level of code coverage has been achieved. Integration tests allow the overall performance of the code to be checked against specifications. The MAUS team provides unit test coverage that executes 70–80 % of the total code base. This level of coverage typically results in a code that performs the major workflows without any problems.

The MAUS codebase is built and tested using a Jenkins [27] continuous integration environment deployed on a cluster of servers. Builds and tests of the development branch are automatically triggered when there is a change to the codebase. Developers are asked to perform a build and test on a personal branch of the codebase using the test server before requesting a merge with the development trunk. This enables the MAUS team to make frequent clean releases. Typically MAUS works on a 4–8 week major-release cycle.

### 3 Monte Carlo

The Monte Carlo simulation of MICE encompasses beam generation, geometrical description of detectors and fields, tracking of particles through detectors and digitization of the detectors' response to particle interactions.

#### 3.1 Beam generation

Several options are provided to generate an incident beam. Routines are provided to sample particles from a multivariate Gaussian distribution or generate ensembles of identical particles (pencil beams). In addition, it is possible to produce time distributions that are either rectangular or triangular in time to give a simplistic representation of the MICE time distribution. Parameters, controlled by data-cards, are available to control random seed generation, relative weighting of particle species and the transverse-to-longitudinal coupling in the beam. MAUS also allows the generation of a polarized beam.

Beam particles can also be read in from an external file created by G4Beamline [28] — a particle-tracking simulation program based on Geant4, or ICOOL [29] — a simulation program that was developed to study the ionization cooling of muon beams, as well as files in user-defined formats. In order to generate beams which are more realistic taking into account the geometry and fields of the actual MICE beamline, we use G4Beamline to model the MICE beamline from the target to a point upstream of the second quad triplet (upstream of Q4). The beamline settings, e.g., magnetic field strengths and number of particles to generate, are controlled through data-cards. The magnetic field strengths have been tuned to produce beams that are reasonably accurate descriptions of the real beam. Scripts to install G4beamline are shipped with MAUS.

Once the beam is generated, the tracking and interactions of particles as they traverse the rest of the beamline and the MICE detectors are performed using Geant4.

#### 3.2 Geant4

A drawing of the MICE Muon Beam line [4] is shown in figure 12. It consists of a quadrupole triplet (Q123) that captures pions produced when the MICE target intersects the ISIS proton beam, a pion-momentum-selection dipole (D1), a superconducting solenoid (DS) to focus and transport the particles to a second dipole (D2) that is used to select the muon-beam momentum, and a transport

channel composed of a further two quadrupole triplets (Q456 and Q789). As described in the next section, the positions and apertures of the beamline magnets were surveyed and are reproduced in the geometry along with windows and materials in the path of the muon beams. The Geant4 simulation within MAUS starts 1 m downstream of the second beamline dipole magnet D2. Geant4 bindings are encoded in the Simulation module. Geant4 groups particles by run, event and track. A Geant4 run maps to a MICE spill; a Geant4 event maps to a single inbound particle from the beamline; and a Geant4 track corresponds to a single particle in the experiment.

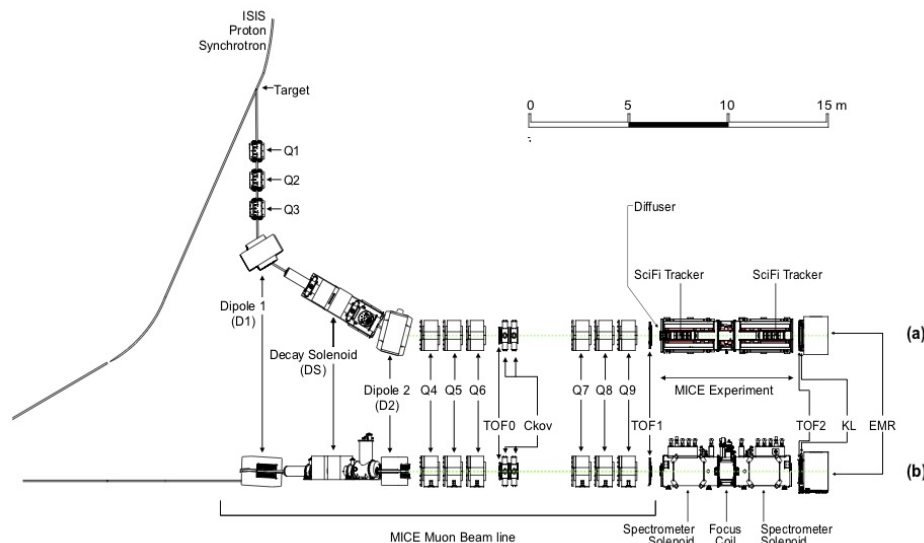


**Figure 12.** (a) Top and (b) side views of the MICE Muon Beamline, its instrumentation, and the experimental configuration. A titanium target dipped into the ISIS proton synchrotron and the resultant spill of particles was captured with a quadrupole triplet (Q1–3) and transported through momentum-selecting dipoles (D1, D2). The quadrupole triplets (Q4–6, Q7–9) transported particles to the upstream spectrometer module. The time-of-flight of particles, measured between TOF0 and TOF1, was used for particle identification.

Geant4 provides a variety of reference physics processes to model the interactions of particles with matter. The default process in MAUS is “*QGSP\_BERT*” which causes Geant4 to model hadron interactions using a Bertini cascade model up to  $10 \text{ GeV}/c$  [30]. MAUS provides methods to set up the Geant4 physical processes through user-controlled data-cards. Finally, MAUS provides routines to extract particle data from the Geant4 tracks at user-defined locations.

### 3.3 Geometry

MAUS uses an online Configuration Database to store all of its geometries. These geometries have been extracted from CAD drawings which are updated based on the most recent surveys and technical drawings available. The CAD drawings are translated to a geometry-specific subset of XML, the Geometry Description Markup Language (GDML) [31] prior to being recorded in the configuration database through the use of the FastRAD [32] commercial software package.

The GDML formatted description contains the beamline elements and the positions of the detector survey points. Beam-line elements are described using tessellated solids to define the

shapes of the physical volumes. The detectors themselves are described using an independently generated set of GDML files using Geant4 standard volumes. An additional XML file is appended to the geometry description that assigns magnetic fields and associates the detectors to their locations in the GDML files. This file is initially written by the geometry maintainers and formatted to contain run-specific information during download.

The GDML files can be read via a number of libraries in Geant4 and ROOT for the purpose of independent validation. The files are in turn translated into the MAUS-readable geometry files either by accessing directly the data using a python extension or through the use of EXtensible Stylesheet Language Transformations (XSLT) [33].

### 3.4 Tracking, field maps and beam optics

MAUS tracking is performed using Geant4. By default, MAUS uses 4<sup>th</sup> order Runge-Kutta (RK4) for tracking, although other routines are available. RK4 has been shown to have very good precision relative to the MICE detector resolutions, even for step sizes of several cm.

In a solenoid focussing lattice a cylindrically symmetric beam can be described by the 4D RMS beam emittance  $\varepsilon_N$  and optical parameters  $\beta_\perp$  and  $\beta'_\perp$ , its derivative with respect to  $z$ .  $\beta_\perp$  is related to the variance of the position of particles  $x$  by [34]:

$$\beta_\perp = \frac{p_z \text{Var}(x)}{\varepsilon_N m c}; \quad (3.1)$$

where  $m$  is the particle mass,  $c$  is the speed of light, and  $p_z$  is the beam longitudinal momentum. In the approximation that particles travel near to the solenoid axis, transport of the beam envelope can be performed by integration of the differential equation:

$$2\beta_\perp\beta''_\perp - (\beta'_\perp)^2 + 4\beta_\perp^2\kappa^2 - 4(1 + \mathcal{L})^2 = 0. \quad (3.2)$$

Transport of individual particles can be performed using numerical integration of the Lorentz force law. Alternately transport can be performed by calculating a transfer map  $\mathbf{M}$  defined by:

$$\vec{u}_{ds} = \mathbf{M}\vec{u}_{us}; \quad (3.3)$$

where  $\vec{u}_{us}$  and  $\vec{u}_{ds}$  are the upstream and downstream transverse phase space vectors  $\vec{u} = (x, p_x, y, p_y)$ . MAUS can calculate the transfer map at arbitrary order by transporting a handful of particles and fitting to a multidimensional polynomial in  $\vec{u}$ .

Electromagnetic field maps are implemented in a series of overlapping regions. The world volume is divided into a number of voxels, and the field maps that impinge on each voxel is stored in a list. At each tracking step, MAUS iterates over the list of fields that impinge on the voxels within which the particle is stepping. For each field map, MAUS transforms to the local coordinate system of the field map, and calculates the field. The field values are transformed back into the global coordinate system, summed, and passed to Geant4. The voxelization enables the simulation of long accelerators without a performance penalty.

Numerous field types have been implemented within the MAUS framework. Solenoid fields can be calculated numerically from cylindrically symmetric 2D field maps, by taking derivatives of an on-axis solenoidal field or by using the sum of fields from a set of cylindrical current sheets.

The use of field maps enables the realistic reproduction of the MICE apparatus, while a derivatives-based approach enables the exclusion of different terms in the higher order parts of the transfer map [35]. Multipole fields can be calculated from a 3D field map, or by taking derivatives from the usual multipole expansion formulae. Linear, quadratic and cubic interpolation routines have been implemented for field maps. Pillbox fields can be calculated by using the Bessel functions appropriate for a TM010 cavity or by reading a cylindrically symmetric field map.

The transport algorithms have been compared with each other and experimental data and show agreement at linear order [36] in  $\vec{u}$ . Work is ongoing to study the effect of aberrations in the optics, indicated by non-linear terms in the transfer map relationship. These aberrations can cause distortion of the beam leading to emittance growth, which has been observed in the tails of the MICE beam. The tracking in MAUS has been benchmarked against ICOOL, G4Beamline, and MaryLie [37], demonstrating good agreement. The routines have been used to model a number of beamlines and rings, including a neutrino factory front-end [38].

### 3.5 Detector response and digitization

The modeling of the detector response and electronics enables MAUS to provide data used to test reconstruction algorithms and estimate the uncertainties introduced by detectors and their readout.

The interaction of particles in materials is modeled using Geant4. For each detector, a “sensitive detector” class processes Geant4 hits in active detector volumes and stores hit information such as the volume that was hit, the energy deposited and the time of the hit. Each detector’s digitization routine then simulates the response of the electronics to these hits, modeling processes such as the photo-electron yield from a scintillator bar, attenuation in light guides and the pulse shape in the electronics. The data structure of the outputs from the digitizers are designed to match the output from the unpacking of real data from the DAQ.

## 4 Reconstruction

The reconstruction chain takes as its input either digitized hits from the MC or DAQ digits from real data. Regardless, the detector reconstruction algorithms, by requirement and design, operate the same way on both MC and real data.

### 4.1 Time of flight

There are three time-of-flight detectors in MICE which serve to distinguish particle type. The detectors are made of plastic scintillator and in each station there are orthogonal  $x$  and  $y$  planes with 7 or 10 slabs in each plane.

Each Geant4 hit in the TOF is associated with a physical scintillator slab. The energy deposited by a hit is first converted to units of photo-electrons. The photo-electron yield from a hit accounts for the light attenuation corresponding to the distance of the hit from the photomultiplier tube (PMT) and is then smeared by the photo-electron resolution. The yields from all hits in a given slab are then summed and the resultant yield is converted to ADC counts.

The time of the hit in the slab is propagated to the PMTs at either end of the slab. The propagated time is then smeared by the PMT’s time resolution and converted to TDC counts. Calibration

corrections based on real data are then added to the TDC values so that, at the reconstruction stage, they can be corrected just as is done with real data.

The reconstruction proceeds in two main steps. First, the slab-hit-reconstruction takes individual PMT digits and associates them to reconstruct the hit in the slab. If there are multiple hits associated with a PMT, the hit which is earliest in time is taken to be the real hit. Then, if both PMTs on a slab have fired, the slab is considered to have a valid hit. The TDC values are converted to time and the hit time and charge associated with the slab hit are taken to be the average of the two PMT times and charges respectively. In addition, the product of the PMT charges is also calculated and stored. Secondly, individual slab hits are used to form space-points. A space-point in the TOF is a combination of  $x$  and  $y$  slab hits. All combinations of  $x$  and  $y$  slab hits in a given station are treated as space-point candidates. Calibration corrections, stored in the Configurations Database, are applied to these hit times and if the reconstructed space-point is consistent with the resolution of the detector, the combination is said to be a valid space-point. The TOF has been shown to provide good time resolutions at the 60 ps level [6].

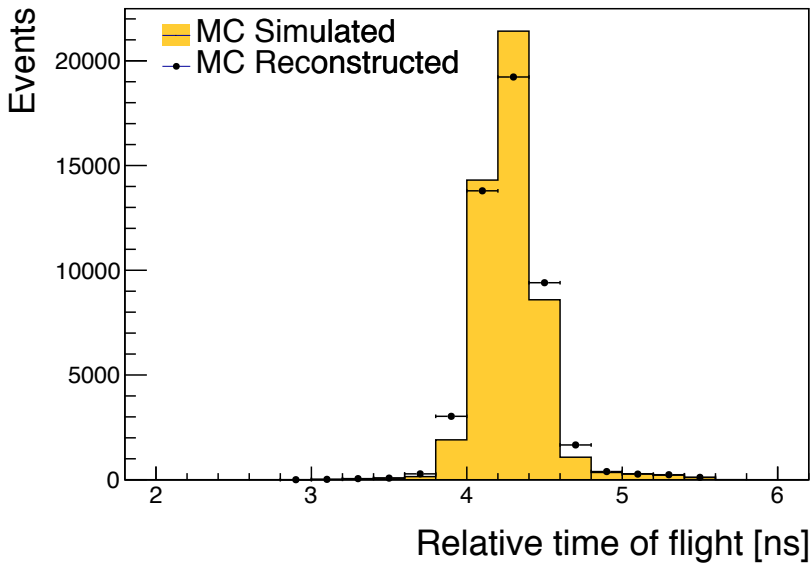


**Figure 13.** Relative time of flight between TOF0 and TOF1. The yellow histogram represents true MC events and the solid markers represent the same sample reconstructed with MAUS.

## 4.2 Scintillating-fiber trackers

The scintillating-fiber trackers are the central piece of the reconstruction. As mentioned in section 1.1, there are two trackers, one upstream and the other downstream of an absorber, situated within solenoidal magnetic fields. The trackers measure the emittance before and after particles pass through the absorber.

The tracker software algorithms and performance are described in detail in [39]. Digits are the most basic unit fed into the main reconstruction module, each digit representing a signal from one channel. Digits from adjacent channels are assumed to come from the same particle and are grouped to form clusters. Clusters from channels which intersect each other, in at least two planes from the

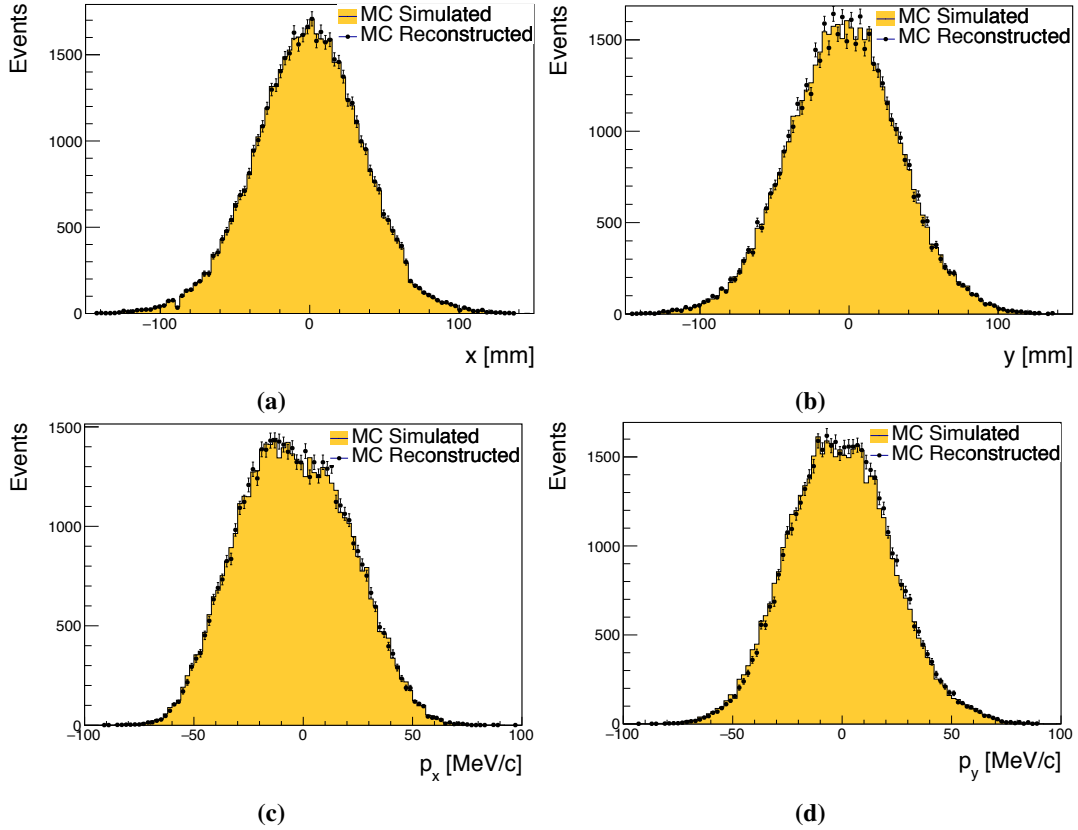


**Figure 14.** Position and momentum distributions of muons reconstructed at upstream tracker station nearest to the absorber: a)  $x$ , b)  $y$ , c)  $p_x$ , d)  $p_y$ . The yellow histograms represent true MC simulations, and the markers represent the MC sample reconstructed using MAUS.

same station, are used to form space-points, giving  $x$  and  $y$  positions where a particle intersected a station. Once space-points have been found, they are associated with individual tracks through pattern recognition (PR), giving straight or helical PR tracks. These tracks, and the space-points associated with them, are then sent to the final track fit. To avoid biases that may come from space-point reconstruction, the Kalman filter uses only reconstructed clusters as input.

### 4.3 KL calorimeter

Hit-level reconstruction of the KL is implemented in MAUS. Individual PMT hits are unpacked from the DAQ or simulated from MC and the reconstruction associates them to identify the slabs that were hit and calculates the charge and charge-product corresponding to each slab hit. The KL has been used successfully to estimate the pion contamination in the MICE muon beamline [9].

### 4.4 Electron-muon ranger

Hit-level reconstruction of the EMR is implemented in MAUS. The integrated ADC count and time over threshold are calculated for each bar that was hit. The EMR reconstructs a wide range of

variables that can be used for particle identification and momentum reconstruction. The software and performance of the EMR are described in detail in [10].

#### 4.5 Cherenkov

The CKOV reconstruction takes the raw flash-ADC data, subtracts pedestals, calculates the charge and applies calibrations to determine the photo-electron yield.

#### 4.6 Global reconstruction

The aim of the Global Reconstruction is to take the reconstructed outputs from individual detectors and tie them together to form a global track. A likelihood for each particle hypothesis is also calculated.

##### 4.6.1 Global track matching

Global track matching is performed by collating particle hits (TOFs 0, 1 and 2, KL, Ckovs) and tracks (Trackers and EMR) from each detector using their individual reconstruction and combining them using a RK4 method to propagate particles between these detectors. The tracking is performed outwards from the cooling channel — i.e., from the upstream tracker to the TOF0 detector, and from the downstream tracker to the EMR detector. Track points are matched to form tracks using an RK4 method. Initially this is done independently for the upstream and downstream sections (i.e., either side of the absorber). As the trackers provide the most accurate position reconstruction, they are used as starting points for track matching, propagating hits outwards into the other detectors and then comparing the propagated position to the measured hit in the detector. The acceptance criterion for a hit belonging to a track is an agreement within the detector's resolution with an additional allowance for multiple scattering. Track matching is currently performed for all TOFs, KL and EMR.

The RK4 propagation requires the mass and charge of the particle to be known. Hence, it is necessary to perform track matching using a hypothesis for each particle type (muons, pions, and electrons). Tracks for all possible PID hypotheses are then passed to the Global PID algorithms.

##### 4.6.2 Global PID

Global particle identification in MICE typically requires the combination of several detectors. The time-of-flight between TOF detectors can be used to calculate velocity, which is compared with the momentum measured in the trackers to identify the particle type. For all events but those with very low transverse momentum ( $p_t$ ), charge can be determined from the direction of helical motion in the trackers. Additional information can be obtained from the CKOV, KL and EMR detectors. The global particle identification framework is designed to tie this disparate information into a set of hypotheses of particle types, with an estimate of the likelihood of each hypothesis.

The Global PID in MAUS uses a log-likelihood method to identify the particle species of a global track. It is based upon a framework of PID variables. Simulated tracks are used to produce probability density functions (PDFs) of the PID variables. These are then compared with the PID variables for tracks in real data to obtain a set of likelihoods for the PIDs of the track.

The input to the Global PID is several potential tracks from global track matching. During the track matching stage, each of these tracks was matched for a specific particle hypothesis. The Global PID then takes each track and determines the most likely PID following a series of steps:

1. Each track is copied into an intermediate track;
2. For each potential PID hypothesis  $p$ , the log-likelihood is calculated using the PID variables;
3. The track is assigned an object containing the log-likelihood for each hypothesis; and
4. From the log-likelihoods, the confidence level, C.L., for a track having a PID  $p$  is calculated and the PID is set to the hypothesis with the best C.L.

#### 4.7 Online reconstruction

During data taking, it is essential to visualize a detector's performance and have diagnostic tools to identify and debug unexpected behavior. This is accomplished through summary histograms of high and low-level quantities from detectors. The implementation is through a custom multi-threaded application based on a producer-consumer pattern with thread-safe FIFO buffers. Raw data produced by the DAQ are streamed through a network and consumed by individual detector *mappers* described in section 3. The reconstructed outputs produced by the *mappers*, are in turn consumed by the *reducers*. The *mappers* and *reducers* are distributed among the threads to balance the load. Finally, outputs from the *reducers* are written as histogram images. Though the framework for the online reconstruction is based on parallelized processing of spills, the reconstruction modules are the same as those used for offline processing. A lightweight tool based on Django [40] provides live web-based visualization of the histogram images as and when they are created. Typical data rates during experimental operations were  $\sim 300$  MB/s. The average event rate varied, depending on the configuration of the beamline, with the maximum instantaneous rate being  $\sim 150$  kHz. MAUS performance matched the data rates and online reconstruction happened virtually "live" with the reconstructed outputs available instantly allowing collaborators to monitor the quality of the data being acquired.

## 5 Summary

The MICE collaboration has developed the MAUS software suite to simulate the muon beamline, simulate the MICE detectors, and reconstruct both simulated and real data. The software also provides global track-matching and particle-identification capabilities. Simplified programming interfaces and testing environments enable productive development. MAUS has been successfully used to reconstruct data online during data collection. In addition, MAUS is routinely used to perform reconstruction of the entire MICE data volume on batch production systems. MICE has collected  $\sim 15$  TB of raw data and a full reconstruction of the data is performed with each released version of MAUS. The batch systems are also used to perform compute-intensive simulations with various configurations of the beamline and the cooling channel.

## Acknowledgments

The work described here was made possible by grants from Department of Energy and National Science Foundation (U.S.A.), the Istituto Nazionale di Fisica Nucleare (Italy), the Science and Technology Facilities Council (U.K.), the European Community under the European Commission Framework Programme 7 (AIDA project, grant agreement no. 262025, TIARA project, grant

agreement no. 261905, and EuCARD), the Japan Society for the Promotion of Science and the Swiss National Science Foundation, in the framework of the SCOPES programme. We gratefully acknowledge all sources of support. We are grateful to the support given to us by the staff of the STFC Rutherford Appleton and Daresbury Laboratories. We acknowledge the use of Grid computing resources deployed and operated by GridPP [41] in the U.K.

## References

- [1] MICE collaboration, *First Demonstration of Ionization Cooling in MICE*, in *Proceedings of the International Particle Accelerator Conference*, Vancouver, Canada, 29 April–May 4 2018, pp. 5035–5040.
- [2] IDS-NF collaboration, *International design study for the neutrino factory: Interim design report*, 2011.
- [3] S. Geer, *Muon Colliders and Neutrino Factories*, *Annu. Rev. Nucl. Part. Sci.* **59** (2009) 345.
- [4] MICE collaboration, *The MICE Muon Beam on ISIS and the beam-line instrumentation of the Muon Ionization Cooling Experiment*, 2012 *JINST* **7** P05009 [[arXiv:1203.4089](#)].
- [5] MICE collaboration, *Characterisation of the muon beams for the Muon Ionisation Cooling Experiment*, *Eur. Phys. J. C* **73** (2013) 2582 [[arXiv:1306.1509](#)].
- [6] MICE collaboration, *The design and commissioning of the MICE upstream time-of-flight system*, *Nucl. Instrum. Meth. A* **615** (2010) 14 [[arXiv:1001.4426](#)].
- [7] KLOE collaboration, *The KLOE electromagnetic calorimeter*, *Nucl. Instrum. Meth. A* **494** (2002) 326.
- [8] F. Ambrosino et al., *Calibration and performances of the KLOE calorimeter*, *Nucl. Instrum. Meth. A* **598** (2009) 239.
- [9] MICE collaboration, *Pion Contamination in the MICE Muon Beam*, 2016 *JINST* **11** P03001 [[arXiv:1511.00556](#)].
- [10] MICE collaboration, *Electron-Muon Ranger: performance in the MICE Muon Beam*, 2015 *JINST* **10** P12012 [[arXiv:1510.08306](#)].
- [11] R. Asfandiyarov et al., *The design and construction of the MICE Electron-Muon Ranger*, 2016 *JINST* **11** T10007 [[arXiv:1607.04955](#)].
- [12] MICE collaboration, *First particle-by-particle measurement of emittance in the Muon Ionization Cooling Experiment*, *Eur. Phys. J. C* **79** (2019) 257 [[arXiv:1810.13224](#)].
- [13] L. Cremaldi, D.A. Sanders, P. Sonnek, D.J. Summers and J. Reidy, Jr, *A Cherenkov Radiation Detector with High Density Aerogels*, *IEEE Trans. Nucl. Sci.* **56** (2009) 1475 [[arXiv:0905.3411](#)].
- [14] M. Ellis et al., *The Design, construction and performance of the MICE scintillating fibre trackers*, *Nucl. Instrum. Meth. A* **659** (2011) 136 [[arXiv:1005.3491](#)].
- [15] <https://scons.org>.
- [16] <https://bazaar.canonical.com>.
- [17] <https://launchpad.net>.
- [18] R. Brun and F. Rademakers, *ROOT: An object oriented data analysis framework*, *Nucl. Instrum. Meth. A* **389** (1997) 81.
- [19] GEANT4 collaboration, *GEANT4: A Simulation toolkit*, *Nucl. Instrum. Meth. A* **506** (2003) 250.

- [20] <https://scientificlinux.org>.
- [21] <https://centos.org>.
- [22] <https://getfedora.org>.
- [23] <https://ubuntu.com>.
- [24] J. Dean and S. Ghemawat, *MapReduce: Simplified data processing on large clusters*, in *Proceedings of OSDI04*, San Francisco, CA, U.S.A., 2004, pp. 137–150.
- [25] <https://json.org>.
- [26] <https://github.com/open-source-parsers/jsoncpp>.
- [27] <https://jenkins-ci.org>.
- [28] T.J. Roberts and D.M. Kaplan, *G4BeamLine programme for matter dominated beamlines*, in *Proceedings of the Particle Accelerator Conference*, Albuquerque, NM, U.S.A., 25–29 June 2007, pp. 3468–3470.
- [29] R.C. Fernow, *Icool: A simulation code for ionization cooling of muon beams*, in *Proceedings of the Particle Accelerator Conference*, New York, NY, U.S.A., 27 March–2 April 1999, pp. 3020–3022.
- [30] J. Apostolakis et al., *Geometry and physics of the geant4 toolkit for high and medium energy applications*, *Radiat. Phys. Chem.* **78** (2009) 859.
- [31] R. Chytrcek, J. McCormick, W. Pokorski and G. Santin, *Geometry description markup language for physics simulation and analysis applications.*, *IEEE Trans. Nucl. Sci.* **53** (2006) 2892.
- [32] <https://fastrad.net>.
- [33] <https://www.w3.org/standards/xml/transformation>.
- [34] G. Penn and J.S. Wurtele, *Beam envelope equations for cooling of muons in solenoid fields*, *Phys. Rev. Lett.* **85** (2000) 764.
- [35] R. Ryne and C. Rogers, *Nonlinear effects in the MICE step iv lattice*, MICE-NOTE-461, 2015.
- [36] S.C. Middleton, *Characterisation of the MICE experiment*, Ph.D. Thesis, Imperial College London (2018).
- [37] R.D. Ryne et al., *Recent progress on the MARYLIE/IMPACT beam dynamics code*, in *Proceedings of the 9<sup>th</sup> International Computational Accelerator Physics Conference*, Chamonix, France, 2–6 October 2006, pp. 157–159.
- [38] C.T. Rogers, D. Stratakis, G. Prior, S. Gilardoni, D. Neuffer, P. Snopok et al., *Muon front end for the neutrino factory*, *Phys. Rev. ST Accel. Beams* **16** (2013) 040104.
- [39] A. Dobbs, C. Hunt, K. Long, E. Santos, M.A. Uchida, P. Kyberd et al., *The reconstruction software for the MICE scintillating fibre trackers*, 2016 *JINST* **11** T12001 [[arXiv:1610.05161](https://arxiv.org/abs/1610.05161)].
- [40] <https://www.djangoproject.com>.
- [41] <https://www.gridpp.ac.uk>.

## MULTIYEAR INDOOR RADON VARIABILITY IN A FAMILY HOUSE – A CASE STUDY IN SERBIA

by

**Vladimir I. UDOVIČIĆ<sup>1\*</sup>, Dimitrije M. MALETIĆ<sup>1</sup>, Radomir M. BANJANAC<sup>1</sup>,  
Dejan R. JOKOVIĆ<sup>1</sup>, Aleksandar L. DRAGIĆ<sup>1</sup>, Nikola B. VESELINOVIĆ<sup>1</sup>,  
Jelena Z. ŽIVANOVIĆ<sup>1</sup>, Mihailo R. SAVIĆ<sup>1</sup>, and Sofija M. FORKAPIĆ<sup>2</sup>**

<sup>1</sup>Institute of Physics, University of Belgrade, Belgrade, Serbia

<sup>2</sup>Department of Physics, Faculty of Science, University of Novi Sad, Novi Sad, Serbia

Scientific paper

<http://doi.org/10.2298/NTRP1802174U>

The indoor radon behavior has complex dynamics due to the influence of the large number of different parameters: the state of indoor atmosphere (temperature, pressure, and relative humidity), aerosol concentration, the exchange rate between indoor and outdoor air, construction materials, and living habits. As a result, indoor radon concentration shows variation, with the usual periodicity of one day and one year. It is well-known that seasonal variation of the radon concentration exists. It is particularly interesting to investigate indoor radon variation at the same measuring location and time period, each year, due to estimation of individual annual dose from radon exposure. The long-term indoor radon measurements, in a typical family house in Serbia, were performed. Measurements were taken during 2014, 2015, and 2016, in February and July, each year. The following measuring techniques were used: active and charcoal canisters methods. Analysis of the obtained results, using multivariate analysis methods, is presented.

*Key words: radon variability, multivariate regression analysis, multi-seasonal radon measurements, indoor radon*

### INTRODUCTION

The research of the dynamics of radon in various environments, especially indoors, is of great importance in terms of protection against ionizing radiation and in designing of measures for its reduction. Published results and development of many models to describe the behavior of indoor radon, indicates the complexity of this research, especially with models for prediction of the variability of radon [1-3]. This is because the variability of radon depends on a large number of variables such as local geology, permeability of soil, building materials used for the buildings, the state of the indoor atmosphere (temperature, pressure and relative humidity), aerosol concentration, the exchange rate between indoor and outdoor air, construction materials, as well as the living habits of people. It is known that the indoor radon concentration variation has periodicity of one day and one year. It is also well-known that the seasonal variation of the radon concentration exists. This is why it is particularly interesting to investigate indoor radon variation at the same measuring location and time period, year after

year, in order to estimate the individual annual dose from radon exposure. In that sense, we performed long-term indoor radon measurements in a typical family house in Serbia. Measurements were taken during the 2014, 2015, and 2016, in February and July, each year. We used the following measuring techniques: active and charcoal canisters methods. The detailed analysis of the obtained results using multivariate analysis (MVA) methods is presented in this paper.

First, MVA methods were tested on the radon variability studies in the Underground Low Background Laboratory in the Institute of Physics, Belgrade [4, 5]. Several climate variables: air temperature, pressure, and humidity were considered. Further advance was made by using all the publicly available climate variables monitored by nearby automatic meteorological station. In order to analyze the dependence of radon variation on multiple variables, multivariate analysis needs to be used. The goal was to find an appropriate method, out of the wide spectrum of multivariate analysis methods that are developed for the analysis of data from high-energy physics experiments, to analyze the measurements of variations of radon concentrations in indoor spaces. Previous

\* Corresponding author; e-mail: [udovicic@ipb.ac.rs](mailto:udovicic@ipb.ac.rs)

analysis were done using the maximum of 18 climate parameters and use and comparison of 8 different multivariate methods. In this paper the number of variables is reduced to the most important ones and new derived variables, like vapor pressure, simple modeled solar irradiance and simple modeled precipitation, which were introduced in the multivariate analysis.

## INDOOR RADON MEASUREMENTS METHODS

Depending on the integrated measurement time, methods of measurement of the indoor radon concentrations may be divided into long-term and short-term ones. The device for the performed short-term radon measurements is SN1029 radon monitor (manufactured by the Sun Nuclear Corporation, NRSB approval-code 31822) with the following characteristics: the measurement range from  $1 \text{ Bqm}^{-3}$  to  $99.99 \text{ kBqm}^{-3}$ , accuracy equal to  $\pm 25 \%$ , sensitivity of 0.16 counts hour per  $\text{Bqm}^{-3}$ . The device consists of two diffused junction photodiodes as the radon detector which is furnished with sensors for temperature, barometric pressure, and relative humidity. The sampling time was set to 2 h. The method for Charcoal Canister used is: EERF Standard Operating Procedures for Radon-222 Measurement Using Charcoal Canisters [6], also used by major laboratories which conduct radon measurements in Serbia [7]. Exposure time of the charcoal canisters was 48 h. The connection between short term and long term measurements has attracted some interest previously [8].

The family house, selected for the measurements and analysis of variations of radon concentrations, is a typical house in Belgrade residential areas, with requirement of existence of cellar. House is built on limestone soil. Radon measurements were carried out in the living room of the family house, which is built of standard materials (brick, concrete, mortar) and isolated with styrofoam. During the period of measurements (winter-summer 2014, 2015, and 2016), the house was naturally ventilated and air conditioning was used in heating mode at the beginning of the measurement period. During the winter period measurements, the electrical heating was used in addition to air conditioning. Measured radon concentrations, room temperature ( $T_{id}$ ), atmospheric pressure ( $P_{id}$ ) and relative humidity ( $H_{id}$ ) inside the house, were obtained using radon monitor. Values of meteorological variables, in the measurement period, were obtained from an automatic meteorological station, located near the house in which the measurement was performed. We used the following meteorological variables: external air temperature ( $T$ ), also at height of 5cm, pressure ( $P$ ) and humidity ( $H$ ), solar irradiation, wind speed, precipitation, temperature of the soil at depths of 10 cm, 20 cm and 50 cm. The natural ventilation routine was not monitored. Since the ventilation is of

crucial importance for the level of radon indoors [9], Multivariate regression analysis was used mainly for winter periods.

## MULTIVARIATE REGRESSION ANALYSIS

In many fields of physics, especially in high-energy physics, there is the demand for detailed analyses of a large amount of data. For this purpose, the data analysis environment ROOT [10], is developed. ROOT is modular scientific software framework, which provides all the functionalities needed to deal with big data processing, statistical analysis, visualization and storage. A specific functionality gives the developed Toolkit for Multivariate Analysis (TMVA) [11]. The TMVA provides an environment for the processing, parallel evaluation and application of multivariate regression techniques.

TMVA is used to create, test and apply all available regression multivariate methods, implemented in ROOT, in order to find methods which are the most appropriate and yield maximum information on the dependence of indoor radon concentrations on the multitude of meteorological variables. Regression methods are used to find out which regression method can, if any, on the basis of input meteorological variables only, give an output that would satisfactorily close match the observed variations of radon concentrations. The output of usage of multivariate regression analysis methods has mapped functional behavior, which can be used to evaluate the measurements of radon concentrations using input meteorological variables only. All the methods make use of training events, for which the desired output is known and is used for training of Multivariate regression methods, and test events, which are used to test the MVA methods outputs.

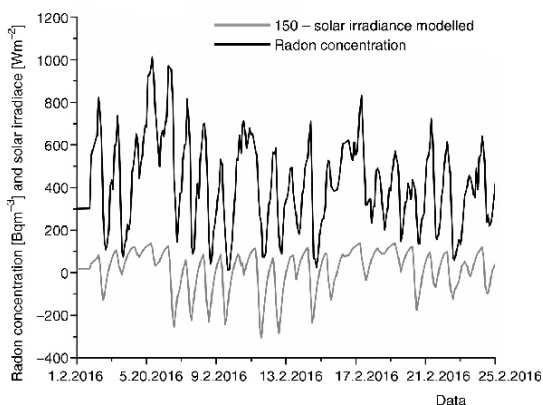
## RESULTS

Measurements were performed during February and July in 2014, 2015, and 2016 using radon monitor and charcoal canister measurements. The descriptive results are summarized in tab. 1. The measurements using radon monitor and charcoal canisters are in good agreement.

Previous work done by researchers from the Low Background Laboratory, Institute of Physics, Belgrade, using the MVA analysis in search of connections between radon concentration and meteorological variables, included only one period of measurement, February or July 2014 [4]. Now the MVA analysis is using all the measured data February/July 2014-2016. New variables introduced in MVA analysis are modeled solar irradiance, modeled precipitation and vapor

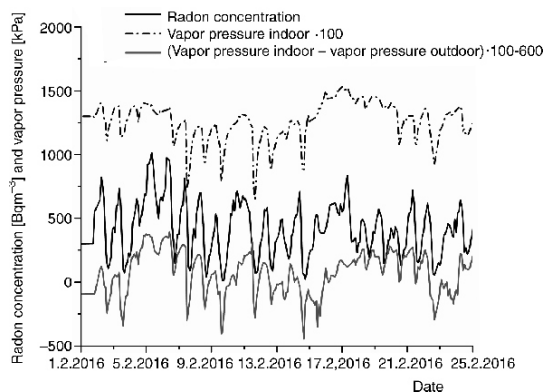
**Table 1. Descriptive results of February and July 2014, 2015, and 2016 measurements, using radon monitor and charcoal canisters (only in February)**

| Results of measurements  | 2014          |               | 2015          |               | 2016          |               |
|--|---------------|---------------|---------------|---------------|---------------|---------------|
|  | Feb.          | July          | Feb.          | July          | Feb.          | July          |
| Minimal radon activity using radon monitor [ $\text{Bqm}^{-3}$ ]                                 | 15            | 0             | 28            | 0             | 12            | 3             |
| Maximal radon activity using radon monitor [ $\text{Bqm}^{-3}$ ]                                 | 1000          | 286           | 915           | 88            | 1013          | 262           |
| Median radon activity using radon monitor [ $\text{Bqm}^{-3}$ ]                                  | 418           | 25            | 524           | 22            | 412           | 28            |
| Arithmetic mean of radon activity using radon monitor (standard deviation) [ $\text{Bqm}^{-3}$ ] | 402<br>(216)  | 40<br>(41)    | 508<br>(207)  | 27<br>(18)    | 423<br>(214)  | 39<br>(32)    |
| Room temperature using radon monitor (standard deviation) [ $^{\circ}\text{C}$ ]                 | 20.4<br>(0.8) | 24.7<br>(0.9) | 21.2<br>(0.6) | 24.9<br>(0.8) | 22.3<br>(0.6) | 24.6<br>(0.8) |
| Relative humidity using radon monitor (standard deviation) [%]                                   | 67.4<br>(5.7) | 67.8<br>(4.8) | 68.2<br>(4.8) | 51.5<br>(4.7) | 64.0<br>(6.4) | 58.9<br>(7.5) |
| Radon activity using charcoal canister (standard deviation) [ $\text{Bqm}^{-3}$ ]                | 432<br>(10)   | /             | 518<br>(6)    | /             | 407<br>(5)    | /             |

**Figure 1. Modeled solar irradiance in comparison with measured radon concentration during February 2016**

pressure. In order to make use of intensity of solar irradiance during the whole day and night, the solar irradiance is modeled so that it includes 80 % of solar irradiance value from the previous measurement (previous hour) with addition of solar irradiance value for the actual hour of measurement (fig. 1). The value of 80 % is chosen so that the modeled solar irradiation has the best correlation with the radon measurements. Similar model of precipitation was used in this analysis. The next new variable is vapor pressure. The vapor pressure variable is calculated using the slope  $s(T)$ , of the relationship between saturation vapor pressure and air temperature and is given by [12, 13], so that the vapor pressure equals relative humidity times saturation vapor pressure, fig. 2.

Before the start of training of Multivariate regression methods using TMVA toolkit in ROOT, the description of input meteorological variables is performed, mainly by looking into inter-correlations of input variables and their connections with the measured radon concentrations. The MVA is using all the measured data. Table 2 presents the meteorological variables and their module value of correlation with the measured radon concentrations (target), which is indicative in finding linear dependence of radon mea-

**Figure 2. Vapor pressure in comparison with measured radon concentration during February 2016**

surements and input variables. The second column in tab. 2 presents us with correlation ratio values which indicate if there are some functional dependence (not only linear) between input variables and radon concentration, and the last column presents the mutual information which indicates if there is a non-functional dependence of input variables and radon measurements [11].

From tab. 2 it can be noticed that linear correlated values are not the only ones which can be used in MVA analysis, for example variable solar irradiance has high mutual information with the radon measurements.

In the data preparation for MVA training the whole dataset is consisting of many events. An event includes time of measurement, radon measurement and meteorological variables. The dataset is randomly split in two halves, one half of the events will be used for training of multivariate regression methods, and the other half of events for testing of methods, mainly to compare the measured and MVA evaluated values for radon concentration.

It turns out that the methods best suited for our purpose is the Boosted Decision Trees (BDT) method. This means that BDT gives the smallest difference be-

**Table 2. Input variable rank and values for correlation, correlation ratio and mutual information, all with the measured radon concentrations (target) for February and July 2014-2016 measurements**

| Variable                             | Correlation with target |       | Correlation ratio |       | Mutual information |       |
|--------------------------------------|-------------------------|-------|-------------------|-------|--------------------|-------|
|                                      | Rank                    | Value | Rank              | Value | Rank               | Value |
| Soil temperature depth 20 cm [°C]    | 1                       | 0.87  | 1                 | 0.60  | 13                 | 1.48  |
| Soil temperature depth 50 cm [°C]    | 2                       | 0.86  | 2                 | 0.57  | 14                 | 1.31  |
| Soil temperature depth 10 cm [°C]    | 3                       | 0.82  | 3                 | 0.54  | 9                  | 1.84  |
| Temperature outdoor [°C]             | 4                       | 0.82  | 5                 | 0.53  | 8                  | 1.85  |
| Vapor indoor – vapor od [mbar]       | 5                       | 0.81  | 9                 | 0.41  | 11                 | 1.73  |
| Temperature od – temperature id [°C] | 6                       | 0.80  | 4                 | 0.53  | 6                  | 1.92  |
| Temperature height 5 cm [°C]         | 7                       | 0.77  | 8                 | 0.48  | 7                  | 1.91  |
| Vapor od [mbar]                      | 8                       | 0.76  | 10                | 0.41  | 5                  | 1.92  |
| Temperature id [°C]                  | 9                       | 0.75  | 7                 | 0.49  | 17                 | 1.16  |
| Solar irradiance [ $Wm^{-2}$ ]       | 10                      | 0.61  | 6                 | 0.50  | 2                  | 2.23  |
| Humidity indoor [%]                  | 11                      | 0.45  | 11                | 0.26  | 1                  | 2.26  |
| Humidity outdoor [%]                 | 12                      | 0.31  | 13                | 0.20  | 10                 | 1.76  |
| Air pressure outdoor [mbar]          | 13                      | 0.27  | 17                | 0.07  | 12                 | 1.55  |
| Wind speed [ $ms^{-1}$ ]             | 14                      | 0.22  | 16                | 0.01  | 16                 | 1.28  |
| Air pressure indoor [mbar]           | 15                      | 0.17  | 18                | 0.04  | 15                 | 1.31  |
| Humidity od – Humidity id [%]        | 16                      | 0.10  | 14                | 0.19  | 4                  | 2.11  |
| Precipitation [ $Lm^{-2}$ ]          | 17                      | 0.01  | 15                | 0.19  | 18                 | 1.13  |
| Vapor indoor [mbar]                  | 18                      | 0.002 | 12                | 0.02  | 3                  | 2.17  |

tween the measured radon concentration from test sample and the evaluation of value of radon concentration using input variables only. This can be seen in fig. 3, which shows the distribution of BDT and BDTG regression method outputs (evaluated values) in comparison with the measured radon concentration during February 2016.

Since TMVA has 12 different regression methods implemented, only some of those will give useful results when evaluating the radon concentration measurements. Table 4 summaries the results of MVA analysis. It shows the MVA methods RMS of difference of evaluated and measured radon concentration. Also, tab. 4 shows the mutual information of measured and MVA evaluated radon concentration. Besides

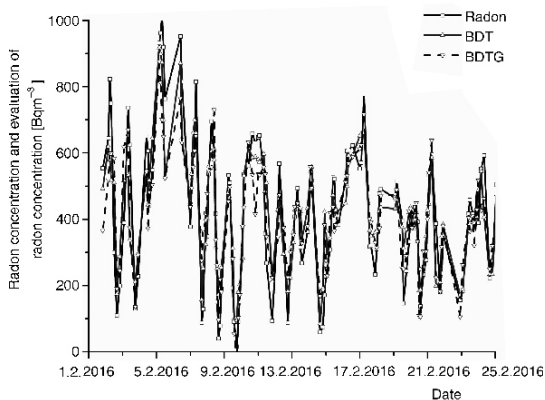


**Figure 3. Comparison of MVA evaluated radon concentration and measured one from the test sample of events during February 2016**

BDT, the Multi-Layer Perceptron (MLP) [10], an implementation of Artificial Neural Network multivariate method, also gives good results.

The MVA regression analysis results in mapped functional behavior and, as opposed to possible existence of theoretical modeling, which is independent of the number of measurements, MVA depends on the number of events. More events, the better mapped function we get as a result. In this sense, if the number of measurements is not great, multivariate analysis can be used only as help, to indicate which variables are more important to be used in theoretical modeling, for comparison of mapped and modeled functions, and modeled function test.

## CONCLUSION

Indoor radon variation at one location in the same periods (February and July), was investigated for three years. Long-term indoor radon measurements show intense seasonal variation. The results obtained with different measuring methods are in good agreement. The radon behavior in the house is almost the same and shows good reproducibility year by year. The small variations in the year by year dynamics are originated mostly from the variations in meteorological variables during winter seasons and mostly due to ventilation habits during summer season. Ventilation habits were not monitored nor taken into account in MVA regression analysis. The preliminary results using multivariate analysis methods in TMVA are shown. Main output of Multivariate regression analy-

**Table 3. Input variable correlation with the measured radon concentrations for February and July 2016**

| Correlation with target              |       |                                      |       |
|--------------------------------------|-------|--------------------------------------|-------|
| February 2016                        |       | July 2016                            |       |
| Variable                             | Value | Variable                             | Value |
| Vapor id-vapor od [mbar]             | 0.58  | Soil temperature depth 20 cm [°C]    | 0.46  |
| Humidity id [%]                      | 0.54  | Soil temperature depth 50 cm [°C]    | 0.42  |
| Vapor id [mbar]                      | 0.52  | Solar irradiance                     | 0.32  |
| Solar irradiance [Wm <sup>-2</sup> ] | 0.48  | Temperature id [°C]                  | 0.30  |
| Temperature od – temperature id [°C] | 0.46  | Soil temperature depth 10 cm [°C]    | 0.24  |
| Temperature [°C]                     | 0.44  | Temperature od [°C]                  | 0.21  |
| Soil temperature depth 10 cm [°C]    | 0.43  | Humidity od [%]                      | 0.20  |
| Soil temperature depth 20 cm [°C]    | 0.42  | Humidity id [%]                      | 0.19  |
| Humidity [%]                         | 0.38  | Air pressure [mbar]                  | 0.17  |
| Temperature height 5 cm [°C]         | 0.32  | Precipitation [Lm <sup>-2</sup> ]    | 0.17  |
| Temperature id [°C]                  | 0.29  | Temperature od – temperature id [°C] | 0.16  |
| Air pressure od [mbar]               | 0.23  | Air pressure_id [mbar]               | 0.16  |
| Air pressure id [mbar]               | 0.21  | Humidity od – humidity id [%]        | 0.14  |
| Soil temperature depth 50 cm [°C]    | 0.20  | Wind speed [ms <sup>-2</sup> ]       | 0.13  |
| Precipitation [Lm <sup>-2</sup> ]    | 0.19  | Temperature height 5 cm [°C]         | 0.12  |
| Humidity od – humidity id [%]        | 0.15  | Vapor id [mbar]                      | 0.06  |
| Vapor od [mbar]                      | 0.08  | Vapor od [mbar]                      | 0.03  |
| Wind speed [ms <sup>-1</sup> ]       | 0.05  | Vapor id – vapor od [mbar]           | 0.02  |

**Table 4. RMS of MVA method's evaluation error and mutual information; February/July 2014-2016**

| MVA method | RMS [Bqm <sup>-3</sup> ] | Mutual information |
|------------|--------------------------|--------------------|
| BDT        | 85.5                     | 1.477              |
| BDTG       | 92.1                     | 1.614              |
| MLP        | 101                      | 1.401              |

sis is the initial version of *mapped* function of radon concentration dependence on multitude of meteorological variables. Simplification of MVA methods can be made by choosing only the most important input variables and exclude the other variables.

#### ACKNOWLEDGEMENTS

The authors acknowledge the financial support of the Ministry of Science, Technology and Development of Serbia within the projects: Nuclear Methods Investigations of Rare Processes and Cosmic Rays (grant number 171002) and Biosensing Technologies and Global System for Continuous Research and Integrated Management (grant number 43002).

#### AUTHORS' CONTRIBUTIONS

The idea for this paper came as a result of discussions of V. I. Udovičić, R. M. Banjanac, D. R. Joković, A. L. Dragić, and D. M. Maletić. Gathering climate data and MVA analysis was done by D. M. Maletić and V. I. Udovičić. Performed indoor radon measurements were done by V. I. Udovičić and S. M. Forkapić. Writing of the paper was done by D. M. Maletić and V. I. Udovičić. A. L. Dragić gave idea about using MVA

methods in cosmic and radon measurements. N. B. Veselinović and M. R. Savić analyzed and validated climate data. J. Z. Živanović helped with MVA analysis. D. R. Joković helped with data analysis and paper technical preparation.

#### REFERENCES

- [1] Collignan, B., *et al.*, Development of a Methodology to Characterize Radon Entry in Dwellings, *Building and Environment*, 57 (2012), Nov., pp. 176-183
- [2] Li, F., Baixeras, C., The RAGENA Dynamic Model of Radon Generation, Entry and Accumulation Indoors, *Science of the Total Environment*, 307 (2003), 1-3, pp. 55-69
- [3] Jelle, B. P., *et al.*, Development of a Model for Radon Concentration in Indoor Air, *Science of the Total Environment*, 416 (2012), Jan., pp. 343-350
- [4] Maletić, D., *et al.*, Comparison of Multivariate Classification and Regression Methods for Indoor Radon Measurements, *Nucl Technol Radiat*, 29 (2014), 1, pp. 17-23
- [5] Udovičić, V., *et al.*, Radon Problem in an Underground Low-Level Laboratory, *Radiation Measurements*, 44 (2009), 9-10, pp. 1009-1012
- [6] EPA 520/5-87-005, Gray D.J, Windham S.T, United States Environmental Protection Agency, Montgomery, 1987
- [7] Živanović, M. Z., *et al.*, Radon Measurements with Charcoal Canisters, *Nucl Technol Radiat*, 31 (2016), 1, pp. 65-72
- [8] Stojanovska, Z., *et al.*, Prediction of Long-Term Indoor Radon Concentrations Based on Short-Term Measurements, *Nucl Technol Radiat*, 32 (2017), 1, pp. 77-84
- [9] Nikolić, M. D., *et al.*, Modelling Radiation Exposure in Homes from Siporex Blocks by Using Exhalation Rates of Radon, *Nucl Technol Radiat*, 30 (2015), 4, pp. 301-305
- [10] Brun, R., Rademakers, F., ROOT – An Object Oriented Data Analysis Framework, *Nucl. Inst. Meth. in Phys. Res.*, A 389 (1997), 1-2, pp. 81-86

- [11] Hoecker, A., *et al.*, TMVA – Toolkit for Multivariate Data Analysis, PoS ACAT 040, arXiv:physics/070303, 2007
- [12] Murray, F. W., On the Computation of Saturation Vapor Pressure, *J. Applied Meteorology*, 6 (1967), 1, pp. 203-204

- [13] Tetens, O., About Some Meteorological Aspects (in German), *Z. Geophys*, 6 (1930), pp. 207-309

Received on October 6, 2018

Accepted on June 8, 2018

---

**Владимир И. УДОВИЧИЋ, Димитрије М. МАЛЕТИЋ, Радомир М. БАЊАНАЦ,  
Дејан Р. ЈОКОВИЋ, Александар Л. ДРАГИЋ, Никола Б. ВЕСЕЛИНОВИЋ,  
Јелена З. ЖИВАНОВИЋ, Михаило Р. САВИЋ, Софија М. ФОРКАПИЋ**

**СТУДИЈА СЛУЧАЈА ВИШЕГОДИШЊЕ ВАРИЈАБИЛНОСТИ РАДОНА  
У ПОРОДИЧНОЈ КУЋИ У СРБИЈИ**

Понашање радона у затвореном простору има сложену динамику због утицаја великог броја различитих параметара који утичу на његову варијабилност: метеоролошких (температура, притисак и релативна влажност), концентрације аеросола, брзине размене између унутрашњег и спољашњег ваздуха, грађевинских материјала и животних навика. Као резултат, концентрација радона у затвореним просторијама показује варијацију, уз стандардну периодичност од једног дана и једне године. Годишња варијабилност је добро позната сезонска варијација концентрације радона. Посебно је интересантно пратити вишегодишње варијације концентрације радона на истој мерној локацији и временском периоду, пре свега због процене индивидуалних годишњих доза од изложености радону. У типичној породичној кући у Србији извршена су дуготрајна мерења радона у дневном боравку. Мерења су рађена током 2014, 2015, и 2016. године, у фебруару и јулу, сваке године. Коришћене су следеће мерне технике: активна и метода коришћења угљених канистера. Добијени резултати анализирани су коришћењем мултиваријантне регресионе анализе.

*Кључне речи: варијабилности радона, мултиваријантна регресиона анализа, радон у затвореним просторијама, вишегодишње мерење радона*



## First steps towards national radon action plan in Serbia

Vladimir Udovičić,  
Dimitrije Maletić,  
Maja Eremić Savković,  
Gordana Pantelić,  
Predrag Ujić,  
Igor Čeliković,  
Sofija Forkapić,  
Dragoslav Nikezić,  
Vladimir M. Marković,  
Vesna Arsić,  
Jovana Ilić

**Abstract.** Radon problem has a special attention in many countries in the world and the most of them have established national radon programmes. The radon issues in Serbia have not been approached in a systematic and organized way. Currently, there are many research groups and institutions working in radon field, and it is a good basis to integrate all these activities into a comprehensive national programme to define the strategic objectives and action plan for the next few years. Also, Serbia as a candidate for membership in the EU is obliged to harmonize its legislation, including the field of radiation protection in which the radon issues has an important role. In this report, a brief history of radon research, present status and plans for the future activity on radon issues in Serbia are presented. Regarding the long-term plans, the establishment and implementation of the Radon Action Plan with the primary goal of raising awareness about the harmful effects of public exposure to radon and implementing a set of measures for its reduction. In that sense, the synergy between the national, regional and local organizations responsible for public health and radiation protection must be achieved.

**Key words:** radon • action plan • survey

V. Udovičić✉, D. Maletić  
Institute of Physics Belgrade,  
University of Belgrade,  
118 Pregrevica Str., 11080 Belgrade, Serbia,  
E-mail: udovicic@ipb.ac.rs

M. Eremić Savković  
Serbian Radiation Protection and Nuclear Safety Agency,  
Belgrade, Serbia

G. Pantelić, P. Ujić, I. Čeliković  
Vinča Institute of Nuclear Sciences,  
University of Belgrade,  
Belgrade, Serbia

S. Forkapić  
Department of Physics,  
Faculty of Science,  
University of Novi Sad,  
Novi Sad, Serbia

D. Nikezić, V. M. Marković  
Faculty of Science,  
University of Kragujevac,  
Kragujevac, Serbia

V. Arsić, J. Ilić  
Serbian Institute of Occupational Health  
“Dr Dragomir Karajović”,  
Belgrade, Serbia

Received: 4 January 2016  
Accepted: 31 March 2016

### Introduction

Radon is a noble, naturally occurring radioactive gas. Radon contribute to almost 50% of the overall high-effective annual dose to the population received from all sources of natural radioactivity. Harmful effects of radon has been proven in a large number of epidemiological studies [1]. The latest recommendation of the International Atomic Energy Agency (IAEA) [2] and Directive EC [3] relating to the field of radiation protection, radon problem got more space and importance because the World Health Organization (WHO) has identified radon as the second biggest cause of cancer lung [4]. In addition, radon is included in the ranks of major pollutants of indoor air [5]. Current knowledge about the mechanisms by which radon is harmful to human health are reflected primarily in harmful, radioactive radon progeny fact. In fact, radon progenies are attached to the aerosol particles from the air and such radioactive particles enter the body through inhalation. These radioactive aerosols deposited in the lungs emit alpha radiation. The harmful activity can be seen in disorders of the cellular structure of DNA, causing the development of cancer cells. Consequently, radon problem has been addressed seriously, and in a number of countries, national radon programme is established, which is basically a multidisciplinary nature and requires the involve-

ment of a large number of experts, researchers involved in radiation physics, geo sciences, chemistry, biology to specialist in various fields of medicine. In that sense, the group of radon professionals decide to start working on establishing and developing national radon programme in Serbia. In this paper, a brief history of radon research, present status and plans for the future activity on radon issues in Serbia are presented.

### International framework

The regulations related to the exposure of the population to radon and its progenies are different worldwide. Based on the researches and a large number of epidemiological studies done in the recent past, the new standards and recommendations have to be incorporated into the national legislation regarding radon issues. Basically, a new approach to the radon issue is to introduce the concept of the reference level (not as strict boundaries between safe and dangerous concentrations of radon, but the annual average indoor radon concentration above which it is necessary to take measures to reduce radon). It differs from action level (the radon concentration above which, if it is found that the measured concentration is greater than defined, gives recommendations to take measures for its reduction). The new concept is incorporated in two new documents. One is developed at the International Atomic Energy Agency (IAEA) [2]. In this new BSS (international Basic Safety Standards), radon is placed in several topics, but the most important is requirements of 50 (Requirement 50: Public exposure because of radon indoors). It defines the reference level, in dwellings of high occupational factors, which must not exceed  $300 \text{ Bq}\cdot\text{m}^{-3}$ . Assuming equilibrium factor for radon 0.4 and the annual occupational factors of 7000 h, the reference level of  $300 \text{ Bq}\cdot\text{m}^{-3}$  corresponds to an annual effective dose of 10 mSv, with dose conversion factor (DCF) of 7.5 mSv per WLM (working level month). The request 52 (Requirement 52: Exposure in workplaces) defines the reference level for radon in workplaces of  $1000 \text{ Bq}\cdot\text{m}^{-3}$ . As the occupation factor for 2000 h with the same factor to balance radon of 0.4 leads to the same effective annual dose of 10 mSv. Important conclusions are based on the collected data and performed radon risk maps, the country has to decide and implement adequate control of the indoor radon, to inform the public and other stakeholders and, finally, to establish and implement Radon Action Plan (RAP).

The second document is EU Directive 2013/59 [3]. In the article 74: Indoor exposure to radon, writes the similar as in the new BSS, accept that the reference level shall not exceed  $300 \text{ Bq}\cdot\text{m}^{-3}$  for the all indoor environment, living and workplaces. Article 103 defines RAP to be developing in member states: The action plan shall take into account the issues set out in Annex XVIII and be updated on a regular basis. Annex XVIII defined 14 items to consider in preparing the national RAP. In the case of Serbia, the first steps towards RAP are described in the next section.

### National radon action plan in Serbia

Serbia did not have a systematic approach to the radon problem. In this sense, there were individual initiatives and research activities dealing with radon:

University of Novi Sad, Faculty of Science, Department of Physics, Chair of Nuclear Physics, Novi Sad

Radon mapping of Autonomous Province of Vojvodina [6], long-term and short-term measurements of radon concentration in soil, water and air using passive devices, active device RAD7, exhalation and diffusion measurements [7], charcoal canisters with gamma spectrometric analysis [8].

University of Belgrade, Vinča Institute of Nuclear Sciences, ECE Lab Belgrade

#### *Department for Nuclear and Plasma Physics*

Mapping radon and thoron throughout south-eastern Serbia, Kosovo and Metohija parts of western Serbia [9, 10] by using different passive devices; electrochemical etch track detectors in a specially designed and built in laboratory [11]; developing method for radon and thoron exhalation from building material [12]; radon measurement campaigns in the schools and houses in the Sokobanja municipality [13].

#### *Radiation and Environmental Protection Department*

Active charcoal detectors are used for testing the concentration of radon in dwellings. The method of measurement is based on radon adsorption on coal and measurement of gamma radiation of radon daughters according to US EPA protocol. Based on this EPA procedure and national and international intercomparison, the laboratory developed a set of procedures for charcoal detector exposure and measurement [14, 15].

University of Belgrade, Institute of Physics Belgrade, Low-Background Laboratory for Nuclear Physics

Radon monitoring in the underground low-background laboratory with the passive and active devices [16]; radon laboratory for chemical etching of the track detectors and automatic counting of the tracks by optical microscopy [17]; modelling of the indoor radon behaviour [18].

Institute of Occupational Health of Serbia  
“Dr Dragomir Karajović”, Center for Radiological Protection, Belgrade

Radon measurements using charcoal canisters with gamma spectrometric analysis, radon monitoring in

schools and kindergartens in the city of Belgrade from 1991 [19] and radon measurements campaigns in schools and kindergartens in Belgrade from 2010 [20].

**University of Kragujevac, Faculty of Science  
Kragujevac, Institute of Physics**

Radon measurement using passive devices with chemical treatment of the track detectors and automatic scanning of the developed detectors; modelling of the behaviour of indoor radon [21]; dosimetric modelling of the effects of the inhalation of radon and its progeny in the lung [22].

Based on the great experience of research related to radon, the group of radon professionals organized Radon Forum in May 2014 and made a decision to start work on RAP in Serbia. The responsibility for the establishment and implementation of RAP is on national regulatory body: Serbian Radiation Protection and Nuclear Safety Agency (SRPNA). We started with Internet radon forum ([www.cosmic.ipb.ac.rs/radon\\_forum](http://www.cosmic.ipb.ac.rs/radon_forum)), which provides an opportunity for radon professionals in Serbia to meet and discuss radon activities and plans. Also, SRPNA formed a 'radon working group' that will manage RAP. The organization chart of the institutions involved in RAP is shown in Fig. 1.

- Short-term plans (to the end of 2015) include
- carrying out initial representative national indoor radon survey for this purpose,
  - developing communication strategy (first basic information leaflet on radon to accompany the measurement explaining the purpose of the measurement, Internet site: <http://cosmic.ipb.ac.rs/radon/index.html>; public relation; etc.).

**First national indoor radon survey in Serbia**

As a first step in RAP, it is the national radon survey in Serbia planned to be done in 2015. In the cooperation with IAEA, SRPNA through radon working

group made the design of the first national radon survey in Serbia. It is well known that regarding the objective of the indoor radon survey, there are two types of survey:

- population-weighted survey by measuring indoor radon levels in randomly selected homes (to estimate the distribution of radon public exposures),
- geographically based survey where homes are randomly selected to obtain a minimum density of measurements per area unit chosen, e.g., a grid square, an administrative unit (to identify radon prone areas, radon map).

Every radon survey needs to check the representativeness (e.g. compare certain parameters in the actual sample with corresponding values in the last census). A carefully designed survey can, in principle, meet the requirements and objectives of both the types of surveys. In the case of Serbia, we choose a stratified (target population is partitioned into separated groups – STRATA) sampling design. We defined STRATA according to the administrative divisions of Serbia into districts.

In principle, our design model can be described as follows:

- SRPNA, in cooperation with the IAEA through the national project SRB9003 – Enhancing the Regulatory Infrastructure and Legislative System,
- Expert mission on National Radon Trial Survey and Raising Awareness of Key Stakeholders held in SRPNA, Belgrade, 2–4 February 2015,
- Equipment: Leasing of 6000 track-etched indoor radon detectors; the distribution of detectors across the Serbian territory should be the responsibility of SRPNA,

and relevant ministries began with the national programme for indoor radon measurements in dwellings and flats in Serbia. The aim of this programme is to determine the radiological exposure risk to radon in residential areas because of the inhalation of this gas as well as to locate areas in Serbia with high concentrations, areas with high radon potential. Within the working group on radon, the division of

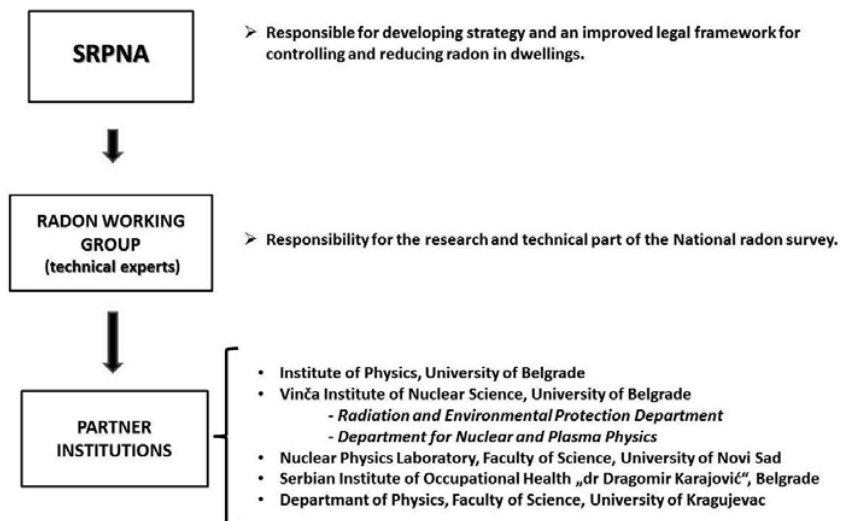


Fig. 1. Organization chart of the institutions involved in RAP.

responsibilities of individual institutions in a given set of administrative regions was established. All owners of houses and apartments (who wish to participate in the project), with the aim of determining the concentration of radon, filled predefined questionnaire on the Web site dedicated to radon in Serbia (<http://cosmic.ipb.ac.rs/radon/index.html>). In this way, they expressed interest to participate in the project. In total, 6000 detectors have been distributed during October 2015 and will be exposed in houses and apartments for six months (till April 2016). Afterwards, the detectors will be sent to an authorized laboratory to be processed, and consequently, we should get data for the first national map radon risk in Serbia. The measurement results will be presented to the owners of houses and apartments that are used for the measurement. Based on these results, in cases where radon concentration exceeds current intervention level of 200 Bq·m<sup>-3</sup> for new developments or 400 Bq·m<sup>-3</sup> for existing facilities, the whole set of measures that could result in a reduction of the radon concentrations and thus reduce the risk of getting lung cancer will be recommended. Additionally, all data collected for the whole of Serbia will enable the determination of the national reference level for radon. During the realization of the national programme for indoor radon measurements, we plan to perform communication strategy (first basic information leaflet on radon to accompany the measurement explaining the purpose of the measurement, internet site, public relation, public education, etc.).

## Conclusions

World Health Organization declared radon as the second most important cause of getting lung cancer. Radon problem being addressed seriously, and in a number of countries, there are established national radon programme. Serbia started work on RAP in 2014, with the first step of preparing, and performed the national indoor radon survey in Serbia, planned to be done in 2015. The responsibility for the establishment and implementation of RAP is on national regulatory body: Serbian Radiation Protection and Nuclear Safety Agency. The results of national radon survey serves to evaluate the existing exposure situation and to define the next steps in establishing and developing RAP in Serbia. Also, the Serbian experience in efforts to have systematic approach to the radon issues, described in this paper, may be useful to the other countries who wish to establish their own RAP.

## References

- Darby, S., Hill, D., Auvinen, A., Barros-Dios, J. M., Baysson, H., Bochicchio, F., Deo, H., Falk, R., Forastiere, F., Hakama, M., Heid, I., Kreienbrock, L., Kreuzer, M., Lagarde, F., Mäkeläinen, I., Muirhead, C., Oberaigner, W., Pershagen, G., Ruano-Ravina, A., Ruostenoja, E., Schaffrath Rosario, A., Tirmarche,

- M., Tomáscaronek, L., Whitley, E., Wichmann, H.-E., & Doll, R. (2005). Radon in homes and risk of lung cancer: collaborative analysis of individual data from 13 European case-control studies. *Brit. Med. J.*, 330, 223–227.
- International Atomic Energy Agency. (2011). *Radiation protection and safety of radiation sources: International basic safety standards Interim edition. General safety requirements Part 3*. Vienna: IAEA. Retrieved from [http://www-pub.iaea.org/MTCD/publications/PDF/p1531interim\\_web.pdf](http://www-pub.iaea.org/MTCD/publications/PDF/p1531interim_web.pdf).
- Council of the European Union. (2014). *Council Directive 2013/59/EURATOM of 5 December 2013 laying down basic safety standards for protection against the dangers arising from exposure to ionising radiation, and repealing Directives 89/618/Euratom, 90/641/Euratom, 96/29/Euratom, 97/43/Euratom and 2003/122/Euratom*. (Official Journal of the European Union 2014; L13). Retrieved from <http://www.srbatom.gov.rs/srbatom/doc/eu-direktive/2013%2059%20eng.pdf>.
- World Health Organization. (2009). *WHO handbook on indoor radon: a public health perspective*. Retrieved from [http://www.who.int/ionizing\\_radiation/env/radon/en/index1.html](http://www.who.int/ionizing_radiation/env/radon/en/index1.html).
- World Health Organization. (2010). *WHO guidelines for indoor air quality: selected pollutants*. Retrieved from <http://www.who.int/indoorair/publications/9789289002134/en/index.html>.
- Forkapić, S., Bikit, I., Slivka, J., Čonkić, Lj., Vesković, M., Todorović, N., Varga, E., Mrda, D., & Hulber, E. (2006). Indoor radon in rural dwellings of the South-Pannonian region. *Radiat. Prot. Dosim.*, 123(3), 378–383.
- Nikolov, J., Todorovic, N., Bikit, I., Petrovic Pantic, T., Forkapić, S., Mrda, D., & Bikit, K. (2014). Radon in thermal waters in South-East part of Serbia. *Radiat. Prot. Dosim.*, 160(1/3), 239–243.
- Todorović, N., Bikit, I., Vesković, M., Krmar, M., Mrda, D., Forkapić, S., Hansman, J., Nikolov, J., & Bikit, K. (2014). Radioactivity in the indoor building environment in Serbia. *Radiat. Prot. Dosim.*, 158(2), 208–215.
- Žunić, Z. S., Yarmoshenko, I. V., Veselinović, N., Zhukovsky, M. V., Ujić, P., Čeliković, I., McLaughlin, J. P., Simopoulos, S. E., Birovljev, A., Fujimoto, K., Paridaens, J., Trotti, F., Tokonami, S., Olko, P., Kozak, K., Bochicchio, F., Ramola, R., Mietelski, J. W., Jakupi, B., Milić, G., Ciotoli, G., Kelleher, K., Budzanowski, M., Sahoo, S. K., Vanmarcke, H., & Waligorski, M. P. R. (2009). Identification and assessment of elevated exposure to natural radiation in Balkan region (Serbia). *Radioprotection*, 44, 919–925.
- Žunić, Z. S., Janik, M., Tokonami, S., Veselinović, N., Yarmoshenko, I. V., Zhukovsky, M., Ishikawa, T., Ramola, R. C., Ciotoli, G., Jovanović, P., Kozak, K., Mazur, J., Celiković, I., Ujić, P., Onischenko, A., Sahoo, S. K., & Bochicchio, F. (2009). Field experience with soil gas mapping using Japanese passive radon/thoron discriminative detectors for comparing high and low radiation areas in Serbia (Balkan region). *J. Radiat. Res.*, 50(4), 355–361.
- Zunic, Z. S., Ujić, P., Nadderđ, L., Yarmoshenko, I. V., Radanović, S. B., Komatina Petrović, S., Čeliković, I., Komatina, M., & Bossew, P. (2014). High variability of indoor radon concentrations in uraniumiferous bedrock areas in the Balkan region. *Appl. Radiat. Isot.*, 94, 328–337.
- Ujic, P., Čeliković, I., Kandić, A., & Žunić, Z. (2008). Development of method for radon/thoron exhalation measurement. *Radiat. Meas.*, 43(8), 1396–1401.

13. Bochicchio, F., Žunić, Z. S., Carpentieri, C., Antignani, S., Venoso, G., Carelli, V., Cordedda, C., Veselinović, N., Töllefsen, T., & Bossew, P. (2014). Radon in indoor air of primary schools: a systematic survey to evaluate factors affecting radon concentration levels and their variability. *Indoor Air*, 24, 315–326.
14. Pantelić, G., Živanović, M., Eremić Savković, M., & Forkapić, S. (2013). Radon concentration inter-comparison in Serbia. In Ž. Knežević, M. Majer, & I. Krajcar-Bronić (Eds.), *Proceedings of the Ninth Symposium of the Croatian Radiation Protection Association, 10–12. April 2013, Krk, Croatia* (pp. 193–198). Zagreb: CRPA.
15. Pantelić, G., Eremić Savković, M., Živanović, M., Nikolić, J., Rajačić, M., & Todorović, D. (2014). Uncertainty evaluation in radon concentration measurement using charcoal canister. *Appl. Radiat. Isot.*, 87, 452–455.
16. Udovičić, V., Aničin, I., Joković, D., Dragić, A., Banjanac, R., Grabež, B., & Veselinović, N. (2011). Radon time-series analysis in the Underground Low-Level Laboratory in Belgrade, Serbia. *Radiat. Prot. Dosim.*, 145(2/3), 155–158.
17. Banjanac, R., Dragić, A., Grabež, B., Joković, D., Markushev, D., Panić, B., Udovičić, V., & Aničin, I. (2006). Indoor radon measurements by nuclear track detectors: Applications in secondary schools. *Facta Universitatis*, 4, 93–100.
18. Maletić, D., Udovičić, V., Banjanac, R., Joković, D., Dragić, A., Veselinović, N., & Filipović, J. (2014). Comparison of multivariate classification and regression methods for indoor radon measurements. *Nucl. Technol. Radiat. Prot.*, 29, 17–23.
19. Eremić-Savković, M., Pantelić, G., Tanasković, I., Vuletić, V., & Javorina, Lj. (2002). Concentration of radon in apartments on the territory of Belgrade in period 1997–2001. *Arch. Toxicol. Kinet. Xenobiot. Metab.*, 10(1/2), 195–197.
20. Arsić, V., Ilić, J., Bogojević, S., Tanasković, I., Eremić-Savković, M., & Javorina, Lj. (2014). Assessment of the effective radon dose, measured in schools and kindergartens in Belgrade during 2012 and 2013. In *Proceedings of Second East European Radon Symposium (SEERAS), May 27–30, 2014, Niš, Serbia* (pp. 17–20).
21. Stevanovic, N., Markovic, V., & Nikezic, D. (2010). Relationship between deposition and attachment rates in Jacobi room model. *J. Environ. Radioact.*, 101(5), 349–352.
22. Jovanovic, B., Nikezic, D., & Stevanovic, N. (2011). Applied mathematical modeling for calculating the probability of the cell killing per hit in the human lung. *J. Radioanal. Nucl. Chem.*, 290(3), 607–613.



# The use of multivariate analysis of the radon variability in the underground laboratory and indoor environment

Jelena Filipović,  
Dimitrije Maletić,  
Vladimir Udovičić,  
Radomir Banjanac,  
Dejan Joković,  
Mihailo Savić,  
Nikola Veselinović

**Abstract.** The paper presents results of multivariate analysis of variations of radon concentrations in the shallow underground laboratory and a family house, depending on meteorological variables only. All available multivariate classification and regression methods, developed for data analysis in high-energy physics and implemented in the toolkit for multivariate analysis (TMVA) software package in ROOT, are used in the analysis. The result of multivariate regression analysis is a mapped functional behaviour of variations of radon concentration depending on meteorological variables only, which can be used for the evaluation of radon concentration, as well as to help with modelling of variation of radon concentration. The results of analysis of the radon concentration variations in the underground laboratory and real indoor environment, using multivariate methods, demonstrated the potential usefulness of these methods. Multivariate analysis showed that there is a potentially considerable prediction power of variations of indoor radon concentrations based on the knowledge of meteorological variables only. In addition, the online system using the resulting mapped functional behaviour for underground laboratory in the Institute of Physics Belgrade is implemented, and the resulting evaluation of radon concentrations are presented in this paper.

**Key words:** multivariate analysis • radon variability

## Introduction

The research of the dynamics of radon in various environments, especially indoors, is of great importance in terms of protection against ionizing radiation and in designing of measures for its reduction. Research of radioactive emanations (of radon ( $^{222}\text{Rn}$ ) and thoron ( $^{220}\text{Rn}$ )) are in the domain of radiation physics, but since a few decades ago, subject of radioactive emanation involves many other scientific disciplines, thus giving a multidisciplinary character to this research. Published results and development of many models to describe the behaviour of indoor radon indicate the complexity of this research, especially with models for the prediction of the variability of radon, simply because the variability depends on large number of variables. Large number of factors (such as local geology, permeability of soil, building materials used to build the buildings as well as the habits of people) impact the variation of radon, and therefore, it is important to study their correlation. In this paper, the results of correlative analysis of indoor radon and meteorological variables are presented. Furthermore, the results of multivariate classification and regression analysis is presented. More details of this study can be found in [1].

Indoor radon variation depends significantly on large number of factors, which include the local ge-

J. Filipović, D. Maletić, V. Udovičić✉, R. Banjanac,  
D. Joković, M. Savić, N. Veselinović  
Institute of Physics Belgrade,  
University of Belgrade,  
118 Pregrevica Str., 11080 Belgrade, Serbia,  
E-mail: udovicic@ipb.ac.rs

Received: 4 January 2016  
Accepted: 24 March 2016

ology, soil permeability, building materials, lifestyle characteristics and meteorological variables. In order to analyse the dependence of radon variation on multiple variables, multivariate analysis needs to be used.

The demand for detailed analyses of large amount of data in high-energy physics resulted in wide and intense development and usage of multivariate methods. Many of multivariate methods and algorithms for classification and regression are already integrated into the analysis framework ROOT [2], more specifically, into the toolkit for multivariate analysis (TMVA [3]). Multivariate analysis toolkit is used to create, test and apply all available classifiers and regression multivariate methods implemented in the TMVA in order to find methods that are the most appropriate and yield maximum information on the dependence of indoor radon concentrations on the multitude of meteorological variables. Classification methods are used to find out if it is possible to classify radon concentrations into low and high concentrations, using arbitrary cut value for radon concentrations. Regression methods are used as a next step with a goal to find out which regression method can, if any, on the basis of input meteorological variables only, give an output that would satisfactorily close match the observed variations of radon concentrations. The output of usage of multivariate regression analysis methods is mapped functional behaviour, which can be used to evaluate the measurements of radon concentrations using input meteorological variables only. The prediction of radon concentrations can be an output of mapped function when the prediction of input meteorological variables exists.

### **Short-term radon measurements in laboratory and real environment**

Depending on the integrated measurement time, methods of measurement of radon concentrations in air may be divided into long-term and short-term ones. For the measurements of radon concentration presented in this paper, the SN1029 radon monitor (manufactured by the Sun Nuclear Corporation, NRSB approval-code 31822) has been used as active, short-term measurement device. The device consists of two diffused junction photodiodes as a radon detector and is furnished with sensors for temperature, barometric pressure and relative humidity. The user can set the measurement intervals from 30 min to 24 h. It was set to record simultaneously the radon concentration, temperature, atmospheric pressure and relative humidity.

For the purposes of determining the best multivariate methods to use in the analysis, the results are obtained using radon monitor are from measurements in two locations, the Low-Background Laboratory for Nuclear Physics in the Institute of Physics in Belgrade and in a family house.

The underground Low-Background Laboratory for Nuclear Physics is selected for measurement and analysis because routine measurements in this labo-

ratory require low levels of radon concentration with minimum temporal variations. Low-background laboratory is located on the right bank of the river Danube in the Belgrade borough of Zemun, on the grounds of the Institute of Physics. The ground level portion of the laboratory, at 75 m above sea level, is situated at the foot of a vertical loess cliff, about 10 m high. The underground part of the laboratory, useful area of 45 m<sup>2</sup>, is dug into the foot of the cliff. Underground laboratory is surrounded with 30-cm thick concrete wall. The overburden of the underground laboratory is thus about 12 m of loess soil. Significant efforts are being made to contain the low radon concentration within the laboratory. The underground laboratory is completely lined with a hermetically sealed, 1-mm thick aluminium foil. The ventilation system maintains the overpressure of 2 mbar, so as to prevent radon diffusion from the soil. Fresh air entering the laboratory is passed through a two-stage filtering system. The first stage is a mechanical filter for dust removal. The second one is a battery of coarse and fine charcoal active filters. The concentration of radon is kept at an average value of about 10 Bq/m<sup>3</sup>.

In the Low-Background Laboratory for Nuclear Physics, radon concentrations were measured in period from 2008 to 2011 and continued later on periodically about a couple of months each year. Measurements of meteorological variables used in the analysis were recorded since 2008 and are taken from the meteorological station located 4 km from the laboratory. Measurements of radon concentrations, room temperature, atmospheric pressure and relative humidity inside the laboratory were obtained using radon monitor. The results obtained from the measurements of radon concentrations and their influence on gamma and cosmic ray measurements in the laboratory were published in several articles in international scientific journals [4–6].

The family house selected for the measurements and analysis of variations of radon concentrations is a typical house in Belgrade residential areas, with requirement of existence of cellar. House is built on limestone soil. Radon measurements were carried out in the living room of the family house, which is built of standard materials (brick, concrete, mortar) and isolated with styrofoam. During the period of measurements (spring–summer), the house was naturally ventilated and air conditioning was used in heating mode at the beginning of the measurement period. During the winter period measurements, the electrical heating was used in addition to air conditioning. Measured radon concentrations, room temperature, atmospheric pressure and relative humidity inside the house were obtained using radon monitor. Values of meteorological variables in measurement period were obtained from an automatic meteorological station located 400 m from the house in which the measurement was performed. We used the following meteorological variables: external air temperature, pressure and humidity, solar radiation, wind speed at a height of 10 m above ground, precipitation, evaporation and temperature and humidity of the soil at a depth of 10, 20, 30 and 50 cm.

**Correlation and regression analysis of the results**

All multivariate methods implemented in the TMVA are used in our search. All multivariate methods in TMVA belong to the family of ‘supervised learning’ algorithms [1]. All methods make use of training events, for which the desired output is known, to determine the mapping function that either describes a decision boundary (classification) or an approximation of the underlying functional behaviour defining the target value (regression). Every MVA methods see the same training and test data. The two best performing multivariate methods for our purposes are boosted decision trees (BDT) and artificial neural networks (ANN).

The determination of correlation coefficients between measured radon concentration and meteorological variables serves as a good tool for identifying the variables with strongest correlation, which are not excluded from the analysis later on. Also, correlation coefficient tables gives a good overview of input data and their intercorrelations. In Fig. 1, the correlation matrix of linear correlation coefficients as an overview of intercorrelations of measured radon concentration and all input meteorological variables are shown for underground laboratory. The input variables in case of analysis of underground laboratory are atmospheric pressure, temperature and humidity in laboratory ( $P_{mm}, T_{mm}, H_{mm}$ ) and outdoor ( $P, T, H$ ) and differences in measured values of pressure ( $P - P_{mm}$ ), temperature ( $T - T_{mm}$ ) and humidity ( $H - H_{mm}$ ) in laboratory and outdoor. Input meteorological variables in case of family house are the same as the list of measured meteorological variables from nearby meteorological station, with the addition of differences in temperature ( $T - T_{mm}$ ) and humidity ( $H - H_{mm}$ ) from indoor and outdoor values, where indoor measurements results were obtained using radon monitor.

Multivariate methods within the package TMVA in ROOT can search for best multivariate approximation of functional behaviour for the classification function of radon concentration depending on meteorological variables. In the analysis, several mul-

|                   | Linear correlation coefficients in % |          |          |     |     |     |              |              |              |       |
|-------------------|--------------------------------------|----------|----------|-----|-----|-----|--------------|--------------|--------------|-------|
| Radon             | 17                                   | 4        | 25       | 14  | 5   | 1   | 13           | 5            | -14          | 100   |
| H-H <sub>mm</sub> | -81                                  | 13       | -73      | -94 | 10  | 79  | -94          | -8           | 100          | -14   |
| P-P <sub>mm</sub> | 9                                    | -15      | 13       | 1   | 15  |     |              | 100          | -8           | 5     |
| T-T <sub>mm</sub> | 80                                   | -14      | 77       | 99  | -14 | -68 | 100          |              | -94          | 13    |
| H                 | -43                                  | 3        | -18      | -65 | 3   | 100 | -68          |              | 79           | 1     |
| P                 | -4                                   | 95       | -12      | -13 | 100 | 3   | -14          | 15           | 10           | 5     |
| T                 | 86                                   | -13      | 80       | 100 | -13 | -65 | 99           | 1            | -94          | 14    |
| H <sub>mm</sub>   | 84                                   | -17      | 100      | 80  | -12 | -18 | 77           | 13           | -73          | 25    |
| P <sub>mm</sub>   | -7                                   | 100      | -17      | -13 | 95  | 3   | -14          | -15          | 13           | 4     |
| T <sub>mm</sub>   | 100                                  | -7       | 84       | 86  | -4  | -43 | 80           | 9            | -81          | 17    |
|                   | $T_{mm}$                             | $P_{mm}$ | $H_{mm}$ | T   | P   | H   | $T - T_{mm}$ | $P - P_{mm}$ | $H - H_{mm}$ | Radon |

Fig. 1. Correlation matrix with linear correlation coefficients as an overview of radon and meteorological variables intercorrelations in case of the Low-Background Laboratory for Nuclear Physics.

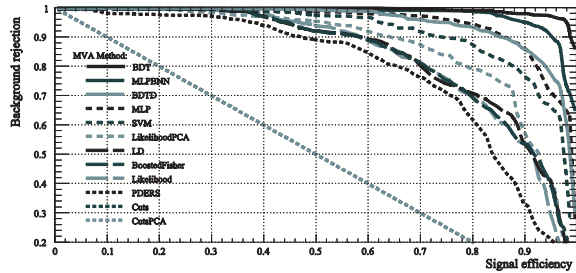


Fig. 2. ROC curve for all multivariate methods in case of house measurements.

tivariate methods were tested, and best performed method was BDT. This can be seen by presenting the receiver operating characteristics (ROC) curve for all tested multivariate methods in case of house measurements (Fig. 2). The BDT method has the highest value of integrated ROC function.

BDT has proven to be the most effective method for the classification of radon concentrations in case of data obtained from the house as well as those obtained from measurements in the Low-Background Laboratory for Nuclear Physics.

The next step in the analysis is the regression analysis, which is the way of finding a mapped function behaviour of dependence of radon concentrations and meteorological input variables. The regression analysis was done using the TMVA packages, already used in classification analysis, and for the same set of measured radon concentration and meteorological variables in underground laboratory and a family house in Serbia. Multivariate method BDT was found to be the best suited for regression analysis also, as was the case in classification analysis.

The data of measured radon concentration in house and BDT evaluated values, using only the values of meteorological variables, without the knowledge of measured values (i.e. in the testing set of multivariate analysis), is presented for comparison in Fig. 3.

One of the possible application of having resulting mapped function, given by multivariate regression analysis, is to have prediction of radon concentration values (evaluated) based on meteorological variables alone. The online application of the regression multivariate analysis can be imple-

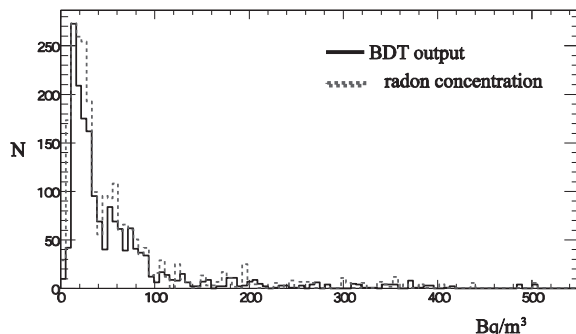
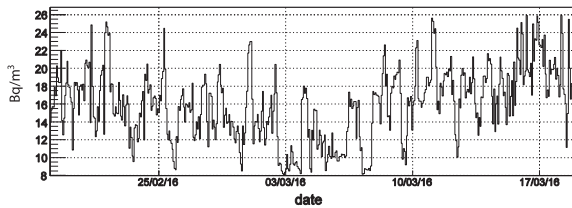


Fig. 3. BDT evaluated (predicted) values of radon concentrations based on meteorological variables using regression analysis within TMVA packages in house (left) and measured values (right).



**Fig. 4.** BDT evaluated (predicted) values of radon concentration, based on meteorological variables alone of underground laboratory posted online and updated daily.

mented, as the one posted online for evaluation (and prediction) based on meteorological variables alone (Fig. 4).

### Limitation of multivariate methods

As the multivariate methods used in the analysis are ‘supervised learning’ algorithms, the performance of the main result of multivariate analysis, the resulting mapped functional behaviour, depends on learning process. Limitation of multivariate analysis in the analysis of radon dependence on meteorological variables are coming from small number of measurements used in learning process, unlike the great number of measurements in high-energy physics experiments. As the next logical step in multivariate analysis presented in this paper should be inclusion of variables such as local geology, permeability of soil, building materials used to build the buildings as well as the habits of people, the requirement for efficient multivariate analysis is to have many measurements in many different houses. Many measurements would help to get good mapped functional behaviour, as opposed to possible existence of theoretical modelling that is independent on number of measurements. In this sense, if the number of measurements is not great, multivariate analysis can be used only as hell to indicate which variables are more important to be used in theoretical modelling, for comparison of mapped and modelled functions, and modelled function test. Another important limitation of multivariate analysis is that no ‘straightforward’ interpretation of mapped functional behaviour is possible, or simply, the mapped function is a ‘black box’. This comes from the fact that the error minimization in learning algorithms, while mapping the functional behaviour, is an important part in learning process.

### Conclusions

The paper presents the results of multivariate analysis of variations of radon concentrations in the shallow underground laboratory and a family house, depending on meteorological variables only. This test of multivariate methods, implemented in the

TMVA software package, applied to the analysis of the radon concentration variations connection with meteorological variables in underground laboratory (with ventilation system turned on and off) and typical house in Serbia, demonstrated the potential usefulness of these methods. It appears that the method can be used for the prediction of the radon concentrations, on the basis of predicted meteorological variables. The next step in multivariate analysis presented in this paper should be inclusion of variables such as local geology, permeability of soil, building materials used to build the buildings as well as the habits of people. The requirement for efficient multivariate analysis is to have many measurements in many different houses, which makes multivariate method very useful only when having many measurement, for instance, during radon mapping campaigns. Many measurements would help to get good mapped functional behaviour, as opposed to possible existence of theoretical modelling that is independent on number of measurements. Generally, multivariate analysis can be used to help indicate which variables are more important to be used in theoretical modelling, furthermore, for comparison of mapped and modelled functions, and modelled function test.

Another usage of the results of classification multivariate analysis presented in this paper is the implementation of online warning system for possible increased radon concentration in family houses based on meteorological variables only.

### References

1. Maletić, D., Udovičić, V., Banjanac, R., Joković, D., Dragić, A., Veselinović, N., & Filipović, J. (2014). Comparison of multivariate classification and regression methods for indoor radon measurements. *Nucl. Technol. Radiat. Prot.*, 29, 17–23.
2. Hoecker, A., Speckmayer, P., Stelzer, J., Therhaag, J., Von Toerne, E., & Voss, H. (2007). TMVA – Toolkit for Multivariate Data Analysis. *PoS ACAT 040*. arXiv:physics/070303.
3. Brun, R., & Rademakers, F. (1997). ROOT – An Object Oriented Data Analysis Framework. *Nucl. Instrum. Methods Phys. Res. Sect. A-Accel. Spectrom. Dect. Assoc. Equip.* 389(1/2), 81–86.
4. Udovičić, V., Grabež, B., Dragić, A., Banjanac, R., Joković, D., Panić, B., Joksimović, D., Puzović, J., & Aničin, I. (2009). Radon problem in an underground low-level laboratory. *Radiat. Meas.*, 44, 1009–1012.
5. Udovičić, V., Aničin, I., Joković, D., Dragić, A., Banjanac, R., Grabež, B., & Veselinović, N. (2011). Radon time-series analysis in the Underground Low-Level Laboratory in Belgrade, Serbia. *Radiat. Prot. Dosim.*, 145(2/3), 155–158.
6. Banjanac, R., Udovičić, V., Dragić, A., Joković, D., Maletić, D., Veselinović, N., & Grabež, B. (2013). Daily variations of gamma-ray background and radon concentration. *Rom. J. Phys.*, 58(Suppl.), S14–S21.

### **6.3 From motivation through the national radon survey to European indoor radon map**

Vladimir Udovičić<sup>1</sup>, Dimitrije Maletić<sup>1</sup>, Maja Eremić Savković<sup>2</sup>, Sofija Forkapić<sup>3</sup>

<sup>1</sup> *Institute of Physics Belgrade, University of Belgrade, Belgrade, Serbia*

<sup>2</sup> *Serbian Radiation Protection and Nuclear Safety Agency, Belgrade, Serbia*

<sup>3</sup> *Department of Physics, Faculty of Science, University of Novi Sad, Novi Sad, Serbia*

E-mail: udovicic@ipb.ac.rs

By 2014, radon issues were treated in Serbia through the scientific research projects. Among radon professionals, there was always the desire to create a radon risk map first of all. In 2014, with a certain amount of lucky circumstances, there was a chance that the radon problem would be raised to the national level. In that sense, Serbia has started to work on the national radon action plan (RAP), and in 2014 made its decision to perform the first national indoor radon survey. The responsibility for the establishment RAP and make indoor radon map in Serbia is on national regulatory body in the field of radiation protection: Serbian Radiation Protection and Nuclear Safety Agency (SRPNA). The project was supported by the IAEA through the technical cooperation programme. In this work, the planning and execution of the survey, including sampling design of the first national indoor radon survey are described in detail. Also, the results from national indoor radon survey and indoor radon mapping based on GPS coordinates was transformed to square map by creating a 10 km x 10 km squares where the starting point (0,0) is the center of Belgrade - Slavia Square are presented. To complete our work, we prepare data from the first Serbian indoor radon survey together with the data from indoor radon survey of Vojvodina, north province of Republic of Serbia performed during 2002-2005, and send to European Indoor Radon Map Group in JRC, Ispra, Italy.

# MEASUREMENT OF PHASE SPACE DENSITY EVOLUTION IN MICE

F. Drielsma\*, Université de Genève, Geneva, Switzerland  
D. Maletic†, Institute of Physics Belgrade, Belgrade, Serbia

## Abstract

The Muon Ionization Cooling Experiment (MICE) collaboration will demonstrate the feasibility of ionization cooling, the technique by which it is proposed to cool the muon beam at a future neutrino factory or muon collider. The position and momentum reconstruction of individual muons in the MICE trackers allows for the development of alternative figures of merit in addition to beam emittance. Contraction of the phase space volume occupied by a fraction of the sample, or equivalently the increase in phase space density at its core, is an unequivocal cooling signature. Single-particle amplitude and nonparametric statistics provide reliable methods to estimate the phase space density function. These techniques are robust to transmission losses and non-linearities, making them optimally suited to perform a quantitative cooling measurement in MICE.

## INTRODUCTION

Future facilities such as the Muon Collider and the Neutrino Factory will require high intensity and low emittance stored muon beams [1, 2]. Muons are produced as tertiary particles ( $p + N \rightarrow \pi + X$ ,  $\pi \rightarrow \mu + \nu$ ) inheriting a large emittance from the isotropic decay of the pions. For efficient acceleration, the phase space volume of these beams must be reduced significantly, i.e. “cooled”, to fit within the acceptance of a storage ring or accelerator beam pipe. Due to the short muon lifetime, ionization cooling is the only practical and efficient technique to cool muon beams [3, 4]. Each muon in the beam loses momentum in all dimensions through ionization energy loss in an absorbing material, reducing the RMS emittance and increasing its phase space density. Subsequent acceleration through radio frequency cavities restores longitudinal energy, resulting in a beam with reduced transverse emittance. A factor of close to  $10^6$  in reduced 6D emittance has been achieved in simulation with a 970 m long channel [5]. The rate of change in normalized transverse RMS emittance,  $\varepsilon_N$ , is given by the ionization cooling equation [3]:

$$\frac{d\varepsilon_N}{ds} \simeq -\frac{\varepsilon_N}{\beta^2 E_\mu} \left| \frac{dE_\mu}{ds} \right| + \frac{\beta_\perp (13.6 \text{ MeV})^2}{2\beta^3 E_\mu m_\mu c^2 X_0}, \quad (1)$$

where  $\beta c$  is the muon velocity,  $|dE/ds|$  is the average rate of energy loss,  $E_\mu$  and  $m_\mu$  are the muon energy and mass,  $\beta_\perp$  is the transverse betatron function and  $X_0$  is the radiation length of the absorber material. The first term on the right can be referred to as the “cooling” term driven by energy loss, while the second term is the “heating term” that uses the PDG approximation for the multiple Coulomb scattering.

\* francois.drielsma@unige.ch

† Speaker

MICE [6] is currently taking data in the Step IV configuration in order to make detailed measurements of the scattering, energy loss [7] and phase space evolution at different momenta and channel configurations, with lithium hydride and liquid hydrogen absorbers. A schematic drawing of MICE Step IV is shown in Figure 1. MICE consists of two scintillating fiber trackers upstream and downstream of the absorber in strong solenoid fields to accurately reconstruct the position and the momentum of individual muons selected in a series of particle identification detectors, including 3 time-of-flight hodoscopes (ToF0/1/2), 2 threshold Cherenkov counters, a pre-shower calorimeter (KL) and a fully active tracker-calorimeter (EMR) [8–11].

## COOLING CHANNEL

The two spectrometer solenoid modules each generate a region of uniform 3 T field in which diagnostic trackers are situated and a matching region that transports the beam from the solenoid to the focus coil module. The focus coil module, positioned between the solenoids, provides additional focusing to increase the angular divergence of the beam at the absorber, improving the amount of emittance reduction that can be achieved. The magnetic field model is shown in Figure 2. The absorber was a single 65 mm thickness lithium hydride disk. Lithium hydride was chosen as an absorber material as it provides less multiple Coulomb scattering for a given energy loss.

In this paper the evolution of phase space density is reported for a single configuration of the cooling apparatus. Results from one transfer line configuration are reported, with the accumulated muon sample having a nominal emittance of 6 mm at momenta around 140 MeV/c in the upstream spectrometer solenoid, denoted as ‘6–140’.

As MICE measures each particle event individually, it is possible to select a particle ensemble from the collection of measured tracks. This enables the study of momentum spread and transverse beam parameters on the cooling. In this analysis, muons have been selected with:

- longitudinal momentum in the range 135 to 145 MeV/c;
- time-of-flight between TOF0 and TOF1 consistent with muons in this momentum range; and
- a single, good quality track formed in the upstream diagnostics.

In order to study the evolution of the phase space density through the whole cooling channel and across the absorber, a realistic simulation of the setting of interest was produced. The betatron function of the selected muon ensemble is shown for the Monte Carlo (MC) simulation, the

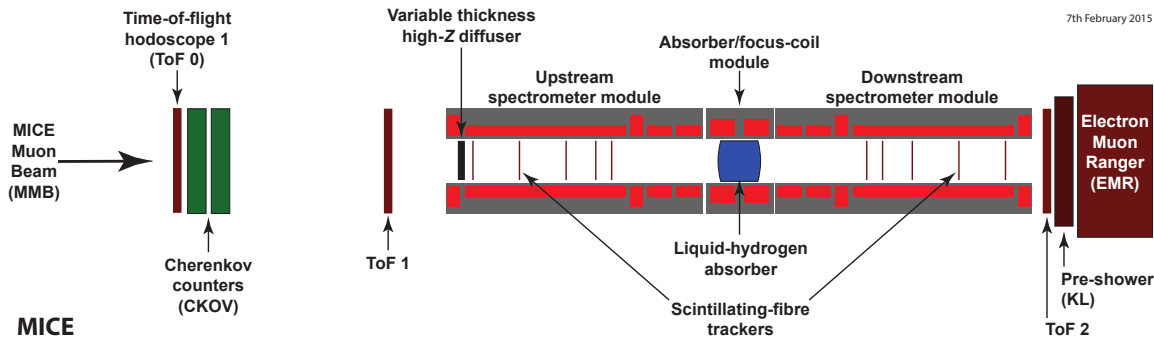


Figure 1: Layout of the MICE Step IV configuration, its absorber module, tracking spectrometers and PID detectors.

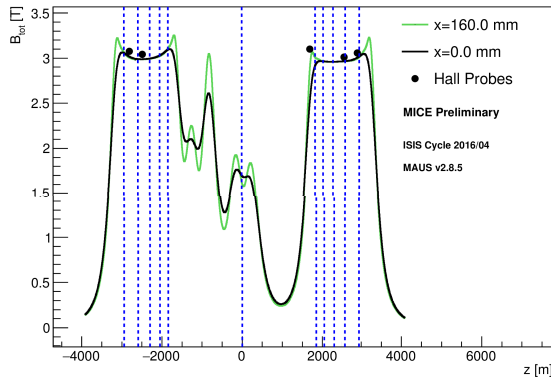


Figure 2: Modelled magnetic field for the configuration on the axis and with 160 mm horizontal displacement from the axis. Hall probes, situated 160 mm from the beam axis, show a 2% discrepancy with the model. Dashed lines show position of the tracker stations and absorber (at  $z = 0$ ).

reconstructed MC and the data for the ‘6–140’ setting in Figure 3. The graph shows a large growth of the beam size in the downstream section due to the absence of the downstream match coils in this configuration. The simulation closely reproduces the function measured in the data.

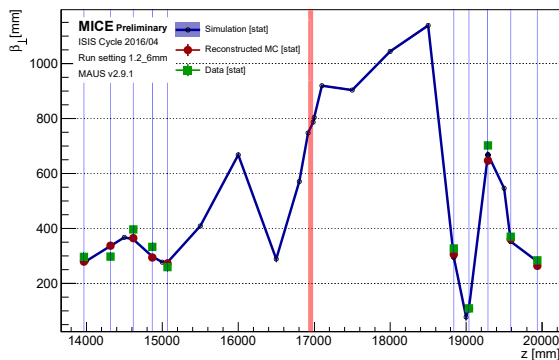


Figure 3: Beta function profile in the MC truth (blue line), reconstructed MC (red circles) and data (green squares).

## PHASE SPACE DENSITY EVOLUTION

### Emittance

The transverse normalized RMS emittance is the most common cooling figure of merit and is defined as

$$\epsilon_N = \frac{1}{m_\mu} |\Sigma|^{1/4}, \quad (2)$$

with  $m_\mu$  the muon mass and  $|\Sigma|$  the determinant of the 4D transverse phase space covariance matrix, i.e.  $\Sigma_{ij} = \langle i \rangle \langle j \rangle - \langle i \rangle \langle j \rangle$  with  $i, j \in [x, p_x, y, p_y]$ . For a Gaussian beam, this quantity is directly related to the volume of the  $1\sigma$  RMS ellipse,  $V_{RMS}$ , through  $\epsilon_N = \sqrt{2V_{RMS}} / (m\pi)$ .

In a fully transmitted beam, emittance reduction is a clean signature of the contraction of transverse phase space volume. For a partially scraped beam, as shown for the ‘6–140’ setting in Figure 4, the emittance evolution exhibits apparent emittance reduction in the downstream section due to the loss of the tails of the distribution. It also experiences significant apparent growth in the downstream tracker due to high field gradient, causing filamentation in the beam.

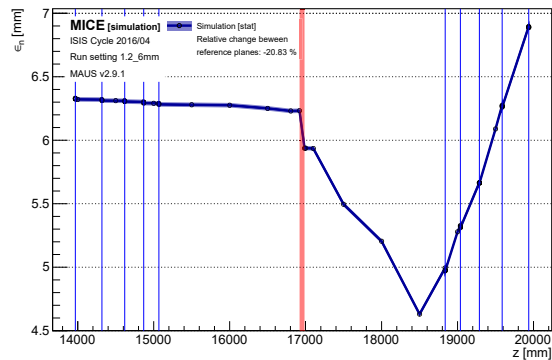


Figure 4: Normalized transverse RMS emittance evolution through the MICE cooling channel.

An alternative to RMS emittance is to study the evolution of the density distribution of the ensemble, as it allows for the selection of a defined and identical fraction of phase space upstream and downstream of the absorber.

## Amplitude

The 4D amplitude of a particle with phase space vector  $\mathbf{v} = (x, p_x, y, p_y)$  is given by

$$A_{\perp} = \epsilon_N (\mathbf{v} - \boldsymbol{\mu})^T \boldsymbol{\Sigma}^{-1} (\mathbf{v} - \boldsymbol{\mu}). \quad (3)$$

with  $\boldsymbol{\mu} = (\langle x \rangle, \langle p_x \rangle, \langle y \rangle, \langle p_y \rangle)$ , the beam centroid. In order to prevent the tails of the distribution from skewing the core, only those events with amplitude less than  $A_{\perp}$  have been included in the calculation of  $\boldsymbol{\mu}$  and  $\boldsymbol{\Sigma}$  for a given event. The high amplitude particles are iteratively removed from the sample first as they are calculated.

The distribution of muons is represented in Figure 5 in the tracker station that is furthest downstream in the  $(x, p_x)$  projection. The color of the points in the scatter plot represents the amplitude of the particle at that position. The distribution exhibits a clear Gaussian core of low amplitudes, while the tails are easily identified as high amplitude points.

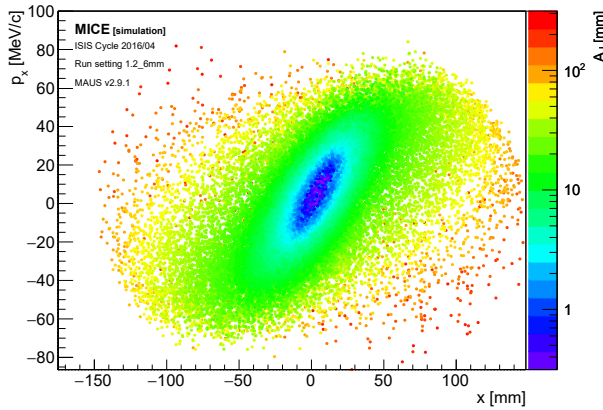


Figure 5: Scatter plot of the particles in the tracker station that is furthest downstream in the  $(x, p_x)$  projection. The color scale represents the individual particle amplitudes.

The amplitude of a particle in a Gaussian beam is related to its local density through

$$\rho(\mathbf{v}) = \frac{1}{4\pi^2 m^2 \epsilon_N^2} \exp\left[-\frac{A_{\perp}}{2\epsilon_N}\right]. \quad (4)$$

A low amplitude sample corresponds to the high density core of the beam.

## Subemittance

The  $\alpha$ -subemittance,  $e_{\alpha}$ , is defined as the RMS emittance of the core fraction  $\alpha$  of the parent beam. For a truncated 4D Gaussian beam of covariance  $S$ , it satisfies

$$\frac{e_{\alpha}}{\epsilon_N} = \frac{|S|^{\frac{1}{4}}}{|\boldsymbol{\Sigma}|^{\frac{1}{4}}} = \frac{1}{2\alpha} \gamma\left(3, Q_{\chi_4^2}(\alpha)/2\right), \quad (5)$$

with  $\gamma(\cdot, \cdot)$  the lower incomplete gamma function and  $Q_{\chi_4^2}(\cdot)$ , the 4-degrees-of-freedom  $\chi^2$  distribution quantiles.

If an identical fraction  $\alpha$  of the input beam is selected upstream and downstream, i.e. the same amount of particles, the measured subemittance change is identical to the normalized RMS emittance change. The evolution of the 9%-subemittance is represented in Figure 6. The choice of 9% is natural in four dimensions as it represents the fraction contained within the 4D RMS ellipsoid of a 4-variate Gaussian. This quantity exhibits a clean cooling signal across the absorber that is unaltered by transmission losses and nonlinearities. The only trade-off is that the relative statistical error on  $\alpha$ -subemittance grows as  $\alpha^{-\frac{1}{2}}$ . The estimated relative emittance change with this technique is  $-7.54 \pm 1.25\%$ , compatible with predictions.

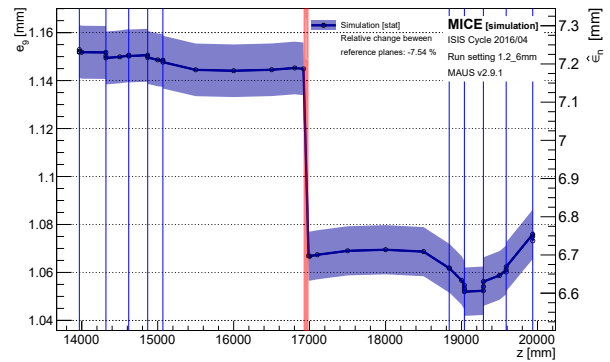


Figure 6: 9%-subemittance evolution through the MICE cooling channel.

## Fractional Emittance

The  $\alpha$ -fractional emittance,  $\epsilon_{\alpha}$ , is defined as the phase space volume occupied by the core fraction  $\alpha$  of the parent beam. For a truncated 4D Gaussian beam, it satisfies

$$\epsilon_{\alpha} = \frac{1}{2} m^2 \pi^2 \epsilon_N^2 Q_{\chi_4^2}^2(\alpha). \quad (6)$$

This volume scales as function of  $\alpha$  only and is proportional to the square of the normalized emittance. For a relative emittance change  $\delta = \Delta\epsilon_N / \epsilon_N^{up}$ , one yields

$$\frac{\Delta\epsilon_{\alpha}}{\epsilon_{\alpha}^{up}} = \delta(2 + \delta) \approx 2 \frac{\Delta\epsilon_N}{\epsilon_N}. \quad (7)$$

The last approximation holds for small fractional changes. The volume of a fraction  $\alpha$  of the beam is reconstructed by taking the convex hull of the selected ensemble [12]. Figure 7 shows the evolution of the 9%-fractional emittance. The estimated relative emittance change with this technique is  $-7.85 \pm 1.08\%$ .

## Nonparametric Density Estimation

Nonparametric statistics are not based on parameterized families of probability distributions. Unlike parametric density estimation, such as amplitude, nonparametric statistics

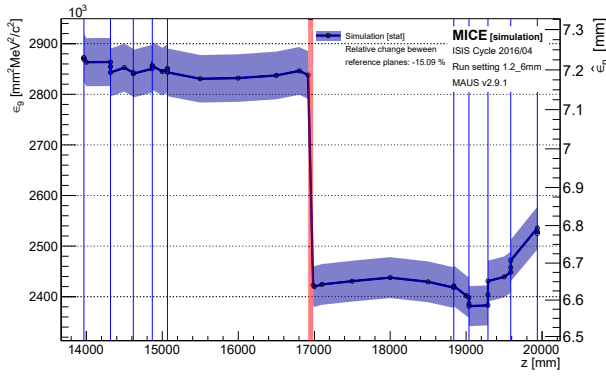


Figure 7: 9 %-fractional emittance evolution through the MICE cooling channel.

make no assumptions about the probability distributions of the variables being assessed.

There are many classes of estimators that have been developed in the last century. Three of them have been considered in this study: optimally binned histograms,  $k$ -Nearest Neighbors ( $k$ NN) and Tessellation Density Estimators (TDEs) [13–16]. Systematic studies showed that the  $k$ NN method is the most efficient and robust technique in four dimensions. For a given phase space vector  $\mathbf{v} = (x, p_x, y, p_y)$ , find the  $k$  nearest points in the input cloud, calculate the distance to the  $k^{\text{th}}$  nearest neighbor,  $R_k$ , and evaluate the density as

$$\rho(\mathbf{v}) = \frac{k}{V_k} = \frac{k\Gamma\left(\frac{d}{2} + 1\right)}{\pi^{\frac{d}{2}} R_k^d}, \quad (8)$$

with  $d$  the dimension of the space,  $V_k$  the volume of the  $d$ -ball of radius  $R_k$  and  $\Gamma(\cdot)$  is the gamma function. The choice of parameter  $k = \sqrt{N}$  has been shown to be quasi-optimal in general [17] and is used in the following. This estimator is applied to the sample in the tracker station that is furthest downstream and is represented in the  $(x, p_x)$  projection for  $(y, p_y) = (0, 0)$  in Figure 8.

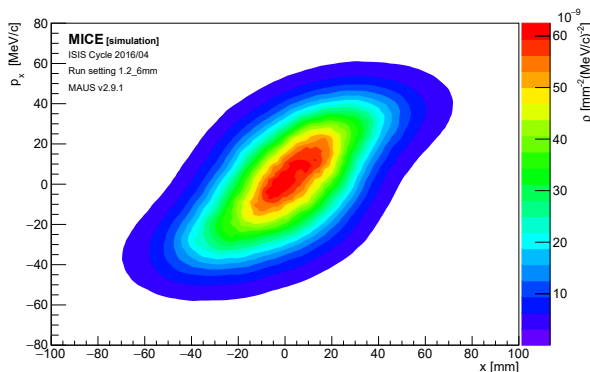


Figure 8:  $k$ -Nearest Neighbors estimate of the phase space density in the  $(x, p_x)$  projection for  $(y, p_y) = (0, 0)$  in the tracker station that is furthest downstream.

This method removes any underlying assumption about a Gaussian core and allows to reconstruct generalized probability contours. The volume of the  $\alpha$ -contour is the  $\alpha$ -fractional emittance, as defined above. An MC method is used to reconstruct the volume of a contour: select the densest fraction  $\alpha$  of the input points and record the level of the lowest point,  $\rho_\alpha$ . Sample  $N$  random points uniformly distributed inside a box that encompasses the contour and record the amount,  $N_\alpha$ , that have a density above the level, i.e.  $\rho > \rho_\alpha$ . The volume of the contour is simply  $\epsilon_\alpha = N_\alpha V_{box} / N$ , with  $V_{box}$  the volume of the 4-box. The 9 %-contour volume evolution is represented in Figure 9. The estimated relative emittance change with this technique is  $-7.97 \pm 1.63 \%$ .

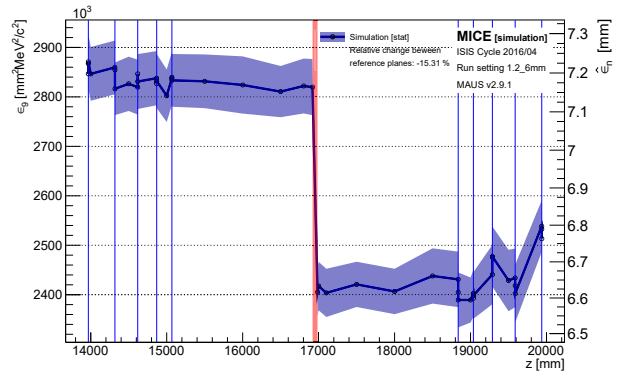


Figure 9: 9 %-contour volume evolution through the MICE cooling channel.

## CONCLUSION

While the traditional normalized RMS emittance measurement is vulnerable to transmission losses and non-linearities in the particle ensemble, density estimation techniques provide the most viable option to recover quantitative cooling measurements. Amplitude-based techniques – subemittance and fractional emittance – rely on a well known quantity to select and study an identical fraction of the beam upstream and downstream of the absorber. Nonparametric density estimators allow to go one step further in removing any assumption on the underlying distribution. Both approaches yield compelling results when applied to a poorly transmitted and highly non-linear beams in a realistic simulation of one of the MICE cooling channel settings.

## ACKNOWLEDGEMENT

Work described here has been made possible through generous funding from the Department of Energy and the National Science Foundation (USA), the Istituto Nazionale di Fisica Nucleare (Italy), the Science and Technology Facilities Council (UK), the European Community under the European Commission Framework Programme 7, the Japan Society for the Promotion of Science and the Swiss National Science Foundation.

## REFERENCES

- [1] IDS-NF Collaboration, M. Apollonio *et al.*, “International Design Study for the Neutrino Factory”, *Nucl. Phys. Proc. Suppl.* 229-232 (2012) 515–515
- [2] Neutrino Factory and Muon Collider Collaboration, M. Alsharova, *et al.*, “Recent progress in neutrino factory and muon collider research within the Muon collaboration”, *Phys. Rev. ST Accel. Beams* 6 (2003) 081001
- [3] D. Neuffer, “Principles and Applications of Muon Cooling”, *Part. Accel.* 14 (1983) 75–90.
- [4] V. Parkhomchuck and A. Skrinsky, “Cooling Methods for Charged Particle Beams”, *Rev. Accel. Sci. Tech.* 1 no. 1 (2008) 237
- [5] D. Stratakis and R. Palmer, “Rectilinear six-dimensional ionization cooling channel for a muon collider: A theoretical and numerical study” *Phy. Rev. ST Accel. Beams* 18 (2015) 031003
- [6] MICE Collaboration, “MICE: An International Muon Ionization Cooling Experiment”, MICE Note 21 (2003). <http://mice.iit.edu/micenotes/public/pdf/MICE0021/MICE0021.pdf>.
- [7] F. Drielsma, “Results from MICE Step IV”, in *Proceedings of “The 2017 European Physical Society Conference on High Energy Physics”* PoS(EPS-HEP2017)534
- [8] C. Heidt, “The tracker systems for the muon ionization cooling experiment”, *Nucl. Instr. Meth.*, vol. 718 (2014), 560–562.
- [9] U. Braver *et al.*, “MICE: the Muon Ionization Cooling Experiment. Step I: First Measurement of Emittance with Particle Physics Detectors”, <https://arxiv.org/abs/1110.1813>.
- [10] D. Adams *et al.*, “Pion contamination in the MICE muon beam”, *JINST* 11 (2016) P03001
- [11] D. Adams *et al.*, “Electron-muon ranger: performance in the MICE muon beam”, *JINST* 10 (2015) P12012
- [12] C.B. Barber, D.P. Dobkin, and H.T. Huhdanpaa, “The Quickhull algorithm for convex hulls”, *ACM Trans. on Mathematical Software*, 22(4) (1996) 469-483, <http://www.qhull.org>.
- [13] D.W. Hogg, “Data analysis recipes: Choosing the binning for a histogram”, <https://arxiv.org/pdf/0807.4820>
- [14] Y.P. Mack and M. Rosenblatt, “Multivariate k-nearest neighbor density estimates”, *Journal of Multivariate Analysis* Volume 9, Issue 1 (1979), 1–15
- [15] M. Browne, “A geometric approach to non-parametric density estimation”, *Pattern Recognition* 40(1) (2007), 134–140
- [16] M. Browne, “Regularized tessellation density estimation with bootstrap aggregation and complexity penalization”, *Pattern Recognition* 45(4) (2012), 1531–1539
- [17] D.O. Loftsgaarden and C.P. Quesenberry, “A nonparametric estimate of a multivariate density function”, *The Annals of Mathematical Statistics* Vol. 36, No. 3 (1965), 1049–1051

## **AN OVERVIEW OF THE RADON RESEARCH IN THE INSTITUTE OF PHYSICS BELGRADE**

*Vladimir Udovičić, Dimitrije Maletić, Aleksandar Dragić,  
Radomir Banjanac, Dejan Joković, Mihailo Savić and Nikola Veselinović*  
Institute of Physics, University of Belgrade, Belgrade, Serbia  
[udovicic@ipb.ac.rs](mailto:udovicic@ipb.ac.rs)

### **INTRODUCTION**

Radon studies in the Institute of Physics Belgrade last a few decades. The first project related to radon was searching for connection between radon variability in soil and water and seismic activity in Montenegro [1]. After that, in the Low-Background Laboratory for Nuclear Physics, Institute of Physics Belgrade, the new research topics of rare nuclear processes was in the scientific focus. There was the need to build up the laboratory space to accomplish this type of research. In the 1997, underground low-background laboratory was built in, with the aim of investigating the rare nuclear processes. In the laboratory of this type, the influence of radon on the natural background radioactivity is dominant and there is an imperative that radon levels must be as low as it possible, with minimal time variation. In that sense, continuous radon monitoring became the mandatory activity. This paper presents the results of many years of radon monitoring in the underground low-background laboratory in the Institute of Physics Belgrade.

Besides radon monitoring in the laboratory, we work on several research topics regarding radon: using multivariate classification and regression methods, as developed for data analysis in high-energy physics and implemented in the TMVA software package, to study connection of climate variables and variations of radon concentrations, modelling of the indoor radon behaviour and radon mapping. All these research activities are presented in this work in more details.

### **RADON MONITORING IN THE UNDERGROUND LOW- BACKGROUND LABORATORY**

The Low-Background Laboratory for Nuclear Physics at the Institute of Physics in Belgrade is a shallow underground laboratory (Figure 1). The laboratory was built in the loamy loess cliff on the bank of the river Danube with the overburden of 12 m of soil. It has an active area of about 60 m<sup>2</sup>.

The walls, the floor and the ceiling of the laboratory are built of reinforced concrete of 30 cm thickness. From the measurements of the absolute flux of cosmic-ray muons in the underground as well as in the ground level laboratory [2] it was estimated that the equivalent depth of the laboratory is about 25 m.w.e. (a shielding thickness of the overburden soil expressed as water equivalent thickness). Description of the laboratory is presented in more detail elsewhere [3].

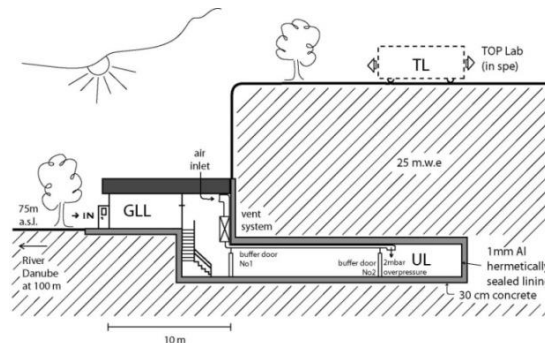


Figure 1. Cross-section of the underground low-background laboratory at the Institute of Physics Belgrade.

The system for the reduction of radon concentration in the laboratory consists of three stages. First, the active area of the laboratory is completely lined up with aluminium foil of 1 mm thickness, which is hermetically sealed with a silicon sealant to minimize the diffusion of radon from surrounding soil and concrete used for construction. The second one is the ventilation system. The laboratory is continuously ventilated with fresh air, filtered through one rough filter for dust elimination followed by the battery of coarse and fine charcoal active filters. The inlet of air is outside of the laboratory, at the height of 2.5 m above the ground. Finally, the parameters of the ventilation system are adjusted so as to result in an overpressure of about 2 mbar over the atmospheric pressure, which further prevents radon diffusion through eventual imperfections in the aluminium layer.

The device for the performed short-term radon measurements is SN1029 radon monitor (manufactured by the Sun Nuclear Corporation, NRSB approval code 31822) with the following characteristics: the measurement range from  $1 \text{ Bq m}^{-3}$  to  $99.99 \text{ kBq m}^{-3}$ , accuracy equal to  $\pm 25 \%$ , sensitivity of 0.16 counts hour per  $\text{Bq m}^{-3}$ . With these characteristics, SN1029 radon monitor is defined as a high-sensitivity passive instrument

for the short-term radon measurements and it is an optimal solution for radon monitoring in the underground laboratory.

The radon data from radon monitor device SN1029 for the period of 3 years are spectrally analysed. The Lomb-Scargle periodogram analysis method has been used in spectral analysis of radon time series. The obtained periodogram show two periodicity, on the 1 day and 1 year [4]. Mean radon value is  $13.8 \text{ Bq m}^{-3}$  with standard deviation of  $9.9 \text{ Bq m}^{-3}$  over the 3 years of continuous measurements with daily and seasonal variability [5]. It has been shown that the radon behaviour in the underground low-level laboratory in Belgrade has the similar characteristics as in the other underground environment (caves, mines, boreholes and so on), because it has the same source and the places are completely surrounded with the soil.

### **MVA METHODS AND MODELLING OF THE INDOOR RADON BEHAVIOUR**

The demand for detailed analyses of large amount of data in high-energy physics resulted in wide and intense development and usage of multivariate methods. Many of multivariate methods and algorithms for classification and regression are already integrated into the analysis framework ROOT, more specifically, into the toolkit for multivariate analysis (TMVA). We use these multivariate methods to create, test and apply all available classifiers and regression methods implemented in the TMVA in order to find the method that would be the most appropriate and yield maximum information on the dependence of indoor radon concentrations on the multitude of climate variables. The first step is to calculate and rank the correlation coefficients between all the variables involved, what will help in setting up and testing the framework for running the various multivariate methods contained in the TMVA. Although these correlation rankings will later be superseded by method specific variable rankings, they are useful at the beginning of the analysis. The next step is to use and compare the multivariate methods in order to find out which one is best suited for classification (division) of radon concentrations into what would be considered acceptable and what would be considered increased concentration in indoor spaces. Main aim is to find out which method can, if any, on the basis of input climate variables only, give an output that would satisfactorily close match the observed variations of radon concentrations. Towards this aim, this work were tested in a many specific cases (underground low-background laboratory and other indoor environment) to

comprise the multitude of possible representative situations that occur in real life.

The test of multivariate methods, implemented in the TMVA software package, applied to the analysis of the radon concentration variations connection with climate variables in different indoor spaces demonstrated the potential usefulness of these methods. It appears that the method can be used with sufficient accuracy (around 15 %) for prediction of the radon concentrations. All the obtained results were published in several research articles [6-8].

### **RADON MAPPING IN SERBIA**

In the last three years, we were involved in the establishing national radon action plan (RAP) and performed first national indoor radon survey as a leading institution in the technical support of the project. The responsibility for the establishment and implementation of RAP is on national regulatory body: Serbian Radiation Protection and Nuclear Safety Agency (SRPNA). As a first step in RAP, it was the national indoor radon survey in Serbia performed during 2015-2016. The project was supported by IAEA through the national project: SRB9003 - Enhancing the Regulatory Infrastructure and Legislative System, with two components:

- Expert mission on „National Radon Trial Survey and Raising Awareness of Key Stakeholders,, held in SRPNA, Belgrade, 2 - 4 February 2015.
- Equipment: Leasing of 6000 track-etched indoor radon detectors; the distribution of detectors across the Serbian territory was the responsibility of SRPNA.

Also, during the realization of the national programme for indoor radon measurements, Institute of Physics Belgrade and other research institutions involved in the project together with the SRPNA, performed good communication strategy (first basic information leaflet on radon to accompany the measurement explaining the purpose of the measurement, internet site, public relation, public education...) which led to high survey efficiency (about 90 %), together with very hard field work. In total 6000 detectors have been distributed during October 2015 and exposed in houses and apartments for six months (till April 2016). Afterwards, the detectors were collected and sent to an authorized laboratory (Landauer Nordic AB) to be processed and consequently, we got data for the first national indoor radon survey. The preliminary results and radon map was presented at the 8th Conference of Protection against Radon at Home and at Work, 12 - 14 September 2016, Prague, Czech Republic [9].

## Acknowledgements

The authors acknowledge the financial support of the Ministry of Education, Science and Technology Development of Serbia within the projects: 171002 - Nuclear Methods Investigations of Rare Processes and Cosmic Rays and 43002 - Biosensing Technologies and Global System for Continuous Research and Integrated Management.

## REFERENCES

- [1] Antanasijević R, Milošević I. Correlation between the concentration of  $^{222}\text{Rn}$  at the Earth's surface and in waters with seismic activities. *Nucl. Tracks Radiat. Meas.* 1990;17:79.
- [2] Dragić A, Joković D, Banjanac R, Udovičić V, Panić B, Puzović J, Aničin I. Measurement of cosmic ray muon flux in the Belgrade ground level and underground laboratories. *Nucl. Instr. Meth. Phys. Res.* 2008;A591:470–475.
- [3] Dragić A, Udovičić V, Banjanac R, Joković D, Maletić D, Veselinović N, Savić M, Puzović J, Aničin I. The new set-up in the Belgrade low-level and cosmic-ray laboratory. *Nucl. Technol. Radiat. Protect.* 2011; 26(3):181–192.
- [4] Udovičić V, Aničin I, Joković D, Dragić A, Banjanac R, Grabež B, Veselinović N. Radon time-series analysis in the underground low-level laboratory in Belgrade, Serbia. *Radiat. Prot. Dosim.* 2011;145:155–158.
- [5] Udovičić V, Filipović J, Dragić A, Banjanac R, Joković D, Maletić D, Grabež B, Veselinović N. Daily and seasonal radon variability in the underground low-background laboratory in Belgrade, Serbia. *Radiat. Prot. Dosim.* 2014;160(1-3):62-64.
- [6] Maletić D, Udovičić V, Banjanac R, Joković D, Dragić A, Veselinović N, Filipović J. Comparison of multivariate classification and regression methods for the indoor radon measurements. *Nucl. Technol. Radiat. Prot.* 2014; 29(1): 17–23.
- [7] Maletić D, Udovičić V, Banjanac R, Joković D, Dragić A, Veselinović N, Filipović J. Correlative and multivariate analysis of increased radon concentration in underground laboratory. *Radiat. Prot. Dosim.* 2014;162:148-151.
- [8] Filipović J, Maletić D, Udovičić V, Banjanac R, Joković D, Savić M, Veselinović N. The use of multivariate analysis of the radon variability in the underground laboratory and indoor environment. *Nukleonika* 2016; 61(3):357-360.
- [9] Udovičić V, Maletić D, Eremić Savković M, Pantelić G, Ujić P, Čeliković I, Forkapić S, Nikezić D, Marković V, Arsić V, Ilić J, Nilsson P. Preliminary results of the first national indoor radon survey in Serbia. In: *Book of Abstracts of 8<sup>th</sup> Conference of Protection against Radon at Home and at Work*, September 12-14, 2016; Prague, Czech Republic.

# Utilization of a shallow underground laboratory for studies of the energy dependent CR solar modulation

N. Veselinović A. Dragić, M. Savić, D. Maletić, D. Joković, R. Banjanac, V. Udovičić,  
*Institute of physics, University of Belgrade, Serbia*

The aim of the paper is to investigate possibility of utilizing a shallow underground laboratory for the study of energy dependent solar modulation process and to find an optimum detector configuration sensitive to primaries of widest possible energy range for a given site. The laboratory ought to be equipped with single muon detectors at ground level and underground as well as the underground detector array for registration of multi-muon events of different multiplicities. The response function of these detectors to primary cosmic-rays is determined from Monte Carlo simulation of muon generation and propagation through the atmosphere and soil, based on Corsika and GEANT4 simulation packages. The simulation predictions in terms of flux ratio, lateral distribution, response functions and energy dependencies are tested experimentally and feasibility of proposed setup in Belgrade underground laboratory is discussed.

## 1. INTRODUCTION

Cosmic rays (CR) are energetic particles, arriving at the Earth from space after interaction with the heliosphere. The interaction of these, primary CRs, with the atmosphere leads to production of a cascade (shower) of secondary particles: hadrons, electrons and photons, muons, neutrinos. CR research has been undertaken at almost every location accessible to humans – from the outer space to deep underground [1].

At the low energy part of the spectrum, lower than 100 GeV, CRs are affected by the solar magnetic field. Modulation effects are energy dependent and have been studied extensively by the neutron monitors, sensitive up to about 10 GeV. Muon detectors at the ground level are sensitive to higher energy primaries [2], and the muons detected underground correspond to even higher energies. The possibility to further extend the sensitivity to higher energies with the detection of multi-muon events underground is the intriguing one. The idea was exploited with the EMMA underground array [3]. For a shallow underground laboratory, exceeding the energy region of solar modulation would open the possibility to study CR flux variations of galactic origin.

## 2. BELGRADE CR STATION

The Belgrade cosmic-ray station is situated at the Laboratory for Nuclear Physics at the Institute of Physics. Its geographic position is: latitude 44° 51' N and longitude 20° 23' E, altitude of 78 m a.s.l., with geomagnetic latitude 39° 32' N and geomagnetic vertical cut-off rigidity 5.3 GV. It is composed of two sections, the underground lab (UL) with useful area of 45 m<sup>2</sup>, dug at the 12-meter shallow depth (equivalent to 25 m.w.e) and the ground level lab (GLL). At UL depth, practically, only the muonic component of the atmospheric shower is present.

The cosmic-ray muon measurements in Belgrade CR station are performed by means of the plastic scintillation detectors, placed both in the GLL and in the UL. With the previous set-ups, monitoring is continuous from 2002.

Measured cosmic-ray intensity data were thoroughly analysed, yielding some results on the variations of the cosmic-ray intensity [4,5,6].

Time series (pressure and temperature corrected) of these measurements can be accessed online at [http://cosmic.ipb.ac.rs/muon\\_station/index.html](http://cosmic.ipb.ac.rs/muon_station/index.html).

In addition to single muon detectors, a small-scale test setup for multi-muon events is installed underground. It consists from three scintillators: one large detector (100cm x 100cm x 5cm) and two small detectors (50cm x 23cm x 5cm) which are placed horizontally on their largest sides. Their mutual position is adaptable. The data acquisition system is based on fast 4-channel flash analog-to-digital converters (FADC), made by CAEN (type N1728B), with 100 MHz sampling frequency. The events are recorded in the list mode. For each event from every input channel the timing and amplitude are saved, together with auxiliary information such as the result of pile-up inspection routine. From this list a time series of single or coincident events could be constructed. The experimental set-up is sketched in Figure 1.

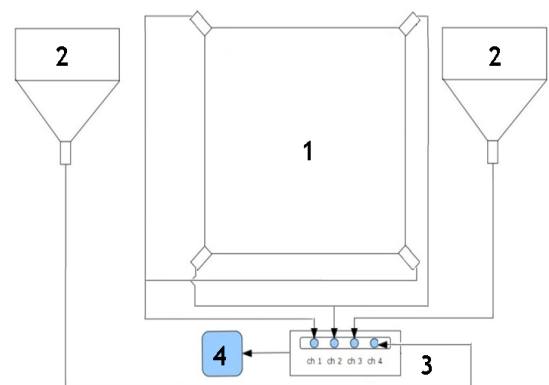


Figure 1 : Sketch of the experimental set-up for the cosmic-ray measurements:

1) Large scintillation detector, 2) small scintillation detectors, 3) flash analog-to-digital Converter (FADC), 4) experiment control and data storage computer

With simultaneous operation of several detector systems, as described, a single facility with the same rigidity cut-off would be used for investigation of solar modulation at different energies. Further integration with the Neutron Monitors data would be beneficial [7, 8, 9].

### 3. SIMULATION DETAILS AND RESULTS

Simulation of the CR shower dynamics up to the doorstep of GLL and UL has been done using Monte Carlo simulation packages CORSIKA and Geant4 [10, 11]. The cosmic-ray muon spatial and momentum distribution at 78m a.s.l. is of our interest. The output of CORSIKA at ground level is used as the input for Geant4 based simulation of particle transport through the soil and simulation of detector response. For this purpose soil analysis is done beforehand. The mean density is found to be  $(2.0 \pm 0.1)$  g/cm<sup>3</sup> and soil type is loess with the assumed composition of Al<sub>2</sub>O<sub>3</sub> 20%, CaO 10% and SiO<sub>2</sub> 70%. For the simulation of underground detector system only those muons with energy sufficient enough to survive passage through soil are taken into consideration (Figure 2).

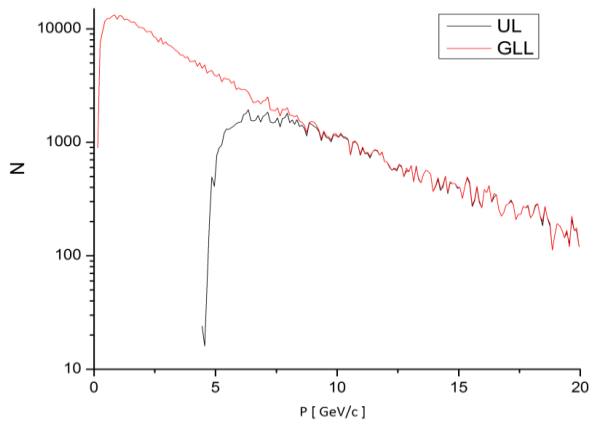


Figure 2: Surface momentum distribution for muons at GLL and muons reaching UL at Belgrade CR station based on GEANT4 and CORSIKA

At lower energies, protons make ~85% of CR, so primary particles used in the simulation were protons. The number of muons reaching UL is not linearly proportional to energy of the primary particle, especially for energies lower than 200 GeV which is energy range of interest, as showed in Figure 3. This correspond to similar work done elsewhere [12]. Probability that a registered event corresponds to a primary particle of certain energy is inferred from the simulation for every detection system:

- Single muon detector at ground level
- Single muon detector underground
- Two-fold muon coincidences underground
- Muon coincidences of higher multiplicity

For these response functions, simulation use 23 million primary protons with energy range from 5 GeV to  $10^{16}$  eV

with zenith angle between  $(0^\circ, 70^\circ)$  and with power law energy spectrum with the exponent  $-2.7$ . Shift toward higher energies is evident for transition from GL to UL and to the events of higher multiplicities.

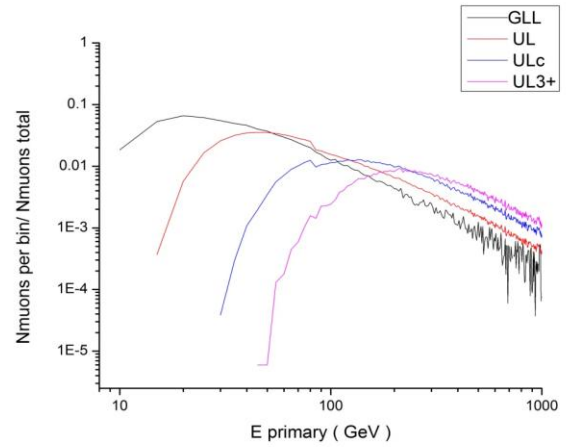


Figure 3: Differential response functions of muon detectors in GLL and UL based on simulation for: single muons at ground level (GLL), underground level (UL), coincident muons at underground level (ULc) and triple and higher multiplicity coincident muons at underground level (UL3+ ) normalized to total number of muons respectively.

For all relevant quantities of the muon flux is given at Table 1. Equivalent depth was found using ratios of integral fluxes of muons at different shallow depth [13].

Table 1: Properties of the flux of the primary particles at Belgrade CR station based on simulation for: ground level (GLL), underground level (UL), coincident muons at underground level (ULc ) and triple and more coincident muons at underground level (UL3+ ).

| Primary protons  | GLL                         | UL                 | ULc             | UL3+             |
|------------------|-----------------------------|--------------------|-----------------|------------------|
| Energy cut-off   | 5 GeV                       | $12.3 \pm 0.7$ GeV | $30 \pm 4$ GeV  | $55 \pm 14$ GeV  |
| Equivalent depth | 0 m.w.e.<br>GLL<br>Belgrade | 25 m.w.e.          | 40 m.w.e.       | 66 m.w.e.        |
| Peak energy      | 20 GeV                      | 45 GeV             | 125 GeV         | 200 GeV          |
| Median energy    | 62 GeV                      | $122 \pm 5$ GeV    | $296 \pm 8$ GeV | $458 \pm 18$ GeV |

Cut-off energy at the ground level is due to geomagnetic cut-off rigidity at Belgrade CR station. For the

underground level, the 25 m.w.e. of soil overburden is the cause of the higher cut-off underground. All the relevant quantities: cut-off, peak and median energies are higher underground and for the events with higher multiplicity. This, in principle, creates a possibility to investigate the CR flux and its variations at different energies of primaries, exceeding the energies relevant to neutron monitors, the most frequently used instrument for study of the low energy side of the CR spectrum. This vindicates the aim of the simulation to investigate possibility of utilizing a shallow underground laboratory for the study of energy dependent solar modulation process and to find an optimum detector configuration sensitive to primaries of different energy range for a given site.

#### 4. DISCUSION ON FEASIBILITY

It is needed, however, to address the questions of reliability of simulation. On the graph 3, the discontinuity at energy of 80 GeV of primary protons is visible, especially muon in UL and muons in UL in coincidence. CORSIKA, by default, uses GHEISHA 2002d particle generator to calculate the elastic and inelastic cross-sections of hadrons below 80 GeV in air and their interaction and particle collisions and for higher energies QGSJET 01C routine is used. Also it is important to know whether sufficient statistics of multi-muon events could be achieved in the limited laboratory space. For this purpose, the flux of single muons is measured at ground level and underground, the rate of double coincidences as a function of detector distance is simulated also. In addition, the rates of double and triple coincidences are also measured for several detector arrangements.

The muon flux is calculated, from simulation, by finding ratio between the number of muons reaching depth of UL ( for single and muons in coincidence) and numbers of muons generated from CORSIKA at the surface and multiplying by experimentally measured value of integrated muon surface flux which is 137(6) muons per m<sup>2</sup>s [14]. The experimental value of integrated flux, compared with number of muons from simulation, is also used to find physical time needed to generate same number of muons at the site as the simulation.

Absolute muon fluxes measured at the site for surface and shallow underground is well reproduced by the simulation (Table 2).

Table 2: Ratio of muon fluxes at Belgrade CR station based on measurements and simulation for: ground level (GLL), underground level (UL), coincident muons at underground level (ULc ) and triple and more coincident muons at underground level (UL3+ )

| Muon flux ratio | Measured GLL/UL | Simulation GLL/UL | Simulation UL/ULc | Simulation UL/UL3+ |
|-----------------|-----------------|-------------------|-------------------|--------------------|
|                 | 3.17(8)         | 3.06(3)           | 1.86(4)           | 2.68(6)            |

Recently with new detector arrangement, the scintillators in Belgrade CR station measured coincident events and triple coincident events at two distances of the detectors: 1.5m and 6m, in UL part of the laboratory. Number of coincidences per unit area of the detector, based on simulation for these distances is 80 and 66 muon coincidences per m<sup>2</sup> per day respectively. Experimental values are higher for closer ( ~350 coincidences a day ) and ~60 coincidences per day for farther arrangement. The ratio of single/coincidence events underground is well reproduced for greater distance of the detector. At shorter distances the measured ratio is higher than predicted by simulation, further study will show is it due to contribution from local EM showers and knock-on electrons. Numbers of measured triple coincidences at same distances are the order of magnitude smaller.

When upgraded, the detector arrangements will cover the whole area of the UL with muon detectors it should provide, based on the simulation, approximately 61k coincidences per day thus allowing to observe ~ 1.2% fluctuation of the CR flux with 3 $\sigma$  certainty originated from Solar modulation ( e.g. Forbush decreases) thus allowing possibility to study solar modulation on three different energy ranges of the primary particles and at higher energies then regular energies detected with NM. To prevent miss-identification of muons, additional methods of sorting muons is needed (lead shielding, hodoscopes...) or to measure only coincidences that occur on reliable distances between detectors, larger then 6m, allowing observation of higher fluctuations (~2.5%) with same certainty.

In principle, larger shallow depth laboratories [15] can be used to investigate solar modulation and extreme solar events on different energies of primary particles, using rate of detected muons on different detectors in coincidence but present small detection area at Belgrade CR station can also give some valuable insight.

#### 5. CONCLUSION

The possibility of utilizing a shallow underground laboratory for the study of energy dependent solar modulation of CR is investigated, by means of computer simulation based on CORSIKA and GEANT packages, combined with the experiment. On the experimental part, the muon flux is measured at ground level and underground at the depth of 25 mwe. In the present feasibility study, the flexible test setup for detection of multiple muons is installed underground in an attempt to achieve sensitivity to higher energy primaries. The rates of double and triple coincidences are measured for several detector distances. The simulation revealed the response functions of each experimental setup. The experimental fluxes are compared with those arising from simulation (Table 2). For single muons, the experimental ratio of

fluxes GLL/UL agrees with the simulated one. The experimental ratio of single/coincident events underground is well reproduced by simulation if the detector distance is greater than 6m. At shorter distances the measured ratio is higher than predicted by simulation, mainly due to contribution from local EM showers and knock-on electrons. When upgraded, the detector arrangements will cover almost the entire area of the UL with muons detectors resulting in expected approximately 61k coincidence per day. One day of measurements will be sufficient to observe  $\sim 1.2\%$  fluctuation of the flux at  $3\sigma$  significance for CRs with several hundred GeV of energy. Together with the single muon measurements at GLL and UL we will have simultaneous measurements centered on three different energies, under the same atmospheric and geomagnetic conditions. Any difference in time series behavior could be attributed to energy dependent response to the forcing. The rate of triple coincidences is too low to be effectively exploited in our conditions.

### Acknowledgments

The present work was funded by the Ministry of Education and Science of the Republic of Serbia, under the Project No. 171002. .

### References

- [1] L.I. Dorman, Cosmic-rays in the Earth's Atmosphere and Underground, Kluwer, Dordrecht, ( 2004)
- [2] I. Braun, J. Engler, J.R. Hörandel, J. Milke, Forbush decreases and solar events seen in the 10 - 20GeV energy range by the Karlsruhe Muon Telescope, ADVANCES IN SPACE RESEARCH 43(4):480-488, (2008)
- [3] Kalliokoski ,L. Bezrukov, T. Enqvist, H. Fynbo, L. Inzhechik, P.J. Jones, J. Joutsenvaara, J. Karjalainen, P. Kuusiniemi, K. Loo, B. Lubsandorzhev, V. Petkov, T. Rähkä, J. Sarkamo, M. Slupecki, W.H. Trzaska, A. Virkajärvi, Can EMMA solve the puzzle of the knee?, Progress in Particle and Nuclear Physics 66, 468-472, ( 2011)
- [4] A.Dragić, V.Udovičić, R.Banjanac, D.Joković, D.Maletić, N.Veselinović, M.Savić, J.Puzović, I.Aničin, The new set-up in the Belgrade low-level and cosmic-ray laboratory, Nucl. Technol. Radiat. 26, 181-192 , (2011)
- [5] A.Dragić, R.Banjanac, V.Udovičić, D.Joković, J.Puzović, I.Aničin, Periodic Variations of CR Muon Intensity in the Period 2002-2004 , Proceedings of the 21st European cosmic-ray Symposium, Košice, Slovakia ,368-373, (2008)
- [6] N. Veselinović, A. Dragić, D. Maletić, D. Joković, M. Savić, R. Banjanac ,V. Udovičić and I. Aničin, Cosmic rays muon flux measurements at Belgrade shallow underground laboratory, AIP Conf. Proc. 1645, 421 (2015); <http://dx.doi.org/10.1063/1.4909614>
- [7] S.N.Karpov ,Z.M. Karpova, A.B. Chernyaev, Multiplicity, yield and response functions for Baksan EAS-arrays and Muon Detector in comparison with similar functions of Neutron Monitors, Proceedings of the 29th International Cosmic Ray Conference, Pune, India, (2005)
- [8] D. Maurin, A. Cheminet, L. Derome, A. Ghelfi, G Hubert, Neutron Monitors and muon detectors for solar modulation studies: Interstellar flux, yield function, and assessment of critical parameters in count rate calculations, Advances in Space Research 55 (1) 363 (2015)
- [9] J.M. Clem and L.I. Dorman, Neutron monitor response functions, Space Science Reviews, Volume 93, Issue 1, pp 335-359,(2000)
- [10] D. Heck et al., CORSIKA: a Monte Carlo code to simulate extensive air showers, Report FZKA 6019, Forschungszentrum Karlsruhe, (1998)
- [11] S. Agostinelli et al., the Geant4 collaboration, Nucl. Instrum. Meth. A 506, 250-303, (2003)
- [12] A. Bogdanov, A. Dmitrieva, R. Kokoulin, A. Petrukhin, D. Timashkov, E. Yakovleva, Coupling functions for primary cosmic rays and ground-level muons at various zenith angles, Proceedings of the 21st European Cosmic Ray Symposium, pp341-346L, (2008)
- [13] N. Bogdanova, M. G. Gavrilo, V. N. Kornoukhov, A. S. Starostin, Cosmic muon flux at shallow depths underground, Phys.Atom.Nucl. 69 , 1293-1298, (2006)
- [14] A. Dragić et al., Measurement of cosmic ray muon flux in the Belgrade ground level and underground laboratories,Nucl. Instrum. Meth. A 591, 470-475, (2008)
- [15] F. Suarez for the Pierre Auger Collaboration, The AMIGA muon detectors of the Pierre Auger Observatory: overview and status, 33rd international cosmic ray conference, (2013)

# Effect of pressure and temperature corrections on muon flux variability at ground level and underground

M. Savic, A. Dragic, N. Veselinovic, V. Udovicic, R. Banjanac, D. Jokovic, D. Maletic  
*Institute of Physics, Belgrade, Pregrevica 118, Serbia*

In Low Background Laboratory at Institute of Physics Belgrade, plastic scintillators are used to continuously monitor flux of the muon component of secondary cosmic rays. Measurements are performed on the surface as well as underground (25 m.w.e depth). Temperature effect on muon component of secondary cosmic rays is well known and several methods to correct for it are already developed and widely used. Here, we apply integral method to calculate correction coefficients and use GFS (Global Forecast System) model to obtain atmospheric temperature profiles. Atmospheric corrections reduce variance of muon flux and lead to improved sensitivity to transient cosmic ray variations. Influence of corrections on correlation with neutron monitor data is discussed.

Belgrade Low Background Laboratory (LBL) is located at Institute of Physics, Belgrade and consists of two interconnected spaces, a ground level laboratory (GLL) and a shallow underground one (UL) [Fig. 1]. GLL is at 75 meters above sea level while UL is dug under a 10 meter cliff and has a 12 meters of loess soil overburden (25 meters of water equivalent) [1]. Geographic latitude for the site is 44.86 and longitude is 20.39 while geomagnetic rigidity cutoff is 5.3 GV.

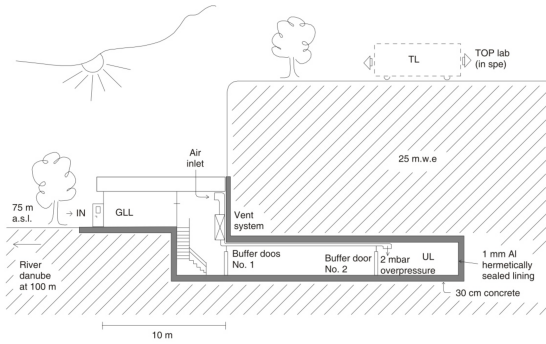


FIG. 1: Layout of the Low Background Laboratory.

Experimental setup consists of two identical sets of detectors and read out electronics, one situated in GLL and the other in UL. Each setup utilizes a plastic scintillator detector with dimensions 100cm x 100cm x 5cm (Amcryst-H, Kharkov, Ukraine) equipped with 4 PMTs (Hamamatsu R1306) directly coupled to the corners [Fig. 2]. Flash ADC (CAEN type N1728B) with 10ns sampling are used for read out [1].

Preamplifier outputs of two diagonally opposing PMTs are summed and fed to a single FADC input thus engaging two inputs of the FADC for two such diagonal pairings. Signals recorded by the two inputs are coincided in offline analysis, resulting in coincidence spectrum which is then used to determine the integral count [Fig. 3]. This procedure almost completely eliminates low-energy environmental background leaving only events induced by cosmic ray muons and muon related EM showers [1].

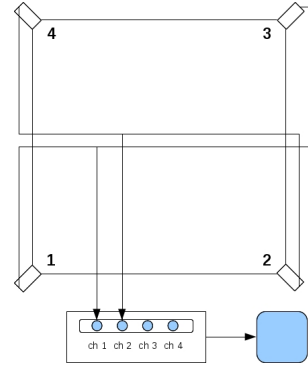


FIG. 2: Experimental setup scheme.

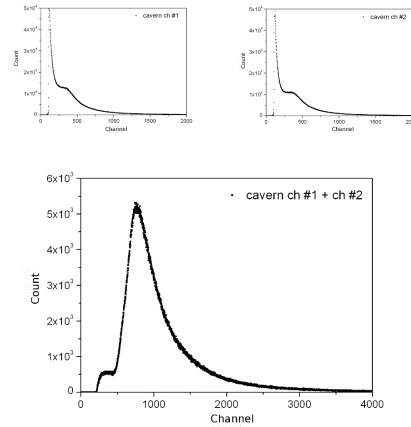


FIG. 3: Single summed diagonal and coincidence spectra.

## I. SIGNIFICANCE OF METEOROLOGICAL EFFECTS

Meteorological effects on muon component of secondary cosmic rays are well known, with pressure and temperature effect being most dominant [2]. Correcting for these effects noticeably increases data usefulness, especially increasing sensitivity to periodic and aperiodic variations of non-atmospheric origin (vari-

ations of primary cosmic rays, different heliospheric processes, etc.)

In Belgrade Low Background Laboratory continual measurements utilizing described setup started in April of 2008 for the GLL and in November of 2008 for the UL, and with some interruptions are still ongoing. Base time resolution for integrated count is 5 minutes but time resolution of 1 hour is also often used in analysis. Link to Belgrade cosmic ray station can be found on the following address: <http://www.cosmic.ipb.ac.rs/>.

### A. Pressure effect

Barometric effect is defined by the following equation:

$$\left(\frac{\delta I}{I}\right)_P = \beta \cdot \delta P \quad (1)$$

where  $\frac{\delta I}{I}$  is the normalized variation of muon flux intensity,  $\beta$  is barometric coefficient and  $\delta P$  is pressure variation. Pressure variation is calculated as  $\delta P = P - P_B$ , where  $P$  is current pressure and  $P_B$  is base pressure value [4].

Since no in situ pressure measurement was performed prior to 2015, current pressure values have mostly been acquired from official meteorological measurements performed by Republic Hydrometeorological Service of Serbia as well as from Belgrade airport meteorological measurements. In all, data from 5 different stations were used. All pressure data was normalized to Belgrade main meteorological station. Stations were sorted according to geographical proximity and consistence of data. Unique pressure time series was composed by using data from the first station with available pressure entries for a given hour. Linear interpolation was then performed and pressure values were sampled with 5 minute step. Normalized variation of muon flux intensity vs. pressure variation was plotted for each year. Only data for the 5 geomagnetically most quiet days of each month were taken into account (selected from International Quiet Days list). Barometric coefficient for each year was determined from linear fits of these plots [Fig. 4].

### B. Temperature effect

Temperature effect on hard muons is well known [2] and there are several methods developed to describe and correct for it. Method we used was integral method, where normalized variation of muon flux dependence on temperature variation is described as:

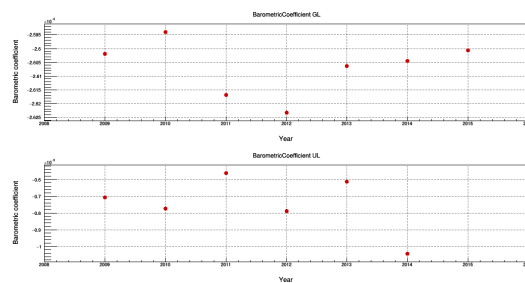


FIG. 4: Yearly values for barometric coefficient for GLL and UL.

$$\left(\frac{\delta I}{I}\right)_T = \int_0^{h_0} \alpha(h) \cdot \delta T(h) \cdot dh \quad (2)$$

$\alpha(h)$  being temperature coefficient density and temperature variation calculated as  $\delta T = T - T_B$ , where  $T$  is current temperature and  $T_B$  is base temperature value [3].

To correct for temperature effect using formula above it is necessary to have most complete information about atmospheric temperature profile for a given geographical location as well as to know temperature coefficient density function. Temperature profile measurements performed by local meteorological service are not done on consistent basis but more detailed information is available from meteorological models. One such model is GFS (Global Forecast System) that, among other data, provides temperatures for 25 isobaric levels for a given geographical location with latitude/longitude precision of 0.5 degrees [3].

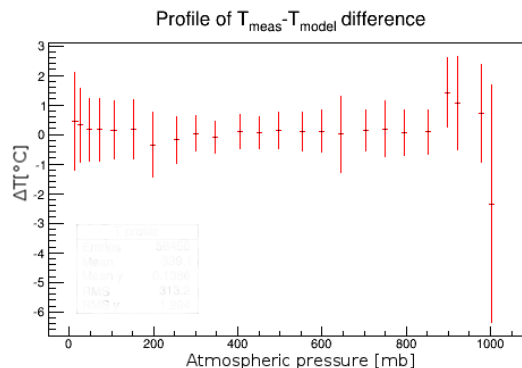


FIG. 5: Distribution of difference between modelled temperatures and temperatures measured by meteorological balloons above Belgrade (where such data was available).

Measured and modelled values seem to be in fairly good agreement [Fig. 5] except for the lowest isobaric level. That is why for this level temperature from local meteorological stations was used, treated in the same manner as described for local pressure data. Time

resolution for modelled temperatures is 6 hours so interpolation was performed using cubic spline [3] and temperature values were sampled in 5 minute steps.

Temperature density functions [Fig. 6] are calculated according to procedure described in [2].

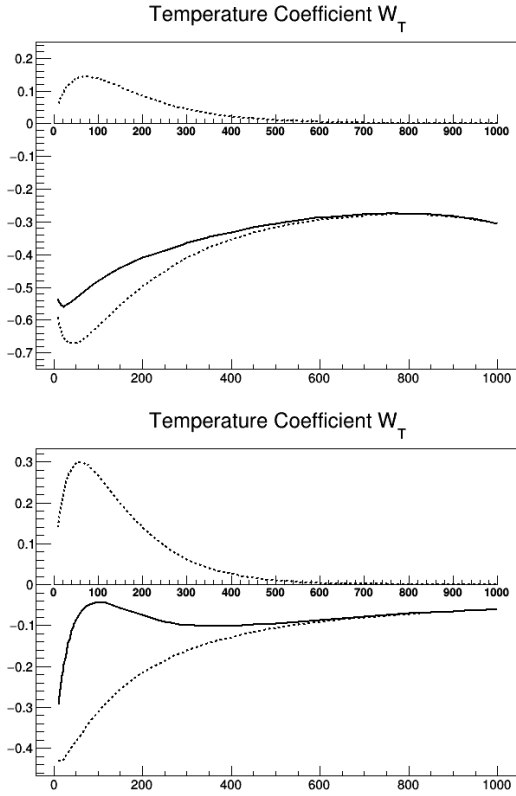


FIG. 6: Temperature coefficient density functions for ground level (above) and depth 25 m.w.e. (below).

## II. RESULTS

### A. PT corrected time series

It would seem that pressure correction successfully removes aperiodic pressure induced fluctuations while temperature correction most significantly affects annual variation induced by atmospheric temperature variations [Fig. 7].

### B. Spectral analysis

Spectral analysis can give us more insight into effect of temperature correction on annual variation of muon count (presented for GLL data in [Fig. 8])

After temperature correction, peak related to annual periodicity in power spectrum appears to be significantly reduced relative to nearby peaks.

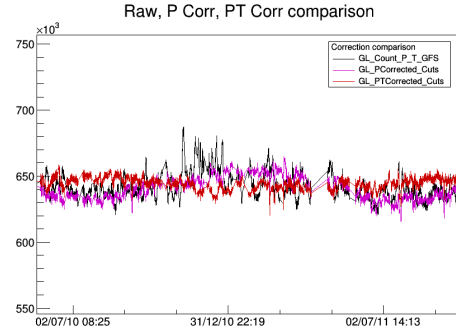


FIG. 7: GLL raw (black), pressure corrected (magenta) and PT corrected (red) muon count time series for a selected period.

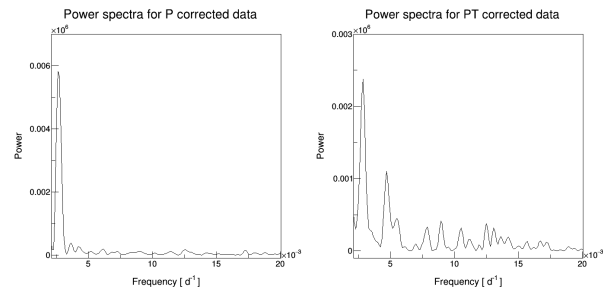


FIG. 8: Power spectra for pressure corrected and temperature and pressure corrected data.

### C. Neutron monitor correlation

Possible validation for correction procedure would be agreement of pressure/temperature corrected muon count time series with neutron monitor data. BAKSAN neutron monitor was selected as a possible reference [Fig. 9].

## III. CONCLUSIONS

Corrections for temperature and pressure effect are essential for muon data gathered at Belgrade LBL. Atmospheric temperature profile for Belgrade seems to be adequately modeled by GFS. Temperature correction utilizing integral method seems to give acceptable results (while quality can still be further improved). Also, other methods could be applied and results compared. Muon flux data after pressure and temperature corrections has increased sensitivity to periodic and aperiodic effects of non-atmospheric origin. Preliminary comparison with neutron monitor data supports this claim with more detailed correlation analysis to follow in the future.

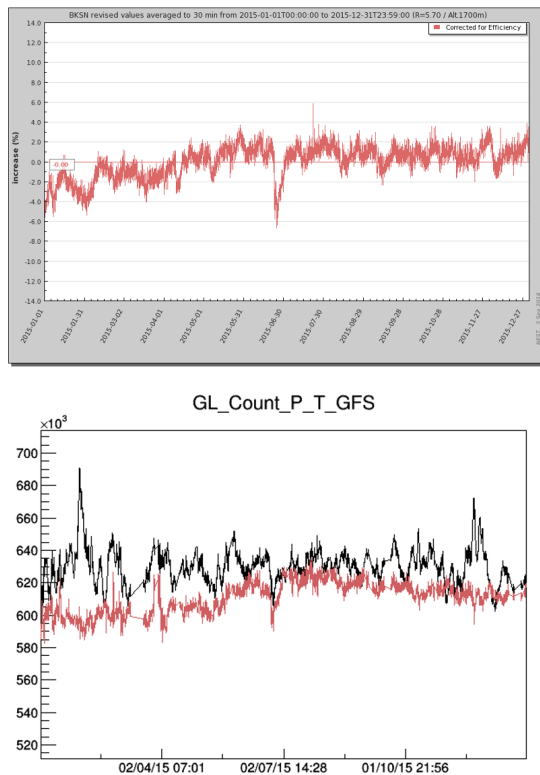


FIG. 9: BAKSAN neutron monitor (above) and GLL raw and pressure/temperature corrected data (below in red) comparison for year 2015.

#### IV. ACKNOWLEDGEMENTS

The present work was funded by the Ministry of Education and Science of the Republic of Serbia, under the Project No. 171002. The Belgrade Laboratory bears the name of Dr. Radovan Antanasijevic, in honour of its early deceased founder and first director.

#### V. REFERENCES

- [1] The new set-up in the Belgrade low-level and cosmic-ray laboratory Nucl. Technol. Radiat. 26 (2011) 181-192. A.Dragic at all
- [2] Dorman, Cosmic Rays in the Earths Atmosphere and Underground
- [3] M. Berkova , A. Belov, E. Eroshenko, and V. Yanke, Temperature effect of muon component and practical questions of how to take into account in real time, Astrophys. Space Sci. Trans., 8, 41-44, 2012
- [4] R. R. S. De Mendona, J. -P. Raulin, E. Echer, V. S. Makhmutov, and G. Fernandez, Analysis of atmospheric pressure and temperature effects on cosmic ray measurements. JOURNAL OF GEOPHYSICAL RESEARCH: SPACE PHYSICS, VOL. 118, 14031409, doi:10.1029/2012JA018026, 2013



## PREDICTABILITY OF LEAD-210 IN SURFACE AIR BASED ON MULTIVARIATE ANALYSIS

Jelena Ajtić <sup>1,\*</sup>, Dimitrije Maletić <sup>2</sup>, Đorđe Stratimirović <sup>3,\*</sup>, Suzana Blesić <sup>4,\*</sup>, Jelena Nikolić <sup>5</sup>, Vladimir Đurđević <sup>6</sup>, and Dragana Todorović <sup>5</sup>

<sup>1</sup> University of Belgrade, Faculty of Veterinary Medicine, Belgrade, Serbia

\* Institute for Research and Advancement in Complex Systems, Belgrade, Serbia

<sup>2</sup> University of Belgrade, Institute of Physics, Belgrade, Serbia

<sup>3</sup> University of Belgrade, Faculty of Dental Medicine, Belgrade, Serbia

<sup>4</sup> University of Belgrade, Institute of Medical Research, Belgrade, Serbia

<sup>5</sup> University of Belgrade, Vinča Institute of Nuclear Sciences, Belgrade, Serbia

<sup>6</sup> University of Belgrade, Faculty of Physics, Institute of Meteorology, Belgrade, Serbia

**Abstract.** Dependence of the lead-210 activity concentration in surface air on meteorological variables and teleconnection indices is investigated using multivariate analysis, which gives the Boosted Decision Trees method as the most suitable for variable analysis. A mapped functional behaviour of the lead-210 activity concentration is further obtained, and used to test predictability of lead-210 in surface air. The results show an agreement between the predicted and measured values. The temporal evolution of the measured activities is satisfactorily matched by the prediction. The largest qualitative differences are obtained for winter months.

**Key words:** lead-210, surface air, meteorological variables, teleconnection indices, multivariate analysis, wavelet transform analysis

### 1. INTRODUCTION

Lead-210 is a naturally occurring radionuclide with a half-life of 22.23 years. The main source of <sup>210</sup>Pb in surface air is its radioactive parent radon-222 that emanates from the soil. After formation, <sup>210</sup>Pb attaches to aerosols whose fate is governed by atmospheric circulation and removal processes.

A number of studies that looked into the <sup>210</sup>Pb activity concentrations at different measuring sites have shown a uniform radionuclide distribution, both in the vertical and horizontal. For example, [1] showed no significant variations in the <sup>210</sup>Pb activity concentration at three locations over distance of approximately 200 km, and still noted a case in which the <sup>210</sup>Pb activity concentration rapidly changed due to a passage of a cold front. Similarly, [2] investigated differences in the <sup>210</sup>Pb activity concentration between two measurement sites at a distance of 12 km in the horizontal and of 800 m in the vertical. Their results also showed that over longer periods of time, the radionuclide was well mixed within the atmosphere. Further, [3] found good correlation between the <sup>210</sup>Pb activity concentrations across two sites 100 km apart, which were influenced by different local conditions, including different prevalent winds.

On the other hand, the vertical profile of the <sup>210</sup>Pb activity concentration in the atmosphere has been shown to reflect the fact that the radionuclide

source is in the lowermost layer - surface air masses are richer in <sup>210</sup>Pb than air masses from higher altitudes, with the sharpest decrease in activity concentration between the ground and an altitude of 3 km [4, 5]. Further, the <sup>210</sup>Pb activity concentration is higher in continental air masses than in air masses originating over a body of water [2, 6, 7], which results in the radionuclide activity concentration variations in the horizontal, and also explains temporal differences in a location under influence of interchangeable winds of either continental or maritime origin [2].

The above mentioned studies, however, did not include an analysis of <sup>210</sup>Pb relation with large-scale atmospheric circulation. The North Atlantic Oscillation (NAO) index is one of the most commonly used teleconnection indices to describe a large-scale circulation pattern over the North Atlantic Ocean and surrounding land masses [8]. The two oscillation phases of NAO induce changes in large-scale circulation patterns [9], which further reflect on local weather conditions especially over eastern North America and across Europe, including Serbia [10]. The Polar/Eurasia pattern [8] is another teleconnection that has an impact on weather in Europe [11]. Further, the East Atlantic/Western Russia pattern [8] influences the amount of precipitation in southeast part of Europe [12], and can thus be a contributing factor in the amount of <sup>210</sup>Pb in surface air.



In contrast to a very limited number of studies looking into an influence of large-scale atmospheric transport on the  $^{210}\text{Pb}$  activity concentrations, a link between local meteorological variables and the radionuclide activities has been extensively investigated [7, 13, 14, 15]. For example, to name only a few: [16] showed a strong positive relationship between the  $^{210}\text{Pb}$  deposition and precipitation; [17] found a positive correlation of  $^{210}\text{Pb}$  activity concentration with temperature, and negative correlation with precipitation, relative humidity and wind speed; [14] showed that washout is the most significant mechanism of  $^{210}\text{Pb}$  removal from the atmosphere.

The goal of our analysis is to combine meteorological data and large-scale atmospheric transport patterns (quantified by teleconnection indices) and treat the  $^{210}\text{Pb}$  concentration in surface air as a result of their interplay. Different statistical tools are employed to achieve this. On one hand, a set of multivariate methods incorporated in the Toolkit for Multivariate Analysis (TMVA) [18] is used. It is complemented by a wavelet transform spectral analysis [19]. A mapped functional behaviour which is obtained in the analysis is then used to test predictability of the  $^{210}\text{Pb}$  activity concentration in surface air.

## 2. DATASETS

In Belgrade, Serbia, at the Vinča Institute of Nuclear Sciences, continual measurements of the  $^{210}\text{Pb}$  activity concentrations in surface air started in 1985. The monthly mean activity concentrations in composite aerosol samples were determined on High Purity Germanium detectors by standard gamma spectrometry. The activity concentrations of  $^{210}\text{Pb}$  were determined using the gamma energy of 46.5 keV. A detailed description of the measurement procedure is given in [15].

The meteorological daily data: minimum, maximum and mean temperature, atmospheric pressure, relative humidity, precipitation, sunshine hours and cloud cover data for Belgrade, were obtained from the European Climate Assessment & Dataset (ECA&D) [20] and the Republic Hydrometeorological Service of Serbia. In addition, a temperature variable, which does not have a local character, was included to investigate the extent to which the local meteorological variables influence the  $^{210}\text{Pb}$  activity concentration in the air. The chosen variable was the Northern Hemispheric mean monthly temperature anomaly over land calculated from historical temperature records ([http://www.cru.uea.ac.uk/cru/data/temperature/C\\_RUTEM4-nh.dat](http://www.cru.uea.ac.uk/cru/data/temperature/C_RUTEM4-nh.dat) visited on 10 March 2015). The temperature anomaly was derived as a deviation from a reference temperature value which, in this data set, was taken as the mean over a reference period 1961–1990. More details on the temperature anomaly calculations can be found in [21, 22].

The data for eight teleconnection indices of large-scale atmospheric circulation: North Atlantic Oscillation (NAO), East Atlantic (EA), East

Atlantic/Western Russia, Scandinavia (SCAND), Polar/ Eurasia, Western Pacific (WP), East Pacific-North Pacific (EP-NP), and Pacific/North American (PNA) were obtained from the data archive of the United States National Oceanic and Atmospheric Administration's Climate Prediction Center (<http://www.cpc.ncep.noaa.gov/data/teledoc/teleconnections.shtml> visited on 18 October 2013). A description of the procedure used to identify the Northern Hemisphere teleconnection patterns and indices is given in [8]. The monthly values of teleconnection indices since 1950 were available.

The temporal resolution of the input variables differed: the  $^{210}\text{Pb}$  activity concentrations and the teleconnection indices, apart from NAO, were available as monthly mean values. This resolution implied a total number of data points that was insufficient for MVA which inherently requires a large number of points to determine the mapped behaviour. To overcome this drawback, an interpolation of the monthly measurements was performed using Fast Fourier Transform smoothing on monthly data (Fig. 1).

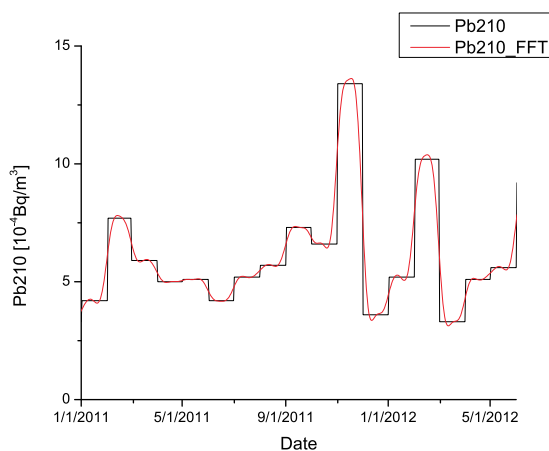


Fig. 1 Fast Fourier Transform of the monthly  $^{210}\text{Pb}$  activity concentrations in surface air. The Fast Fourier Transform curve gives interpolated daily  $^{210}\text{Pb}$  values which were used in the MVA classification and regression analysis.

## 3. CALCULATIONS

### 3.1. Multivariate Analysis

Many multivariate methods and algorithms for classification and regression are integrated in the analysis framework ROOT [23], and the Toolkit for Multivariate Analysis (TMVA) [18]. Multivariate analysis is used to create, test and apply all available classifiers and regression methods to single out one method that is the most appropriate and yields maximum information on the dependence of an investigated variable on a multitude of input variables. Thus, in TMVA there is no need to choose *a priori* a method for the data classification and regression – all of the techniques incorporated in TMVA are tested and the most suitable one is chosen for further analysis.

The TMVA package includes various techniques, such as multi-dimensional likelihood estimation, linear and nonlinear discriminant analysis, artificial neural networks, support vector machine, and boosted/bagged decision trees. All the techniques in TMVA belong to the family of "supervised learning" algorithms. They make use of training events, for which the desired output is known, to determine the mapping function that either describes a decision boundary (classification) or an approximation of the underlying functional behaviour defining the target value (regression). All MVA methods see the same training and test data.

The multivariate methods are compared within the procedure in order to find one which, on the basis of input variables, gives a result satisfactorily close to the observed values of the output variable. More details on calculation procedure are given in [24].

In our analysis, the output variable was the activity concentration of  $^{210}\text{Pb}$  in surface air, while the input variables were the nine meteorological variables, one derived variable, and eight teleconnection indices, adding to 18 input variables in total. A multivariate method that gave the best regression results in our study was the Boosted Decision Trees method.

### 3.1.1. Boosted Decision Trees

Boosted Decision Trees (BDT) is a method in which a decision is reached through a majority vote on a result of several decision trees. A decision tree consists of successive decision nodes which are used to categorise the events in a sample, while BDT represents a forest of such decision trees. The (final) classification for an event is based on a majority vote of the classifications done by each tree in the forest, which ultimately leads to a loss of the straightforward interpretation in a decision tree. More detailed information on training in BDT can be found in [24].

An importance of an input variable is measured by a "variable rank". In BDT, this measure is derived by counting the number of times a specific variable is used to split decision tree nodes, and then weighting each split occurrence by the separation gain-squared it achieved and by the number of events in the node [18].

### 3.2. Wavelet Transform Analysis

Wavelet transform (WT) is a standard analytical tool in investigation of time series with nonstationarities at different frequencies [19]. In WT analysis, a calculated global wavelet power spectrum (which corresponds to Fourier power spectrum) is smooth and can therefore be used to estimate characteristic periods in the data sets. To detect these characteristic periods, a standard peak analysis was performed by searching the maximum and saddle (for hidden peaks) points in the global wavelet power spectra of the  $^{210}\text{Pb}$  activities.

## 4. RESULTS AND DISCUSSION

The WT analysis showed a number of characteristic periods in the  $^{210}\text{Pb}$  activity concentration in surface air (Fig. 2). The periods are given by the time coordinates of the local maxima in the  $^{210}\text{Pb}$  activity concentration power spectrum. Three short characteristic periods were found, with a seasonal one (at 2.6 months) most pronounced. The annual cycle (at 11.8 months) was also evident, as well as a longer period of approximately three years (at 36.5 months). Apart from the annual cycle [2, 14, 15], the other  $^{210}\text{Pb}$  periodicities have not been studied in detail.

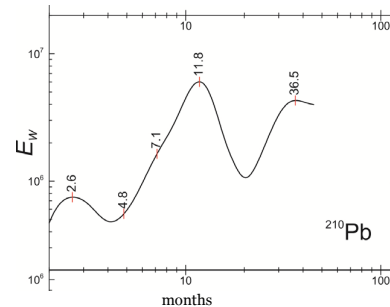


Fig. 2 Power spectrum of the  $^{210}\text{Pb}$  activity concentration in surface air. Positions of the maximum and saddle points are marked with the assigned values of characteristic time in months.

To allow for the prominent annual cycle in the  $^{210}\text{Pb}$  activity concentration in surface air, another input variable, called MonthDay, was introduced in the analysis. The MonthDay variable is purely mathematical – its values represent a sum of the month number (1 to 12) and the day number in a month divided by the total number of days in the given month. For example, a MonthDay value for 10 January is  $1+10/31$ . This variable has an annual cycle and thus serves as a proxy of any contributing variable which is not specified in the analysis but also exhibits an annual cycle.

Prior to the multivariate analysis, the Pearson's linear correlation coefficients for the input variables and  $^{210}\text{Pb}$  activity concentrations were calculated (Tab. 1) using the monthly means. The strongest correlation was found with temperature anomaly. However, that correlation was not significant at the 0.05 level. Statistically significant linear correlation was obtained only for atmospheric pressure and three teleconnection indices: EP-NP, East Atlantic/Western Russia, and Polar/Eurasia.

The calculated correlation coefficients describe the measure of linear correlation between the  $^{210}\text{Pb}$  activity concentrations and the input variables. However, apart from linear, other types of dependence between variables could exist. Each method incorporated in the MVA gives its own ranking (as one of the results), which does not necessarily coincide with a ranking of another method, or with the order given by the linear correlation coefficients.

Table 1. Pearson's linear correlation coefficients ( $r$ ) of the input variables and the  $^{210}\text{Pb}$  activity concentration in surface air, and the BDT variable ranking. The correlation coefficients significant at the 0.05 level are given in bold.

| Variable                     | $r$          | BDT rank |
|------------------------------|--------------|----------|
| Temperature anomaly          | -0.47        | 1        |
| Precipitation                | -0.22        | 18       |
| Atmospheric pressure         | <b>+0.21</b> | 15       |
| EP-NP                        | <b>+0.19</b> | 6        |
| Cloud cover                  | -0.16        | 17       |
| East Atlantic/Western Russia | <b>+0.14</b> | 8        |
| Polar/Eurasia                | <b>+0.12</b> | 7        |
| NAO                          | +0.10        | 4        |
| SCAND                        | +0.08        | 9        |
| Mean temperature             | -0.08        | 11       |
| Minimum temperature          | -0.08        | 12       |
| Maximum temperature          | -0.07        | 14       |
| Relative humidity            | +0.07        | 16       |
| Sunshine hours               | -0.07        | 13       |
| PNA                          | +0.04        | 5        |
| WP                           | +0.03        | 3        |
| EA                           | +0.008       | 10       |
| MonthDay value               | N/A          | 2        |

#### 4.1. Regression Analysis

A result of MVA regression method training is an approximation of the underlying functional behaviour that defines the dependence of the target value, the  $^{210}\text{Pb}$  activity concentrations in our analysis, on the input variables. This set of calculations was based on the measurements performed during the training period, which was from 1985 to 2010 in our case. Predictability of the  $^{210}\text{Pb}$  activity concentration in surface air was tested in the ensuing calculations, in which the measurements for 2011 and 2012 were used.

The analysis indicated that the best regression method, in which the output values (evaluated, or predicted,  $^{210}\text{Pb}$  activity concentrations) were closest to the measured concentrations, was BDT. In an ensemble of multivariate methods, the average quadratic deviation between the evaluated and measured values was the least for BDT (Fig. 3). The BDT output deviation from the measurements over the training period was close to zero for the majority of data points (Fig. 4), which confirmed the good quality of the regression method.

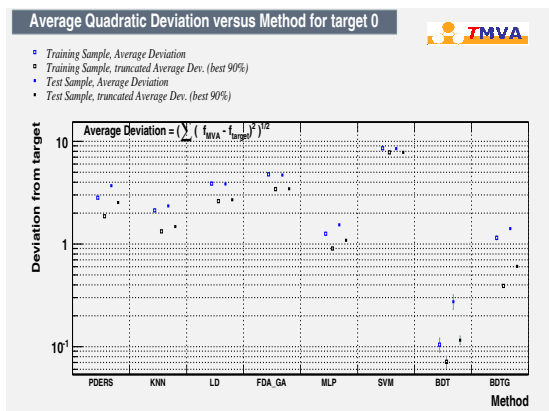


Fig. 3 Average quadratic deviation for multivariate regression methods. The deviation was the least for BDT.

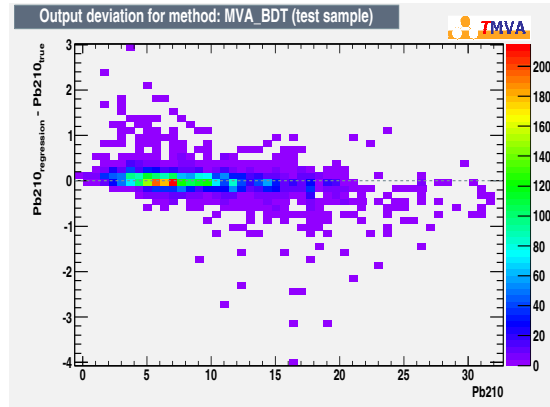


Fig. 4 Difference between the BDT evaluated and the measured  $^{210}\text{Pb}$  activity concentrations. The colour bar on the right gives the number of data points.

One of the results given by the BDT method is a variable ranking (Table 1). Apart from temperature anomaly (rank 1), all other meteorological variables were ranked as less important than the teleconnection indices. The influence of the large-scale circulation is not well understood, but the local  $^{210}\text{Pb}$  activity concentration could be significantly influenced by mesoscale and synoptic scale variations in atmospheric pressure (as quantified by the teleconnection indices). The local variations in atmospheric pressure, on the other hand, could play a minor role (low BDT rank in Table 1).

Similarly, a high rank obtained for temperature anomaly (Table 1) may imply that the  $^{210}\text{Pb}$  activity concentration in surface air is to a certain extent insensitive to relatively fast variations in local temperature.

The high rank of the MonthDay variable could indicate an existence of another contributing factor with a strong annual cycle.

#### 4.2. $^{210}\text{Pb}$ activity concentration prediction

The final step in our analysis was an evaluation of the  $^{210}\text{Pb}$  activity concentration outside the training period for which the mapped functional behaviour was obtained. In other words, the input variables for 2011 and the first half of 2012 were used to calculate the output variable which was then compared to the measured  $^{210}\text{Pb}$  activity concentration over that period (Fig. 5).

The standard deviation of all the absolute and relative differences between the BDT evaluated and measured  $^{210}\text{Pb}$  values were  $0.64 \cdot 10^{-4}$  Bq/m<sup>3</sup> and 0.12, respectively.

The temporal evolution of the  $^{210}\text{Pb}$  activity concentration was satisfactorily captured by the regression method (Fig. 5). However, the regression was not able to quantitatively predict the observed values in winter periods, when the radionuclide activity concentration reached maximum values. Thus, during January and February 2011, the evaluated values were conspicuously higher than the measured ones, while in November and December of the same year, the evaluation first underestimated and then overestimated the  $^{210}\text{Pb}$

activity concentration. It can, however, be argued that the sum of the predicted  $^{210}\text{Pb}$  activity concentrations for these two months matched the sum of the measured values. Furthermore, a local maximum seen in February 2012 was satisfactorily reproduced by the method.

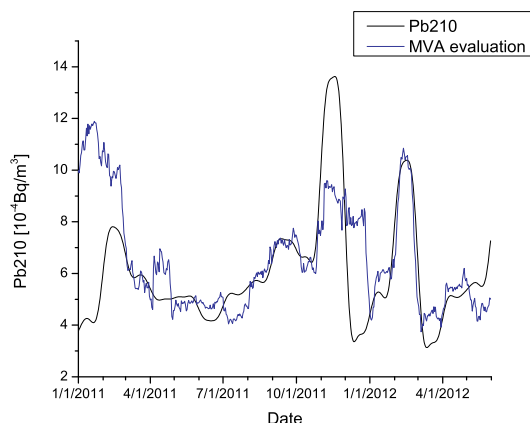


Fig. 5  $^{210}\text{Pb}$  activity concentration measured in surface air (black line) and evaluated by MVA (blue line) during 2011 and the first half of 2012.

The above results may indicate that in winter some additional processes play a key role in the  $^{210}\text{Pb}$  activity concentration in surface air. Emanation of radon-222, the parent radionuclide, could be affected by soil conditions, such as snow cover, soil temperature and moisture, and it could thus induce changes in the  $^{210}\text{Pb}$  source abundance. Future choice of input variables should include some soil parameters in an attempt to increase the accuracy of the  $^{210}\text{Pb}$  prediction in winter months.

Further assessments and refinements of the prediction should also address the limitation given by the temporal resolution of the measured  $^{210}\text{Pb}$  activity concentration in the air. The interpolation of the monthly data performed to obtain daily values (Fig. 1) could give rise to spurious relations between the  $^{210}\text{Pb}$  activity concentration and input variables, which could reflect on the mapped functional behaviour, and in turn, on the prediction of  $^{210}\text{Pb}$  in surface air. A possible way to check the validity of our method is to run the prediction using only the measured monthly values, while still employing the daily data in the training period. However, a preferred approach to our method refinement would be to use a more comprehensive database with the measured  $^{210}\text{Pb}$  activity concentration of higher temporal resolution.

## 5. CONCLUSIONS

The dependence of the  $^{210}\text{Pb}$  activity concentration in surface air on different meteorological variables and indices of large-scale circulation was investigated using multivariate analysis.

Boosted Decision Trees was singled out as the best regression method with the least average

quadratic deviation between the evaluated and measured activity concentrations. The importance variable ranking given by the BDT method implied a greater influence of large-scale transport than of the local meteorological variables.

The prediction of the  $^{210}\text{Pb}$  activity concentrations showed an agreement with the measurements, except in winter months when the largest differences were obtained.

**Acknowledgement:** The paper is a part of the research done within the projects "Climate changes and their influence on the environment: impacts, adaptation and mitigation" (No. 43007), "Nuclear research methods of rare events and cosmic radiation" (No. 171002), and "Phase transitions and their characterization in inorganic and organic systems" (No. 171015) financed by the Ministry of Education, Science and Technological Development of the Republic of Serbia (2011-2014). The authors would also like to thank the Republic Hydrometeorological Service of Serbia for data provision.

## REFERENCES

1. T. Abe, T. Kosako and K. Komura, "Relationship between variations of  $^7\text{Be}$ ,  $^{210}\text{Pb}$  and  $^{212}\text{Pb}$  concentrations and sub-regional atmospheric transport: Simultaneous observation at distant locations", *J. Environ. Radioact.*, vol. 101, pp. 113-121, 2010.
2. L. Bourcier, O. Masson, P. Laj, J. M. Pichon, P. Paulat, E. Freney and K. Sellegri, "Comparative trends and seasonal variation of  $^7\text{Be}$ ,  $^{210}\text{Pb}$  and  $^{137}\text{Cs}$  at two altitude sites in the central part of France", *J. Environ. Radioact.*, vol. 102, pp. 294-301, 2011.
3. R. L. Lozano, M. A. Hernández-Ceballos, J. F. Rodrigo, E. G. San Miguel, M. Casas-Ruiz, Eason, R. García-Tenorio and J. P. Bolívar, "Mesoscale behavior of  $^7\text{Be}$  and  $^{210}\text{Pb}$  in superficial air along the gulf of Cadiz (south of the Iberian Peninsula)", *Atmos. Environ.*, vol. 80, pp. 75-84, 2013.
4. L. Kownacka, Z. Jaworowski and M. Suplinska, "Vertical distribution and flows of lead and natural radionuclides in the atmosphere", *Sci. Total Environ.*, vol. 91, pp. 199-221, 1990.
5. J. Braziewicz, L. Kownacka, U. Majewska and A. Korman, "Elemental concentrations in tropospheric and lower stratospheric air in a Northeastern region of Poland", *Atmos. Environ.*, vol. 38, pp. 1989-1996, 2004.
6. F. P. Carvalho, "Origins and concentrations of  $^{222}\text{Rn}$ ,  $^{210}\text{Pb}$ ,  $^{210}\text{Bi}$  and  $^{210}\text{Po}$  in the surface air at Lisbon, Portugal, at the Atlantic edge of the European continental landmass", *Atmos. Environ.*, vol. 29, pp. 1809-1819, August 1995.
7. A. S. Likuku, "Factors influencing ambient concentrations of  $^{210}\text{Pb}$  and  $^7\text{Be}$  over the city of Edinburgh (55.9°N, 03.2°W)", *J. Environ. Radioact.*, vol. 87, pp. 289-304, 2006.
8. A. G. Barnston and R. E. Livezey, "Classification, seasonality and persistence of low-frequency atmospheric circulation patterns", *Mon. Wea. Rev.*, vol. 115, pp. 1083-1126, June 1987.
9. J. W. Hurrell, "Decadal trends in the North Atlantic Oscillation: regional temperatures and precipitation", *Science*, vol. 269, pp. 676-679, August 1995.

## BACKGROUND SPECTRUM CHARACTERISTICS OF THE HPGE DETECTOR LONG-TERM MEASUREMENT IN THE BELGRADE LOW-BACKGROUND LABORATORY

Radomir Banjanac, Vladimir Udovičić, Dejan Joković, Dimitrije Maletić, Nikola Veselinović, Mihailo Savić, Aleksandar Dragić, Ivan Aničin

Institute of Physics, Belgrade, Serbia

**Abstract.** The Belgrade low-level background laboratory, built in 1997, is shallow (25 m.w.e) underground space (45m<sup>2</sup>) which is constantly ventilated with fresh air against radon. The muon intensity (about 3.5 times less than at ground level), radon concentration (suppressed to averaged value of 15 Bqm<sup>-3</sup>), as well as gamma-ray background are monitoring for more than eight years. After long-term measurement using the radiopure HPGe detector with 35% relative efficiency, the measured data includes radionuclide concentration of detector surroundings, estimation of background time variation due to radon and cosmic-rays as well as MDA values for typical samples of water matrix. The detailed characteristics of gamma-ray background spectra are here presented.

**Key words :** Underground laboratory, Low-level background, long-term gamma-ray measurement

### 1. INTRODUCTION

Various experiments which strive for the detection of very rare events require the lowest possible background radiation which can be achieved only in a deep underground laboratory. Some of recent the most interesting are double beta-decay experiments, [1] and dark matter searches, [2]. In any applied measurements of low activities, a goal that is pursued by all gamma spectroscopist is to lower the minimum detectable activity (MDA) of their detection system obtaining more statistical evidence in less time.

But, any long and even short-term gamma-ray background measurement is subject to certain temporal variations due to time variability of two prominent contributors to background, cosmic-rays and radon. The most of the low background laboratories that deal with low activity measurements have developed routine measurements of background. The duration of these measurements may be from one day to even a month and they are designed to produce results with sufficiently low statistical errors for the envisaged measurements. These measurements yield only average values of the background, what in principle may lead to systematic errors in later measurements, especially of NORM samples.

The averaged values of the background, gamma lines and continuum, nuclide concentrations or MDA presenting a "personal card" of used detector system for certain samples in any low-level background laboratory, [3]. Here is attempt to present our low-level background laboratory in a similar way. First of all, the detailed description of the laboratories and used detector system are described.

### 2. DESCRIPTION OF THE LABORATORIES AND EQUIPMENT

The Belgrade underground low-level laboratory (UL), built in 1997 and located on the right bank of the river Danube in the Belgrade borough of Zemun, on the grounds of the Institute of Physics. The overburden of the UL is about 12 meters of loess soil, equivalent to 25 meters of water. It is equipped with ventilation system which provides low radon concentration of 15(5) Bq/m<sup>3</sup>. The "passive" shield consists of 1 mm thick aluminum foil which completely covers all the wall surfaces inside the laboratory, including floor and ceiling. As the active radon shield the laboratory is continuously ventilated with fresh air, filtered through one rough filter for dust elimination followed by active charcoal filters for radon adsorption. The UL has an area of 45m<sup>2</sup> and volume of 135m<sup>3</sup> what required the rate of air inlet adjusted to 800m<sup>3</sup>/h. This huge amount of fresh air contributes to greater temperature variations and the long-term mean value of temperature inside the UL is 19(4)°C. The rate of air outlet (700m<sup>3</sup>/h) was adjusted to get an overpressure of about 200 Pa over the atmospheric pressure, what prevents radon diffusion through eventual imperfections in the aluminum layer. Relative humidity is controlled by a dehumidifier device, what provides that the relative humidity in the underground laboratory does not exceed 60%. The muon intensity (which is about 3.5 times less than at ground level), radon concentration and gamma-ray background are monitoring for more than eight years. Comparative background study is performing in the GLL (at ground level) which is equipped with a Ge detector (13% relative efficiency and not intrinsically low-radioactivity level, named SGe) and a big plastic scintillator (1m<sup>2</sup>, named BPS) in veto position. The GLL is air-conditioned (average radon concentration of

50(30) Bq/m<sup>3</sup>) has an area of 30m<sup>2</sup> and volume of 75m<sup>3</sup>. The Fig. 1 presents veto arrangement of the HPGe detector (BGe, in 12cm lead shield) and big plastic scintillator, inside the UL.

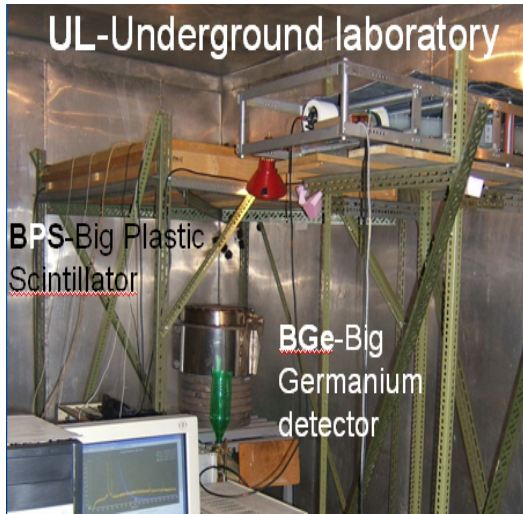


Fig. 1 Veto arrangement of the HPGe detector (BGe) and big plastic scintillator inside the UL

### 3. DESCRIPTION OF DETECTOR SYSTEMS IN THE UL

The low-level background detector system in the UL includes an intrinsically low-radioactivity level p-type Ge detector (35% relative efficiency, named BGe) and another plastic veto scintillator (1m<sup>2</sup>, named BPS) situated coaxially above the BGe detector. The BGe is a GEM30 model (made by ORTEC) in LB-GEM-SV cryostat configuration with magnesium end cap. The energy resolution at 1332.5keV, measured by analog data acquisition system, is 1.72keV, 0.65keV at 122keV as well as the Peak to Compton ratio at 1332.5keV has value of 68. The cylindrical lead shielding of the BGe, with a wall thickness of 120 mm and an overall weight of about 900kg, was cast locally out of scratch plumbing retrieved after the demolition of some old housing. Radon monitoring inside the laboratories was performed by radon monitor, model RM1029 manufactured by Sun Nuclear Corporation. The device consists of two diffused junction photodiodes as a radon detector, and is furnished with sensors for temperature, pressure and relative humidity. A pair of plastic scintillator detectors is used for CR muon measurements at both laboratories. One of them is a larger (100cmx100cmx5cm) detector (BPS), equipped with four PMT directly coupled to the corners beveled at 45°, made by Amcryst-H, Kharkov, Ukraine. The other, a smaller 50cmx23cmx5cm plastic scintillator detector, with a single PMT looking at its longest side via a Perspex light guide tapering to the diameter of a PMT, made by JINR, Dubna, Russia, and assembled locally. The smaller detector may serve as a check of stability of the muon time series obtained from the larger detector, which is important for long term measurements. Two flash analog to digital converters (FADC), made by C.A.E.N (type N1728B), which sample at 10 ns intervals into 214 channels were used

to analyze spectra from Ge detectors as well as corresponding BPS. User-friendly software was developed to analyze the C.A.E.N data with the possibility to choose the integration time for further time-series analysis that corresponds to integration time of the radon monitor. The performances of digital acquisition system as well as software developed for analysis were described in detail, [4].

### 4. THE RESULTS OF BACKGROUND MEASUREMENTS IN THE UL

Additional to intrinsically low-radioactivity level of the BGe itself, environmental radioactivity is low, too. The UL was built from low activity concrete about 12 Bq/kg of U-238 and Th-232, and of 23 Bq/kg and 30 Bq/kg of surrounding soil, respectively. Radioactivity of aluminum wall-lining is negligible. Pb-210 activity of used lead shield of 30Bq/kg is measured. After long-term cosmic-ray, [5], radon concentration, [6] and gamma-ray background measurements, no significant long-term time variations of gamma background was found, [7]. After several years of almost continuously background measurements, the integral background rate in the region from 40keV to 2700keV has mean value of about 0.5 cps. The lines of Co-60 are absent in the background spectrum, while the line of Cs-137 with the rate of  $1 \times 10^{-4}$  cps starts to appear significantly only if the measurement time approaches one month. Fukushima activities, though strongly presented in our inlet air filters samples, did not enter the background at observable levels, in spite of the great quantities of air that we pump into the UL to maintain the overpressure, and it seems that the double air filtering and double buffer door system, along with stringent radiation hygiene measures, is capable of keeping the UL clean in cases of global accidental contaminations. No signatures of environmental neutrons, neither slow nor fast, are present in direct background spectra.

The Fig. 2 shows a characteristic shape of background spectrum obtained in the UL after about 6 months of measuring, with distinctive Pb X-ray lines at the beginning of the spectrum, annihilation line, and lines from <sup>40</sup>K and <sup>208</sup>Tl (2614.5keV) at the end of the spectrum with a lot of post-radon lines between them.

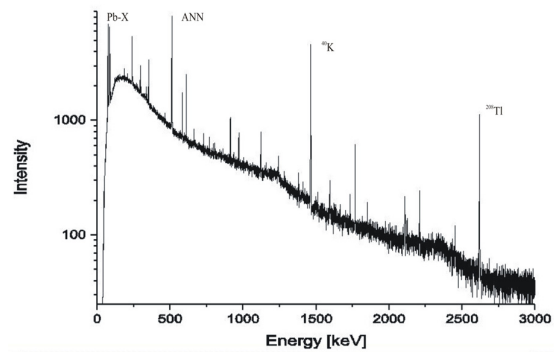


Fig. 2 Background spectrum of the HPGe detector (BGe) inside the UL after about 6 months of measuring

The table 1 in the third column presents gamma-ray background values of typical spectrum measured in

the UL using the BGe in direct (no veto) mode. The measurement time was about 6 months.

Table 1 The background characteristics of the BGe inside the UL

| Line/<br>region<br>(keV) | Radionuclide/<br>series/<br>nuclear<br>reaction | Intensity<br>( $10^{-3} \text{ s}^{-1}$ ) | MDA<br>(mBq)<br>for<br>100ks<br>Water<br>matrix |
|--------------------------|---|---|---|
| 40-2700                  | -   | 500                                       | -   |
| 46.5                     | Pb-210/U-238                                    | 0.38(11)                                  | 1500  |
| 53.2                     | U-234   | -   | 9400  |
| 63.3                     | Th-234  | -   | 700   |
| 72.8                     | Pb-X-K $\alpha_2$                               | 3.1(1)                                    | -   |
| 75                       | Pb-X-K $\alpha_1$                               | 6.2(1)                                    | -   |
| 84.9                     | Pb-X-K $\beta_1$                                | 4.2(1)                                    | -   |
| 87.3                     | Pb-X-K $\beta_2$                                | 1.49(6)                                   | -   |
| 92.5                     | Th-234  | -   | 100   |
| 143.8                    | U-235   | -   | 20  |
| 163.4                    | U-235   | -   | 110   |
| 200.3                    | U-235   | -   | 100   |
| 238.6                    | Pb-212/Th-232                                   | 0.83(4)                                   | 40  |
| 242                      | Pb-214/U-238                                    | 0.20(2)                                   | -   |
| 295.2                    | Pb-214/U-238                                    | 0.71(4)                                   | 40  |
| 338.3                    | Ac-228/Th-232                                   | 0.15(2)                                   | -   |
| 351.9                    | Pb-214/U-238                                    | 1.26(5)                                   | 30  |
| 477.6                    | Be-7  | -   | 40  |
| 510.8+511                | Tl-208/Th-232/ANN                               | 7.0(1)                                    | -   |
| 583.2                    | Tl-208/Th-232                                   | 0.30(3)                                   | 56  |
| 609.2                    | Bi-214/U-238                                    | 1.08(5)                                   | 60  |
| 661.7                    | Cs-137  | 0.10(5)                                   | 9   |
| 727.3                    | Bi-212  | -   | 200   |
| 803.3                    | Pb-206 (n,n $\gamma$ )<br>Pb-206                | 0.11(2)                                   | -   |
| 911.2                    | Ac-228/Th-232                                   | 0.25(2)                                   | 110   |
| 969                      | Ac-228/Th-232                                   | 0.11(2)                                   | 80  |
| 1001                     | Pa-234m   | -   | 1300  |
| 1120.4                   | Bi-214/U-238                                    | 0.28(3)                                   | -   |
| 1173.2                   | Co-60   | -   | 19  |
| 1332.5                   | Co-60   | -   | 11  |
| 1238.1                   | Bi-214/U-238                                    | 0.09(2)                                   | -   |
| 1460.8                   | K-40  | 3.27(9)                                   | 850   |
| 1764.6                   | Bi-214/U-238                                    | 0.49(3)                                   | 230   |
| 2103.7                   | 2614.5SE/Tl-208                                 | 0.13(2)                                   | -   |
| 2204.2                   | Bi-214/U-238                                    | 0.15(2)                                   | -   |
| 2614.5                   | Tl-208/Th-232                                   | 1.05(5)                                   | -   |

The fourth column of the same table presents minimum detectable activity (MDA) calculated for predicted measurement time of 100000 seconds (approximately one day) for cylindrical sample (volume of 120cm<sup>3</sup>) situated on the top of the detector. Efficiency calibration was obtained by GEANT4 simulation toolkit as well as experimentally using appropriate standard. The difference between the two efficiency calibration curves is less than 5% for sample of water matrix, which MDA is here presented. MDA values are calculated as  $MDA=L_D/(t \times \text{Eff} \times p)$ , where the  $L_D=2.71+4.65B^{1/2}$  is detection limit. B is background at the energy of gamma-ray line with

absolute detection efficiency Eff and emission probability p. If the predicted measurement time t is valued in seconds then MDA values have Bq unit. The obtained MDA values are presented for water matrix cylindrical samples in bottles with volume of 120cm<sup>3</sup>.

With the BPS currently positioned rather high over the detector top, at a vertical distance of 60cm from the top of the lead castle, in order to allow for the placing of voluminous sources in front of the vertically oriented detector, the off-line reduction of this integral count by the CR veto condition is only about 18%. Up to a factor of two might be gained if the veto detector were to be positioned at the closest possible distance over the BGe detector. This configuration requires some changes of the lead shield including introducing a sliding lead lid. Such a new shielding and veto configuration would be additionally reduce gamma-ray background up to the same factor that corresponds to factor of reduction expected for cosmic rays.

We do not insist on the lowering of statistical errors which depend on background levels solely and are difficult to reduce further with available means, but rather emphasize its stability due to the low and controlled radon concentration in the laboratory. This is essential, especially in NORM measurements, and makes our system virtually free of systematic errors as compared to systems which operate in environments where radon is not controlled. In that systems the reduction of post-radon background activities is achieved by flushing the detector cavity with liquid nitrogen vapor, where the transient regimes during sample changes and possible deposition of radon progenies may introduce systematic uncertainties which are difficult to estimate.

**Acknowledgement:** The paper is a part of the research done within the projects OI171002 and III43002.

#### REFERENCES

1. W.G. Kang, *et al.*, "Ultra-low gamma-ray measurement system for neutrinoless double beta decay", *Appl. Radiat. Isot.* (2013), vol. 81, pp. 290–293.
2. G. Angloher, *et al.*, "Results from 730 kg days of the CRESST-II Dark Matter search", *Eur. Phys. J.* (2012), vol. C72, pp. 1971
3. L. Dragounová and P. Rulík, "Low level activity determination by means of gamma spectrometry with respect to the natural background fluctuation", *Appl. Radiat. Isot.* (2013), vol. 81, pp. 123–127
4. A. Dragić *et al.*, "The new set-up in the Belgrade low-level and cosmic-ray laboratory", *Nucl. Techn. Radiat. Prot.* (2011), vol. 26/3, pp. 181-192
5. A. Dragić *et al.*, "Variations of CR-muon intensity in the declining phase of the 23<sup>rd</sup> solar cycle in ground and shallow underground data", 29th International Cosmic Ray Conference, Pune (2005), vol. 1, pp. 249-252
6. V. Udovičić *et al.*, "Daily and seasonal radon variability in the underground low-background laboratory in Belgrade, Serbia", *Radiation Protection Dosimetry* (2014), vol. 160, Issue 1-3, pp. 62-64
7. R. Banjanac *et al.*, "Variations of gamma-ray background in the Belgrade shallow underground low-level laboratory", *Applied Radiation and Isotopes*, (2014), vol. 87, pp. 70-72

## CORRELATIVE AND PERIODOGRAM ANALYSIS OF DEPENDENCE OF CONTINUOUS GAMMA SPECTRUM IN THE SHALLOW UNDERGROUND LABORATORY ON COSMIC RAY AND CLIMATE VARIABLES

Dimitrije Maletić, Radomir Banjanac, Dejan Joković, Vladimir Udovičić,  
Aleksandar Dragić, Mihailo Savić, Nikola Veselinović

Institute of Physics University of Belgrade, Serbia

**Abstract.** *The continuous gamma spectrum, Cosmic ray intensity and climate variables; atmospheric pressure, air temperature and humidity were continually measured in the Underground laboratory of Low Background Laboratory in the Institute of Physics Belgrade. Same three climate variables for outside air were obtained from nearby meteorological station. The obtained gamma spectrum, measured using HPGe detector, is split into three energy ranges, low, intermediate and high ending with energy of 4.4 MeV. For each of the energy intervals periodogram and correlative analysis of dependence of continuous gamma spectrum on cosmic ray intensity and climate variables is performed. Periodogram analysis is done using Lomb-Scargle periodograms. The difference of linear correlation coefficients are shown and discussed, as well as the differences in resulting periodograms.*

**Key words:** *gamma spectroscopy, surface air, underground laboratory, correlative analysis, periodogram analysis.*

### 1. INTRODUCTION

The low-level and cosmic-ray laboratory in the Low-Background laboratory for Nuclear Physics in the Institute of Physics Belgrade is dedicated to the measurements of low activities and to the studies of the muon and electromagnetic components of cosmic rays at the ground level and at the shallow depth under-ground, and in particular to the detailed studies of the signatures of these radiations in HPGe spectrometers situated shallow underground. The ground level part of the laboratory (GLL), at 75 m above sea level, is situated at the foot of the vertical loess cliff, which is about 10 meters high. The underground part of the laboratory (UL), of the useful area of 45 m<sup>2</sup>, is dug into the foot of the cliff and is accessible from the GLL via the 10 meters long horizontal corridor, which serves also as a pressure buffer for a slight overpressure in the UL (Fig.1). The overburden of the UL is about 12m of loess soil, equivalent to 25 meters of water. [1]

In the UL laboratory the gamma spectrum is recorded using HPGe detector and fast ADC unit made by CAEN, and analysed using software developed in our laboratory. Besides HPGe measurements the air pressure, temperature and humidity were recorded in UL also. Values for temperature, pressure and humidity of outside air was taken from publicly available web site. The time period from which the

measurements were used in this analysis is from beginning of December 2009 till end of April 2010.

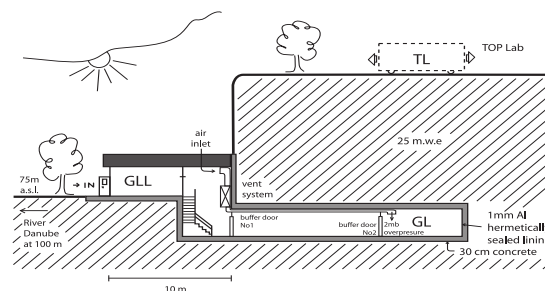


Figure 1. Cross-section of the low-level and CR laboratory at IOP, Belgrade, 44°49'N, 20°28'E, vertical rigidity cut off 5.3 GV.

Continuous Cosmic rays' (CR) spectrum measurements by means of a pair of small plastic scintillators [(50x25x5)cm] started in the GLL and UL back in 2002 and lasted for about 5 years. It agrees to the spectrum of relatively shallow underground laboratories worldwide [2]. These measurements yielded the precise values of the integral CR muon flux at the ground level and underground level laboratory, at the location of Belgrade [3]. Different analyses of the time series of these measurements have also been performed [4, 5]. Since the UL is completely lined with the hermetically sealed 1 mm thick aluminum lining, and the ventilation system keeps the overpressure of 2 mbars of doubly filtered air, the concentration of radon is kept at the low average value of about 10 Bq/m<sup>3</sup>.

Measurements and analysis of periodicity of gamma-rays in underground laboratory had been reported [6-7], and also for Radon measurements and periodicity [8-9] including advanced Multivariate Analysis techniques [10-11].

Most recent research done in our laboratory [12] addresses the question of determination of origin of low energy gamma-rays detected by HPGe detector, which are coming either from environmental radiation or from CR. In this paper the correlative analysis is used to address the same question of composition of low-energy gamma-rays spectrum, thus giving us the new approach to the research done in [12].

The correlative analysis in this paper was done using Toolkit for Multivariate Analysis TMVA[13] package as part of the ROOT[14] software, widely used in analysis, especially for High Energy Physics experiments. The TMVA was used for analysis extensively in our laboratory, and it was the natural choice to use the software for correlative analysis also. Lomb-Scargle periodograms were produced using software developed in Low-Background laboratory.

## 2. EXPERIMENTAL SETUP

In the UL 35% efficiency radiopure HPGe detector, made by ORTEC, is used. The HPGe is surrounded by 12 cm thick cylindrical lead castle. Cosmic ray setup consists of a single [(100x100x5)cm] plastic scintillator detector equipped with four PMTs directly coupled to the corners beveled at 45°, made by Amcrys-H of Kharkov, Ukraine. The signals from HPGe detector and plastic scintillators give output to fast ADC unit with four independent inputs each, made by CAEN, of the type N1728B. CAEN units are versatile instruments capable of working in the so-called energy histogram mode, when they perform like digital spectrometers, or/and in the oscillogram mode, when they perform like digital storage oscilloscopes. In both modes they sample at 10 ns intervals, into  $2^{14}$  channels. The full voltage range is  $\pm 1.1V$ .

CAEN units are capable of operating in the list mode, when every analyzed event is fully recorded by the time of its occurrence over the set triggering level, and its amplitude, in the same PC, which controls their workings. This enables to off-line coincide the events at all four inputs, prompt as well as arbitrarily delayed, with the time resolution of 10 ns, as well as to analyze the time series not only of all single inputs, but also of arbitrary coincidences, with any integration period from 10 ns up. The flexible software that performs all these off-line analyses is user-friendly and is entirely homemade.

The preamplifier outputs of the PMTs of detectors are paired diagonally, the whole detector thus engaging the two inputs of the CAEN unit. The signals from these inputs are later off-line coincided and their amplitudes added, to produce the singles spectra of these detectors. Offline coincidence allows that the high intensity but uninteresting low energy portion of the background spectrum of this detector (up to some 3 MeV), which is mostly due to environmental radiations, is practically completely suppressed, leaving only the high energy-loss events due to CR muons and EM showers that peak at about 10 MeV, as shown in Figure 2.

Since event of HPGe gamma spectrum and Cosmic rays consists of time-stamp and the amplitude, off-line analysis is used to create time series of arbitrary time window with selection of specific part of gamma spectrum as well as the time series of Cosmic ray flux in UL (Figure 3.). This enables that whole gamma spectrum can be divided into energy ranges, and analyze each energy range separately. The spectrum separation is done on channel numbers, and after the energy calibration, the energy ranges used in our analysis are 180-440 keV, 620-1330 keV and 1800-4440 keV. The full gamma spectrum is recorded in range of 180-6670 keV. The part of gamma spectrum of the HPGe is shown in Figure 4.

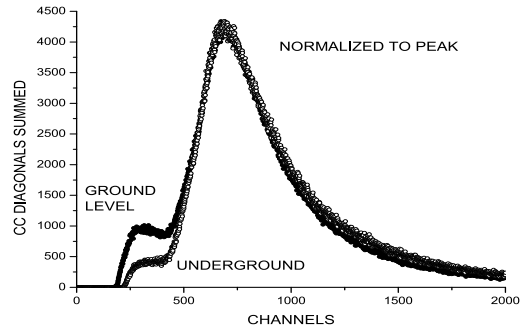


Fig. 2. The sum spectra of two diagonals of big plastic detectors in the UL and GLL .

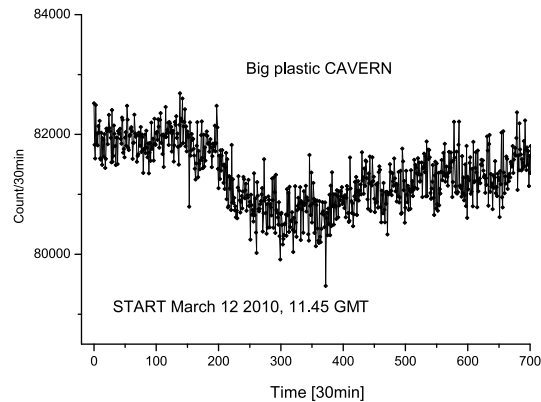


Fig. 3. The time series of the CR muon count of the big plastic detector in the UL.

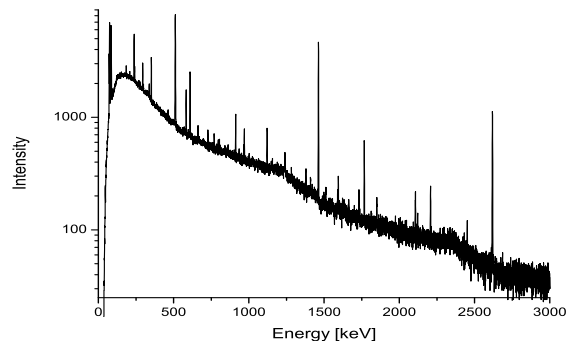


Figure 4. Gamma spectrum of the HPGe detector in 12cm lead castle in the Underground laboratory.

### 3. RESULTS AND DISCUSSIONS

The analysis starts with correlation analysis. The software for correlative analysis is a part of TMVA package. Hourly time series of variables, atmospheric pressure P, temperature T, and humidity H for UL (P\_R, T\_R, H\_R), and outside (P,T,H) are used, Cosmic ray time series (CR) as well as T (DT) and H (DH) difference of UL and outside values make the number of nine input variables. The table summarizing the linear correlation coefficients is shown in Table 1. We can see correlation between each input variable and HPGe gamma spectrum for full energy range in Table 1 also.

|      |      |     |     |     |     |     |     |     |     |     |
|------|------|-----|-----|-----|-----|-----|-----|-----|-----|-----|
| DH   | -10  | 69  | -9  | -86 | 57  | -22 | 51  | -25 | -64 | 100 |
| DT   | 7    | -98 | 7   | 60  | -30 | 10  | -24 | 42  | 100 | -64 |
| CR   | -14  | -42 | -65 | 36  | -14 | -52 | 13  | 100 | 42  | -25 |
| H_R  | -2   | 30  | -44 | -1  | 42  | -59 | 100 | 13  | -24 | 51  |
| P_R  | 14   | -13 | 80  | -8  | -22 | 100 | -59 | -52 | 10  | -22 |
| T_R  | 1    | 43  | -16 | -41 | 100 | -22 | 42  | -14 | -30 | 57  |
| H    | 10   | -63 | -15 | 100 | -41 | -8  | -1  | 36  | 60  | -86 |
| P    | 11   | -9  | 100 | -15 | -16 | 80  | -44 | -65 | 7   | -9  |
| T    | -6   | 100 | -9  | -63 | 43  | -13 | 30  | -42 | -98 | 69  |
| HPGe | 100  | -6  | 11  | 10  | 1   | 14  | -2  | -14 | 7   | -10 |
|      | HPGe | T   | P   | H   | T_R | P_R | H_R | CR  | DT  | DH  |

Table 1. Summary table of linear correlation coefficient for all 9 input variables' 1 hour time series and 1 hour time series of HPGe gamma spectrum for full energy range.

Correlation analysis was done also for three mentioned energy ranges, the Table 2. summarizes the results.

|                    | 180-6670 keV  | 180-440 keV   | 620-1330 keV  | 1780-4440 keV |
|--------------------|---------------|---------------|---------------|---------------|
| T                  | -0.070        | -0.045        | -0.041        | -0.096        |
| <b>P</b>           | <b>+0.111</b> | <b>+0.124</b> | <b>+0.033</b> | <b>+0.010</b> |
| H                  | +0.106        | +0.056        | +0.047        | +0.101        |
| T <sub>UG</sub>    | +0.013        | -0.029        | +0.014        | -0.012        |
| P <sub>UG</sub>    | +0.149        | +0.111        | +0.091        | +0.061        |
| H <sub>UG</sub>    | -0.029        | -0.068        | -0.030        | +0.028        |
| <b>CR</b>          | <b>-0.140</b> | <b>-0.179</b> | <b>-0.030</b> | <b>+0.036</b> |
| T <sub>UG</sub> -T | +0.076        | +0.043        | +0.046        | +0.100        |
| H <sub>UG</sub> -H | -0.105        | -0.083        | -0.055        | -0.072        |

Table 2. Linear correlation coefficients in % for full and three narrower energy ranges.

All the correlation of HPGe gamma spectrum hourly time series and input variables are not significant. The biggest correlation coefficient with HPGe time series is pressure time series measured underground followed by Cosmic ray time series. It is interesting to notice the change of correlation coefficients with HPGe for atmospheric pressure and Cosmic rays time series. While pressure correlation coefficients tend to drop going towards higher gamma energies, Cosmic rays' correlation coefficients are increasing from negative sign to positive one. This observation is in agreement with the fact that the Cosmic rays are contributing

more to the the gamma spectrum of higher energies, as it was shown in [12]. Since Cosmic rays and pressure are anti-correlated with correlation coefficient of -65%, as can be seen in Table 1, increase in atmospheric pressure will give negative correlation coefficient of HPGe and Cosmic rays' time series. This can be explained by having in mind that Cosmic rays are contributing insignificantly to gamma spectrum on lower energies [12] behaving like constant in low energy range, while increase in pressure increases the air density, thus more gamma scattering events are contributing to low energy gamma spectrum.

In the periodogram analysis the Lomb-Scargle periodograms were produced for atmospheric variables P, T, H and HPGe gamma spectrum. The periodograms show only daily periodicity of T, H time series as shown on figures 5 and 6. The P periodogram on Figure 7. Shows expected daily and mid-daily periodicity. It is noticeable that the periodogram for P has lowest spectral powers, which means that periodicity of P is less noticeable. Also, the unexpected 1/3 day periodicity is with low spectral power. The periodogram analysis showed that there is no significant periodicity in HPGe gamma spectrum time series, as shown on Figure 8.

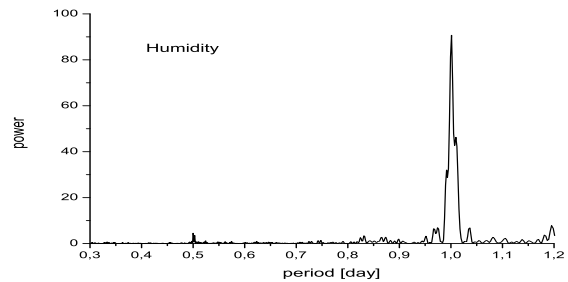


Figure 5. Lomb-Scargle periodogram of air humidity.

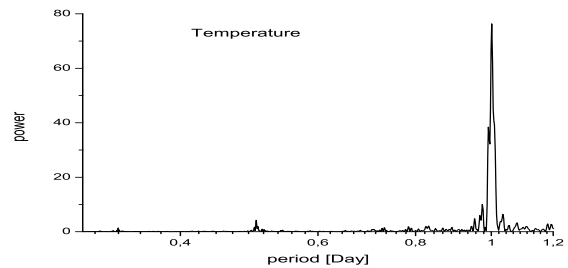


Figure 6. Lomb-Scargle periodogram of air temperature.

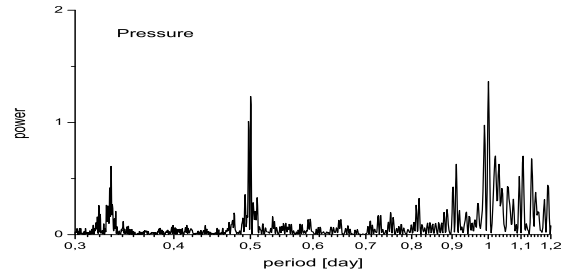


Figure 7. Lomb-Scargle periodogram of air pressure.

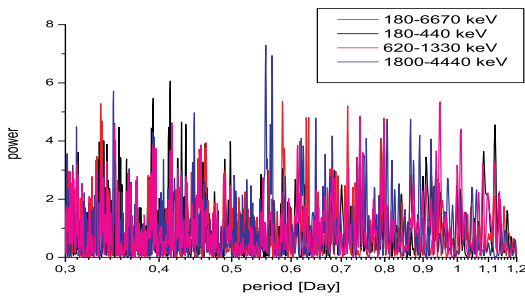


Figure 8. Lomb-Scargle periodogram of full and three different energy range HPGe gamma spectrum time series.

## CONCLUSION

In the Underground laboratory of Low Background Laboratory in the Institute of Physics Belgrade the continuous HPGe gamma spectrum, Cosmic ray intensity and climate variables were continually measured in the period from beginning of December 2009 till the end of April 2010. The HPGe gamma spectrum is split into three energy ranges, low, intermediate and high. For each of the energy intervals periodogram and correlative analysis of dependence of continuous gamma spectrum on cosmic ray intensity time series and climate variables time series is performed. Periodogram analysis is done using Lomb-Scargle periodograms. The correlation coefficient between air pressure and Cosmic rays is -65%. The correlation coefficients between HPGe gamma spectrum and input variables are not significant. The decrease of values of correlation coefficients of gamma spectrum and air pressure is present. The increase of values of correlation coefficients of gamma spectrum and Cosmic rays is present also. Increase in atmospheric pressure is resulting in negative correlation coefficient between HPGe and Cosmic rays' time series for low energy gamma spectrum. The more significant contribution of Cosmic rays in high energy gamma spectrum, as opposite to insignificant contribution of Cosmic rays to low energy gamma spectrum is evident. Lomb-Scargle periodograms showed daily periodicity for air temperature and humidity, and additional mid-daily periodicity for air pressure. There is no noticeable periodicity for each of energy ranges of gamma spectrum.

**Acknowledgement:** *The paper is a part of the research done within the project "Nuclear research methods of rare events and cosmic radiation" (No. 171002) financed by the Ministry of Education, Science and Technological Development of the Republic of Serbia (2011-2015).*

## REFERENCES

1. Dragic Aleksandar, Udovicic Vladimir I, Banjanac Radomir M, Jokovic Dejan R, Maletic Dimitrije M, Veselinovic Nikola B, Savic Mihailo, Puzovic Jovan M, Anicin Ivan V "The New Set-Up in the Belgrade Low-

- Level and Cosmic-Ray Laboratory", NUCLEAR TECHNOLOGY & RADIATION PROTECTION, vol. 26, br. 3, pp. 181-192, 2011
2. S. Niese, "Underground laboratories for low-level radioactivity measurements", Analysis of Environmental Radionuclides, Ed. P.Povinec, Elsevier, Amsterdam, pp.209-239, 2008
3. A.Dragić, D.Joković, R.Banjanac, V.Udovičić, B.Panić, J.Puzović and I.Anićin, "Measurement of cosmic ray muon flux in the Belgrade ground level and underground laboratories", Nucl. Instr. and Meth. in Phys. Res. A591, pp. 470 – 475, 2008
4. A. Dragić, R. Banjanac, V. Udovičić, D. Joković, I. Anićin and J. Puzović, "Comparative study of power spectra of ground and shallow underground muon data", Int. Journal of Modern Physics A, Vol. 20 pp. 6953-6955, 2005
5. A. Dragić, R. Banjanac, V. Udovičić, D. Joković, J. Puzović, I. Anićin, "Periodic Variations of CR Muon Intensity in the Period 2002-2004", Proc. 21st European Cosmic Ray Symposium, Košice, Slovakia, pp.368-373, 2008.
6. Banjanac Radomir M, Udovicic Vladimir I, Dragic Aleksandar, Jokovic Dejan R, Maletic Dimitrije M, Veselinovic Nikola B, Grabez Bojana S "Daily Variations of Gamma-Ray Background and Radon Concentration", ROMANIAN JOURNAL OF PHYSICS, vol. 58, br. , pp. S14-S21, 2013
7. Banjanac Radomir M, Dragic Aleksandar, Udovicic Vladimir I, Jokovic Dejan R, Maletic Dimitrije M, Veselinovic Nikola B, Savic Mihailo "Variations of gamma-ray background in the Belgrade shallow underground low-level laboratory", APPLIED RADIATION AND ISOTOPES, vol. 87, br. , pp. 70-72, 2014
8. V. Udovičić, B. Grabež, A. Dragić, R. Banjanac, D. Joković, B. Panić, D. Joksimović, J. Puzović, I. Anićin, "Radon problem in an underground low-level laboratory", Radiation Measurements 44 pp. 1009-1012. 2009
9. V. Udovičić, I. Anićin, D. Joković, A. Dragić, R. Banjanac, B. Grabež, N. Veselinović, "Radon Time-series Analysis in the Underground Low-level Laboratory in Belgrade, Serbia", Radiation Protection Dosimetry 145 (2-3) pp. 155-158, 2011
10. Maletic Dimitrije M, Udovicic Vladimir I, Banjanac Radomir M, Jokovic Dejan R, Dragic Aleksandar L, Veselinovic Nikola B, Filipovic Jelena Z "Comparison of Multivariate Classification and Regression Methods for the Indoor Radon Measurements", NUCLEAR TECHNOLOGY & RADIATION PROTECTION, vol. 29, br. 1, pp. 17-23 (2014)
11. Maletic Dimitrije M, Udovicic Vladimir I, Banjanac Radomir M, Jokovic Dejan R, Dragic Aleksandar L, Veselinovic Nikola B, Filipovic Jelena Z "Correlative and Multivariate Analysis of Increased Radon Concentration in Underground Laboratory", RADIATION PROTECTION DOSIMETRY, vol. 162, br. 1-2, pp. 148-151, 2014
12. Banjanac Radomir M, Maletic Dimitrije M, Jokovic Dejan R, Veselinovic Nikola B, Dragic Aleksandar, Udovicic Vladimir I, Anicin Ivan V "On the omnipresent background gamma radiation of the continuous spectrum", NUCLEAR INSTRUMENTS & METHODS IN PHYSICS RESEARCH SECTION A, vol. 745, br. , str. 7-11, 2014.
13. R. Brun and F. Rademakers, "ROOT - An Object Oriented Data Analysis Framework", Nucl. Inst. Meth. in Phys. Res. A 389, 81, 1997
14. A. Hoecker, P. Speckmayer, J. Stelzer, J. Therhaag, E. von Toerne, and H. Voss, "TMVA - Toolkit for Multivariate Data Analysis", PoS ACAT 040 (2007), arXiv:physics/070303

PAPER • OPEN ACCESS

## Pressure and temperature effect corrections of atmospheric muon data in the Belgrade cosmic-ray station

To cite this article: M Savi *et al* 2015 *J. Phys.: Conf. Ser.* **632** 012059

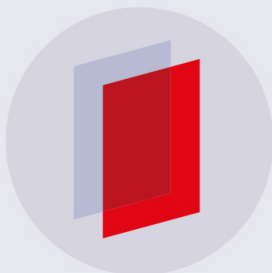
View the [article online](#) for updates and enhancements.

### Related content

- [Temperature effect correction for muon flux at the Earth surface: estimation of the accuracy of different methods](#)  
A N Dmitrieva, I I Astapov, A A Kovylyayeva *et al.*
- [Temperature effect correction for the cosmic ray muon data observed at the Brazilian Southern Space Observatory in São Martinho da Serra](#)  
C R Braga, A Dal Lago, T Kuwabara *et al.*

### Recent citations

- [A novel method for atmospheric correction of cosmic-ray data based on principal component analysis](#)  
M. Savi *et al*
- [Rigidity dependence of Forbush decreases in the energy region exceeding the sensitivity of neutron monitors](#)  
M. Savi *et al*



**IOP | ebooks™**

Bringing you innovative digital publishing with leading voices to create your essential collection of books in STEM research.

Start exploring the collection - download the first chapter of every title for free.

# Pressure and temperature effect corrections of atmospheric muon data in the Belgrade cosmic-ray station

**M Savić, D Maletić, D Joković, N Veselinović, R Banjanac, V Udovičić, A Dragić**  
Institute of Physics, University of Belgrade  
Pregrevica 118, 11080 Belgrade, Serbia

E-mail: yokovic@ipb.ac.rs

**Abstract.** We present results of continuous monitoring of the cosmic-ray muon intensity at the ground and shallow underground level at the Belgrade cosmic-ray station. The cosmic-ray muon measurements have been performed since 2002, by means of plastic scintillation detectors. The scintillator counts are corrected for atmospheric pressure for the whole period of measurements and, as well, for vertical temperature profile for the period of the last six years. The results are compared with other correction methods available. One-hour time series of the cosmic-ray muon intensity at the ground level are checked for correlation with European neutron monitors, with emphasis on occasional extreme solar events, e.g. Forbush decreases.

## 1. Introduction

The Belgrade cosmic-ray station, situated in the Low-level Laboratory for Nuclear Physics at Institute of Physics, Belgrade, have been continuously measuring the cosmic-ray intensity since 2002. The station is at near-sea level at the altitude of 78 m a.s.l.; its geomagnetic latitude is 39° 32' N and geomagnetic vertical cut-off rigidity is 5.3 GV. It consists of two parts: the ground level lab (GLL) and the underground lab (UL); the UL is located at a depth of 12 metres below the surface, i.e. 25 metre water equivalent. At this depth practically only the muonic component is present. The cosmic-ray muon measurements are performed by means of plastic scintillation detectors, a pair of which is, along with instrumentation modules for data acquisition, placed in both the GLL and the UL. The set-up is quiet flexible, as the scintillators could be arranged in different ways, which allows conducting different experiments. The analyses of the measurements yielded some results on variations of the cosmic-ray muon intensity and on precise values of the integral muon flux at the ground level and at the depth of 25 m.w.e. [1,2,3,4].

## 2. Experimental set-up

The experimental set-up in both the GLL and the UL consists of a large plastic scintillation detector (rectangular shape, 100cm x 100cm x 5cm) and a data acquisition system (DAQ). The scintillator is polystyrene based UPS-89, with four 2-inch photomultiplier tubes attached to its corners, so that each PM tube looks at the rectangle diagonal. Preamplifier signals from two PM tubes looking at the same diagonal are summed in one output signal, thus two output signals are led to the DAQ from each scintillator.

The summed signals from the PM tubes on the same diagonal of the detectors are stored and digitized by the DAQ, which is based on 4-channel flash analog-to-digital converters (FADC), made by CAEN (type N1728B), with 100 MHz sampling frequency. The FADCs are capable of operating in



the event-list mode, when every analyzed event is fully recorded by the time of its occurrence and its amplitude. This enables the correlation of events, both prompt and arbitrarily delayed, at all four inputs with the time resolution of 10 ns. Single and coincident data can be organized into time series within any desired integration period. The FADCs can also be synchronized with each other for the additional coinciding of the events in the GLL and the UL.

For both the GLL and the UL detector, two input channels on the corresponding FADC are reserved for events recorded by each of detector's diagonals. The cosmic-ray events recorded by a single diagonal are drown in the background. Coinciding of the prompt events from two diagonals within a narrow time window gives the resulting experimental spectrum of the plastic scintillator, which is the energy deposit ( $\Delta E$ ) spectrum of the cosmic-ray particles (figure 1). Interpretation of the experimental spectra and their features as well as their calibration have been done using Geant4 based Monte Carlo simulation [4,5]. The spectra peak at  $\sim 11$  MeV and have the instrumental thresholds at  $\sim 4$  MeV. Comparing the spectra of the GLL detector and the UL detector one can notice the obvious difference in their shape, especially in the low-energy part below  $\sim 6$  MeV. This difference points to the contribution of the cosmic-ray electrons and gammas (electromagnetic component) to the  $\Delta E$  spectra at the ground level, which is absent in case of the underground detector.

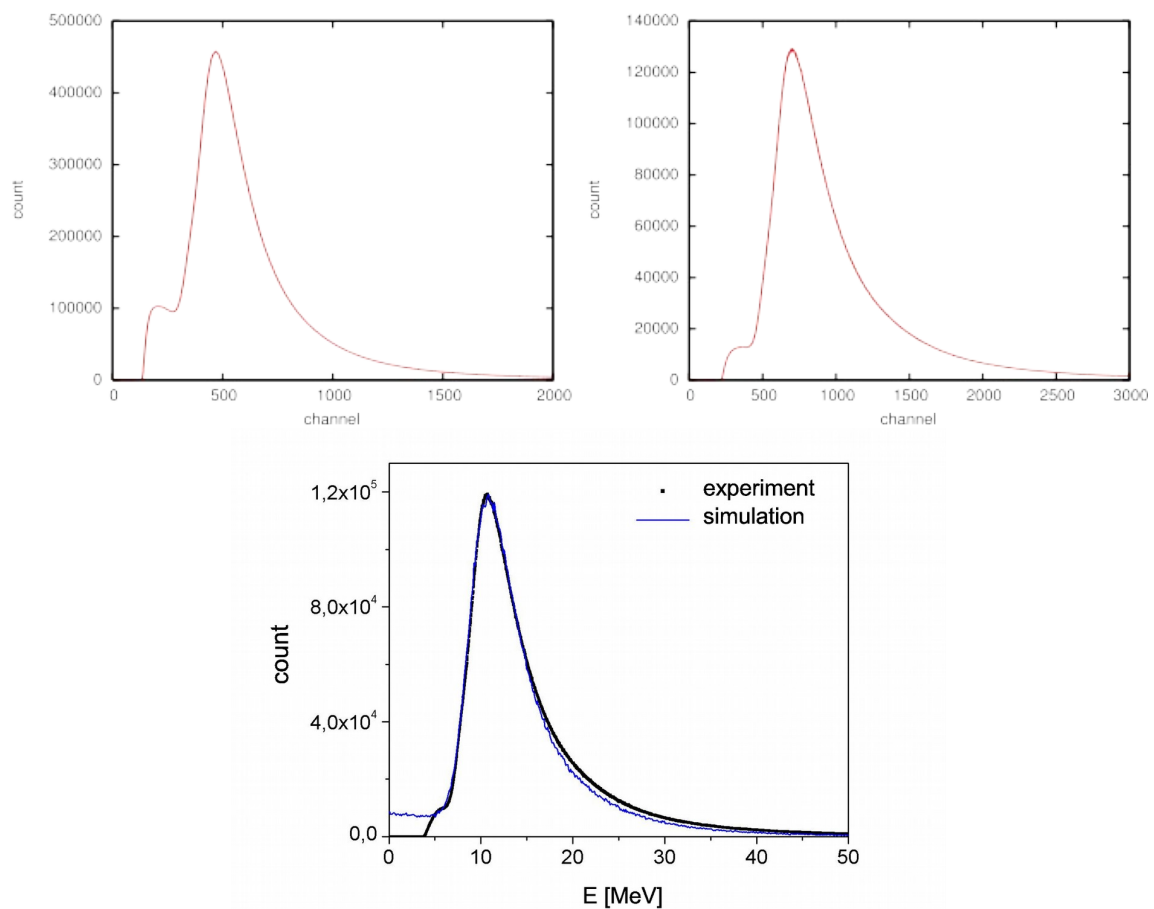


Figure 1. The cosmic-ray  $\Delta E$  spectra of the GLL detector (top left) and the UL detector (top right). Experimental and simulated  $\Delta E$  spectra of the UL detector (bottom).

### 3. Results and discussion

The cosmic-ray intensity data are automatically processed, using a web-based “robot” developed for this purpose, and published online at [www.cosmic.ipb.ac.rs/muon\\_station](http://www.cosmic.ipb.ac.rs/muon_station). The online available data are raw scintillator counts in time series with resolution of 5 min or 1 h. Time series of the raw data are corrected for pressure and temperature effect; pressure corrections have been done for the whole data taking period and temperature effect corrections have been done for the the time period of the last six years.

#### 3.1. Efficiency corrections

The first data corrections are related to detector assembly efficiency. As mentioned, the instrumental thresholds cut the spectra at  $\sim 3$  MeV. However, the thresholds may vary, thus changing the initial spectrum and resulting in fluctuations of the integral spectrum count. Related to this, the necessary correction has been done by means of constant fraction discriminator (CFD) function (figure 2); with use of the CFD cut the spectrum fluctuations decreased significantly. The CFD is based on cut on chosen height as a percentage of peak height where the spectrum is cut. The simulation tells us that, for the underground detector,  $\sim 6\%$  of muon events is also cut (figure 1).

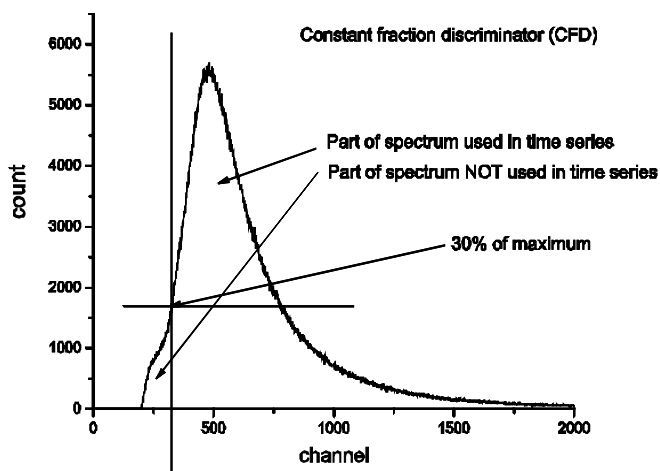


Figure 2. Constant fraction discriminator (CFD) applied in efficiency corrections. The obtained truncated spectrum is used for calculating time series.

The next step in the efficiency corrections is a correction of 5-min count values that are clearly lower than a mean 5-min count in surrounding time intervals. This undershoot comes at the beginning/end of runs, where events are not collected for all 5 min of measurement. The last and smallest correction is a correction of fluctuations of spectrum due to fluctuation in amplification which influence the cut on diagonals and efficiency of coincidence of two diagonals. We found that the CFD cut is proportional to efficiency of coincidence.

#### 3.2. Corrections for atmospheric pressure and for temperature

Significant part of variation of cosmic ray muon component intensity can be attributed to meteorological effects. Here, two main contributors are barometric and temperature effect [6].

Barometric effect is caused by variation of the atmospheric mass above the detector. These pressure corrections are done by finding the linear regression coefficient, using only International Quiet Days, i.e. time series data from periods with more or less constant intensity of galactic cosmic rays, for creation of the distribution of scintillator counts vs. atmospheric pressure. Atmospheric pressure data are available due to on-site continuous measurement.

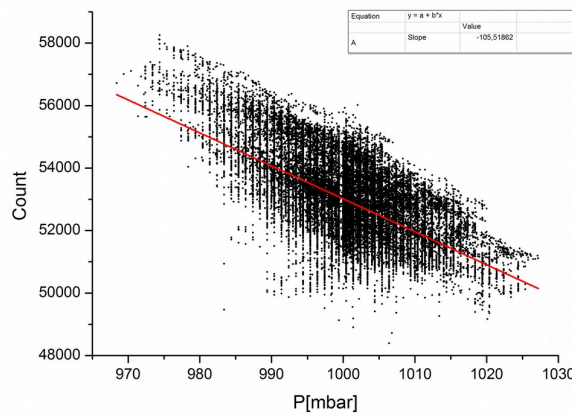


Figure 3. Dependence of 5-min counts on atmospheric pressure.

The temperature effect is related to the variation of the atmospheric temperature profile. The effect is two-fold, as it affects pion decay (positive contribution) as well as muon ionization losses and possible decay (negative contribution). To correct for these effects, integral correction method was applied [6,7]. The variation of the muon intensity due to temperature variations is calculated by using the formula:

$$\delta I_T = \int_0^{h_0} \alpha(h) \cdot \delta T(h) \cdot dh$$

where  $\delta I_T$  is the variation of the muon intensity due to the temperature effect,  $\delta T(h)$  is the variation of the atmospheric temperature, which is calculated in reference to the mean temperature value for a given time period (denoted by index M):  $\delta T(h) = T_M(h) - T(h)$ , where  $h$  is atmospheric depth. Temperature coefficient densities  $\alpha(h)$  are calculated according to [6].

Available meteorological models make it possible to have hourly atmospheric temperature profiles for 17 standard isobaric levels at the geographic position of the Belgrade muon station, necessary for application of formula shown above. The procedure used here is as described in [7]. Temperature profiles have been obtained from [ftp://cr0.izmiran.rssi.ru/COSRAY!/FTP\\_METEO/blgd\\_Th/](ftp://cr0.izmiran.rssi.ru/COSRAY!/FTP_METEO/blgd_Th/), courtesy of IZMIRAN laboratory.

### 3.3. Time series of the cosmic-ray intensity

In Figure 4 the count rate time series is shown for all corrections. First, the corrected count rate for efficiency corrected data is shown. Also, the atmospheric pressure and combined atmospheric pressure and temperature corrections time series of count rates are shown.

One-hour time series of the cosmic-ray muon intensity at the ground level are checked for correlation with European neutron monitors (NM), with emphasis on occasional extreme solar events, e.g. Forbush decreases.

In Figure 5 the comparison of time series of pressure corrected and pressure and temperature corrected count rates for the Belgrade muon station and Jungfrauoch, Rome, Baksan and Oulu neutron monitors is presented for Forbush candidate in March 2012. The count rates of neutron monitors are shifted to be close to each-other for visibility. The count rate for the Belgrade station is shown in percentages with additional shift down for visibility. The count rate drop for the neutron monitors is clearly more pronounced than for Belgrade muon monitor.

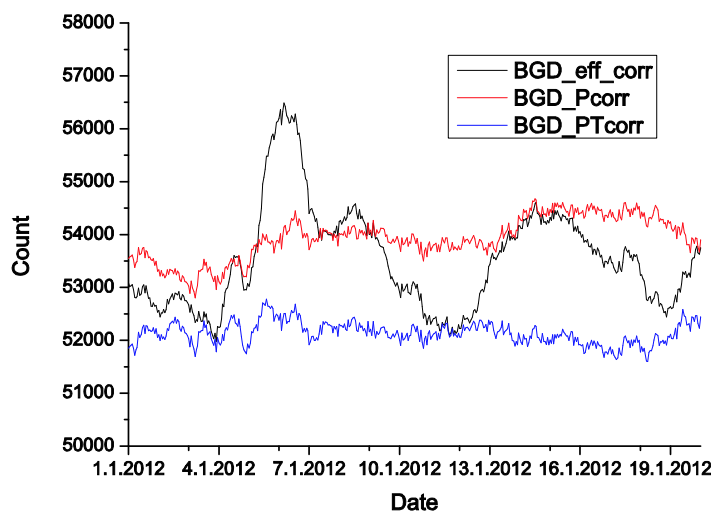


Figure 4. Time series of efficiency corrected, pressure corrected and pressure and temperature corrected counts.

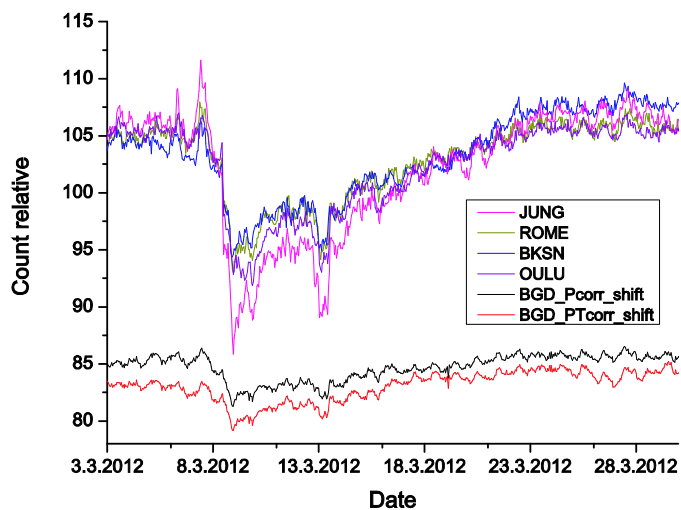


Figure 5. Comparison of time series of pressure corrected and pressure and temperature corrected count rates for the Belgrade muon monitor station and neutron monitors. Count rates are shifted for comparison.

In Figure 6 the comparison of time series of pressure corrected count rates for the Belgrade muon station Jungfrauoch, Rome, Baksan and Oulu neutron monitors is presented. The count rates of neutron monitors are shifted to be close to each-other for visibility. The count rate for Belgrade station is scaled in the way that the drop in count rate is similar to most of the stations (except Jungfrauoch, which is at high altitude). The visual comparison shows the good correlation of the count rates of Belgrade muon monitor and neutron monitors, previously noticed using correlative analyses of count rates. The pressure corrected count rates from Belgrade muon monitor is only dataset used for visual comparison, since neutron monitor data are also only pressure corrected. This was also observed previously using correlative analyses of count rates.

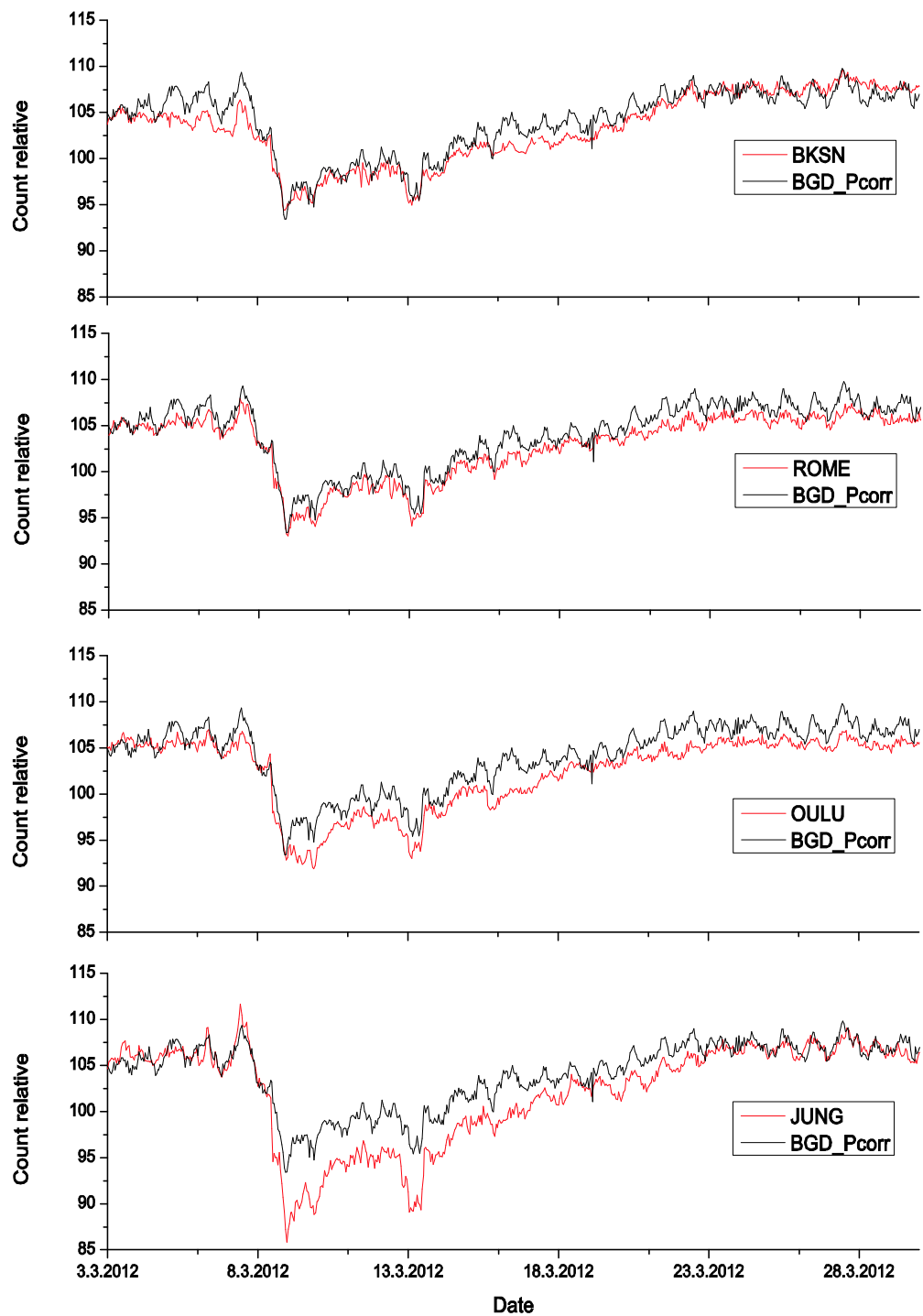


Figure 6. Comparison of time series of pressure corrected count rates for the Belgrade muon monitor station and neutron monitors. Count rates are shifted and scaled for comparison.

#### 4. Conclusions

The results of continuous monitoring of the cosmic-ray muon intensity at the ground and shallow underground level at the Belgrade cosmic-ray station are presented. The scintillator counts are corrected for atmospheric pressure for the whole period of measurements and, as well, for vertical temperature profile for the period of the last six years. The results are compared with other correction methods available and showed excellent agreement. One-hour time series of the cosmic-ray muon intensity at the ground level are checked for correlation with European neutron monitors, with emphasis on occasional extreme solar events, e.g. Forbush decreases. As a result of correlative analysis, the Forbush candidate in March 2012 is the best choice to be used for visual comparison presented in this work. The comparison showed high correlation of the Belgrade muon monitor with neutron monitors, especially geographically closer neutron monitors such as Rome NM. In some specific time periods, like during the Forbush candidate in March 2012, we showed that our muon measurement system has sensitivity comparable to European neutron monitors in this period, but still not as efficient as NM with better geographical position (at high altitude), e.g. Jungfraujoch in the Swiss Alps.

#### 5. Acknowledgements

This work is supported by the Ministry of Education, Science and Technological Development of Republic of Serbia, project no. OI171002. We acknowledge the NMDB database ([www.nmdb.eu](http://www.nmdb.eu)), founded under the European Union's FP7 programme (contract no. 213007) for providing data. We acknowledge the Department of Physical Sciences, University of Oulu, Finland, as the source of data used in publications. Jungfraujoch neutron monitor data were kindly provided by the Cosmic Ray Group, Physikalisches Institut, University of Bern, Switzerland. We acknowledge the ROME neutron monitor data. SVIRCO NM is supported by IFSI/INAF-UNIRoma3 collaboration. We acknowledge the Baksan Neutrino Observatory of Institute for Nuclear Research of Russian Academy of Science, Moscow, for providing data.

#### 6. References

- [1] Dragić A, Banjanac R, Udovičić V, Joković D, Aničin I and Puzović J 2005 *Int. J. Mod. Phys. A* **20** 6953
- [2] Dragić A, Banjanac R, Udovičić V, Joković D, Puzović J and Aničin I 2008 *Proc. 21<sup>st</sup> European Cosmic Ray Symposium (Košice, Slovakia)* p 368
- [3] Dragić A, Banjanac R, Udovičić V, Joković D, Aničin I and Puzović J 2009 *Proc. 31<sup>st</sup> Int. Cosmic Ray Conf. (Lodz, Poland)*
- [4] Dragić A, Joković D, Banjanac R, Udovičić V, Panić B, Puzović J and Aničin I 2008 *Nucl. Instrum. Meth. A* **591** 470
- [5] Joković D, Dragić A, Udovičić V, Banjanac R, Puzović J and Aničin I 2009 *Appl. Radiat. Isot.* **67** 719
- [6] Dorman L.I. 2004 *Cosmic Rays in the Earth's Atmosphere and Underground* (Berlin: Springer)
- [7] Berkova M, Belov A, Eroshenko E and Yanke V 2012 *Astrophys. Space Sci. Trans.* **8** 41

# Cosmic rays muon flux measurements at Belgrade shallow underground laboratory

Cite as: AIP Conference Proceedings **1645**, 421 (2015); <https://doi.org/10.1063/1.4909614>  
Published Online: 25 February 2015

N. Veselinović, A. Dragić, D. Maletić, D. Joković, M. Savić, R. Banjanac, V. Udovičić, and I. Aničin



View Online



Export Citation

## ARTICLES YOU MAY BE INTERESTED IN

[A shallow underground laboratory for low-background radiation measurements and materials development](#)

Review of Scientific Instruments **83**, 113503 (2012); <https://doi.org/10.1063/1.4761923>

[Cosmic ray topography](#)

American Journal of Physics **85**, 840 (2017); <https://doi.org/10.1119/1.4996874>

[Estimation of m.w.e \(meter water equivalent\) depth of the salt mine of Slanic Prahova, Romania](#)

AIP Conference Proceedings **1304**, 331 (2010); <https://doi.org/10.1063/1.3527218>

Lock-in Amplifiers

Find out more today



Zurich Instruments

# Cosmic Rays Muon Flux Measurements at Belgrade Shallow Underground Laboratory

N. Veselinović <sup>a)</sup>, A. Dragić, D. Maletić, D. Joković, M. Savić, R. Banjanac, V. Udovičić, I. Aničin

*Institute of Physics, University of Belgrade, Pregrevica 118, Belgrade, Serbia*

<sup>a)</sup> Corresponding author: veselinovic@ipb.ac.rs

**Abstract.** The Belgrade underground laboratory is a shallow underground one, at 25 meters of water equivalent. It is dedicated to low-background spectroscopy and cosmic rays measurement. Its uniqueness is that it is composed of two parts, one above ground, the other below with identical sets of detectors and analyzing electronics thus creating opportunity to monitor simultaneously muon flux and ambient radiation. We investigate the possibility of utilizing measurements at the shallow depth for the study of muons, processes to which these muons are sensitive and processes induced by cosmic rays muons. For this purpose a series of simulations of muon generation and propagation is done, based on the CORSIKA air shower simulation package and GEANT4. Results show good agreement with other laboratories and cosmic rays stations.

## Belgrade Cosmic Rays Station

Cosmic rays are energetic particles from outer space that continuously bombard Earth atmosphere, causing creation of secondary showers made of elementary particles. For last hundred years, after Hess' discoveries, cosmic rays ( CR ) has been studied at almost every location accessible to research, from deep underground to above atmosphere [1]. Low-level and cosmic-ray lab in Belgrade is dedicated to the measurement of low activities and CR muon component. One of the objectives is also intersection of these two fields, namely, muon-induced background in gamma spectroscopy. Belgrade lab is relatively shallow underground laboratory [2] located at the right bank of river Danube on the ground of Institute of Physics in Belgrade. It is located at near-sea level at the altitude of 78 m a.s.l. and its geographic position is 44° 51' N and longitude 20° 23' E with geomagnetic latitude 39° 32' N and geomagnetic vertical cut-off rigidity 5.3 GV. The lab has two portions, ground level portion ( GL ) is situated at the foot of the vertical loess cliff. Other portion, the underground level ( UL ) is dug into the foot of the cliff and is accessible from the GL via horizontal corridor as can be seen at Fig.1. Working area of UL has three niches for independent experiments.

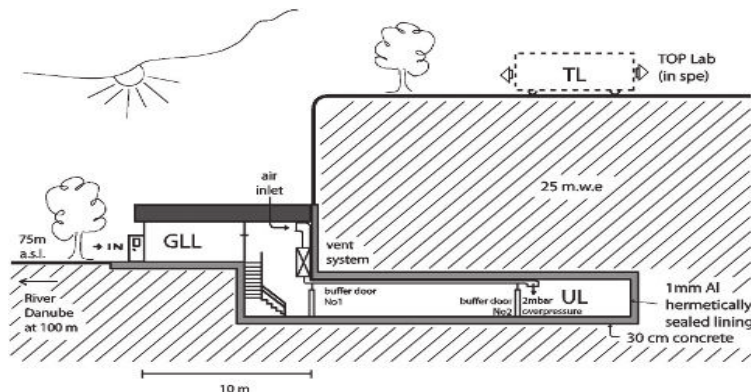


**FIGURE 1.** Scheme of low-level and CR laboratory at Institute of Physics, Belgrade

The overburden of the UL is about 12 meters of loess soil, which is equivalent to 25 meters of water. The walls are made of 30 cm thick reinforced concrete and covered with the hermetically sealed Al lining 1 mm thick, to

prevent the radon from the soil to diffuse into the laboratory. The low-level laboratory is equipped with an air ventilation system which keeps 2 mbar overpressure in the UL, in order to minimize radon diffusion through eventual imperfections in the Al lining.

## Experimental Set-up

The equipment of the lab consists of two identical set of detectors and analyzing electronics. One set is situated in the GL and other in the UL. Each set is composed of gamma spectrometer and muon detectors. For muon measurements a pair of plastic scintillator detectors is used. One of the detectors is small, 50 cm x 23 cm x 5 cm plastic scintillator detector, with a single PMT looking at its longest side via a Perspex light guide tapering to the diameter of a PMT, made by JINR, Dubna, Russia, and assembled locally. The other, larger one has dimensions of 100 cm x 100 cm x 5 cm, equipped with four PMT directly coupled to the corners beveled at 45°, made by Amcrys-H, Kharkov, Ukraine. The smaller detector may serve as a check of stability of the muon time series obtained from the larger detector, which is important for long term measurements. It can also be used (in coincidence with the larger detector ) for measurements of the lateral spread of particles in CR showers and decoherence. Plastic scintillation detectors are also employed for active shielding of gamma spectrometers. In the UL, a 35% efficiency radio-pure p-type HPGe detector, made by ORTEC, 12 cm thick cylindrical lead castle is deployed around the detector. One of the set-ups is presented at Fig.2. Another HPGe detector, of 10% efficiency, is placed in GL.



**FIGURE 2.** Detectors in the underground laboratory. Large scintillator detector is placed above HPGe and small scintillator can change position.

Data acquisition system is identical both in UL and GL and it has two flash analog to digital converter (FADC), one in each laboratory, made by CAEN (type N1728B). These are versatile instruments, capable of working in two modes, energy histogram mode when performing as digital spectrometers or, in the oscillogram mode, when they perform as digital storage oscilloscopes. In both modes, they sample at 10 ns intervals into  $2^{14}$  channels in four independent inputs. The full voltage range is  $\pm 1.1$  V. They are capable of operating in the list mode, when every analyzed event is fully recorded by the time of its occurrence and its amplitude. This enables the correlation of events, both prompt and arbitrarily delayed, at all four in puts with the time resolution of 10 ns. Single and coincident data can be organized into time series within any integration period from 10 ns up. The two N1728B units are synchronized, enabling coincidence/correlation of the events recorded in both of them. The flexible software encompassing all above said off-line analyses is user-friendly and entirely homemade. The preamplifier outputs of the PMT of the larger detectors are paired diagonally. Signals from these paired inputs are later coincided off-line and their amplitudes added to produce the single spectra. This procedure suppress low-energy portion of the background spectrum (up to some 3 MeV), mostly environmental radiation, leaving only high-energy loss events due to CR muons and EM showers that peak at about 10 MeV, shown at Fig 3. The output of the PMT of the smaller detector is fed to the third input of FADC. [3]

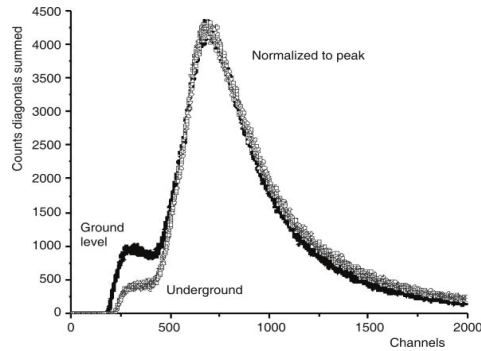


**FIGURE 3.** The sum spectra of two diagonals of the large plastic detectors in the UL and GLL. For comparison, the spectra are normalized for the peaks to coincide. Channel 650 corresponds to the muon energy loss of 10 MeV.

### Simulation and Results

The experimental set-up is rather flexible, thus allowing different studies of the muon and electromagnetic components of cosmic rays at the ground level and at the shallow depth underground. The cosmic-ray muon flux in the underground laboratory has been determined from data taken from November 2008 till June 2013 (there were some small gaps in recording data during this period). These measurements yielded the precise values of the integral cosmic ray muon flux at the location of Belgrade. Measured muon flux is:  $137(6) \text{ m}^{-2}\text{s}^{-1}$  at the ground level and  $45(2) \text{ m}^{-2}\text{s}^{-1}$  at the underground level [4]. Different analyses of time series of these measurements have also been performed. Interpretation and calibration of the experimental spectra has been done using Monte Carlo simulation packages CORSIKA and Geant4 [5, 6]. CORSIKA simulates extensive air showers generated by the primary cosmic-rays in interactions with air nuclei at the top of the atmosphere. It gives spectra of the secondary cosmic-rays at the preferred observation level. These secondary particles, their energy and momentum direction distribution, obtained by CORSIKA, are then used as an input for the Geant4 based simulation of the detectors. In this simulation, particles first traverse through soil and infrastructure of the UL lab before hitting the detector. Then the response of the plastic scintillation detectors is simulated. For the UL scintillators, the simulated spectra are shown in Fig. 4.[7]

They agree very well with the experimental ones, except in the low-energy part where the ambient gamma radiation is mostly present and where the cuts are applied. We also used these simulation packages to simulate different experimental set-ups and to obtain information about lower cut-of energy of primary cosmic rays at our site and for single muons and muons in coincidence. Energy of the primary particles from which detected muons originate increases for UL compared to GL but also for muons in coincidence compared with single detected muons.

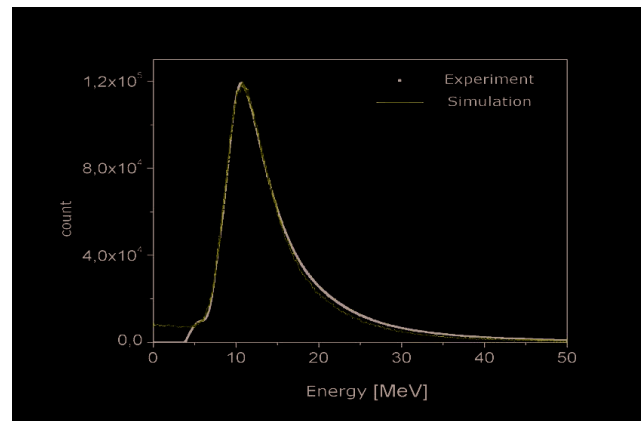


**FIGURE 4.** Experimental vs simulated spectrum of large plastic scintillator detector at UL

These measurements allow us to study fluctuations in muon flux intensity during the rising phase of Solar Cycle 24 and to make five-minutes or one-hour time series of the flux. The scintillator counts are corrected for atmospheric pressure for the whole period of measurements and, as well, for vertical temperature profile for the period of last six years. The results are compared with other correction methods available. One-hour time series of the cosmic ray muon intensity at the ground level are checked for correlation with European neutron monitors ( NM ), with emphasis on occasional extreme solar events, e.g. Forbush decreases ( FD ) in order to investigate claims of influence of cosmic-rays on cloud formation and climate [8,9] In some specific time periods, like during the FD in March 2012, we showed that our muon measurement system has sensitivity comparable to European neutron monitors in this period, but still not as efficient as NM with better geographical position (at high altitude), e.g. Jungfraujoch in the Swiss Alps. These results are presented at Fig. 5. Due to fact that muons detected underground originate from primary particles with energy around and above the limit for solar modulation time series from UL are less sensitive to these Solar events.

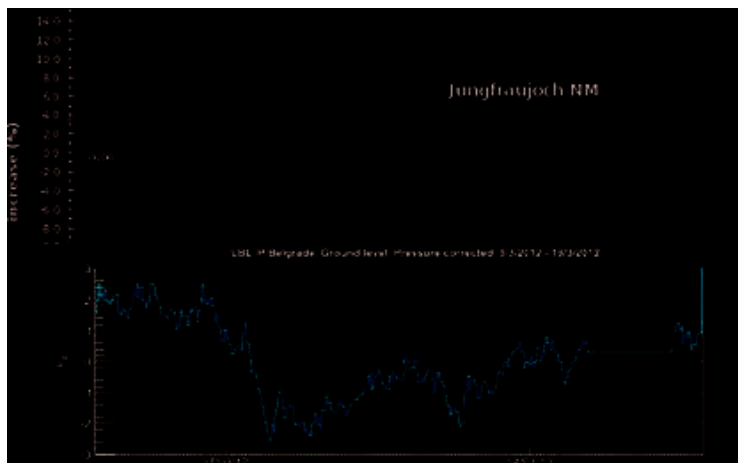


**FIGURE 5.** Time series for March 2012 recorded at NM at Jungfraujoch compared to time series obtained at Belgrade cosmic-rays station

#### Acknowledgement

The present work was funded by the Ministry of Education and Science of the Republic of Serbia, under the Project No. 171002.

#### References

- [1] L.I. Dorman, *Cosmic-rays in the Earth's Atmosphere and Underground*, Kluwer, Dordrecht, 2004.
- [2] S. Niese, *Underground laboratories for low-level radioactivity measurements. Analysis of Environmental Radionuclides*, 209-240, (2008 ) P.P. Povinec, ed., Elsevier, Amsterdam.
- [3] A. Dragić, V. Udovičić, R. Banjanac, D. Joković, D. Maletić, N. Veselinović, M. Savić, J. Puzović, I. Aničin, *The new set-up in the Belgrade low-level and cosmic-ray laboratory*, Nucl. Technol. Radiat. 26 (2011) 181-192
- [4] A. Dragić, D. Joković, R. Banjanac, V. Udovičić, B. Panić, J. Puzović, I. Aničin, *Measurement of cosmic ray muon flux in the Belgrade ground level and underground laboratories*, Nuclear Instruments and Methods in Physics Research A 591 (2008) 470-475.

- [5] D. Heck, *CORSIKA: a Monte Carlo code to simulate extensive air showers*, Report FZKA 6019, Forschungszentrum Karlsruhe, 1998.
- [6] S. Agostinelli et al., *the Geant4 collaboration*, Nucl. Instrum. and Meth. A 506 (2003) 250-303
- [7] A.Dragić, R. Banjanac, V. Udovičić, D. Joković, J.Puzović, I Aničin, I., *Periodic Variations of CR Muon Intensity in the Period 2002-2004* Proceedings of the 21st European cosmic-ray Symposium, Košice, Slovakia (2008) 368-373.
- [8] A.Dragić, I.Aničin, R.Banjanac, V.Udovičić, D.Joković, D.Maletić, J.Puzović, *Forbush decreases - clouds relation in the neutron monitor era*, Astrophys. Space Sci. Trans. 7 (2011) 315-318.
- [9] H. Svensmark, *Cosmoclimatology: a new theory emerges*, Astron. Geophys. 48 (2007) 1.18-1.24.

## 10. Прилози

RAD2014 - BEST PAPERS AWARDS

<http://www.rad2014.elfak.rs/bestpapers.php>



The Second International Conference on Radiation and Dosimetry in Various Fields of Research  
[www.rad2014.elfak.rs](http://www.rad2014.elfak.rs)

MAY 27 - 30, 2014 | FACULTY OF ELECTRONIC ENGINEERING | NIŠ | SERBIA



Gold sponsor  


Silver sponsor  


### Awards – RAD 2014 Conference and SEERAS Symposium

The winners are awarded by not paying the conference fee for the next RAD Conference. Moreover, a Certificate will be given to the winners at the next RAD Conference.

Since we had two events with a large number of participants and a lot of high-quality papers, we have decided to give 5 awards – 2 for the best oral contributions, 1 for the best poster contribution and 2 for the best student contributions (one for oral and one for poster).

**Awards for the best oral contribution go to:**

**Jorge Sampaio**  
for the contribution:  
J. Sampaio, M<sup>a</sup>. Conceição Abreu, P. Sousa, Scatter fraction with simulations. revisiting radiation scatter in x-ray imaging and

**Mikhail Zhukovsky**  
for the contribution:  
M. Rogozina, M. Zhukovsky, A. Ekidin, M.Vasyanovich, Thoron decay products size distribution in Monazite Storage Facility

**Award for the best poster contribution goes to:**

**Dimitrije Maletić**  
for the contribution:  
D. M. Maletić, V. I. Udovičić, R. M. Banjanac, D. R. Joković, A. L. Dragić, N. B. Veselinović, J. Filipović, Correlative and multivariate analysis of increased radon concentration in underground laboratory

**Awards for the best student contribution go to:**

**Karolina Krefft**  
for the contribution:  
K. Krefft, B. Drogoszewska, J. Kamińska, M. Juniewicz, G. Wołakiewicz, I. Jakacka, B. Ciesielski, Application of EPR dosimetry in bone for verification of doses in radiotherapy patients and

**Ziyafer Gizem Portakal**  
for the contribution:  
Z. G. Portakal, C. Tunali, A comparative treatment planning study of intensity modulated radiotherapy and 3-d conformal radiotherapy for head & neck cancer

We congratulate to all the nominees and to all the awarded contributions and participants, and are looking forward to see you at the next RAD Conference!

**Nominations for:**

**I – Best oral contribution**

1. T. Wysokinski, G. Okada, G. Belev, C. Koughia, A. Edgar, L. D. Chapman, J. Ueda, S. Tanabe, S. Kasap, QA dosimetry for the biomedical imaging and therapy facility at CLSI
2. A. Y. Kilcar, F. Z. Biber Muftuler, H. Enginar, E. I. Medine, V. Tekin, P. Unak, A novel brain imaging agent including Alzheimer's disease diagnosis potential: <sup>99m</sup>Tc-BIOQUIN-HMPO
3. A. Esposito, B. Caccia, C. Andenna, GEANT4 simulation of a helical tomotherapy unit
4. G. Žauhar, S. Jurković, Đ. Smilović Radojčić, D. Dobravac, Testing of ultrasound trasducers by use of thermocromic tile
5. B. Obryk, P. Bilski, K. Hodyr, P. Mika, High-level TL dosimetry for high-temperature environment
6. M. Cuijić, J. Petrović, M. Đorđević, R. Dragović, S. Dragović, The radiological hazard due to



## Way to go, Dimitrije!

R<sup>6</sup>

With new reads,  
your research items  
Were the **most read**  
research items from

## your institution

### Achieved in 2020:

January 6, 13, 27, February 3

### Achieved in 2019:

December 2, 9, 23, 30  
November 4, 11, 18, 25  
October 7, 21, 28,  
September 2, 9, 16, 23, 30,  
August 5, 12, 19, July 29,  
June 3, 10, May 13, 20, 27,  
Apr 1, 8, 15, 22,  
Mar 4, 11, 18, 25,  
Feb 5, 11, 18, 25, Jan 28

---

### Achieved in 2018:

Jun 4, 11, 18,  
May 11, 21, 28

With new reads, your research items were  
the **most read** research items  
from **Serbia**

### Achieved in 2019

October 14,  
July 1, 8, 15, 22,  
June 17, 24,  
May 6  
Apr 29



# НАСТАВНО НАУЧНОМ ВЕЋУ ФИЗИЧКОГ ФАКУЛТЕТА УНИВЕРЗИТЕТА У БЕОГРАДУ

Пошто смо на VI седници Нучно-наставног Већа Физичког факултета Универзитета у Београду одржаној 27. марта 2019. године одређени за чланове Комисије за припрему извештаја о докторском раду "Моделовање утицаја атмосфере на мионску компоненту секундарног космичког зрачења" из научне области Физика језгара и честица, коју је кандидат Михаило Савић предао Физичком факултету у Београду, подносимо следећи

## РЕФЕРАТ

### 1 Основни подаци о кандидату

#### 1.1 Биографски подаци

Михаило Савић рођен је 31.12.1975. године у Београду. Дипломирао је 2009. године а затим 2011. године завршио и мастер студије године на Физичком факултету у Београду. Исте године уписао је докторске студије на Физичком факултету Универзитета у Београду.

У периоду од 2009. до 2011. године био је запослен на Физичком факултету у Београду, где је у оквиру катедре за Физику језгра и честица држао рачунске и експерименталне вежбе из неколико предмета. Од 2011. године запослен је на Институту за физику у Београду као члан Нискофонске лабораторије за нуклеарну физику.

Од 2011. до 2014. године, као члан Београдског SHINE Team-а, био је део NA61/-SHINE колаборације. Од 2015. године, као члан Београдског MICE Team-а, део је MICE колаборације.

#### 1.2 Научна активност

Као члан Нискофонске лабораторије за нуклеарну физику, у оквиру пројекта ОИ 171002, "Нуклеарне методе истраживања ретких догађаја и космичког зрачења", ради на анализи утицаја атмосферских параметара на мионску компоненту секундарног космичког зрачења, као и на проблематици ефикасности мерења исте. Дао је значајан допринос и коаутор је два рада M21 категорије, једног рада M22 и једног рада M23 категорије. Резултати су презентовани на три међународне конференције.

У оквиру NA61/SHINE колаборације радио је на анализи продукције барионских резонанци, продукцији података, одржавању и надгледању Time-Of-Flight (TOF) поддетектора, калибрацији TOF података, одржавању и развоју софтвера за калибрацију, реконструкцију и геометрију. Дао је допринос и коаутор је на четири рада M21 категорије.

У оквиру МІСЕ колаборације радио је на развоју апликације за визуелизацију догађаја (EventViewer) снимљених у оквиру МІСЕ експеримента. Дао је допринос и коаутор је на једном раду М23 категорије.

## 2 Опис предатог рада

### 2.1 Основни подаци

Ова дисертација урађена је под руководством др Димитрија Малетића, вишег научног сарадника Института за физику у Београду. Др Димитрије Малетић испуњава услове за менторство обзиром да има велико искуство у најужој области истраживања и техникама коришћеним у изради дисертације. Осим ментора, значајан допринос у раду и публикацијама дали су и остали чланови Нискофонске лабораторије за нуклеарну физику Института за физику у Београду, а нарочито др Александар Драгић, виши научни сарадник Института за физику у Београду.

Дисертација има 148 страна, не рачунајући насловне и стране са општим информацијама, садржај, литературу, списак слика и табела и биографију. Текст садржи 66 слика, 10 табела и 109 референци.

Текст дисертације подељен је на седам поглавља, од којих прво представља увод.

У другом поглављу представљени су извори и механизми убрзања, неке основне карактеристике (хемијски састав, енергетски спектар и др.), главни механизми модулатије и асоциране варијације интензитета примарног космичког зрачења. Такође, описани су неки основни процеси у оквиру честичне физике значајни за формирање и пропагацију каскада секундарног космичког зрачења, дат је преглед главних карактеристика пропагације ових каскада, као и неке особине мионске компоненте.

У трећој глави представљени су различити емпиријски и теоријски модели метеоролошких ефеката на мионску компоненту секундарног космичког зрачења, методи за корекцију развијени на основу датих модела, као и резултати примене ових метода на подацима мереним у Нискофонској лабораторији.

У четвртом поглављу описана је експериментална поставка, формат и основне технике процесирања мерених података, као и извори и обрада метеоролошких параметара неопходних за анализу.

У петом поглављу уводи се емпиријска анализа метеоролошких ефеката применом технике декомпозиције на основне компоненте и демонстрира ефикасност одговарајуће корекције.

У шестом поглављу се уводи емпиријска анализа метеоролошких ефеката применом метода за мултиваријантну регресију, имплементираних у TMVA пакету у оквиру ROOT окружења за анализу.

Седмо поглавље представља закључак који сумира и пореди уведене методе.

Универзитет у Београду ФИЗИЧКИ ФАКУЛТЕТ  
Студентски трг 12, 11000 Београд  
Поштански фах 44  
Тел. 011 7158 151, 3281 375  
ПИБ 100039173, Мат. бр. 07048190



University of Belgrade FACULTY OF PHYSICS  
Studentski trg 12, 11000 Belgrade  
Postal Box 44  
Phone +381 11 7158 151, Fax +381 11 3282 619  
www.ff.bg.ac.rs, dekanat@ff.bg.ac.rs

УНИВЕРЗИТЕТ У БЕОГРАДУ  
ФИЗИЧКИ ФАКУЛТЕТ  
Бр. 348/12  
05.07.2019 год.  
БЕОГРАД, СТУДЕНТСКИ ТРГ 12-19  
П. ФАХ 44

На основу члана 29 Закона о општем управном поступку («Службени гласник РС» број 18/2016 и 95/2018), и члана 149 Статута Универзитета у Београду - Физичког факултета, по захтеву МИХАИЛА САВИЋА, мастер физичара, издаје се следеће

## У В Е Р Е Њ Е

**МИХАИЛО САВИЋ**, мастер физичар, дана 4. јула 2019. године, одбранио је докторску дисертацију под називом

„МОДЕЛОВАЊЕ УТИЦАЈА АТМОСФЕРЕ НА МИОНСКУ КОМПОНЕНТУ СЕКУНДАРНОГ КОСМИЧКОГ ЗРАЧЕЊА“

пред Комисијом Универзитета у Београду - Физичког факултета, и тиме испунио све услове за промоцију у ДОКТОРА НАУКА – ФИЗИЧКЕ НАУКЕ.

Уверење се издаје на лични захтев, а служи ради регулисања права из радног односа и важи до промоције, односно добијања докторске дипломе.

Уверење је ослобођено плаћања таксе.



ДЕКАН ФИЗИЧКОГ ФАКУЛТЕТА

Проф. др Иван Белча

# dr Tijana Prodanovic

Professor of astrophysics @ Physics Department, Faculty of Sciences

## Colloquium

**Welcome to Astronomy and Physics Colloquium/Seminar Page!**

**Colloquia are held on Fridays at 14h, at the lecture room VII at the ground floor of the Physics Department.**

15. mart 2019. 14:00, amfiteatar VII, Departman za fiziku

**Др Марко Војиновић, Институт за физику Београд:**

### **Квантна гравитација — шта, како и зашто**

Конструкција теорије квантне гравитације (КГ) представља један од најфундаменталнијих проблема модерне теоријске физике. У овом предавању, даћемо увод и преглед разних приступа овом проблему, са конкретним циљем да на једноставан начин објаснимо (а) зашто хоћемо да квантујемо гравитацију, (б) шта тачно ту треба да се квантује, и (в) како то може да се изведе. Продискутоваћемо разна решена и нерешена питања везана за истраживање КГ. На крају ћемо дефинисати један конкретан модел КГ, као илустрацију једног од могућих приступа истраживању КГ.

\*\*\*

23. novembar 2018. 14:00, amfiteatar V, Departman za fiziku

**Prof. dr Dragutin Mihailović, Poljoprivredni fakultet, Novi Sad:**

### **Fizika u potrazi za skrivenim strukturama**

Kao po nekom pravilu, razvoj fizike zastane ispred zida za koji su se fizičari uvek nadali da će da se is-

rističe se Ljapunovljevi eksponenti i Kolmogorovljeva kompleksnost. na kraju će se ispitati ponašanje sistema jednačina za prognozu temperature na površini i u dubljem sloju zemljišta, proisteklog iz jednačine energijskog bilansa.

PETAK 4. decembar 2015. 14:00, amfiteatar V, Departman za fiziku

**MSc Arpad Toth,**

**Departman za fiziku, Novi Sad: Simulacija protoka krvi kroz aneurizmu abdominalne aorte: nove mogućnosti**

Klinički kriterijum za predviđanje rupture aneurizme abdominalne aorte (AAA) baziran je samo na dijametru AAA. Ovaj kriterijum ne uzima u obzir kompleksne hemodinačke sile koje deluju na zid AAA kao ni mehaničke osobine zida. U okviru našeg istraživanja pokušali smo da kroz četiri primera AAA dijagnostikovana kod muškaraca starijih od 65 godina pokažemo da trodimenzioni modeli krvnih sudova rekonstruisani na osnovu podataka dobijenih kompjuterizovanom tomografijom mogu dati mnogo bolja predviđanja rupture AAA. Za matematičko modelovanje i simulacije korišćena je računarska dinamika fluida. Na ovaj način smo bili u mogućnosti da pratimo dinamičko ponašanje protoka krvi u trodimenzionom prostoru. Rezultati simulacija provereni su doplerskom ultrazvučnom tehnikom. Validnost našeg modela potvrđena je dobrim slaganjem za vrednosti brzina protoka krvi dobijenih simulacijama i izmerenih doplerskom ultrazvučnom tehnikom. Nove informacije dali su nam i proračuni *Von Mises* napona što je još jedna od novih mogućnosti u proceni potencijalne rupture zida AAA.

PETAK 27. novembar 2015. 14:00, amfiteatar V, Departman za fiziku

**dr Dimitrije Maletić,**

**Institut za fiziku, Beograd: Neutrinska i fizika kosmičkog zračenja korišćenjem relativističkih miona**

U eksperimentima detekcije neutrina postoji problem slabe interakcije neutrina i detektora. Proces jonizacionog hladjenja relativističkih miona, koji se po prvi put ispituje na eksperimentu MICE, u Rutherford Appleton Laboratoriji u okolini Oksforda, Engleska, omogućiće da se višestruko poveća broj neutrina na neutrinским detektorima. Pored toga, proces jonizacionog hladjenja miona omogućiće razvoj kolajdera mnogo manjih dimenzija nego što su potrebne za ubrzanje elektrona ili protona. Saradnici Instituta za fiziku iz Beograda članovi su MICE kolaboracije.

Izučavanje fizike kosmičkog zračenja, u Niskofonskoj laboratoriji Instituta za fiziku u Beogradu, ko-

risti metod kontinualnog snimanja spektra i odbroja plastičnih scintilatora koji su indukovani prolaskom relativističkih miona kosmičkog zračenja kroz ove detektore. Prvenstveno se izučavaju promene odbroja dobijenih prolaskom miona iz kosmičkog zračenja i veza ovih promena sa aktivnošću Sunca. Beogradska mionska stanica je jedna od većeg broja svetskih stanica koja vrši monitorisanje intenziteta kosmičkog zračenja.

PETAK 20. novembar 2015. 14:00, amfiteatar V, Departman za fiziku

**MSc Marko Pavlović**

**Katedra za astronomiju, Matematički fakultet, Beograd: Ubrzanje čestica na udarnim talasima i njihov uticaj na hidrodinamičku i radio-evoluciju ostataka supernovih**

Ostaci supernove su objekti koji nastaju nakon eksplozije supernove. Materijal izbačen u eksploziji nastavlja život kroz interakciju sa okolnom medjuzvezdanom materijom hiljadama, pa čak i do milion godina nakon eksplozije. Ostaci supernovih su kosmicki akceleratori, predstavljaju glavne izvore galaktickih kosmickih zraka. Ovi objekti ubrzavaju cestice do visokih energija u procesu koji nazivamo difuzno ubrzanje. Koriscenjem superkompjutera i kompleksnih magnetohidrodinamickih kodova, modeliramo ostatke supernovih i proucavamo njihovu hidrodinamicku i radio evoluciju. Efikasno ubrzanje cestica na udarnih talasima modifikuje strukturu udarnog talasa i medjuzvezdanog magnetnog polja. Evolutivne trake ostataka supernovih koristice buduci projekti kao sto su SKA i ALMA, za procenu mnogih parametara samih ostataka ali i okolne medjuzvezdane sredine.

PETAK 13. novembar 2015. 14:00, amfiteatar V, Departman za fiziku

**dr Slobodan Radošević,**

**Departman za fiziku, Prirodno-matematički fakultet, Novi Sad: Primena lokalne  $SU(2)$  algebre na opis spinskih sistema – za ili protiv**

Sistemi lokalizovanih spinova (feromagnetni, antiferomagnetni itd.) su danas zanimljivi iz mnogo brojnih praktičnih i teorijskih razloga. Zbog toga je poželjno imati teorijske alate koje omogućavaju precizno i pouzdano predviđanje njihovih termodinamičkih karakteristika. Standardne metode koje se baziraju na direktnoj analizi lokalne  $su(2)$  algebre, poput Monte-Karlo simulacija ili metoda jednačina kretanja, poseduju fundamentalni nedostatak usled odsustva jasno definisanih interakcija u sistemu što može da dovede do pogrešnih interpretacija dobijenih rezultata. Sa druge strane, metod efektivnih lagranžijana se zasniva na sistematskom uračunavanju interakcija između Nambu-

## MICE Institutional Contacts

| Country                  | Institute  | Name  | email   | Comments     |
|--------------------------|--|---|---|--------------|
| Bulgaria                 | Sofia  | Tsenov, R   | tsenov@phys.uni-sofia.bg  |              |
| China                    | IHEP<br>Sichuan  | Tang, J<br>Li, Z  | tangjy@ihep.ac.cn<br>lizhihui@scu.edu.cn  |              |
| Italy                    | INFN Milano Bicocca<br>INFN Napoli<br>INFN Pavia ...<br>INFN Roma III ...  | Bonesini, M<br>Palladino, V<br>A de Bari<br>Orestano, D   | bonesini@mi.infn.it<br>Vittorio.Palladino@na.infn.it<br>antonio.debari@unipv.it<br>domizia.orestano@roma3.infn.it   |              |
| Korea                    | UNIST  | Chung, M  | chung.moses@gmail.com   |              |
| Netherlands              | NIKHEF   | Filthaut, F   | F.Filthaut@science.ru.nl  |              |
| Serbia                   | Belgrade<br>Novi Sad   | D Maletic<br>J Nikolov  | maletic@ipb.ac.rs<br>jovana.nikolov@df.uns.ac.rs  |              |
| Switzerland              | DPNC, Geneva<br>CERN   | Blondel, A<br>Vretenar, M   | Alain.Blondel@cern.ch<br>Maurizio.Vretenar@cern.ch  |              |
| UK                       | Brunel Univ<br>Daresbury Lab<br>Glasgow Univ<br>Imperial College<br>Liverpool Univ<br>Oxford Univ<br>RAL<br>Sheffield Univ<br>Strathclyde<br>Warwick | Kyberd, P<br>Grant, A<br>Soler, P<br>Pasternak, J<br>Gamet, R<br>Cobb, J<br>Rogers, C<br>Hodgson, P<br>Ronald, K<br>Boyd, S | Paul.Kyberd@brunel.ac.uk<br>alan.grant@STFC.AC.UK<br>p.soler@physics.gla.ac.uk<br>j.pasternak@imperial.ac.uk<br>gam@hep.ph.liv.ac.uk<br>j.cobb1@physics.ox.ac.uk<br>chris.rogers@STFC.AC.UK<br>p.hodgson@sheffield.ac.uk<br>k.ronald@strath.ac.uk<br>s.b.boyd@warwick.ac.uk | CB Secretary |
| USA                      | BNL<br>Fermilab<br>Illinois Inst Tech<br>Iowa Univ<br>LBL<br>Mississippi Univ<br>Riverside   | Witte, H<br>Popovic, M<br>Kaplan, D<br>Onel, Y<br>Li, D<br>Summers, D<br>Hanson, G  | hwitte@bnl.gov<br>popovic@fnal.gov<br>kaplan@iit.edu<br>yonel@newton.physics.uiowa.edu<br>Dli@lbl.gov<br>summers@phy.olemiss.edu<br>gail.hanson@ucr.edu   |              |
| Chairperson<br>Secretary |  | Booth, C<br>Kyberd, P   | C.Booth@sheffield.ac.uk<br>Paul.Kyberd@brunel.ac.uk   |              |

## MICE Collaborator list

| Country     | Institute           | Name               | Number | Comments      |
|-------------|---------------------|--------------------|--------|---------------|
| Bulgaria    | Sofia               | R Tsenov           | 3      |               |
|             |                     | M Bogomilov        |        |               |
|             |                     | G Vankova-Kirilova |        |               |
| China       | IHEP                | Jingyu Tang        | 6      |               |
|             |                     | Yingpeng Song      |        | Grad. Student |
|             |                     | Weibin Liu         |        |               |
|             |                     | Meifen Wang        |        | Engineer      |
|             |                     | Weichai Yao        |        | Engineer      |
|             |                     | Jianping Dai       |        |               |
| Italy       | Sichuan             | Zhihui Li          | 1      |               |
|             | INFN Milano Bicocca | M Bonesini         | 5      |               |
|             |                     | R Bertoni          |        | Engineer      |
|             |                     | R Mazza            |        | Technician    |
|             |                     | F Chignoli         |        | Technician    |
|             |                     | S Banfi            |        | Technician    |
|             | INFN Napoli         | V Palladino        | 1      |               |
| INFN Pavia  | A de Bari           | 1                  |        |               |
| Netherlands | INFN Roma III       | D Orestano         | 2      |               |
|             |                     | L Tortora          |        |               |
|             |                     |                    |        |               |
| Serbia      | NIKHEF              | F Filthaut         | 1      |               |
| Serbia      | Belgrade            | D Maletic          | 3      |               |
|             |                     | D Jokovic          |        |               |
|             |                     | M Savic            |        |               |
| Switzerland | Novi Sad            | J Nikolov          | 3      |               |
|             |                     | N Jovancevic       |        |               |
|             |                     | D Knezevic         |        |               |
| Switzerland | DPNC, Geneva        | A Blondel          | 4      |               |
|             |                     | F Drielsma         |        | Grad. Student |
|             |                     | Y Karadzhov        |        |               |
|             |                     | E Noah             |        |               |
| UK          | CERN                | M Vretenar         | 1      |               |
|             | Brunel Univ         | P Kyberd           | 2 or 3 |               |
|             |                     | H Nebrensky        |        |               |
|             |                     | Vacancy            |        | Grad. student |
| UK          | Daresbury Lab       | A Grant            | 17     |               |
|             |                     | N Collomb          |        |               |
|             |                     | A Muir             |        |               |
|             |                     | G Stokes           |        |               |
|             |                     | S Griffiths        |        |               |
|             |                     | I Mullacrane       |        |               |
|             |                     | A Gallagher        |        |               |

## MICE Collaborator list

| Country | Institute        | Name          | Number | Comments      |
|---------|------------------|---------------|--------|---------------|
|         |                  | T Hartnett    |        |               |
|         |                  | C Whyte       |        |               |
|         |                  | A Oates       |        |               |
|         |                  | P Warburton   |        |               |
|         |                  | P Owens       |        |               |
|         |                  | P Hindley     |        |               |
|         |                  | N Rimmer      |        |               |
|         |                  | D Abrams      |        |               |
|         |                  | A Moss        |        |               |
|         |                  | K Dumbell     |        |               |
|         | Glasgow Univ     | P Soler       | 3      |               |
|         |                  | R Bayes       |        |               |
|         |                  | J Nugent      |        | Grad. student |
|         | Imperial College | J Pasternak   | 14     |               |
|         |                  | D Colling     |        |               |
|         |                  | P Dornan      |        |               |
|         |                  | K Long        |        |               |
|         |                  | S Alsari      |        |               |
|         |                  | G Barber      |        |               |
|         |                  | V J Blackmore |        |               |
|         |                  | A Dobbs       |        |               |
|         |                  | A Kurup       |        |               |
|         |                  | J-B Lagrange  |        |               |
|         |                  | J Martyniak   |        |               |
|         |                  | S Middleton   |        | Grad. Student |
|         |                  | M A Uchida    |        |               |
|         |                  | C Hunt        |        | Grad. Student |
|         | Liverpool Univ   | R Gamet       | 1      |               |
|         | Oxford Univ      | J Cobb        | (1)    | Retired       |
|         | RAL              | C Rogers      | 21     | ISIS          |
|         |                  | A Nichols     |        | TD            |
|         |                  | B Anderson    |        | ISIS          |
|         |                  | C Brew        |        | PPD           |
|         |                  | C MacWaters   |        | TD            |
|         |                  | D Adams       |        | ISIS          |
|         |                  | E Capocci     |        | TD            |
|         |                  | J Tarrant     |        | TD            |
|         |                  | J Govans      |        | PPD           |
|         |                  | J Boehm       |        | TD            |
|         |                  | M Tucker      |        | PPD           |
|         |                  | M Hughes      |        | ISIS          |
|         |                  | M Courthold   |        | TD            |
|         |                  | O Kirichek    |        | ISIS          |
|         |                  | P Barclay     |        | TD            |
|         |                  | R Down        |        | ISIS          |
|         |                  | R Hale        |        | ISIS          |
|         |                  | S Watson      |        | TD            |
|         |                  | T Stanley     |        | ASTeC         |
|         |                  | T Bradshaw    |        | TD            |
|         |                  | V Bayliss     |        | TD            |

## MICE Collaborator list

| Country            | Institute      | Name        | Number                           | Comments      |
|--------------------|----------------|-------------|----------------------------------|---------------|
| USA                | Sheffield Univ | C Booth     | 5                                | Grad. Student |
|                    |                | E Overton   |                                  |               |
|                    |                | P Hodgson   |                                  |               |
|                    |                | S Wilbur    |                                  |               |
|                    |                | J Langlands |                                  |               |
|                    | Strathclyde    | K Ronald    | 4                                | Grad. Student |
|                    |                | A Young     |                                  |               |
|                    |                | C Whyte     |                                  |               |
|                    |                | A Dick      |                                  |               |
|                    | Warwick        | S Boyd      | 3                                | Grad. Student |
|                    |                | P Franchini |                                  |               |
|                    |                | J Greiss    |                                  |               |
|                    | Brookhaven     | H Witte     | 2                                |               |
|                    |                | M. Palmer   |                                  |               |
| Fermilab           | M Popovic      | 5           | May leave before end step IV     |               |
|                    | D Bowring      |             |                                  |               |
|                    | A Bross        |             |                                  |               |
|                    | A Liu          |             |                                  |               |
|                    | D Neuffer      |             |                                  |               |
| Illinois Inst Tech | D Kaplan       | 6           | Grad. Student<br>Undergraduate   |               |
|                    | P Snopok       |             |                                  |               |
|                    | Y Torun        |             |                                  |               |
|                    | D Rajaram      |             |                                  |               |
|                    | T Mohayai      |             |                                  |               |
|                    | V Suezaki      |             |                                  |               |
| Iowa Univ          | Y Onel         | 1           |                                  |               |
| LBNL               | D Li           | 5           | Engineer<br>Engineer<br>Engineer |               |
|                    | T Luo          |             |                                  |               |
|                    | A DeMello      |             |                                  |               |
|                    | A Lambert      |             |                                  |               |
|                    | S Virostek     |             |                                  |               |
| Mississippi Univ   | D Summers      | 3           |                                  |               |
|                    | L Cremaldi     |             |                                  |               |
|                    | D Sanders      |             |                                  |               |
| Riverside          | G Hanson       | 2           | Grad. Student                    |               |
|                    | C Heidt        |             |                                  |               |

----- Forwarded Message -----

**Subject:** EuCARD-2 Transnational Access Funding

**Date:** Mon, 11 May 2015 07:30:59 +0000

**From:** roy.preece@stfc.ac.uk

**To:** maletic@ipb.ac.rs

Dear Dimitrije

The allocations panel for the Transnational Access to the ICTF at STFC have deliberated your application for funding. The outcome has been to award you an amount of €-- for the period of 24 months.

The EuCARD-2 project is now half way through its lifetime. To enable the allocations panel to effectively and efficiently grant the access funding to applicants I would like to be able to provide them with up to date and accurate forecasts of how the money is being and will be spent during the allocation period you have been granted. If you can provide me with your forecast of how the grant will be spent over the 24 months of your allocation period I'd be grateful. The details I would be interested to see are the number of people to visit, the number of days and the dates they will attend the ICTF.

There is the mid-term review in CERN for the project and I would like to be able to present the spending profile that you will provide, if you can get the details to me by Wednesday 20th May I'd be very grateful.

I look forward to seeing you at the Rutherford Appleton Laboratory soon.

Best regards

Roy

**DECISIONS  
OF THE 4<sup>th</sup> JOINT COORDINATION COMMITTEE  
OF THE MINISTRY OF EDUCATION, SCIENCE AND TECHNOLOGICAL  
DEVELOPMENT  
OF THE REPUBLIC OF SERBIA  
AND THE JOINT INSTITUTE FOR NUCLEAR RESEARCH  
8<sup>th</sup> February 2017, Dubna-Belgrade**

**Participants from Serbia:**

**Dr. S. Petrović** –Principal Research Fellow, Vinča Institute of Nuclear Sciences, Belgrade

**Dr. Lj. Simić** – Principal Research Fellow, Institute of Physics, Belgrade

**Dr. M. Aničić Urošević** – Senior Research Associate, Institute of Physics, Belgrade

**Dr. Dimitrije Maletić** – Senior Research Associate, Institute of Physics, Belgrade

**Participants from JINR:**

**Prof. R. Lednicky** – Vice Director

**Prof. S. Pakuliak** – Director of the University Centre

**Dr. D. Kamanin** – Deputy Chief Scientific Secretary

**Dr. O. Culicov** – Deputy Director, Frank Laboratory of Neutron Physics

**Prof. V. Scuratov** – Division Head, Laboratory of Nuclear Reactions

**Mrs. Yu. Polyakova** – Coordinator, Department of International Cooperation

On 8 February 2017, the session of the 4<sup>th</sup> Joint Coordination Committee (JCC) was held as the video conference, the participants were present in JINR, Dubna, and in Vinča Institute of Nuclear Sciences, Belgrade. During this meeting, the Committee discussed the status and the main tasks of the cooperation, financial issues and the next steps. The representatives from Serbia and JINR (hereinafter also referred to as the “Parties”) recorded as follows.

1. Prof. Lednicky made an introduction, and the Parties confirmed the list of JCC members:
  - D. Kamanin, S. Pakuliak and O. Culicov from the JINR side;
  - S. Petrović, D. Maletić and M. Aničić Urošević from the Serbian side.Prof. R. Lednicky as well as the State Secretary of Serbia will be considered as the Heads of the Parties being available.
2. The parties endorsed the roadmap of the development of cooperation to submit it subsequently to the Government of Serbia.
3. The Parties agreed to hold the forthcoming celebration of 10 Years JINR-Serbia cooperation on 15-17 March 2017 in Belgrade. The program will include participation in Russia-Serbia EXPO, launching of the roadmap, round table with the minister, lecture of JINR director at the Serbian academy of sciences etc. JINR will assign the representative delegation including the directorate of the JINR Laboratories and the project leaders, while Serbian part will provide with a program by 1 March 2017 and secure a quorum. The celebration should attract attention to the wide perspectives of the development of the cooperation between JINR and Serbian universities and research organizations.
4. The parties concluded that it is necessary to foster the new cooperation lines (IT, Radiobiology, gamma-activation). Both parties agreed to identify the respective experts on new cooperation lines by celebration or during it.

**Subject:** Invitation to future MEMOs ...

**From:** "Long, Kenneth R" <k.long@imperial.ac.uk>

**Date:** 1/22/19, 5:48 PM

**To:** Maletic Dimitrije <maletic@ipb.ac.rs>, Kyberd Paul  
<Paul.Kyberd@brunel.ac.uk>

**CC:** Dr Rogers Chris <Chris.Rogers@stfc.ac.uk>, Franchini Paolo  
<p.franchini@warwick.ac.uk>

Dimitrije, Paul — Hi —

This is to invite you to future meetings of the MEMO — we meet once per month on a Tuesday at 15:30 UK time. The reason for the invite is that we need to be sure to address issues that arise related to the GRID processing as it affects MICE.

I hope you don't mind!

With best wishes ...

Ken

*Kenneth Long*

*[EMail: K.Long@Imperial.AC.UK](mailto:K.Long@Imperial.AC.UK)*

*Mobile: work : +44-(0)7824 560302*

*home: +44-(0)7890-595138*

## MICE Experiment Management Office

### Membership

- Spokesperson: K. Long (Chair)
- Deputy: A. Bross
- Experimental Integration Scientist: P. Hodgson
- Operations Coordinator: S. Boyd
- Physics Coordinator: C. Rogers
- Software and Computing Coordinator: D. Rajaram
- Co-opted:
  - Project Manager: C. Whyte
  - P. Kyberd, D. Maletic

|                                   |
|-----------------------------------|
| MICE Experiment Management Office |
| Membership                        |
| Organisation                      |
| Mailing list                      |
| Meetings:                         |
| Reviews:                          |
| Documents:                        |
| Uplinks:                          |

### Organisation

- MEMO organigram: [MEMO.pdf](#)
- Operations organigram: [Ops.pdf](#)
- Software and computing organigram: [SWandC.pdf](#)
- Physics and analysis organigram: [Physics1.pdf](#)

### Mailing list

- mice-memo\_at\_jiscmail.ac.uk

### Meetings:

- 2019: joint MEMO/MIPO -- or MEMO alone
  - [2020-01-07](#)
  - [2019-07-23](#)
  - [2019-06-11](#)
  - [2019-03-12](#)
  - [2019-02-12](#)
  - [2019-01-22](#)
- [2018](#)
- [2017](#)
- [2016](#)
- [2015](#)
- [2014](#)
- [2013](#)

### Reviews:

- **2017: Tracker s/w review:**
  - Meetings:
    - [Meeting 1, 2017-04-27](#)
    - [Meeting 2, 2017-05-26](#)
    - [Meeting 3, 2017-06-19](#)
    - [Meeting 4, 2017-07-19](#)
    - [Meeting 5, 2017-08-02](#)
    - [Meeting 6, 2017-08-16](#)
    - [Meeting 7, 2017-09-08](#)
    - [Meeting 8, 2017-11-01](#)
- [2016/17: Controls and monitoring review](#)

### Documents:

- **2016:**
  - *MEMO 2016(01):* [MICE bimonthly project update 7](#)
- **2015:**
  - *MEMO 2015(01):* [Response to feedback from the RLSR panel and the MPB](#)

### Uplinks:

[Back to Collaboration](#)

[Back to Governance](#)

[MEMO.pdf](#) (17.6 KB) Long, Kenneth, 29 May 2014 22:48  
[Physics1.pdf](#) (41.9 KB) Long, Kenneth, 29 May 2014 23:03  
[SWandC.pdf](#) (40.2 KB) Long, Kenneth, 29 May 2014 23:05  
[Ops.pdf](#) (82.6 KB) Long, Kenneth, 29 May 2014 23:12



Fuel



# Certificate of Reviewing

Awarded since June 2018 (1 review)

presented to

**DIMITRIJE MALETIC**

in recognition of the review contributed to the journal

The Editors of Fuel





Environmental Pollution

# Certificate of Reviewing

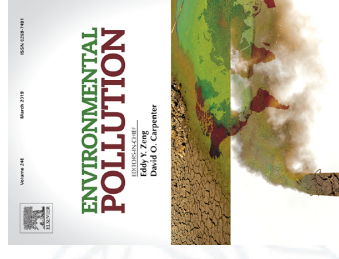
Awarded since February 2019 (1 review)

presented to

**DIMITRIJE MALETIC**

in recognition of the review contributed to the journal

The Editors of Environmental Pollution





Atmospheric Pollution Research



# Certificate of Reviewing

Awarded since May 2019 (1 review)

presented to

**DIMITRIJE MALETIC**

in recognition of the review contributed to the journal

The Editors of Atmospheric Pollution Research





Building and Environment



# Certificate of Reviewing

Awarded since June 2019 (1 review)

presented to

**DIMITRIJE MALETIC**

in recognition of the review contributed to the journal

The Editors of Building and Environment



**NUCLEAR TECHNOLOGY & RADIATION PROTECTION**  
**Vol. XXXIII, 2018**

**List of Reviewers**

Aleksandar Kandić, Vinča Institute of Nuclear Sciences, University of Belgrade,  
Belgrade, Serbia  
Asghar Mesbahi, Tabriz University of Medical Sciences, Tabriz, Iran  
Borislava Petrović, Institute of Oncology, Sremska Kamenica, Serbia  
Boško Bojović, Vinča Institute of Nuclear Sciences, University of Belgrade,  
Belgrade, Serbia  
Branka Mihaljević, Rudjer Bošković Institute, Zagreb, Croatia,  
Costas J. Hourdakakis, Greek Atomic Energy Commission (EEAE), Athens, Greece  
Dejan Joković, Institute of Physics, University of Belgrade, Belgrade, Serbia  
Desanka Šulić, Faculty of Ecology and Environmental Protection,  
Union – Nikola Tesla University, Belgrade, Serbia  
Dimitrije Maletić, Institute of Physics, University of Belgrade, Belgrade, Serbia  
Djordje Lazarević, Vinča Institute of Nuclear Sciences, University of Belgrade,  
Belgrade, Serbia  
Dragana Krstić, Faculty of Sciences, University of Kragujevac, Kragujevac, Serbia  
Dragana Todorović, Vinča Institute of Nuclear Sciences, University of Belgrade,  
Belgrade, Serbia  
Dragoslav Nikezić, Faculty of Sciences, University of Kragujevac, Kragujevac, Serbia  
Hosein Ghiasi, Tabriz University of Medical Sciences, Tabriz, Iran  
Igor Čeliković, Vinča Institute of Nuclear Sciences, University of Belgrade,  
Belgrade, Serbia  
Ivan Knežević, Public Company 'Nuclear Facilities of Serbia', Belgrade, Serbia  
Ivana Smičiklas, Vinča Institute of Nuclear Sciences, University of Belgrade,  
Belgrade, Serbia  
Ivana Vukanac, Vinča Institute of Nuclear Sciences, University of Belgrade,  
Belgrade, Serbia  
Jelena Ajtić, Faculty of Veterinary Medicine, University of Belgrade, Belgrade, Serbia  
Jelena Radovanović, Faculty of Electrical Engineering, University of Belgrade,  
Belgrade, Serbia  
Jelena Stajić, Faculty of Sciences, University of Kragujevac, Kragujevac, Serbia  
Jelena Stanković Petrović, Vinča Institute of Nuclear Sciences, University of Belgrade,  
Belgrade, Serbia  
Joanna Domienik, Nofer Institute of Occupational Medicine, Lodz, Poland  
Koviljka Stanković, Faculty of Electrical Engineering, University of Belgrade,  
Belgrade, Serbia  
Ljiljana Gulan, University of Priština, Kosovska Mitrovica, Serbia

Marija Janković, Vinča Institute of Nuclear Sciences, University of Belgrade,  
Belgrade, Serbia

Marija Šljivić-Ivanović, Vinča Institute of Nuclear Sciences, University of Belgrade,  
Belgrade, Serbia

Matthias Krause, University of Utah, Salt Lake City, Utah, USA

Maurice O. Miller, University of the West Indies, Kingston, Jamaica

Milan Pešić, Vinča Institute of Nuclear Sciences, University of Belgrade,  
Belgrade, Serbia

Milan Tanić, Serbian Army, Kruševac, Serbia

Milica Vujković, Faculty of Physical Chemistry, University of Belgrade, Belgrade, Serbia

Miloš Živanović, Vinča Institute of Nuclear Sciences, University of Belgrade,  
Belgrade, Serbia

Milutin Jevremović, Public Company 'Nuclear Facilities of Serbia', Belgrade, Serbia

Mladen Nikolić, College of Applied Technical Sciences, Kruševac, Serbia

Nace Stojanov, Institute of Physics, University of Scopje, Scopje, North Macedonia

Nenad Stevanović, Faculty of Sciences, University of Kragujevac, Kragujevac, Serbia

Nikola Vukelić, Faculty of Physical Chemistry, University of Belgrade, Belgrade, Serbia

Olivera Ciraj-Bjelac, Vinča Institute of Nuclear Sciences, University of Belgrade,  
Belgrade, Serbia

Petar Beličev, Vinča Institute of Nuclear Sciences, University of Belgrade,  
Belgrade, Serbia

Peter Bossew, German Federal Office for Radiation Protection, Berlin, Germany

Predrag Kolarž, Institute of Physics, University of Belgrade, Belgrade, Serbia

Predrag Osmokrović, Faculty of Electrical Engineering, University of Belgrade,  
Belgrade, Serbia

Rodoljub Simović, Vinča Institute of Nuclear Sciences, University of Belgrade,  
Belgrade, Serbia

Saša Ćirković, Institute of Physics, University of Belgrade, Belgrade, Serbia

Sladjana Tanasković, Faculty of Pharmacy, University of Belgrade, Belgrade, Serbia

Srboljub Stanković, Vinča Institute of Nuclear Sciences, University of Belgrade,  
Belgrade, Serbia

Suzana Bogojević, 'Karajović' Institute, University of Belgrade, Belgrade, Serbia

Svetlana Štrbac, ICTM, University of Belgrade, Belgrade, Serbia

Taško Grozdanov, Institute of Physics, University of Belgrade, Belgrade, Serbia

Tatjana Jevremovic, University of Utah, Salt Lake City, Utah, USA

Venkat H. Deshraj, International Atomic Energy Agency, Vienna, Austria

Vesna Gershan, Faculty of Natural Sciences and Mathematics, Skopje, North Macedonia

Vladan Ljubenov, International Atomic Energy Agency, Vienna, Austria

Vladimir Marković, Faculty of Sciences, University of Kragujevac, Kragujevac, Serbia

Vladimir Udovičić, Institute of Physics, University of Belgrade, Belgrade, Serbia

Vladimir Vukić, Institute of Electrical Engineering Nikola Tesla, University of Belgrade,  
Belgrade, Serbia

Zoran Mirkov, 'Karajović' Institute, University of Belgrade, Belgrade, Serbia

Zoran Radovanović, Faculty of Medicine, University of Belgrade, Belgrade, Serbia



# MICE CM48

27-29 June 2017  
Europe/Belgrade timezone

- Overview
- Timetable
- Contribution List
- Registration
- Participant List

## Timetable

### Tue 27/6

|       |  |   |
|-------|--|---|
| 09:00 | <b>Analysis, software and computing</b><br><i>Chris Rogers, Durga Rajaram</i>  |   |
| 10:00 | <i>D. Popovic, IPB</i> <span style="float: right;">09:00 - 10:30</span>  |   |
|       | <b>Coffee</b> <span style="float: right;">10:30 - 11:00</span>   |   |
| 11:00 | <b>Beam selection</b> <i>Christopher Hunt</i><br><i>D. Popovic, IPB</i> <span style="float: right;">11:00 - 11:20</span>             | <b>Tracker</b> <i>Edward Overton</i><br><i>Z. Maric, IPB</i> <span style="float: right;">11:00 - 11:20</span>       |
|       | <b>Event viewer</b> <i>Mihailo Savic</i><br><i>D. Popovic, IPB</i> <span style="float: right;">11:20 - 11:40</span>                  | <b>LH2 Installation</b> <i>colin whyte</i><br><i>Z. Maric, IPB</i> <span style="float: right;">11:20 - 11:55</span> |
|       | <b>EMR performance</b> <i>Francois Elie Rene Drielsma</i><br><i>D. Popovic, IPB</i> <span style="float: right;">11:40 - 12:00</span> | <b>SS Magnets</b> <i>Alan Bross</i><br><i>Z. Maric, IPB</i> <span style="float: right;">11:55 - 12:15</span>        |
| 12:00 | <b>Cuts tool</b> <i>Mr Misha Fedorov</i><br><i>D. Popovic, IPB</i> <span style="float: right;">12:00 - 12:10</span>                  | <b>Operations</b> <i>Steven Boyd</i><br><i>Z. Maric, IPB</i> <span style="float: right;">12:15 - 12:35</span>       |
|       | <b>Magnetic field map analysis</b> <i>Joe Langlands</i><br><i>D. Popovic, IPB</i> <span style="float: right;">12:10 - 12:30</span>   |   |
|       | <b>Discussion</b><br><i>D. Popovic, IPB</i> <span style="float: right;">12:30 - 13:00</span>   |   |
| 13:00 | <b>Lunch</b> <span style="float: right;">13:00 - 14:00</span>  |   |
| 14:00 | <b>Welcome</b> <i>Aleksandar Bogojevic</i><br><i>D. Popovic, IPB</i> <span style="float: right;">14:00 - 14:10</span>                |   |
|       | <b>Introduction</b> <i>Kenneth Richard Long</i><br><i>D. Popovic, IPB</i> <span style="float: right;">14:10 - 14:30</span>           |   |
|       | <b>Recent results from MUCOOL</b> <i>Alan Bross</i>  |   |





# MICE CM48

27-29 June 2017  
Europe/Belgrade timezone


[Overview](#)
[Timetable](#)
[Contribution List](#)
[Registration](#)
[Participant List](#)

## Participant List

27 participants

| First Name      | Last Name | Affiliation                          |
|-----------------|-----------|--------------------------------------|
| Alan            | Bross     | Fermi National Accelerator Lab. (US) |
| Alexandre       | Zaitsev   | NRC KI IHEP, Protvino                |
| Azeez Adesina   | Akerekan  |                                      |
| Chris           | Rogers    | Rutherford Lab                       |
| Christopher     | Hunt      | Imperial College                     |
| Colin           | Whyte     | mice                                 |
| Daniel          | Kaplan    | Illinois Institute of Technology     |
| David           | Neuffer   | Fermilab                             |
| Dejan           | Joković   | Institute of Physics Belgrade        |
| Dimitrije       | Maletic   |                                      |
| Durga           | Rajaram   | Illinois Institute of Technology     |
| François        | Drielsma  | University of Geneva                 |
| Henry           | Nebrensky | Brunel University                    |
| Janusz          | Martyniak | Imperial College London              |
| Jaroslaw        | Pasternak | Imperial College London              |
| John            | Cobb      | Oxford Unoversity                    |
| John            | Nugent    | University of Glasgow                |
| Kenneth Richard | Long      | Imperial College (GB)                |
| Maurizio        | Bonesini  | Sezione INFN Milano Bicocca          |
| Melissa         | Uchida    | Imperial College London              |
| ...             | ...       | ...                                  |





# MICE CM48

27-29 June 2017  
Europe/Belgrade timezone

Overview

Timetable

Contribution List

Registration

Participant List

**The 48th Muon Ionization Cooling Experiment (MICE) Collaboration Meeting will be held at the Institute of Physics Belgrade, Serbia from 27th to 29th June 2017 inclusive**

**Registration 30 EUR      Collaboration Dinner 25 EUR**

**Payment method: Bank transfer. Instructions bellow. Or in Belgrade upon arrival.**

**(as this meeting is being held in Belgrade, registration via the ISIS database is NOT required)**

Some photos taken at the event:

<http://147.91.87.151/foto/micecm48/>



**Starts** 27 Jun 2017, 09:00  
**Ends** 29 Jun 2017, 18:00  
Europe/Belgrade



Institute of Physics Belgrade  
Pregrevica 118, 11080 Zemun-Belgrade  
Republic of Serbia  
GPS: 44.855121, 20.390716  
<http://www.ipb.ac.rs/index.php/en/>  
local contact: maletic@ipb.ac.rs



Instructions\_EUR.doc  
 Instructions\_USD.doc



Hotels we know:  
Hotel Zlatnik, Theater Hotel Belgrade, IN Hotel Belgrade  
Hotel Yugoslavia, Tulip Inn, Crowne Plaza Belgrade, Hyatt Regency Belgrade

Downtown hotels:  
Palace, Majestic Hotel, Courtyard by Marriott

Many other options. Please check online, for example on: [Booking.com](http://Booking.com)



**Registration**  
Registration for this event is currently open.

**Register now** >



Powered by [Indico](#)

[Help](#) | [Contact](#) | [Terms and conditions](#) | [URL Shortener](#)





# Одељење Друштва физичара Србије за научна истраживања и високо образовање

## Одсеци Одељења НИВО ДФС

Братислав Обрадовић, председник, [obrat@ff.bg.ac.rs](mailto:obrat@ff.bg.ac.rs)  
Горан Ђорђевић, потпредседник, [gorandj@junis.ni.ac.rs](mailto:gorandj@junis.ni.ac.rs)

### 1. Одсек за квантну и математичку физику (7)

Милан Дамњановић, ФФ, председник, [yqoq@afrodita.rcub.bg.ac.rs](mailto:yqoq@afrodita.rcub.bg.ac.rs)  
Татјана Вуковић, ФФ, [tanja37@afrodita.rcub.bg.ac.rs](mailto:tanja37@afrodita.rcub.bg.ac.rs)  
Мирољуб Дугић, ПМФ Крагујевац, [dugic@kg.ac.rs](mailto:dugic@kg.ac.rs)  
Ненад Милојевић, ПМФ Ниш, [nenad81@pmf.ni.ac.rs](mailto:nenad81@pmf.ni.ac.rs)  
Милан Пантић, ПМФ Нови Сад, [mpantic@df.uns.ac.rs](mailto:mpantic@df.uns.ac.rs)  
Бранислав Цветковић, ИФ, [branislav.cvetkovic@ipb.ac.rs](mailto:branislav.cvetkovic@ipb.ac.rs)  
Далибор Чевизовић, Винча, [cevizd@vinca.rs](mailto:cevizd@vinca.rs)

### 2. Одсек за физику језгра, елементарних честица и основних интеракција (8)

Петар Аџић, ФФ, председник, [adzic@ff.bg.ac.rs](mailto:adzic@ff.bg.ac.rs)  
Иванка Божовић-Јелисавчић, Винча, [ibozovic@vinca.rs](mailto:ibozovic@vinca.rs)  
Драгољуб Димитријевић, ПМФ Ниш, [ddrag@pmf.ni.ac.rs](mailto:ddrag@pmf.ni.ac.rs)  
Димитрије Малетић, ИФ, [dimitrije.maletic@ipb.ac.rs](mailto:dimitrije.maletic@ipb.ac.rs)  
Јована Николов, ПМФ Нови Сад, [jovana.nikolov@df.uns.ac.rs](mailto:jovana.nikolov@df.uns.ac.rs)  
Воја Радовановић ФФ, [rvoja@ff.bg.ac.rs](mailto:rvoja@ff.bg.ac.rs)  
Светислав Савовић, ПМФ Крагујевац, [savovic@kg.ac.rs](mailto:savovic@kg.ac.rs)  
Ковиљка Станковић, ЕТФ, [kstankovic@etf.bg.ac.rs](mailto:kstankovic@etf.bg.ac.rs)

### 3. Одсек за астрономију и астрофизику (9)

Лука Поповић, АО, председник, [lpopovic@aob.bg.ac.rs](mailto:lpopovic@aob.bg.ac.rs)  
Весна Борка Јовановић, Винча, [vborka@vinca.rs](mailto:vborka@vinca.rs)  
Драган Гајић, ПМФ Ниш, [dgaja@junis.ni.ac.rs](mailto:dgaja@junis.ni.ac.rs)  
Мирослав Мићић, АО, [micic@aob.rs](mailto:micic@aob.rs)  
Тијана Продановић, ПМФ Нови Сад, [prodanvc@df.uns.ac.rs](mailto:prodanvc@df.uns.ac.rs)  
Владимир Срећковић, ИФ, [vladimir.sreckovic@ipb.ac.rs](mailto:vladimir.sreckovic@ipb.ac.rs)  
Саша Симић, ПМФ Крагујевац, [ssimic@kg.ac.rs](mailto:ssimic@kg.ac.rs)  
Зорица Цветковић, АО, [zcvetkovic@aob.bg.ac.rs](mailto:zcvetkovic@aob.bg.ac.rs)  
Кристина Чајко, ПМФ Нови Сад,

### 4. Одсек за физику кондензоване материје и статистичку физику (9)

Антун Балаж, ИФ, председник, [antun@ipb.ac.rs](mailto:antun@ipb.ac.rs) , [antun.balaz@scl.rs](mailto:antun.balaz@scl.rs)  
Наташа Бибић, Винча, [natasabi@vinca.rs](mailto:natasabi@vinca.rs)  
Ивица Брадарич, Винча, [bradaric@vinca.rs](mailto:bradaric@vinca.rs)  
Владимир Миљковић, ФФ, [miljko@ff.bg.ac.rs](mailto:miljko@ff.bg.ac.rs)  
Милица Павков Хрвојевић, ПМФ Нови Сад, [milica@df.uns.ac.rs](mailto:milica@df.uns.ac.rs)  
Јована Гојановић, ЕТФ, [jovana@etf.bg.ac.rs](mailto:jovana@etf.bg.ac.rs)  
Ђорђе Спасојевић, ФФ, [djordjes@ff.bg.ac.rs](mailto:djordjes@ff.bg.ac.rs)

**Subject:** URGENT REPLY DUE: a MICE contribution of yours at COOL 2017?

**From:** Vittorio Palladino <palladin@na.infn.it>

**Date:** 8/24/17, 3:54 PM

**To:** Mariyan.Bogomilov@CERN.CH, P.Hodgson@SHEFFIELD.AC.UK, Maletic Dimitrije <maletic@ipb.ac.rs>

**CC:** mauchida <m.a.uchida@imperial.ac.uk>, Ken Long <K.Long@Imperial.AC.UK>, Daniel Kaplan <kaplan@iit.edu>

Dear Dimitrije, Mariyan, Paul,

would you be in condition to be one of the four champions presenting MICE results at COOL 2017

<https://indico-jsc.fz-juelich.de/event/48/> ?

If so, would you have a preference for one of the three abstracts below?

The same three talks are being prepared for NuFact 2017 by C. Hunt, J. Nugent and F. Drielsma. So your task would not be so difficult. NB each of them will rehearse his talk at the MICE VC of Sep 7.

Our fourth presentation at COOL 2017 will precede these three and will be a general introduction to MICE also in preparation (by Melissa) for Sep 7.

Please reply literally as soon as possible. Especially if your answer had unfortunately to be negative.

Vittorio  
for the MICE Speakers Bureau

- >
- > 2) Recent results from MICE on multiple Coulomb scattering and energy
- > loss
- >
- > Multiple coulomb scattering and energy loss are well known phenomena
- > experienced by charged particles as they traverse a material and
- > energy loss is a similarly well studied phenomenon for particles in
- > matter. However, from recent measurements by the MuScat
- > collaboration, it is known that the available simulation codes,
- > specifically GEANT4, overestimate the scattering of muons in low Z
- > materials. This is of particular interest to the Muon Ionization
- > Cooling Experiment (MICE) collaboration which has the goal of

## COOL 2017

from Monday, 18 September 2017 at **08:30** to Friday, 22 September 2017 at **18:00** (Europe/Berlin)  
at **Gustav-Stresemann-Institut, Bonn**

Langer Grabenweg 68 D-53175 Bonn

### Description News:

- [Dieter-Möhl-Medal 2017 for Prof. Takeshi Katayama](#)
- [Dieter-Möhl-Medal 2017 for Dr. Markus Steck](#)
- [Dieter-Möhl-Award 2017 for Dr. Vsevolod Kamerzhiev](#)
- [Conference Photos](#)

Dear Colleagues,

we are delighted to invite you to join us for the 11th bi-annual COOL workshop on the 18th to 22nd of September 2017 at the Gustav-Stresemann-Institute Bonn. This year's workshop will be touching on topics from all across the field of beam cooling, including:

- electron cooling
- stochastic cooling
- muon cooling
- cooled beam dynamics
- new concepts and theoretical advancements in beam cooling
- facility status updates and beam cooling reviews

There will be lots of opportunity to gather and exchange thoughts, ideas and opinions in a relaxed environment. We would like to invite anyone from the field, accelerator physicists, engineers and students, to participate in this year's event. There will be oral presentations, both invited and contributed, as well as poster sessions during the week. Conference Proceedings will be published electronically on JACoW a couple of weeks after the workshop.

There will be an option for accommodation at the Gustav-Stresemann-Institut. If you would like to reserve a room there please indicate so during your registration. The price will be 73€ per person and night including breakfast. If you are arriving by car, there is parking available at the rate of 8€ per day for hotel guests. The workshop will also feature a banquet to facilitate informal exchange and gathering. Please let us know whether you would like to attend on the registration form.

The workshop fee will be 450€ per person. This will include the conference dinner as well as full board (lunch and dinner). It is to be paid in advance electronically. After registration you will be contacted by Forschungszentrum Jülich with instructions how to pay. Both credit card payment as well as bank transfer will be possible.

For those colleagues who need to apply for a visa we are happy to provide a letter of invitation on [request](#).

We hope to see you all in September.

The organisation committee.

Registration and abstract submission are now open.

Please register by September 8th. Abstracts are due September 8th and contributions to the proceedings must be submitted by September 18th.

Conference fee announced: 450€

Hotel rate announced: 73€ per person and night

Material:  

[Go to day](#)

### Monday, 18 September 2017

- |               |                          |
|---------------|--------------------------|
| 10:00 - 11:00 | Registration             |
| 11:00 - 11:30 | Coffee Break             |
| 11:30 - 12:50 | Registration             |
| 13:00 - 14:00 | Lunch Break              |
| 14:00 - 16:00 | Muon I                   |
|               | Convener: Dieter Prasuhn |
| 14:00         | <b>Welcome 20'</b>       |
|               | Speaker: Dieter Prasuhn  |

- 14:20 **MICE muon ionization cooling – progress and first results** 50'  
 Speaker: M.A. Uchida  
 Material: [Slides](#) 
- 15:10 **Measurement of phase-space density evolution in MICE** 50'  
 Speaker: D. Maletic  
 Material: [Slides](#) 
- 16:00 - 16:30 Coffee Break
- 16:30 - 17:50 Muon II  
 Convener: Yuhong Zhang
- 16:30 **Recent results from the study of emittance evolution in MICE** 40'  
 Speaker: M.A. Uchida  
 Material: [Slides](#) 
- 17:10 **Recent results from MICE on multiple Coulomb scattering and energy loss** 40'  
 Speaker: D. Maletic  
 Material: [Slides](#) 

## Tuesday, 19 September 2017

- 09:00 - 11:00 E-Cooling I / L-Cooling  
 Convener: Markus Steck
- 09:00 **Low Energy Cooler for NICA Booster** 40'  
 Speaker: Alexander Bubley  
 Material: [Slides](#) 
- 09:40 **Scaling Laser Cooling of Ion Beams towards High Beam Energies** 40'  
 Speaker: M.H. Bussmann  
 Material: [Slides](#) 
- 10:20 **Electron cooling at COSY – status and perspectives** 40'  
 Speaker: Vsevolod Kamerzhiev  
 Material: [Slides](#) 
- 11:00 - 11:30 Coffee Break
- 11:30 - 13:00 E-Cooling II  
 Convener: Jürgen Dietrich
- 11:30 **The High Voltage cooler for NICA, Status and Ideas** 30'  
 Speaker: Vladimir Borisovich Reva  
 Material: [Slides](#) 
- 12:00 **Model Development for the Automated Setup of the 2 MeV Electron Cooler Transport Channel** 30'  
 Speaker: Arthur Johannes Halama  
 Material: [Slides](#) 
- 12:30 **Status of the Turbine Concept for Relativistic electron coolers** 30'  
 Speaker: Kurt Aulenbacher  
 Material: [Slides](#) 
- 13:00 - 14:00 Lunch Break
- 14:00 - 17:50 Poster
- 14:00 **Beam Tracking Studies of Electron Cooling in ELENA** 3h50'  
 Speaker: Javier Resta-López
- 14:00 **Towards Laser Cooling of Relativistic  $^{16}\text{O}^{5+}$  Ion Beams at the CSR** 3h50'  
 Speaker: Hanbing Wang
- 14:00 **Muon Cooling Research at Fermilab** 3h50'  
 Speaker: David Vincent Neuffer
- 14:00 **Stochastic cooling theory based on Langevin equations** 3h50'  
 Speaker: Nikolay Shurkhno
- 14:00 **Emittance Measurement of Cooled Beams** 3h50'

Talk on bulk MC production at MPB ...

**Subject:** Talk on bulk MC production at MPB ...  
**From:** Kenneth Long <k.long@imperial.ac.uk>  
**Date:** 2/23/17, 9:06 AM  
**To:** Dimitrije Maletic <maletic@ipb.ac.rs>  
**CC:** Durga Rajaram <durga@fnal.gov>, Dr Chris Rogers <Chris.Rogers@stfc.ac.uk>

Dimitrije,

I have been working on the agenda for teh next MICE Project Board (where we report on the project to the funders). One issue that they have pressed us on in the past is the MC processing. We're now OK with that thanks to your work to make batch production on the grid.

Would you be willing to explain the way we do the processing and demonstrate that this is not an issue for the MICE analysis? The talk will be at RAL on 07Mar17.

I do hope you will be able to do this!

K

*Kenneth Long*

*EMail: [K.Long@Imperial.AC.UK](mailto:K.Long@Imperial.AC.UK)*

*Mobile: work : +44-(0)7824 560302*

*home: +44-(0)7890-595138*

## MICE Project Board and Resource Loaded Schedule Review, March 2017

[Back](#)

### Documentation

- **Resource Loaded Schedule Review:**
  - [Resource Loaded Schedule, costs and risks to complete MICE](#)
- **MICE Project Board:**
  - [MICE report to the MICE Project Board](#)
- **Funding Agency Committee:**
  - <http://micewww.pp.rl.ac.uk/attachments/8384/Common-Fund.pdf>
- **Supporting documents:**
  - Step IV Hydrogen Project Plan: [170307\\_MICE\\_LH2\\_system\\_plan.mpp](#)
- **Recent reviews:**
  - [UK Cost-to-Completion Review](#)
  - [Meeting 28th June 2016 - Agenda and Files can be found with this link](#)
- **Responses to "homework questions":**
  - **Q1:** MICE Muon Beam; simulation and tuning:
    - Please give an example of a comparison between simulation and measured data through the beamline from the target to the EMR.
    - What are the physical quantities used in the comparison? (Phase-space plots and what else?)
    - What are the parameters that are used in fitting the optics tuning data? (For example initial particle distribution, magnet settings, absorber settings, et cetera?)
    - How are the multiple Monte Carlo and other simulations integrated together? Why are the interface locations where they are?
  - **Q1 Response:** C. Rogers, P. Franchini, D. Rajaram: [homework-question-1.pdf](#)
  - **Q2:** What is the capability of U.S. members of the MICE collaboration to take part in the 2017/02 cycle (from September 19 to October 27) if such a data-taking run occurs? What would be the optimum (approximate) distribution between shifters and hardware experts?
  - **Q2 Response:** M. Palmer: [MPB\\_Q2\\_Response.pdf](#)

[Back](#)

### RLSR, MPB & FAC outline agendas - 07 & 08 March 2017

Venue: Conference Room 12/13, Building R68, RAL

Tuesday, 07 March 2017 and Wednesday, 08 March 2017

#### RLSR & MPB-11 outline agendas

| 07 March 2017 |  |              |           |
|---------------|--|--------------|-----------|
| 09:00-09:20   | RLSR closed session - introduction   |              |           |
| 09:20-10:00   | Project overview: <a href="#">01-2017-03-07-Long.pptx</a>                                | K. Long      | 30' + 10' |
| 10:00-10:15   | Coffee   |              | 15'       |
| 10:15-12:15   | RLSR presentations & questions   |              |           |
| 10:15-10:55   | Project Manager's report: <a href="#">02-2017-03-07-Whyte.pdf</a>                        | C. Whyte     | 30' + 10' |
| 10:55-11:20   | Status of the liquid-hydrogen project: <a href="#">03-2017-03-07-Bayliss.pdf</a>         | V. Bayliss   | 20' + 5'  |
| 11:20-11:55   | Completion of the US construction project: <a href="#">04-2017-03-07-Bross.pptx</a>      | A. Bross     | 25' + 10' |
| 11:55-12:15   | MICE project in the US; completion of efforts: <a href="#">05-2017-03-07-Palmer.pptx</a> | M. Palmer    | 15' + 5'  |
| 12:15-13:00   | Lunch  |              |           |
| 13:00-13:30   | RLSR closed session session--critical findings   |              |           |
| 13:30-15:00   | MPB: Operations, software and computing  |              |           |
| 13:30-13:55   | Commissioning and operation: <a href="#">06-2017-03-07-Hodgson.pdf</a>                   | P. Hodgson   | 20' + 5'  |
| 13:55-14:20   | Operation of the magnetic channel: <a href="#">07-2017-03-07-Boehm.pdf</a>               | J. Boehm     | 20' + 5'  |
| 14:20-14:40   | Bulk production of Monte Carlo: <a href="#">08-2017-03-07-Maletic_v2.pptx</a>            | D. Maletic   | 15' + 5'  |
| 14:40-15:00   | Software and computing overview: <a href="#">09-2017-03-07-Rajaram.pdf</a>               | D. Rajaram   | 15' + 5'  |
| 15:00-15:15   | Tea  |              |           |
| 13:30-15:00   | MPB: MICE Muon Beam and MICE experiment  |              |           |
| 15:15-15:45   | Tuning the MICE Muon Beam: <a href="#">10-2017-03-07-Franchini.pdf</a>                   | P. Franchini | 25' + 5'  |
| 15:45-16:15   | Detector performance: <a href="#">11-2017-03-07-Overton.pdf</a>                          | E. Overton   | 25' + 5'  |

Using the Grid For Data Analysis

Authors: Paul Keyberd, Maletic Dimitrije, Paolo Francini  
Event date: Thursday, April 18, 2019 5:45:00 PM  
MICE Video Conference 210

Hybrid MC Update

Authors: Maletic Dimitrije  
Start Date: Thursday, December 06, 2018 4:25:00 PM  
Event: MICE Video Conference 207

MC Batch Production Status

Authors: Maletic Dimitrije  
Start Date: Friday, October 12, 2018 3:20:00 PM  
Event: MICE CM52

MC Status

Authors: Maletic Dimitrije  
Start Date: Wednesday, October 04, 2017 10:00:00 AM  
Event: MICE CM48

Batch/MC

Authors: Maletic Dimitrije  
Start Date: Monday, October 02, 2017 12:50:00 PM  
Event: MICE CM49

MC Status

Authors: Maletic Dimitrije  
Start Date: Thursday, June 29, 2017 10:00:00 AM  
Event: MICE CM48

MC Production

Authors: Maletic Dimitrije  
Start Date: Monday, February 13, 2017 6:00:00 PM  
Event: MICE CM47

GRID MC Production

Authors: Maletic Dimitrije  
Start Date: Thursday, July 28, 2016 3:20:00 PM  
Event: MICE CM45

Energy Loss 2

Authors: Maletic Dimitrije  
Start Date: Wednesday, March 30, 2016 5:30:00 PM  
Event: MICE CM44

Batch MC

Authors: Maletic Dimitrije  
Start Date: Wednesday, March 30, 2016 4:55:00 PM  
Event: MICE CM44

Measurement of Energy Loss (2)

Authors: Maletic Dimitrije  
Start Date: Thursday, October 29, 2015 10:20:00 AM  
Event: MICE CM43

Energy Loss Measurement

Authors: Maletic Dimitrije  
Start Date: Monday, June 22, 2015 1:10:00 PM  
Event: MICE CM42

Visit Computer Centre

Authors: Dordevic Milos, Maletic Dimitrije

Start Date: Sunday, November 11, 2012 1:00:00 PM

Event: Novi Sad University Students

Physics with the CMS ECAL

Authors: Maletic Dimitrije

Start Date: Thursday, October 29, 2009 11:30:00 AM

Event: Serbian and Montenegrin Teachers Programme 2009

Event Details

## 9. решење о претходном избору у звање

Република Србија  
МИНИСТАРСТВО ПРОСВЕТЕ,  
НАУКЕ И ТЕХНОЛОШКОГ РАЗВОЈА  
Комисија за стицање научних звања

Број:660-01-00042/543  
26.03.2015. године  
Београд

|                         |       |        |       |
|-------------------------|-------|--------|-------|
| ИНСТИТУТ ЗА ФИЗИКУ      |       |        |       |
| ПРИЈАВА БРОЈ 17-04-2015 |       |        |       |
| Рад. јед.               | Број  | Серија | рилог |
| 0801                    | 493/1 |        |       |

На основу члана 22. става 2. члана 70. став 6. Закона о научноистраживачкој делатности ("Службени гласник Републике Србије", број 110/05 и 50/06 – исправка и 18/10), члана 2. става 1. и 2. тачке 1 – 4.(прилози) и члана 38. Правилника о поступку и начину вредновања и квантитативном исказивању научноистраживачких резултата истраживача ("Службени гласник Републике Србије", број 38/08) и захтева који је поднео

*Инстџиџуџи за физику у Београду*

Комисија за стицање научних звања на седници одржаној 26.03.2015. године, донела је

### ОДЛУКУ О СТИЦАЊУ НАУЧНОГ ЗВАЊА

*Др Димџирије Малџиџић*

стиче научно звање

*Виџи научни сарадник*

у области природно-математичких наука - физика

О Б Р А З Л О Ж Е Њ Е

*Инстџиџуџи за физику у Београду*

утврдио је предлог број 1437/1 од 28.10.2014. године на седници научног већа Института и поднео захтев Комисији за стицање научних звања број 1455/1 од 12.11.2014. године за доношење одлуке о испуњености услова за стицање научног звања *Виџи научни сарадник*.

Комисија за стицање научних звања је по претходно прибављеном позитивном мишљењу Матичног научног одбора за физику на седници одржаној 26.03.2015. године разматрала захтев и утврдила да именовани испуњава услове из члана 70. став 6. Закона о научноистраживачкој делатности ("Службени гласник Републике Србије", број 110/05 и 50/06 – исправка и 18/10), члана 2. става 1. и 2. тачке 1 – 4.(прилози) и члана 38. Правилника о поступку и начину вредновања и квантитативном исказивању научноистраживачких резултата истраживача ("Службени гласник Републике Србије", број 38/08) за стицање научног звања *Виџи научни сарадник*, па је одлучила као у изреци ове одлуке.

Доношењем ове одлуке именовани стиче сва права која му на основу ње по закону припадају.

Одлуку доставити подносиоцу захтева, именованом и архиви Министарства просвете, науке и технолошког развоја у Београду.

ПРЕДСЕДНИК КОМИСИЈЕ

Др Станислава Стоџиџић-Груџиџић,  
научни саветник

*С. Станислава Стоџиџић-Груџиџић*

ДРЖАВНИ СЕКРЕТАР

Др Александар Белџић

*Александар Белџић*